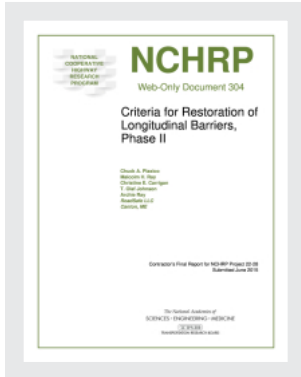


This PDF is available at <http://nap.edu/26321>

SHARE



Criteria for Restoration of Longitudinal Barriers, Phase II (2021)

DETAILS

480 pages | 8.5 x 11 | PAPERBACK

ISBN 978-0-309-08529-8 | DOI 10.17226/26321

CONTRIBUTORS

Chuck A. Plaxico, Malcolm H. Ray, Christine E. Carrigan, T. Olaf Johnson, Archie Ray; National Cooperative Highway Research Program; Transportation Research Board; National Academies of Sciences, Engineering, and Medicine

SUGGESTED CITATION

National Academies of Sciences, Engineering, and Medicine 2021. *Criteria for Restoration of Longitudinal Barriers, Phase II*. Washington, DC: The National Academies Press. <https://doi.org/10.17226/26321>.

GET THIS BOOK

FIND RELATED TITLES

Visit the National Academies Press at NAP.edu and login or register to get:

- Access to free PDF downloads of thousands of scientific reports
- 10% off the price of print titles
- Email or social media notifications of new titles related to your interests
- Special offers and discounts



Distribution, posting, or copying of this PDF is strictly prohibited without written permission of the National Academies Press. (Request Permission) Unless otherwise indicated, all materials in this PDF are copyrighted by the National Academy of Sciences.

Copyright © National Academy of Sciences. All rights reserved.

NCHRP

Web-Only Document 304

Criteria for Restoration of Longitudinal Barriers, Phase II

Chuck A. Plaxico
Malcolm H. Ray
Christine E. Carrigan
T. Olaf Johnson
Archie Ray
RoadSafe LLC
Canton, ME

Contractor's Final Report for NCHRP Project 22-28
Submitted June 2015

NATIONAL COOPERATIVE HIGHWAY RESEARCH PROGRAM

Systematic, well-designed, and implementable research is the most effective way to solve many problems facing state departments of transportation (DOTs) administrators and engineers. Often, highway problems are of local or regional interest and can best be studied by state DOTs individually or in cooperation with their state universities and others. However, the accelerating growth of highway transportation results in increasingly complex problems of wide interest to highway authorities. These problems are best studied through a coordinated program of cooperative research.

Recognizing this need, the leadership of the American Association of State Highway and Transportation Officials (AASHTO) in 1962 initiated an objective national highway research program using modern scientific techniques—the National Cooperative Highway Research Program (NCHRP). NCHRP is supported on a continuing basis by funds from participating member states of AASHTO and receives the full cooperation and support of the Federal Highway Administration (FHWA), United States Department of Transportation, under Agreement No. 693JJ31950003.

COPYRIGHT INFORMATION

Authors herein are responsible for the authenticity of their materials and for obtaining written permissions from publishers or persons who own the copyright to any previously published or copyrighted material used herein.

Cooperative Research Programs (CRP) grants permission to reproduce material in this publication for classroom and not-for-profit purposes. Permission is given with the understanding that none of the material will be used to imply TRB, AASHTO, FAA, FHWA, FTA, GHSA, NHTSA, or TDC endorsement of a particular product, method, or practice. It is expected that those reproducing the material in this document for educational and not-for-profit uses will give appropriate acknowledgment of the source of any reprinted or reproduced material. For other uses of the material, request permission from CRP.

DISCLAIMER

The opinions and conclusions expressed or implied in this report are those of the researchers who performed the research. They are not necessarily those of the Transportation Research Board; the National Academies of Sciences, Engineering, and Medicine; the FHWA; or the program sponsors.

The information contained in this document was taken directly from the submission of the author(s). This material has not been edited by TRB.

The National Academies of
SCIENCES • ENGINEERING • MEDICINE



TRANSPORTATION RESEARCH BOARD

The National Academies of **SCIENCES • ENGINEERING • MEDICINE**

The **National Academy of Sciences** was established in 1863 by an Act of Congress, signed by President Lincoln, as a private, non-governmental institution to advise the nation on issues related to science and technology. Members are elected by their peers for outstanding contributions to research. Dr. Marcia McNutt is president.

The **National Academy of Engineering** was established in 1964 under the charter of the National Academy of Sciences to bring the practices of engineering to advising the nation. Members are elected by their peers for extraordinary contributions to engineering. Dr. John L. Anderson is president.

The **National Academy of Medicine** (formerly the Institute of Medicine) was established in 1970 under the charter of the National Academy of Sciences to advise the nation on medical and health issues. Members are elected by their peers for distinguished contributions to medicine and health. Dr. Victor J. Dzau is president.

The three Academies work together as the **National Academies of Sciences, Engineering, and Medicine** to provide independent, objective analysis and advice to the nation and conduct other activities to solve complex problems and inform public policy decisions. The National Academies also encourage education and research, recognize outstanding contributions to knowledge, and increase public understanding in matters of science, engineering, and medicine.

Learn more about the National Academies of Sciences, Engineering, and Medicine at www.nationalacademies.org.

The **Transportation Research Board** is one of seven major programs of the National Academies of Sciences, Engineering, and Medicine. The mission of the Transportation Research Board is to provide leadership in transportation improvements and innovation through trusted, timely, impartial, and evidence-based information exchange, research, and advice regarding all modes of transportation. The Board's varied activities annually engage about 8,000 engineers, scientists, and other transportation researchers and practitioners from the public and private sectors and academia, all of whom contribute their expertise in the public interest. The program is supported by state transportation departments, federal agencies including the component administrations of the U.S. Department of Transportation, and other organizations and individuals interested in the development of transportation.

Learn more about the Transportation Research Board at www.TRB.org.

COOPERATIVE RESEARCH PROGRAMS

CRP STAFF FOR NCHRP WEB-ONLY DOCUMENT 304

Christopher J. Hedges, *Director, Cooperative Research Programs*

Lori L. Sundstrom, *Deputy Director, Cooperative Research Programs*

David Jared, *Senior Program Officer*

Clara Schmetter, *Senior Program Assistant*

Natalie Barnes, *Director of Publications*

Kathleen Mion, *Senior Editorial Assistant*

NCHRP PROJECT 22-28 Panel

Field of Design—Area of Vehicle Barrier Systems

Bernie L. Clocksin, *South Dakota DOT, Pierre, SD (Chair) (retired)*

Michael S. Bline, *Office of Licking County (OH) Engineer, Newark, OH*

D. Lance Bullard, Jr., *Texas A&M Transportation Institute, College Station, TX*

Mark Burkhead, *Harrisburg, PA*

Scott Gardner Capps, *North Carolina DOT, Raleigh, NC*

Douglas Gabauer, *Bucknell University, Lewisburg, PA*

Armando Garcia, *Coffman Specialties, Inc., San Diego, CA*

David L. Little, *Iowa DOT, Mason City, IA*

Eduardo Arispe, *FHWA Liaison*

Nicholas Artimovich, II, *FHWA Liaison*

James Bryant, Jr., *TRB Liaison*

CONTENTS

Chapter 1 – Introduction.....	1
Project Objective.....	1
Background.....	2
Roadmap of the Report.....	4
Chapter 2 – A Summary of Common Non-Proprietary Guardrails (Basic Design and Crash Performance).....	6
Crash Testing for Federal Aid Eligibility.....	6
Summary of Common Non-Proprietary Strong-Post Guardrail Systems.....	7
Modified G4(1S) with Routed Wood Blockouts.....	7
G4(2W).....	13
G4(1W).....	15
MGS.....	15
MGS with Round Wood Posts.....	16
G9 Thrie-Beam Guardrail.....	17
Thrie-Beam Guardrail with Wood Blockouts.....	21
Modified Thrie-Beam Guardrail.....	21
Summary of Full-Scale Tests Conducted on Strong-Post Guardrail.....	23
Typical System Damage in Low-Speed Full-Scale Tests.....	23
Chapter 3 – Literature Review.....	28
General Crash Phenomena that Lead to Poor Performance.....	28
Pocketing.....	28
Wheel Snag.....	29
Barrier Override.....	29
Rail Rupture.....	30
General Functions and Influences of Guardrail Components.....	30
Posts and Soil.....	30
Blockouts.....	47
Rail-to-Post Connection.....	54

Rail Element.....	57
End Terminals.....	64
Summary of Literature Review.....	68
Chapter 4 – Survey of Practice	69
Chapter 5 – Prioritization of Damage Modes	71
Introduction.....	71
Methods for Evaluating Damage Modes	71
Full-Scale Testing	71
Pendulum Testing	72
Computer Simulation.....	72
Guardrail Systems.....	73
Critical Damage Modes	73
G4(1W) and G4(2W) Wood-Post W-Beam Guardrails.....	75
Thrie-Beam Steel Post Guardrail.....	85
Modified Thrie-Beam Guardrail.....	90
MGS – Steel Post W-Beam Guardrail	92
G2 – Weak-Post W-Beam Guardrail	95
End Terminals.....	96
Guardrail Transitions	99
Combination Damage Modes	99
Combination of Post and Rail Deflection and Rail-to-Post Connection.....	99
Combination of Rail Deflection and Splice Damage.....	100
Combination of Post and Rail Deflection and Anchor Damage	100
Combination of Post/Rail Deflection and Missing Post(s).....	101
Other Considerations	101
Traffic Exposure	101
Evaluating Impact Upstream or Downstream of Damaged Section:	101
Hazard Being Shielded	101
Recommendations.....	102
Chapter 6 – General Research Approach.....	105
Finite Element Analysis.....	105
Pendulum Testing	108
Chapter 7 – Development and Validation of the G4(2W) Guardrail Model	109
Model Development.....	109

W-Beam	109
Splice Connection Model.....	111
Bolt Hardware	113
Guardrail Posts.....	114
Soil Model.....	118
Vehicle Model.....	126
Validation of the G4(2W) Guardrail Model	126
Simulation of Test 471470-26	126
Qualitative Validation.....	129
Quantitative Validation.....	143
Conclusions.....	154
Chapter 8 – Evaluation of Guardrail Post Deterioration for the G4(2W).....	155
Scope.....	156
Procurement of Guardrail Post Test Articles	156
Resistograph Measurements and Processing	157
Resistograph Measurements	157
Data Processing and Interpretation	157
Statistics for Resistograph Measurement of Test Articles.....	161
Pendulum Testing of Post-in-Rigid-Foundation.....	163
Scope.....	163
Test Specimen Mounting Condition	167
Equipment and Instrumentation.....	168
Impact Conditions.....	170
Results.....	171
Correlation of Resistograph Measurements to Test Results	174
Quantifying Wood Post Deterioration Damage Levels	186
Visual and Auditory Cues.....	191
Pendulum Testing of Posts-in-Soil	191
Scope.....	191
Soil Strength Tests	194
Wood Post Strength Test	196
Effects of Post Shape (Round vs. Rectangular) on Load Capacity.....	196
Finite Element Analysis.....	200
Calibration of FE Models for Deteriorated Posts	200

Evaluate Effects of Post Deterioration on Guardrail Performance	212
Summary and Discussion.....	226
Recommendations.....	228
Chapter 9 – Effects of Anchor Strength on Performance of the G4(2W).....	230
Research Approach	231
Physical Testing.....	232
Quasi-Static Pull-Test on End-Anchor	232
Evaluate Effects of Anchor Strength on Guardrail Performance.....	240
Results.....	241
Summary and Discussion.....	251
Recommendations.....	254
Chapter 10 – Combination Damage Mode of Rail Deflection and Rail-Post Connection for the G4(2W)	255
Evaluate Effects of Rail Deflection and Rail-to-Post Connection Strength	255
Low Severity Crash-Induced Damage	255
High-Speed Impact into Pre-Damaged Guardrail.....	259
Summary and Discussion.....	266
Recommendations.....	269
Chapter 11 – Re-Assess Cause of Failure in Test C08C3-027 for the Modified G4(1S) with Pre-Crash-Induced Deflection.	271
Simulation of Test C08C3-027-1	272
Test C08C3-027-1 Summary	272
FEA Model Development.....	273
FEA Simulation	275
Simulation of Test C08C3-027-2.....	279
Test C08C3-027-2 Summary	279
Model Setup – Including Pre-Damage.....	279
FEA Simulation	280
Summary and Discussion.....	299
Conclusions.....	301
Recommendations.....	302
Chapter 12 – Effects of Soil Erosion at Guardrail Posts for the G4(2W).....	303
Research Approach	304
Physical Testing.....	304
Equipment and Instrumentation.....	307
Impact Conditions.....	308
Results.....	309

Finite Element Analysis.....	315
Calibration/Validation of FE Soil-Erosion Model.....	315
Effects of Soil Erosion on Guardrail Performance	326
Summary and Discussion.....	337
Recommendations.....	338
Chapter 13 – Anchor Strength Quantified in Terms of Anchor Damage	340
Research Approach	341
Test Set-up	342
Equipment and Instrumentation.....	347
Test Procedure	349
Test Results	350
Missing or Non-Functioning Groundline Strut.....	354
Reduced Embedment Depth	356
Slack Anchor-Cable	363
Summary and Discussion.....	368
Discussion of Failure Modes	368
Missing Groundline Strut.....	369
Reduced Embedment Depth for the Foundation Tubes.....	369
Slack in Anchor Cable	371
Recommendations.....	371
Future Work.....	373
Chapter 14 – Effects of W-Beam Splice Damage on Rail Capacity.....	375
Research Approach	375
Procurement and Assessment of Damaged W-Beam Splices.....	376
Inspection of Fully Assembled Splice (General Field-Type Measurements).....	376
Inspection of Unassembled Splice (for Hidden Damages in the Splice-Holes)	387
Physical Testing.....	387
Equipment and Instrumentation.....	387
Test Setup.....	389
Impact Conditions	393
Scope.....	393
Results.....	395
Discussion of Test Results	406
Rail Flattening.....	406
Longitudinal Displacement (Slip) in the Splice Connection	407

Vertical Crush	408
Lateral Separation of Rails at Splice.....	408
Conclusions.....	408
Recommendations.....	409
Chapter 15 – Development of Field Guide Materials and Field Testing.....	411
The Field Manual.....	411
Online Interactive Field Guide.....	412
Chapter 16 – Field Guide Application Examples	417
Example 1	418
User Input for Question 1:	418
User Input for Question 2:	419
User Input for Question 3:	419
User Input for Question 4:	419
User Input for Question 5:	420
User Input for Question 6:	420
User Input for Question 7:	420
User Input for Question 8:	421
User Input for Question 9:	421
User Input for Question 10:	421
User Input for Question 11:	422
User Input for Question 12:	422
User Input for Question 13:	422
User Input for Question 14:	423
User Input for Question 15:	423
Assessment Results:.....	424
Example 2	425
User Input for Question 1:	425
User Input for Question 2:	426
User Input for Question 3:	426
User Input for Question 4:	426
User Input for Question 5:	427
User Input for Question 6:	427
User Input for Question 7:	427

User Input for Question 8:	428
User Input for Question 9:	428
User Input for Question 10:	428
User Input for Question 11:	429
User Input for Question 12:	429
User Input for Question 13:	429
User Input for Question 14:	430
User Input for Question 15:	430
User Input for Question 16:	430
User Input for Question 17:	431
Assessment Results:.....	432
Example 3	433
User Input for Question 1:	433
User Input for Question 2:	434
User Input for Question 3:	434
User Input for Question 4:	434
User Input for Question 5:	435
Assessment Results:.....	436
Chapter 17 – Conclusions	437
Damage Modes Investigated.....	437
Recommendations for Future Work.....	438
Recommendations for Additional Barrier Types	439
REFERENCES	440

LIST OF FIGURES

Figure 1. Modified G4(1S) with wood blockouts.[<i>Bullard96</i>]	8
Figure 2. Sequential views of Crash Test 405421-1.[<i>Bullard96</i>]	8
Figure 3. Sequential views of Crash Test 2214-WB2.[<i>Polivka06b</i>]	8
Figure 4. Sequential views of Crash Test 2214-WB1.[<i>Polivka06b</i>]	8
Figure 5. Drawing of the strong-post w-beam guardrail (SGR04a-c).....	9
Figure 6. Drawing of the 8-inch wood blackout for the modified G4(1S) with wood blackout guardrail (PDB01b).....	10

Figure 7. Drawing of the W6x9 guardrail post (PWE01).	11
Figure 8. Drawing of the bolt used to fasten the rail element to guardrail posts.	12
Figure 9. Photo of the G4(2W) guardrail Test 476460-1-5 test installation.[<i>Bullard10</i>]	13
Figure 10. Sequential views of full-scale crash Test 471470-26.[<i>Mak99</i>].....	13
Figure 11. Sequential views of full-scale crash Test RF476460-1-5.[<i>Bullard10</i>]	13
Figure 12. Drawing of the rectangular wood post used in the G4(2W) and G4(1W) guardrail systems (i.e., AASHTO designator SGR04b).....	14
Figure 13. Photo of the MGS guardrail system. [<i>Sicking02</i>]	16
Figure 14. MGS with (a) 7.25-inch diameter round Douglas Fir posts and (b) 8-inch diameter round Ponderosa Pine posts.	16
Figure 15. Test MGSDF-1 of the MGS guardrail with 7.25-inch diameter Douglas Fir posts. [<i>Hascal07</i>].....	17
Figure 16. Test MGSPP-1 of MGS with 8-inch diameter Ponderosa Pine posts. [<i>Hascal07</i>].....	17
Figure 17. Photo of the standard thrie-beam guardrail (G9; SGR09a)	18
Figure 18. Sequential photos of Test 471470-31 on the G9 thrie-beam guardrail. [<i>Mak99</i>].....	18
Figure 19. AASHTO-AGC-ARTBA drawings for the SGR09 guardrail systems. [<i>AASHTO04</i>].	19
Figure 20. AASHTO-AGC-ARTBA drawings for the W6x9 steel blockout for the G9 thrie-beam guardrail.[<i>AASHTO04</i>].....	20
Figure 21. Photo of the thrie-beam guardrail with routed wood blockouts. [<i>Bullard10</i>]	21
Figure 22. Sequential photos for Test 476460-1-8 on the thrie-beam guardrail with routed wood blockouts (MASH Test 3-11).[<i>Bullard10</i>].....	21
Figure 23. Photo of the modified thrie-beam guardrail (SGR09b).	22
Figure 24. Sequential photos for Test 471470-30 on the modified thrie-beam guardrail (SGR09b) under <i>NCHRP Report 350</i> Test 3-11 conditions. [<i>Mak99</i>].....	22
Figure 25. Sequential photos for Test 404211-5a on the modified thrie-beam guardrail under <i>NCHRP Report 350</i> Test 4-12 conditions.[<i>Buth99c</i>].....	22
Figure 26. AASHTO-AGC-ARTBA drawings for the M14x17.2 steel blockout for the modified thrie-beam guardrail.[<i>AASHTO04</i>]	24
Figure 27. Low-speed Test C08C3-027.1 on the modified G4(1S) with routed wood blockouts. [<i>Fleck08</i>]	27
Figure 28. Barrier deflections recorded after Test C08C3-027.1. [<i>Fleck08</i>]	27
Figure 29. Guardrail damage in Test C08C3-027.1. [<i>Fleck08</i>]	27
Figure 30. Example of pocketing during a simulated impact with a w-beam median barrier. [<i>Fang10</i>].....	29
Figure 31. Modified Eccentric Loader Breakaway Cable Terminal. [<i>Patzner99</i>]	32
Figure 32. Illustration of wood post with failure fuse.....	35

Figure 33. Summary of TTI Test 0482-1 on the G4(2W) with 12.5-ft post spacing. [Mak93]	37
Figure 34. Maximum rail tension as a function of missing posts.[Gabler10]	38
Figure 35. Maximum dynamic deflection comparison plots: (a) KSWB-1, (b) KSWB-2, (c) KSWB-3, (d) KSWB-4. [Rosson96]	43
Figure 36. Typical steel post test installation for bogie impact testing.[Polivka00b].....	44
Figure 37. W-beam guardrail adjacent to 2:1 foreslope for full-scale crash test.[Polivka00b]	46
Figure 38. Illustration of how blockouts help reduce possibility of wheel-s snag.[Ray04].....	47
Figure 39. Wheel snag against guardrail post in TTI Test 471470-26.[Mak94].....	48
Figure 40. Illustration of how blockouts help to maintain critical rail height during post deflection.....	49
Figure 41. Peak tire-post impact force as a function of blockout depth for Report 350 TL-3 impacts.[Karlsson00]	49
Figure 42. Modified thrie-beam guardrail (SGR09b).[Sheikh09]	52
Figure 43. Deformation of thrie-beam guardrail during impact with 4,577-lb vehicle at 85 mph and 25 degree impact.[Sheikh09]	53
Figure 44. Position of bolt in slotted hole in w-beam for each load case.[Plaxico03].....	56
Figure 45. Results from uniaxial tests on rail-to-post connections.[Plaxico03]	56
Figure 46. Effective plastic strains in the back layer of w-beam in a guardrail splice showing the formation of a plastic hinge. [Ray01b].....	58
Figure 47. Von Mises stress contour plot showing relatively low stresses on the top layer of rail in the rail splice.[Ray01b]	58
Figure 48. Pendulum test setup for the Gabler et al. study. [Gabler10]	59
Figure 49. Fabricated splice damage mode evaluated by Gabler et al. [Gabler10].....	60
Figure 50. Test 473750-1 on a weak-post w-beam guardrail resulting in rail rupture. [Buth00a] 62	
Figure 51. Sequential view of Report 350 Test 3-11 on the modified G2 at 32.25 inch rail height.[Buth00c].....	63
Figure 52. Sequential view of Report 350 Test 3-10 on the modified G2 at 32.25 inch rail height.[Buth00e].....	63
Figure 53. FEA results for Report 350 Test 3-11 on the G4(1S) guardrail with rail heights of (a) 27 inches, (b) 25.5 inches and (c) 24 inches.[Marzougui07a]	63
Figure 54. Full-scale test results for Report 350 Test 3-11 on the G4(1S) guardrail with rail heights of (a) 27 inches and (b) 24.5 inches.[Marzougui07a]	64
Figure 55. Sketch of typical guardrail anchor system.	65
Figure 56. Generic end-terminal used in full-scale Crash Test 2214-WB1 of a strong-post guardrail system.[Polivka06a]	65

Figure 57. Test results for Test NEC-1 on modified G4(1S) with wood blockouts and 4-inch curb. [Polivka00a].....	66
Figure 58. Guardrail damage in Test TTI 404201-1.[Bullard00]	67
Figure 59. Typical damage modes for wood post guardrails.[Bullard00;Mak95].....	75
Figure 60. Typical damage mode for steel wide-flange posts.[Fleck08b]	75
Figure 61. Post-test photo for Test MGA C08C3-027.2 showing the un-failed rail-post connection which resulted in the post pulling the rail down during impact.[Fleck08b]	76
Figure 62. Post-test photo for Test MGA C08C3-027.2 showing the excessive anchor movement that occurred during the test.[Fleck08b]	77
Figure 63. Post fracture below groundline due to rot. [Photo provided by Mark Bloschok]	78
Figure 64. Illustration of possible splice deformation mode resulting from a split blockout.	81
Figure 65. Blockout split during Test NEC-1 (left) and in Test 405160-1-1 (right).[Polivka00a; Buth06].....	81
Figure 66. Splice damage mode investigated in Report 656.[Gabler10].....	84
Figure 67. Splice rupture initiated at downstream splice bolts in (a) Test NEC-1, (b) Test 405160-1-1 and (c) Test C08C3-027.1. [Polivka00a; Buth06; MGA08b].....	84
Figure 68. Effective plastic strain contour plot at a splice connection. [Ray01b].....	85
Figure 69. Photo of the standard thrie-beam guardrail.....	87
Figure 70. Flow chart for developing damage assessment criteria for the G4(2W) and the generic end-terminal.	106
Figure 71. Flow chart for developing damage assessment criteria for the G4(1S)......	107
Figure 72. Finite element model of the G4(2W) guardrail.....	110
Figure 73. Angle perspective view illustrating typical components of guardrail model.	110
Figure 74. Components of the finite element model of a weak-post w-beam guardrail splice used in Ray <i>et al.</i> [Ray01a]	112
Figure 75. Splice connection model used in current study.	112
Figure 76. Test setup and axial force-displacement graphs from uniaxial tension tests of guardrail splices. [Engstrand00]	113
Figure 77. Test set-up and FEA model used in wood-model validation.....	117
Figure 78. Force vs. deflection plots from dynamic impact tests 13009K and 13009L at impact speed of 20 mph.	117
Figure 79. Energy vs. deflection plots from dynamic impact tests 13009K and 13009L at impact speed of 20 mph.	118
Figure 80. Force vs. deflection plots from dynamic impact analysis with pre-defined properties in MAT143 for (a) clear wood, (b) grade DS-65 and (c) grade 1.	119

Figure 81. Energy vs. deflection plots from dynamic impact analysis with pre-defined properties in MAT143 for (a) clear wood, (b) grade DS-65 and (c) grade 1.....	119
Figure 82. Sequential views of (a) Test 13009L and analyses for post model with pre-defined MAT143 properties for (b) clear wood, (c) grade DS-65 and (d) grade 1.....	120
Figure 83. Force vs. deflection plots from dynamic impact analysis using properties for (1) Grade 1 and (2) quality factors set to $Q_T=0.60$ and $Q_C=0.7$	121
Figure 84. Energy vs. deflection plots from dynamic impact analysis using properties for (1) Grade 1 and (2) quality factors set to $Q_T=0.60$ and $Q_C=0.7$	121
Figure 85. Soil springs attached directly to post. [Patzner99].....	123
Figure 86. Soil modeled with non-linear springs and contact plates.	124
Figure 87. Sequential views illustrating typical model response to simulated bogie impact load.	124
Figure 88. Force vs. displacement results from FE analysis compared with Test 13010F.	125
Figure 89. Energy vs. displacement results from FE analysis compared with Test 13010F.	125
Figure 90. Comparison of properties for the test and analysis vehicle.	128
Figure 91. Comparison of G4(2W) guardrail after crash event for Test 471470-26 and FE analysis.....	130
Figure 92. Sequential views of TTI Test 471470-26 and FE analysis from overhead viewpoint.	132
Figure 93. Sequential views of TTI Test 471470-26 and FE analysis from downstream viewpoint.	134
Figure 94. Sequential views of TTI Test 471470-26 and FE analysis from an oblique viewpoint behind the system.....	136
Figure 95. Location of accelerometer in FE model.....	139
Figure 96. Longitudinal acceleration-time history plot from accelerometer at c.g. for full-scale Test 471470-26 and FEA (10-ms and 50-ms moving averages).....	141
Figure 97. Lateral acceleration-time history plot from accelerometer at c.g. for full-scale Test 471470-26 and FEA (10-ms and 50-ms moving averages).	141
Figure 98. Vertical acceleration-time history plot from accelerometer at c.g. for full-scale Test 471470-26 and FEA (10-ms and 50-ms moving averages).	141
Figure 99. Yaw-time history plot from accelerometer at c.g. for full-scale test 471470-26 and FEA (angular rate and displacement).	142
Figure 100. Roll-time history plot from accelerometer at c.g. for full-scale test 471470-26 and FEA (angular rate and displacement).....	142
Figure 101. Pitch-time history plot from accelerometer at c.g. for full-scale test 471470-26 and FEA (angular rate and displacement).....	142
Figure 102. Plot of global energy-time histories from the analysis.	146

Figure 103. RSVVP metric selection for validation assessment.....	147
Figure 104. Posts from Ohio DOT procured for the Physical Test Program.	156
Figure 105. IML Resi-F400 S Resistograph.	157
Figure 106. Schematic of typical (a) Free-body and (b) strain and stress diagrams for non-homogeneous beam under bending load.	158
Figure 107. Schematic illustrating internal force distribution through cross-section of a circular shaped post.	159
Figure 108. Resistograph results for Post A.....	159
Figure 109. Schematic illustrating the local moduli and subareas associated with the various points through the post thickness at $y = y_i$	160
Figure 110. Cumulative distribution plot for M^*	161
Figure 111. Cumulative distribution plot for U^*	162
Figure 112. Resistograph data corrected for drift.....	162
Figure 113. Photo of post specimen soaking in tank of water.	167
Figure 114. Rigid steel sleeve used for post mounting.	167
Figure 115. 2,372-lb pendulum device with semi-rigid nose.....	168
Figure 116. Schematic of the accelerometer instrumentation for the pendulum tests.	169
Figure 117. High-speed camera specifications and placement.	170
Figure 118. Photo of Test 13009G1 showing Post 71 breaking below groundline.	171
Figure 119. Typical force and energy curves annotated to illustrate location of peak force, initial rupture energy, and rupture energy computed from pendulum test results.....	172
Figure 120. Cumulative distribution plot for the peak force values measured in Test Series 13009 (Group 2).	177
Figure 121. Cumulative distribution plot for the strain energy in the post at initiation of rupture measured in Test Series 13009 (Group 2).	177
Figure 122. Cumulative distribution plot for the total energy absorbed by the post at complete rupture measured in Test Series 13009 (Group 2).	178
Figure 123. Peak Force vs. M^* for Test Series 13009 Group 2 (all data).	178
Figure 124. Peak Moment vs. M^* for Test Series 13009 Group 2 (all data).	179
Figure 125. Energy at rupture initiation vs. U^* for Test Series 13009 Group 2 (all data).	179
Figure 126. Rupture Energy vs. U^* for Test Series 13009 group 2 (all data).	180
Figure 127. Test Summary Sheet for Test 13009Q1.....	181
Figure 128. Test Summary Sheet for Test 13009S1.	182
Figure 129. Peak Force vs. M^* for Test Series 13009 Group 2 (revised data set).	183
Figure 130. Energy at Initial Break vs. U^* for Test Series 13009 Group 2 (revised data set).	183

Figure 131. Test Summary Sheet for Test 13009T1.	184
Figure 132. Test summary sheet for Test 13009Y1.	185
Figure 133. Pendulum impact tests from Series 13009 corresponding to deterioration damage level 1 (DL1).	188
Figure 134. Pendulum impact tests from Series 13009 corresponding to deterioration damage level 2 (DL2).	188
Figure 135. Pendulum impact tests from Series 13009 corresponding to deterioration damage level 3 (DL3).	188
Figure 136. Examples of aged posts corresponding to deterioration levels DL1 through DL3...	189
Figure 137. Graphical representation of damage levels with respect to resi-score, S_M , and load capacity.	190
Figure 138. Graphical representation of damage levels with respect to resi-score, S_U , and strain energy capacity.	190
Figure 139. Tests 13010A, B and C resulted in relatively little soil displacement.	194
Figure 140. Force vs. deflection results for soil strength tests.	195
Figure 141. Energy vs. deflection results for soil strength tests.	195
Figure 142. Summary sheet for Test 13010G.	197
Figure 143. Summary sheet for Test 13010H.	198
Figure 144. Summary sheet for Test 13010I.	199
Figure 145. Section modulus for round posts with radius ranging from 7 to 8 inches compared to the 6x8 rectangular post.	201
Figure 146. Finite element model used for calibrating material property values for various deterioration levels of wood posts.	203
Figure 147. Force vs. deflection for DL1(a) wood post model corresponding to Test 13009H1 (ductile response).	203
Figure 148. Energy vs. deflection for DL1(a) wood post model corresponding to Test 13009H1 (ductile response).	204
Figure 149. Force vs. deflection for DL1(b) wood post model corresponding to Test 13009L1 (brittle response).	204
Figure 150. Energy vs. deflection for DL1(b) wood post model corresponding to Test 13009L1 (brittle response).	205
Figure 151. Sequential views of Test 13009H1 and FE analysis DL1(a).	206
Figure 152. Sequential views for Test 13009L1 and FE analysis DL1(b).	207
Figure 153. Force vs. deflection for DL1(a) wood post model corresponding to Test 13009H1 (ductile response).	208

Figure 154. Energy vs. deflection for DL1(a) wood post model corresponding to Test 13009H1 (ductile response).	209
Figure 155. Force vs. deflection for DL3(a) wood post model and Tests 13009S1 and 13009N1 (more ductile response).	210
Figure 156. Force vs. deflection for DL3(b) wood post model and Tests 13009S1 and 13009N1 (more brittle response).	210
Figure 157. Energy vs. deflection for DL3(a) wood post model and Tests 13009S1 and 13009N1 (more ductile response).	211
Figure 158. Energy vs. deflection for DL3(b) wood post model and Tests 13009S1 and 13009N1 (more brittle response).	211
Figure 159. Analysis setup for evaluation of uniform deterioration of posts in the impact region.	213
Figure 160. Summary of barrier damage evaluation from analysis of uniform post deterioration.	214
Figure 161. Summary of anchor displacement at rail height from analysis of uniform post deterioration.	215
Figure 162. Effective plastic strain contour plot for w-beam in splice connection at Post 16.	216
Figure 163. Summary of occupant impact velocity evaluation of uniform post deterioration. ...	218
Figure 164. Summary of maximum occupant ridedown acceleration evaluation of uniform post deterioration.	218
Figure 165. Summary of 50-ms running average acceleration evaluation of uniform post deterioration.	219
Figure 166. Summary of maximum effective plastic strains occurring at the splice-bolt locations at Post 16.	219
Figure 167. Analysis setup for evaluation of mixed deterioration of posts in the impact region.	220
Figure 168. Summary of barrier damage evaluation from mixed post deterioration analyses. ...	221
Figure 169. Summary of anchor displacement at rail height from mixed post deterioration analyses.	222
Figure 170. Summary of occupant impact velocity evaluation of uniform post deterioration. ...	224
Figure 171. Summary of maximum occupant ridedown acceleration evaluation of uniform post deterioration.	224
Figure 172. Summary of 50-ms running average acceleration evaluation of uniform post deterioration.	225
Figure 173. Summary of maximum effective plastic strains occurring at the splice-bolt locations at Post 16.	225
Figure 174. Sketch of typical guardrail anchor system.	230

Figure 175. Generic end-terminal used in full-scale crash test 2214-WB1 of a strong-post guardrail system.[Polivka06a].....	231
Figure 176. Example – finite element model for computing force-deflection response of the standard two-post guardrail anchor system.[Plaxico03]	232
Figure 177. Test set-up for measuring force-deflection response of a standard two-post guardrail end-terminal anchor.	233
Figure 178. Photograph of anchor tubes with soil plates during installation.	234
Figure 179. Cable and pulley system used to apply tensile loading on end-terminal anchor.	234
Figure 180. Video camera specifications and placement.	235
Figure 181. Displacement- and displacement rate-time histories measured at the load point on the end of the rail.	236
Figure 182. Force-displacement response of the anchor system measured at the load point on the end of the rail.	237
Figure 183. Displacement-time history at the end-of the rail and at the groundline of Post 2. ...	237
Figure 184. Sequential views of Test 13011B.	238
Figure 185. Damage to end-terminal anchor in full-scale crash Test MGSDf-1.[Hascal07].....	239
Figure 186. Measured and approximated force-deflection response for the end-anchor.....	240
Figure 187. Analysis setup for evaluating effects of anchor strength on the performance of the G4(2W).	241
Figure 188. Summary of barrier damage evaluation from analyses of undamaged G4(2W) guardrail with various anchor strengths.	242
Figure 189. Summary of anchor displacement at rail height from analyses of undamaged G4(2W) guardrail with various anchor strengths.	243
Figure 190. Summary of occupant impact velocity (OIV) from analyses of undamaged G4(2W) guardrail with various anchor strengths.	244
Figure 191. Summary of occupant ridedown accelerations (ORA) from analyses of undamaged G4(2W) guardrail with various anchor strengths.....	245
Figure 192. Summary of occupant risk measures from analyses of undamaged G4(2W) guardrail with various anchor strengths.	245
Figure 193. Summary of maximum effective plastic strains occurring at the splice-bolt locations at Post 16.....	246
Figure 194. Summary of barrier damage evaluation from analyses of G4(2W) with combination of weak anchor and deteriorated posts.	247
Figure 195. Summary of anchor displacement at rail height from analyses of G4(2W) with combination of weak anchor and deteriorated posts.	248
Figure 196. Summary of occupant impact velocity (OIV) from analyses of G4(2W) with combination of weak anchor and deteriorated posts.	249

Figure 197. Summary of occupant ridedown accelerations (ORA) from analyses of G4(2W) with combination of weak anchor and deteriorated posts.	250
Figure 198. Summary of occupant risk measures from analyses of G4(2W) with combination of weak anchor and deteriorated posts.	250
Figure 199. Summary of maximum effective plastic strains occurring at the splice-bolt locations at Post 16.	251
Figure 200. Snapshot from Test C08C3-2 illustrating torsion behavior of posts upstream of impact on the G4(1S).[Fleck08b].....	252
Figure 201. Snapshot from 471470-26 illustrating torsion behavior of posts upstream of impact on the G4(2W).[Mak99a].....	252
Figure 202. System damage at upstream anchor resulting from Test MGSDf-1.[Hascall07]	253
Figure 203. Impact locations, IP01 and IP02, for low-speed impact cases.....	256
Figure 204. Example of low-severity impact damage illustrating final position of post-bolts relative to the slotted hole in w-beam.	258
Figure 205. Extent of damage resulting from impact on G4(2W) at 30 mph at Impact Point.	259
Figure 206. Initial conditions used in evaluating effects of low-level guardrail deflection on the performance of the G4(2W).	260
Figure 207. Summary of barrier damage resulting from analysis of high-speed impact into the G4(2W) with pre-existing low-severity rail deflection.	262
Figure 208. Summary of anchor displacement at rail height from analysis of high-speed impact into the G4(2W) with pre-existing low-severity rail deflection.	262
Figure 209. Summary of maximum effective plastic strains occurring at splice-bolt locations..	263
Figure 210. Summary of occupant impact velocity (OIV) from analysis of high-speed impact into the G4(2W) with pre-existing low-severity rail deflection.	265
Figure 211. Summary of occupant ridedown accelerations (ORA) from analysis of high-speed impact into the G4(2W) with pre-existing low-severity rail deflection.	265
Figure 212. Summary of 50-ms average acceleration from analysis of high-speed impact into the G4(2W) with pre-existing low-severity rail deflection.	266
Figure 213. Results of Test MGA C08C3-027.2 illustrating torsional deformation of the W6x8 steel guardrail posts during vehicle collision.[Fleck08b]	268
Figure 214. Results of Test 471470-26 illustrating the response of the wooden guardrail posts during vehicle collision.[Mak99]	268
Figure 215. Results of Test 404201-1 illustrating brittle fracture of wood posts due to tensile forces in the w-beam rail.[Bullard00].....	269
Figure 216. Anchor used in evaluation of the modified G4(1S) with wood blockouts in tests (a) 405421-1 [Bullard96], (b) 2214-WB2 [Polivka06b] and (c) C08C3-027 [Fleck08a;08b].....	271
Figure 217. Damage to guardrail in low-speed impact test C08C3-027-1.[Fleck08a]	272

Figure 218. Damage to guardrail in low-speed test C08C3-027-1 (overhead view).[Fleck08a]	273
Figure 219. Finite element model of G4(1S) for simulation of Test C08C3-027-1.....	274
Figure 220. Sequential views of FEA results compared with Test C08C3-027-1.	276
Figure 221. Impact response at 0.18 seconds for (a) full-scale test and (b) FEA illustrating wheel orientation.	277
Figure 222. Comparison of guardrail damage for (a) Test C08C3-027-1 and (b) FEA model....	278
Figure 223. Photo of upstream anchor after Test C08C3-027-1.[Fleck08a]	278
Figure 224. Contours of effective plastic strain for the initial state of the guardrail model for simulation of Test C08C3-027-2.....	280
Figure 225. Sequential Views of Test C08C3-027-2 and FE analysis Case 1 from downstream-backside view perspective.....	282
Figure 226. Sequential Views of Test C08C3-027-2 and FE analysis Case 1 from an upstream view perspective.....	284
Figure 227. Vehicle impacts against Post 15 in analysis Case 1.....	286
Figure 228. Longitudinal acceleration-time history at C.G. of pickup truck model in local coordinates for analysis Case 1.....	286
Figure 229. Lateral acceleration-time history at C.G. of pickup truck model in local coordinates for analysis Case 1.	287
Figure 230. Vertical acceleration-time history at C.G. of pickup truck model in local coordinates for analysis Case 1.	287
Figure 231. Acceleration-time history at C.G. of pickup truck model in local coordinates for analysis Case 1.	287
Figure 232. Summary report of occupant risk measures for the analysis Case 1.	288
Figure 233. Test setup for low-speed test C08C3-027-1 illustrating the limited distance to the back-edge of the soil-pit for the test article.....	289
Figure 234. Snapshots from low-speed test C08C3-027-1 illustrating the position of the guardrail posts relative to the backside of the soil pit at the beginning of the test and at 0.16 seconds.	290
Figure 235. Test setup for high-speed test C08C3-027-2 illustrating the reduced distance from the back of Posts 11 and 12 to the back-edge of the soil-pit.....	290
Figure 236. FE model for Case 2 with vertical “rigidwall” located just below grade to simulate back-edge of soil pit (overhead viewpoint).....	291
Figure 237. FE model for Case 2 with vertical “rigidwall” located just below grade to simulate back-edge of soil pit (downstream viewpoint).....	291
Figure 238. Sequential Views of Test C08C3-027-2 and FE analysis from downstream-backside view perspective.....	293

Figure 239. Sequential views of Test C08C3-027-2 and FE analysis from an upstream view perspective.....	295
Figure 240. Permanent displacement of the upstream anchor in Test C08C3-027-2.	298
Figure 241. Displacement of upstream rail boundary in FEA analysis Case 2 (modeled with 47% baseline anchor stiffness).	298
Figure 242. Maximum rotation displacement of Post 10 in (a) full-scale test and (b) FEA analysis Case 2.	299
Figure 243. Anchor stiffness used in FEA model compared to anchor stiffness measured in physical tests.	301
Figure 244. Example of soil erosion at a guardrail post.....	303
Figure 245. Example of severe soil erosion at multiple posts.....	304
Figure 246. Test set-up for pendulum tests.	305
Figure 247. 2,372-lb pendulum device with semi-rigid nose.....	307
Figure 248. Schematic of the accelerometer instrumentation for the pendulum tests.	307
Figure 249. High-speed camera specifications and placement.	308
Figure 250. Repair to the pendulum head included adding a steel “slide Plate” underneath the head.	310
Figure 251. Force vs. deflection curves for Test Series 14003 from primary accelerometer.	312
Figure 252. Force vs. deflection curves for Test Series 14003 from secondary accelerometer...	312
Figure 253. Energy vs. deflection curves for Test Series 14003 from primary accelerometer....	313
Figure 254. Energy vs. deflection curves for Test Series 14003 from secondary accelerometer.	313
Figure 255. Peak “impulse” force in Test Series 14003.....	314
Figure 256. Total energy vs. erosion for Test Series 14003 – energy values correspond to point when pendulum overrides the post.....	314
Figure 257. Total energy vs. erosion for Test Series 14003 – average of primary and secondary accelerometers – including linear curve fit to the data.	315
Figure 258. Finite element model used for validating/calibrating soil-spring stiffness corresponding to various levels of soil erosion.....	316
Figure 259. Force vs. deflection for DL0 soil model compared to Tests 14003B and 14003F. ..	317
Figure 260. Energy vs. deflection for DL0 soil model compared to Tests 14003B and 14003F.	317
Figure 261. Sequential views of Test 14003F and FE analysis on baseline post-soil case, DL0.	318
Figure 262. Force vs. deflection for soil model with 3” erosion compared to Test 14003A.	319
Figure 263. Energy vs. deflection for soil model with 3” erosion compared to Test 14003A.....	319
Figure 264. Sequential views of Test 14003A and FE analysis for 3-inch erosion case.	320
Figure 265. Force vs. deflection for soil model with 6” erosion compared to Test 14003C.	321

Figure 266. Energy vs. deflection for soil model with 6” erosion compared to Test 14003C.....	321
Figure 267. Sequential views of Test 14003C and FE analysis for 6-inch erosion case.	322
Figure 268. Force vs. deflection for soil model with 9” erosion compared to Test 14003D.....	323
Figure 269. Energy vs. deflection for soil model with 9” erosion compared to Test 14003D.....	323
Figure 270. Sequential views of Test 14003D and FE analysis for 9-inch erosion case.	324
Figure 271. Force vs. deflection for soil model with 12” erosion compared to Test 14003E.	325
Figure 272. Energy vs. deflection for soil model with 12” erosion compared to Test 14003E..	325
Figure 273. Sequential views of Test 14003E and FE analysis for 12-inch erosion case.....	326
Figure 274. Analysis setup for evaluating effects of anchor strength on the performance of the G4(2W).	327
Figure 275. Summary of barrier damage evaluation from analyses of undamaged G4(2W) guardrail with various levels of soil erosion at a single post.	328
Figure 276. Summary of anchor displacement at rail height from analyses of undamaged G4(2W) guardrail with various levels of soil erosion at a single post.	329
Figure 277. Summary of occupant impact velocities for undamaged G4(2W) guardrail with various levels of soil erosion at a single post.....	330
Figure 278. Summary of maximum occupant ridedown accelerations for undamaged G4(2W) guardrail with various levels of soil erosion at a single post.	331
Figure 279. Summary of maximum 50-ms running average accelerations for undamaged G4(2W) guardrail with various levels of soil erosion at a single post.	331
Figure 280. Summary of maximum effective plastic strains occurring at the splice-bolt locations at Post 16.....	332
Figure 281. Summary of barrier damage evaluation from analyses of undamaged G4(2W) guardrail with various levels of soil erosion at two consecutive posts.	333
Figure 282. Summary of anchor displacement at rail height from analyses of undamaged G4(2W) guardrail with various levels of soil erosion at two consecutive posts.	334
Figure 283. Summary of occupant impact velocities for undamaged G4(2W) guardrail with various levels of soil erosion at two consecutive posts.....	335
Figure 284. Summary of maximum occupant ridedown accelerations for undamaged G4(2W) guardrail with various levels of soil erosion at two consecutive posts.	336
Figure 285. Summary of maximum 50-ms running average accelerations for undamaged G4(2W) guardrail with various levels of soil erosion at two consecutive posts.	336
Figure 286. Summary of maximum effective plastic strains occurring at the splice-bolt locations at Post 16.....	337
Figure 287. Example – finite element model for computing force-deflection response of the standard two-post guardrail anchor system.[Plaxico03].....	341

Figure 288. Typical test set-up for measuring force-deflection response of the guardrail end-terminal anchor.....	344
Figure 289. Photograph of anchor tubes with soil plates during installation (from preliminary Test 14011B).....	344
Figure 290. Photo of the simulated terminal-head bracket mounted onto the end-post.....	345
Figure 291. Cable and pulley system used to apply tensile loading on end-terminal anchor.	345
Figure 292. Idler-pulley mount used to maintain vertical position of loading cable.	346
Figure 293. Comparison of the two post types used in the end-terminal tests.....	346
Figure 294. Displacement transducers mounted to (a) w-beam rail at load point and (b) top of foundation tube at Post 1.....	347
Figure 295. Video camera specifications and placement.	348
Figure 296. Displacement- and displacement rate-time histories measured at the load point on the end of the rail and at the groundline of Post 1 for baseline case.....	349
Figure 297. Force-displacement response of the anchor system measured at the load point on the end of the rail for undamaged end-terminal case.	350
Figure 298. Sequential views of quasi-static test conducted for undamaged end-terminal case (Test 14011E).....	351
Figure 299. Pre-test photo of Test 14001D (front view).....	354
Figure 300. Post-test photo of Test 14001D (back view).	355
Figure 301. Force vs. deflection response for the standard end-terminal with missing groundline strut.....	355
Figure 302. Displacement and displacement rate vs. time for Test 14001D.	356
Figure 303. Typical position of groundline strut in a standard two-post-strut anchor system relative to (a) Post 2 and (b) Post 1.....	356
Figure 304. Procedure for measuring reduced embedment depth.....	357
Figure 305. Pre-test photo of Test 14001M for 2-inch reduced embedment case.	358
Figure 306. Pre-test photo of Test 14001F for 4-inch reduced embedment case.....	359
Figure 307. Pre-test photo of Test 14001L for 6-inch reduced embedment case.	359
Figure 308. Pre-test photo of Test 14001G for 8-inch reduced embedment case.	360
Figure 309. Post-test photo of Test 14001M for 2-inch reduced embedment case.....	360
Figure 310. Post-test photo of Test 14001F for 4-inch reduced embedment case.	361
Figure 311. Post-test photo of Test 14001L for 6-inch reduced embedment case.	361
Figure 312. Post-test photo of Test 14001G for 8-inch reduced embedment case.	362
Figure 313. Force vs. deflection response for the standard end-terminal with 0 to 8 inches reduced embedment depth of foundation tubes.	362

Figure 314. Illustration showing procedure for measuring slack in cable-anchor.	363
Figure 315. Pre-test photo of Test 14001H for 1” slack-cable case.	364
Figure 316. Pre-test photo of Test 14001I for 2” slack-cable case.	364
Figure 317. Pre-test photo of Test 14001K for 3” slack-cable case.	365
Figure 318. Pre-test photo of Test 4001J for 4” slack-cable case.	365
Figure 319. Post-test photos of Test 14001H for 1” slack-cable case.	366
Figure 320. Post-test photos of Test 14001I for 2” slack-cable case.	366
Figure 321. Post-test photos of Test 14001K for 3” slack-cable case.	366
Figure 322. Post-test photos of Test 14001J for 4” slack-cable case.	367
Figure 323. Force vs. deflection response for the standard end-terminal with 0 to 4 inches of slack in the anchor-cable.	367
Figure 324. Test 14001H showing continuing effectiveness of anchor after Post 2 fails.	369
Figure 325. Rail flattening – Rail flattening and rail crush at each quadrant of the splice is measured from the center of the w-beam to the top/bottom edge at the splice bolts.	378
Figure 326. Rail separation - Lateral gap between rail elements at splice connection (measurements taken at locations adjacent to the eight splice bolts).	378
Figure 327. Rail separation – Longitudinal slip in splice connection.	379
Figure 328. Gouging – Gouging of splice-bolts into w-beam panel is evidenced by rotation of the bolt about the vertical axis.	379
Figure 329. Splice bolt hole stretching – Stretching of the splice bolt hole is evidenced in this photo by the apparent longitudinal movement of the splice bolt relative to its original position.	380
Figure 330. Horizontal tear in post bolt hole – This photo shows evidence of both stretching and a horizontal tear in the post bolt hole.	380
Figure 331. Horizontal and vertical tears – tears were measured and categorized according to location on upstream and downstream panel as denoted here.	381
Figure 332. 4,360-lb pendulum device with semi-rigid nose.	387
Figure 333. Schematic of the accelerometer instrumentation for the pendulum tests.	388
Figure 334. High-speed camera specifications and placement.	389
Figure 335. Sequential views of a pendulum test performed in Gabler’s study.	390
Figure 336. Pocketing during full-scale crash test C08C3-27.2.[<i>Fleck08b</i>]	390
Figure 337. Test set-up for Test Series 14004.	391
Figure 338. Anchoring of the downstream end of the rail for Test Series 14004.	392
Figure 339. Anchoring of the upstream end of the rail for Test Series 14004.	392

Figure 340. Typical mounting position for post-bolt was on the downstream side of the slotted hole on the rail.....	392
Figure 341. Peak impact force for each damage mode case investigated in test series 14004F-O.	396
Figure 342. Peak impact energy for each damage mode case investigated in test series 14004F-O.	396
Figure 343. (a) Force vs. Deflection and (b) Energy vs. Deflection curves for damaged splices with flattened cross-section compared to undamaged cases.	397
Figure 344. (a) Force vs. Deflection and (b) Energy vs. Deflection curves for damaged splices with longitudinal slip compared to undamaged cases.	398
Figure 345. (a) Force vs. Deflection and (b) Energy vs. Deflection curves for damaged splice with vertical crush compared to undamaged cases.	399
Figure 346. (a) Force vs. Deflection and (b) Energy vs. Deflection curves for damaged splice with combination of lateral rail separation and flattened rail compared to undamaged cases.	400
Figure 347. Sequential views of Tests 14004F and 14004G.....	401
Figure 348. Sequential views of Tests 14004H and 14004I.....	402
Figure 349. Sequential views of Tests 14004J and 14004K.	403
Figure 350. Sequential views of Tests 14004L and 14004M.....	404
Figure 351. Sequential views of Tests 14004N and 14004O.....	405
Figure 352. Overhead view of Test 14004K from high-speed video camera.	406
Figure 353. Results of Test 14004F with rail tear passing through all four downstream splice-bolt holes.	407
Figure 354. Flow chart for the online guide’s guardrail assessment.....	413
Figure 355. Photos of the crash site for Example 1.	418
Figure 356. Photos of the crash site for Example 2.	425
Figure 357. Photos of the crash site for Example 3.	433

LIST OF TABLES

Table 1. Methods for evaluating damage modes in <i>NCHRP Report 656</i> . [<i>Gabler10</i>].....	3
Table 2. <i>NCHRP Report 350</i> and <i>MASH TL-3</i> for Guardrail.	7
Table 3. Summary of guardrail systems that have been full-scale crash tested under TL-3 conditions.....	25
Table 4. Summary of full-scale test results on guardrail systems tested under TL-3 conditions. 26	
Table 5. Pendulum tests on wood and steel posts. [<i>Bronstad88; Hascall07</i>].....	34

Table 6. TL-2 computer simulation results. [Marzougui10].....	40
Table 7. Full-Scale crash test impact conditions and results. [Rosson96].....	41
Table 8. Test matrix for post-in-soil bogie tests. [Rosson96].....	41
Table 9. BARRIER VII post input variables. [Rosson96].....	42
Table 10. BARRIER VII maximum dynamic deflection results. [Rosson96].....	44
Table 11. Steel post bogie impact test matrix. [Polivka00b].....	44
Table 12. Steel post bogie test results. [Polivka00b].....	45
Table 13. BARRIER VII computer simulation results. [Polivka00b].....	45
Table 14. Comparison of full-scale test results for MGS with 12-inch blockouts, 8-inch blockouts and no blockouts.[Rosenbaugh12].....	50
Table 15. Summary of pendulum test and model results. [Hampton10].....	54
Table 16. Summary of generic end terminal repair guidance. [Gabler10].....	67
Table 17. Summary of common strong and weak post guardrail systems.....	74
Table 18. Summary of possible methods for assessing damage modes for the G4(1W) and G4(2W) guardrail systems.	86
Table 19. Summary of possible methods for assessing damage modes for thrie-beam guardrail systems.....	90
Table 20. Summary of possible methods for assessing damage modes for the modified thrie- beam guardrail system.	92
Table 21. Summary of possible methods for assessing damage modes for the MGS with steel posts.	93
Table 22. Summary of possible methods for assessing damage modes for MGS with wood posts.	94
Table 23. Summary of possible methods for assessing damage modes for the Modified G2 guardrail.	96
Table 24. Summary of generic end terminal repair guidance. [Gabler10].....	98
Table 25. Summary of possible methods for assessing damage modes for generic end terminals.	98
Table 26. Guardrail damage modes.	100
Table 27. Prioritization of damage modes.	103
Table 28. Predefined material parameters values for *MAT_WOOD_PINE in LS-DYNA for various quality factor settings (units: Mg, mm, sec, N, MPa).	116
Table 29. Groundline deflections of posts for Test 471470-26 and FE analysis.....	130
Table 30. Summary of phenomenological events of full-scale test 471470-26 and FEA simulation.	138

Table 31. Summary of occupant risk measures computed from Test 471470-26 and FEA simulation.	140
Table 32. Analysis solution verification table.	146
Table 33. Roadside safety validation metrics rating table – time history comparison (single-channel option).	149
Table 34. Roadside safety validation metrics rating table – (multi-channel option).	150
Table 35. Report 350 crash test criteria with the applicable test numbers.	151
Table 36. Roadside safety phenomena importance ranking table (structural adequacy).	152
Table 37. Roadside safety phenomena importance ranking table (occupant risk).	153
Table 38. Roadside safety phenomena importance ranking table (vehicle trajectory).	154
Table 39. Test Series 13009 Group 1 (2,372-lb pendulum, velocity = 20 mph, impact point = 21.5 inches).	164
Table 40. Test Series 13009 Group 2 (2,372-lb pendulum, velocity = 10 mph, impact point = 21.5 inches).	165
Table 41. Test Results for Test Series 13009 Group 1 (2,372-lb pendulum, velocity = 20 mph, impact point = 21.5 inches).	173
Table 42. Test Results for Test Series 13009 Group 2 (2,372-lb pendulum, velocity = 10 mph, impact point = 21.5 inches).	175
Table 43. Statistics for Post Strength Capacity from Pendulum Test Series 13009 (Group 2).	177
Table 44. Deterioration damage levels for posts in Test 13009 Series 2 based on strain energy.	187
Table 45. Damage levels for guardrail post deterioration.	189
Table 46. Post-in-Soil Test Group 1 (2,372-lb pendulum, v = 20 mph, impact point = 24.88 inches, embedment 40 inches).	193
Table 47. Post-in-Soil Test Group 2 (2,372-lb pendulum, v = 20 mph, impact point = 21.5 inches, embedment 40 inches).	193
Table 48. Material properties for wood post model corresponding to damage levels 1 through 3.	202
Table 49. Analysis matrix for deteriorated wood post study.	212
Table 50. Summary of barrier damage evaluation from uniform post deterioration analyses.	213
Table 51. Summary of occupant risk measures from evaluation of uniform post deterioration analyses.	217
Table 52. Summary of barrier damage evaluation from mixed post deterioration analyses.	221
Table 53. Summary of occupant risk measures from mixed post deterioration analyses.	223
Table 54. Recommendations for wood post deterioration damage.	229
Table 55. Analysis matrix for Task 4A-2.	232

Table 56. Summary of barrier damage evaluation from analyses of undamaged G4(2W) guardrail with various anchor strengths.	242
Table 57. Summary of occupant risk measures from analyses of undamaged G4(2W) guardrail with various anchor strengths.	244
Table 58. Summary of barrier damage evaluation from analyses of G4(2W) with combination of weak anchor and deteriorated posts.	247
Table 59. Summary of occupant risk measures from analyses of G4(2W) with combination of weak anchor and deteriorated posts.	249
Table 60. Recommendations for end-terminal damage for the G4(2W).	254
Table 61. Simulation matrix for creating low-severity guardrail deflection damage cases.	256
Table 62. Summary of results for the low-severity impact analyses.	257
Table 63. Summary of barrier damage resulting from analysis of high-speed impact into the G4(2W) with pre-existing low-severity rail deflection.	261
Table 64. Summary of occupant risk measures from analysis of high-speed impact into the G4(2W) with pre-existing low-severity rail deflection.	264
Table 65. Recommendations for post and rail deflection damage.	270
Table 66. Summary of phenomenological events of full-scale test C08C3-027-2 and FEA simulation.	297
Table 67. Dry density of soil for each test case measured at 6-inch lifts.	306
Table 68. Pendulum test matrix for erosion study showing post embedment, soil properties and impact conditions.	306
Table 69. Summary of results for Test Series 14003.	311
Table 70. Simulation matrix for evaluating soil erosion around creating low-severity guardrail deflection damage cases.	326
Table 71. Summary of barrier damage evaluation from analyses of undamaged G4(2W) guardrail with various levels of soil erosion at a single post.	328
Table 72. Summary of occupant risk measures from evaluation of undamaged G4(2W) guardrail with various levels of soil erosion at a single post.	330
Table 73. Summary of barrier damage evaluation from analyses of undamaged G4(2W) guardrail with various levels of soil erosion at two consecutive posts.	333
Table 74. Summary of occupant risk measures from evaluation of undamaged G4(2W) guardrail with various levels of soil erosion at two consecutive posts.	335
Table 75. Recommendations for soil erosion around guardrail posts for the G4(2W).	339
Table 76. Summary of generic end terminal repair guidance. [Gabler10]	340
Table 77. Test matrix for the anchor system damage study.	343
Table 78. Quasi-static test results for end-terminal damage modes (Table 1 of 2).	352

Table 79. Quasi-static test results for end-terminal damage modes (Table 2 of 2).	353
Table 80. Recommendations for end-terminal damage for the G4(2W).	373
Table 81. Summary of “rail flattening” damage mode for MEDOT crash-damaged splice specimens – listed in descending order, w.r.t maximum degree of flattening.....	382
Table 82. Summary of “rail crush” damage mode for MEDOT crash-damaged splice specimens – listed in descending order, w.r.t maximum degree of crush.	383
Table 83. Summary of “rail separation” damage mode for MEDOT crash-damaged splice specimens – listed in descending order, w.r.t maximum separation.	384
Table 84. Summary of “visible splice bolt and splice bolt hole” damage mode for MEDOT crash-damaged splice specimens.	385
Table 85. Summary of “non-bolt-hole tear” damage mode for MEDOT crash-damaged splice specimens – listed in descending order w.r.t maximum vertical tear, then maximum horizontal tear.	386
Table 86. Pendulum test matrix for the splice damage study.	394
Table 87. Results of pendulum test series 14004.....	395
Table 88. Recommendations for assessment criteria for w-beam splice damage.....	410

LIST OF APPENDICES

- Appendix A:** A Guide for W-Beam Guardrail Damage Assessment – A Field Manual for Highway Maintenance Personnel
- Appendix B:** Survey of Practice
- Appendix C:** Validation/Verification Report Forms
- Appendix D:** Assess Effects of Guardrail Post Deterioration on Performance of G4(2W) – FOIL Tests 13009 B-W Summary Sheets (Posts in Rigid Foundation)
- Appendix E:** Assess Effects of Guardrail Post Deterioration on Performance of G4(2W) – FOIL Tests 13009 Y-K2 Summary Sheets (Posts in Rigid Foundation)
- Appendix F:** Assess Effects of Guardrail Post Deterioration on Performance of G4(2W) – FOIL Tests 13010 Summary Sheets (Posts in Soil)
- Appendix G:** Sequential Views from FEA Evaluation of Uniform Post Deterioration in Impact Region
- Appendix H:** Sequential Views from FEA Evaluation of Deteriorated Posts Located Upstream of Undamaged Posts
- Appendix I:** Sequential Views from FEA Evaluation of G4(2W) with Various Anchor Strengths
- Appendix J:** Sequential Views from FEA Evaluation of G4(2W) with Combination of Weak Anchor and Deteriorated Posts

- Appendix K:** Sequential Views from FEA Evaluation of G4(2W) Under Low-Speed Impact (To Induce Low-Severity Rail Deflection)
- Appendix L:** Sequential Views from FEA Evaluation of High-Speed Impact into G4(2W) with Low-Severity Rail Deflections
- Appendix M:** Assess Effects of Soil Eroded Away from Posts on Performance of G4(2W) – FOIL Tests 14003 Summary Sheets (Pendulum Tests on Posts in Soil)
- Appendix N:** Sequential Views from FEA Evaluation of G4(2W) with Various Levels of Erosion at a Single Post
- Appendix O:** Sequential Views from FEA Evaluation of G4(2W) with Various Levels of Erosion at Two Consecutive Posts
- Appendix P:** Construction Drawings for the Baseline Generic End-Terminal
- Appendix Q:** Quantify Anchor Strength in Terms of Anchor Damage Modes
- Appendix R:** Visual Inspection of Crash-Damaged Splice Specimens – Damage Summary Sheets
- Appendix S:** Quantify Effects of W-Beam Splice Damage on Capacity of Railing – FOIL Tests 14004 Summary Sheets (Pendulum Impact Study)

Note: The appendices listed here can be found on the TRB website (www.trb.org) by searching for *NCHRP Web-Only Document 304: Criteria for Restoration of Longitudinal Barriers, Phase II*.

CHAPTER 1 – INTRODUCTION

Guardrails are an important feature of the roadside that are used to shield errant motorists from becoming involved in even more catastrophic crashes by redirecting vehicles away from fixed hazards (trees, poles, etc.) and terrain hazards (steep roadside slopes, fill embankments, etc.). A properly installed and maintained guardrail is a very effective roadside safety device. Occasionally, however, guardrails are struck by errant vehicles and incur damage. Sometimes this damage is extensive and the guardrail must be replaced or reconstructed to bring it back into its fully operational condition. More frequently though, these impacts result in only moderate or minor damage to the device and may only compromise the safety performance a little, if at all. It is not well understood just how much these minor-damage crash events affect the operational performance of the system. Making decisions about the maintenance and repair of these systems are important but challenging tasks for transportation agencies. It is their responsibility to ensure that these safety barriers function as they were originally designed, yet they must make the best use of their constrained maintenance budgets.

Repair efforts are costly and often consume a considerable amount of a transportation agency's resources. Making repairs quickly is also challenging in many circumstances. It is not always clear what constitutes performance altering damage. Damage to these systems is not always characterized by obvious repair signs such as large rail deflections, sheared or twisted posts, or broken components – all of which are characteristic of high severity crashes. The damage is more often the result of low-speed collisions and side-swipes which cause only minor or moderate damage. These systems also suffer deterioration from environmental factors and frequently incur minor impact damage during roadway maintenance operations such as snow plowing and mowing. Unfortunately, very little information has been available to quantify degradation in barrier performance that these seemingly minor damages cause. Regardless of the cause of the damage, failure to repair a system that has been damaged beyond some critical level may lead to serious injuries in a crash and expose the agency to tort liability claims. On the other hand, repairing a system that is still largely functional may unnecessarily consume valuable time and funding resources that could be put to better use elsewhere.

One of the oft-touted advantages of strong-post w-beam guardrails, for example, is that they can retain some effectiveness even after having been struck and damaged. Maintenance and repair personnel need to have specific guidance about when a guardrail is so badly damaged that it needs to be repaired and when they can defer the repair of a barrier that is still largely effective even though somewhat damaged. Making such decisions maximizes the overall safety of the roadway by ensuring that barriers are still effective even when damaged while minimizing the overall cost of maintenance and repair by focusing on the guardrails most in need of the limited resources of the Department of Transportation (DOT).

Project Objective

Historically, each agency has developed its own repair guidelines based on “perceived” level of damage using their own experience and engineering judgment. The primary objective of this study was to develop a Field Guide to assist maintenance personnel in making decisions about repairing damaged guardrail installations. The Field Guide provides quantitative criteria for assessing guardrail damage and repair priority based on measureable damage metrics. The repair priority relates only to the reduced performance of the guardrail for various types and

levels of incurred damage modes. There are other benefit-cost and risk factors to consider in deciding which systems most warrant repair (e.g., traffic exposure, operating speeds, site conditions, crash history, etc.). Those aspects were outside the scope of this study; however, the guidance for assessing the need for repair based on quantifiable measures of damage will greatly aid in the decision making process.

Background

Probably the first widely available guide for the repair of guardrails aimed at DOT maintenance personnel was developed by Iowa State University and published by the FHWA in 1990.[*Brewer90*] This guide, titled “W-Beam Guardrail Repair and Maintenance: A Guide for Street and Highway Maintenance Personnel,” provides very practical instructions and guidance on repairing and maintaining strong-post w-beam guardrails and has been useful to many DOT maintenance engineers. The guide provided examples including photographs of typical damage, methods for estimating the quantities of materials for repairs, methods for estimating the crew size and time required for repairs, lists of equipment needed for different types of repairs and example forms and worksheets for keeping records of the repairs. The main deficiency of the 1990 Iowa State/FHWA guide is that at the time, no one knew just how effective guardrails with various types of damage might be if struck again. There were no crash tests of damaged guardrails and, at the time, finite element simulations of damaged guardrails were not even possible so the only option for the authors then was to use experience and engineering judgment to assess the degree of damage. Prioritizing which repairs were essential and which could be deferred was based largely on intuition and field experience.

In 2006 the National Cooperative Highway Research Program (NCHRP) Project 22-23 was initiated in order to develop specific criteria that would answer these lingering questions on the effectiveness of damaged strong-post w-beam guardrail installations. The result of NCHRP Project 22-23 was *NCHRP Report 656*. [*Gabler10*] Report 656 focused on a single barrier type, which was a semi-rigid w-beam guardrail with steel posts and routed wood or plastic blockouts called the modified G4(1S). This system was selected because it is one of the most widely used semi-rigid barriers in the U.S. The Project 22-23 research team used a combination of pendulum impact experiments, finite element simulations, and full-scale crash tests to evaluate performance degradation due to varying degrees of damage for each of these damage modes. Table 1 lists the eleven damage modes that were investigated in Report 656, as well as the methods used to evaluate each damage mode.

The performance assessment guidelines for damaged guardrails in Report 656 provide maintenance personnel with a process to determine the repair priority for each damage mode based on quantifiable measures of component damage. The priority levels were defined as high, medium or low and a brief description of each priority level is provided below from *NCHRP Report 656*:

- “High Priority: Indicates damage where the crash performance of the barrier has been compromised to such a degree that a second impact to the damaged barrier would result in unacceptable vehicle and/or barrier performance. This would include vehicle penetration of the barrier (i.e., rail rupture, vehicle override, or vehicle under-ride) and vehicle rollover.”
- “Medium Priority: Indicates damage where the crash performance of the barrier has likely been compromised to some degree but the damage is less likely to

result in unacceptable vehicle and/or barrier performance than high-priority damage.”

- “Low Priority: Indicates damage where the crash performance of the barrier is indistinguishable from the undamaged condition.”[Gabler10]

Table 1. Methods for evaluating damage modes in *NCHRP Report 656*. [Gabler10]

Damage Mode	Pendulum Tests	Full-Scale Crash Tests	Finite Element Modeling
Rail / Post Deflection	x	x	x
Vertical Tear	x		
Horizontal Tear	x		
Twisted Blockout	x		
Missing Blockout	x		
Splice Damage	x		
Hole in Rail	x		
Missing Posts			x
Post-Rail Separation			x
Rail Flattening			x
Generic End Terminal Damage			

Report 656 provided much needed quantitative information on the effectiveness of damaged strong-post w-beam guardrail installations and guidance on determining repair priority. Due to the limited funds available for the project, however, Report 656 only focused on a single guardrail type (i.e., the modified G4(1S)) and performance assessments were based on the assumption that each damage mode exists in isolation (i.e., there was no attempt to assess the performance of a system that exhibited multiple damage modes).

Further guidance was needed in assessing barrier installations with multiple damage modes, as well as further development of the guidelines to include a number of other damage modes and additional barrier systems beyond what is provided in Report 656. A list of additional research needs suggested by Gabler in *NCHRP Report 656* is summarized below:

- Conduct a more thorough sensitivity analysis for each damage mode.
- Include more applicable methodology for assessing component failures due to fracture (e.g., rail tears, fractured blockouts, etc.).
- Conduct additional full-scale crash tests of damaged barriers as a means to both evaluate crash performance and to provide additional data for validation of analytical models.
- Assess implications of damage based on performance criteria outlined in Manual for Assessing Safety Hardware (*MASH*) – the current FHWA approved crash testing guidelines.
- Assess performance degradation and develop repair criteria for barriers with multiple damage modes.
- Assess performance degradation and develop repair criteria for other types of guardrail systems, such as wood post systems, three-beam systems, etc.
- Assess performance degradation and develop repair criteria for transition systems.
- Provide more quantitative assessment and guidance for repair of generic end treatments.

- Evaluate the effects that damage to barriers near energy absorbing end terminals will have on the ability of those end terminals to activate and function properly.

Roadmap of the Report

It was not the intent of this study to re-do any of the work already accomplished in Report 656, but rather to expand the work to include damage assessment and repair guidelines for additional strong-post guardrail systems, additional damage modes, and more in-depth sensitivity analyses of select damage modes. The basic approach used in this project was similar to that used in Report 656 and involved a combination of pendulum testing and computational analyses to assess performance degradation of a guardrail for various damage modes. The report is organized into 17 chapters as follows:

- Chapter 1 gives an introduction to the report, the study objectives and background information regarding the project.
- Chapter 2 provides a summary of current and past testing requirement for obtaining “eligibility” for a roadside device for use on federal-aid projects, and a summary of the design and crash performance of common non-proprietary strong-post guardrails.
- Chapter 3 provides a literature review that describes (1) general crash phenomena that lead to poor guardrail performance and (2) the general function and influences of various guardrail components.
- Chapter 4 summarizes the results of a survey of practitioners which was conducted to identify which damage modes and system elements should be evaluated in this research.
- Chapter 5 discusses which additional guardrail systems should be included in the field guide, evaluates the importance of addressing each damage mode associated with each of those systems, identifies the research methods that could be used in quantifying the effects of various levels of damage for each case, and prioritizes a list of damage modes and system elements for inclusion in the research.
- Chapter 6 discusses the research approach and includes the scope of work performed in this study.
- Chapter 7 details the development and validation for the finite element model that will be used for assessing the performance of the guardrail with various types and levels of damage.
- Chapters 8 through 14 discuss the evaluations and results for assessing the performance of guardrails with various damage modes. The recommended assessment procedures and the criteria for repair priority are provided at the end of each of these chapters. The damage modes include:
 - Guardrail post deterioration (e.g., rot and insect damage),
 - End-terminal damages that may affect anchor strength,
 - Combination damage modes of rail deflection and rail-to-post connection,
 - Soil erosion around guardrail posts, and

- Additional splice damages that were not investigated in Phase I
- Chapter 15 discusses the development and formatting for the field guide.
- Chapter 16 provides a series of real-world examples performed using the on-line version of the Field Guide at <http://www.roadsafellc.com/GCA/index.php> to illustrate the basic assessment procedure.
- Chapter 17 provides the conclusions and recommendations for future research.

The result of this research is a relatively comprehensive field guide for assessing damages for two of the most widely used strong-post w-beam guardrails –the modified G4(1S) and the G4(2W). The field guide was assembled in two basic formats: (1) a field manual, which is provided as Appendix A to this report and (2) an online interactive website which can be accessed at <http://www.roadsafellc.com/GCA/index.php>. The field manual and the on-line guide are meant to be used together; the online version is intended to facilitate and automate the assessment procedure, while the field manual provides additional details and commentary on how to carry out the assessments.

CHAPTER 2 – A SUMMARY OF COMMON NON-PROPRIETARY GUARDRAILS (BASIC DESIGN AND CRASH PERFORMANCE)

Crash Testing for Federal Aid Eligibility

Full-scale crash testing is the method used by the Federal Highway Administration to ensure that a barrier system is crashworthy for use on federally funded highways. Roadside safety barriers should meet the performance standards accepted by the FHWA. The current procedures are published in the *Manual for Assessing Safety Hardware (MASH)*. [AASHTO09] From the first testing procedures specified in HRB 482 until those of *NCHRP Report 350*, the 4500-lb (2040-kg) passenger sedan served as the crash test vehicle representing the large end of the passenger vehicle fleet. The large passenger sedan had virtually disappeared from the vehicle population by the late 1980's and new vehicle types such as minivans, sport utility vehicles and pickup trucks had emerged in their place. *Report 350* replaced the large car with a 4409-lb (2000-kg) pickup truck. The challenges that the pickup truck introduced to the crash testing procedures were due to its higher center of gravity, making it much more unstable during impacts than its predecessor, the low center of gravity large car sedan.

In *Report 350*, the 4409-lb pickup was chosen as a replacement for the 4500-lb passenger sedan for several reasons. First, both vehicles had similar mass and were therefore thought to represent similar barrier loadings. Second, the pickup truck was chosen as a surrogate for the much broader class of vehicles known at the time as ISTEAs (e.g., pickup trucks, SUVs, minivans, vans, etc.). The U.S. Congress required the FHWA to address the issue of the crashworthiness of the emerging light truck fleet (e.g., SUV, vans and mini vans) in the ISTEAs act. The FHWA responded by adopting the 4409-lb pickup in *Report 350* as a surrogate for the entire class of SUVs (e.g., pickup trucks, SUVs, vans, minivans, etc.). There were two tests in *Report 350* for evaluating the crashworthiness of guardrail systems for test level three (*Report 350* TL-3) which are described in Table 2.

In 2002, NCHRP Project 22-14 was initiated to assess the need for updating *Report 350*. Since publication of *Report 350*, several changes have occurred in vehicle fleet characteristics, testing technology and crashworthiness research. The result of Project 22-14 was a document with revised criteria for evaluating roadside safety features. The new test guidelines and evaluation criteria were published in 2009 by the American Association of State Highway and Transportation Officials (AASHTO) in the *Manual for Assessing Safety Hardware (MASH)* and have been adopted by the FHWA for eligibility testing of barrier systems to be installed on federal funded highways. [AASHTO09] The most significant changes in *MASH* were that both the small car and light truck test vehicles increased in mass, as shown in Table 2.

Table 2. NCHRP Report 350 and MASH TL-3 for Guardrail.

	Report 350	MASH
Test 3-10		
Vehicle Classification	820C	1100C
Mass (lb)	1,807	2,425
Minimum C.G. Height (in)	N/A	N/A
Impact Speed (mph)	62.1	62.1
Impact Angle (deg)	20	25
Test 3-11		
Vehicle Classification	2000P	2270P
Mass (lb)	4,400	5,000
Minimum C.G. Height (in)	27.6	28
Impact Speed (mph)	62.1	62.1
Impact Angle (deg)	25	25

Summary of Common Non-Proprietary Strong-Post Guardrail Systems

Modified G4(1S) with Routed Wood Blockouts

The Modified G4(1S) with routed wood blockouts is constructed with 6-ft long W6x9 steel guardrail posts spaced at 6 feet- 3 inches center-to-center; the 12-gauge w-beam rail is offset 8 inches from the posts using routed wood blockouts with dimensions 6 x 8 x 14 inches. The w-beam and blockout are fastened to the post using a 5/8-inch diameter bolt 10 inches long. Drawings for the system (i.e., AASHTO-AGC-ARTBA designator SGR04c) are shown in Figure 5. (AASHTO-AGC-ARTBA designator SGR04c), drawings of the blockout are shown in Figure 6 (PDB01b), drawings of the post are shown in Figure 7 (PWE01), and drawings of the rail-to-post fastener are shown in Figure 8 (FBB03).

A photo of the modified G4(1S) with routed wood blockouts is shown in Figure 1. This guardrail system was successfully crash tested at Texas Transportation Institute (TTI Test 405421-1) on November 16, 1995 under *NCHRP Report 350* Test 3-11 impact conditions.[*Bullard96*] A sequence of snapshots from the crash test video is shown in Figure 2.

The modified G4(1S) with wood blockouts was also successfully tested under *MASH* Test 3-11 impact conditions on April 8, 2005 at the Midwest Roadside Safety Facility (MwRSF). A sequence of snapshots from the test video from Test 2214-WB2 is shown in Figure 3. In an earlier test, 2214-WB1, which was conducted under test conditions very similar to the *MASH* Test 3-11 requirements, the system failed to safely contain and redirect the vehicle.[*Polivka06a*] The standard test vehicle for *MASH* Test 3-11 is the 2270P, which is a 5,000-lb ½-ton quad-cab pickup. The test vehicle used in Test 2214-WB1 was a 5,000-lb ¾-ton standard cab pickup. During Test 2214-WB1, the rail ruptured at a w-beam splice connection allowing the vehicle to penetrate behind the system. A sequence of snapshots from the test video for Test 2214-WB1 is shown in Figure 4. The failed test caused many in the roadside safety community to wonder if the modified G4(1S) was being tested very close to its performance limit if a slightly different (but still common) vehicle type resulted in a failed test. This led to the development of the Midwest Guardrail System (MGS) and other 31-inch w-beam guardrails.



Figure 1. Modified G4(1S) with wood blockouts.[Bullard96]



Figure 2. Sequential views of Crash Test 405421-1.[Bullard96]



Figure 3. Sequential views of Crash Test 2214-WB2.[Polivka06b]



Figure 4. Sequential views of Crash Test 2214-WB1.[Polivka06b]

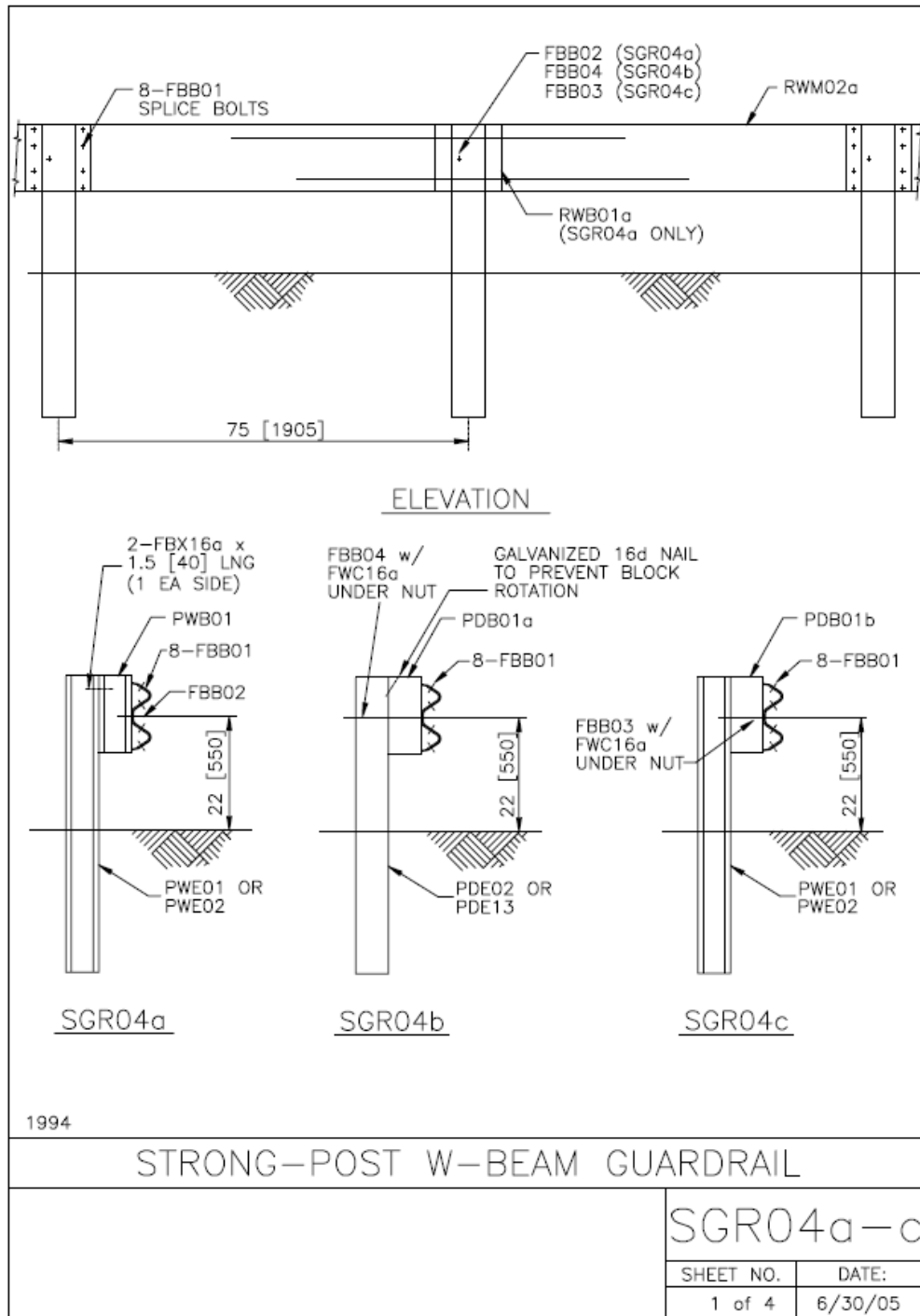


Figure 5. Drawing of the strong-post w-beam guardrail (SGR04a-c).

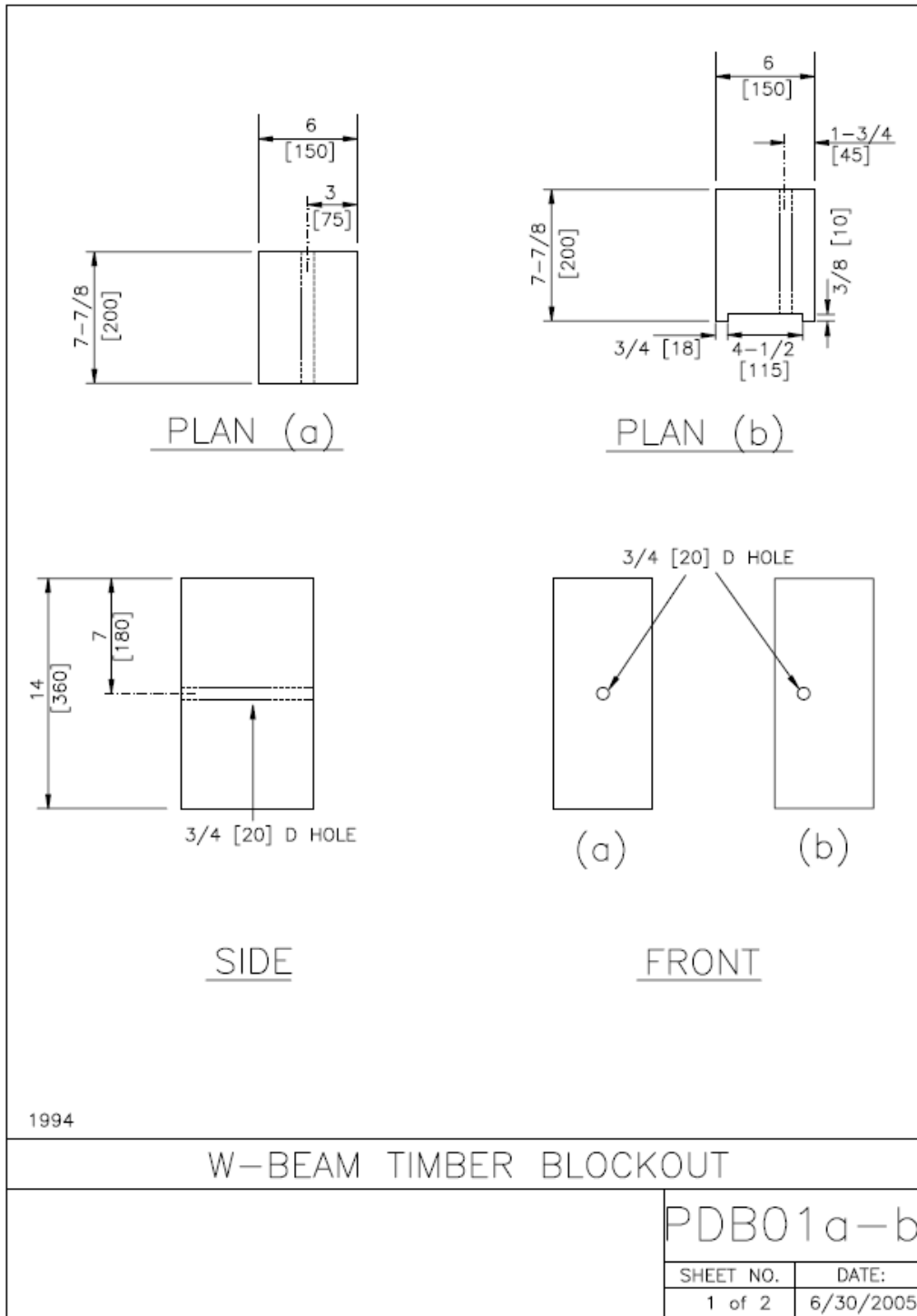


Figure 6. Drawing of the 8-inch wood blockout for the modified G4(1S) with wood blockout guardrail (PDB01b).

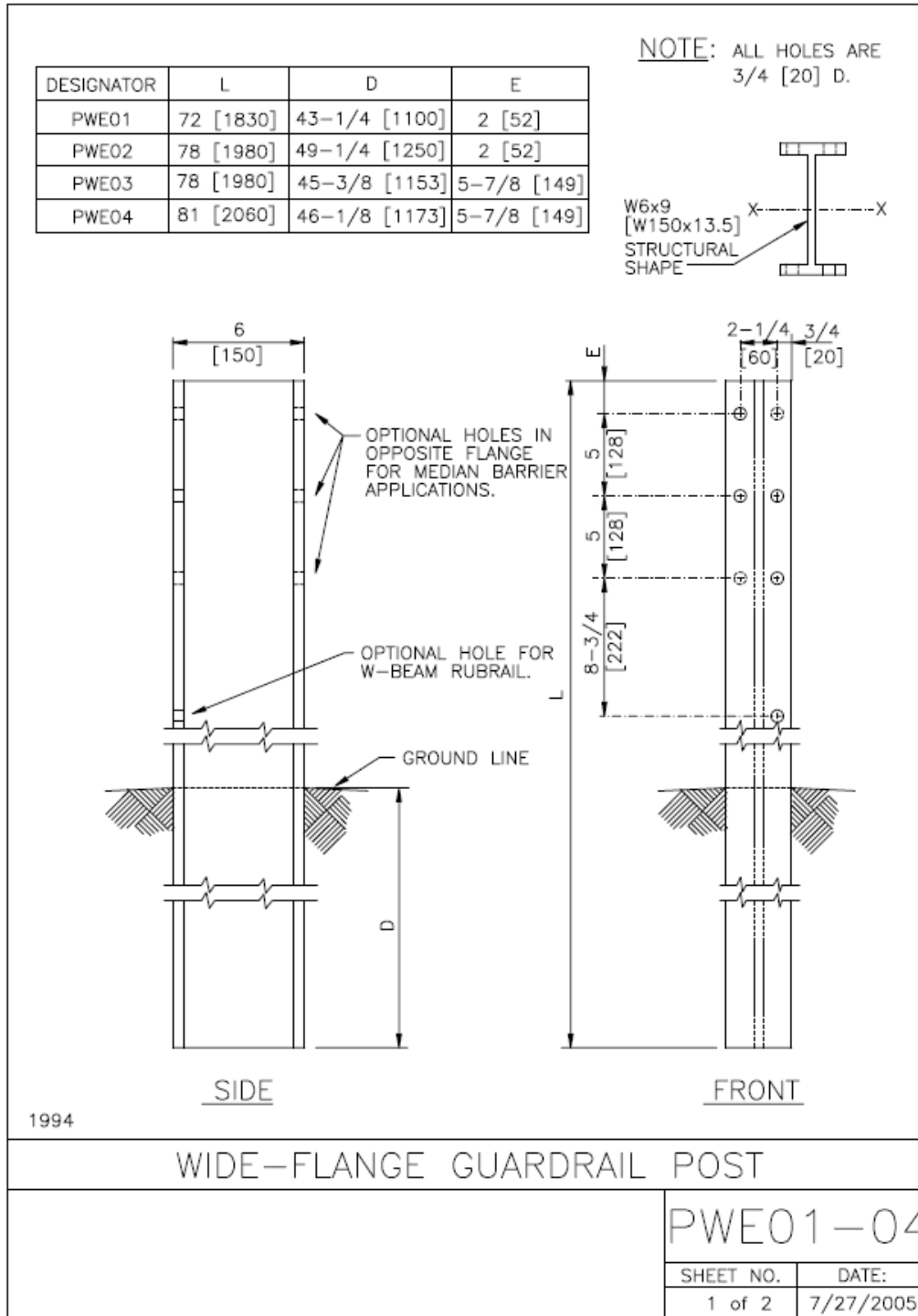


Figure 7. Drawing of the W6x9 guardrail post (PWE01).

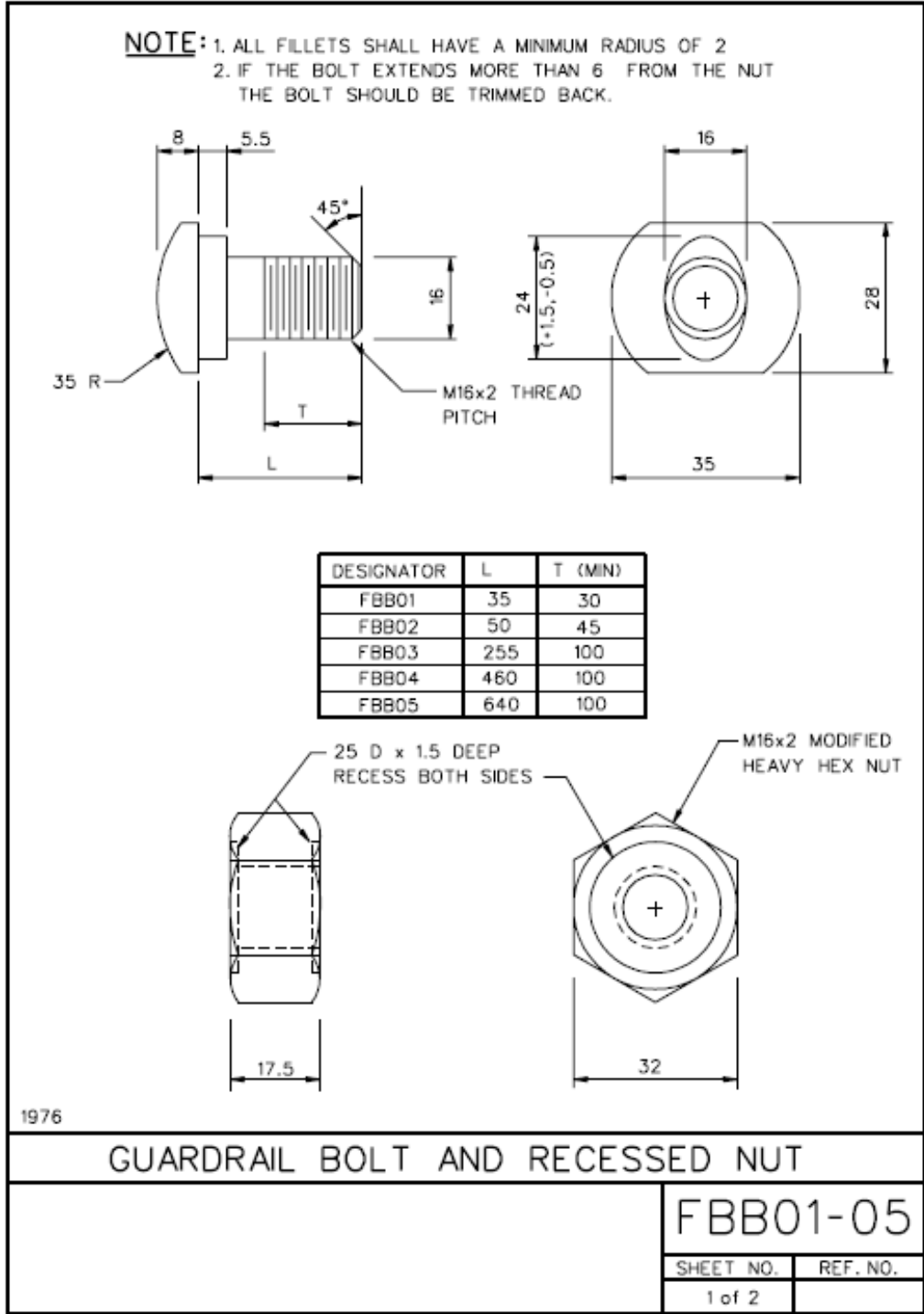


Figure 8. Drawing of the bolt used to fasten the rail element to guardrail posts.

G4(2W)

The G4(2W) guardrail is constructed with 6x8-inch rectangular timber posts spaced at 6 feet- 3 inches center-to-center; the 12-gauge w-beam rail is offset 8 inches from the posts using wood blockouts with dimensions 6 x 8 x 14 inches. The w-beam and blockout are fastened to the post using a 5/8-inch diameter bolt 18 inches long. A photo of the G4(2W) guardrail is shown in Figure 9. Drawings for the system are shown in Figure 5 (SGR04b), drawings of the blockout are shown in Figure 6 (PDB01a), drawings of the post are shown in Figure 12 (PDE01 and PDE02), and drawings of the rail-to-post fastener are shown in Figure 8 (FBB04).

The G4(2W) was successfully crash tested at Texas Transportation Institute (TTI Test 471470-26) on May 25, 1994 under *NCHRP Report 350* Test 3-11 impact conditions.[*Mak99*] For this test installation the posts were 64 inches long with a 36-inch embedment depth (PDE01). The test, however, was classified as “marginally acceptable” due to severe wheel snag and subsequent vehicle instability after redirection from the system. A sequence of snapshots from the crash test video is shown in Figure 10.



Figure 9. Photo of the G4(2W) guardrail Test 476460-1-5 test installation.[*Bullard10*]



Figure 10. Sequential views of full-scale crash Test 471470-26.[*Mak99*]

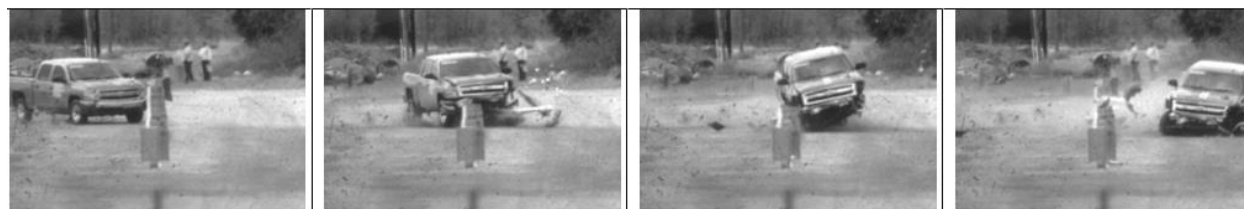


Figure 11. Sequential views of full-scale crash Test RF476460-1-5.[*Bullard10*]

The G4(2W) was also tested (Test RF476460-1-5) under MASH test conditions, in which the guardrail ruptured at a splice connection allowing the vehicle to penetrate behind the guardrail.[Bullard10] Test RF476460-1-5 was conducted at the Transportation Research Institute on March 4, 2009. In this case, the posts were 72 inches long with an embedment depth of 44 inches. A sequence of snapshots from the test video is shown in Figure 11.

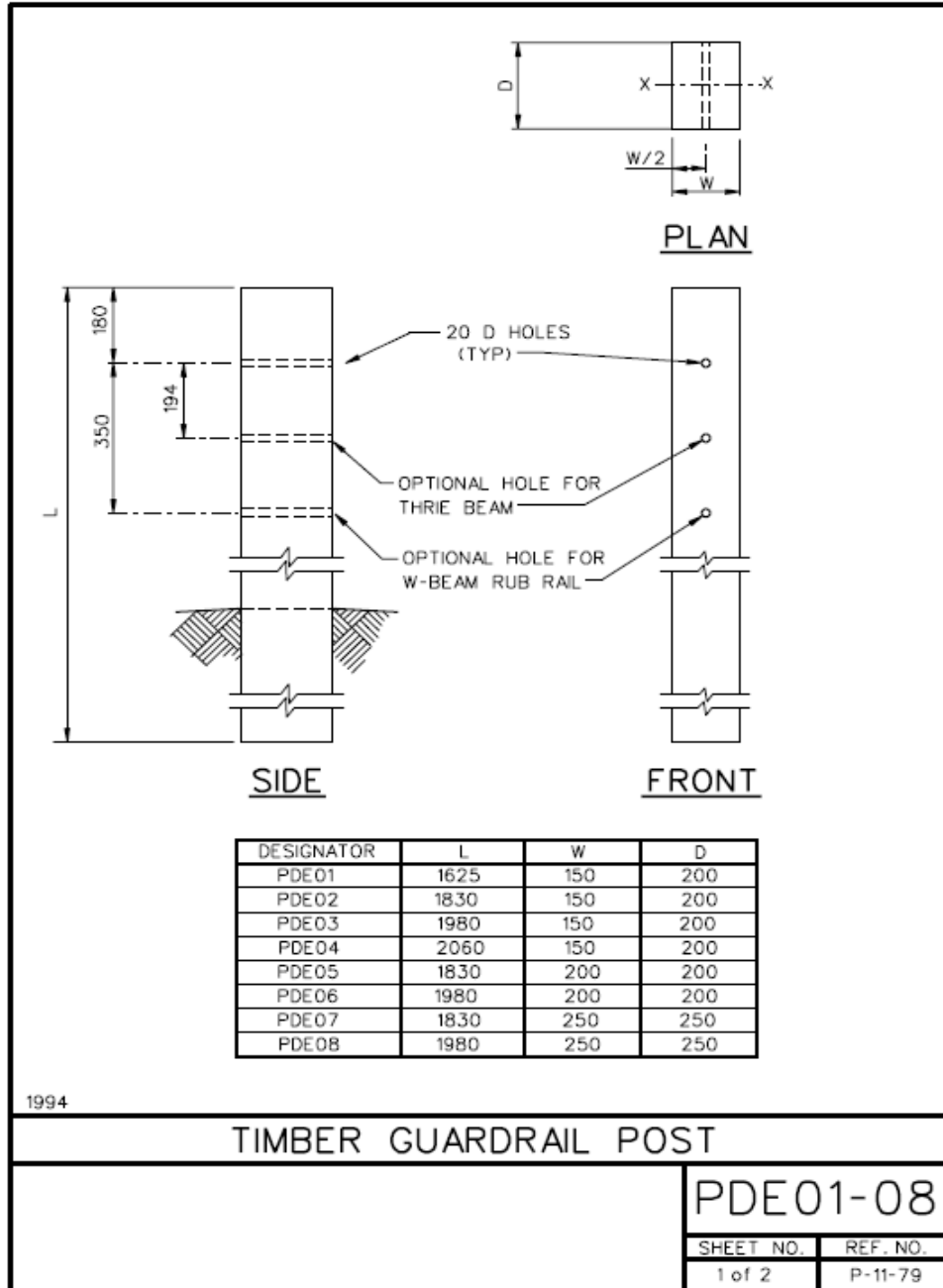


Figure 12. Drawing of the rectangular wood post used in the G4(2W) and G4(1W) guardrail systems (i.e., AASHTO designator SGR04b).

G4(1W)

The G4(1W) guardrail is constructed with 6-ft long, 8x8-inch rectangular timber spaced at 6 feet- 3 inches center-to-center; the 12-gauge w-beam rail is offset 8 inches from the posts using wood blockouts with dimensions 8 x 8 x 14 inches. The w-beam and blockout are fastened to the post using a 5/8-inch diameter bolt 18 inches long. Drawings of the G4(1W) guardrail system are shown in Figure 5(SGR04b), drawings of the blockout are shown in Figure 6 (PDB01a), drawings of the post are shown in Figure 12 (PDE05), and drawings of the rail-to-post fastener are shown in Figure 8 (FBB04).

While the G4(2W) has been used in a number of states, the G4(1W) is now commonly used only in the state of Iowa. Though the performance of the two guardrails have been presumed to be equivalent, only one full-scale crash test has ever been performed on the G4(1W) and that test was performed over 40 years ago. That successful test involved a 2000-kg passenger car striking the barrier at 100 km/hr and 22 degrees using the recommendations of Highway Research Board Circular 482, the first full-scale crash testing guidelines published in 1962.[*Michie71; HRB62*]

In a study performed by Plaxico, Ray, and Hiranmayee for the State of Iowa, finite element analysis was used to evaluate the G4(1W) guardrail.[*Plaxico00*] The only difference between the G4(1W) system and the G4(2W) system is the cross-sectional dimensions of the wood posts (i.e., the posts in the G4(1W) system are 50 mm wider than the posts in the G4(2W) system). Analyses were conducted to simulate *NCHRP Report 350* Test 3-11 impact conditions. Crash performance of the G4(1W) was compared to the G4(2W) with respect to guardrail deflection, vehicle redirection and occupant risk factors. Although the larger posts in the G4(1W) provided more lateral stiffness to the system, the dynamic deflections of the posts in the finite element analysis were comparable to the deflections of the posts in the G4(2W) system. The maximum total deflection of the G4(1W) system was only about 4% less than the maximum total deflection of the G4(2W) system.

MGS

Sicking and other researchers at the Midwest Roadside Safety Facility (MwRSF) developed a new strong-post w-beam guardrail system designed to provide better performance for high center-of-gravity (c.g.) light trucks, allow additional tolerance for low mounting heights, and maintain acceptable safety performance for small automobiles.[*Sicking02*] Sicking suggested that the existing strong-post w-beam guardrails were at their performance limits in *Report 350* Test 3-11 impact conditions and that a reasonable proportion of the passenger vehicle fleet are larger and have higher c.g.'s than the then-current test vehicles. The new design essentially involved modifications to the G4(1S) guardrail system, including: (1) raising the rail height from 27 inches to 31 inches, (2) moving rail splices to the midspan between posts, (3) increasing blockout depth from eight inches to twelve inches, (4) increasing the size of the post-bolt slots, and (5) decreasing embedment depth. A photo of the MGS guardrail is shown in Figure 13. Finite element analysis was used to explore the effects of changes in these barrier attributes. The performance of the new barrier system was verified with full-scale crash testing.[*Sicking02*] This system has been successfully crash tested to *Report 350* and MASH for Test Level 3 (TL-3).[*Sicking02; Polivka06c-e*]

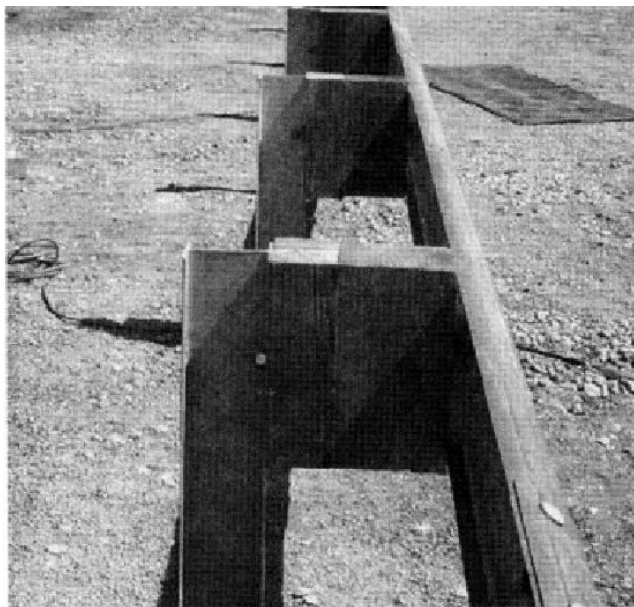


Figure 13. Photo of the MGS guardrail system. [Sicking02]

MGS with Round Wood Posts

The MGS with round wood posts has also been successfully crash tested at the Midwest Roadside Safety Facility. [Hascal07] Two full-scale crash tests were performed to evaluate system performance according to the testing and evaluation requirements of *NCHRP Report 350* Test 3-11. Test MGSDF-1 used guardrail posts made from 7.25-inch diameter Douglas Fir, and Test MGSDF-2 used guardrail posts made from 8-inch diameter Ponderosa Pine. The test results showed that the MGS functioned adequately with posts made from either species. Photographs of the guardrail system with Douglas Fir and Ponderosa Pine are shown in Figure 14. A sequence of snapshots from the test videos are shown in Figure 15 and Figure 16.



(a) 7.25-in. dia. Douglas Fir



(b) 8-in. dia. Ponderosa Pine

Figure 14. MGS with (a) 7.25-inch diameter round Douglas Fir posts and (b) 8-inch diameter round Ponderosa Pine posts.



Figure 15. Test MGSDF-1 of the MGS guardrail with 7.25-inch diameter Douglas Fir posts. [Hascal07]



Figure 16. Test MGSPP-1 of MGS with 8-inch diameter Ponderosa Pine posts. [Hascal07]

G9 Thrie-Beam Guardrail

The standard thrie-beam guardrail (G9) is constructed with 6.5-ft long W6x9 steel guardrail posts spaced at 6 feet- 3 inches center-to-center; the 12-gauge w-beam rail is offset 6 inches from the posts using a 21.81 inches long W6x9 steel flanged section. The top of the thrie-beam rail is 31-5/8 inches above grade and the bottom of the rail is 12 inches above grade. The thrie-beam rail is connected to the blockout using two 5/8-inch diameter button-head guardrail bolts (FBB01). The blockout is fastened to the posts using two 5/8-inch diameter hex bolts (FBX16a). Drawings for the system (i.e., AASHTO-AGC-ARTBA designator SGR09a) are shown in Figure 19, drawings of the blockout are shown in Figure 20, drawings of the post are shown in Figure 7 (PWE03), and drawings of the rail-to-blockout fastener are shown in Figure 8 (FBB01).

A photo of the G9 guardrail is shown in Figure 17. The G9 system was crash tested at Texas Transportation Institute (TTI Test 471470-31) on April 14, 1995 under *NCHRP Report 350* Test 3-11 impact conditions.[Mak99] The system failed to meet the safety requirements of Report 350. A sequence of snapshots from the crash test video is shown in Figure 18. “After the vehicle exited the installation, it rolled two and a quarter revolutions and came to rest on its left side 138 feet downstream of the impact point.”



Figure 17. Photo of the standard three-beam guardrail (G9; SGR09a)



Figure 18. Sequential photos of Test 471470-31 on the G9 three-beam guardrail. [Mak99]

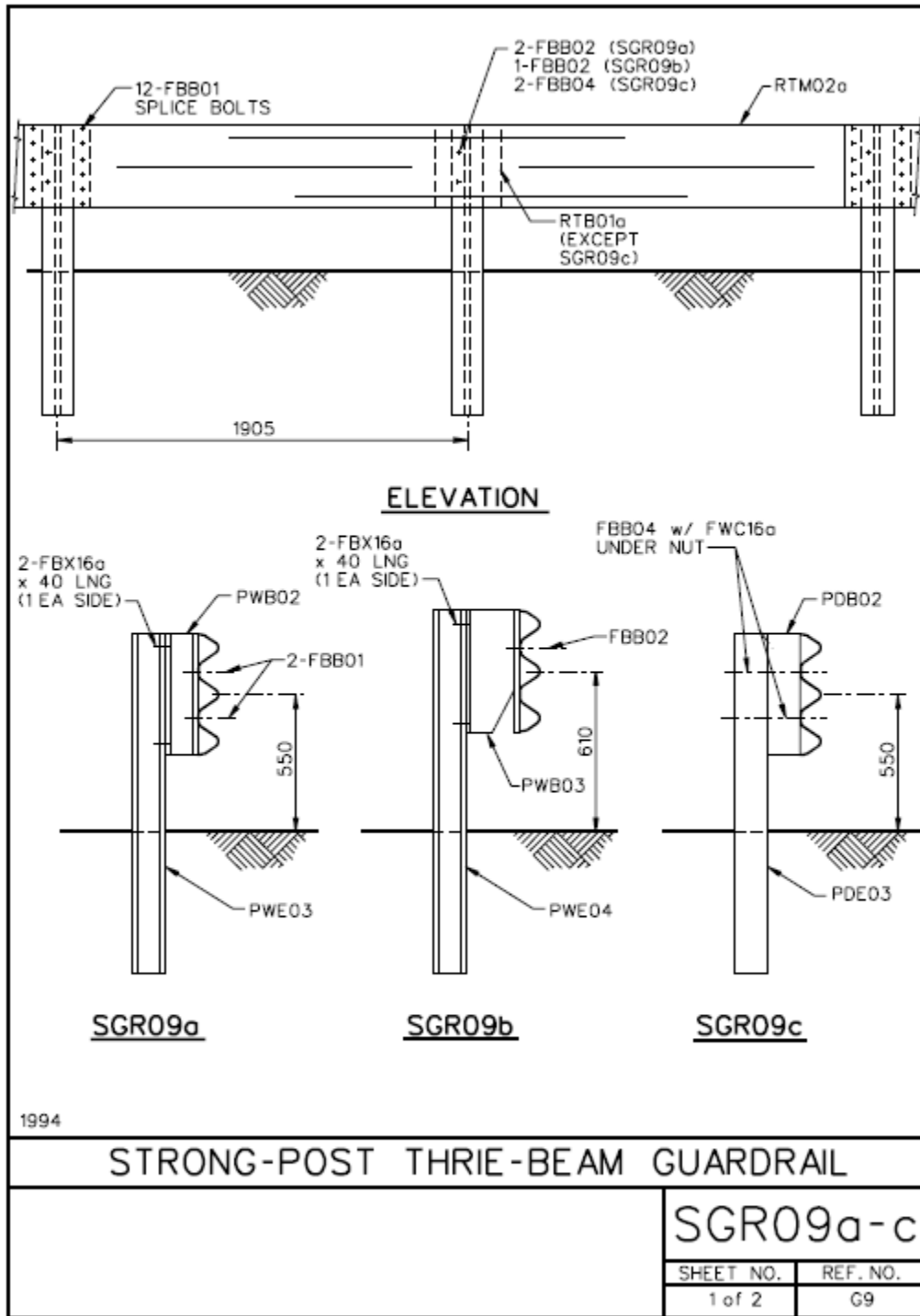


Figure 19. AASHTO-AGC-ARTBA drawings for the SGR09 guardrail systems. [AASHTO04]

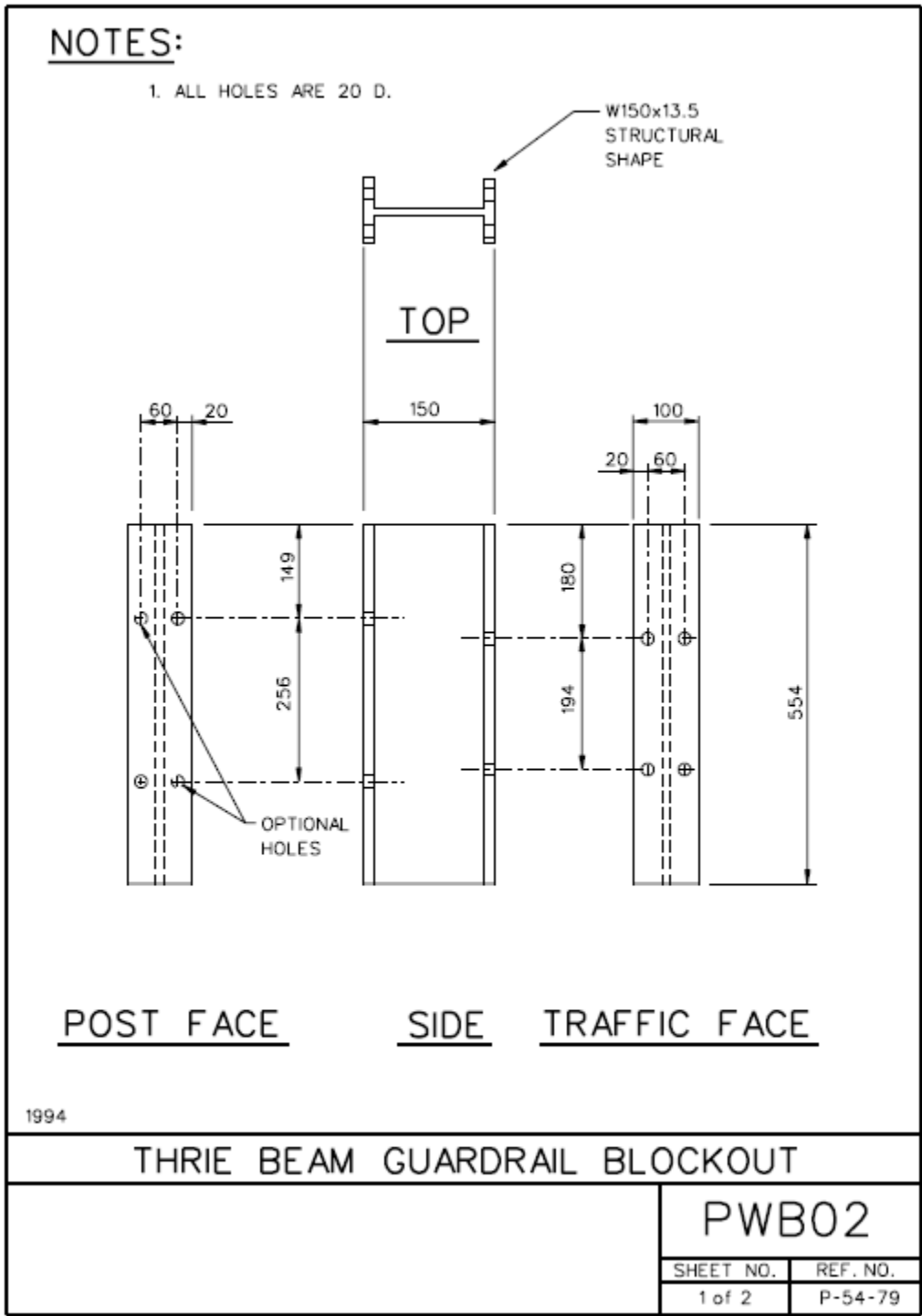


Figure 20. AASHTO-AGC-ARTBA drawings for the W6x9 steel blockout for the G9 thrie-beam guardrail.[AASHTO04]

Thrie-Beam Guardrail with Wood Blockouts

The thrie-beam guardrail with wood blockouts is constructed with 6.5-ft long W6x9 steel guardrail posts spaced at 6 feet- 3 inches center-to-center; the 12-gauge w-beam rail is offset 8 inches from the posts using a 22 inches long 6x8-inch routed wood blockout. The top of the thrie-beam rail is 32.5 inches above grade and the bottom of the rail is 12.5 inches above grade. The thrie-beam rail and blockout are connected to the blockout using two 5/8-inch diameter button-head guardrail bolts (FBB03). There currently are no AASHTO-SGC-ARTBA drawings for the assembled guardrail system; however, drawings of the blockout are shown in Figure 6, drawings of the post are shown in Figure 7 (PWE03), and drawings of the rail-to-blockout fastener are shown in Figure 8 (FBB03). The wood blockout component shown in Figure 6 was modified by routing 4 inches wide x 3/8 inches deep on the back-side of the block to fit over the flange of the W6x9 steel posts.

A photo of the guardrail system is shown in Figure 21. The system was successfully crash tested at Texas Transportation Institute (TTI Test 476460-1-8) on February 26, 2009 under MASH Test 3-11 impact conditions.[*Bullard10*] However, the vehicle appeared to be very unstable upon exiting the guardrail, as shown in the sequential photos of the full-scale test in Figure 22.



Figure 21. Photo of the thrie-beam guardrail with routed wood blockouts. [*Bullard10*]



Figure 22. Sequential photos for Test 476460-1-8 on the thrie-beam guardrail with routed wood blockouts (MASH Test 3-11).[*Bullard10*]

Modified Thrie-Beam Guardrail

The modified thrie-beam guardrail (AASHTO-AGC-ARTBA designator SGR09b) is constructed with 6.75-ft long W6x9 steel guardrail posts spaced at 6 feet- 3 inches center-to-center; the 12-gauge thrie-beam rail is offset 14-inches from the posts using a 21.8 inches long M14x17.2 steel flanged section with a unique cutout at the bottom of the web, as shown in the drawing in Figure 26. The top of the thrie-beam rail is 34 inches above grade and the bottom of the rail is 14 inches above grade. The thrie-beam rail is connected to the blockout using two 5/8-

inch diameter button-head guardrail bolts (FBB02). The blackout is fastened to the posts using two 5/8-inch diameter hex bolts (FBX16a). Drawings for the system (i.e., AASHTO-AGC-ARTBA designator SGR09b) are shown in Figure 19, drawings of the blackout are shown in Figure 26, drawings of the post are shown in Figure 7 (PWE04), and drawings of the rail-to-blackout fastener are shown in Figure 8 (FBB02)¹.

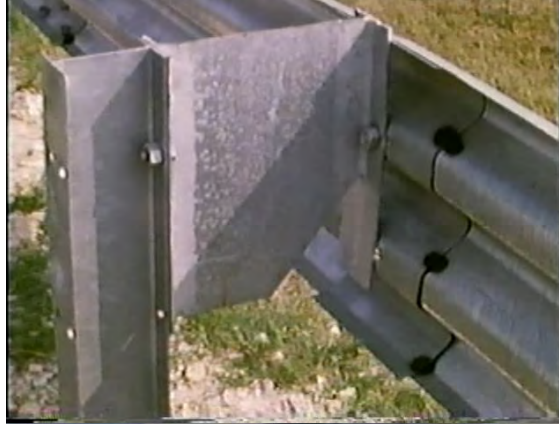


Figure 23. Photo of the modified three-beam guardrail (SGR09b).

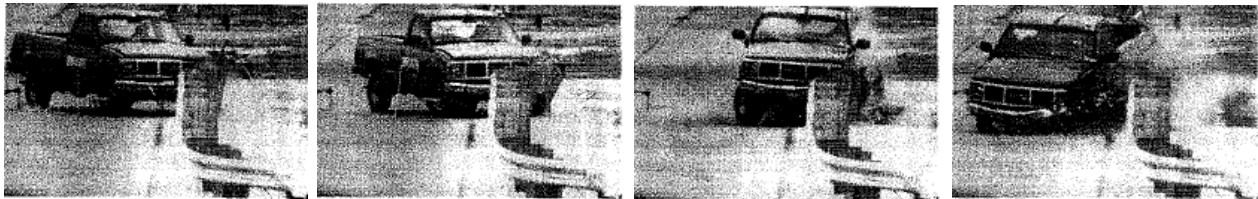


Figure 24. Sequential photos for Test 471470-30 on the modified three-beam guardrail (SGR09b) under NCHRP Report 350 Test 3-11 conditions. [Mak99]



Figure 25. Sequential photos for Test 404211-5a on the modified three-beam guardrail under NCHRP Report 350 Test 4-12 conditions. [Buth99c]

The 14-inch depth of the M14x17.2 creates a greater separation between the rail and post (e.g., 8 inches deeper than the SGR09a); while the cutout at the bottom of the web allows the lower section of the rail to deflect inward during impact and helps to keep the face of the rail vertical as the posts rotate back in collisions.

A photo of the modified three-beam guardrail is shown in Figure 23. The guardrail system was successfully crash tested at Texas Transportation Institute (TTI Test 471470-30) on January 1, 1995 under NCHRP Report 350 Test 3-11 impact conditions. [Mak99] A sequence of

¹ See <http://www.youtube.com/watch?v=qmNJabGIETk>

snapshots from the crash test video is shown in Figure 13. The system was also successfully crash tested on June 12, 1998 at the Texas Transportation Institute with the 18,000-lb single unit truck according to *NCHRP Report 350* Test 4-12 test conditions.[*Buth99c*] A sequence of snapshots from the crash test video is shown in Figure 25.

Summary of Full-Scale Tests Conducted on Strong-Post Guardrail

Table 3 shows a summary of guardrail systems that have been tested for FHWA eligibility under *Report 350* or *MASH* TL-3 conditions; Table 4 shows a summary of the test results. Many of these systems are composed of essentially the same components and many have very similar designs. The differences in design are primarily limited to post type (e.g., 6x8 inch wood or W6x9 steel), rail type (e.g., w-beam or thrie-beam), blockout type (e.g., steel wide-flange or wood), blockout depth, post embedment depth, and rail height. The similarity in the design of these systems indicates that they may be susceptible to similar damage modes.

Typical System Damage in Low-Speed Full-Scale Tests

In Report 656, Gabler, Gabauer and Hampton evaluated the performance of the modified G4(1S) guardrail with wood blockouts with pre-existing low- to moderate crash-induced damage.[*Gabler10*] The evaluation was carried out using full-scale testing and was comprised of two parts: (1) an initial, low-speed impact to induce realistic damage to the guardrail and (2) a subsequent test conducted at *NCHRP Report 350* test 3-11 impact conditions. To the authors' knowledge, this is the only crash test that has been conducted on a guardrail system with pre-existing crash damage.

The low speed test (i.e., Test C08C3-027.1) was conducted by MGA Research Corporation on August 6, 2008.[*Fleck08*] The test involved a 4,632-lb $\frac{3}{4}$ -ton pickup impacting the undamaged guardrail at 30 mph and 26 degrees. The impact point was 23.27 inches upstream of post 11. The test installation, including end-terminals, was 162.4 ft. long. A sequence of photographs from the crash event is shown in Figure 27. The results of the low-speed test provide information regarding the types and magnitude of damage that can commonly be expected in low-speed collisions with this and similar guardrail types.

The deflection of the guardrail was recorded and is shown in Figure 28. Rail and post deflections were the primary damage modes resulting from the impact. There were no torsional deformations of any of the posts, no twisted blocks, nor rail tears, and no significant damage to the splice connection (other than rail bending), as shown in Figure 29.

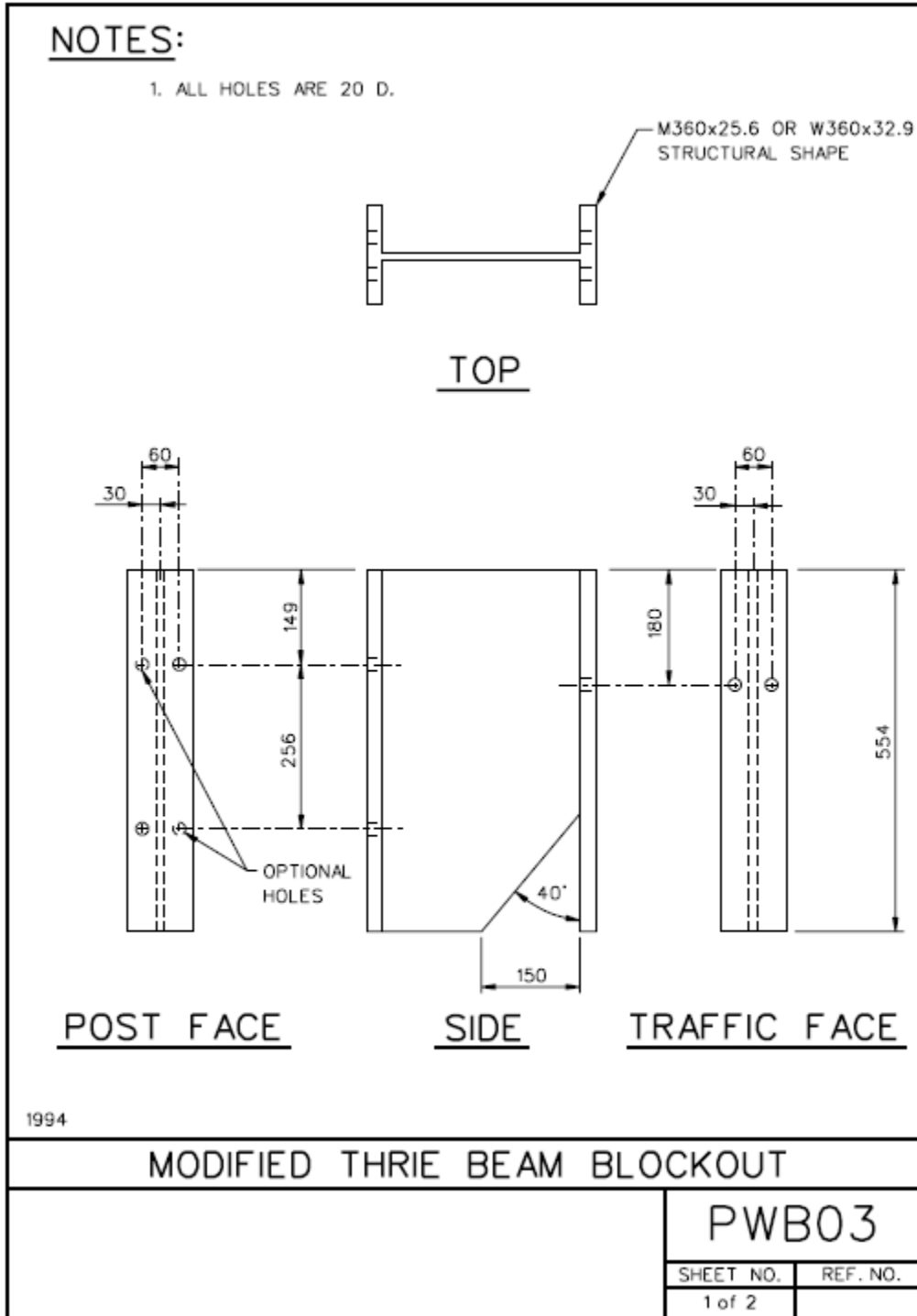


Figure 26. AASHTO-AGC-ARTBA drawings for the M14x17.2 steel blockout for the modified thrie-beam guardrail.[AASHTO04]

Table 3. Summary of guardrail systems that have been full-scale crash tested under TL-3 conditions.

Reference	Test	System	System Length (ft)	Rail		Post				Blockout	
				Type	Height (in)	Type	cross-section	Embed. (in)	spacing (in)	Type	depth (in)
Polivka06a	2214WB-1	Modified G4(1S)	175	W	27.8	Steel	W6x9	43	75	Wood	8
Polivka06b	2214WB-2	Modified G4(1S)	175	W	27.8	Steel	W6x9	43	75	Wood	8
Polivka06c	2214MG-1	MGS	175	W	31	Steel	W6x9	40	75	Wood	12
Polivka06d	2214MG-2	MGS	175	W	31	Steel	W6x9	40	75	Wood	12
Polivka06e	2214MG-3	MGS	175	W	31	Steel	W6x9	40	75	Wood	12
Sicking02	NPG-1	MGS	175	W	32	Steel	W6x9	37.2	75	Wood	12
Faller04	NPG-4	MGS	175	W	31	Steel	W6x9	40	75	Wood	12
Faller04	NPG-5	MGS w/6-in curb	175	W	31	Steel	W6x9	40	75	Wood	12
Faller04	NPG-6	MGS	175	W	31	Steel	W6x9	40	37.5	Wood	12
Buth99a	405421-2	G4(1S)	175	W	27.8	Steel	W6x8.5	44	75	W6x12	6
Mak99a	471470-27	G4(1S)	225	W	27	Steel	W6x8.5	44	75	W6x8.5	6
Bullard96	405421-1	Modified G4(1S)	174	W	27.8	Steel	W6x8.5	43	75	Wood	8
Bligh97	439637-1	Modified G4(1S)	175	W	27.8	Steel	W6x9	38	75	Routed Wood	6
Bligh97b	400001-MPT1	Modified G4(1S) with recycled blockouts		W	27.8	Steel	W6x9	43	75	Recycled Plastic	7.9
Bullard09	476460-1-5	G4(2W)		W	27	Wood	6x8 inch	44	75	Wood	8
Bligh95	405391-1	G4(2W) round post		W	27.8	Wood	7.25-in Dia.	46	75	Wood	5.75
Mak99a	471470-26	G4(2W)	225	W	27	Wood	6x8 inch	36	75	Wood	8
Faller06	MGSDf-1	MGS with Douglas Fir wood posts	175	W	31	Wood	7.25-in Dia.	38	75	Wood	13
Faller06	MGSPp-1	MGS with Ponderosa Pine wood posts	175	W	31	Wood	8-in Dia.	38	75	Wood	13
Buth99b	404211-11	Thrie-Beam	262	Thrie	32	Wood	6x8 inch	48	75	Wood	7.9
Mak99a	471470-30	Modified Thrie-Beam	212	Thrie	34	Steel	W6x9			M14x17.2	14

Table 4. Summary of full-scale test results on guardrail systems tested under TL-3 conditions.

Reference	Test	System	System Length (ft)	Vehicle		Impact Conditions		Result					Comment	
				Type	Mass (lb)	Speed (mph)	Angle (deg)	Deflection (in)	ORA (G)		OIV (ft/s)			Result
									x-dir	y-dir	x-dir	y-dir		
Polivka06a	2214WB-1	Modified G4(1S)	175	3/4-ton standard-cab	5000	61	25.6		19.8	8.5	17.3	16.2	Fail	Rail rupture at splice Override
Polivka06b	2214WB-2	Modified G4(1S)	175	1/2-ton quad-cab 2270P	5000	62.4	25.8	47.1	6.9	6.6	17.7	13.1	Pass	Rail tear at splice Wheel removed
Polivka06c	2214MG-1	MGS	175	3/4-ton standard-cab	5000	62.6	25.2	57	8.8	5.3	17.1	14.8	Pass	minor rail-tear at post-bolt resulting from hand-fabricated rail slot Wheel removed
Polivka06d	2214MG-2	MGS	175	1/2-ton quad-cab 2270P	5000	62.9	25.5	43.9	8.2	6.9	15.3	15.6	Pass	minor rail-tear at post-bolt resulting from hand-fabricated rail slot Wheel removed
Polivka06e	2214MG-3	MGS	175	1100C	2425	60.8	25.4		16.1	8.4	14.9	17.1	Pass	
Sicking02	NPG-1	MGS	175	820C	1956	63.9	18.7		6.1	8	11.5	18.6	Pass	
Faller04	NPG-4	MGS	175	2000P	4378	61	25.6	43.1	9.5	6.9	18.3	12.8	Pass	
Faller04	NPG-5	MGS w/6-in curb	175	2000P	4383	60	25.8	40.3	10.5	8.7	17.2	12.9	Pass	
Faller04	NPG-6	MGS	175	2000P	4411	60.2	25.6	17.6	10.7	9	25	18.4	Pass	
Buth99a	405421-2	G4(1S)	175	2000P	4572	61.9	25.7		15.8	8.9	30.1	15.2	Fail	Rail Rupture
Mak99a	471470-27	G4(1S)	225	2000P	4570	63	26.1		7.8	6.2	24.8	16	Fail	Severe wheel snag Rollover after redirection
Bullard96	405421-1	Modified G4(1S)	174	2000P	4577	63	25.5	39.4	7.9	8.4	23.3	14.4	Pass	
Bligh97	439637-1	Modified G4(1S)	175	2000P	4409	63.3	24.9	29.5	7.76	6.54	24.2	17.1	Pass	improper release of rail caused rail to pull down and vehicle to ramp
Bligh97b	400001-MPT1	Modified G4(1S) with recycled blockouts		2000P									Pass	
Bullard09	476460-1-5	G4(2W)		2270P	5009	64.4	26.1		10.2	9.6	21.6	14.1	Fail	Rail Rupture
Bligh95	405391-1	G4(2W) round post		2000P	4409	63.5	25.4	43.3	10.9	11.8	22.2	14.6	Pass	
Mak99a	471470-26	G4(2W)	225	2000P	4568	62.6	24.3	32.3	11.6	11.4	24.5	19.3	Pass	
Faller06	MGSDF-1	MGS with Douglas Fir wood posts	175	2000P	4449	62.1	25.5	60.2	8.76	5.69	13.22	13.22	Pass	7 posts fractured
Faller06	MGSPP-1	MGS with Ponderosa Pine wood posts	175	2000P	4464	62.3	25.5	37.6	5.9	4.09	22.5	23.6	Pass	4 posts fractured
Buth99b	404211-11	Thrie-Beam	262	2000P	4575	61.9	23.6		8.4	9	20.7	18.4	Pass	2 posts fractured
Mak99a	471470-30	Modified Thrie-Beam	212	2000P	4573	62.3	25.1	40.8	9.7	9	25.6	17.1	Pass	excessive deflection due to posts twisting



Figure 27. Low-speed Test C08C3-027.1 on the modified G4(1S) with routed wood blockouts. [Fleck08]

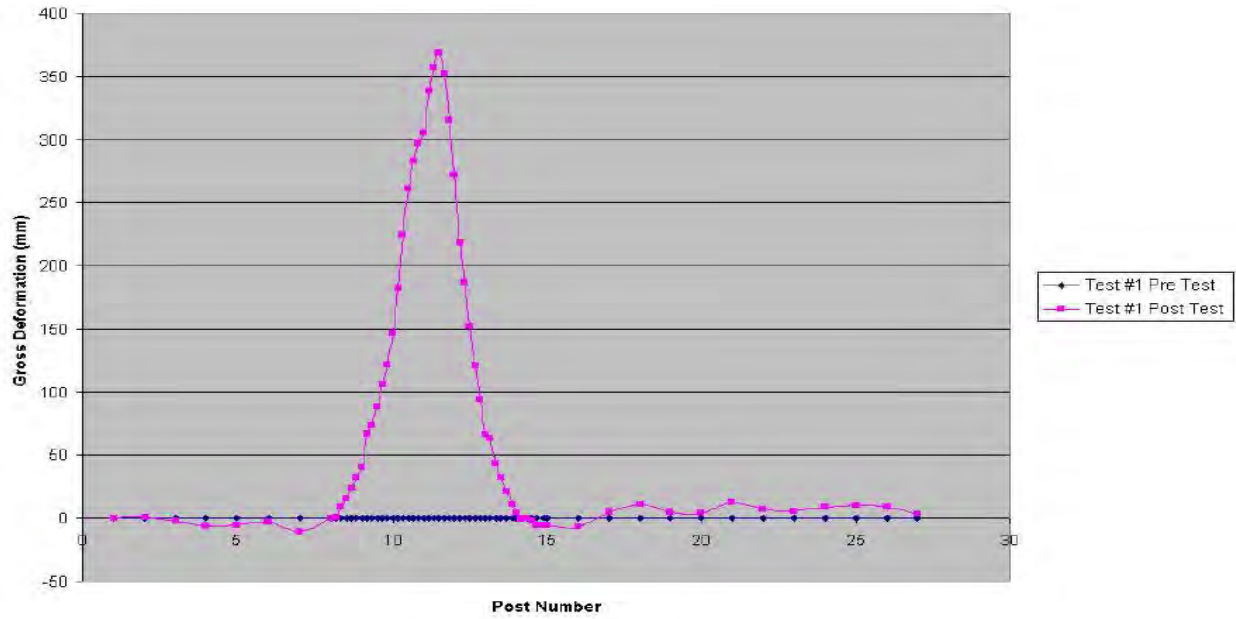


Figure 28. Barrier deflections recorded after Test C08C3-027.1. [Fleck08]



Figure 29. Guardrail damage in Test C08C3-027.1. [Fleck08]

CHAPTER 3 – LITERATURE REVIEW

The literature search conducted in Report 656 focused primarily on published guidelines for assessment of barrier damage and repair. That study effort was relatively comprehensive and thus is not repeated here. The literature review herein was focused primarily on the many studies related to analysis and design/redesign of guardrail systems that have been conducted in the past two decades. From this general area of research, the literature to be searched, reviewed, and summarized is extensive; however, a great deal of the analysis work from these studies remains unpublished - that is, the final reports and published papers generally only include performance data related to final designs and not the analysis and testing details that lead up to the final design.

In an attempt to gather some of the unpublished data, the roadside safety research community was asked to provide information or references involving parametric studies of guardrail system component design and analysis. Unfortunately, these data are often incomplete, documented in private notebooks, or deemed “fully privileged” (e.g., proprietary products, NCHRP quarterly reports, etc.); and researchers are generally not privileged to, or willing to, share the information. However, even without the complete detailed analysis data, the published reports provide a great deal of information about how the various elements of a barrier system function as well as their respective role in overall system performance, and were thus useful in identifying:

- The guardrail types to be considered in the study,
- The critical damage modes associated with each guardrail type,
- The combination(s) of damage modes that are considered most likely to be characteristic of damaged systems, and
- Which of those combinations are considered most critical to system performance.

General Crash Phenomena that Lead to Poor Performance

There are, in general, four crash phenomena that lead to poor performance of strong-post guardrail: (1) pocketing, (2) wheel snag, (3) barrier override/underide, and (4) rail rupture. These phenomena are described below with a brief explanation of their causes and effects.

Pocketing

Pocketing is the crash event in which the impacting vehicle causes a large deflection in a relatively low-stiffness section of a guardrail upstream and adjacent to a relatively high-stiffness section of the guardrail, which forms a “pocket” shape in the rail. For strong-post w-beam guardrails, this phenomenon occurs when the w-beam rail experiences relatively high lateral deflections in the span between guardrail posts, as shown in Figure 30. As the vehicle approaches the downstream end of the pocket, the rail element tends to bend around the post. This generally causes high stress concentrations in the rail element at the post location, particularly when a splice connection exists at that post, and often results in rupture of the rail element.

Pocketing can be alleviated by making the stiffness along the guardrail more uniform. For example, by reducing post stiffness (e.g., weak-post guardrail systems) the downstream posts

will more readily deflect as the vehicle approaches. In this case the post stiffness is reduced to better match that of the unsupported section of rail. However, reducing post stiffness will generally result in greater system deflections, which may not be appropriate in many situations.

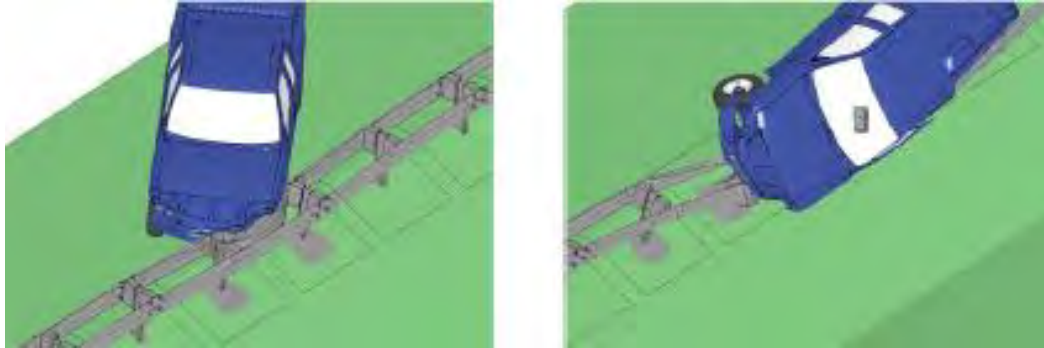


Figure 30. Example of pocketing during a simulated impact with a w-beam median barrier. [Fang10]

Another means of reducing the effects of pocketing is to decrease the spacing between posts. As the posts are placed closer together, the unsupported length of the w-beam becomes shorter and, consequently, more stiff. In this case the stiffness of the unsupported section of rail is increased to better match that of the stiff guardrail posts. However, the added increase in system cost (i.e., additional materials and construction costs), is generally not feasible for most guardrail applications.

Wheel Snag

Wheel snagging is a crash event in which the tire or rim of the vehicle directly impacts against a relatively stiff component of the system, usually a guardrail post, causing high vehicle decelerations and extensive damage to the wheel assembly. Increased vehicle decelerations are directly associated with increased occupant impact forces and decelerations; while a damaged wheel assembly is often times attributed to causing vehicle instability and rollover during redirection.

Wheel snag may be caused by several factors, such as pocketing, underride of the rail element, shallow blockout depth or collapsed blockout. Wheel snag is seldom preventable in high speed, high angle impacts with standard strong-post guardrail; however, its effects are often reduced when the contact area between the vehicle and post is minimized and/or the capacity of the post (e.g., failure load and energy absorption) is reduced with respect to the longitudinal direction of the guardrail.

Barrier Override

Barrier override, as the name implies, is a crash event in which the impacting vehicle vaults over the barrier, exposing the vehicle to the hazards behind the barrier. Barrier override may be caused by many factors, such as low mounting height of the rail element, improper release of rail-to-post connection, pocketing, and ramping of a vehicle tire on a guardrail post, to name a few.

The top of the rail element should be high enough to prevent the front bumper of an impacting vehicle from going over the top of the rail; this is particularly true for the case of pickup trucks and SUV's where, once the bumper goes over the rail, the rail will be in direct contact with the vehicle tire. The spinning tire and the friction between the tire and the rail are often sufficient to push the rail down, allowing the vehicle to override the system.

The rail-to-post connection is also a critical aspect of a guardrail system. The post-rail connection must fail consistently and at the appropriate time to prevent the rail from being pulled down with the post during impact.[*Engstrand00; Ray01a*] As discussed in the preceding paragraph, if the rail drops enough to allow the front bumper of the vehicle to override, then there is an increased chance for the vehicle to override the barrier.[*Bligh97a; Engstrand00; Ray01a; Gabler10*] As will be discussed later, increased blockout depth can help alleviate the sensitivity of the rail-to-post release on system performance.

Rail Rupture

Rail rupture refers to the event of complete rupture or tearing of the metal guardrail component which allows the vehicle to penetrate the system, thereby exposing the vehicle to hazards behind the barrier. An additional hazard associated with rail rupture is subsequent vehicle rollover resulting from the "loose end" of the rail wrapping around a tire and tripping the vehicle or penetrating the occupant compartment of the vehicle.[*Buth99a; Buth00a; Bullard10*] One of the leading causes of rail rupture for most standard strong-post guardrail is pocketing and subsequent failure of the splice connection.[*Bullard10; Buth99a; Buth06; Mak99b; Polivka99; Ross99*]. It has been determined, based in part on the results of tensile tests on specimens taken from the failed w-beam, that guardrail rupture is not usually caused by defective or substandard material; but rather due to stress concentrations in the splice-bolt holes as the rail splice is bent around guardrail posts during impact.[*Engstrand00; Polivka00a; Ray01a*]

Another cause of rail rupture is small tears in the rail that occur when the rail is directly exposed to other guardrail components with sharp edges, such as steel wide-flange posts when no blockouts are used (e.g., weak post guardrails) or when steel blockouts are used.[*Engstrand00; Ray01a*] Regardless of how the tear initiates, the tension in the rail element may cause the tear to propagate and lead to rail rupture. The various phenomena leading to rail rupture are discussed in more detail later in this review.

General Functions and Influences of Guardrail Components

The general function and influences of the various guardrail components are presented and discussed in this section. There are several studies that provide information directly related to the sensitivity of various components, while others provide supporting information from full-scale testing, component testing or numerical analyses. The discussion presented herein references specific studies which directly or indirectly support the conclusions with only brief summaries of the studies.

Posts and Soil

Strong-Axis Loading

Sometimes, essentially identical full-scale tests can result in dramatically different outcomes.[*Strybos97*] One of the causes of these variations could be the result of varying post

strengths and soil conditions.[Patzner97; Patzner99] The response of the post has a significant effect on the energy absorption of the post-soil system in guardrail impacts. For example, typical deformation modes of a post-soil system include post rotation in the soil, fracture of the post, post bending, post twisting or a combination of these modes. The maximum energy absorption of the post-soil system occurs when all deformation occurs in the soil (i.e., post rotates through the soil with no post deformation or failure); therefore, the stiffness of the post should be greater than the stiffness of the soil for optimal performance.[Reid97] When evaluating guardrail strengthening techniques, Rossen *et al.* determined via computer simulation that, although dynamic deflection was consistently higher for guardrail systems using the steel W6x8.5 posts than for those with the 6x8-inch wood posts, the difference was relatively small compared to the differences in deflection arising from variation in soil type and soil density.[Rossen96]

Patzner, Plaxico and Ray while at the University of Iowa conducted a study for the Federal Highway Administration to investigate the effects of post and soil strengths on the performance of a common generic guardrail terminal called the Modified Eccentric Loader Breakaway Cable Terminal (MELT), shown in Figure 31.[Patzner97; Patzner99] The MELT was tested at the Southwest Research Institute in San Antonio, Texas in 1997 and it was found that the system would meet performance criteria for *NCHRP Report 350* Test 3-35 only after optimizing the post and soil conditions (i.e., “Grade 1 structural grade lumber for the posts and dry compacted strong soil”).[Mayer99]

Although the current study is mainly concerned with strong-post guardrail systems, guardrail terminals such as the MELT are designed to function like a guardrail when struck along the side downstream of the end. For example, NCHRP Test 3-35 involves the 4,409-lb pickup impacting on the side of the guardrail terminal at 62.1 mph and 20 degrees. The posts used in the MELT are designed to break with relatively low forces when impacted in the weak direction (i.e., end-on impacts where it is desired to have the posts shear at the groundline as the vehicle passes over them) but are designed to function as guardrail line-posts when loaded in the strong direction (e.g., vehicle impact on the face of the w-beam rail).

Patzner, *et al.* used finite element analysis to conduct a parametric study to examine the effects of post and soil strength on the overall performance of the MELT under impact conditions corresponding to *Report 350* Test 3-35. The study included a matrix of twelve cases varying only post strength and soil conditions. Three post strengths and four soil strengths were investigated. The three post strengths corresponded to a Grade 1 Dense, Grade 2, and a Grade 2 with 30% strength reduction. The four soil strengths were modeled using properties of a granular soil (e.g., similar to the soil type used in the full-scale crash tests) with four different moisture conditions of 50, 75, 87.5 and 100 percent saturation.



Figure 31. Modified Eccentric Loader Breakaway Cable Terminal. [Patzner99]

The results of the analyses showed that certain combinations of soil and post strengths increase the hazardous possibilities of wheel snagging, pocketing, or rail penetration and they identified conditions that would maximize the safety and reliability of the guardrail terminal system. In particular, the analyses indicated that the potential for pocketing tended to increase as soil stiffness increased and as post strength decreased. [Patzner99] In such cases, the premature failure of the posts resulted in significant reduction in stiffness of the unsupported section of rail leading up to the next downstream post, thereby increasing the potential for pocketing. The results from the study were also evidenced in full-scale tests. “In Test MLT-3 Grade No. 2 posts were installed in a very stiff soil. The posts in this test had been used in an earlier full-scale test and it was believed that some of the posts may have been damaged. This test resulted in several posts breaking and guardrail rupture. Test MLT-4, in which Grade No. 1 Dense posts were mounted in very wet soil conditions, resulted in wheel snag which caused the vehicle to roll over. In Test MLT-5 the Grade No.1 Dense posts were mounted in very stiff soil at near optimum moisture conditions and the test was successful.”[Mayer99]

Hascall *et al.* performed a study for the U.S. Department of Agriculture to design and test a wood-post guardrail system for Report 350 TL-3 application.[Hascall07] The primary objective of the project was to determine the acceptable diameter and grading for three species of wood posts for use in the MGS guardrail system. A series of static and dynamic bogie impact testing was carried out on 8-, 10- and 12-inch diameter wood posts made from Douglas Fir, Ponderosa Pine, and Southern Yellow Pine to determine appropriate post diameter and length. Two full-scale crash tests were performed to evaluate system performance according to the testing and evaluation requirements of *NCHRP Report 350 Test 3-11*. Test MGSDF-1 used guardrail posts made from 7.25-inch diameter Douglas Fir, and Test MGSDF-2 used guardrail posts made from 8-inch diameter Ponderosa Pine. The test results showed that the MGS functioned adequately with posts made from either species. Although a full-scale test was not performed for the guardrail system with posts made from Southern Yellow Pine, the 7.5-inch diameter Southern Yellow Pine posts were also determined to be an acceptable for use in the

MGS system, based on comparable strength of the Southern Yellow Pine relative to the other two species.

Another very useful result of the Hascall *et al.* study was the extensive literature review on wood-post testing and the comparison of the performance between wood and steel posts. The reader is referred to [Hascall07] for the complete review. A few of the relevant studies from that review are summarized here:

- Jeyapalan *et al.* concluded, based on static testing of posts with embedment depths of 38 inches, that the 7-inch diameter Southern Pine posts had similar peak force and energy dissipation to that of the W6x8.5 steel posts regardless of soil type. In the dynamic tests, the peak force and energy dissipation for the 7-inch diameter Southern Yellow Pine post were lower, but within 10% of the values for the W6x8.5 steel posts installed in cohesive soil; dynamic response comparisons in noncohesive soils, however, could not be made since the wooden post fractured almost immediately upon impact. [Jeyapalan84]
- Bronstad *et al.* conducted a study in 1988 involving pendulum tests on both wood and steel posts. The tests involved various sizes of wood posts with embedment depth of 36 inches and two types of steel posts (i.e., W6x8.5 and W6x15.5) with embedment depth of 44 inches. The results of those tests, as shown in Table 5, showed that the W6x8.5 steel posts at 44-inch embedment provided 1.6 times more stiffness in the strong axis than the 6x8-inch wood posts at 36-inch embedment; whereas the wood post provided 1.7 times more stiffness than the steel post in the weak direction.[Bronstad88]
- Rohde and Reid conducted a study regarding grading specifications and requirements for wood posts used in w-beam guardrail systems, and concluded that there was no significant benefit to using Grade 1 over Grade 2 posts, and that “use of the Grade 2 posts would lower cost of guardrail installations without adversely impacting its safety performance”. [Rhode95]
- Coon *et al.* showed that when wooden posts fractured the energy absorption was significantly lower than when the posts rotated in the soil.[Coon99]

Hascall *et al.* concluded from their review of pendulum impact tests on guardrail posts embedded in soil that the response of the 6x8-inch wood post performed similarly to the W6x8.5 steel post when loaded in the strong direction.[Hascall07] Full-scale crash tests seem to indicate, however, that although performance is similar between these two systems, all other system components being the same, the steel-post systems provide lower impact forces in full-scale tests. For example, as shown in Table 5, tests on the modified G4(1S) with wood blockouts resulted in longitudinal Occupant Ridedown Accelerations (ORA) values of 7.9 G and 7.6 G [Bullard96; Bligh97]; while tests on the G4(2W) resulted in longitudinal ORA values of 10.2 G, 10.9 G and 11.6 G.[Bullard09; Bligh95; Mak99a]

Table 5. Pendulum tests on wood and steel posts. [Bronstad88; Hascall07]

	Post Type	Max. Force		Avg. Stiffness		Total Impulse		Failure Type
		kN	(kips)	kN/mm	(kips/in.)	kN-sec	(kip-sec)	
Square	305 mm x 305 mm (12 in. x 12 in.) Wood	92.08	(20.7)	0.597	(3.41)	10.12	(2.274)	Soil Yield
	305 mm x 305 mm (12 in. x 12 in.) Wood	105.87	(23.8)			10.10	(2.271)	Soil Yield
	254 mm x 254 mm (10 in. x 10 in.) Wood	72.51	(16.3)	0.447	(2.55)	6.87	(1.544)	Soil Yield
	254 mm x 254 mm (10 in. x 10 in.) Wood	72.95	(16.4)			NA	NA	Post Fracture
	203 mm x 203 mm (8 in. x 8 in.) Wood	58.72	(13.2)	0.292	(1.67)	5.72	(1.287)	Soil Yield
203 mm x 203 mm (8 in. x 8 in.) Wood	51.60	(11.6)	4.85			(1.091)	Soil Yield	
Strong Axis	W152x23.0 (W6x15.5) With paddles	90.74	(20.4)	0.420	(2.40)	11.01	(2.475)	Soil Yield
	W152x23.0 (W6x15.5) With paddles	81.40	(18.3)			10.90	(2.450)	Soil Yield
	W152x23.0 (W6x15.5)	85.41	(19.2)	0.399	(2.28)	11.73	(2.637)	Soil Yield
	W152x23.0 (W6x15.5)	76.95	(17.3)			9.85	(2.215)	Soil Yield
	W152x13.4 (W6x8.5)	56.49	(12.7)	0.431	(2.46)	2.54	(0.572)	Soil Yield
	W152x13.4 (W6x8.5)	56.49	(12.7)			3.91	(0.879)	Soil Yield
	W152x13.4 (W6x8.5)	45.37	(10.2)			2.22	(0.500)	Soil Yield
	W152x13.4 (W6x8.5)	36.92	(8.3)			2.97	(0.667)	Soil Yield
	152 mm x 203 mm (6 in. x 8 in.) Wood	52.04	(11.7)	0.273	(1.56)	3.11	(0.699)	Soil Yield
	153 mm x 203 mm (6 in. x 8 in.) Wood	28.47	(6.4)			2.29	(0.514)	Soil Yield
	154 mm x 203 mm (6 in. x 8 in.) Wood	32.47	(7.3)			2.35	(0.529)	Soil Yield
	155 mm x 203 mm (6 in. x 8 in.) Wood	32.03	(7.2)			1.94	(0.437)	Soil Yield
Weak Axis	W152x23.0 (W6x15.5)	48.04	(10.8)	0.228	(1.30)	7.74	(1.740)	Post Yield
	W152x23.0 (W6x15.5)	46.71	(10.5)			7.64	(1.717)	Post Yield
	W152x13.4 (W6x8.5)	21.35	(4.8)	0.201	(1.15)	1.25	(0.280)	Post Yield
	W152x13.4 (W6x8.5)	18.24	(4.1)			1.08	(0.243)	Post Yield
	W152x13.4 (W6x8.5)	22.69	(5.1)			1.28	(0.287)	Post Yield
	W152x13.4 (W6x8.5)	19.13	(4.3)	0.341	(1.95)	1.26	(0.284)	Post Yield
	152 mm x 203 mm (6 in. x 8 in.) Wood	49.82	(11.2)			0.69	(0.154)	Post Fracture
	153 mm x 203 mm (6 in. x 8 in.) Wood	28.91	(6.5)			0.46	(0.103)	Post Fracture
	154 mm x 203 mm (6 in. x 8 in.) Wood	35.59	(8.0)			NA	NA	Soil Yield
	155 mm x 203 mm (6 in. x 8 in.) Wood	49.38	(11.1)			0.83	(0.186)	Post Fracture

Weak-Axis Loading

Posts with high bending stiffness about the weak-axis (i.e., loading of the posts in the longitudinal direction with respect to the guardrail system) can also result in *severe* wheel snags when contact between the tire and posts occurs. The steel W6x9 posts used in the modified G4(1S) and MGS guardrail systems, as well as the 6x8-inch wood posts used in the G4(2W) guardrail system, tend to have appropriate strength in the weak-direction to alleviate severe wheel snags during impacts with pickups (i.e., in Test 3-11). The steel posts tend to bend over when struck in the weak direction at high speeds by heavier passenger vehicles, while the wood posts tend to rupture in such cases. [Bullard96; Mak99a] On the other hand, when these posts are directly impacted by small and midsize passenger cars (e.g., Report 350 and Mash 3-10 test vehicles), the effects of the wheel snag are more pronounced, and in some cases result in relatively high vehicle decelerations and occupant compartment intrusion.[Ray04] This effect is magnified as the overlap between the posts and vehicle wheel increases, which will be discussed in more detail in the next section on blockouts.

Karlsson investigated the use of failure fuses on timber guardrail posts to reduce the impact forces when vehicles directly impact against the side of the posts during collisions with strong-post guardrail systems.[Karlsson00] Karlsson's study included evaluation of a 6x8-inch wood post that was modified by drilling a 3.5-inch diameter hole through the side of the post at approximately two-inches above the groundline, as illustrated in Figure 32. The study was carried out using finite element analysis, where it was shown that the post provided

approximately the same stiffness and load carrying ability as the standard 6x8-inch wood post when loaded in the strong direction (i.e., impacts on front of post), but would fail at 60% of the impulse required to fail the standard post in the weak direction (i.e., impacts on the side of the posts). The same basic technique has been widely used in the design of the breakaway mechanism in guardrail terminals for decades.

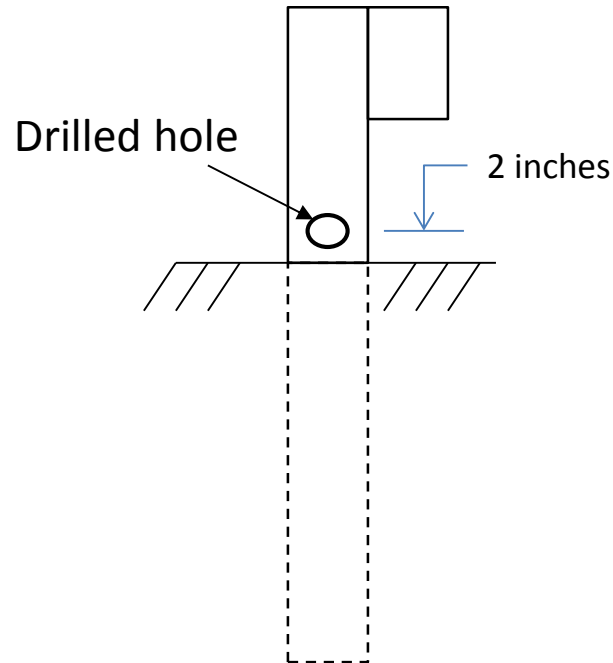


Figure 32. Illustration of wood post with failure fuse.

An existing post type, the CRT post, was also investigated in Karlsson's study. The CRT post includes two 3.5-inch diameter holes, one at the ground line and another at 15.75 inches below ground. This post is used in most guardrail terminals (e.g., MELT, FLEAT, SKT, etc.) as well as in the MGS long-span guardrail. It was determined that the CRT post did not possess adequate strength in the strong direction for application in a length-of-need section of guardrail with standard post spacing of 75 inches. The weakened post could lead to excessive lateral deflections. The modified post concept was never evaluated in full-scale crash tests for a standard length-of-need section of guardrail.

Embedment Depth

The embedment depth of guardrail posts must be optimized to achieve the desired resistance and energy absorption from the post-soil system. The stiffness of the soil increases as embedment depth increases. Recall that pocketing can be alleviated by ensuring that the stiffness along the guardrail is more or less uniform. Thus, if the stiffness of the post-soil system greatly exceeds that of the unsupported section of rail, pocketing may result.

When the soil stiffness exceeds that of the post, the deformation of the post-soil system is primarily due to bending of the post (e.g., steel posts) or rupture of the post (e.g., wood posts) with minimal soil displacement. This tends to (1) cause posts in the immediate impact area to yield or fail prematurely, (2) decrease deflection of the posts located immediately down-stream of the impact, due to the increased rigidity of the post-soil system, (3) reduce the amount of

energy dissipation absorbed by the post-soil system, and (4) cause the posts to rotate about a point nearer to ground level. Issues (1) through (3) may result in pocketing due to an increase in relative deflection between the unsupported section of rail and the downstream post. Issue (4) results in an increased potential for the rail to be pulled down with the posts as the posts rotate about a shorter radius. In this case, the release of the rail-to-post connection becomes more critical.

Kuipers and Reid conducted a series of bogie impact tests on W6x16 steel guardrail posts with embedment depths ranging from 34 to 43 inches. [Kuipers03] The purpose of the tests was to determine the appropriate embedment depth for the posts in the MGS guardrail system. They determined that embedment depths less than 40 inches resulted in the posts being pulled out of the ground during impact with little or no post deformation, while embedment depths equal to or greater than 40 inches resulted in higher levels of soil failure with slight deformations of the posts.

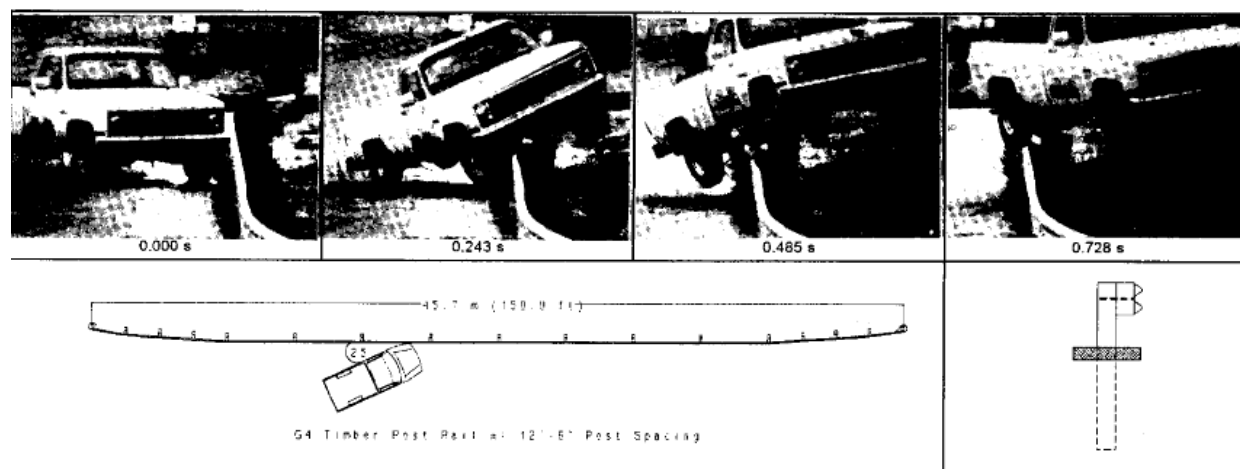
In the development of the MGS long-span guardrail system, Bielenberg *et al.* used a reduced embedment depth for the posts at the up- and down-stream ends of the long-span section of the guardrail system.[Bielenberg07] The long-span system was developed to shield culvert headwalls and was designed to accommodate up to 25 feet of unsupported w-beam rail. The unsupported length is composed of a single layer of w-beam rail, which may experience relatively large deflections during collisions. The reduced embedment depth of the posts adjacent to this unsupported section prevents pocketing by acting as a transition from the low-stiffness of the long-span section to the high-stiffness of the standard MGS guardrail section. This transition allows deflections to be spread over longer distances of the guardrail, creating a more effective load distribution along the rail, which reduces the rail force and rail strain.

Increased Post Spacing

Mak and other researchers at TTI performed a study for the Washington State Department of Transportation to crash test and evaluate a strong-post guardrail system with 12.5-ft post spacing under Report 350 TL-2 impact conditions. At the time of the study, Washington state was using TL-3 guardrail systems for both low-speed and high-speed facilities. If successful, the modified strong-post guardrail with reduced post-spacing would provide a more cost-effective alternative for installations on low-volume, low-speed roadways.

The test installation consisted of a 100-foot long section of guardrail and two 25-foot long end-terminals. The guardrail was a standard G4(2W) with modified post spacing of 12.5 feet (double post spacing). The wooden posts were 6 inch x 8 inch in cross-section and 6 feet long. The wooden blockouts were also 6 inch x 8 inch cross-section and were 14 inches long. The w-beam rail was attached to the posts with standard 20-inch long, 5/8-inch diameter bolts. The mounting height of the guardrail was 27-inches.

The test resulted in the vehicle vaulting over the barrier, as shown in Figure 33 (taken from the test report).[Mak93] The vaulting was attributed to “lack of torsional rigidity of the w-beam rail element and increased post spacing.” As the rail deflected the w-beam twisted allowing the front bumper to slide over the top of the rail. This exposed the front tire to direct contact with the w-beam rail, which resulted in the tire immediately beginning to climb the rail. The damage to the guardrail was minor and was confined to a 12.5-ft section of the rail. The maximum dynamic deflection was 20.4 inches.



General Information		Impact Conditions		Test Article Deflections (m)	
Test Agency	Texas Transportation Institute	Speed (km/h)	69.5 (43.2 mi/h)	Dyanmic	0.5 (1.7 ft)
Test No.	04820-1	Angle (deg)	24.5	Permanent	0.3 (1.0 ft)
Date	05/18/93				
Test Article		Exit Conditions		Vehicle Damage	
Type	W-Beam Guardrail	Speed (km/h)	58.5 (36.4 mi/h)	Exterior	
Installation Length (m)	30.5 (100.0 ft)	Angle (deg)	14.0	VDS	11LFQ-1
Size and/or dimension and material of key elements	12'-6" Post Spacing			CDC	11LFLW3
Soil Type and Condition	Strong soil	Occupant Risk Values		Interior	
Test Vehicle		Impact Velocity (m/s)		OCDI	
Type	1985 Chevrolet Truck	x-direction	3.3 (10.7 ft/s)	Post-Impact Behavior	
Designation	2000P	y-direction	1.9 (6.1 ft/s)	Max. Roll Angle (deg)	20.1
Model	C-20	THIV (optional)		Max. Pitch Angle (deg)	12.3
Mass (kg) Curb	2097 (4,623 lb)	Ridedown Accelerations (g's)		Max. Yaw Angle (deg)	5.8
Test Inertial	2000 (4,409 lb)	x-direction	3.4		
Dummy		y-direction	2.9		
Gross Static		PHD (optional)			
		ASI (optional)			

Figure 33. Summary of TTI Test 0482-1 on the G4(2W) with 12.5-ft post spacing. [Mak93]

Gabler, Gabauer and Hampton evaluated the effects of missing guardrail posts in a modified G4(1S) guardrail with routed wood blockouts under *NCHRP Report 350* Test 3-11 conditions using finite element simulations. [Gabler10] Two impact points were used in the analyses: (1) at a post located at the upstream end of the unsupported section and (2) at the midspan of the unsupported section. The analyses indicated that, for the case of a single post missing, impacts at the mid-span of the unsupported section resulted in 25 percent higher rail deflections compared to the results of the undamaged system; however, the potential for system override was not evident in the simulations.

As discussed earlier, a major concern of pocketing is rail-splice rupture. Gabler *et al.* evaluated the potential for splice rupture by recording and assessing increased magnitude in rail tension through the unsupported section of rail. The results indicate that rail tension increases as the damaged section included more and more missing posts, as shown in Figure 34. It was concluded by Gabler *et al.* that “the likelihood of the rails rupturing during impact increased as more posts were removed.”

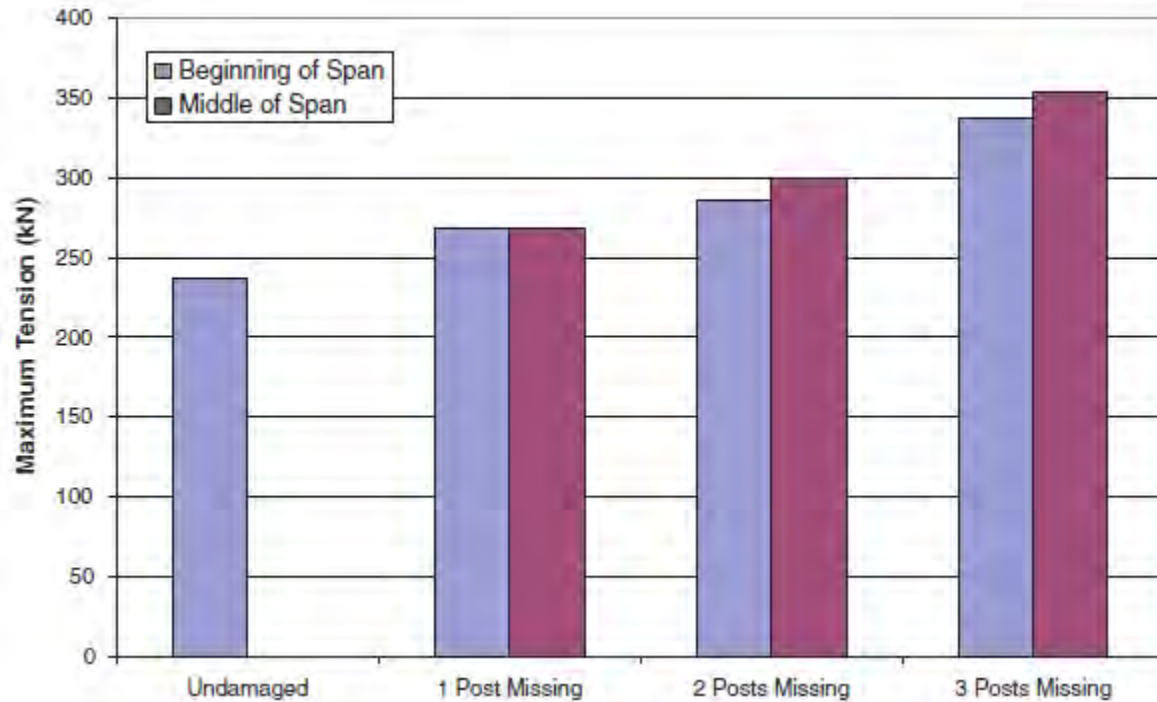


Figure 34. Maximum rail tension as a function of missing posts.[Gabler10]

Marzougui, Mahadevaiah, and Opiela used finite element analysis to evaluate various design modifications to the MGS guardrail for TL-2 applications.[Marzougui10] Five design alternatives were explored which involved doubling post spacing and reducing blockout depth, as listed below:

1. Doubling the post spacing from 6.25 ft. to 12.5 ft.,
2. Reducing the blockout depth by half; from 11.811 in. to 5.906 in.,
3. A combination of doubling the post spacing and reducing the blockout depth by half,
4. A combination of doubling the post spacing and having no blockouts, and
5. A combination of doubling the post spacing, having no blockouts, and lowering the height of the rail from 31 in. top of rail height to 27.75 in.

Simulations of TL-2 impact tests were made for each design option, under both *NCHRP Report 350* and *MASH* test requirements.

Modification #1 – Doubled Post Spacing

The simulations for both the small car and the 2000P pickup truck showed a smooth redirection and limited rail deflection. Major bending of only one post was observed with the pickup truck. The simulation of the heavier pickup with the higher center of gravity at a sharper angle resulted in greater system deflection, pull-out of two posts from the soil, and significant bending at one post in the *MASH* test. The vehicle's front wheel was partially severed in the impact. The analyses of the system indicated that the system would pass all required safety performance criteria of *Report 350* and *MASH*. The *Report 350* tests showed a potential for

intrusion into adjacent traffic lanes for both the passenger car and the pickup, with both exit angles at 14 degrees.² This criterion is preferable but not required.

Modification #2 – Reduced Blockout Depth

The small car simulation showed smooth redirection, but increased deflection and minor wheel snagging on the posts. For the *Report 350* 2-11 test there was a greater amount of deflection and more post bending than there was for the increased post spacing modification, but both were well within limits and both tests passed *Report 350* criteria.

The simulation results for the *MASH* 2-11 test were very similar to the increased post spacing modification, including the indication of the vehicle's front tire being partially severed during impact. The critical values of occupant ridedown velocity and acceleration were higher than with the increased post spacing modification, but still within desired levels. The analyses of the simulations indicated that the system would pass all required safety performance criteria of *Report 350* and *MASH*, and as such the researchers deemed reducing the blockout depth to be a viable design option.

Modification #3 – Doubled Post Spacing and Reduced Blockout Depth

As would be expected, there was increased deflection and minor wheel snagging on the posts for the small car when compared to either of the individual previous modifications. The results were still well within the limits of *NCHRP Report 350*, and were considered as passing. The *Report 350* Test 2-11 simulation was not performed on this design modification, but the more stringent *MASH* test with the larger test vehicle was evaluated with computer simulation. The vehicle in this scenario behaved similarly to its response in each of the two previous individual design alternatives and met all *MASH* TL-2 criteria.

Modification #4 – Doubled Post Spacing and No Blockouts

For this design alternative, the researchers conducted both 2-10 and 2-11 simulations to *MASH* standards. The small car test met all of the crashworthiness requirements but exhibited significant wheel snagging. The pickup truck test also passed all the crashworthiness requirements, but displayed greater instability and greater lift as it was redirected. As such, the researchers stated that although the design met all safety performance requirements, it was considered less desirable than the previous design alternatives.

Modification #5 – Doubled Post Spacing, No Blockouts, and Lowered Rail Height

MASH Tests 2-10 and 2-11 simulations were performed for the system with double post spacing, no blockouts, and a 27.75-inch rail height. Although the lower rail height reduces the amount of underride for the small vehicle in the Test 2-10 simulation, it was noted that the vehicle experienced greater vertical trajectory and greater pitch. The Test 2-11 simulation showed similar deflection behavior as the same system with the higher rail height, but also showed more lift during redirection. The degree of upward pitch was greater for this modification than in any of the other tests. As with Modification #4, the high degree of vehicle instability renders this design alternative less desirable than the previous design options.

² Note that this test is similar to the test conducted on the Washington State guardrail, but the guardrail in this case was the steel post MGS with double post spacing, whereas the Washington State guardrail was the G4(2W) with double post spacing.

Table 6 shows the results for the different simulation cases. Although all of the design alternatives met safety performance requirements, the authors stated that "...other considerations may render some of these alternatives undesirable (i.e., potentials for snagging, costs, sensitivity to factors)."

Table 6. TL-2 computer simulation results. [Marzougui10]

Design Option	Report 350 Criteria		MASH Criteria	
	Test 2-10	Test 2-11	Test 2-10	Test 2-11
	820C 43.5 mph (70 km/h) 20 degrees	2000P 43.5 mph (70 km/hr) 20 degrees	1100C 43.5 mph (70 km/h) 25 degrees	2270P 43.5 mph (70 km/hr) 25 degrees
Modification #1 - Increased Post Spacing	Pass	Pass		Pass
Modification #2 - Reduced Blockout Width	Pass	Pass		Pass
Modification #3 - Increased Post Spacing & Reduced Blockout Width	Pass			Pass
Modification #4 - Increased Post Spacing & No Blockout			Pass	Pass
Modification #5 - Increased post Spacing, No Blockout, & Lower Rail Height			Pass	Pass

Reduced Post Spacing

Rosson, Bierman and Rhode conducted a study for the Midwest States Regional Pooled Fund Research Program to assess the effectiveness of three common strengthening techniques for strong-post w-beam guardrail: (1) nesting w-beam rail, (2) reduce post spacing by half (i.e., 3.1-ft post spacing), and (3) combination of nested w-beam rails and half post-spacing. The evaluations were carried out using computer simulation and full-scale crash testing.[Rosson96]

Four full-scale tests were conducted and the results are shown in Table 7. The baseline test included the standard G4(1S) with W6x8.5 steel posts and blockouts with a single layer of 12-gauge w-beam rail and post spacing of 6ft-3in. All tests were conducted under the crash testing guidelines in NCHRP Report 230 Service Level 2, which involved a 4400-lb large car sedan impacting at a nominal speed and angle of 60 mph and 25 degrees, respectively. [Michie81].

Test KSWB-3 with the half-post spacing resulted in a 16 percent reduction in dynamic rail deflection, compared to the baseline test KSWB-1. Test KSWB-4 with the combination of nested rail and half-post spacing resulted in a 37 percent reduction in dynamic deflection, compared to the baseline test. Test KSWB-2 with the nested rails, on the other hand, resulted in an increase in lateral deflection, compared to the baseline test. It was stated by the researchers that they believed that the moisture content of the soil on the day that KSBW-2 was tested was

higher than it was when KSWB-1 was tested, “despite attempts to ensure the same density of soil for both tests.”

Table 7. Full-Scale crash test impact conditions and results. [Rosson96]

	KSWB-1 (single w-beam with standard post spacing)	KSWB-2 (nested w-beam with standard post spacing)	KSWB-3 (single w-beam with 1/2 post spacing)	KSWB-4 (nested w-beam with 1/2 post spacing)
Test Vehicle Weight - lbs. (kg)	4398.2 (1995)	4486.4 (2035)	4486.4 (2035)	4501.8 (2042)
Impact Speed - mi/hr (km/hr)	61.8 (99.6)	60.5 (97.4)	59.7 (96.1)	60.3 (97.2)
Impact Angle - deg.	25.1	25.4	24.8	28.4
Impact Severity - ft lbf (kJ)	101783.5 (138)	101046 (137)	93670.3 (127)	123910.4 (168)
Exit Speed - mi/hr (km/hr)	40 (64.5)	52.6 (84.7)	46.1 (74.2)	46.7 (75.3)
Exit Angle - deg.	14.5	12.9	9.6	14.1
Maximum Dynamic Deflection - in. (cm)	27.9 (71.1)	32.4 (82.5)	23.5 (59.7)	17.6 (44.8)
Maximum Permanent Set Deflection - in. (cm)	22.9 (58.4)	24.8 (63)	20.3 (51.6)	15.9 (40.4)

In order to better isolate the variables in the system to only those variables being studied, computer simulation was undertaken to evaluate the three strengthening techniques. The computational analyses were carried out using the BARRIER VII program. In addition to the three strengthening alternatives, the parametric study also included three different soil conditions: high density clay, (2) low density clay and (3) granular soil.

Table 8. Test matrix for post-in-soil bogie tests. [Rosson96]

Class No.	Post Type	Soil Type	Moisture Content	Embedment Depth	No. of Tests Conducted
1	Timber	Clay	Low	Standard	2
2	Timber	Clay	Low	Extended	2
3	Timber	Clay	Optimum	Standard	2
4	Timber	Clay	High	Standard	2
5	Timber	Sand	Unsaturated	Standard	2
6	Steel	Clay	Low	Standard	2
7	Steel	Clay	Low	Extended	1
8	Steel	Clay	Optimum	Standard	2
9	Steel	Clay	High	Standard	2
10	Steel	Sand	Unsaturated	Standard	2

Table 9. BARRIER VII post input variables. [Rosson96]

Class	Post Material	Soil Material	Embedment	Moisture Content (%)	K _B (kip-ft)	M _A (kip-ft)	D _B (in)	F _B (kip)
1	Timber	Clay	Standard	Low	443	19.8	20	14.1
2	Timber	Clay	Extended	Low	324	21.2	15	15.2
3	Timber	Clay	Standard	Optimum	359	23.8	20	17.0
4	Timber	Clay	Standard	High	190	8.4	17.5	6.0
5	Timber	Sand	Standard	Unsaturated	347	11.3	20	8.0
6	Steel	Clay	Standard	Low	349	16.1	20	11.5
7	Steel	Clay	Extended	Low	339	18.8	20	13.4
8	Steel	Clay	Standard	Optimum	587	17.2	20	12.3
9	Steel	Clay	Standard	High	139	8.2	20	5.8
10	Steel	Sand	Standard	Unsaturated	291	9.1	20	6.5

The input parameters for the BARRIER VII program for the material and mechanical properties of the post-soil model were determined through physical testing of guardrail posts embedded in different soil types and at different embedment depths. A total of 21 dynamic bogie-impact tests were conducted in the test series, as shown in Table 8. Five different soil types were used in the tests including a well-graded medium grain unsaturated sand, silty clay with low moisture content, silty clay with high moisture content, and silty clay with optimum moisture content. Two post types were used: a W6 X 8.5 steel post and a 6x8-inch timber post. Two embedment depths were used: 44 inches and 50 inches. The BARRIER VII properties which were derived from the tests are presented in Table 9.

The BARRIER VII model for each of the four guardrail cases were then performed and compared to the results of the four full-scale tests KSWB-1, KSWB-2, KSWB-3, and KSWB-4 as shown in Figure 35. The BARRIER VII model was then used to conduct a parametric investigation to evaluate the effectiveness of three different strengthening techniques and the effects of soil properties on the dynamic deflection of the systems. The results from the BARRIER VII simulations, shown in Table 10, indicated that soil density has a much greater influence on dynamic deflection than any of the other variables, while nesting of the w-beam rails was shown to have the least effect on deflection. As can be seen, the posts with the highest dynamic deflection are those that were embedded in either low density clay or sand. Although the dynamic deflection is consistently higher for steel posts than for wood posts, the difference is much smaller in all cases than it is for the soil type/density variation.

Low Soil Confinement/Support

Polivka et al. performed a study for the Midwest States Regional Pooled Fund Research Program to design and test a w-beam guardrail for installation at the break point of 2:1 slopes.[Polivka00b] The guardrail was to be evaluated according to *NCHRP Report 350* Test 3-11 requirements. The study involved (1) conducting dynamic bogie-impact tests on guardrail posts installed in soil to determine post-soil response, (2) develop and calibrate a post-soil for use in the BARRIER VII program based on the results from the dynamic bogie-impact tests, (3) use

BARRIER VII to determine optimum barrier design, and (4) verify new barrier design via full-scale testing.

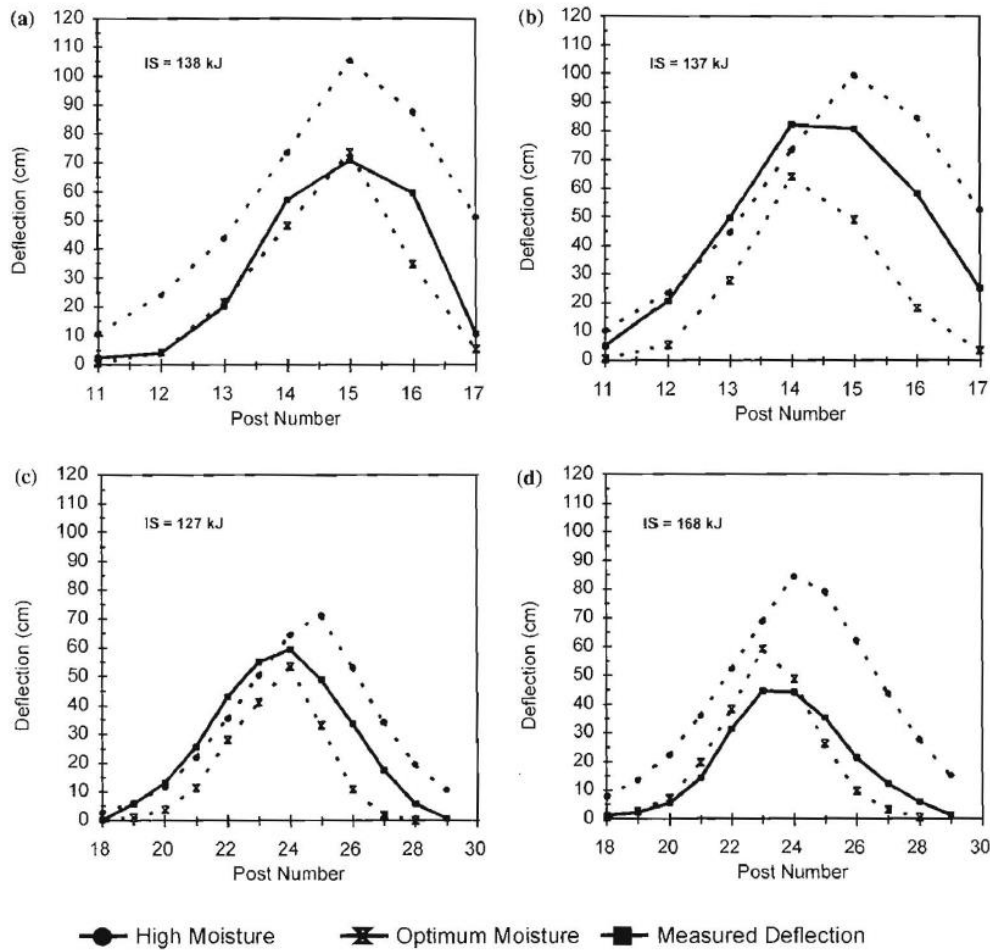


Figure 35. Maximum dynamic deflection comparison plots: (a) KSWB-1, (b) KSWB-2, (c) KSWB-3, (d) KSWB-4. [Rosson96]

Six bogie tests on steel posts installed at the break point of a 2:1 foreslope were conducted. The soil conformed to AASHTO M147-65 gradation "B" specifications (*NCHRP Report 350 Strong Soil*). The posts were impacted with a 2,143 lb bogie vehicle at the target speeds of 15 mph for the first five tests and 20 mph for the last test. The impact point in all tests was at 21.65 in. above the ground line and perpendicular to the front face of the posts. The test matrix for the six bogie tests is provided in Table 11 and a typical test-installation is shown in Figure 36. The bogie test results are shown in Table 12. The primary mode of failure occurred in the soil rather than post yielding in all six tests.

Table 10. BARRIER VII maximum dynamic deflection results. [Rosson96]

			Maximum Dynamic Deflection (cm) (% Decrease of Max. Defl. Compared with Std. Installation)			
			Standard Installation	W-Beam Nesting Only	Half-Post Spacing Only	Both Nesting & Half-Post Spacing
Clay	High Density	Steel	68.1	62.7 (8%)	54.4 (20%)	46.2 (32%)
		Timber	62.7	59.9 (4%)	48.0 (23%)	41.4 (34%)
	Low Density	Steel	102.4	95.8 (6%)	72.9 (29%)	69.6 (32%)
		Timber	98.8	91.9 (7%)	73.4 (26%)	69.1 (30%)
Sand		Steel	94.7	88.6 (6%)	69.3 (27%)	65.0 (31%)
		Timber	88.9	80.8 (9%)	65.0 (27%)	59.9 (33%)

Table 11. Steel post bogie impact test matrix. [Polivka00b]

Test No.	Post Type ASTM Designation	Embedment Depth (in)	Target Speed (mph)
MSB-1	W6x12 by 8 ft long	67	15
MSB-2	W6x12 by 8 ft long	55	15
MSB-3	W6x9 by 7 ft long	55.25	15
MSB-4	W6x9 by 7 ft long	55.25	15
MSB-5	W6x9 by 7 ft long	55.25	15
MSB-6	W6x12 by 9.68 ft long	87.25	20



Figure 36. Typical steel post test installation for bogie impact testing. [Polivka00b]

The researchers used the results from the bogie tests to develop and calibrate a post-soil model for use in the BARRIER VII program. BARRIER VII was then used to evaluate four W-beam guardrail design alternatives on both level and sloped terrain conditions:

1. A system with 7-ft posts spaced 6.25 feet on center
2. A system with 8-ft posts spaced 6.25 feet on center
3. A system with 7-ft posts spaced 3.125 feet on center
4. A system with 8-ft posts spaced 3.125 feet on center

The BARRIER VII results are shown in Table 13. The results of the analyses indicated that excessive guardrail deflections would occur with posts installed on the break-point of slopes for the standard post spacing of 6.25 feet for both embedment depths. It was theorized that the excessive deflection would greatly increase the possibility of severe wheel snag on posts. The analyses also indicated that for both embedment depths the guardrail with post spacing at 3.125 feet (i.e., half post-spacing) would result in less dynamic deflection than standard strong-post w-beam on level terrain conditions. The design selected for full-scale testing included 7-ft posts with 3.125-ft post spacing.

Table 12. Steel post bogie test results. [Polivka00b]

Test No.	Impact Speed (mph)	Peak Load (kip)	Deflection at Peak Load (in)	Results
MSB-1	14.5	26.5	2.67	Small soil failure at front of post, post rotation
MSB-2	15.7	17.8	2.39	Large soil failure at front of post
MSB-3	14.4	14.5	2.5	18-in radius soil failure at front of post
MSB-4	14.4	17.4	2.11	15-in radius soil failure at front of post
MSB-5	13.5	9.3	2.87	12-in radius soil failure at front of post
MSB-6	21.2	30.6	3.79	No soil failure at the front of the post, post slightly twisted during rotation, post bent 55 in from the top with maximum deflection of 4.75 in.

Table 13. BARRIER VII computer simulation results. [Polivka00b]

Run No.	Impact Node	Impact Conditions		Maximum Dynamic Rail Deflection ¹ (mm)	Terrain Condition	Post Length (mm)	Post Spacing (mm)	Description Summary
		Speed (km/hr)	Angle (deg)					
Slope5d	52	101.5	25.5	993 @ Node 70	Level	1,829	1,905	Calibration to TTI test no. 405421-1.
Slope6d	83	100.0	25.0	889 @ Node 101	Level	1,829	1,905	Baseline simulation with 1,829-mm posts and standard spacing.
Slope7d	83	100.0	25.0	1,031 @ Node 103	Sloped	2,438	1,905	Sloped fill and 2,438-mm posts.
Slope8d	83	100.0	25.0	1,194 @ Node 101	Sloped	2,134	1,905	Sloped fill and 2,134-mm posts.
Slope6dHPS	83	100.0	25.0	566 @ Node 97	Level	1,829	952.5	Level fill and 1,829-mm posts with half-post spacing.
Slope7dHPS	83	100.0	25.0	668 @ Node 97	Sloped	2,438	952.5	Sloped fill and 2,438-mm posts with half-post spacing.
Slope8dHPS	83	100.0	25.0	757 @ Node 99	Sloped	2,134	952.5	Sloped fill and 2,134-mm posts with half-post spacing.

¹ - Lateral distance measured at the center height of the rail.

The test installation, shown in Figure 37, was constructed adjacent to a pit with 2:1 slope, 9 ft wide, 3 ft deep and 62.5 ft. long. The guardrail system was impacted with a 1994 GMC 2500 ¾-ton pickup weighing 4,462 lbs., in accordance with *NCHRP Report 350* TL-3 testing standards. The guardrail safely contained and redirected the vehicle and successfully met all safety performance criteria specified in *NCHRP Report 350*. The researchers noted, however, that "...it may be possible to obtain acceptable safety performance from a guardrail design which incorporates longer posts, a wider post spacing, or combinations thereof."

Marzougui *et al.* recently performed a study for the Federal Highway Administration to investigate the effects of raising the rail height of the G4(2W) strong-post w-beam guardrail placed at the break-point of a 2:1 slope.[*Marzougui09*] The increase in rail height was achieved by raising the blockouts three inches which, in effect, achieves the increase in rail height without altering post height or embedment depth.



Figure 37. W-beam guardrail adjacent to 2:1 foreslope for full-scale crash test.[*Polivka00b*]

The study involved the use of finite element analysis to simulate *Report 350* Test 3-11 on four different cases:

- Case 1: Standard G4(2W) on level terrain (baseline case)
- Case 2: Standard G4(2W) placed at break-point of 2:1 slope
- Case 3: G4(2W) with blockouts raised 3 inches, placed at break-point of 2:1 slope
- Case 4: Same as Case 3, but with two bolts used to fasten the blockout to the post

The results of the analyses indicated that the standard G4(2W) placed at the break-point of a 2:1 slope would result in an increase in rail deflection of approximately 2-inches, relative to the baseline rail deflection of 22.4 inches. The performance of the modified system with raised

blockouts was essentially the same as the standard system regarding barrier response, vehicle response and occupant risk measures. They concluded that there is no evidence from this analysis that the raised blockout design would increase the likelihood of barrier failure or have adverse effects on impacting vehicles. It was also stated that the proposed method of adjusting guardrail height by raising the rails and blockouts may be a low cost option for retrofitting existing field installations until system upgrades can be made. It was not stated in the report, however, what the embedment depths were.

Blockouts

The blockouts used in most strong-post guardrail systems serve a dual function: (1) to reduce the possibility of wheel-snap on the guardrail posts by creating separation distance between post and rail and (2) to ensure that the rail element maintains a critical height as the system deflects to allow enough time for the rail-to-post connection to release properly. The connection of the rail to blockout (or post if no blockout is used) is designed to release under relatively low loads. The failure mechanism for standard strong-post guardrails involves the bolt-head pulling through the slot in the w-beam rail. Although this release occurs rather quickly, it is not instantaneous so it is important that the rail remain above the critical height until it is released.

Effects of Blockout Depth

Figure 38 shows an illustration of how the blockouts serve to reduce the probability of wheel snag. In Figure 38(a) the eight-inch blockout provides adequate separation of the rail from the post to prevent wheel contact with the post; whereas in Figure 38(b) the wheel impacts against the post even at very low rail deflection. Full-scale tests on w-beam guardrail systems have shown that the front wheel on the impact side of the vehicle often snags on the guardrail posts as the top of the posts are pushed back by the rail element, exposing the lower section of the post to impact by the wheel, as shown in the test photo in Figure 39.[Mak94]

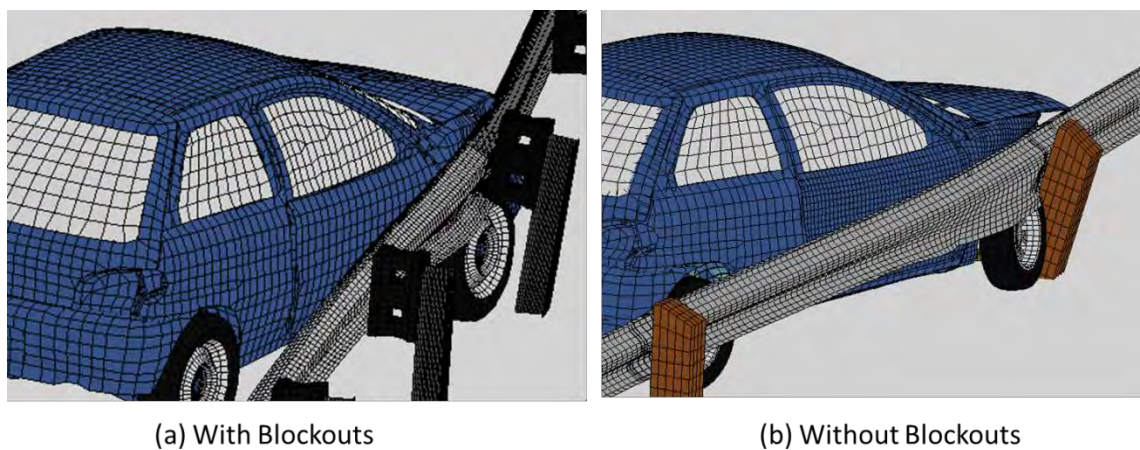


Figure 38. Illustration of how blockouts help reduce possibility of wheel-snap.[Ray04]



Figure 39. Wheel snag against guardrail post in TTI Test 471470-26.[Mak94]

For small, light-weight vehicles, a direct impact with a guardrail post can lead to high decelerations and occupant compartment intrusion, and/or vehicle instability.[Ray04] In such cases, the release of the rail from the post may be critical in reducing the effective resistance of the post. That is, if the rail does not release properly from the post, then the post is effectively a “fixed-pinned” beam restrained at the top by rail-to-post connection and at the ground line by the soil, which will not easily yield, particularly under the impact forces from a small car.

Figure 40 shows an illustration of how the blockouts function to keep the rail above the critical height as the posts deflect. During impact, the rail element imposes a lateral load on the posts and as the posts are pushed back they rotate at a point below grade. For a 6-ft long strong-post with a rail height of 27 inches, the rotation point is typically between 25 and 30 inches below grade.[Rohde96] At post rotations less than approximately 30 degrees, the post with the blockout (Figure 40(a)) maintains the critical rail height, while the post without the blockout (Figure 40(b)) results in the rail being pulled down significantly by the rotating post. The release of the rail from the post is therefore much more critical when a blockout is not present.

Karlsson used finite element analysis to evaluate the interaction between the vehicle wheel and guardrail posts in simulations of *Report 350 TL-3* impact conditions.[Karlsson00] Several design alternatives for alleviating the effects of wheel snagging were investigated, including the use of longitudinal failure fuses on the posts as discussed earlier. Another alternative was the use of deeper blockouts to increase the separation distance between the rail and posts. The results from Karlsson’s study are shown in Figure 41 where the peak force between tire and post is plotted as a function of blockout depth. These results correspond to strong-post guardrails with a 27-inch rail-mounting height. The analyses indicated that (1) the impact forces decrease with increasing blockout depth, (2) the impact forces are approximately constant for blockout depths between 4 to 8 inches, and (3) a minimum blockout depth of 10 inches would be required to avoid wheel snag on strong-post w-beam guardrails (Note: the standard blockout depth on most strong-post guardrail systems is 8 inches). Figure 41 also suggests there are diminishing returns for using block-outs much greater than 10 inches (254 mm).

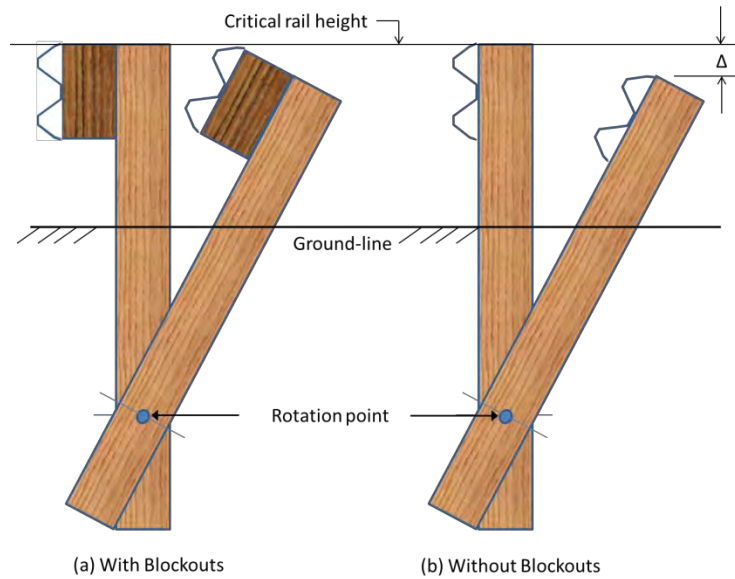


Figure 40. Illustration of how blockouts help to maintain critical rail height during post deflection.

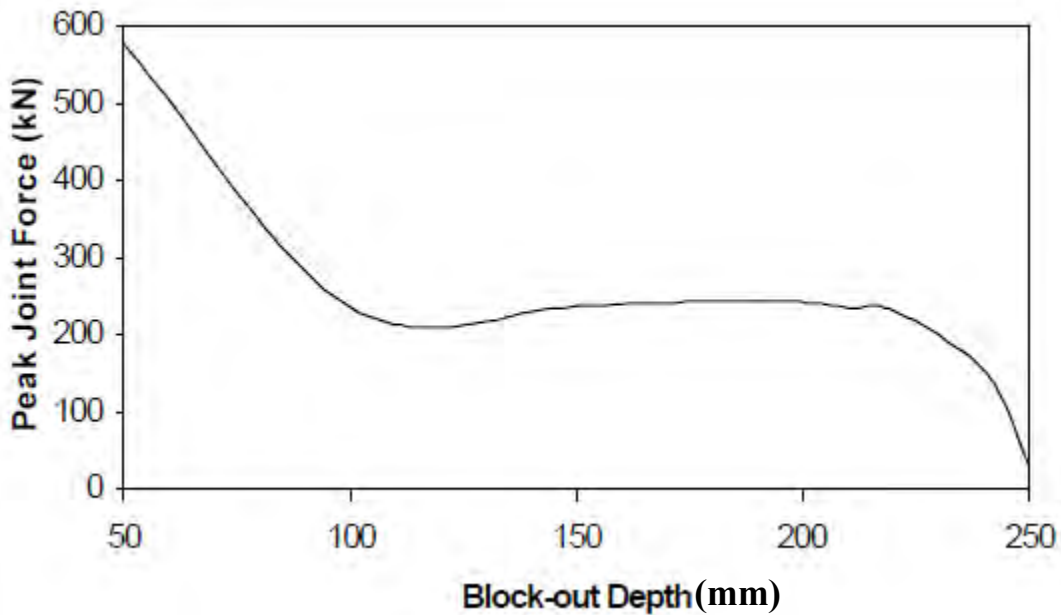


Figure 41. Peak tire-post impact force as a function of blockout depth for Report 350 TL-3 impacts.[Karlsson00]

Karlsson’s conclusions were similar to those made by Sicking and Ross in their 1987 study on structural optimization of strong-post w-beam guardrail.[Sicking87] The results of the Sicking and Ross study indicated that a blockout depth of 10 inches for strong-post w-beam guardrails was sufficient to prevent wheel snag for both the small car and full-size sedan.

It is worth noting, that the MGS guardrail uses a 12-inch blockout but still experiences slight to moderate wheel snag on guardrail posts in Report 350 TL-3 tests.[*Sicking02*] Recall that the MGS has a standard rail height of 31 inches; whereas the earlier studies by [*Sicking87*] and [*Karlsson00*] pertained to strong-post guardrail with a 27-inch height so there is clearly a geometric relationship between the rail height and the optimal blockout depth.

In a recent study at MwRSF, full-scale crash tests were conducted on the MGS guardrail with 8-inch blockouts and no blockouts.[*Rosenbaugh12*] The tests were performed according to *MASH* TL-3 criteria. This work is not yet published, however, a brief summary of the test results regarding occupant risk measures were presented at the Transportation Research Board (TRB) Roadside Safety Design Committee (AFB20) mid-year meeting in Irvine, California; those results are shown in Table 14. The results showed that occupant risk measures generally increase as blockout depth decreases. The pickup test for the non-blocked MGS resulted in increases of 12 percent and 20 percent for longitudinal and lateral occupant impact velocities, respectively, and increases of 40 percent and 87 percent for longitudinal and lateral occupant ridedown accelerations, respectively, compared to the MGS with 12-inch blocks. For the small car test, reducing blockout depth primarily results in increased occupant impact velocity (e.g., higher accelerations at the beginning of the impact event), where the MGS with 8-inch block results in a 42 percent increase in longitudinal Occupant Impact Velocity (OIV) compared to the 12-inch block; and the MGS without blocks results in a 111 percent increase in longitudinal OIV compared to the 12-inch block.

Table 14. Comparison of full-scale test results for MGS with 12-inch blockouts, 8-inch blockouts and no blockouts.[*Rosenbaugh12*]

	Pickup		Small Car		
	MGS – 12" Block	MGS – No Block	MGS – 12" Block	MGS – 8" Block	MGS – No Block
OIV: Longitudinal (ft/s)	15.3	17.1	14.8	21.0	31.3
OIV: Lateral (ft/s)	15.6	18.7	17.1	17.4	15.8
ORA: Longitudinal (g's)	8.2	11.5	16.1	8.8	10.2
ORA: Lateral (g's)	6.9	12.9	8.4	6.8	6.3
IS (kip-ft)	122.3	115.1	55.0	55.4	59.3

Ray, Plaxico and Oldani evaluated the performance of the Alberta weak-post w-beam guardrail under *Report 350* TL-3 impact conditions using finite element analysis.[*Ray04*] The Alberta weak-post system is composed of 6x8 inch wooden posts supporting a w-beam rail. The posts are spaced at 12.5 ft and the rail is fastened to the posts using 5/8-inch diameter bolts. This system is basically the G4(2W) strong-post system with increased post spacing and no blockouts.

The results of Ray's study indicated that vehicle decelerations caused by wheel-snag during the simulation of *Report 350* Test 3-10 (i.e., small car test) would result in Occupant Ridedown Accelerations (ORA's) that would only marginally pass the *Report 350* safety criteria and it was suggested that small changes in event timing could lead to unacceptable results. The forces induced by the wheel-snag also resulted in excessive deformation inside the occupant compartment, which was deemed unacceptable based on *Report 350* criteria. The results from

the simulation of *Report 350 Test 3-11* (i.e., pickup truck test) indicated marginal performance of the guardrail system. The analysis results showed that the vehicle was very unstable when exiting the system, as the vehicle was airborne with a maximum roll angle of more than 45 degrees.

Several design alternatives were investigated involving a smaller size wood post (5-inch diameter), different rail-to-post connection strengths (5.6k, 6.7k and 9.0k), w-beam splice moved to midspan between posts, and rail height (27, 30 and 32 inches). The use of this smaller sized post was based on the results of an earlier study performed by Bronstad and Burkett for the State of Ohio who recommended the use of 5-inch posts with ¼-inch bolts inserted through a pipe sleeve in the post for weak-post w-beam guardrail systems.[*Bronstad71*] Ray *et al.* concluded that “good performance cannot be expected consistently unless the guardrail height is at least 32-inches above grade and the connection strength is below 6.7k. The recommend design included:

- Standard 12-gauge w-beam rail
- Splices moved to the mid-span
- 32-inch rail-mounting height (top of rail)
- 5-inch diameter wood posts
- Rail connected to posts with standard 5/8-inch diameter button-head bolts

It was also suggested that post types other than wood be considered, which may provide better performance. The new design was never put in place since a suitable anchor system was not available.

Effects of Collapsed Blockouts

Blockouts used for most strong-post guardrail systems are designed to be “non-collapsible.” Earlier versions of the G4(1S) guardrail (i.e., steel-post w-beam guardrail) used W6x9 steel blockouts which have a relatively low torsional rigidity. The poor performance of that system was a direct result of the blockout collapsing in a lateral torsional buckling mode during impact, leading to wheel snag on the posts.[*Mak96a; Mak99a*] The wheel-snag was exacerbated by the twisting deformation mode of the blockout which caused the posts to fail prematurely in torsion resulting in low deflection of the posts at the groundline. The solution was to replace the steel blockout with the 6x8 inch wooden blockout that performed successfully in the G4(2W) guardrail.[*Bullard96*] Other versions of the modified G4(1S) incorporate “non-collapsible” blockout designs made from other materials (e.g., recycled plastic).[*Bligh97b*]

This behavior is common in all strong-post guardrail systems that use structural-steel posts with low torsional rigidity (e.g., wide-flange posts), including the modified thrie-beam guardrail system shown in Figure 42. The modified thrie-beam guardrail (SGR09b) uses the same W6x9 steel posts as the G4(1S) system with a W14x22 blockout. This system was successfully tested for *NCHRP Report 350 TL-3* at the Texas Transportation Institute. [*Mak99a*] It was concluded from the results of the test (i.e., Test 471470-30) that:

“The relatively large deflection sustained by the guardrail system and snagging of the left wheel assembly with post 17 were somewhat unexpected given the stiffness of the thrie-beam element and the (14-inch) deep blockout. The soil condition was checked and found to be a little damp, but not to the extent that it would adversely affect the bearing

capacity of the soil. Review of the high-speed film showed that posts 16-18 were severely twisted from the vehicle impact as the thrie-beam element deflected. The W6x9 steel posts are relatively weak in torsion to begin with. The added moment arm due to the deep blockout aggravated the torsional moment acting on the posts. As the posts twisted, the blockouts essentially collapsed. This in effect increased the dynamic deflection of the guardrail by 18 inches ... Also, the collapse of the blockout allowed the left front wheel assembly of the vehicle to come into direct contact with post 17 ... ”[Mak99a]

Sheikh and other researchers at the Texas Transportation Institute recently used finite element analysis to evaluate the performance of the SGR09b for high-speed impact conditions (i.e., 4,577-lb pickup, 85 mph, 25 degrees) for the Texas Department of Transportation (TxDOT).[\[Sheikh09\]](#) TxDOT embarked on an effort to expand the state’s transportation system and expressed interest in the development of road systems with higher design speeds.

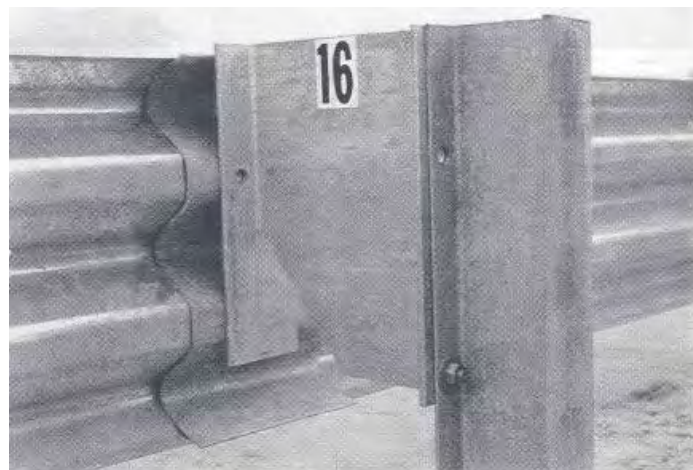


Figure 42. Modified thrie-beam guardrail (SGR09b).[\[Sheikh09\]](#)

The results of their analyses indicated that the performance of the SGR09b guardrail would not likely be acceptable in high-speed (e.g., 85 mph) impact events. They also concluded that the overall deformation mode of the blockout-and-post components, shown in Figure 43, leads to the poor performance of the system and suggested that these components be replaced by wood posts and blockouts. Although this system has been shown to perform well in *Report 350* TL-4 conditions, it was concluded that performance would be further improved if the post and blockout were designed such that they had sufficient lateral stiffness to allow the post to rotate properly in the soil as the system deflected to reduce the potential for wheel-snap on the posts.

Recall that the thrie-beam guardrail with 6x8-inch routed wood blockouts met the crash test requirements of *MASH*, but the vehicle appeared to be very unstable during redirection.[\[Bullard10\]](#) It is not known, however, how a solid block (e.g., wood, plastic, etc.) would affect the performance of the modified thrie-beam guardrail. Recall that the modified thrie-beam rail is 34 inches high (1.5 inches higher than the standard thrie-beam system) and has a 14-inch deep blockout with a unique cutout at the bottom of the blockout to help to keep the face of the rail vertical as the posts rotate back during collisions.

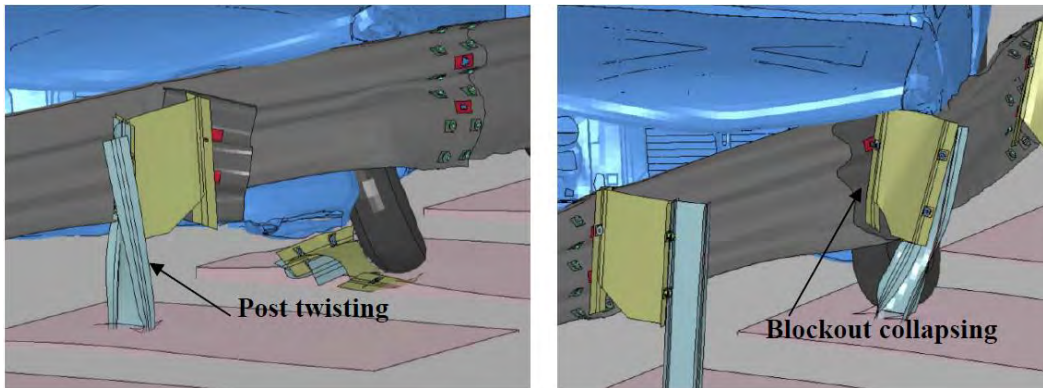


Figure 43. Deformation of three-beam guardrail during impact with 4,577-lb vehicle at 85 mph and 25 degree impact.[Sheikh09]

Effects of Missing Blockouts

Hampton and Gabler conducted pendulum testing on missing blockouts in Report 656.[Hampton10] The problem with pendulum testing alone is that it cannot predict the possibility of wheel-snagging due to the missing blockout. To account for this, the researchers continued on their previous work by conducting finite element modeling of the pendulum testing using LS-DYNA software. The model was created by modifying an existing model of the modified G4(1S) guardrail with routed wood blockouts obtained from the National Crash Analysis Center (NCAC). Parts of the model were deleted until only a small section that matched the original setup remained. They also increased the strength of the connections between the splice bolts and nuts, increased the mesh density of the rail, and lowered the strength of the soil in which the posts were embedded to better replicate the results of the actual pendulum tests. As a result, the pendulum simulations were able to predict the same test outcome as was observed in the real tests, as can be seen in Table 15.

The researchers then combined the modified guardrail model with a model of a Chevrolet 2500 pickup truck obtained from the same NCAC library. They conducted a series of eight simulations (four impact points for each missing blockout location), keeping the initial vehicle speed and angle constant for all simulations (62.1 mph and at 25 degrees). “In all of the missing blockout simulations, the vehicle was observed to show more roll and pitch than was seen in a simulation of an impact into a guardrail not missing any blockouts... [however] ...the roll and pitch were not high enough to conclude that the vehicle was unstable.” Most notably, however, is that no evidence was found in any of the simulations of major snagging of the vehicle tires.[Gabler10]

Table 15. Summary of pendulum test and model results. [Hampton10]

	Pendulum Test 1		Pendulum Test 2		Pendulum Test 3	
	Real Test	Model	Real Test	Model	Real Test	Model
Test Outcome	Contained	Contained	Splice Fail	Splice Fail	Contained	Contained
Maximum Rail Deflection (inch)	25.9	25.5	27.2	27.2	24.9	25.2
Splice Post Bolt	Intact	Intact	Broken	Pulled out	Intact	Intact
Non-splice Post Bolt	Pulled out	Intact	Pulled out	Pulled out	Pulled out	Intact

Rail-to-Post Connection

As mentioned earlier, the release of the rail-to-post connection is critical for proper performance of the guardrail. If the release forces are too low, the rail will release too soon allowing the rail to drop ahead of the vehicle, increasing the probability of the vehicle overriding the rail and penetrating behind the system. If the release forces are too high, the rail may release too late, or not at all, resulting in the rail being pulled down by the posts during impact.[Bligh97] Thus, the post-rail connection must fail consistently and at the appropriate time to ensure that the rail maintains the proper height during impact.[Engstrand00; Ray01a; Sicking02] It was also demonstrated earlier that increased blockout depth can help alleviate the sensitivity of the rail-to-post release on system performance (refer to the section on blockouts for more information).

Ray, Engstrand and Plaxico at Worcester Polytechnic Institute and McGinnis at Bucknell University conducted a study for the Pennsylvania Department of Transportation to improve the crash performance of the weak post w-beam guardrail system (G2);[Engstrand00; Ray01a] This system is very popular in Connecticut, New York, Pennsylvania and, to a lesser extent, in Virginia and North Carolina. The original G2 design successfully met performance criteria of Report 230 but failed to meet that of Report 350.

The weak-post W-beam guardrail is composed of W-beam rails supported on weak S3x5.7 steel posts with rectangular soil plates. The system performs much like the cable guardrail in that the posts hold up the rail at the proper height until the guardrail is struck by an errant vehicle. The posts are spaced at 12.5 feet and the rail is connected to the posts using 5/16-inch diameter bolts with 1.75 inch square washers under the head. The bolts are designed to fail in an impact allowing the rail to separate easily from the post. The rail separation from the post is an important feature of the design since this action allows the rail to remain in contact with the vehicle instead of being pulled to the ground by the post. Once the rail is separated from the post, the posts are bent back as the w-beam deflects and slips over the top of the posts. The W-beam rail then redirects the vehicle, acting like a cable that is anchored at the ends. Although the basic functionality of weak post systems is quite different from its strong-post “cousin,” the weak post w-beam guardrail shares many of the same components which perform the same basic functions at the local component level.

Ray *et al.* demonstrated that relatively small changes in several important design details can significantly affect performance of the weak-post w-beam guardrail.[Ray01a] They found that: (1) the post-rail connection must fail consistently and at the appropriate time to prevent the rail from being pulled down with the post during impact; (2) rupture of guardrail splices were largely a result of high stress concentrations around the splice-bolt holes as the splice bends

about the post and blockout, which could easily be avoided by simply moving the splices to the mid-span (i.e., non-post locations); (3) backup plates are needed when the rail is directly exposed to other components with sharp edges, such as steel I-beam posts when blockouts are not used, to prevent small tears in the rail; and (4) that guardrail height must be sufficient to prevent override of vehicles with high centers of gravity (e.g., pickup trucks) while still preventing under-ride of smaller vehicles (e.g., small cars). These modifications were initially investigated through FEA analysis and later through a series of four full-scale crash tests conducted at TTI from November 1999 through June 2000. [Buth99a-c; Buth00e] The final modified system consists of the following components:

- 12 gauge w-beam guardrail mounted 32.25 inches (820 mm) above the ground with splices at mid-span,
- S3x5.7 (S75x8.5) weak steel posts with soil plates spaced at 12.5 ft (3,810 mm) and attached to the rail at non-splice locations
- W-beam backup plates at each post, and
- A post-rail connection consisting of one 5/16-in diameter ASTM F568 Class 4.6 bolt with two 1.6-in square washers and two nuts.

The resulting modified design was successfully crash tested to both *Report 350* and *MASH* performance criteria.[Buth00c; Buth00d; Bullard10] The importance of this study is that many of the design modifications that were made to the G2 system were later implemented into the strong-post system (i.e., the MGS guardrail), which demonstrated marked improvement over the standard G4(1S) and G4(2W) systems.[Sicking02]

As with the design of the weak post w-beam guardrail [Engstrand00; Ray01a], the rail-to-post connection is also an important design consideration for strong post systems. In a study by Plaxico *et al.*, the force and energy required to fail the post-bolt connection (i.e., bolt head pulling through the w-beam slot) in strong post guardrail systems was determined through quasi-static laboratory testing.[Plaxico03] Four scenarios were investigated which are illustrated in Figure 44:

- Case 1. One layer of w-beam with the bolt positioned in the center of the slot in the w-beam,
- Case 2. One layer of w-beam with the bolt positioned at the edge of the slot in the w-beam,
- Case 3. Two layers of w-beams (e.g., a splice connection at a post) with the bolt positioned at the center of the slots in both sections, and
- Case 4. Two layers of w-beams with the bolt positioned at the edge of the slots in both sections.

The results of the tests are shown in Figure 45. The minimum pull-through force required to fail the connection occurred in case 1 (i.e., one layer of w-beam with the bolt in the center of the slot) with an average load of 4,046 lb (18 kN). The maximum pull-through force occurred in case 4 (i.e., two layers of w-beams with the bolt positioned at the corner of the slot) with an average load of 14,545 lb (64.7 kN); which was a difference of 3.6 times compared to the minimum failure force. The results shown here were measured from quasi-static tests, thus the

effects of strain-rate were not invoked in the tests but the relative difference in magnitude between the four connection cases should be similar in impact events.

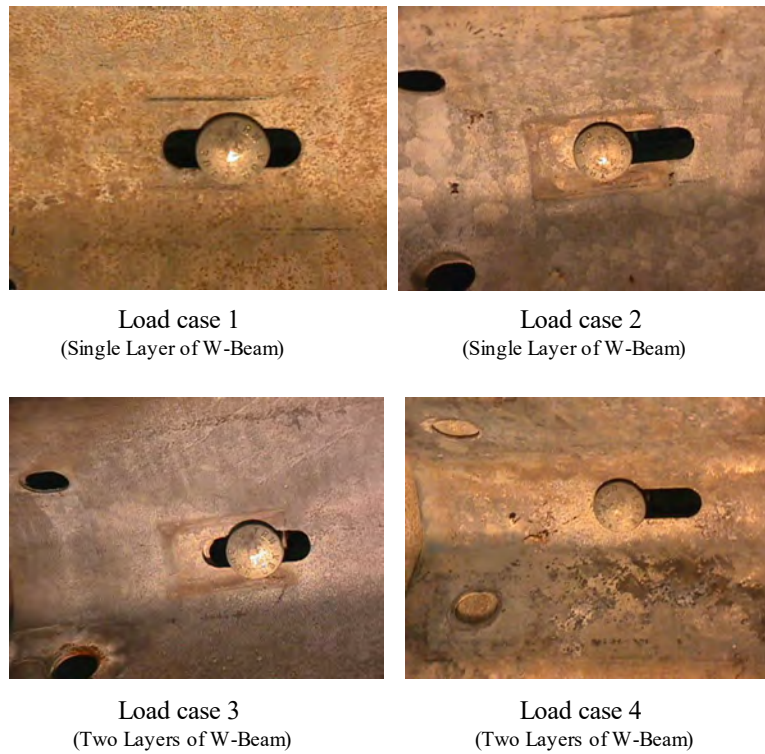


Figure 44. Position of bolt in slotted hole in w-beam for each load case.[Plaxico03]

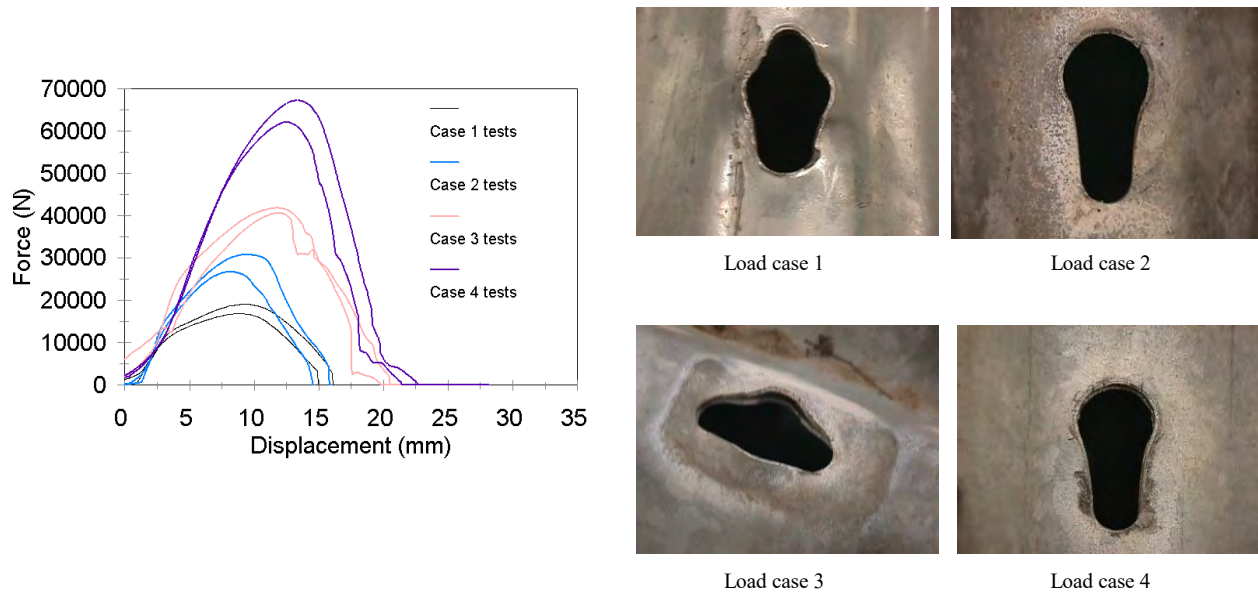


Figure 45. Results from uniaxial tests on rail-to-post connections.[Plaxico03]

Moving the rail splice to the mid-span between guardrail posts improves crash performance for strong post guardrail systems by serving two very important functions: (1) it

alleviates high-stresses in the splice connection by moving the splice away from the post (see earlier discussion) and (2) results in a more consistent failure load for the rail-to-post connection by limiting the connection to a single layer of w-beam, as illustrated in load cases 1 and 2 in Figure 45.[*Engstrand00; Polivka00a; Plaxico03*] Recall that in the development of the MGS guardrail, the rail splice was also moved to the midspan for these reasons.[*Sicking02*] The design of the rail-to-post connection was further improved for the MGS by lengthening the post-bolt slot in the w-beam rail, which further reduces the connection strength and improves consistency of the failure load by making it less likely for a post-bolt to be positioned near the edge of the slot during installation.[*Sicking02*]

Rail Element

Splice Failures

Splice failures have been observed in a wide variety of w-beam guardrail types, including weak-post w-beam guardrail [*Kilareski99*], strong-post w-beam guardrail [*Buth99a; Ross99; Mak99b; Polivka00a*], as well as w-beam end-terminals and transitions [*Mak96b; Mak96c*]. Essentially all w-beam barriers use the same 8-bolt splice connection for connecting the ends of w-beam rails to each other and all such systems occasionally experience splice failures. Based on a comprehensive review of these tests it was found that:

- Guardrail rupture is not usually caused by defective or substandard material, based on the results of tensile tests on specimens taken from the failed w-beam,
- In every case where it could be determined, the rupture occurred downstream of the vehicle,
- In the only test that was instrumented with a strain gauge on the rail, rail tension was no more than 29.2 kip (i.e., approximately 32% of the tensile capacity of the splice connection),
- Dynamic deflections when noted were usually modest,
- Failures were observed with both large and small vehicles
- Tears always pass through at least one splice hole and the bottom-downstream hole is *usually* located on the tear line – the only exception being Test RF476460-1-5 on the G4(2W).

These results suggest that splice failures cannot be adequately explained by material deficiencies or axial rail capacity. The splice connections in most guardrail and guardrail terminal systems are located at the guardrail posts so the loading experienced by the splice is a combination of the axial guardrail tension, torsion in the guardrail section about its longitudinal axis as well as lateral bending due to displacements of the posts. Ray explored the mechanics of w-beam splice connections using finite element analysis, laboratory tests and full-scale tests. While rail ruptures occur on all types of w-beam guardrail systems, Ray's study focused on the weak-post w-beam guardrail. The results of his study demonstrated that rail ruptures are commonly caused by (1) high stress concentrations in the splice connection (e.g., as the splice bends around the post), as illustrated in Figure 46 and Figure 47, and (2) small tears/cuts in the rail caused by the rail sliding over relatively sharp edges (e.g., top of posts) while the rail is in tension.

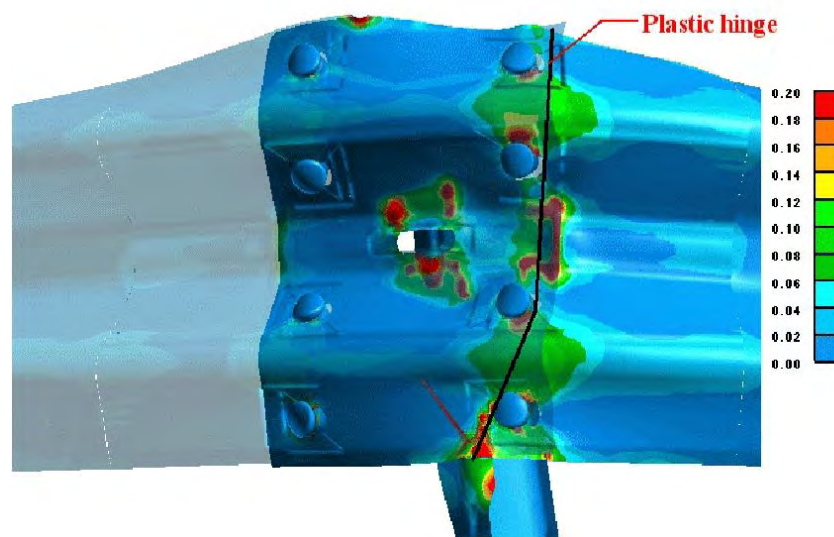


Figure 46. Effective plastic strains in the back layer of w-beam in a guardrail splice showing the formation of a plastic hinge. [Ray01b]

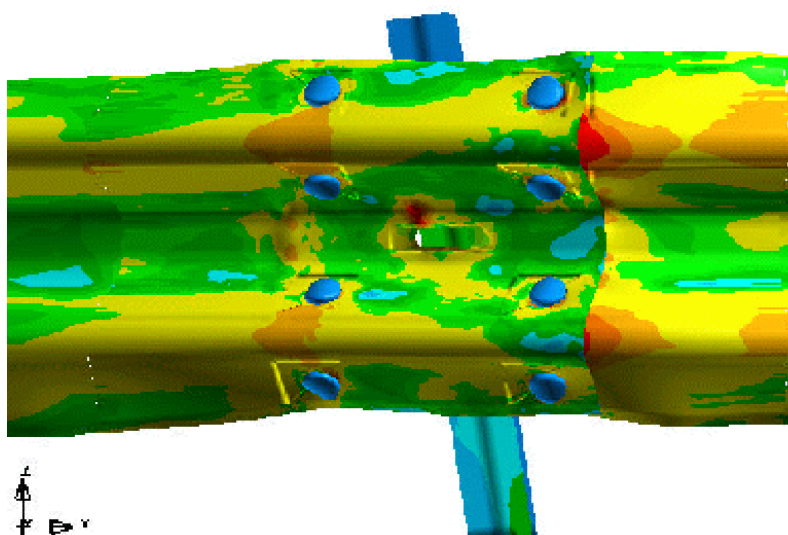


Figure 47. Von Mises stress contour plot showing relatively low stresses on the top layer of rail in the rail splice.[Ray01b]

Ray *et al.* concluded that W-beam guardrail splice failures are usually caused by the complex multi-axial state of strain experienced by the splice when it is located near a guardrail post. When subjected to these multidirectional loads, stress concentrations develop around the bolt holes in the back layer of w-beam in the splice connection and this often results in a small fracture or tear in those locations. Once a tear is initiated, the tension in the rail may cause the tear to propagate through the whole w-beam section causing the guardrail to rupture completely.[Engstrand00; Ray01a]

A similar conclusion was also made by Polivka *et al.* in a study for the Midwest States Regional Pooled Fund Research Program to investigate the effects of curbs placed in combination with strong-post guardrail.[Polivka00a] In their study a four-inch tall curb was

placed under a G4(1S) guardrail with the edge of the curb flush with the w-beam rail. The test (i.e., NEC-1) resulted in rupture at a w-beam splice. It was stated that the “reduction in (w-beam) cross-section (at splice connections) tends to localize strain in the splice region and leads to rail rupture near the point that the full cross-section begins to yield ... Subsequently, a tear in the w-beam rail was observed at the bottom downstream bolt location of the rail splice which later propagated upward through the reduced-area cross-section.”[*Polivka00a*]

Gabler, Gabauer and Hampton evaluated the effects of splice damage using pendulum tests in Report 656.[*Gabler10*] The test article was an 18-ft section mockup of the modified G4(1S) with routed wood blockouts, as illustrated in Figure 48. Each end of the w-beam rail was anchored to rigid posts with two 3/4-inch diameter swaged cables (i.e., AASHTO component FCA01).

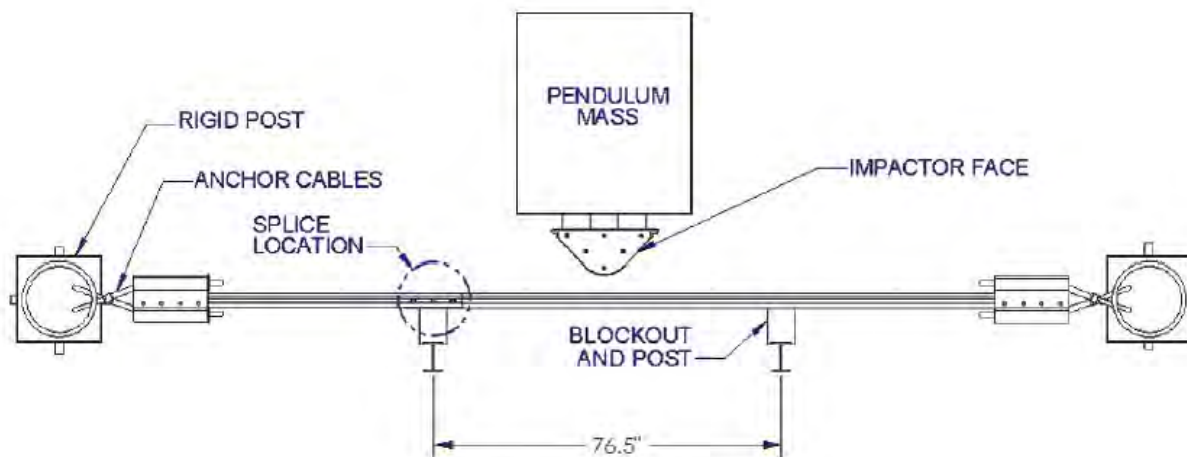


Figure 48. Pendulum test setup for the Gabler et al. study. [*Gabler10*]

In their tests the damage mode was fabricated by cutting out the material around one of the bottom splice bolts, as shown in Figure 49. The damage mode was essentially representative of a missing splice bolt at that location. The test article was impacted perpendicular to the face of the rail with a 4,545-lb pendulum at a nominal speed of 20 mph. The test article contained the pendulum and “no serious splice separation was observed.” The results of the Gabler et al. study verifies the conclusions from Ray *et al.* and Polivka *et al.* that splice failure is not likely the result of reduced rail capacity.

A simple yet very effective means of minimizing the chance of a guardrail rupture is to relocate the splice to the mid-span of the guardrail. As discussed earlier, this design alternative was implemented in the modified weak-post w-beam guardrail system [*Engstrand00; Ray01a*] and the MGS strong post guardrail system.[*Sicking02*] The splice connection performed well in all cases and both systems passed all safety and structural adequacy requirements of *Report 350* and *MASH*. [*Buth00c; Buth00d; Bullard10; Sicking02; Polivka06c-e*]



Figure 49. Fabricated splice damage mode evaluated by Gabler et al. [Gabler10]

Rail Tear

Another critical failure mode related to rail rupture is small tears in the rail that propagate when the rail is tensioned. This type of damage is typically caused during an impact event when the rail slides over, or bends around, sharp edges such as the edge of a steel guardrail post. In most strong-post guardrails the rail element is not directly exposed to such dangers since the rail is generally separated from the posts by wooden or plastic blockouts. In the case of weak-post guardrail systems, however, the rail is fastened directly to the post. The posts used in the weak-post w-beam system are structural steel, small-flange posts (i.e., I-shape with small flanges) which twist as they deflect due to their low torsional stiffness. During impact, as the rail detaches and slides up and over the top of post, the rail element is exposed directly to the edge of the twisted post.

This failure mode was demonstrated in a full-scale test on the weak-post w-beam system conducted by the Texas Transportation Institute under *Report 350* Test 3-11 impact conditions.[Buth00a] A small “nick” formed at the bottom edge of the w-beam rail as the rail was pulled over the top of the second post downstream of the impact point, as shown in the top photo of Figure 50. During impact, the friction between the vehicle and the w-beam rail causes the section of rail upstream of the vehicle (i.e., behind the vehicle) to be under much higher tension than the down-stream sections of rail. As soon as the vehicle moved past the tear, the tear was suddenly on the tension side of the rail, resulting in crack propagation and, finally, complete rupture of the rail, as shown in Figure 50.

The solution to the problem was to use a w-beam back-up plate as a sacrificial element to shield the rail from the sharp edges of the post. Ray *et al.* determined, through the use of finite element analysis, that the backup plate would reduce the effective plastic strain in the rail by 38 percent.[Ray01a] Subsequent tests on the weak-post w-beam system with this modification successfully met performance requirements for *Report 350* and *MASH* for TL-3.[Buth00c; Buth00d; Bullard10]

Gabler, Gabauer and Hampton evaluated the effects of vertical tears in the w-beam rail using pendulum tests in Report 656.[*Gabler10*] The test setup was shown earlier in Figure 48. Three tests were conducted: Test 01-3 and Test 03-5 included a 4-inch cut made on the top of the rail element, and Test 08-2 included a 0.5-inch cut on the top of the rail. In each test case, the test article was impacted perpendicular to the face of the rail with a 4,545-lb pendulum at a nominal speed of 20 mph. The “tear” propagated in all three tests and resulted in complete rupture in Tests 01-3 and 03-5. It was concluded that “no vertical tear is safe” and that “vertical rail tears of any length ... should be repaired with high priority.” [*Gabler10*]

Effects of Rail Height

Another important design change made by Ray *et al.* to the weak-post w-beam guardrail was to raise the height of the rail from 27 inches to 32.25 inches.[*Engstrand00; Ray01a*] A full-scale test of the modified weak-post w-beam system (i.e., improved rail-to-post connection, splices moved to the mid-span and back-plates at the posts) with the rail height at 27 inches resulted in the 2000P test vehicle (i.e., 4409-lb pickup) overriding the rail in a full-scale test conducted by TTI (Test 473750-2) under *Report 350* Test 3-11 conditions.[*Buth00b*] Finite element analysis was used to investigate the effects of rail height and it was determined that a rail height of 32.25 inches was sufficient to prevent override of the pickup truck while preventing underide of the 820C test vehicle (i.e., 820 kg small car).

The modified weak-post w-beam guardrail system with the higher 32.25 mounting height was subjected to a full-scale crash test according to *NCHRP Report 350* Test 3-10 (i.e., small car test) and Test 3-11 (e.g., pickup test), as shown in Figure 51 and Figure 52, respectively. The tests demonstrated that the modified design met all *Report 350* performance requirements for TL-3 [*Buth00c; Buth00e*] The system was later successfully tested under *MASH* TL-3 conditions.[*Bullard10*]

Marzougui *et al.* performed a study for the Federal Highway Administration to investigate the effects of rail height on the safety performance of the modified G4(1S) with routed wood blockouts using finite element analysis and full-scale testing.[*Marzougui07b*] Marzougui’s analyses involved simulations of *Report 350* Test 3-11 on a model of the modified G4(1S) with the rail height of ± 1.5 inches and ± 3 inches, relative to the standard rail height of 27 inches (i.e., rail heights of 24, 25.5, 27, 28.5 and 30 inches).

The results of Marzougui’s study indicated that a rail height of 27 inches for the G4(1S) guardrail would successfully redirect the pickup under *Report 350* TL-3 conditions; however, “reducing rail height by as little as 1.5 inches could hinder the ability of the barrier to redirect pickup trucks and large SUVs.” Figure 53 shows the results of the analyses for rail heights of 27 inches (i.e., standard height), 25.5 inches (i.e., rail lowered 1.5 inches) and 24 inches (i.e., rail lowered 3 inches). Figure 54 shows the results of the full-scale tests for rail heights of 27 inches and 24.5 inches (i.e., rail lowered 2.5 inches).



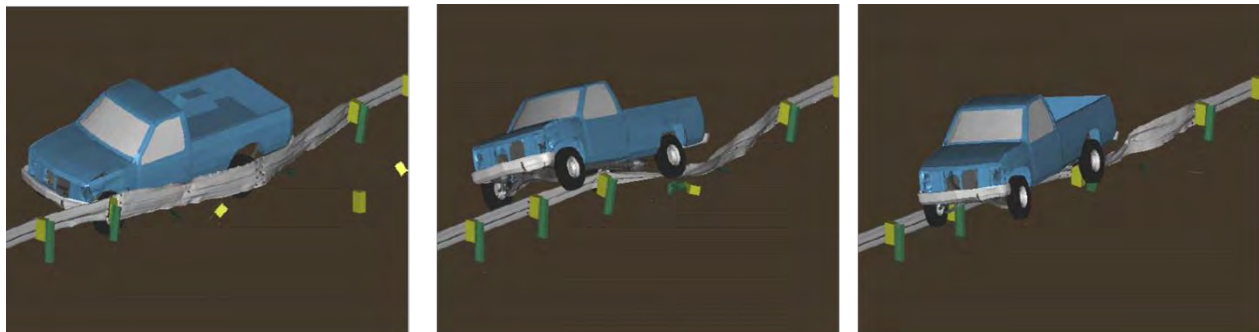
**Figure 50. Test 473750-1 on a weak-post w-beam guardrail resulting in rail rupture.
[Buth00a]**



Figure 51. Sequential view of Report 350 Test 3-11 on the modified G2 at 32.25 inch rail height.[Buth00c]



Figure 52. Sequential view of Report 350 Test 3-10 on the modified G2 at 32.25 inch rail height.[Buth00e]



(a) 27-inch rail height

(b) 25.5-inch rail height

(c) 24-inch rail height

Figure 53. FEA results for Report 350 Test 3-11 on the G4(1S) guardrail with rail heights of (a) 27 inches, (b) 25.5 inches and (c) 24 inches.[Marzougui07a]



(a) 27-inch rail height



(a) 24.5-inch rail height

Figure 54. Full-scale test results for *Report 350* Test 3-11 on the G4(1S) guardrail with rail heights of (a) 27 inches and (b) 24.5 inches.[Marzougui07a]

End Terminals

The primary purpose of end-terminals is to anchor the ends of a guardrail, but end-terminals must also be crashworthy themselves. In fact, end-terminals are much more complex systems than guardrails. Guardrails are designed for one basic type of loading, (i.e., lateral impact on the traffic-facing side of the system). Accordingly, only two tests are required in *MASH* to assess the crashworthiness of guardrails: Test 3-10 (small car impact at 62 mph and 25 degrees) and Test 3-11 (pickup truck impact at 62 mph and 25 degrees).[AASHTO09]

End-terminals, on the other hand, can be impacted on the side or on the end. The loading of an end-terminal's components, and hence their intended function, will vary depending on several factors, including: (1) which end of the guardrail the end-terminal is located (e.g., downstream or upstream), (2) where the end-terminal is struck (side hit or end-on), (3) the orientation of the vehicle (frontal impact or side impact), (4) impact direction relative to up-stream or down-stream placement (forward or reverse hit) and (5) the end-release function of the end-terminal (i.e., gating or non-gating). These additional functions of an end-terminal are reflected in the number of tests and impact conditions that are required in the crash testing guidelines.

The buried-in-backslope end-terminal is the only non-proprietary end-terminal that meets FHWA eligibility for *NCHRP Report 350* TL-3; this system, however, has limited application since it can only be installed in locations where there is a backslope. There are several older, obsolete end-terminal installations still in service, but it is expected that most of these will be replaced by proprietary systems in the near future. Unfortunately, proprietary systems all function somewhat differently (e.g., some are gating, some are non-gating, each has a unique energy absorbing mechanism, etc.). Because of the complexity and the proprietary nature of these systems, a comprehensive assessment would require the consent and participation from manufacturers.

Although a great deal of attention was focused on the crashworthy design of guardrail terminals in the late 1990's and early 2000's, little change was made to the basic design of the guardrail anchor mechanism. For example, the anchor mechanism used on most FHWA eligible end terminals including the BEST, SKT, ET2000, ETplus, and FLEAT, were adopted from a non-proprietary design developed for the Modified Eccentric Loader breakaway cable Terminal

(MELT). The basic design of the anchor mechanism, illustrated in Figure 55, entails an anchor cable (3/4-inch diameter) with one end fastened to the rail element and the other fastened to the end-post near the groundline. A bearing plate is used to prevent the cable from pulling through the hole in the end-post and to distribute the load to the foundation tube (i.e., the bearing plate overlaps the top of the foundation tube). The end-post and the adjacent post are both installed in 5-foot long steel foundation tubes with a soil-bearing-plate (18 inches long by 24 inches wide) attached to provide additional resistance from the soil. A steel strut is then laid at the groundline which connects the two foundation tubes together making them work as a system. When the guardrail is struck, the anchor cable transfers the load to the foundation tubes to resist axial movement of the rail; the resulting tension in the rail helps to limit lateral deflections of the guardrail in the impact zone. Figure 56 shows a photo of a generic end-anchor for the modified G4(1S) with wood blockouts that was used in full-scale crash test 2214-WB1.[*Polivka06a*]

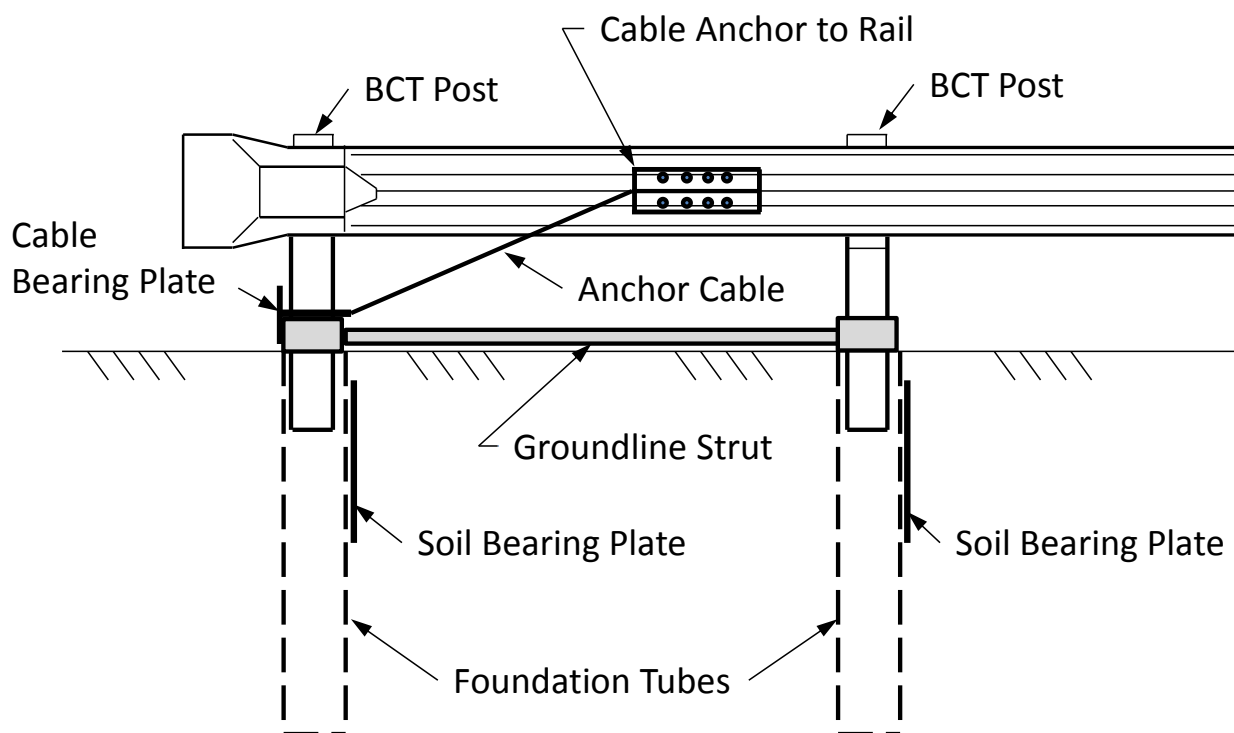


Figure 55. Sketch of typical guardrail anchor system.



Figure 56. Generic end-terminal used in full-scale Crash Test 2214-WB1 of a strong-post guardrail system.[*Polivka06a*]

If the anchor fails or experiences excessive movement during loading, the “slack” in the rail generally results in pocketing. For example, Polivka *et al.* and Bullard *et al.* showed through full-scale testing that poor guardrail performance is often associated with large anchor movement. [Polivka00a; Bullard00] In a full-scale test (i.e., Test NEC-1) conducted at the Midwest Roadside Safety Facility at the University of Nebraska-Lincoln to evaluate the effects of a 4-inch curb placed flush behind the face of a modified G4(1S) guardrail system, the anchor posts split during the collision, as shown in Figure 57, causing a loss of tension in the w-beam which resulted in pocketing. The test was conducted under *NCHRP Report 350 TL-3* conditions. [Polivka00a] The guardrail ruptured at a splice connection allowing the vehicle to penetrate behind the system. The splice failure was attributed to contact and snagging of the post blackout against the w-beam rail splice. The post twisted as it was pushed back in the soil, causing the bottom corner of the blackout to push up against the corner of the w-beam rail splice. This resulted in a tear in the w-beam at the lower downstream bolt location.

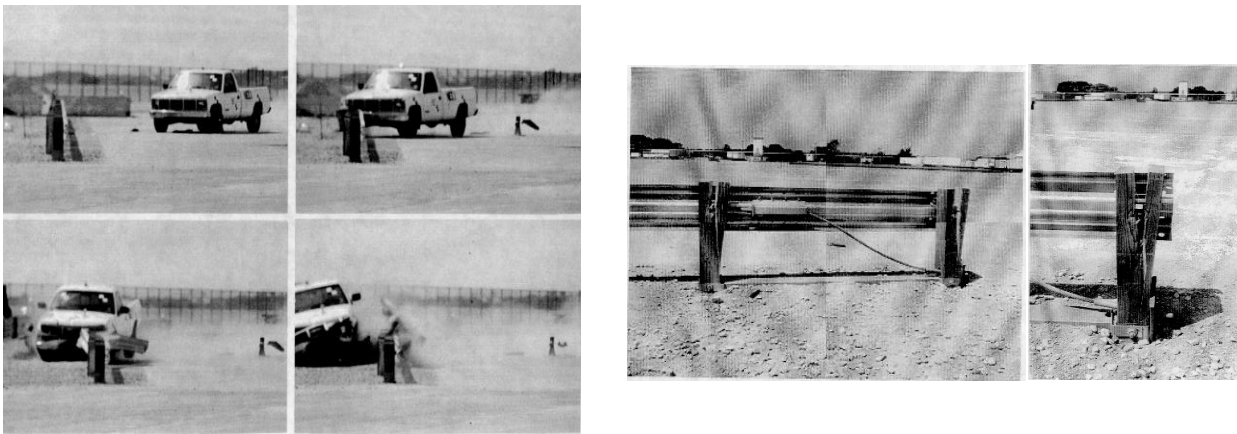


Figure 57. Test results for Test NEC-1 on modified G4(1S) with wood blockouts and 4-inch curb. [Polivka00a]

Researchers at the Texas Transportation Institute conducted a *NCHRP Report 350 TL-3* test on a G4(2W) guardrail with a 4-inch curb set out one inch from the face of the w-beam rail (i.e., Test 404201-1). [Bullard00] During the test, there was significant movement of the anchor system as the foundation of the anchor posts moved in excess of 2.75 inches. The test was successful; however, there was considerable damage to the guardrail system due to the movement of the anchor, as shown in Figure 58, and it was stated in the test report that the guardrail was at its performance limit.



Figure 58. Guardrail damage in Test TTI 404201-1.[Bullard00]

Report 656 provides some guidance on criteria for repair of generic end-terminals which was based on Ohio Department of Transportation’s check list for repairing energy absorbing end terminals.[Gabler10] The repair criteria shown in Table 16 “was based solely on engineering judgment; no finite element simulations of pendulum tests evaluating these end terminal damage modes were conducted.”[Gabler10]

Table 16. Summary of generic end terminal repair guidance. [Gabler10]

Damage	Repair Threshold	Relative Priority
Damaged end post	Not functional (sheared, rotted, severely cracked)	High
Anchor cable	Missing	High
	Loose—more than 1 inch of movement when pushed down by hand	Medium
Cable Anchor Bracket	Loose or not firmly seated in rail	Medium
Stub height of steel tube or hinged post	Height which exceeds 4 inches	Medium
Lag bolts on impact head (Energy Absorbing Terminals Only)	Missing or failed lag bolts	High
Bearing Plate	Loose or Misaligned	Medium
	Missing	High

Summary of Literature Review

A review of the literature on guardrail design and evaluation studies was conducted to garner information regarding how the various elements of a guardrail system function as well as their respective role in overall system performance. The review considered four crash phenomena that lead to poor performance of strong-post guardrail: (1) pocketing, (2) wheel snag, (3) barrier override/underide, and (4) rail rupture. The results of several studies related to the sensitivity of various components were presented, including supporting information from full-scale testing, component testing and/or numerical analyses. These studies provided a great deal of information on the general function and influences of post strength, soil strength, post embedment depth, blockout material, blockout depth, blockout shape, rail-to-post connections, rail height, splice damage and rail tears.

The information presented here was used for identifying:

- The guardrail types to be considered in the study
- The critical damage modes associated with each guardrail type,
- The combination(s) of damage modes that are considered most likely to be characteristic of damaged systems, and
- Which of those combinations are considered most critical to system performance.

CHAPTER 4 – SURVEY OF PRACTICE

A survey was conducted to determine Transportation Agency plans for implementing *NCHRP Report 656* and to identify damage modes and other system elements (e.g., wood posts, transitions, end treatments) that should be added to those covered by Report 656. This information was considered important for several reasons. First, it was essential to understand the issues facing the user base of the Field Guide. Additionally, it was essential to understand what obstacles users have or may face when implementing the research recommendation into practice.

The survey had two target audiences (1) those with direct maintenance responsibilities in the state DOT's and (2) those involved in barrier design and evaluation. The two groups have very different perspectives on the performance of these systems, but only the maintenance group is able to provide feedback regarding the usefulness of the field guide. In particular, only certain entities in the DOT maintenance groups have reasonable knowledge of the existence of Report 656 and whether its recommendations have been implemented in their state's maintenance practices.

Two separate surveys were developed and sent to the two groups with survey questions designed according to each's respective field and expected knowledge base. Survey 1 was designed to target maintenance engineers with the states and providences; therefore the survey was sent to the member list for the AASHTO Subcommittee on Maintenance which included 104 members on their email list. Survey 2 was designed to target researchers and policy makers familiar with ongoing and recently completed research in this field. The second survey was sent to the chair of TRB AFB20 to forward to the TRB AFB20 "committee members and friends" list. It was not known exactly how many people were on this list but the number was likely in the many hundreds.

The surveys were assembled and made available using the on-line tool [surveymonkey.com](http://www.surveymonkey.com) (i.e., www.surveymonkey.com). The advantage to using an internet-based facility like Survey Monkey was that very sophisticated surveys can be developed and easily disseminated to recipients by email. The intent of the two surveys was to analyze the unique perspectives from these separate functional fields (i.e., maintenance and research); however, since the TRB AFB20 committee and subcommittees encompass many professional groups, the respondents to Survey 2 included a significant proportion of maintenance engineers, as well as researchers, policy makers, manufacturers and others. Therefore, where appropriate the results of the two surveys were combined and reorganized into two profession groups: (1) Maintenance and (2) Research/Policy/Other.

The results of the surveys are presented in Appendix B. Unfortunately, the response rate on the survey was relatively low with a total of only 29 respondents. Twenty of the respondents were involved in maintenance related fields, and nine respondents were involved in research/policy/other. The survey results (see Appendix B) are presented graphically and include the average response from each of the two individual groups, as well as, the overall average response of the combined groups. The questions included (but were not limited to):

- What types of barrier should be included in the study,
- What types of damage modes are most common for each barrier type,

- What types of damages are associated with each specific component of the barrier,
- What combination of damage modes are typical of crash damaged guardrail and which of those damage combinations should be considered for this study.

The two groups generally agreed on questions related to the G4(2W) wood-post guardrail and the standard thrie-beam guardrails, which are both widely used systems; but often disagreed on the answers to questions related to the modified thrie-beam and the weak-post w-beam guardrail systems. It was assumed that these differences were due to the different perspectives of the two groups; however, it was also possible that there was confusion regarding those two particular guardrail systems. For example, as shown in the Background section, the blockout on the standard G9 thrie-beam guardrail was changed to a wooden blockout in the late 90's to improve crash performance, thus some respondents may have considered the wood-block thrie-beam system to be a modified thrie-beam guardrail. Likewise, the weak-post w-beam guardrail, which is a TL-3 system very common throughout the northeastern States, may have been confused with other so-called "weak-post" systems that use *standard strong-posts* (i.e., W6x9 steel posts or 6x8-inch wood posts) with *wider post spacing* (i.e., 12.5-ft post spacing) and *no blockouts*. These so-called "weak-post" systems are very common throughout the country but are generally installed on low-speed roadways since they are rated as TL-2 or lower.

It was also possible that respondents from the research field may have rated damage modes based on their perceived "effect on performance" rather than how common the damage mode was for the system. For example, in almost every case the research/policy/other group gave higher ratings for damage modes, regardless of system, compared to the maintenance group.

Overall, the results of the survey were not too surprising. With such a low number of respondents it was not clear, however, how much merit could be given to the results. Where appropriate, the results of the survey in combination with the information garnered from the literature review were used for prioritize of the guardrail system(s) and damage modes considered for investigation in this study.

CHAPTER 5 – PRIORITIZATION OF DAMAGE MODES

Introduction

The objectives of this task were to: (1) identify which additional guardrail systems should be included in the field guide, (2) evaluate the importance of addressing each damage mode associated with each of those systems, (3) identify the research methods that could be used in quantifying the effects of various levels of damage for each case, and (4) prioritize the list of damage modes and system elements for inclusion in this study.

The basic research approach used in Report 656 for assessing performance degradation of damage to the Modified G4(1S) guardrail involved a combination of pendulum tests, computational analyses and full-scale crash testing. Finite element analysis was used to investigate damage modes that were cost prohibitive to investigate using full-scale tests and that could not be adequately assessed with pendulum testing. In particular, finite element analysis was used to assess performance degradation due to (1) post and rail deflection, (2) missing or damaged posts, (3) post and rail separation, and (4) rail flattening. Physical testing was used to assess the effects of damage modes for cases where finite element analysis was not well suited, such as fracture of system elements (e.g., rail tears). Physical tests were also used to validate the accuracy of the finite element models and gain confidence in their results. Crash performance of the damaged systems was assessed based on *NCHRP Report 350* Test 3-11 test conditions (i.e., 2000-kg pickup impacting at 100 km/hr and 25 degrees) and evaluation criteria.

This study resumed where Report 656 left off, expanding on the information already in the field guide by including additional guardrail systems and/or additional damage assessment criteria for the modified G4(1S). For example, some of the damage modes evaluated in Report 656 warranted additional investigation so that damage thresholds could be better defined, or to further confirm and strengthen the already-established guidelines. Alternative methods of analysis may be used to confirm previous analysis results, or additional analyses may be conducted to encompass a broader range of damage levels in the assessments.

The evaluations may also be expanded to investigate damage characterized by multiple damage modes. When a guardrail system is damaged, for example in a low-speed impact, the damage is usually characterized by several minor damage modes such as a flattened and deflected rail, deflected and twisted posts, loose soil around posts, damaged bolt connection, etc. As such, the guidelines should be expanded to include guardrails with multiple combined damage modes to better aid highway maintenance personnel faced with making repair decisions.

Methods for Evaluating Damage Modes

Full-Scale Testing

While full-scale crash tests are the most conclusive method for determining crashworthy performance of roadside safety hardware, they tend to be expensive and yield relatively little information about the contribution of each specific component to overall performance. In other words, full-scale crash tests are definitive in terms of assessing performance but information poor in terms of knowing the stresses, strains and failure conditions of individual components. Since this project is concerned with detailed damage and failure mechanisms, full-scale crash testing is of limited use. For example, Report 656 demonstrated that pre-existing guardrail

deflection can affect the performance of the system in subsequent collisions. If one were only using full-scale tests to determine the threshold of lateral deflection where performance is compromised, a series of three, four or five tests would be required until the performance limit was identified. This would cost well over \$100,000 to quantify this single damage mode. Using pendulum testing or finite element simulations, on the other hand, can provide the same basic information at dramatically lower cost. The research team believes it is more important to provide as much quantitative guidance for the broadest possible range of systems and damage modes than it is to definitively establish only one or two damage modes with full-scale crash testing. For this reason, full-scale crash testing is not the preferred method for studying damage effects, although one or two tests may be warranted for confirming results from pendulum testing or simulation.

Full-scale testing of the *undamaged* systems will not be required since that data should be available from the original acceptance testing. The most recent crash test guidelines for assessing crash performance of roadside safety hardware are detailed in the AASHTO Manual for Assessing Safety Hardware (MASH).[MASH09] Most strong-post guardrail systems, however, have been around for many years and were tested under *NCHRP Report 350*, the then-current crash testing procedures. As such, the evaluations of the *damaged* systems should be consistent with crash testing procedures used in evaluating the original undamaged systems, so that performance degradation can be directly assessed. Full-scale testing was not within the scope of this study.

Pendulum Testing

As mentioned previously, the advantage of pendulum testing is that it allows for more precise control of boundary and loading conditions so that response behavior can be more accurately quantified. The disadvantage is that it is difficult (when at all possible) to extrapolate these results to overall crash performance of the system. In the context of this project, pendulum testing was used to (1) quantify strength degradation due to various damage modes (e.g., reduction in stiffness or energy absorption capacity of a post-and-rail system due to a damage mode or combination of damage modes), (2) evaluate failure modes that were not well suited for finite element analysis (e.g., tears and ruptures) and (3) for sub-system validation of the finite element models (e.g., pendulum test conditions were simulated to verify that specific aspects of the model were providing accurate response for those particular loading and boundary conditions).

Computer Simulation

Whereas full-scale crash testing is definitive but information poor, finite element simulation, in comparison, is less definitive because it is a mathematical simulation but extremely rich in detailed structural mechanical information. Stresses and strains of each part of the structure can be examined at every point in time and space of the crash allowing the analyst to determine exactly how close the system is to failure.

Finite element analysis has become a reliable and widely accepted tool for investigating crashworthiness of roadside safety structures in simulated collision events. LSDYNA is a nonlinear, dynamic, explicit finite element code that is very efficient for the analysis of vehicular impact and is used extensively by the automotive industry to analyze vehicle crashworthiness.[LSDYNA03]

Guardrail Systems

General descriptions of several common non-proprietary strong-post guardrail systems and their crash test results were provided in the “Background” section of this report. A summary of each of those system’s components is shown below in Table 17. As indicated in the table, many of these systems have similar designs and share several of the same components and are therefore susceptible to similar damage modes as the modified G4(1S) examined in Report 656. In many of these cases, the performance degradation due to a particular damage mode should likewise be similar; thus, analysis results for a particular damage mode may be used to infer the response for systems that share those same system elements. For example, the G4(1W), G4(2W) and the G4(2W) with round posts all use slightly different shaped wooden posts but otherwise share the same system components and over-all system design (e.g., rail height, post spacing, etc.). Although the posts are different (e.g., square, rectangular, and circular, respectively), they are similar in that they are all wood and are of similar dimensions (i.e., 8-10 inches in width/diameter and 6 ft in length); thus it could be inferred that each of these systems incur similar performance degradation due to each type and combination of damage mode(s). Similarly, all three systems use the same w-beam guardrail, blockout type and connection hardware, so it is likely that the effects of horizontal or vertical tears and holes will be very similar in all three systems as well.

The results from the survey of practitioners indicated a strong desire for including damage assessment criteria for wood strong-post guardrail systems in the field guide (refer to Appendix B). Combining the responses from both survey groups resulted in the wood-post systems having the highest rating and the weak-post w-beam guardrail having the second highest rating; however, given the small number of respondents and the similarity in the weighted average scores for the thrie-beam guardrail, the modified thrie-beam guardrail and the weak-post w-beam guardrail, a case could be made for including any or all systems in the study.

Critical Damage Modes

As mentioned in the introduction, this study will expand on the information already in the field guide by including additional guardrail systems and/or additional damage assessment criteria for the modified G4(1S). The following sections discuss the common damage modes for several of the guardrail systems listed in Table 17, the importance of addressing them in this study, and the research methods that could be used in quantifying the effects of various levels of damage for each case.

Table 17. Summary of common strong and weak post guardrail systems.

Guardrail Type	Rail				Post					Blockout			Rail-to-Block	
	Material	Type	Height (inches)	Gauge	Material	Type	Length (inches)	Embedment (inches)	Spacing (inches)	Material	Type	Depth (inches)	Diameter (inches)	Length (inches)
Modified G4(1S)	Steel	W-beam	27	12	Steel	W6x9	72	43.3	42	Wood	6 x 8 x 14	8	0.625	10
G4(2W)	Steel	W-beam	27	12	Wood	6 x 8	72	43.3	42	Wood	6 x 8 x 14	8	0.625	18
G4(2W) - Round Wood	Steel	W-beam	27	12	Wood	8-in Dia.	72	43.3	42	Wood	6 x 8 x 14	8	0.625	18
G4(1W)	Steel	W-beam	27	12	Wood	8 x 8	72	43.3	42	Wood	8 x 8 x 14	8	0.625	18
MGS	Steel	W-beam	31	12	Steel	W6x9	69	37.2	42	Wood	8 x 12 x 14	12	0.625	18
MGS - Wood Post	Steel	W-beam	31	12	Wood	8-in Dia.	69	37.2	42	Wood	8 x 12 x 14	12	0.625	22
G9 Thrie-Beam	Steel	Thrie-beam	31.6	12	Steel	W6x9	78	45.4	42	Steel	W6x9	5.9	0.625	1.38
G9 Thrie-Beam - Wood post	Steel	Thrie-beam	32.5	12	Wood	6x8	78	45.4	42	Wood	8 x 8 x 14	8	0.625	10
Modified Thrie-Beam	Steel	Thrie-beam	34	12	Steel	W6x8	81	46	42	Steel	M14x17.2	14	0.625	1.38
Modified G2 (Weak-Post W-Beam)	Steel	W-beam	32.3	12	Steel	S3x5.7	63	30.7	84	-	-	-	0.775	1.38

G4(1W) and G4(2W) Wood-Post W-Beam Guardrails

The G4(1W) and G4(2W) guardrail systems contain many of the same components and dimensions as the modified G4(1S) guardrail. Thus, many of the common damage modes for these systems are very similar to those of the modified G4(1S), such as w-beam damage, splice damage, twisted or missing blockouts, missing posts, post-rail separation, rail flattening and end terminal damage. As such, the damage assessment criteria developed in Report 656 for those specific damage modes on the G4(1S) should be applicable to the G4(1W) and G4(2W) systems.

Damage modes related to the guardrail posts, on the other hand, may result in a different response for wood post systems when compared to the response for steel post systems. For example, under relatively severe impact conditions, as shown in Figure 59, wooden posts tend to either fracture at the ground line, split along the vertical direction of the post, or remain essentially undamaged (i.e., the posts simply rotate in the soil); whereas the steel W6x9 posts of the G4(1S) system, which have relatively low torsional rigidity, tend to twist as they are pushed back during impacts and subsequently bend about the weak axis of the post, as illustrated in Figure 60. Although the impact performance may be somewhat similar for these two systems when struck either in their undamaged state or when damage levels are relatively low, their performance under somewhat higher levels of damage *may* change due to the differing damage modes associated with the two very different guardrail post types.



Figure 59. Typical damage modes for wood post guardrails.[Bullard00;Mak95]

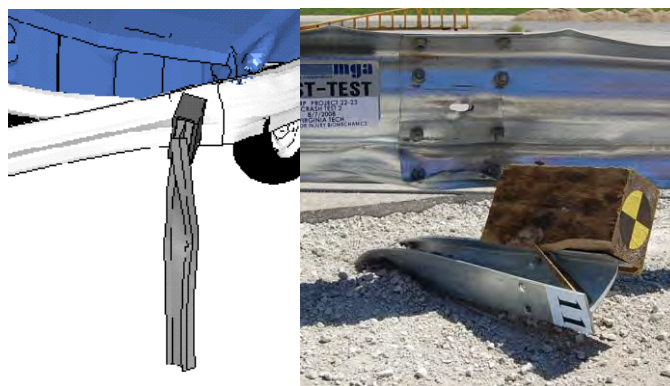


Figure 60. Typical damage mode for steel wide-flange posts.[Fleck08b]

Posts

There are five basic damage modes for wood guardrail posts: (1) deflection, (2) rotted or weakened, (3) soil eroded away from post, (4) split post and (5) missing or fractured post.

Based on the survey of practitioners, the most common damage mode for wooden posts in strong-post guardrails is post deflection, followed by rotted (or weakened) posts (see Appendix B). The effects of these two damage modes were evaluated and quantified for the G4(2W) wood-post guardrail in this study (see Chapter 8).

Post Deflection

Recall that this damage mode was evaluated in full-scale Crash Test C08C3-027.2 in Report 656 which showed that the damaged guardrail was unable to contain the vehicle and the vehicle overrode the guardrail.[*Fleck08b; Gabler10*] It was stated in Report 656 that,

“The first MGA impact, a low-speed collision intended to cause a minor amount of deflection, was successfully reproduced. A simulation speed of 32 mph (52 km/hr) was required to reproduce the 14.5 inches (368 mm) of deflection observed in the 30 mph (48.3 km/hr) crash test. For the second MGA crash test, initial attempts at reproducing the results were unsuccessful. After an investigation, a critical factor in the outcome of the crash test was found to be the failure of a single post, located roughly 12.8 feet (3.9 meters) downstream of the impact point, to separate from the rail during both the first and second impacts. The addition of a constraint on the same post in the finite element model resulted in a drastic change in the predicted outcome of the impact, changing a successful crash into a failure with the vehicle vaulting over the guardrail.”[*Gabler10*]

It was thus implied in Report 656 that the reason for the override was the result of a post-rail connection that did not release properly, as shown in Figure 61. As the guardrail post located downstream of the impact point deflected and rotated back, the undetached rail was pulled down with the post, allowing the vehicle to override the system.



Figure 61. Post-test photo for Test MGA C08C3-027.2 showing the un-failed rail-post connection which resulted in the post pulling the rail down during impact.[*Fleck08b*]

Since the rail-post connection is “designed” to release as post deflection increases, it was not clear that the test was successful in confirming the effects of rail deflection on guardrail performance; but rather in confirming the effects of improper release of the rail-post connection. So, the real question was then, “*What caused the rail-post connection to function improperly in the test?*” The most likely answer was a loss of tension in the rail resulting from the excessive movement of the anchor system, as shown in Figure 62.



Figure 62. Post-test photo for Test MGA C08C3-027.2 showing the excessive anchor movement that occurred during the test.[Fleck08b]

The most cost effective method for quantifying the effects of post/rail deflection on system performance is to conduct finite element analyses of crash events. The basic methodology would be to (1) simulate impact of the guardrail at a low velocity; (2) save all nodal deformations and residual stresses in the barrier components; (3) re-initialize the guardrail under gravity; and (4) simulate impact on the damaged system at MASH or Report 350 TL-3 conditions. FEA should provide reasonably accurate information regarding vehicle stability, potential for barrier override, the relative increase in rail forces due to increased pocketing, the relative increase in stress concentration around connection points (e.g., splice bolt holes) due to increased rail forces, etc.

The effects of post-rail deflection for the modified G4(1S) guardrail was investigated using finite element analysis in Report 656. It was shown that, when other damage modes were eliminated, there was very little difference in guardrail performance when guardrail deflections were less than 11 inches. Although it is expected that low levels of post/rail deflection will have similar effect for the G4(1W) and G4(2W) as it did for the G4(1S), it was necessary to investigate this damage mode for the G4(2W) to verify this assumption and to better quantify rail-post deflection for wood post systems as will be discussed in a later section.

Rotted or Weakened Post

One challenge regarding evaluation of rotted or weakened posts was how to quantify the degree of rot or insect damage in terms of post strength. Figure 63 shows a photo of a wooden guardrail post that fractured just below the groundline due to rot. Although deterioration at the

location of the break seems evident in the photo, the fact that the damage was below grade and not visible makes this type of damage difficult to identify.



Figure 63. Post fracture below groundline due to rot. [Photo provided by Mark Bloshock]

As stated by Dave Olson of Washington State DOT, “perhaps the answer is that any detectable rot or insect damage is sufficient reason to replace the posts, knowing that these conditions would be expected to progress and worsen over time. (Experience has taught that) visual inspection is not sufficient as rot typically starts below ground and often starts from the inside of the post and works outward” [Olson12] The Washington State DOT is currently promoting research into methods for identification of in situ test methods for determining degradation of wood posts.[Olson12]

There have been studies conducted to evaluate the effects of different strengths of posts on guardrail performance, such as wood grade (refer to the literature review), but those studies involved cases in which all the posts in the guardrail system were of the same type and grade of wood (i.e., same strength). A more critical situation may be when a damaged post (including impact damage such as split posts) is upstream and adjacent to an undamaged post, which would increase the chance for pocketing during impact.

The suggested methodology for evaluating this damage mode was to use pendulum testing to quantify the loss of post strength as a function of rot or weakness of the post. Crash analyses could then be performed using FEA to quantify the effects of the various degrees of post damage on system performance. The pendulum tests would also be used to validate the FEA models of the damaged posts.

Soil Eroded Away From Posts

A similar approach could be used to investigate the effects of soil eroded away from the posts (e.g., environmental or crash induced soil loss). This type of damage would effectively reduce the stiffness of the post-soil system and may have similar effects on guardrail

performance as that of weakened posts described above. For cases in which soil confinement is reduced by the same degree at every post, such as when posts are installed at the edge of a foreslope, the increased deflection is not expected to significantly degrade system performance. Recall from the literature review that the w-beam guardrail adjacent to 2:1 foreslope was successfully tested to *NCHRP Report 350 TL-3*. A more critical situation may be when the soil is eroded away from one or two isolated posts. In this case, the increased deflection of the guardrail when impacted at the lower stiffness section may result in pocketing as the vehicle approaches the stiffer downstream posts.

The suggested methodology for evaluating this damage mode would be to use pendulum testing to quantify the loss of post strength as a function of the depth of soil erosion behind the post. Then conduct finite element analyses to simulate the effects of the various degrees of soil erosion on system performance – using the pendulum tests to validate the FEA models of the post-soil models.

Missing Posts

The damage modes involving missing posts are considered to be of lower priority for this study. In particular, the effects of missing posts in the G4(2W) system are expected to be similar to that for the modified G4(1S) studied in Report 656. Thus the assessment criteria for the modified G4(1S) should be applicable to the G4(2W) and G4(1W) for that particular damage mode.

W-Beam Rail

There are six basic damage modes for the rail element in a guardrail system: (1) deflection, (2) flattened, (3) vertical crush, (4) vertical tear, (5) horizontal tear and (6) hole in the rail. Each of these damage modes were evaluated for the modified G4(1S) in Report 656, except for the vertical crush damage mode. Based on the survey of practitioners, the most common damage mode for the rail element for the wood-post w-beam guardrail is rail deflection, followed by rail flattening and vertical crush (see Appendix B).

The similarity in the overall design of the G4(1W) and G4(2W) wood-post guardrails to the design of the modified G4(1S) suggests that the effects of damage to the w-beam rail element would be similar for these systems. Thus the assessment criteria for the modified G4(1S) developed in Report 656 should be applicable to the G4(2W) and G4(1W) for all w-beam rail damage modes.

Rail-Only Deflection

As discussed in the literature review, the potential for rail rupture increases when the w-beam experiences excessive deflection leading up to a relatively stiff guardrail post (i.e., pocketing). Report 656 provides guidance for guardrail repair priority for this damage mode based on analyses at 3 and 6 inches of rail deflection with standard soil conditions. Higher rail deflections were not investigated since it was assumed that “since larger rail deflections generally do not occur without also deflecting the posts.”[*Gabler10*] However, there are some potential crash scenarios that may lead to such conditions, including low-speed impact on the mid-span between posts under high impact angle or rigid ground conditions (e.g., frozen soil, posts driven through asphalt, etc.). In each of these cases there could be significant rail deflections with little or no post deflections, other than slight twisting of the posts.

The damage mode of rail-only deflection was considered to be of low priority for this study. It did not make sense to evaluate the effects of pocketing on guardrail with rigid soil conditions unless the response of the undamaged guardrail under these soil conditions was known. The authors agree with the Report 656 conclusion that larger rail deflections are not likely to occur without some post deflection for the standard soil condition. However, it was expected that the evaluation criteria for this damage mode would be applicable to both the G4(2W) and G4(1S) system due to the similarity between these systems.

Vertical Rail Crush

Although it was not expected that vertical rail crush would significantly affect the structural capacity of the rail, the reduction in the cross-sectional height of the rail could affect the ability of the rail to “capture” and contain the vehicle (i.e., increase the potential for underride or override). Since this damage mode was not investigated in Report 656, it was therefore considered for the current study. The most efficient and effective analysis method for evaluating this damage mode would be to use finite element analysis to quantify the increase in the potential for override/underride (i.e., for pickup and small car, respectively) for various degrees of vertical crush.

Wooden Blockouts

There are four basic damage modes for guardrail blockouts: (1) twisted, (2) split, (3) rotted, and (4) missing. These damage modes are common to all strong-post guardrail systems that use wooden blockouts. Based on the survey of practitioners, the most common damage mode for blockouts on the wood-post guardrails was “twisted blockouts,” followed fairly closely by “split blockouts.” (see Appendix B)

Twisted Blockouts

Twisted blockouts were evaluated in Report 656 for the modified G4(1S) guardrail. It was determined that a twisted blockout was of low priority for repair based on the results of pendulum tests that showed that “the performance of (the) damaged barrier section was virtually identical to that of the undamaged strong-post barrier section.”[*Gabler10*] Recall that the overall design of the G4(1W) and G4(2W) are similar to the modified G4(1S) and that all three systems share the same 6x8x14-inch wooden blockout. The effects of a twisted blockout on the wood post guardrail systems are expected to be similar to the effects of this same damage mode on the steel post guardrail. Thus the assessment criteria for the modified G4(1S) developed in Report 656 should be applicable to the G4(2W) and G4(1W) for twisted blockouts.

Split Blockouts

As discussed in the literature section, the primary function of blockouts is to create separation between the post and rail, which (1) reduces the possibility of a vehicle’s tire impacting against the post and (2) helps to maintain critical rail height during guardrail deflection. In order to perform this function, the blockout must effectively transfer the loads from the rail element to the post. A split blockout should not significantly affect the ability of the blockout to transfer load to the post, but the reduction in width of the split blockout may affect the contact area between the rail and blockout, which may result in a different deformation mode for the splice. It does not seem likely that a split blockout would adversely affect the potential for splice rupture, based on the illustration in Figure 64; however, many of the full-scale crash tests that resulted in splice rupture also involved split blockouts, as shown in Figure 65.

The most appropriate analysis method for this damage mode would be to use pendulum tests to quantify the potential for splice rupture as a function of blockout width (measured at the interface between the block and the w-beam).

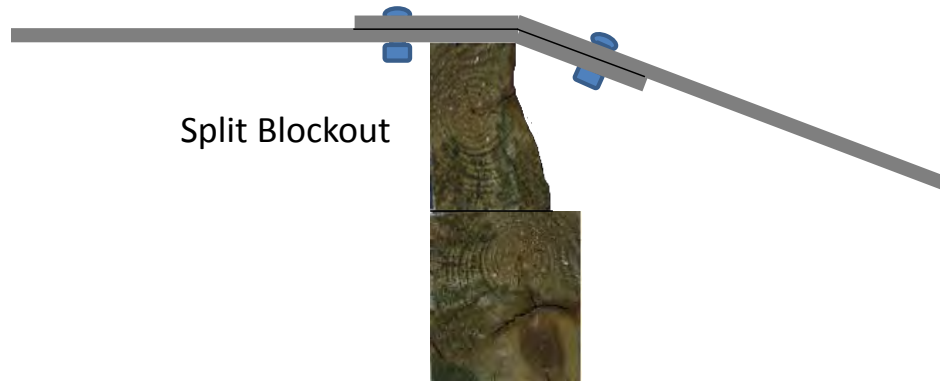


Figure 64. Illustration of possible splice deformation mode resulting from a split blockout.



Figure 65. Blockout split during Test NEC-1 (left) and in Test 405160-1-1 (right). [Polivka00a; Buth06]

Missing Blockouts

The effects of missing blockouts for the modified G4(1S) guardrail was addressed in Report 656. It was shown that the missing blockout on the steel wide-flange post could lead to rail tear as the w-beam pushes back against the post during impact. Recall from the literature review that Test No. 473750-1 of the weak-post guardrail resulted in rail rupture after a small “nick” formed at the bottom edge of the w-beam rail as the rail was pulled over the top of a post downstream of the impact point (refer to Figure 50). The 9-inch tear in the rail that occurred during the pendulum test in Report 656 would likely have resulted in complete rupture of the rail if such a tear occurred during a vehicle collision event. That is, the high tensile force in the rail

upstream of the vehicle would likely propagate the tear as the vehicle passed down-stream of the tear location.

The dangers of the rail directly contacting steel wide-flange posts are well known, which is why backup plates are generally used in guardrail designs that do not use blockouts (e.g., weak-post w-beam guardrail) and for those that use wide-flange steel sections as blockouts (e.g., standard G4(1S) and modified three-beam). However, as mentioned in Report 656, there is less of a propensity for tearing when the w-beam interacts directly with solid wooden posts.

FEA was used in Report 656 to evaluate vehicle stability due to missing blockout(s), and it was determined that, “the missing blockout case does result in elevated vehicle instability, but not to the extent of the missing post case.” As such, the damage modes of “missing blockouts” and “rotted blockouts” on wood-post guardrail systems are also considered to be of low priority in this study. There seems to be little evidence for an increased chance of rail rupture and it is expected that the vehicle kinematic response would be similar to that of the modified G4(1S) evaluated in Report 656. Thus the assessment criteria for the modified G4(1S) developed in Report 656 should be applicable to the G4(2W) and G4(1W) for missing (or rotted) blockouts.

Connections

There are three basic damage modes for guardrail connections in wood-post guardrails: (1) post-rail separation, (2) splice damage, and (3) end-anchor damage. Based on the survey of practitioners, each of these damage modes have similar rate of occurrence (see Appendix B).

Post-Rail Separation

The effects of a separated rail-to-post connection on guardrail performance was evaluated in Report 656 for the modified G4(1S) guardrail using finite element analysis. The similarity in the overall design of the G4(1W) and G4(2W) wood-post guardrails to that of the modified G4(1S) suggests that the effects of post-rail separation would be similar for these systems. Thus, the assessment criteria for the modified G4(1S) in report 656 should be applicable to the G4(2W) and G4(1W) regarding rail-to-post separation.

Report 656 indicates that the separation of the rail from the post actually improved vehicle stability during impact and redirection. When only a single connection was broken, the deflection of the system was essentially identical to the undamaged guardrail performance; whereas when two posts were detached from the rail with a separation distance of three inches, guardrail deflection was increased 5.6 percent. The improvement in vehicle stability should be expected since early release of the rail from the post as the vehicle approaches the post is a fundamental part of the design of the post-rail connection, which is necessary for reducing the potential for severe snag on the post as well as for reducing the risk of the post pulling the rail down as the post rotates back during impact (refer to the literature review for more discussion). In fact, a more critical case would be a non-failed connection on a deflected system, such as occurred in Test C08C3-027.2 and shown in Figure 61.

As mentioned earlier, the effects of post-rail separation was sufficiently addressed in Report 656. If further study on post-rail connection is considered, the focus should be on how much post-rail deflection is permissible before a *non-released* connection becomes critical. FEA may prove to be an effective analysis method for evaluating this damage mode. The challenge will be how to set up the analysis in such a way that the non-released connection is accurately

modeled (e.g., correct pre-damage to bolt and to the w-beam slot). There may be several factors that cause the connection not to release, such as:

- Low deflection of the guardrail (i.e., insufficient deflection to fail the connection),
- Bolt head installed too close to the edge of the w-beam slot (see further discussion in the literature review), or
- Loss of tension in the rail which causes the rail to slip, resulting in the bolt head “jamming” into the corner of the slot, as shown earlier in Figure 61.

Recall from the literature review that the force required to pull the bolt head through the slot at a splice connection when the bolt head is located at the edge of the slot is almost four times the amount of force required to pull the bolt head through the slot when the bolt head is located at the center of the slot at a non-splice connection.[*Plaxico03*] In fact, the MGS design includes moving the splices to the mid-span and increasing the slot-length in the rail specifically to alleviate this problem.[*Sicking02*]

Further, as shown in the literature review, the force magnitude required to detach the rail from the post can vary from 4,050 lb to 14,500 lb depending on the position of the bolt head in the slotted rail, and if the connection is at a splice (refer to Figure 44). Therefore, analyses may indicate that the criteria for assessing rail-post connections at a splice may differ from that for connections at non-splice locations.

Rail Splice

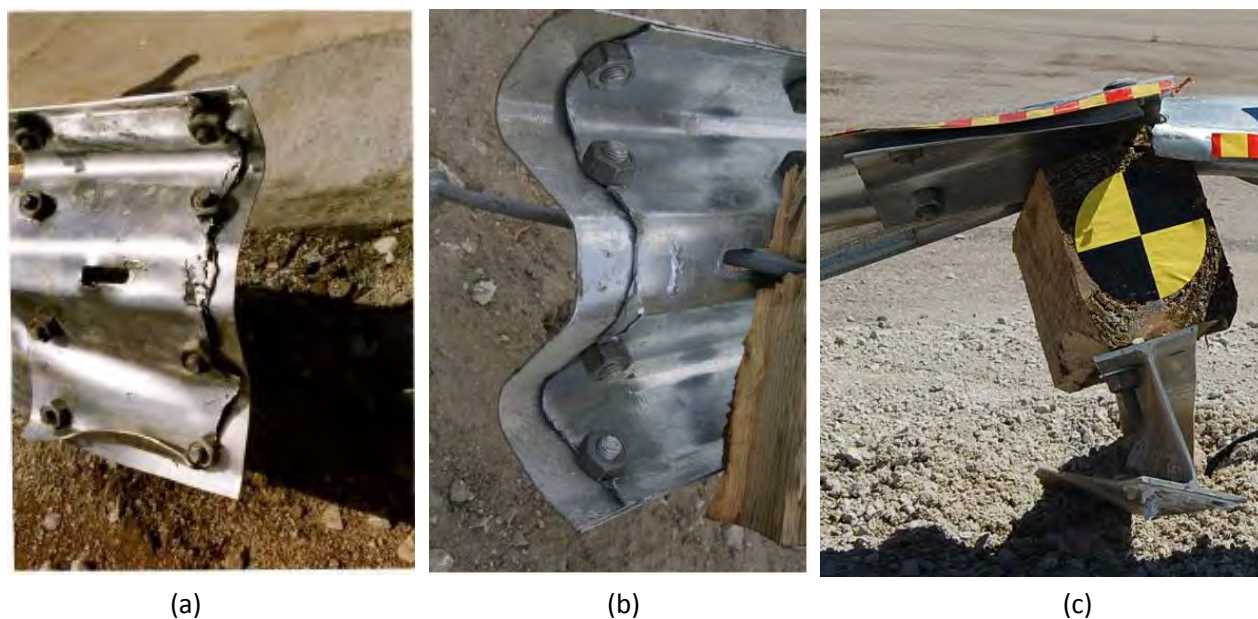
Although w-beam splice damage was addressed in Report 656, additional splice damage modes should be considered for further investigation in this study to more thoroughly quantify their effects on rail capacity. For example, Report 656 evaluated the damage mode shown in Figure 66, which involved a simulated tear-out of a splice bolt at the lower up-stream section of the splice. Note, however, that the field installation photo in Figure 66 (left photo) shows the damage being located at the lower, downstream splice bolt, which would result in different loading (or stress concentrations around the bolt holes) than the one studied in Report 656 (right photo).

For example, impact on a guardrail either upstream or downstream of the splice connection will cause the two rail elements to tend to separate at the downstream splice bolts; whereas the two sections of rail at the upstream splice bolts tend to compress together. Thus, rail rupture should be more likely when the downstream splice bolt holes are damaged, compared to similar damage in the upstream splice bolt location. This is particularly true for reverse impact cases, such as when a vehicle crosses the roadway and strikes the guardrail on the opposing roadside (e.g., vehicle approaches the splice connection in Figure 66(a) from the right). In such a case, the rail element on the right side of the splice in Figure 66(a) would bend back and “tend” to tear the splice bolt through the w-beam. Further, note that the rupture of the w-beam splice in full-scale crash Tests NEC-1, 405160-1-1 and C08C3-027 involved tearing along the bolt-line at the downstream splice bolts of the back-side rail, as shown in Figure 67.[*Polivka00a; Buth06; MGA08b*] Additional full-scale tests that resulted in w-beam rupture at the downstream splice bolts include TTI Tests 471470-23 and 405421-2.[*Buth99a; Mak96c*] Although the potential for splice rupture at the upstream splice bolts exists, the research team has only identified one full-scale test which resulted in rupture at that location – Test RF476460-1-5.[*Bullard10*]



(a) Field Installation damage

(b) Simulation damage

Figure 66. Splice damage mode investigated in Report 656. [Gabler10]

(a)

(b)

(c)

Figure 67. Splice rupture initiated at downstream splice bolts in (a) Test NEC-1, (b) Test 405160-1-1 and (c) Test C08C3-027.1. [Polivka00a; Buth06; MGA08b]

To evaluate splice damage, the damage modes for the splice connection should be imposed onto the test sample by a pre-impact test, since this type of damage is difficult (if not impossible) to achieve otherwise. Since small tears in the splice bolt holes are likely to be hidden by the bolt head and/or nut, it may be reasonable to quantify the degree of damage by such parameters as degree of flattening, angle of bend in the splice, measure of separation between the two rail elements at the downstream end of the splice, etc. The evaluation for quantifying the reduction in rail capacity as a function of splice damage could be achieved through pendulum testing or a combination of pendulum testing and finite element analysis. Pendulum tests will obviously indicate when failure has occurred, but the relative increase in stress levels at the critical locations in the splice would be better assessed through FEA, as illustrated in the effective-plastic-strain contour plot of the weak-post w-beam system in Figure 68.

Methods for Damage Assessment for the G4(1W) and G4(2W)

Table 18 provides a summary of possible methods for evaluating the various damage modes for the strong-post w-beam guardrail systems (i.e., G4(1W) and G4(2W)). An “x” indicates that the analysis method is applicable; an “x” in a shaded cell indicates the preferred method for analysis; and a “blank” cell indicates that the analysis method is not applicable. The table also includes a rating scale which indicates the damage modes considered most common for this system, based on the weighted average summary of the survey results.

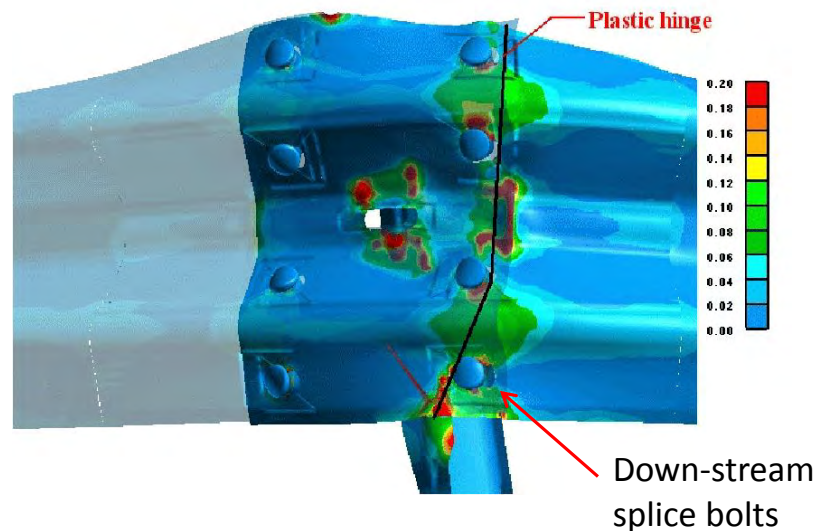


Figure 68. Effective plastic strain contour plot at a splice connection. [Ray01b]

Thrie-Beam Steel Post Guardrail

The primary components of the standard G9 thrie-beam guardrail system include 12-gauge thrie-beam rails, W6x9 steel posts, W6x9 steel blockouts, and standard connection hardware. Like the G4(1S) w-beam, the steel-post thrie-beam guardrail was modified from its original design by replacing the 6-inch deep W6x9 blockout with an 8-inch deep wooden blockout. This design change increased the blockout distance and reduced the tendency for torsional failure of the posts as the posts deflected back during impacts, resulting in improved crashworthiness of the system.[Bullard10]

Although the current FHWA approved system includes 8-inch wooden blockouts, installations of the original G9 design with W6x9 blockouts likely still exist throughout the country. According to the survey of practitioners, the interest in including the strong-post thrie-beam guardrail in the update to the field guide was rated “medium” based on the weighted average of responses (i.e., weighted average value = 3.08 on a scale of 1 to 5). Approximately 1/5 of the respondents rated it as “medium”, 2/5 of the respondents rated it as “high” or “very high” and the remaining 2/5 of respondents rated it as “low” or “very low,” which indicates that there were very mixed opinions among the groups (see Appendix B).

Based on the fact that the thrie-beam guardrail is expected to have different sensitivities to damage than strong-post w-beam guardrails, and the fact that current funding levels may not permit development of repair evaluation guidelines that are sufficiently comprehensive for

immediate field use, this system was considered to be of medium priority for inclusion in this study.

Table 18. Summary of possible methods for assessing damage modes for the G4(1W) and G4(2W) guardrail systems.

Component	Damage Mode	Weighted Avg. Priority from Survey (Scale 1-5)*	Possible Methods for Evaluation		
			Extrapolate from Report 656	Pendulum Test	FEA
Posts	Deflection	4.26	x		x
	Rotted or Weakened	3.65		x	x
	Soil Eroded from Post	3.13		x	x
	Split Posts	3.09		x	x
	Missing Posts	2.73	x		
	Twisted Posts	2.48			
Rail Element	Deflection	4.25	x		x
	Flattening	3.54	x		
	Vertical Crush	2.91			x
	Vertical Tear	2.65	x		
	Horizontal Tear	2.52	x		
	Hole in Rail	2.39	x		
Blockouts	Twisted Blockouts	3.82	x		
	Split Blockouts	3.26		x	x
	Rotted Blockouts	2.61		x	x
	Missing Blockouts	2.48	x		
Connections	Post-Rail Separation	2.82	x	x	x
	Splice Damage	2.81	x	x	x
	End Anchor Damage	2.77	x		x

* Priority is rated on a scale of 1 (very low) to 5 (very high)

Legend

x	<i>Preferred method for analysis.</i>
x	<i>Analysis method is applicable.</i>
N.A.	<i>Not applicable</i>

Posts

Based on the survey of practitioners, the most common damage mode for guardrail posts in strong-post thrie-beam guardrails is post deflection, followed by soil erosion around the post and twisted posts (see Appendix B).

Post-Rail Deflection

The suggested methods for evaluating post-rail deflection for the G4(1W) and G4(2W) guardrails also apply to the thrie-beam guardrail systems. However, due to the additional height of the thrie-beam guardrail, compared to the common strong-post w-beam guardrail systems (i.e., 32.5 inches compared to 27 ¾ inches, respectively), deflection damage will not likely result in the same level of performance degradation for the thrie-beam guardrail. Also, as shown in Figure 69, the rail-to-post connection for the standard thrie-beam guardrail consists of two bolts at each post, which increases the chances for the connection to remain intact during low severity

impacts. In such cases, the rail element would rotate back at an angle with the undetached post and effectively act as a ramp for the vehicle to climb and vault over the guardrail. As a side note, a possible design improvement for this system may be to exclude or weaken the upper bolt connection. Recall that one of the design changes for the modified thrie-beam guardrail was the exclusion of the lower bolt connection.



Figure 69. Photo of the standard thrie-beam guardrail.

This damage mode was considered to be of high priority for the G9 thrie-beam guardrail system due to the fact that post-rail deflection is a common damage mode for thrie-beam guardrail in low severity impacts; and also due to the increased potential for vaulting the deflected system - especially if the connections do not fail correctly or consistently. Finite element analysis would be the most practical method for evaluating performance degradation of deflected guardrail systems. Although full-scale testing is not in the scope of this study, the conclusions made from the computational analyses should be confirmed through full-scale testing if future work is performed.

Soil Eroded Away From Posts

This damage mode was considered to be of medium priority for evaluation in this study. The approach used to investigate the effects of soil eroded away from the posts for the G4(1W) and G4(2W) wood post guardrail systems also applies here for the G9 thrie-beam guardrail. Pendulum tests could be used to quantify the loss of post strength as a function of the depth of soil erosion behind the post. FEA could then be used to simulate the effects of the various degrees of soil erosion on system performance – using the pendulum tests to validate the FEA models of the post-soil models.

Twisted Posts

Steel wide-flange posts, unlike rectangular wooden posts, tend to twist and bend during impacts, as opposed to fracturing. As such, “twisted posts” are an inherent part of the damage mode of a deflected system and were thus considered to be of low priority for additional study beyond that of post-rail deflection. However, if the twisted post damage mode is included, then the most effective analysis method would be FEA.

Thrie-Beam Rail

Based on the survey of practitioners, the most common damage mode for the rail element in a strong-post thrie-beam guardrail is deflection, followed by rail flattening (see Appendix B). Rail deflection was included as part of the post-deflection damage mode since it is not likely that one can exist without the other. Thus, rail deflection is considered to be of low priority for additional study beyond that of the combination post-rail deflection damage mode.

Although rail tearing was not considered to be a common damage mode for thrie-beam rail elements, evaluation of vertical tears in thrie-beam rail may be warranted since that particular damage mode has been shown to be critical for w-beam guardrail systems. Alternatively, the damage assessment and repair criteria developed in Report 656 for the w-beam rail may serve as conservative assessment criteria for the thrie-beam rail.

Evaluation of horizontal tears and holes in the thrie-beam rail are considered to be of low priority based on the pendulum test results from Report 656 which showed that those damage modes were of lower significance than a vertical tear for the w-beam rail. Rail crush is also considered to be of low priority in this study since the cross-section height of the thrie-beam is not likely to be reduced enough to significantly affect the ability of the rail to capture and contain the vehicle. In other words, even with substantial vertical crush the thrie-beam would still be taller than the undeformed w-beam, and thus should have sufficient vertical height to capture an impacting vehicle unless other damage modes are also present.

In Report 656 it was shown that vehicle instability and vaulting were likely when the w-beam rail was 75% or more flattened. The flattened rail increased the probability for the vehicle's tire to mount and climb the rail. The bottom edge of the thrie-beam rail is lower to the ground than the w-beam, thus rail flattening may pose a greater risk for the thrie-beam systems.

Blockouts

Based on the survey of practitioners, the most common damage mode for blockouts in the thrie-beam steel post guardrail is twisted blockout, followed by split blockout and missing blockout (see Appendix B). Based on the responses of the survey respondents, it is assumed that these damage modes were rated based on the thrie-beam guardrail with wood blockouts. Since there may be many G9 guardrails with steel blockouts still in existence, the evaluation criteria should include both the steel and wood blockout versions of the system.

Twisted Blockouts

Since the blockout is fastened to the post with two bolts in the G9 guardrail, it seems unlikely that the blockout could rotate unless one of the bolted connections failed. It is difficult to say for certain that a twisted blockout in the G9 guardrail would be of higher or lower risk for system failure than it was for the G4(1S) guardrail studied in Report 656, but the risk was considered to be relatively low for the wood blockouts compared to other critical damage modes. For the standard G9 with wide-flange steel blockouts, on the other hand, there may be an increased risk for tearing the rail against the sharp edges at the top and bottom of the wide-flange blockout when the blockout is rotated on the post. Finite element analysis could be used to investigate the potential for increased stress concentrations and overall crash performance; then if the results indicate that twisted blockouts may lead to poor performance (e.g., rail rupture), pendulum tests could be used to confirm the results.

The research team considers the evaluation of the twisted blockout to be low priority in this study, since this damage mode is unlikely to occur unless (1) the rail is detached from the blockout and (2) the blockout is detached from the post. For the wood blockout system, it is probable that the rail could separate from the block, but much less probable that the blockout would also be detached from the post at the same location. This seems to be a highly unlikely event unless bolts were either left out during installation or there was significant damage to the system.

Split Blockouts

The split blockout damage mode only pertains to wooden blockouts. As discussed for the G4(2W) system, a split blockout should not significantly affect the ability of the blockout to transfer load to the post, but the reduction in width of the split blockout may affect the contact area between the rail and blockout, which may result in a different deformation mode for the splice. If this damage mode is determined to be critical to the performance of the G4(2W) guardrail, then it would likewise be considered to be of higher priority for the G9 as well. Otherwise, this damage mode was considered to be of low priority in this study.

Missing Blockouts

As was shown in the Report 656, a missing blockout on the steel wide-flange post could lead to rail tear as the w-beam pushes back against the post during impact. The effects of missing and rotted blockouts for the thrie-beam guardrail should be similar to, or less severe than, that for the G4(1S). Thus the assessment criteria for the modified G4(1S) developed in Report 656 may be extrapolated to the thrie-beam guardrail systems. The damage modes of “missing blockouts” and “rotted blockouts” were considered to be of low priority in this study.

Connections

The post-rail connection was considered to be high priority for evaluation of the G9 system since, as mentioned previously, proper release of the connection may prove to be a critical aspect of system performance. The release of the connection is not only a function of deflection but is also a function of bolt-position in the rail-slot and rail tension (e.g., anchoring). Further, these aspects are not likely independent of each other. For example, if the anchor system yields and releases the tension in the rail, the forces on the connection would reduce, which could result in large deflections, as well as undetached rail-post connections.

Pendulum testing may be appropriate for evaluating the release of the post-rail connection as a function of (1) rail deflection, (2) bolt-position relative to slots in the thrie-beam rail, and (3) longitudinal movement of the rail element during lateral deflection. Care should be taken to ensure that the bolts are properly position in the thrie-beam slot so that the effects of bolt position can be adequately quantified. Finite element analysis would be the most effective method of quantifying the effects of various levels of damage on guardrail performance, given that the finite element models can be adequately validated with results of the pendulum tests.

Methods for Damage Assessment for the G9

Table 19 provides a summary of possible methods for evaluating the various damage modes for G9 thrie-beam guardrail.

Table 19. Summary of possible methods for assessing damage modes for thrie-beam guardrail systems.

Component	Damage Mode	Weighted Avg. Priority from Survey (scale of 1-5)	Possible Methods for Evaluation		
			Extrapolate from Report 656	Pendulum Test	FEA
Posts	Deflection	3.80			x
	Soil Eroded from Post	2.93		x	x
	Twisted Posts	2.87			x
	Missing Posts	2.43			x
	Rotted Posts	1.93			x
	Split posts	1.50		x	x
Rail Element	Deflection	3.83			x
	Flattening	3.08	x		x
	Horizontal Tear	2.50	x	x	
	Vertical Crush	2.45			x
	Vertical Tear	2.42	x	x	
	Hole in Rail	2.17	x	x	
Steel Blockouts	Twisted Blockouts	3.17	x	x	x
	Missing Blockouts	2.17	x		x
	Bent Blockouts	2.00	x		x
Wood Blockouts	Twisted Blockouts	3.17	x	x	x
	Split Blockouts	2.42		x	x
	Rotted Blockouts	1.83		x	x
	Missing Blockouts	2.17	x		x
Connections	End Anchor Damage	2.90	x		x
	Splice Damage	2.73		x	
	Post-Rail Separation	2.27		x	x

* Priority is rated on a scale of 1 (very low) to 5 (very high)

Legend

x	<i>Preferred method for analysis.</i>
x	<i>Analysis method is applicable.</i>
N.A.	<i>Not applicable</i>

Modified Thrie-Beam Guardrail

The primary components of the modified thrie-beam guardrail system include the same 12-gauge thrie-beam rails, W6x9 steel posts, and standard connection hardware as the standard G9 thrie-beam guardrail. In addition to a taller rail height, the modified thrie-beam guardrail also has a unique deep structural steel blockout, which is designed to help keep the face of the rail vertical during impacts, but is unfortunately susceptible to bending through the web (see Figure 42). So, although many damage modes will be similar for these two systems, the differences in the damage modes for the blockout may result in significant differences in guardrail performance.

The modified thrie beam is not widely used; therefore, this system was considered to be of low priority in this study. The G9 guardrail was considered to be of higher priority than the modified thrie-beam due to the fact that (1) the G9 is more widely used than the modified thrie-beam and (2) many of the damage assessment criteria developed for the G9 would also apply to the modified thrie-beam guardrail. The damage mode evaluations for the modified thrie-beam guardrail would be similar to those discussed for the standard G9 guardrail in the previous section. The primary differences in damage assessment would arise from the differences in the blockout design and the reduced number of connections for the rail-to-blockout.

Posts

Based on the survey of practitioners, the damage mode for posts that is most common with the modified thrie-beam is post deflection, followed by posts with soil erosion around them, and posts that are missing (see Appendix B). Refer to the earlier section of standard thrie beam guardrail posts for discussion of damage types and proposed evaluation methods. It is expected, however, that additional damage modes will be introduced for impacts on the modified thrie-beam system at relatively low rail deflections due to the low collapse load of the blockouts. Thus, it may not be possible to fully evaluate the post-rail deflection without considering a more involved multi-damage mode evaluation study.

Rail

Based on the survey of practitioners, the damage mode for rail elements that is most common for the modified thrie-beam guardrail is rail deflection. Tearing and crushing of the rail both vertically and horizontally were all rated roughly the same by the respondents, and rated much lower than rail deflection. (see Appendix B).

Blockouts

Based on the survey of practitioners, the damage mode for blockouts most common in the modified thrie-beam guardrail is a twisted blockout, followed by missing blockout and bent steel blockout (see Appendix B). However, as was the case with the standard G9 thrie-beam guardrail, it does not seem likely that the blockout could twist unless one of the bolts connecting the blockout to the post was broken or missing. It is also unlikely that a low-speed impact would result in breaking one of these bolts, which are 5/8-in diameter high-strength steel bolts. In order for a blockout to be missing, both bolts would need to be broken. It is likely, however, that the blockout could be bent as the result of a low-speed impact. A bent blockout would result in a reduced blockout distance between the rail and post, which would increase the chance for vehicle impact against the posts. The bending of the blockout also induces a torsional moment onto the posts, which may reduce its effective stiffness. Based on these observations, the bent blockout was considered to be of high priority for the modified thrie-beam guardrail system.

Connections

Based on the survey of practitioners, the most common damage mode regarding connection elements for the modified thrie-beam guardrail is splice damage, followed by damage to the guardrail cable anchor (see Appendix B). These damage modes are similar to those for the standard thrie-beam guardrail discussed in a previous section. The effects of rail-to-post connection will be different for the modified G9 system compared to the standard G9, since the modified thrie-beam guardrail only uses a single bolt to connect the rail to the blockout at each

post. In this case, the evaluation methods would be similar to those described for evaluating the rail-to-post connection for the G4(2W).

Methods for Damage Assessment for the Modified Thrie-Beam

Table 20 provides a summary of possible methods for evaluating the various damage modes for the modified G9 thrie-beam guardrail.

Table 20. Summary of possible methods for assessing damage modes for the modified thrie-beam guardrail system.

Component	Damage Mode	Weighted Avg. Priority from Survey (scale of 1-5)	Possible Methods for Evaluation		
			Extrapolate from Report 656	Pendulum Test	FEA
Posts	Deflection	2.89			x
	Soil Eroded from Post	2.56		x	x
	Missing Posts	2.25			x
	Twisted Posts	2.11			x
Rail Element	Deflection	3.50			x
	Flattening	2.63	x		
	Horizontal Tear	2.50	x	x	
	Vertical Tear	2.50	x	x	
	Vertical Crush	2.38			x
	Hole in Rail	2.00	x	x	
Steel Blockouts	Twisted Blockouts	3.00		x	x
	Missing Blockouts	2.29			x
	Bent Blockouts	2.14			x
Connections	Splice Damage	2.71		x	
	End Anchor Damage	2.33			x
	Post-Rail Separation	1.86		x	x

* Priority is rated on a scale of 1 (very low) to 5 (very high)

Legend

x	<i>Preferred method for analysis.</i>
x	<i>Analysis method is applicable.</i>
N.A.	<i>Not applicable</i>

MGS – Steel Post W-Beam Guardrail

Although the MGS guardrail consists of the same w-beam rail, W6x9 steel posts, and connection hardware used in the modified G4(1S), there are several fundamental design differences between these two systems. The primary differences being that the MGS is four inches higher, the splices are moved to the mid-span, the posts have shallower embedment depth, and the blockout distance is 50% greater. In minor impacts, it is expected that the damage modes for the MGS would be similar to that of the modified G4(1S); however, the response of these two systems, given the same level of damage, may differ considerably due to the fundamental differences of their designs. For example, the increased height of the MGS makes it less sensitive to small decreases in rail height, but may make it more sensitive to small increases

in rail height (e.g., increase potential for under-ride); the splice connection located at the mid-span between posts results in less severe loading on the splice (e.g., no bending), which means less sensitivity to splice damage. Likewise, a missing post in combination with a deflected rail may result in a higher probability for a vehicle with low profile (e.g., Geo Metro) to push underneath the higher rail element and impact with the adjacent downstream post.

The MGS guardrail was not included in the survey of practitioners, and none of the survey respondents included the MGS system when asked “which additional guardrail systems should be included in this study.” The MGS was therefore considered to be of lower priority for this study; however, given the success of the MGS in crash testing, it is likely that the MGS (or systems with similar design) will see increased use in the near future and may be considered with higher priority in future projects.

Methods for Damage Assessment for the MGS with Steel Post

Table 21 provides a summary of possible methods for evaluating the various damage modes for the MGS with steel posts.

Table 21. Summary of possible methods for assessing damage modes for the MGS with steel posts.

Component	Damage Mode	Weighted Avg. Priority from Survey (scale of 1-5)	Possible Methods for Evaluation		
			Extrapolate from Report 656	Pendulum Test	FEA
Posts	Deflection	N.A.			x
	Soil Eroded from Post	N.A.		x	x
	Missing Posts	N.A.			x
	Twisted Posts	N.A.			x
Rail Element	Deflection	N.A.			x
	Flattening	N.A.			x
	Vertical Crush	N.A.			x
	Vertical Tear	N.A.	x		
	Horizontal Tear	N.A.	x		
	Hole in Rail	N.A.	x		
Blockouts	Twisted Blockouts	N.A.		x	x
	Split Blockouts	N.A.		x	x
	Rotted Blockouts	N.A.		x	x
	Missing Blockouts	N.A.		x	x
Connections	Post-Rail Separation	N.A.			x
	Splice Damage	N.A.		x	x
	End Anchor Damage	N.A.			x

* Priority is rated on a scale of 1 (very low) to 5 (very high)

Legend

x	Preferred method for analysis.
x	Analysis method is applicable.
N.A.	Not applicable

MGS – Wood Post W-Beam Guardrail

The wood-post version of the MGS is expected to experience the same basic damage modes under low speed impact as the standard steel-post MGS system. As such, the assessment criteria for damage modes that are common to both systems should be applicable to both. However, damage modes specific to the guardrail posts, as discussed previously, may result in a different response between the wood post MGS and the steel post MGS. Thus, the additional damage modes that would need to be included for assessing the wood-post version would essentially include quantification of performance degradation due to (1) post/rail deflection and (2) rotted or weakened posts.

Methods for Damage Assessment for the MGS with Wood Posts

Table 22 provides a summary of possible methods for evaluating the various damage modes for the MGS guardrail with wood posts.

Table 22. Summary of possible methods for assessing damage modes for MGS with wood posts.

Component	Damage Mode	Weighted Avg. Priority from Survey (scale of 1-5)	Possible Methods for Evaluation		
			Extrapolate from Report 656	Pendulum Test	FEA
Posts	Deflection	N.A.			x
	Rotted or Weakened	N.A.		x	x
	Soil Eroded from Post	N.A.		x	x
	Split Posts	N.A.			x
	Missing Posts	N.A.			x
	Twisted Posts	N.A.			x
Rail Element	Deflection	N.A.			x
	Flattening	N.A.			x
	Vertical Crush	N.A.			x
	Vertical Tear	N.A.	x		
	Horizontal Tear	N.A.	x		
	Hole in Rail	N.A.	x		
Blockouts	Twisted Blockouts	N.A.		x	x
	Split Blockouts	N.A.		x	x
	Rotted Blockouts	N.A.		x	x
	Missing Blockouts	N.A.		x	x
Connections	Post-Rail Separation	N.A.			x
	Splice Damage	N.A.		x	x
	End Anchor Damage	N.A.			x

* Priority is rated on a scale of 1 (very low) to 5 (very high)

Legend

x	<i>Preferred method for analysis.</i>
x	<i>Analysis method is applicable.</i>
N.A.	<i>Not applicable</i>

G2 – Weak-Post W-Beam Guardrail

The G2 weak-post guardrail was described in the Background section and is repeated here for convenience. The weak-post w-beam guardrail is composed of w-beam rails supported on weak S3x5.7 steel posts with rectangular soil plates. The system performs much like the cable guardrail in that the posts hold up the rail at the proper height until the guardrail is struck by an errant vehicle. The posts are spaced at 12.5 feet and the rail is connected to the posts using 5/16-inch diameter bolts with 1-3/4 inch square washers under the head. The bolts are designed to fail in an impact allowing the rail to separate easily from the post. The rail separation from the post is an important feature of the design since this action allows the rail to remain in contact with the vehicle instead of being pulled to the ground by the post. Once the rail is separated from the post, the posts bend at the ground-line allowing the w-beam to slip over the top of the posts. As the rail continues to deflect, tension develops and the rail effectively behaves as a cable (or ribbon) anchored at the ends. Ray *et al.* demonstrated that relatively small changes in several important design details can significantly affect performance of the weak-post w-beam guardrail.[Ray01a]

Although the weak post w-beam guardrail shares many of the same components as the strong-post systems, the basic function of weak post systems is quite different and is expected to have different sensitivities to various levels of damage. As discussed in the literature review, the performance of the weak-post guardrail is likely to be much more sensitive to: (1) post-rail connection damage due to weaker posts and no blockouts; (2) rail tears due to higher tensile forces in rail during impact; (3) guardrail height due to the potential for over-ride and underride given the large rail deflections and length of unsupported section of rail at the point of maximum deflection; (4) and missing backup plates which protect the w-beam rail from the sharp edges of the small-flange posts. Recall from the literature review that rail rupture occurred in Test 473750-1 as a result of a small nick in the rail as the w-beam was pulled over the top of one of the guardrail posts.[Buth00a]

Finite element analysis would be the most cost effective analysis method for studying/quantifying many of the damage effects for the G2. For example, a low severity crash could be simulated (e.g., low-speed low angle) for the purpose of imposing realistic damage modes onto the system, including the associated residual stresses in the system components. Then, additional specific damage modes could be directly imposed onto the model such as:

- Additional detached rail-post connections (which under gravity would result in lower rail height over a relatively long span of the rail),
- Undetached post-rail connections (which would result in lower rail height due to post pulling the rail down),
- Various levels of rail-tear damage and
- End-terminal damage which would allow greater rail deflections.

Pendulum testing may be applicable for evaluating rail tears on the w-beam rail element, if appropriate boundary conditions can be achieved for the sub-system tests. Also, weak post guardrails have much larger deflections than strong post guardrails, and it may not be possible to achieve a constant loading height on the rail as the pendulum swings into its arc. These issues will have to be considered when developing the testing plan for the G2 system.

Based on the fact that the G2 weak-post guardrail is expected to have significantly different sensitivities to damage than strong-post guardrails, and the fact that current funding

levels may not permit development of repair evaluation guidelines sufficiently comprehensive for immediate field use, the G2 guardrail was considered to be of medium priority for this study.

Although the modified G2 guardrail (i.e., 32.25 inch tall, splice at mid-span, modified rail-post connection, and backup plates at posts) is the only weak-post w-beam guardrail that currently meets crashworthiness criteria for both Report 350 and MASH, installations of the original G2 are still common in the field. It is suggested that any damage to an original G2 system should warrant high priority for repair, due to its susceptibility to unacceptable performance even in its undamaged state.

Methods for Damage Assessment for the Modified G2 Weak-Post Guardrail

Table 23 provides a summary of possible methods for evaluating the various damage modes for the modified G2 weak-post guardrail.

Table 23. Summary of possible methods for assessing damage modes for the Modified G2 guardrail.

Component	Damage Mode	Weighted Avg. Priority from Survey (scale of 1-5)	Possible Methods for Evaluation		
			Extrapolate from Report 656	Pendulum Test	FEA
Posts	Deflection	4.00			x
	Twisted Posts	3.00			x
	Soil Eroded from Post	2.94			x
	Missing Posts	2.82			x
Rail Element	Deflection	4.13			x
	Flattening	3.19			x
	Vertical Crush	2.69			x
	Vertical Tear	2.60		x	x
	Hole in Rail	2.20		x	x
	Horizontal Tear	2.13		x	x
Connections	Post-Rail Separation	3.07			x
	Splice Damage	3.00		x	x
	Missing Back-Up Plate	N.A.		x	x
	End Anchor Damage	2.14			x

* Priority is rated on a scale of 1 (very low) to 5 (very high)

Legend

x	Preferred method for analysis.
x	Analysis method is applicable.
N.A.	Not applicable

End Terminals

The primary purpose of end-terminals is to anchor the ends of a guardrail, but end-terminals must also be crashworthy themselves. In fact, end-terminals are much more complex systems than guardrails. Guardrails are designed for one basic type of loading, (i.e., lateral impact on the traffic-facing side of the system). Accordingly, only two tests are required in *MASH* to assess the crashworthiness of guardrails: Test 3-10 (small car impact at 62 mph and 25 degrees) and Test 3-11 (pickup truck impact at 62 mph and 25 degrees).

End-terminals, on the other hand, can be impacted on the side or on the end. The loading of an end-terminal's components, and hence their intended function, will vary depending on several factors including: (1) which end of the guardrail the end-terminal is located (e.g., downstream or upstream), (2) where the end-terminal is struck (side hit or end-on), (3) the orientation of the vehicle (frontal impact or side impact), (4) impact direction relative to up-stream or down-stream placement (forward or reverse hit), and (5) the end-release function of the end-terminal (i.e., gating or non-gating). These additional functions of an end-terminal are reflected in the number of tests and impact conditions that are required in the crash testing guidelines.[*Ross93; AASHTO09*] Because of these basic differences in function, the damage criteria assessments derived from guardrail performance studies may not correspond directly to end-terminals; thus damage modes for end-terminals will need to be evaluated using criteria appropriate for the various functions of those systems.

The buried-in-backslope end-terminal is the only non-proprietary end-terminal that meets FHWA eligibility for *NCHRP Report 350 TL-3*; this system, however, has limited application since it can only be installed in locations where there is a backslope. Although several older, largely obsolete end-terminal installations are still in service, it is expected that most of these will eventually be replaced by accepted systems; thus, any damage assessment criteria developed in this study for end-terminals would likely be focused on proprietary systems. Unfortunately, there are several of these systems and they all function somewhat differently (e.g., some are gating, some are non-gating, each has a unique energy absorbing mechanism, etc.). Because of the complexity and the proprietary nature of these systems, it would be difficult to conduct comprehensive assessments without the consent and participation from manufacturers.

Concerning their function as part of a guardrail system, however, essentially all proprietary end-terminals share many of the same basic features and components that function to ensure that the guardrail maintains proper tension during impacts (e.g., cable anchor mechanism, soil foundation tubes, ground-line strut, bearing plates, etc.). End-terminals also function in much the same way as guardrails when hit on the side. Thus, evaluation criteria for damage modes which affect an end-terminal's function as a guardrail anchor system or which affect its performance as a guardrail (i.e., side hits) were considered to be of high importance.

Report 656 did not evaluate damage modes for guardrail end-terminals, but did provide rationale for repair criteria based on an Ohio Department of Transportation Energy Absorbing End Terminal Maintenance Checklist. The assessment criteria for end-terminals included damaged end-post, missing or slack anchor cable, improper stub height, missing or failed lag bolts on impact head, and bearing plate. A summary of generic end terminal repair guidance from Report 656 is shown in Table 24. Evaluation criteria for additional damage modes should be included, such as soil eroded away from anchor posts and missing or damaged ground-line strut. These damage modes could affect the end-terminal's ability to properly anchor the guardrail during impacts, which could in turn lead to excessive rail deflection, improper release of rail-post connection, and pocketing. Further, whereas local damage to a guardrail results in a relatively isolated damage-affected section of the guardrail (i.e., limited exposure to future impacts in the damage region), a damaged anchor will affect the performance of the entire guardrail system (i.e., increased risk of exposure). Due to the importance of the end-terminal to guardrail performance, the research team considers that the additional damage evaluations for end-terminals to be of high priority.

Table 24. Summary of generic end terminal repair guidance. [Gabler10]

Damage	Repair Threshold	Relative Priority
Damaged end post	Not functional (sheared, rotted, severely cracked)	High
Anchor cable	Missing	High
	Loose—more than 1 inch of movement when pushed down by hand	Medium
Cable Anchor Bracket	Loose or not firmly seated in rail	Medium
Stub height of steel tube or hinged post	Height which exceeds 4 inches	Medium
Lag bolts on impact head (Energy Absorbing Terminals Only)	Missing or failed lag bolts	High
Bearing Plate	Loose or Misaligned	Medium
	Missing	High

Methods for Damage Assessment for Generic End-Terminal

Table 25 provides a summary of possible methods for evaluating the various damage modes for a generic end-terminal.

Table 25. Summary of possible methods for assessing damage modes for generic end terminals.

Component	Damage Mode	Possible Methods for Evaluation		
		Included in Report 656	Pendulum Test	FEA
Posts	Deflection			x
	Rotted or Weakened	x	x	x
	Split Posts	x	x	x
Foundation	Stub Height	x	x	x
	Bearing Plate	x	x	x
	Soil Eroded from Post		x	x
	Groundline Strut		x	x
Connections	Anchor Cable	x	x	x
	Cable Anchor Bracket	x		x

Legend

x	<i>Preferred method for analysis.</i>
x	<i>Analysis method is applicable.</i>
N.A.	<i>Not applicable</i>

Guardrail Transitions

Transition systems are used to join two barriers of different stiffness, such as a strong-post guardrail to a rigid bridge rail. The function of these systems is to provide a gradual transition from the more flexible system to the stiffer system to prevent “pocketing” and “snagging” on the approach end of the stiffer system. These systems generally share the same (or similar) components that are used in strong-post guardrail (e.g., w-beam or thrie-beam rail, steel or wood posts, rail-to-post fasteners, splice connections, etc.). The increase in stiffness is accomplished simply by using smaller spacing of the posts and stronger posts as the system approaches the more rigid structure. So, although they share the same components, the resulting response of the components may be quite different. For example, as the transition approaches the stiffer barrier, the w-beam rail functions more as a shear-beam transferring load to the posts, which results in less tensile force being developed in the rail element compared to the same impact on a guardrail. Thus transition systems will have different sensitivities to w-beam damage modes compared to typical strong-post guardrails.

Guardrail transitions were not included in this study; however, the results from the survey of practitioners indicated that the “steel-post w-beam to rigid barrier transition” and the “thrie-beam to rigid barrier transition” was of greater interest than other transition types and should therefore be considered in future studies involving damage assessment of roadside safety barriers (see Appendix B).

Combination Damage Modes

The damage analyses in Report 656 consisted primarily of isolated damage modes. In most real-world impacts any given damage mode is usually associated with several other damage modes. For instance, rail/post deflection is usually accompanied at a minimum by a deformed w-beam rail and post-rail separation. The net effect for a given group of damage modes will not always be the sum of the individual effects. As mentioned earlier, rail-post separation is generally considered to be a damage mode, but when rail deflection is in excess of some critical amount, an undetached rail-post connection would likely be a more hazardous situation than a detached connection. As stated in Report 656, “*A critical contribution to the vaulting of the vehicle in the MGA crash test was believed to be the failure of some of the posts to detach from the guardrail.*”

All post and beam guardrails can experience any of the damage modes listed in Table 26. Any of these modes can be observed in combination with any of the others. The net effect on barrier performance may be somewhat different for each type of guardrail system but in principal each system has the same potential range of combinations. Several specific combinations of damage modes that may be of interest in this study are discussed below.

Combination of Post and Rail Deflection and Rail-to-Post Connection

Recall that FEA was used in Report 656 to evaluate guardrail response as a function of rail-post deflections; rail deflections of 3, 6, 9, 11 and 14 inches were investigated in that study. Two series of analyses were conducted in order to bracket the crash performance. In the first series, the rail was allowed to detach normally from the post during the impact event. In the second series, the rail was constrained from releasing at a critical post location. The first series indicated that even with 14 inches of pre-deflection of the rail the guardrail performance was acceptable when the rail detached normally from the post. On the other hand, when the rail-post

connection was prevented from releasing, vehicle instability resulted due to severe wheel snags on the undetached post, increased potential for pocketing, and increased potential for override as the rail was pulled down by the post. The second series of analyses provided interesting information about the dangers of a rigidly constrained rail-post connection; however, the connection should not be expected to remain fixed in all cases. If so, then essentially all rail damage would need to be repaired, because even an undamaged system will not perform successfully with a fixed post-rail connection.

Table 26. Guardrail damage modes.

Damage Region	Damage Mode
Post Damage	1. Post/Rail Deflection
	2. Missing Posts
	3. Split Posts
	4. Rotted/Weakened Posts
	5. Twisted Posts
	6. Soil Eroded Away From Posts
Rail Damage	7. Rail Deflection
	8. Vertical Tear in W-Beam
	9. Horizontal Tear in W-Beam
	10. Hole in Rail
	11. Rail Flattening
	12. Rail Crushing (vertical)
Blockout Damage	13. Twisted Blockout
	14. Split Blockout
	14. Rotted Blockout
	15. Missing Blockout
Connection Damage	16. Bent Blockout (steel)
	17. Splice Damage
	18. Post-Rail Separation
	19. End Anchor Damage
	20. Missing Backup Plates

Combination of Rail Deflection and Splice Damage

Because the potential for rail rupture increases when excessive rail deflections occur just upstream of a post (i.e., pocketing) at splice connections, the combination of pocketing and splice damage should warrant higher consideration for repair. Although this combination mode was not addressed in *NCHRP Report 656*, evaluation was considered to be of low priority for this study.

Combination of Post and Rail Deflection and Anchor Damage

The anchor is a critical component of a guardrail system, and a damaged section of guardrail may be further compromised if the anchor system is compromised in any way. Quantification of this combination damage mode was considered to be of low to medium priority

for the study. The individual assessment criteria for post/rail deflection and for anchor damage should be sufficient for establishing repair priority for this combination mode.

Combination of Post/Rail Deflection and Missing Post(s)

A damaged guardrail may sometimes exhibit broken or missing posts. Quantification of this combination damage mode was considered to be of low priority for this study. The individual assessment criteria for post/rail deflection and for damage or missing posts should be sufficient for establishing repair priority for this combination mode. Particularly, since Report 656 recommended that even one missing post in an otherwise undamaged guardrail should be given a high priority for repair.

Other Considerations

Traffic Exposure

When assessing the need to repair a damaged section of guardrail, it may be important to consider its exposure to future impacts. For example, if the damaged section is located on the outside of a curve and there is a history of frequent impacts at that location, then the damaged section may warrant a higher priority for repair. On the other hand, if the damaged section were located along a tangent section of a low-volume, low-speed roadway which had little or no history of impacts at that specific location, then the priority for repair may be deferred to other guardrails with equal or less damage but higher exposure. From the Survey of States in Report 656 it was reported that "... the survey respondents could provide almost no documented cases of vehicles impacting previously damaged barriers." [Gabler10]

Evaluating Impact Upstream or Downstream of Damaged Section:

Another important factor to consider when evaluating guardrail damage is its effect on performance when the rail is struck at locations upstream or downstream of the damaged section. For example, repair of a *ruptured rail element* should have increased priority, since the damage will not only affect subsequent impacts at the rupture location, but will also effect impacts over a significant length of the guardrail both up- and down-stream of the rupture (i.e., a ruptured rail is essentially an unanchored system). The same is true for damage to the end-terminals which are necessary for maintaining proper tension in the rail and limiting guardrail deflections, regardless of where an impact occurs along the length of the guardrail.

The two above scenarios are relatively obvious signs for guardrail repair; however, it is not known how lower levels of damage to a local section of guardrail will affect performance of the system when struck at points up- and down-stream of the damaged area. For example, impact down-stream of a damaged section, may result in higher rail deflection due to reduced tension in the rail element as the previously damaged section "straightens out" during the impact. As discussed earlier, excessive deflections of an unsupported section of rail results in an increased potential for pocketing. Thus, when assessing damage to guardrails, one must include the total damage affected region of the guardrail.

Hazard Being Shielded

The level of crash severity for the hazard being shielded should also be considered when deciding repair priority. For example, if a guardrail is shielding a hazard is likely to result in

severe injuries if struck, then that damage may warrant higher priority for repair compared to other damaged guardrails that are shielding hazards of lower risk severities.

Recommendations

The ultimate goal of this study is to develop damage assessment and repair criteria that will lead to a comprehensive and highly valued field guide for assessing guardrail damage and establishing priority for repair. So it was necessary to carefully select which of the damage modes were to be included in the study to make the most effective use of the available funding.

The G4(2W) guardrail was rated the highest for inclusion in this study. The wood-post w-beam guardrail is the second most commonly installed guardrail system used in the U.S. and was also rated the highest by the survey respondents for inclusion in this study. As indicated in Table 17, the G4(2W) is composed of the same components and same basic design as the G4(1S), with the exception of the guardrail posts and is thus expected to be susceptible to similar damage modes. In many of these cases the performance degradation due to a particular damage mode will also be similar between these two systems; therefore evaluation criteria for several damage modes for the G4(1S) should be directly applicable to the G4(2W) guardrail. Further, some of the additional damage modes of the G4(1S) that warrant more investigation could be studied as part of the assessment for the G4(2W) and then “extrapolated” to the G4(1S), or vice versa.

The assessment criteria for the G4(2W) should apply to all wood post w-beam guardrails that are of the same basic design and that use guardrail posts of similar dimensions to those of the G4(2W). For example, the G4(1W), G4(2W), and the ODOT Type 5 guardrail all use slightly different shaped wooden posts, but otherwise share the same system components. Although the posts are different (e.g., square, rectangular, and round, respectively), they are similar in that they are all wood and are of similar dimensions (i.e., 8-10 inches in width/diameter and 6 ft in length); thus it could be inferred that each of these systems incur similar performance degradation due to each type and combination of damage mode(s).

The G2 weak-post guardrail was considered to be the next highest rated system for evaluation in this study. This system was also rated second highest for inclusion in the study by the survey respondents. The thrie-beam guardrail was considered to be the third highest rated system for inclusion in the study. The thrie-beam is not as popular as the strong-post w-beam, but most states have limited installations of these systems. Although the G2 weak-post guardrail received the second highest rating from the survey respondents for inclusion in the study, the rating for the thrie-beam guardrail was very similar (see Appendix B), thus a case could be made for selecting either system. Consideration should also be given to the fact that the thrie-beam guardrail will require fewer damage mode evaluations for developing a comprehensive set of assessment criteria compared to the weak-post system.

The guardrail systems and damage modes were prioritized for evaluation in this study, as shown in Table 27, based on considerations of

- (1) Has the damage mode been quantitatively assessed before?
- (2) Applicability of damage assessment criteria to multiple systems.
- (3) How widely used is the guardrail system?
- (4) Can a sufficient number damage modes for a given system be evaluated (e.g., considering budget constraints) to ensure comprehensive damage assessment and repair guidance?

Table 27. Prioritization of damage modes.

Guardrail Type	Priority Order	Damage Mode	Evaluation Method	Comments
G4(2W)	A1	Validate G4(2W) Model	FEA	Simulate tests 471470-26 and/or RF476640-1-5 to validate the model for use in subsequent analyses
	A2	Weak Anchor	FEA	Evaluate the effects of anchor stiffness and strength on guardrail performance. Results for this system should also correspond to the G4(1S) .
	A3	Rotted/Weakened Posts	Pendulum / FEA	Pendulum test to quantify loss of post strength and validate FEA model. FEA to evaluate system performance
	A4	Combination Mode: Post/Rail Deflection and rail-post separation	Pendulum / FEA / Full-Scale Test?	Combination Modes: Pendulum tests to determine amount of rail deflection at which rail detachment should occur. FEA to evaluate barrier performance for a range of barrier deflections w.r.t. varying connection strength. Full-scale test to validate model.
	A5	Splice Damage	Pendulum	Evaluate damage to downstream splice bolt holes (damage to front and back layers). Results should also be applicable to the G4(1S) and vice versa.
	A6	Soil Eroded Away from Posts	Pendulum / FEA	Pendulum test to quantify loss of post strength and FEA to evaluate system performance.
	A7	Split Blockouts	Pendulum	Pendulum tests to quantify the potential for splice rupture.
	A8	Post/Rail Deflection and Flattened Rail	FEA	Combination Modes: Rail flattening was shown to increase probability for system vaulting in R656. A deflected system in combination with rail flattening may further increase potential for vaulting.
Generic Anchor	B1	Reduced Embedment of Anchor Foundation Tubes	Static Testing / Pendulum / FEA	Measure force-deflection response (i.e., stiffness and strength) of anchor for each damage mode and level of damage. Combine with A2, C2, D2 and E2 to establish repair criteria.
	B2	Missing Grounline Strut	Static Testing / Pendulum	
	B3	Slack Cable	Static Testing / Pendulum / FEA	
	B4	Rotted / Weakened Anchor Posts	Pendulum	
G4(1S)	C1	Validate G4(1S) Model	FEA	Simulate tests C08C3-027 using appropriate anchor strength to verify research team's hypothesis that the weak anchor was the cause of failed test.
	C2	Weak Anchor	FEA	Use FEA to evaluate effects of anchor strength on guardrail performance.
G2	D1	Validate G2 Model	FEA	Simulate full-scale crash test to validate the model for use in subsequent analyses
	D2	Post/Rail Deflection	FEA + Full-Scale Test(?)	FEA to simulate low-speed impacts followed by high-speed impact (analogous to Report 656 methodology). Full-scale test to validate model?
	D3	Anchor Damage	FEA	The weak-post system will have different sensitivity to anchor strength than strong-post systems.
	D4	Horizontal Tear	Pendulum / FEA	This damage mode may be more critical for weak-post systems than strong-post systems due to higher tensile loads in rail
	D5	Hole in rail	Pendulum / FEA	This damage mode may be more critical for weak-post systems than strong-post systems due to higher tensile loads in rail
	D6	Soil Eroded Away from Posts	Pendulum / FEA	The weak-post system will have a different sensitivity to this damage mode compared to strong post systems.
	D7	Splice Damage	FEA	Splice damage will be less critical for the modified G2 (e.g., splice at mid-span) than the original G2
	D8	Rail-Post Separation	FEA	FEA could be used to evaluate this mode; however, a detached rail-post connection would also indicate a missing back-up plate which is not acceptable.
	D9	Missing Back-up Plate	Pendulum / FEA	FEA or Pendulum testing could be used to evaluate this damage mode; however, test results have already proven that a missing back-up plate is not acceptable.

Table 27. Prioritization of damage modes. (continued)

Guardrail Type	Priority Order	Damage Mode	Evaluation Method	Comments
G9	E1	Validate G9 Model	FEA	Simulate full-scale crash test to validate the model for use in subsequent analyses
	E2	Anchor Damage	FEA	Evaluate the effects of anchor stiffness and strength on guardrail performance. These results could be combined with the damage vs stiffness evaluations above.
	E3	Combination Mode: Post/Rail Deflection and rail-post separation	Pendulum / FEA / Full-Scale Test?	Combination Modes: Pendulum tests to determine amount of rail deflection at which rail detachment should occur. FEA to evaluate barrier performance for a range of barrier deflections w.r.t. varying connection strength. Full-scale test to validate model.
	E4	Combination Mode: Post/Rail Deflection and rail flattening	FEA	Parametric study to determine critical degree of rail flattening for varying degrees of rail deflection.
	E5	Soil Eroded Away from Posts	Pendulum / FEA	Pendulum test to quantify loss of post strength and FEA to evaluate system performance.
	E6	Twisted Posts	FEA	FEA to evaluate system performance due to various degrees of twisted posts.
	E7	Rotted/Weakened Posts	Pendulum / FEA	Pendulum test to quantify loss of post strength and validate FEA model (note: May be able to extrapolate from G4(2W) study). FEA to evaluate system performance.
MGS	F1	Validate MGS Model	FEA	Simulate full-scale crash test to validate the model for use in subsequent analyses
	F2	Combination Mode: Post/Rail Deflection and rail-post separation	Pendulum / FEA / Full-Scale Test?	Combination Modes: Pendulum tests to determine amount of rail deflection at which rail detachment should occur. FEA to evaluate barrier performance for a range of barrier deflections w.r.t. varying connection strength. Full-scale test to validate model.
	F3	Anchor Damage	FEA	Evaluate the effects of anchor stiffness and strength on guardrail performance. Combine with results of anchor study to develop repair criteria.
	F4	Soil Eroded Away from Posts	FEA	Results from the pendulum tests in Tasks 4A-6 and 4E-5 will be used to calibrate the soil model for use in the finite element analyses.
	F5	Combination Mode: Post/Rail Deflection and rail flattening	FEA	Parametric study to determine critical degree of rail flattening for varying degrees of rail deflection.
	F6	Twisted Posts	FEA	FEA to evaluate system performance due to various degrees of twisted posts.
	F10	Rotted/Weakened Posts	FEA	Pendulum test to quantify loss of post strength and validate FEA model (note: May be able to extrapolate from G4(2W) study). FEA to evaluate system performance.

CHAPTER 6 – GENERAL RESEARCH APPROACH

The performance of common strong-post guardrail systems subjected to each damage mode or combination of damage modes identified in Chapter 5 was evaluated. The basic research approach was similar to that used in Report 656 and involved a combination of pendulum testing and computational analyses to assess performance degradation of guardrails due to various damage modes.

Pendulum testing was used to quantify strength degradation due to various damage modes, to evaluate failure modes that are not well suited for finite element analysis, and to validate finite element models. Finite element analysis was used to evaluate damage modes that could not be adequately assessed with pendulum testing and to investigate the effects of damage modes on overall system performance, which would be cost prohibitive to investigate using full-scale tests. For example, pendulum tests were used to quantify reduction in post strength due to rotted or weakened post; the results of the pendulum tests were then used to validate/calibrate the finite element model of the post-soil system(s); then FEA was used to evaluate the effects of the various levels of damage on system performance.

Figures 70 and 71 show a flow chart illustrating the scope of work performed in the study, which included the damage assessments listed in Table 27 under Tasks 4A-1 through 4A-6 for the G4(2W), Tasks 4B-1 through 4B-4 for the generic end-terminal, and Task 4C-1 for the G4(1S).

Finite Element Analysis

The finite element analyses were performed using the LS-DYNA software versions SMP R6.1.1 and SMP R7.1.1. The performance of each damaged guardrail case was evaluated based on vehicle stability, guardrail capacity, and occupant risk measures. The impact conditions and evaluation procedures were consistent with those used to evaluate the original undamaged system so that performance degradation could be directly assessed. The G4(2W) guardrail was not successfully crash tested to MASH, so its performance evaluations were assessed based on *NCHRP Report 350 TL-3* test conditions.

Each analysis case was carried out for 0.6 seconds of the impact event. For the majority of analysis cases this was sufficient time for the vehicle to impact and redirect from the guardrail. For those cases in which the vehicle was still in contact with the guardrail at the time of analysis termination, the guardrail had in all cases reached maximum deflections and the exit conditions of the vehicle could be readily projected.

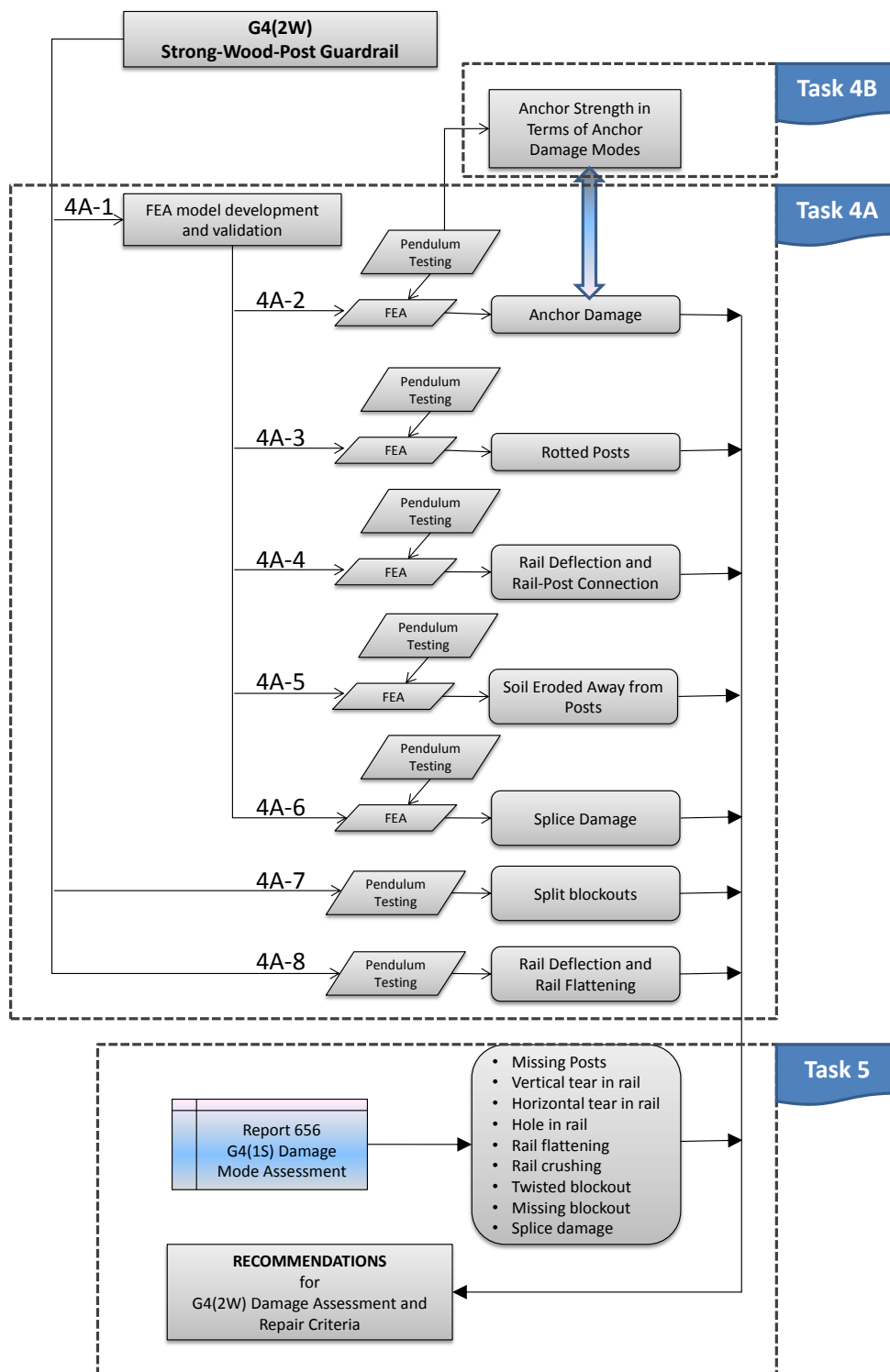


Figure 70. Flow chart for developing damage assessment criteria for the G4(2W) and the generic end-terminal.

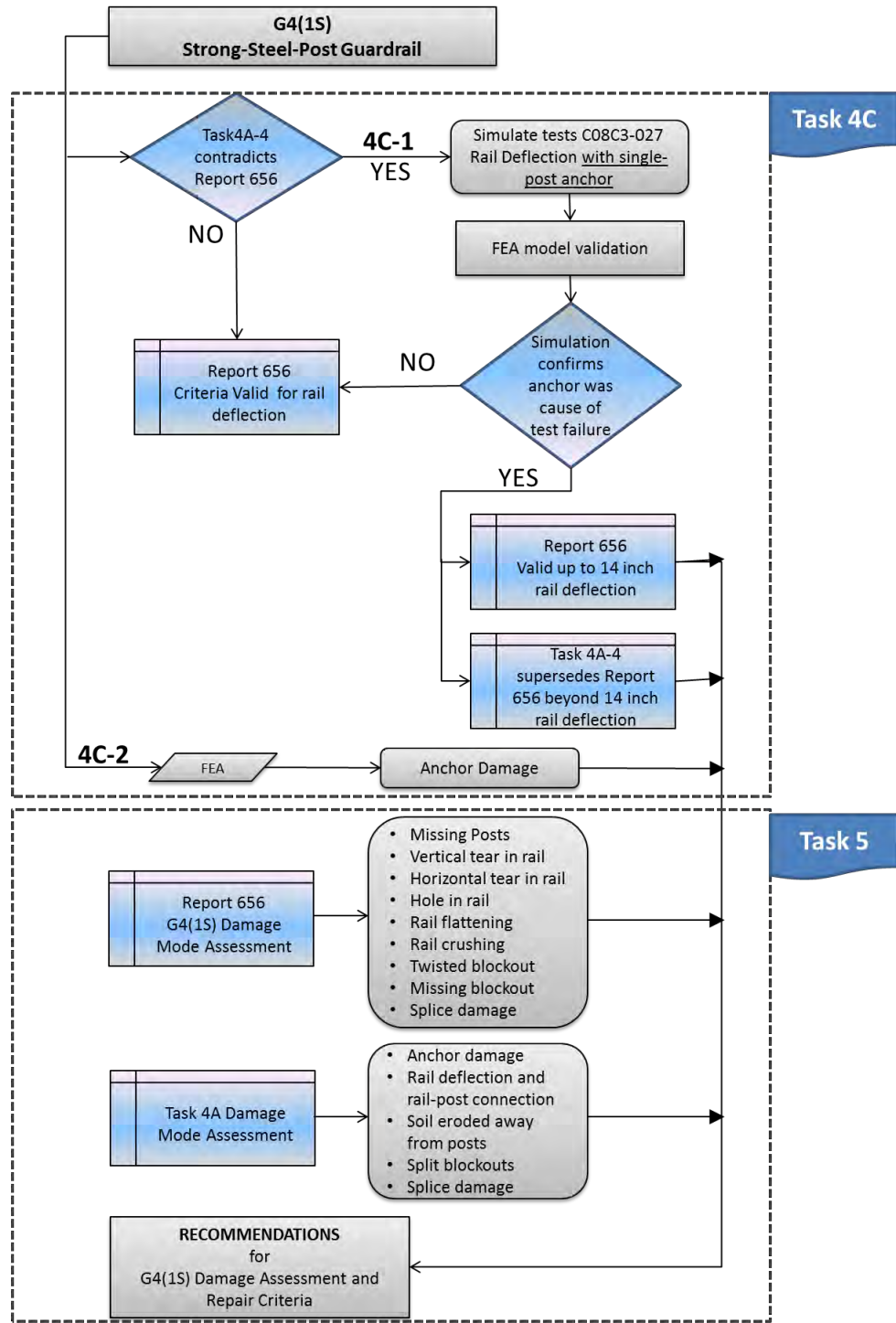


Figure 71. Flow chart for developing damage assessment criteria for the G4(1S).

The strength capacity of the guardrail was assessed based on the potential for rail rupture and on the potential for the vehicle to override the guardrail. For crash simulations involving damage modes for the G4(2W) guardrail, the capacity failures were generally associated with potential ruptures at a w-beam splice connection. The potential for rail rupture was assessed by comparing the plastic strains in the w-beam rail with critical failure strain values for the w-beam material. In most rail-rupture cases, the rupture occurs at a splice connection and the tear usually passes through one or more of the splice-bolt holes. [Bullard10; Buth99a; Buth06; Mak99b; Polivka00] This is a strong indicator that rupture generally initiates at a splice-bolt hole. Once a tear is initiated, the tension in the rail then causes the tear to propagate vertically through the w-beam cross-section. The failure strain for w-beam material was determined via tensile coupon tests to be approximately 0.66.[Wright96] Thus, when the local strains in the w-beam material at the splice-bolt holes reached a value of 0.66, it was assumed that there was a potential for tear initiation.

In most cases, the highest plastic strains in the rail occurred in the splice connection that was located immediately downstream of the impact point. These high magnitude strains were due to the splice-bolts bearing against the edges of the slotted holes in the w-beam, resulting in very high compressive stresses in very localized regions (i.e., at the end-edge of the splice-bolt holes). The magnitude of these strains was generally in excess of the stated failure strain of the material; however since the strains were largely compressive, the potential for tear initiation was much lower than the same magnitude of strain in a tensile region of the w-beam (e.g., on the upper or lower edges of the splice-bolt holes).

The strain computed for an element is actually the average strain for that element. So, as mesh refinement increases (i.e., element size gets smaller) the magnitude of strain for elements in high stress concentration regions of the model will increase. Because strain is mesh dependent it cannot be used to definitively predict the onset of rupture, especially when the strains arise from a stress concentrator, such as the bearing of a splice-bolt on the edge of the slotted hole of a w-beam. In this study, there was no failure condition set for the w-beam material. Instead, the finite element mesh for the w-beam and all other components of the guardrail system were kept constant throughout this study; so that the values of effective plastic strain computed for each damage mode case could be directly compared to those from the baseline case for assessing relative increase in strain magnitudes.

It is important to note that the degree of “pocketing,” which corresponds to the relative deflection and/or bend angle of the rail immediately upstream of a post, was not measured in the analyses. However, the effect of pocketing is higher magnitudes of strain in the splice; those quantities were computed for each analysis case and are reported herein.

Pendulum Testing

The pendulum tests were performed at the Federal Outdoor Impact Laboratory (FOIL) at the Turner-Fairbank Highway Research Center in McLean, Virginia. The materials used in the pendulum test program were donated to the study by two state agencies (Ohio Department of Transportation and Maine Department of Transportation) and three guardrail manufacturers (Gregory Industries, Trinity Industries, and Road Systems). Additional details regarding specific research methodology used for each evaluation case is presented at the beginning of each corresponding chapter.

CHAPTER 7 – DEVELOPMENT AND VALIDATION OF THE G4(2W) GUARDRAIL MODEL

Model Development

A detailed finite element model of the G4(2W) guardrail system was developed and the finite element analysis code LS-DYNA was used to conduct crash analyses of the barrier system. The G4(2W) guardrail system includes many of the same components used in other common strong-post guardrail systems, thus valid models for most of the guardrail components were readily available from previous projects conducted by the authors. The development of the components of the G4(2W) model were based largely on the modeling methodology used for G4(2W) and G4(1S) models developed at Worcester Polytechnic Institute in the late 1990's and early 2000's. [Plaxico98; Plaxico02; Plaxico07] The improvements of the current model were primarily related to mesh refinement of critical components.

The guardrail model consisted of 13.5 ft (4.13 m) lengths of 12-gauge w-beam rail (RWM02a), 6x8 inch cross-section wood posts with lengths of 64 inches (PDE01), and 6x8x13 inch wood blockouts (PDB01). The splice bolts (FBB01) connecting the w-beam rail elements together were modeled in geometric detail with rigid material properties. The bolts fastening the w-beam rail to the posts (FBB04) were modeled with beam elements with material properties modeled as piecewise linear plasticity. The nuts and the bolt heads were modeled with rigid material properties since deformations of those components were considered insignificant to the results. [Component designators refer to the AASHTO-ARTBA-AGC hardware Guide AASHTO04]. The nuts were tightened onto the bolts using nonlinear springs and dampers. The posts were spaced at 75 inches (1.905 m) center-to-center. The w-beam rail was positioned such that the top of rail was 27-5/8 inches (650.9 mm) above ground.

The boundary conditions on the upstream and downstream ends of the guardrail model were modeled with nonlinear springs attached to the ends of the w-beam rail. The stiffness properties of the boundary springs were intended to correspond to a two-BCT post anchor system with foundation tubes and groundline strut, as defined in [Plaxico03]. The post-soil interaction was modeled with the post model supported by an array of non-linear springs based on the subgrade reaction approach. Figure 72 shows the overall dimensions of the guardrail model, and Figure 73 shows a close up view illustrating the level of detail in the geometry and finite element mesh.

W-Beam

The cross-sectional dimensions of the rails were modeled according to the standard drawing RWM02a for 12-gauge w-beam (designation from AASHTO's *A Standardized Guide to Highway Barrier Hardware*). The material properties were characterized based on the properties determined in an earlier study by Wright and Ray. [Wright96] This model has been used in numerous analyses over the past decade by members of the research team and others, and has been validated based on full-scale crash testing. [Engstrand00; Plaxico02]

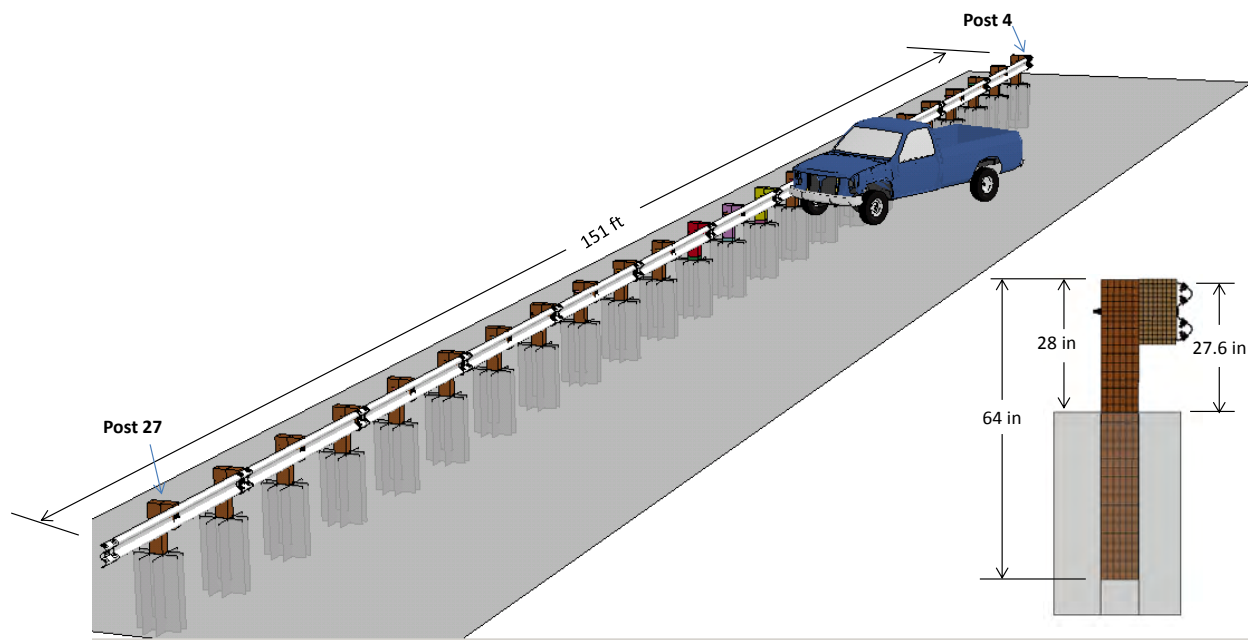


Figure 72. Finite element model of the G4(2W) guardrail.

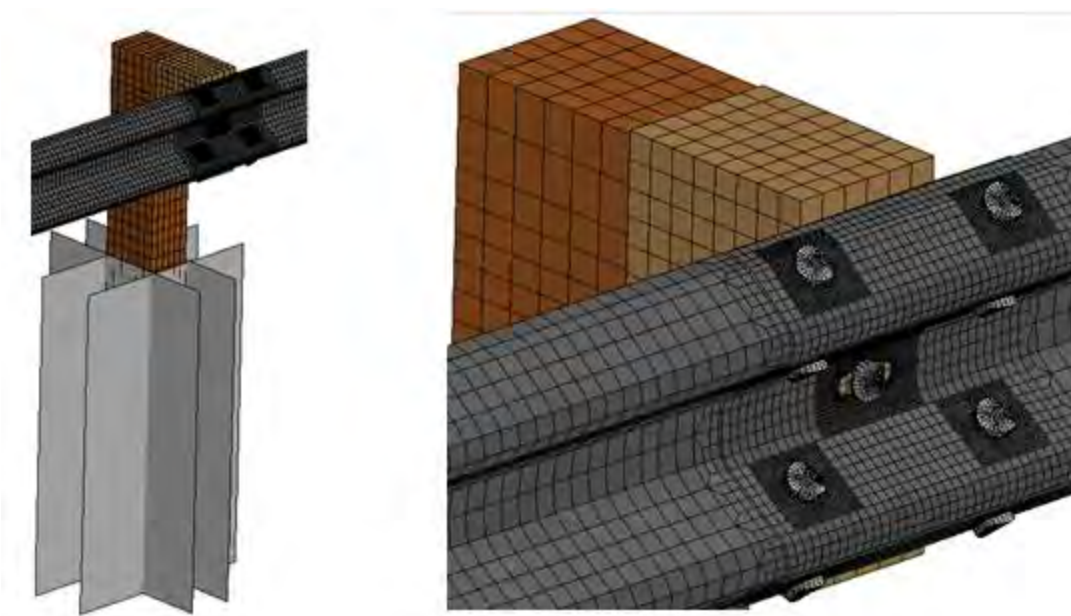


Figure 73. Angle perspective view illustrating typical components of guardrail model.

Splice Connection Model

An important consideration in modeling the w-beam rails is the splice connections that fasten the individual rail sections together. The splice is often the point where structural failure occurs during impact. W-beam guardrails are connected by overlapping the ends of the rail sections and clamping them together using eight 16-mm diameter bolts and nuts, as shown in Figure 74. In a study conducted by Ray *et al.*, the performance of w-beam splices were analyzed using the results of full-scale crash tests, laboratory experiments and finite element simulation.[Ray01a; Ray01b] In the G4(2W) and many other guardrails and guardrail terminal systems, the w-beam splice is located at the posts where the splice is subjected to a combination of axial tension, torsion in the guardrail section about its longitudinal axis, and lateral bending of the splice against the guardrail posts. Incorporating failure into the model of the splice connection would require a very fine mesh in order to capture the local stress concentrations around the splice bolt connections, as demonstrated by Engstrand.[Engstrand00] The finite element model of the splice and guardrail used in their study is shown in Figure 74. Using such a fine mesh in the current model would require a time-step on the order of 0.1 microseconds which was not feasible for analysis of a full-scale impact event which lasts 0.6 to 1.2 seconds (*e.g.*, the analysis would require 6,000,000 to 12,500,000 time-steps to complete the simulation).

In order to approximate the behavior of the splice connection, the mesh around the splice hole was modeled with a moderately refined mesh (element size 7 mm nominally). This mesh size provides reasonable accuracy up to the point of failure, but will not properly capture the fracture of the material around the hole when ultimate stress of the material is exceeded. A refined mesh (with null material properties) was overlaid and tied to the deformable mesh around the splice connection hole in the rail element, in order to provide sufficient load points between the w-beam and bolt hardware to more accurately model the force distribution at these critical locations. The splice connection details are shown in Figure 75 (note that the null mesh for the top-right bolt hole is hidden from view in order to show the mesh for the deformable elements). The bolt hardware is the same as that shown in Figure 74.

At the start of the analysis the w-beam rails are in an unstressed state and positioned such that the overlapping rails in the splice connection are only in “slight” contact with each other. As the analysis begins, the splice bolts tighten and clamp the w-beam splice together, resulting in a pre-stressed state of the w-beam material which approximates that of the actual splice connection. More details on modeling of the splice bolts are provide in the following section.

The behavior of the splice connection was validated by comparing model results to physical laboratory tests. In the study by Engstrand, the force-displacement relationship of the splice connection in pure tension was determined by conducting a series of quasi-static laboratory uniaxial tensile tests of the guardrail splice connection using a Tinius-Olsen 400,000-lb uniaxial load test machine.[Engstrand00] The splice-test conducted by Engstrand was simulated using the finite element model shown in Figure 76.

The FE results are accurate up to approximately 89.9 kips (400 kN) – the point when the splice bolts began to tear through the holes in the laboratory tests. The model experiences severe element distortion at this load, which is an apparent indication of the potential for rupture. Since the model does not incorporate failure directly, the results from the model must be carefully monitored at critical locations, such as splice connections, to evaluate model results and discern onset of potential failure.

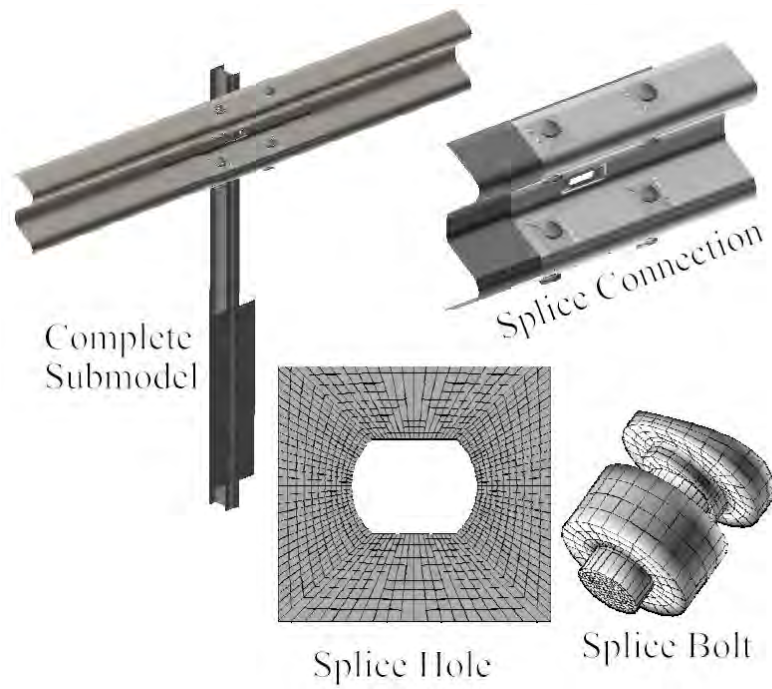


Figure 74. Components of the finite element model of a weak-post w-beam guardrail splice used in Ray *et al.* [Ray01a]

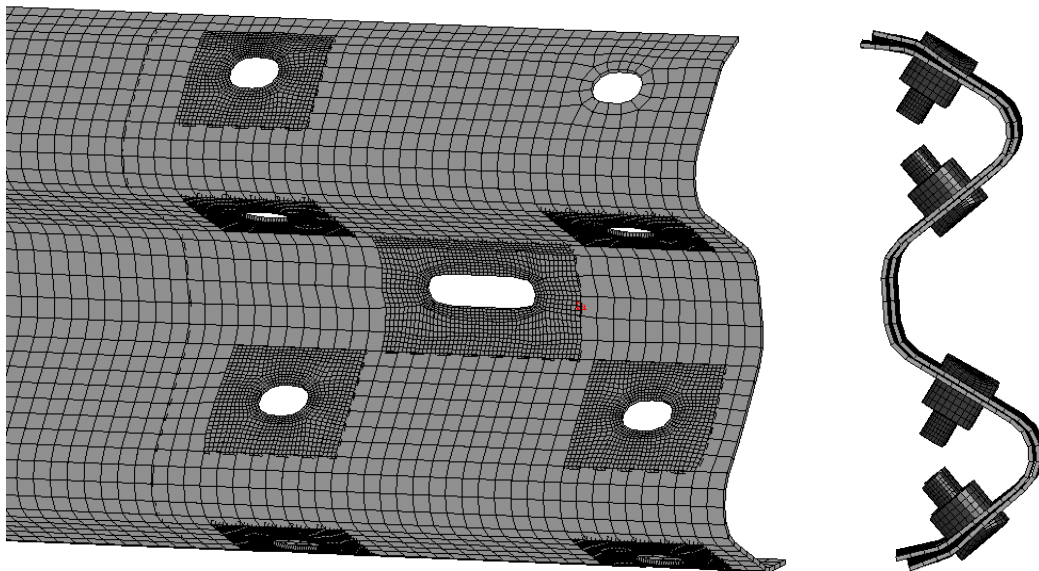


Figure 75. Splice connection model used in current study.

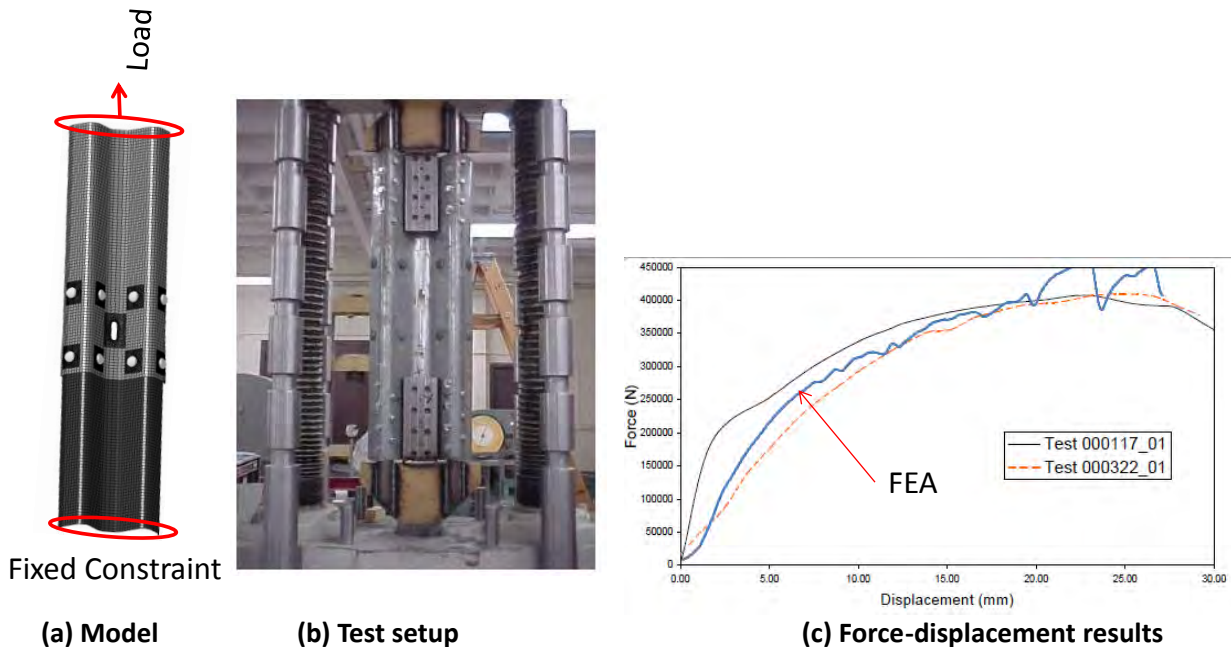


Figure 76. Test setup and axial force-displacement graphs from uniaxial tension tests of guardrail splices. [Engstrand00]

Bolt Hardware

Splice-bolt hardware seldom fails during impact, thus the material properties for the bolts and nuts were modeled with rigid material behavior. Failure of the splice connection is generally due to the “rigid” bolts rotating and tearing through the relatively thin w-beam material. Therefore, the bolts were modeled with geometric fidelity in order to obtain accurate force distribution and stress concentrations in the w-beam splice holes. The dimensions of the bolt hardware were modeled according to the standard drawing FBB01 for guardrail bolt and recessed nut (designation from AASHTO’s *A Standardized Guide to Highway Barrier Hardware*).

The details of the splice bolts, however, do not include the bolt-threads. Non-linear springs and damper elements are used to tighten nut onto the bolts. The stiffness of bolt springs was set to achieve an appropriate clamping force applied to each bolt, while linear dampers were used control the speed of the clamping process (i.e., prevent the nut from impacting against the w-beam during clamping). For example, the clamping process occurs over a 0.001 second time interval. Once the nut is in the desired clamped position, it is necessary to ensure that it is securely “fixed” to the bolt (i.e., simulate the nut being locked to the bolt by threads) to prevent the nut from “backing off” during crash simulations. A set of non-linear one-way dampers were included on the bolt model for this purpose, which was more than sufficient to hold the nut in place during the crash simulations.

Guardrail Posts

The cross-section dimensions of the wood guardrail posts and blockouts were 6 x 8 inches; the length of the posts was 64 inches. The wood material was modeled with mechanical properties consistent with Southern Yellow Pine. Two different LS-DYNA material models were used for the posts. In the impact region of the guardrail, the material model *Mat_Wood (material type 143) was used, which is a transversely isotropic elasto-plastic damage model with rate effects. In the non-impact regions of the guardrail, a much simpler and less computationally demanding constitutive model called *Mat_Isotropic_Elastic_Plastic_Failure (material type 13) was used.

The material model *MAT_WOOD (i.e., material type 143 in LS-DYNA) was developed by APTEK through a study sponsored by the Federal Highway Administration.[*Murray07*] This material model was developed specifically for conducting finite element analyses of vehicle collisions into wooden guardrail posts. The constitutive model in *MAT_WOOD is characterized as a transversely isotropic material with yield surfaces. The model effectively simulates the stiffness, strength and post-peak softening behavior in the two primary directions of wood (i.e., parallel and perpendicular to wood grain). The model also includes rate effects which effectively increase the strength properties of the material as a function of strain rate.

The user has the option of inputting his or her own material properties or requesting default material properties for Southern Yellow Pine or Douglas Fir. The material property data stored in LS-DYNA for MAT 143 corresponds to clear wood properties for these two species, whereas most structural wood, such as guardrail posts, are graded. Clear wood properties correspond to the highest strength properties for the wood material (i.e., no knots or defects). In order to obtain the appropriate strength reduction for graded wood, MAT 143 applies *quality factors* (e.g., strength-reduction factors) to the clear-wood property values. In particular, two quality factor parameters may be defined, Q_T and Q_C , whose values range from 0 to 1. Q_T is applied to the tensile and shear strength properties, and Q_C is applied to the compressive strength properties. Predefined values for these quality factors are provided with this material model for Pine and Douglas Fir. These values were developed based on correlation to static bending tests and bogie impact tests of guardrail posts.[*Murray07*] The default quality factors for Grade 1 and DS-65 Southern Yellow Pine are:

- Grade 1: $Q_T=0.47$ and $Q_C=0.63$
- Grade DS-65: $Q_T=0.80$ and $Q_C=0.93$

Table 28 shows a summary of the resulting material property values for *MAT_WOOD_PINE in LS-DYNA for clear wood, DS-65 and Grade 1. (NOTE: Table 28 lists the values for the material parameters in the units used in the FE model (i.e., Mg, mm, sec, N and MPa)). These properties correspond to Southern Yellow Pine under saturated conditions (e.g., moisture content is greater than or equal to 30 percent).

Wood Post Model Calibration/Validation

The material properties for the baseline guardrail post model were determined through the process of trial and error by comparing the dynamic impact response of the post model to the results of full-scale pendulum tests. The tests used for this evaluation were conducted as part of Task 4A-3 of this study (see Chapter 8) to assess the dynamic failure properties of deteriorated guardrail posts. The tests were performed at the FOIL. The nominal impact conditions for the

tests involved a 2,372-lb rigid-nose pendulum striking the posts at 21.5 inches above grade. The posts were 66 inches long and were embedded 38 inches inside a 12x12 inch steel tubular sleeve with “rigid” fixity. See Chapter 8 for more details regarding the test setup. Figure 77 shows a side-by-side view of the physical test set-up and the finite element model.

Two series of tests were performed: Series 1 included 22 tests with impact speed of 20 mph and Series 2 included 31 tests with impact speed of 10 mph. The tests specimens ranged from highly deteriorated posts (e.g., rot and insect damage) to relatively sound posts. Unfortunately, only two of the posts tested were new, unused posts. These were labeled as Post A and Post B and were tested in Series 1 at 20 mph; the corresponding test numbers are 13009L and 13009K, respectively (see Chapter 8). The finite element model of the wood post was used to simulate these test conditions and the results are presented below. Additional validation/calibration of the model was also made based on comparison to pendulum tests performed on guardrail posts embedded in soil. The results of those comparisons are presented in the following section of this report.

The posts used in Tests 13009K and 13009L were very similar in that both had a diameter of 7.24 inches; the mass densities were 44.8 lb/ft³ and 45.4 lb/ft³ for 13009K and 13009L, respectively; and the moisture content for both cases was greater than 30 percent (i.e., saturated condition). The most notable difference between the two tests was the ring density of the posts. The post in test 13009K had an average ring density of 5.8 rings/inch and the post in Test 13009L had an average ring density of 9.4 rings/inch.

The force vs. deflection and the energy vs. deflection results from the tests are shown in Figure 78 and Figure 79, respectively. Post A, which had the higher ring density, resulted in a peak impact force of 19 kips and total energy absorption of 37 kip-inches. Post B resulted in a peak impact force of 16 kips and total energy absorption of 24.9 kip-inches.

These impact conditions were simulated using the finite element model shown in Figure 77. As a starting point, the pre-defined material parameters in LS-DYNA for clear wood, Grade DS-65 and Grade 1 were used to model the wood material (refer to Table 28). The results from those three analysis cases are shown in Figures 80 through 82. The dashed lines in the plots correspond to the results from the physical tests.

The analysis results using Grade 1 properties matched reasonably close to the results from the physical tests. The peak impact force for the analysis was 20.8 kips and the total energy absorption was 34 kip-inches. The Grade 1 properties also resulted in a more brittle failure response of the post, as illustrated in the sequential views in Figure 82.

The peak impact forces for the Grade DS-65 and clear wood material properties were 20.7 kips and 23.9 kips, respectively; while the total energy absorption was 72 kip-in and 95 kip-in, respectively. The higher strength properties also resulted in a more ductile failure of the post with significantly more energy absorption after reaching peak force. The initial peak in the force-deflection plots, which accounted for a notable portion of the energy in the event, was attributed in part to the impulse of the rigid pendulum head impacting the post and in part to the post's boundary conditions. This spike was generally of lower force magnitude and larger displacement in the tests but varied slightly from test to test; whereas in the FEA analyses, the spike was exactly the same in every analysis case conducted since the material properties at the top of the post (i.e., DS65) and the boundary conditions were modeled the same in every analysis case.

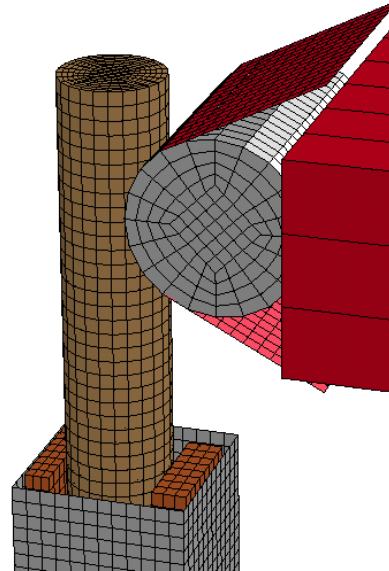
The differences between the FEA results and tests indicate that the pendulum head, as well as the boundary conditions, were softer in the test.

Table 28. Predefined material parameters values for *MAT_WOOD_PINE in LS-DYNA for various quality factor settings (units: Mg, mm, sec, N, MPa).

Variable	Description	Clear Wood	DS-65	Grade 1	User Defined
			($Q_T=0.8$ $Q_C=0.93$)	($Q_T=0.47$ $Q_C=0.63$)	($Q_T=0.60$ $Q_C=0.70$)
General					
RO	Density (Mg/mm ³)	6.73E-10	6.73E-10	6.73E-10	6.73E-10
NPLOT	Parallel damage written to D3PLOT	1	1	1	1
ITERS	Number of plasticity iterations	1	1	1	1
IRATE	Rate effects (0=off; 1=on)	1	1	1	1
GHARD	Perfect plasticity override (0=perfect plasticity)	0.05	0.05	0.05	0.05
IFAIL	Erosion perpendicular to grain (0=No; 1=Yes)	1	1	1	1
IVOL	Erode on negative volume (0=No; 1=Yes)	0	0	0	0
Stiffness					
EL	Parallel Normal Modulus (MPa)	11352	11352	11352	11352
ET	Perpendicular Normal Modulus (MPa)	246.8	246.8	246.8	246.8
GLT	Parallel Shear Modulus (MPa)	715.2	715.2	715.2	715.2
GTR	Perpendicular Shear Modulus (MPa)	87.5	87.5	87.5	87.5
PR	Parallel Major Poisson's Ration	0.157	0.157	0.157	0.157
Strength					
XT	Parallel Tensile Strength (MPa)	85.1	68.1	40	51.1
XC	Parallel Compressive Strength (MPa)	21.1	19.7	13.3	14.8
YT	Perpendicular Tensile Strength (MPa)	2.05	1.6	0.96	1.23
YC	Perpendicular Compressive Strength (MPa)	4.08	3.8	2.6	2.9
SXY	Parallel Shear Strength (MPa)	9.1	7.3	4.3	5.5
SYZ	Perpendicular Shear Strength (MPa)	12.7	10.2	6	7.6
Damage					
GF1	Parallel Fracture Energy in Tension (MPa-mm)	42.7	34.1	20	25.6
GF2	Parallel Fracture Energy in Shear (MPa-mm)	88.3	70.6	41.5	53
BFIT	Parallel Softening Parameter	30	30	30	30
DMAX	Parallel Maximum Damage	0.9999	0.9999	0.9999	0.9999
GF1 _⊥	Perpendicular Fracture Energy in Tension (MPa-mm)	0.4	0.4	0.4	0.4
GF2 _⊥	Perpendicular Fracture Energy in Compression (MPa-mm)	0.83	0.83	0.83	0.83
DFIT	Perpendicular Softening Parameter	30	30	30	30
DMAX _⊥	Perpendicular Maximum Damage	0.99	0.99	0.99	0.99
Rate Effects					
FLPAR	Parallel Fluidity Parameter Tension/Shear	9.42E-06	7.54E-06	4.43E-06	5.65E-06
FLPARC	Parallel Fluidity Parameter Compression	9.42E-06	8.76E-06	5.94E-06	6.60E-06
POWPAR	Parallel Power	0.107	0.107	0.107	0.107
FLPER	Perpendicular Fluidity Parameter Tension/Shear	1.97E-04	1.58E-04	9.27E-05	1.18E-04
FLPERC	Perpendicular Fluidity Parameter Compression	1.97E-04	1.84E-04	1.24E-04	1.38E-04
POWPER	Perpendicular Power	0.104	0.104	0.104	0.104
Hardening					
NPAR	Parallel Hardening Initiation	0.50	0.50	0.50	0.5
CPAR	Parallel Hareding Rate (/s)	400.0	462.5	1010.0	816.3
NPER	Perpendicular Hardening Initiation	0.40	0.40	0.40	0.4
CPER	Perpendicular Hardening Rate (/s)	100.0	115.6	252.0	204.08



(a) Test 13009L



(b) FEA Model

Figure 77. Test set-up and FEA model used in wood-model validation.

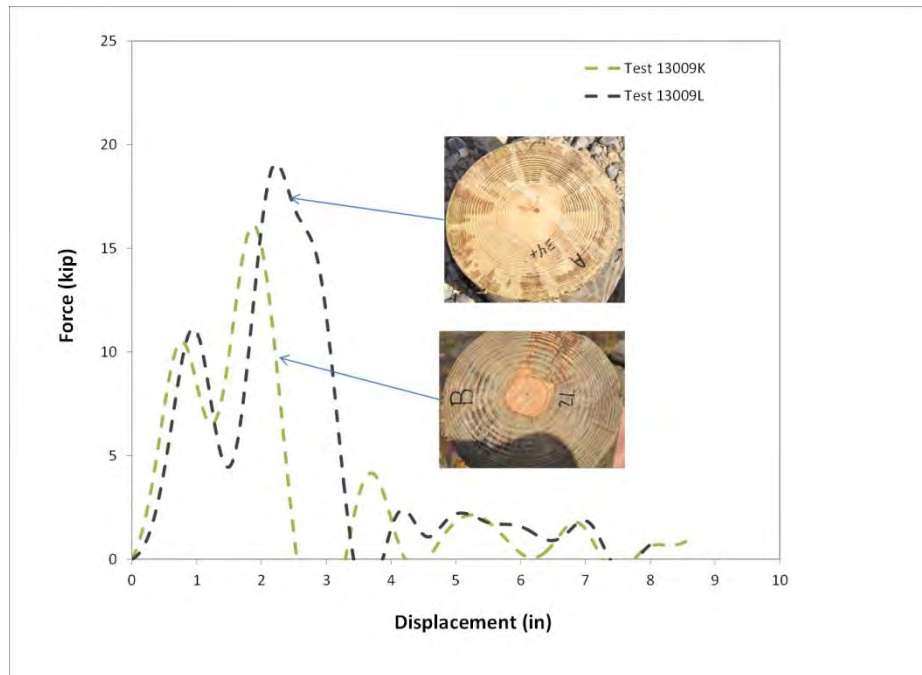


Figure 78. Force vs. deflection plots from dynamic impact tests 13009K and 13009L at impact speed of 20 mph.

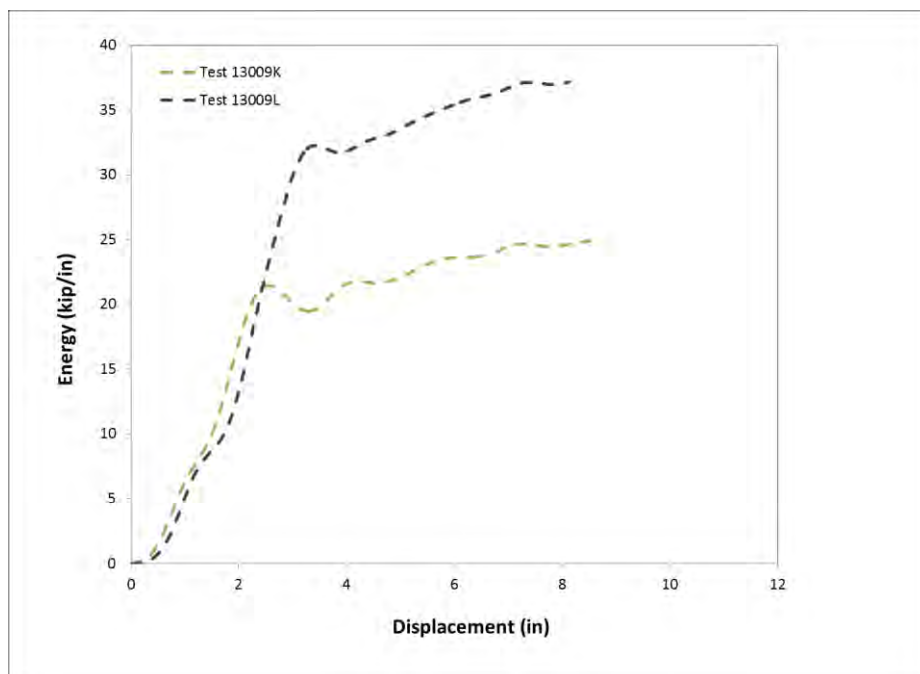


Figure 79. Energy vs. deflection plots from dynamic impact tests 13009K and 13009L at impact speed of 20 mph.

An additional analysis was conducted using a set of quality factors with slightly higher values than those pre-defined for Grade 1. For this case, the quality factor Q_T was set to 0.60 and the quality factor Q_C was set to 0.7. The purpose for this analysis will become apparent in the next section which compares model results to pendulum impact tests on posts embedded in soil. The results for this analysis case are shown in Figure 83 and Figure 84, where the peak forces are identical to those for the Grade 1 analysis case. The post-peak response, however, was somewhat less brittle for the analysis case using $Q_T = 0.60$ and the quality factor $Q_C = 0.7$.

Soil Model

The posts of the G4(2W) guardrail were 6x8 inches in cross-section and were embedded 36 inches into the soil. There are several approaches that may be used for modeling the soil in analyses of guardrail posts embedded in soil. Some common approaches include:

1. Post embedded in a soil continuum of solid finite elements,
2. Post embedded in a continuum of meshless finite elements,
3. Subgrade reaction approach in which the post is supported by an array of uncoupled springs.

The finite element formulations available in LS-DYNA include:

1. Lagrangian,
2. Eulerian,
3. Arbitrary Lagrangian-Eulerian (ALE),
4. Element Free Galerkin (EFG),
5. Smooth Particle Hydrodynamics (SPH), and
6. Discrete springs and dampers.

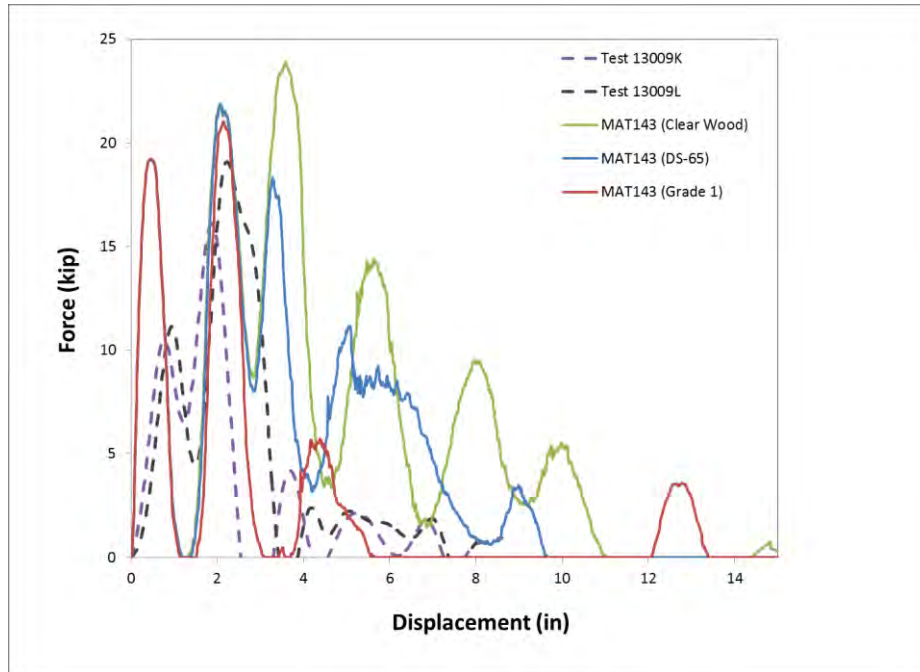


Figure 80. Force vs. deflection plots from dynamic impact analysis with pre-defined properties in MAT143 for (a) clear wood, (b) grade DS-65 and (c) grade 1.

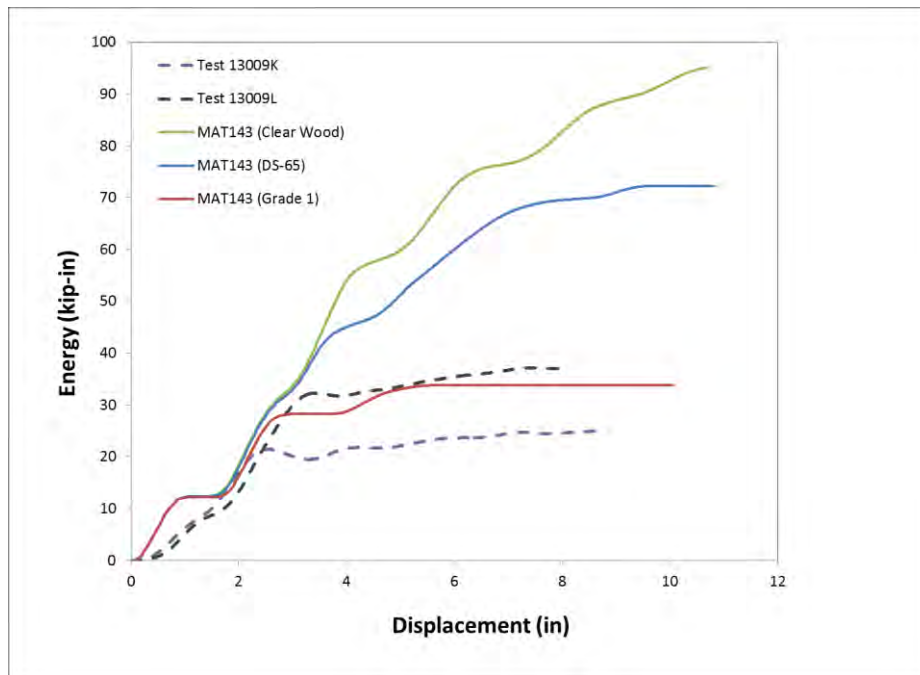


Figure 81. Energy vs. deflection plots from dynamic impact analysis with pre-defined properties in MAT143 for (a) clear wood, (b) grade DS-65 and (c) grade 1.



(a) Test 13009L



(b) Clear Wood



(c) Grade DS-65



(d) Grade 1

Figure 82. Sequential views of (a) Test 13009L and analyses for post model with pre-defined MAT143 properties for (b) clear wood, (c) grade DS-65 and (d) grade 1.

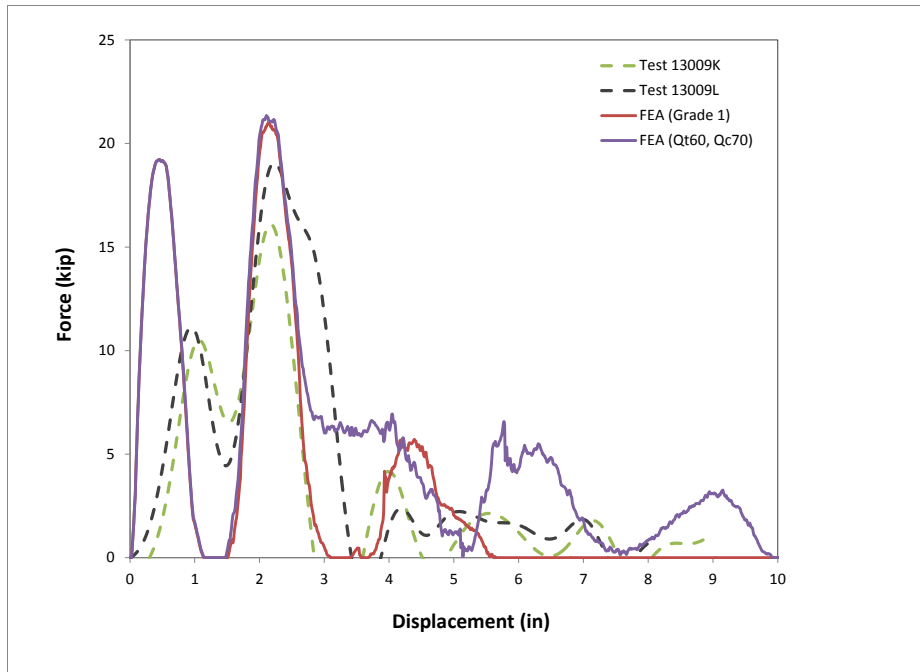


Figure 83. Force vs. deflection plots from dynamic impact analysis using properties for (1) Grade 1 and (2) quality factors set to $Q_T=0.60$ and $Q_C=0.7$.

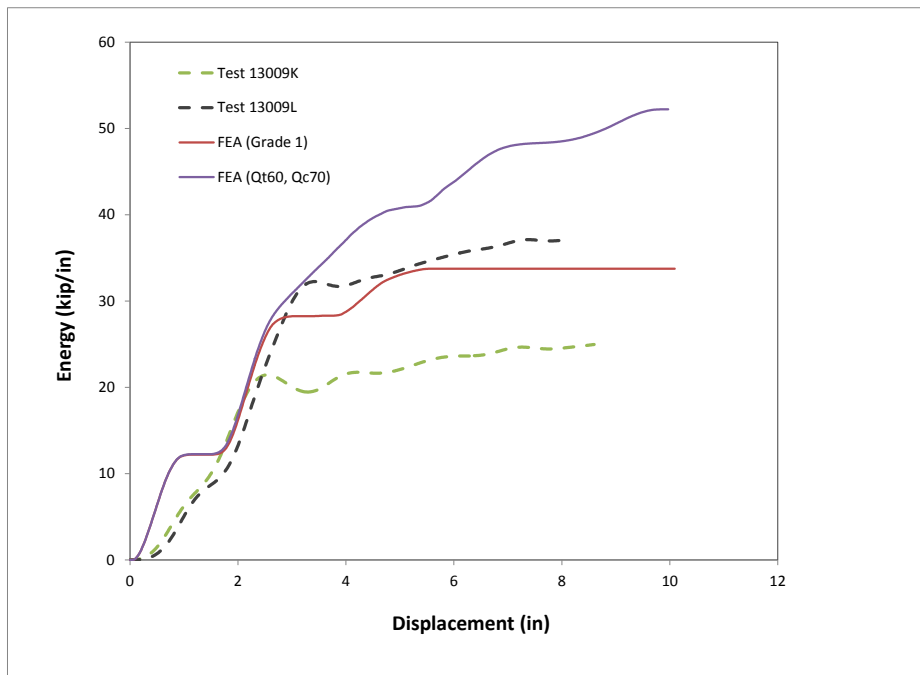


Figure 84. Energy vs. deflection plots from dynamic impact analysis using properties for (1) Grade 1 and (2) quality factors set to $Q_T=0.60$ and $Q_C=0.7$.

The Lagrangian and Eulerian element types are the traditional formulations used in stress analysis as well as crash analysis; although ALE, EFG and SPH formulations may be better suited to modeling fluid type behavior. All these element formulations can be mixed and often are to model fluid-structure interactions. The research team has used each of these methods to model soil in various projects with limited success.

The most commonly used method for modeling guardrail posts in soil is to model the soil as a continuum of solid Lagrangian elements. However, the solid Lagrangian based meshes generally do not provide very accurate response for the case of large soil deformation, where the post is shearing through the soil (e.g., typical of wood post systems). In these cases the soil often demonstrates more fluid like behavior. For the current study, the soil model was developed based on the subgrade reaction approach and validated through comparison with full-scale pendulum tests.

The subgrade modulus is influenced by many factors such as the relative density and moisture content of the soil, the cohesiveness of the soil, the overburden pressure, the nature of the applied load, the post deflection, and the properties and geometry of the post. Refer to Plaxico *et al.* for more details on the development of the force-deflection relationship of the soil springs.[Plaxico98] The soil for *NCHRP Report 350* and MASH tests is assumed to be non-cohesive. The parameters that are needed to characterize the soil model include:

- Unit weight of soil
- Void ratio
- Relative density
- Degree of saturation
- Moisture content of soil at saturation
- Critical moisture content
- Current moisture content (calculated using void ratio and degree of saturation)
- Effective unit weight of soil (calculated based on unit weight of soil, moisture content and degree of saturation)
- Angle of internal friction
- Post shape
- Depth of each layer of springs
- Distance between rows of springs

Patzner *et al.* used the subgrade reaction approach to model the post-soil interaction for wooden guardrail posts used in the Modified Eccentric Loader Terminal (MELT) with reasonable success.[Patzner99] In their model the soil springs were attached directly to the post, as illustrated in Figure 85, which provides adequate response for low to moderate rotation of the guardrail post. However, as post rotation continues to increase and the post begins to extract from the soil, the accuracy of the model starts to decline. This is because the force-deflection curves for the discrete spring elements were defined based on their initial position (e.g., initial overburden stress). When these springs are attached directly to the post, their vertical position will change as the posts rotate during loading (e.g., they generally rise toward the ground surface). The lateral resistance of the springs in such a model will not automatically readjust as the post rotates in the “soil.”

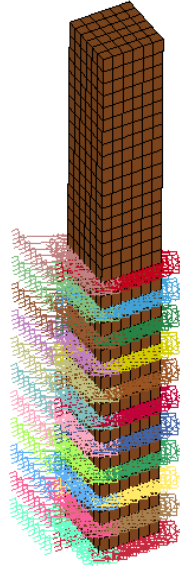


Figure 85. Soil springs attached directly to post. [Patzner99]

To correct this issue, a shell element interface was included to separate the soil springs from the post, as shown in Figure 86. The shell elements were meshed such that the element size was consistent with the element size of the posts and each line of nodes of the mesh was spaced at 1.97 inches (50 mm). A single discrete spring element was attached to each row of nodes at the center of the shell section. The shell elements were modeled with null material properties so that the resistance to the elements movement/deformation was due solely to the discrete springs. Each row of nodes was constrained to move as a rigid body with its corresponding spring element. That is, for the elements representing y-direction displacement of the soil, each individual row of nodes were constrained in the x- and z-directions using the *CONSTRAINED_NODAL_RIGIDBODY_SPC option in LS-DYNA. Figure 87 shows sequential views illustrating the typical response of the post-soil model to an impact load at approximately 21.6 inches (550 mm) above grade with a post embedment depth of 44 inches.

Soil Model Validation

The soil model was qualitatively validated based on comparison with impact tests of guardrail posts embedded 40 inches in soil with impact height of approximately 25 inches. Test 13010F involved a 2,372-lb rigid-nose pendulum impacting a W6x16 steel post at an impact speed of 20 mph. The post was 72 inches long and embedded 40 inches in the soil. The impact point was 24.88 inches above ground.

The soil conformed to Grading B of AASHTO M147-95 and was compacted in 6-inch lifts using a pneumatic tamper. The density, moisture content and degree of compaction of the soil was measured in front of and behind the post after each compaction process using a Troxler-model 3440 Surface Moisture-Density Gauge. There were a total of twelve readings which were averaged to determine the effective soil conditions, which were a 92 percent soil compaction with average soil density of 138 pcf.

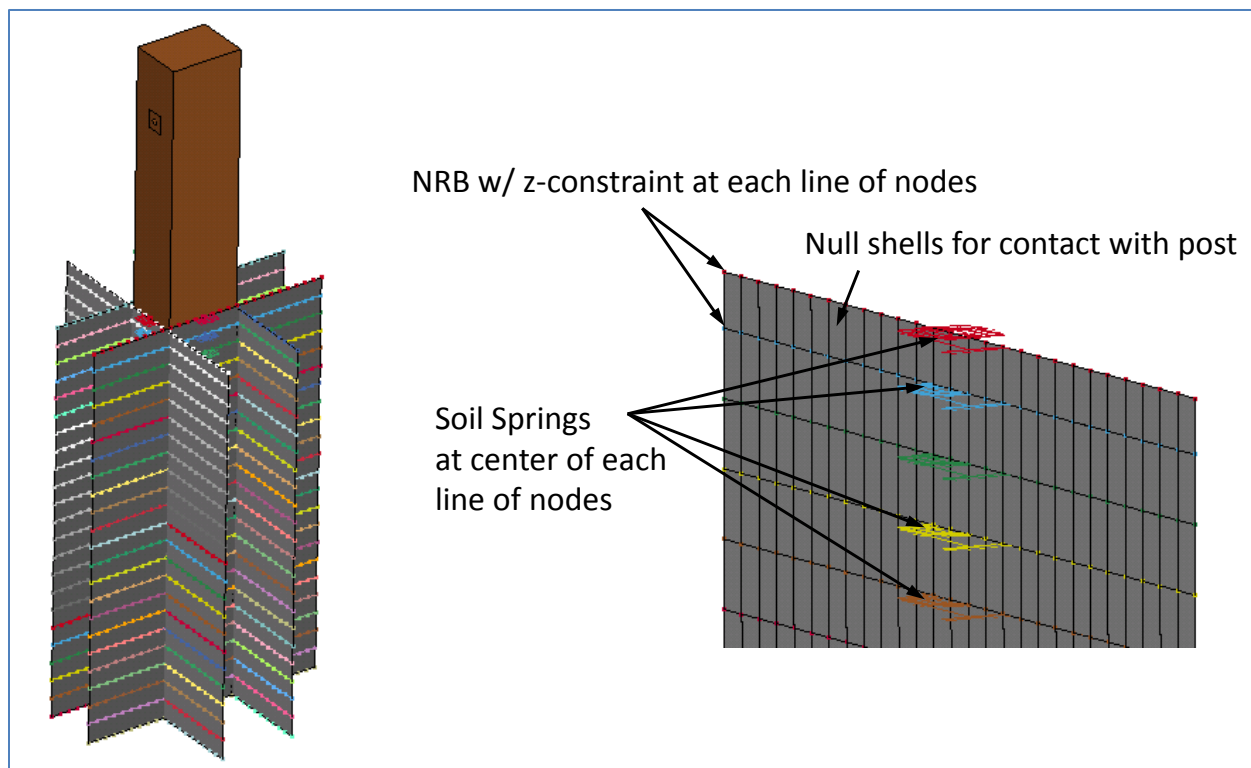


Figure 86. Soil modeled with non-linear springs and contact plates.

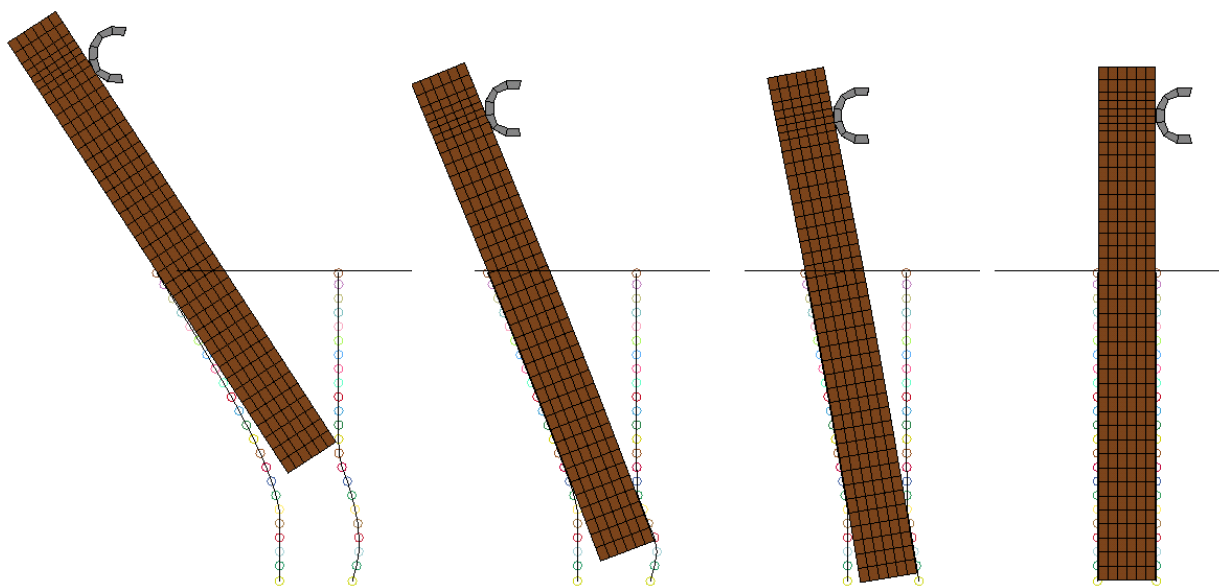


Figure 87. Sequential views illustrating typical model response to simulated bogie impact load.

A finite element model was developed to simulate Test 13010F using the soil-spring model. The properties of the spring elements were defined according to [Plaxico98] using a soil density of 134 pcf. The striker head used in the simulation was modeled with rigid material

properties with the dimensions similar to those of the physical device. The pendulum model struck the face of the post at 24.88 inches above grade at an impact speed of 20.0 mph. Acceleration data was collected at the rear of the pendulum model and used to compute the force-displacement response. The results from the finite element analysis are compared to those from full-scale Test 13010F in Figure 88 and Figure 89. The response of the soil-spring model with the stiffness of the soil-springs adopted directly from [Plaxico98] matched very well with the test results. The total energy absorption for the analysis was 288 kip-in compared to 274 kip-in in the test.

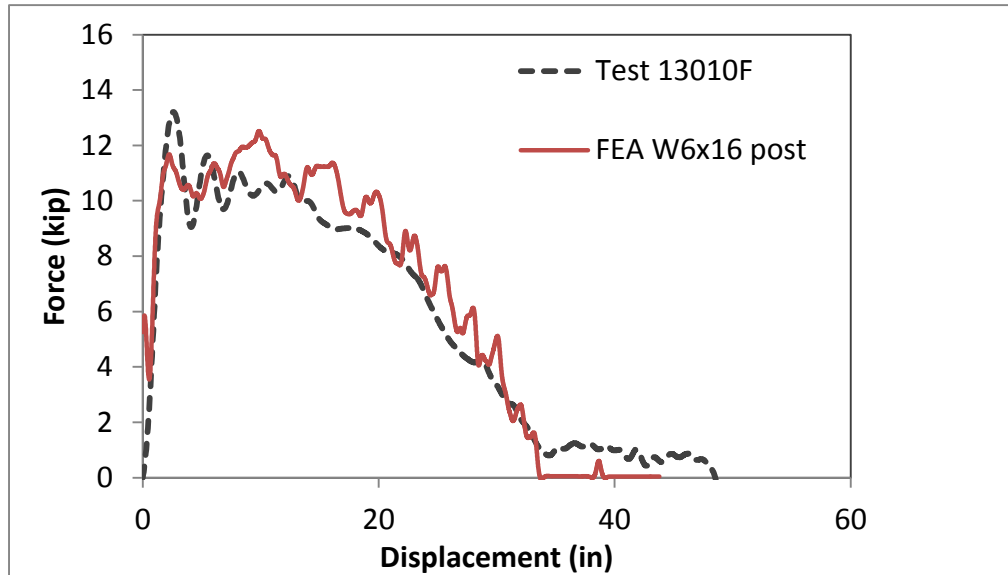


Figure 88. Force vs. displacement results from FE analysis compared with Test 13010F.

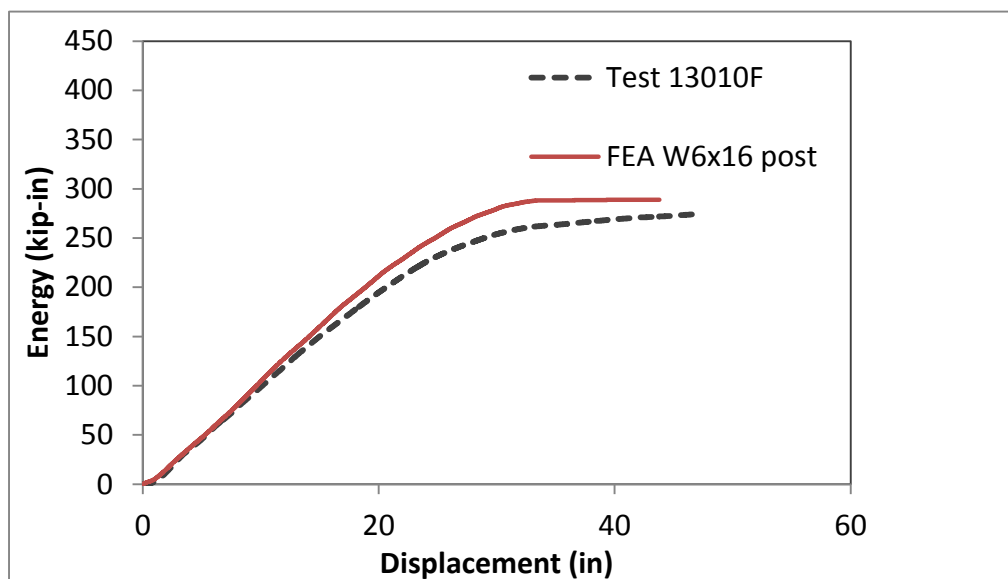


Figure 89. Energy vs. displacement results from FE analysis compared with Test 13010F.

Limitations of the model

- The effects of dynamic loading of the soil (e.g., inertial spikes) are not accounted for in this model, although they could be modeled using discrete damper elements with empirically defined properties.
- The springs only provide lateral resistance for the posts. For the soil-plate model described here, the vertical resistance to pull-out comes from the vertical constraint on the plates. That is, the nodes of the soil-plates can move laterally but not vertically. It is assumed that this would become less of an issue as the vertical distance between springs is reduced (i.e., mesh refinement); however, accuracy in simulating large post rotation would likely be improved if the vertical response of the soil were included in the model.

Vehicle Model

C2500D-v5b

The C2500D-v5b vehicle model was developed through the process of reverse engineering by the National Crash Analysis Center (NCAC).[NCAC08] The model version used in these analyses is version 5b. Minor modifications were made to the model by RoadSafe to improve hourglass modes, contact stability and wheel assembly failure. The FE model was developed based on a 1994 Chevrolet C2500 pick-up truck and corresponds to the 2000P large passenger vehicle specification in *NCHRP Report 350*. The C2500D-v5b model closely matches the mass and dimensional properties of the test vehicle used in the full-scale crash test of the G4(2W) guardrail in Test No. 471470-26.[Mak99]

Validation of the G4(2W) Guardrail Model

A finite element model of the standard G4(2W) (SGR04b) wood post guardrail system was developed. In order to gain confidence in the model's results, it was necessary to validate the model's predictions against full-scale crash test results. The validation procedures presented in NCHRP Web Document 179 were used to assess the fidelity of the model.

Full-scale crash test 471470-26 conducted by the Texas Transportation Institute (TTI) in College Station, Texas on May 25, 1994 was used for the validation.[Mak99] The test was conducted under *NCHRP Report 350* Test 3-11 impact conditions. The guardrail system successfully passed Report 350 performance criteria; however, the test was classified as "marginally acceptable" due to severe wheel snag and subsequent vehicle instability after redirection from the system.[Mak99]

Simulation of Test 471470-26

TTI Test 471470-26 involved an impact with a 1989 Chevrolet C-2500 pickup truck striking a standard G4(2W) wood post guardrail system. The gross static mass of the test vehicle was 4,568 lbs including a restrained 50th percentile male anthropomorphic dummy placed in the driver's position. The test guardrail system included 150 ft of standard G4(2W) guardrail, with a Modified Eccentric Loader Terminal (MELT) at the upstream end of the system and a Breakaway Cable Terminal (BCT) at the downstream end to provide anchorage. The total length of the complete system, including terminals, was 225 ft. The test vehicle struck the G4(2W) guardrail at an angle of 24.3 degrees and a speed of 62.6 mph (100.8 km/h), traveling in the

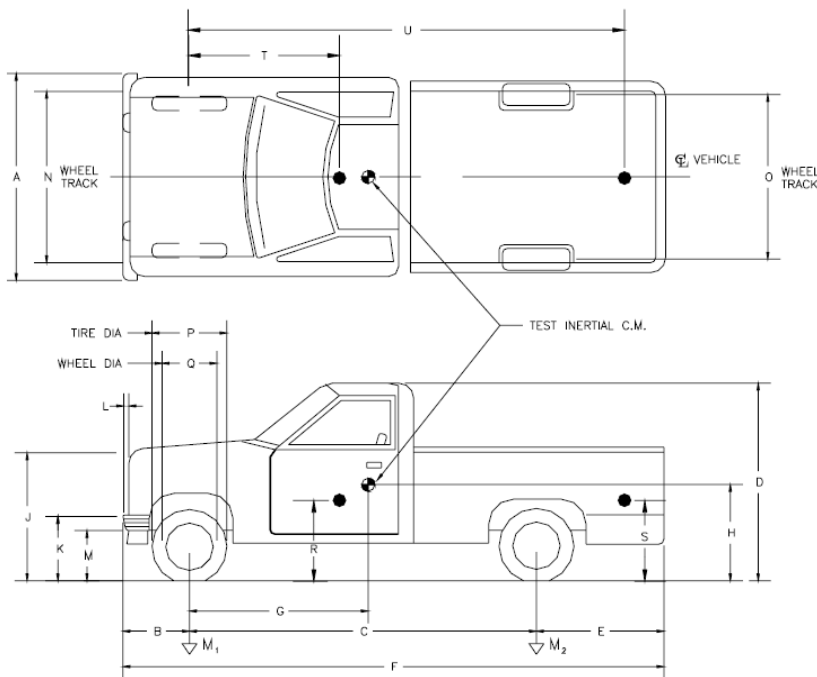
downstream direction. The initial point of contact was approximately 2-ft upstream of the w-beam rail splice connection at Post 14.

The guardrail model consisted of twelve 13.5 ft (4.13 m) lengths of 12-gauge w-beam rail, twenty-four 6x8x64 inch wood posts, and twenty-four 6x8x13 inch wood blockouts. The posts were spaced at 75 inches (1.905 m) center-to-center and the w-beam rail was positioned such that the top of rail was 27-5/8 inches (650.9 mm) above ground. The posts were embedded 36 inches in the ground. The total length of the guardrail model, excluding end anchors, was 151 ft.

The vehicle model used in the analysis was the NCAC C2500D version 5B. The model was modified in order to calibrate the mass inertial properties of the vehicle to the properties of the test vehicle. This was achieved through the use of the **Constrained_Nodal_Rigid_Body_Inertia* card in LS-DYNA, with the added mass concentrated at the center of gravity of the vehicle model. The mass of the vehicle model was increased by 573 lb to match the gross static mass of the test vehicle. However, the mass moments of inertia of the test vehicle were not measured, so the inertial properties of the model were calibrated to a similar vehicle type (i.e., 1998 Chevrolet C1500) which were documented in a NHTSA report.[*Garret98*] A comparison of the physical and inertial properties of the test and analysis vehicles is provided in Figure 90. The most notable difference was the location of the center of gravity of the vehicle in the longitudinal direction. The c.g. of the vehicle model was located approximately 10 inches forward of that measured for the test vehicle, which corresponded to a 17 percent error.

Additional modifications to the model included remeshing various parts in the impact region of the model and changing the element type to the fully integrated shell element (i.e., type 16 in LS-DYNA). A failure condition was also included on the spherical joints which simulate the attachment of the wheel assembly to the upper and lower A-Frames. The failure force for the joint was set to 14.6 kips based on the tests conducted at the FOIL by Stefano Dolci of Polytechnico di Milano.[*Dolci12*] Dolci measured the static load required to fail the wheel assembly joint of a 2007 Chevrolet Silverado 1500 Crew-Cab pickup, where the joint failed at a static load of 9.98 kips. The failure load used in the finite element model was approximated, by assuming a strain-rate magnification factor of 1.5 for the component.

The analysis was conducted with a time-step of 1.26 microseconds for a time period of 0.6 seconds. The exact timing of phenomenological events was not possible, because plot states were only collected at 0.005 second intervals throughout the analysis. Therefore, a 0.005 second time window corresponding to range of time for which the event could have occurred in the analysis was reported.



Vehicle Geomerty (inches)

	Test Vehicle	FE Model	Error %
A	73.2	73.3	0.2
B	31.5	35.6	12.9
C	131.9	144.3	9.4
D	70.9	73.2	3.3
E	52.8	52.8	0.1
F	216.1	232.7	7.7
G	60.7	50.3	-17.1
H	-	27.8	-
J	41.1	42.3	2.8
K	25.6	26.0	1.5
L	3.5	4.1	16.7
M	16.9	18.0	6.3
N	61.8	65.2	5.4
O	63.8	65.2	2.2
P	31.1	28.0	-9.9
Q	17.3	16.4	-5.5
R	28.0	27.6	-1.4
S	40.6	-	-
T	59.1	54.6	-7.5
U	163.8	-	-

Mass -Properties

		Curb			Test Inertial			Gross Static		
		Test Vehicle	FE Model	Error %	Test Vehicle	FE Model	Error %	Test Vehicle	FE Model	Error %
M₁	(lb)	2,394	-	-	2,381	-	-	2,478	-	-
M₂	(lb)	1,682	-	-	2,028	-	-	2,094	-	-
M_{Total}	(lb)	4,076	3,995	-2.0	4,409	-	-	4,572	4,568	-0.1
I₁₁	(lb - ft ²)	-	-	-	-	-	-	* 18,082	17,997	-0.5
I₂₂	(lb - ft ²)	-	-	-	-	-	-	* 103,985	104,080	0.1
I₃₃	(lb - ft ²)	-	-	-	-	-	-	* 11,650	111,341	-0.3

*Properties for 1998 C1500 [NHTSA]

Figure 90. Comparison of properties for the test and analysis vehicle.

The vehicle model impacted the guardrail at 22 inches upstream of Post 14, traveling at a speed of 62.6 mph and at an angle of 24.3 degrees. Redirection began at 0.044 seconds. The vehicle contacted Post 15 at 0.085 – 0.090 seconds and tire contact with Post 15 occurred at 0.100 - 0.105 seconds. The front impact side tire assembly separated shortly after wheel impact with Post 15 from the vehicle at 0.124 seconds. The vehicle contacted Post 16 at 0.155 – 0.160 seconds and tire contact with Post 16 occurred at 0.190 – 0.195 seconds. The rear of the vehicle made contact with the guardrail at 0.190 – 0.195 seconds. The vehicle contacted Post 17 at 0.240 – 0.245 seconds. The vehicle was parallel to the guardrail at 0.256 seconds, traveling at 41.0 mph. The vehicle lost contact with the installation at 0.600 seconds, traveling at a speed of 37 mph and at an exit angle of 26 degrees. As the vehicle exited the rail, its roll angle was 30.3 degrees.

The analysis was terminated at 0.6 seconds, at which time:

- The roll angle of the vehicle was 30.3 degrees and increasing,

- The pitch angle was 9.1 degrees and decreasing,
- The yaw angle was 26.15 degrees relative to the barrier, and
- The forward velocity of the vehicle was 37.3 mph.

Damage to Test Installation

The installation received moderate damage as shown in Figure 91. None of the posts were broken in either simulation or the test but there was significant deflection of some of the posts as they were pushed back in the soil. The groundline deflections of the posts are shown in Table 29. The post displacements in the impact region in the simulation showed good correlation with the full-scale test; whereas the post deflections just outside the impact region were slightly lower in the analysis compared to the test measurements. Although it cannot be confirmed, it also appears from visual inspection that the posts in the full-scale test showed greater rotation angles compared to the simulation.

The W-Beam rail element was deformed from Posts 13 through 18 as shown in Figure 91. The maximum deformation of the guardrail during the simulated impact event was 27.2 inches between Posts 15 and 16, which correlates exactly to the rail deformation reported in the full-scale test. Overall, the simulated barrier response was essentially identical to that observed in the full-scale test.

Qualitative Validation

Sequential Views

A qualitative assessment was made by comparing sequential snapshots of the full-scale crash test with the results of the simulation to verify vehicle kinematic response as well as sequence and timing of key phenomenological events. The results from the FE analysis compare reasonably well with the results from full-scale crash test 471470-26. Figure 92, Figure 93 and Figure 94 show sequential snapshots of the impact event from an overhead viewpoint, a downstream viewpoint, and from an oblique (downstream and behind the barrier) viewpoint, respectively. The model appears to simulate the basic kinematic behavior of the pickup and adequately captures the basic phenomenological events that occur during impact. Table 2 provides a list of phenomenological events and their corresponding time of occurrence for both the full-scale test and the FE analysis.

Occupant Risk Measures

Acceleration-time histories and angular rate-time histories were collected from several locations in the model using the *Element-Seatbelt-Accelerometer option in LS-DYNA, which is the preferred method suggested by LS-DYNA for collecting acceleration data.[*LSDYNA13*] The accelerometers were connected to the vehicle model using *Nodal-Rigid-Body-Constraints (NRBs). The time-history data was collected from each accelerometer in a local reference coordinate system that was fixed to the vehicle with the x-direction coincident with the forward direction of the vehicle; which is consistent with the way the test data was collected from physical accelerometers. The data was collected at a frequency of 30 kHz which was determined to be sufficient to avoid aliasing of the data. The model was instrumented with eight accelerometers with one positioned near the center of gravity of the vehicle on the cabin floor, as identified in Figure 95.

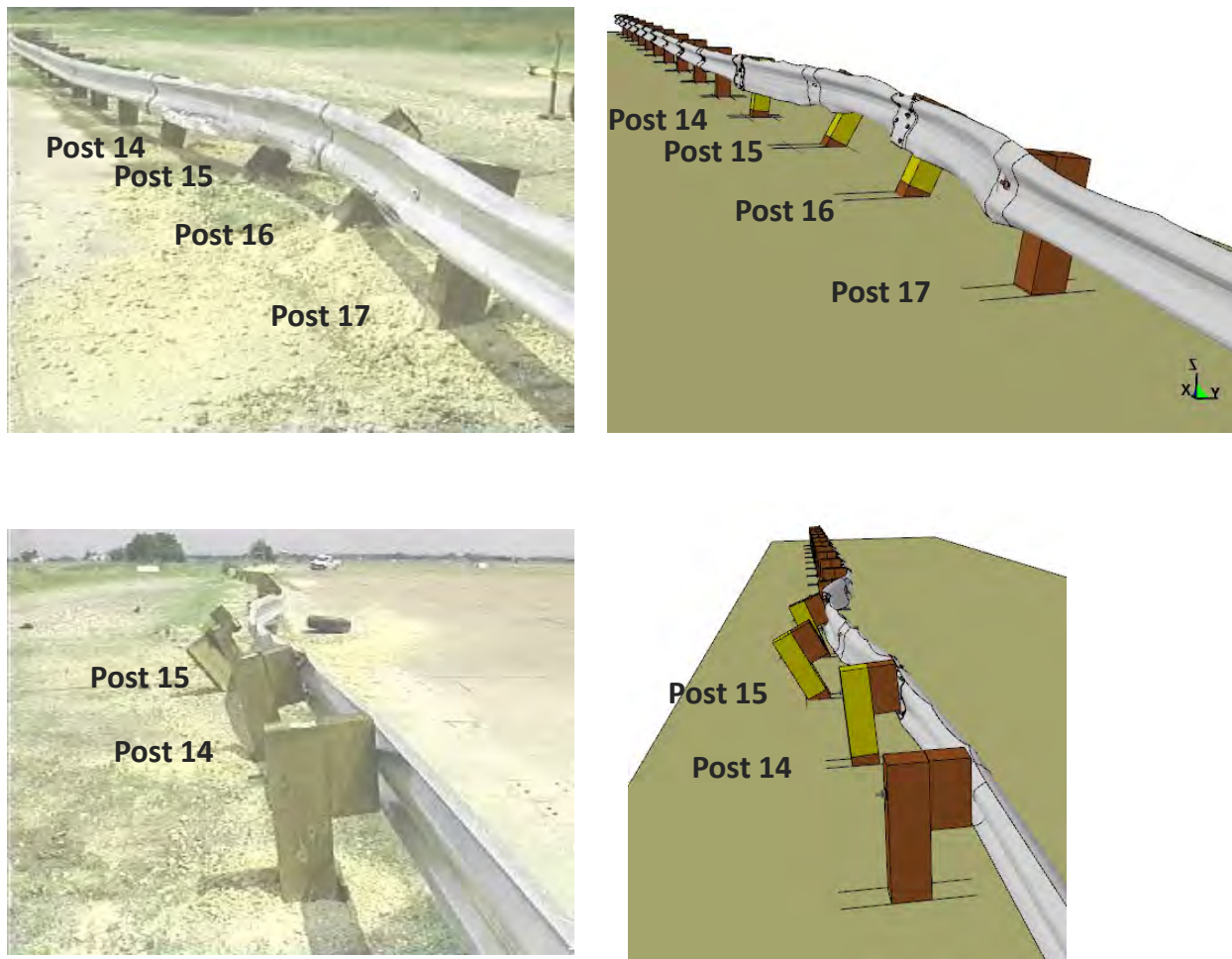


Figure 91. Comparison of G4(2W) guardrail after crash event for Test 471470-26 and FE analysis.

Table 29. Groundline deflections of posts for Test 471470-26 and FE analysis.

Post Number	Test 471470-26 (in)	FEA (in)
Post 13	2.0	0.5
Post 14	5.0	5.0
Post 15	13.0	13.0
Post 16	13.5	12.5
Post 17	4.75	4.0
Post 18	1.5	0.25
Post 19	0.25	0.00

The occupant risk assessment measures were computed using the three acceleration time-histories and the three angular-rate time histories collected at the center of gravity of the vehicle. The Test Risk Assessment Program (TRAP) calculates standardized occupant risk factors from vehicle crash data in accordance with the National Cooperative Highway Research Program (NCHRP) guidelines and the European Committee for Standardization (CEN). (TTI98)

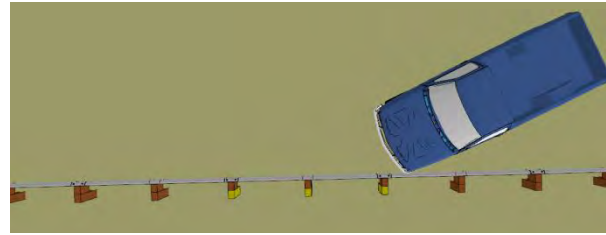
The analysis results obtained from TRAP for the full-scale test and the FE analysis are shown in Table 31. The acceleration data used in the TRAP program was filtered using the SAE Class 180 filter. The table shows the two occupant risk factors recommended by *NCHRP Report 350*: 1) the lateral and longitudinal components of Occupant Impact Velocity (OIV) and 2) the maximum lateral and longitudinal component of resultant vehicle acceleration averaged over 10 millisecond interval after occupant impact called the Occupant Ridedown Acceleration (ORA). Also provided in the table are the CEN risk factors: the Theoretical Head Impact Velocity (THIV), the Post Impact Head Deceleration (PHD) and the Acceleration Severity Index (ASI).

The results indicate that the occupant risk factors for both the full-scale test and the simulation are similar. The occupant impact velocity in the longitudinal direction was predicted from the simulation to be 5.3-m/s (15 percent higher than the test OIV of 4.6 m/s) at 0.1442 seconds. In the transverse direction, the occupant impact velocity predicted in the simulation was 5.8-m/s (same as test OIV). The highest 0.010-second occupant ridedown acceleration in the longitudinal direction was 10.2 g (11.3 percent lower than test ORA of 11.5 g) between 0.1791 and 0.1891 seconds. In the transverse direction, the highest 0.010-second occupant ridedown acceleration was 11.1 (0.9 percent lower than test ORA of 11.2) between 0.2152 and 0.2248 seconds. The THIV, PHD and ASI predicted from the simulation were 7.4 m/s (7.3 percent higher), 13.6 g's (16 percent higher), and 0.99 (2 percent higher), respectively. With the exception of the PHD, both the test and the simulation values agree within ± 15 percent.

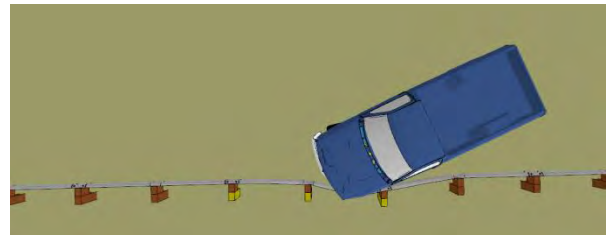
The most notable differences between the analysis and the test were the angular displacements of the vehicle. The increased pitch of the vehicle in the analysis allowed the rear bumper to pass over the top of the rail. Refer to Figure 94 starting at time 0.241 seconds. This event resulted in an increased yaw angle of the vehicle during redirection in the analysis and was likely caused by too high of friction between the vehicle and barrier.

Time-History Data Comparison

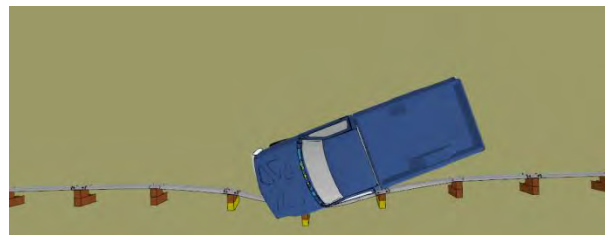
Figure 96, Figure 97, and Figure 98 show a comparison of the 10-millisecond moving average and the 50-millisecond moving average acceleration-time history at the c.g. of the pickup (i.e., longitudinal, transverse and vertical channels, respectively) for the test and FE analysis. Figure 99, Figure 100, and Figure 101 show comparisons of the yaw, roll, and pitch rates and displacements at the c.g. of the pickup for the test and FE analysis. Values for the quantitative evaluation metrics are also shown on the time-history plots. These quantities were computed from the raw acceleration data and are shown with these plots only for reference. The values in red font indicate poor correlation between test and analysis results, while the values in black font indicate good correlation. The quantitative metrics are discussed in more detail in the Quantitative Evaluation section of this chapter.



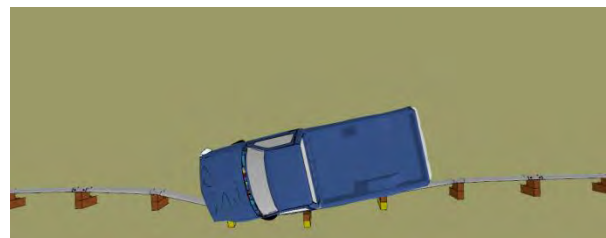
0.000 seconds



0.061 seconds



0.119 seconds



0.180 seconds

Figure 92. Sequential views of TTI Test 471470-26 and FE analysis from overhead viewpoint.

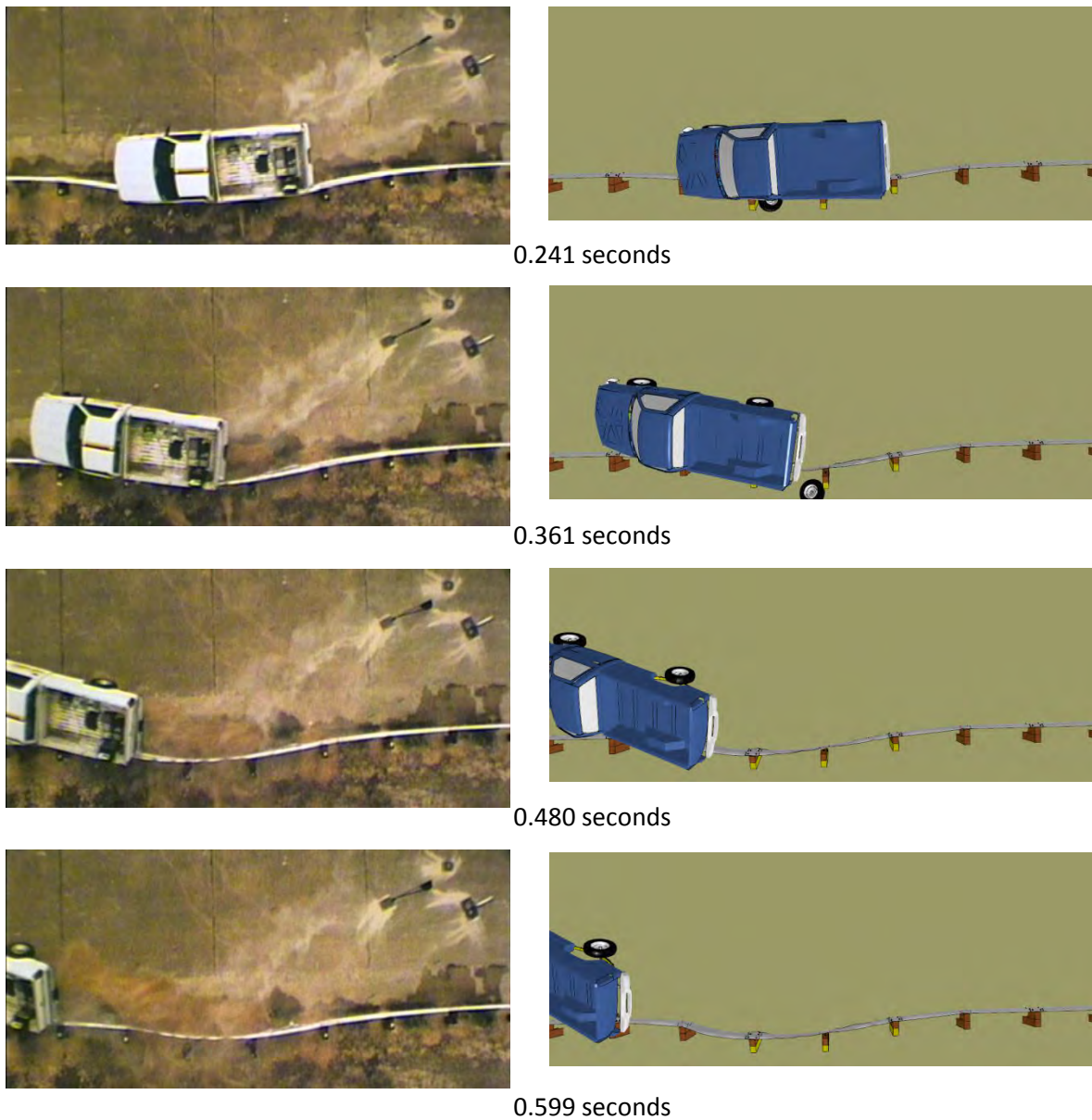


Figure 92. [CONTINUED] Sequential views of TTI Test 471470-26 and FE analysis from overhead viewpoint.

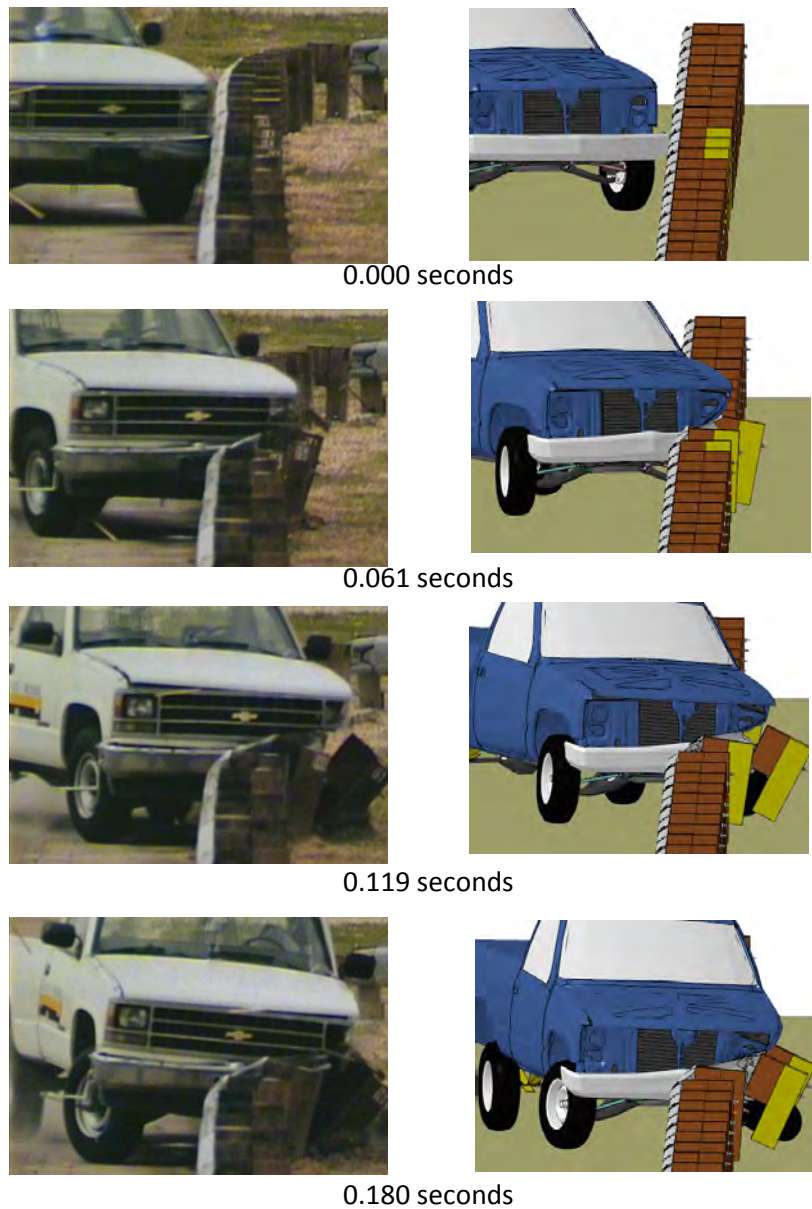


Figure 93. Sequential views of TTI Test 471470-26 and FE analysis from downstream viewpoint.

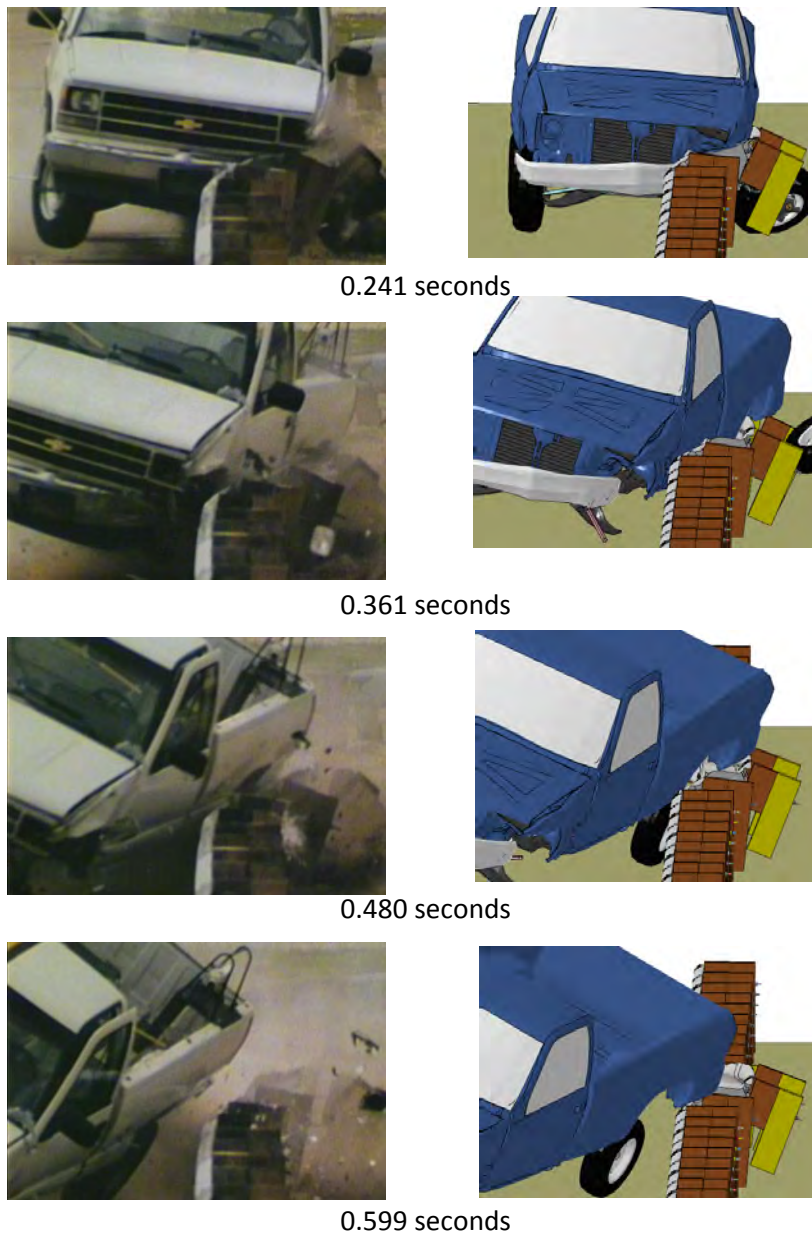


Figure 93. [CONTINUED] Sequential views of TTI Test 471470-26 and FE analysis from downstream viewpoint.

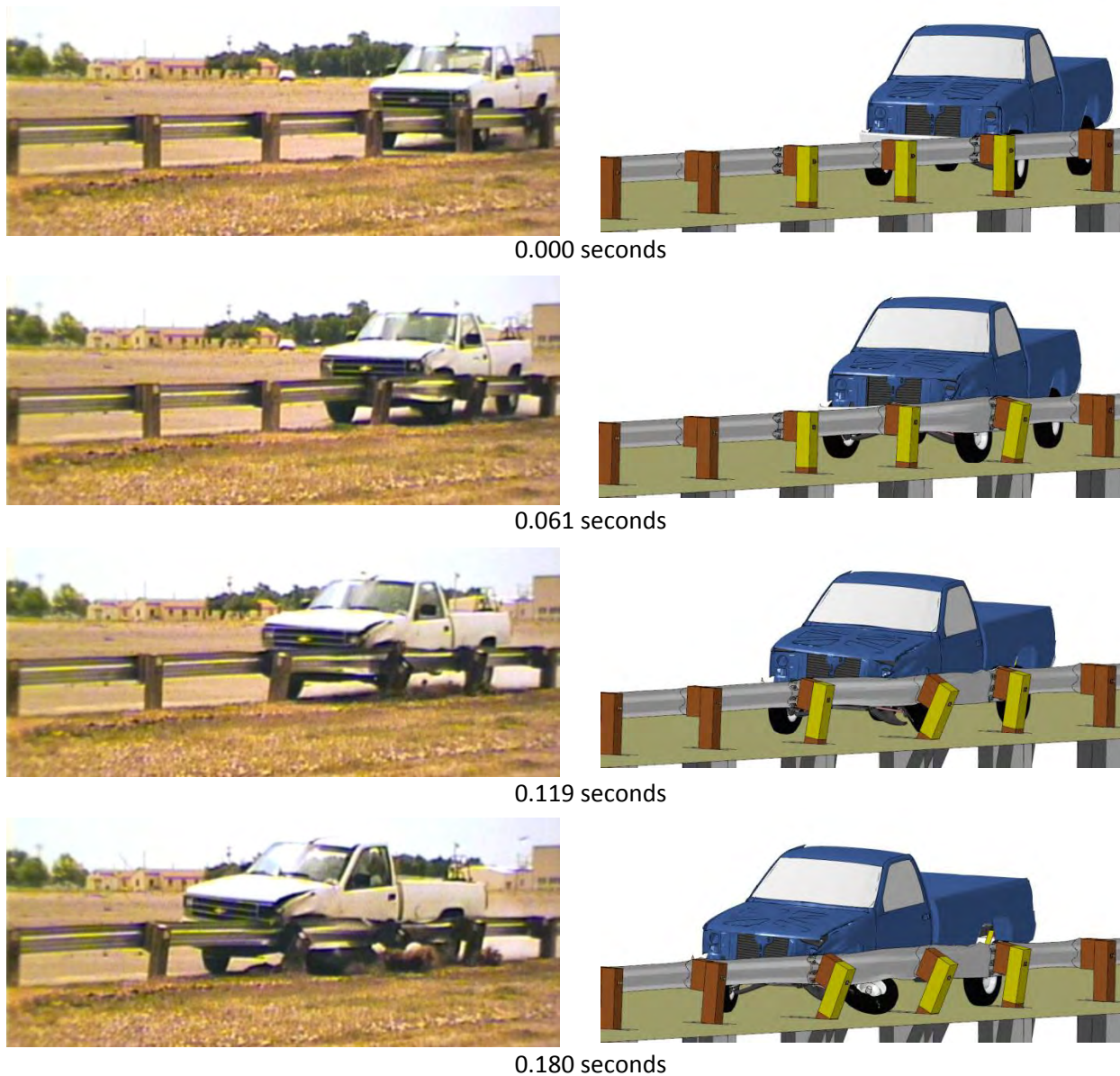


Figure 94. Sequential views of TTI Test 471470-26 and FE analysis from an oblique viewpoint behind the system.

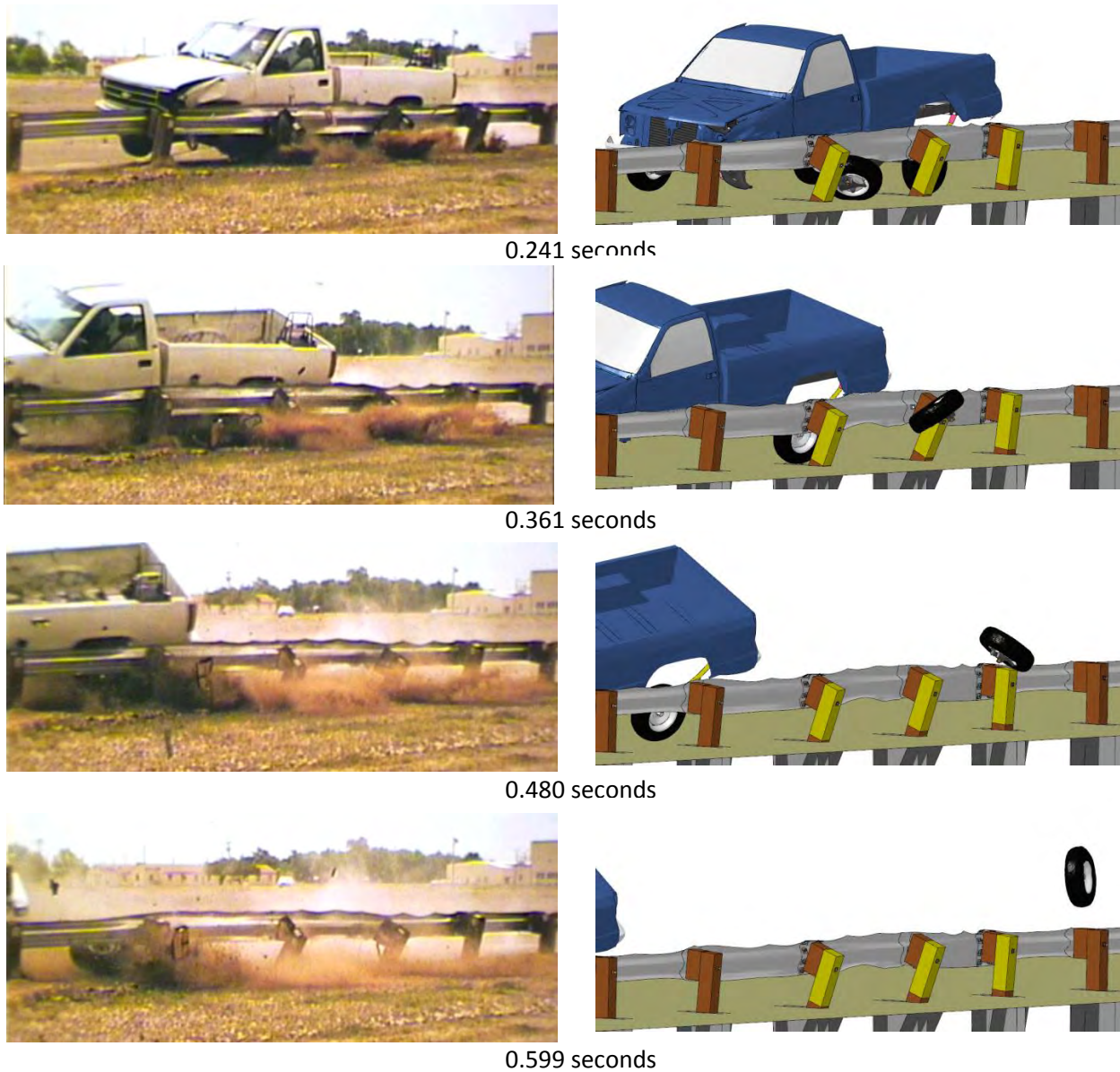


Figure 94. [CONTINUED] Sequential views of TTI Test 471470-26 and FE analysis from an oblique viewpoint behind the system.

Table 30. Summary of phenomenological events of full-scale test 471470-26 and FEA simulation.

Event	Test 471470-26	FE Analysis
Start of redirection	0.056 sec	0.044 sec
Vehicle contact with Post 15	0.086 sec	0.085 - 0.090 sec
Tire contact with Post 15	0.104 sec	0.100 – 0.105 sec
Wheel assembly separated	0.104 – 0.193 sec	0.124 seconds
Vehicle contacts Post 16	0.157 sec	0.155 – 0.160 sec
Tire contact with Post 16	0.193 sec	0.190 – 0.195 sec
Rear of vehicle contacts rail	0.203 sec	0.190 – 0.195 sec
Vehicle contact with Post 17	0.236 sec	0.240 – 0.245 sec
Vehicle parallel with guardrail	0.249 sec	0.256 sec
Speed at parallel	46.3 mph (74.5 km/h)	41.0 mph (66.0 km/h)
Vehicle contact with Post 18	0.356 sec	N.A.
Maximum deflection of guardrail	27.2 in (691 mm)	27.2 in (691 mm)
Vehicle loses contact with guardrail	0.513 sec	0.600 sec
Speed at exit	44.0 mph (70.8 km/h)	37.3 mph (60.0 km/h)
Angle at exit	8.1 deg	26.0 deg
Roll angle at exit	25 deg	30.3 deg
Maximum roll angle	39 deg @ 0.709 s	N.A.
Total contact length	22.7 ft (6.92 m)	25.1 ft (7.65 m)

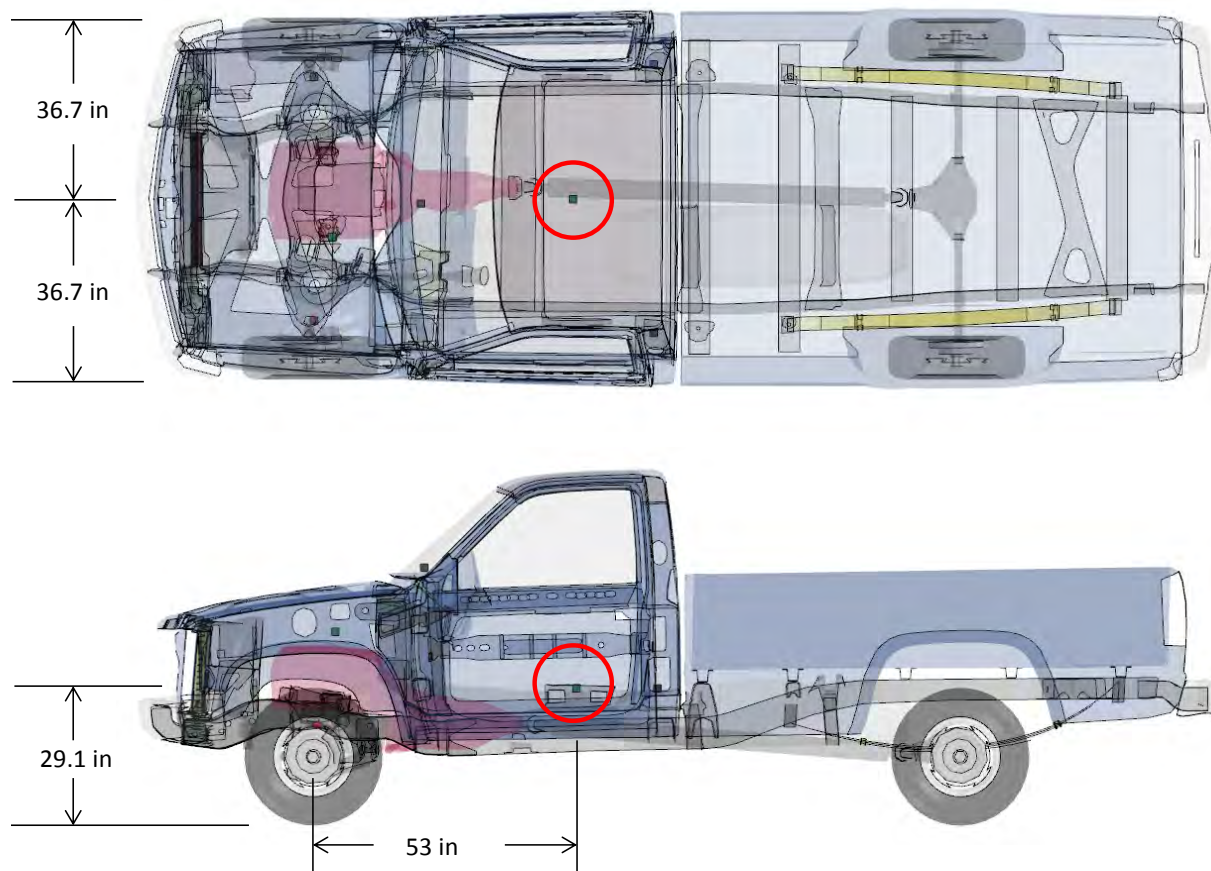


Figure 95. Location of accelerometer in FE model.

Table 31. Summary of occupant risk measures computed from Test 471470-26 and FEA simulation.

Event	Test 471470-26	FE Analysis
Start of redirection	0.056 sec	0.044 sec
Vehicle contact with Post 15	0.086 sec	0.085 - 0.090 sec
Tire contact with Post 15	0.104 sec	0.100 – 0.105 sec
Wheel assembly separated	0.104 – 0.193 sec	0.124 seconds
Vehicle contacts Post 16	0.157 sec	0.155 – 0.160 sec
Tire contact with Post 16	0.193 sec	0.190 – 0.195 sec
Rear of vehicle contacts rail	0.203 sec	0.190 – 0.195 sec
Vehicle contact with Post 17	0.236 sec	0.240 – 0.245 sec
Vehicle parallel with guardrail	0.249 sec	0.256 sec
Speed at parallel	46.3 mph (74.5 km/h)	41.0 mph (66.0 km/h)
Vehicle contact with Post 18	0.356 sec	N.A.
Maximum deflection of guardrail	27.2 in (691 mm)	27.2 in (691 mm)
Vehicle loses contact with guardrail	0.513 sec	0.600 sec
Speed at exit	44 mph (70.8 km/h)	37.3 mph (60.0 km/h)
Angle at exit	8.1 deg	26.0 deg
Roll angle at exit	25 deg	30.3 deg
Maximum roll angle	39 deg @ 0.709 s	N.A.
Total contact length	22.7 ft (6.92 m)	25.1 ft (7.65 m)

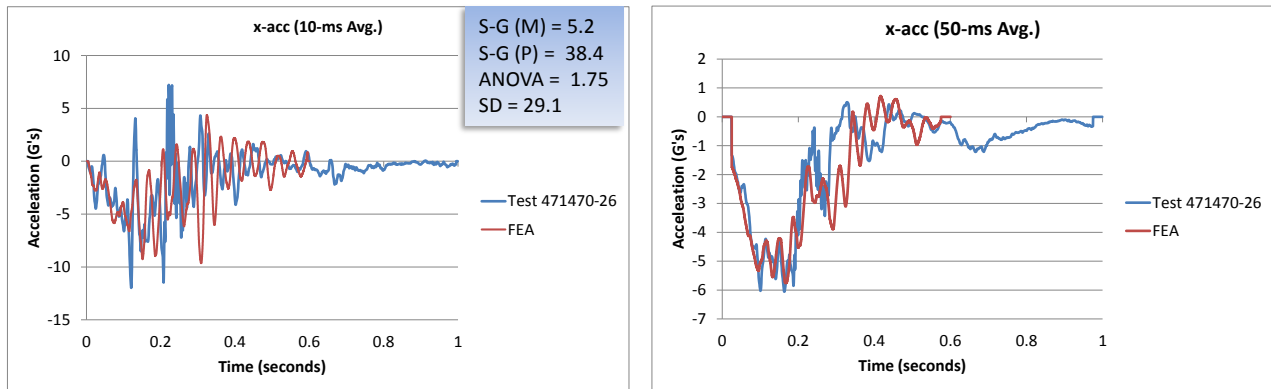


Figure 96. Longitudinal acceleration-time history plot from accelerometer at c.g. for full-scale Test 471470-26 and FEA (10-ms and 50-ms moving averages).

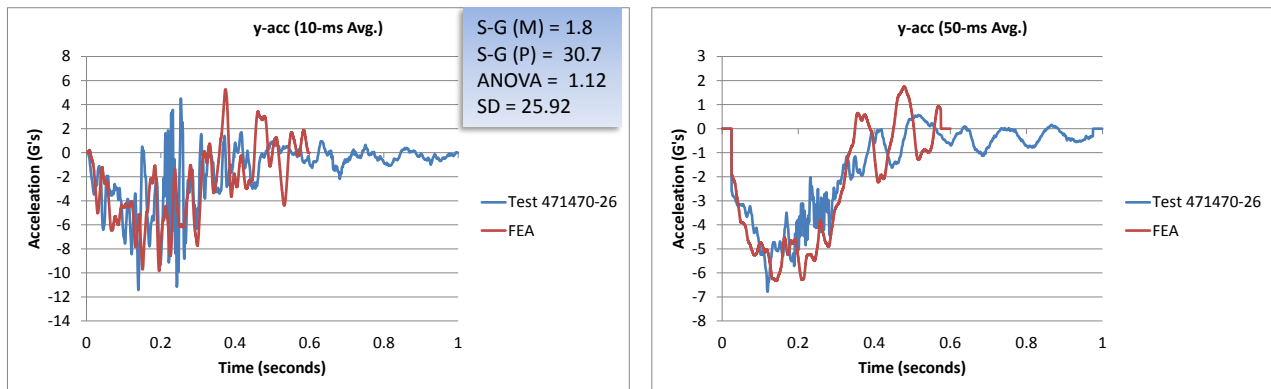


Figure 97. Lateral acceleration-time history plot from accelerometer at c.g. for full-scale Test 471470-26 and FEA (10-ms and 50-ms moving averages).

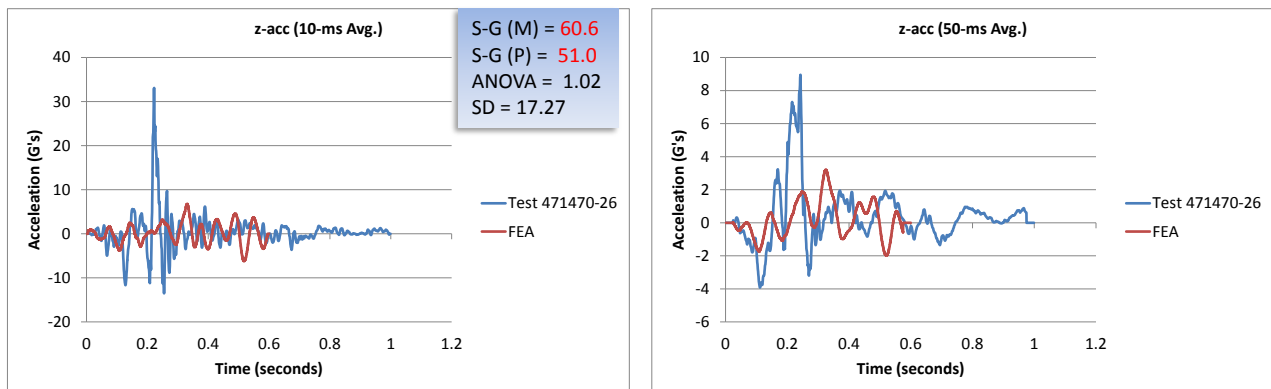


Figure 98. Vertical acceleration-time history plot from accelerometer at c.g. for full-scale Test 471470-26 and FEA (10-ms and 50-ms moving averages).

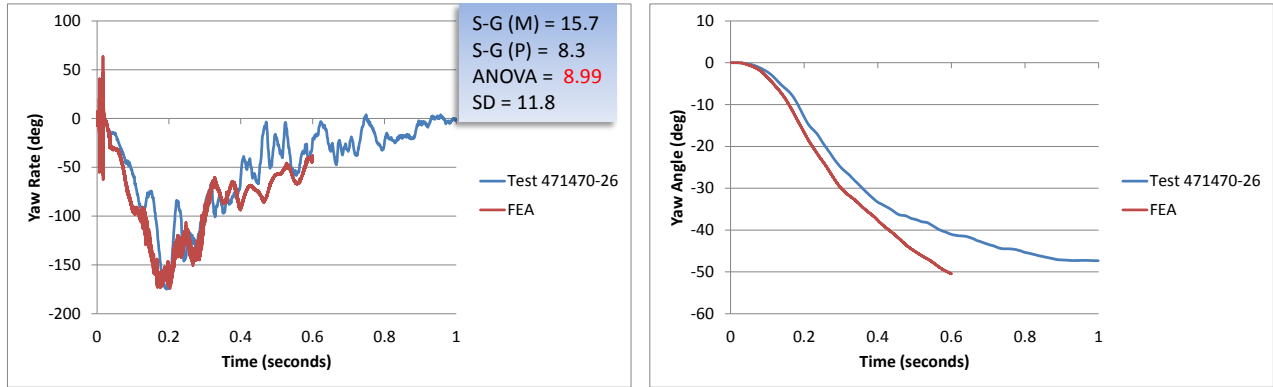


Figure 99. Yaw-time history plot from accelerometer at c.g. for full-scale test 471470-26 and FEA (angular rate and displacement).

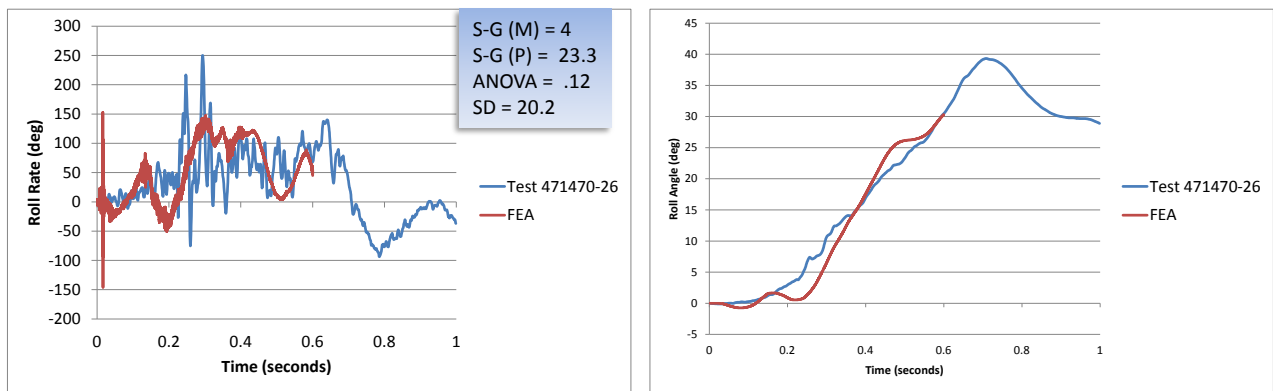


Figure 100. Roll-time history plot from accelerometer at c.g. for full-scale test 471470-26 and FEA (angular rate and displacement).

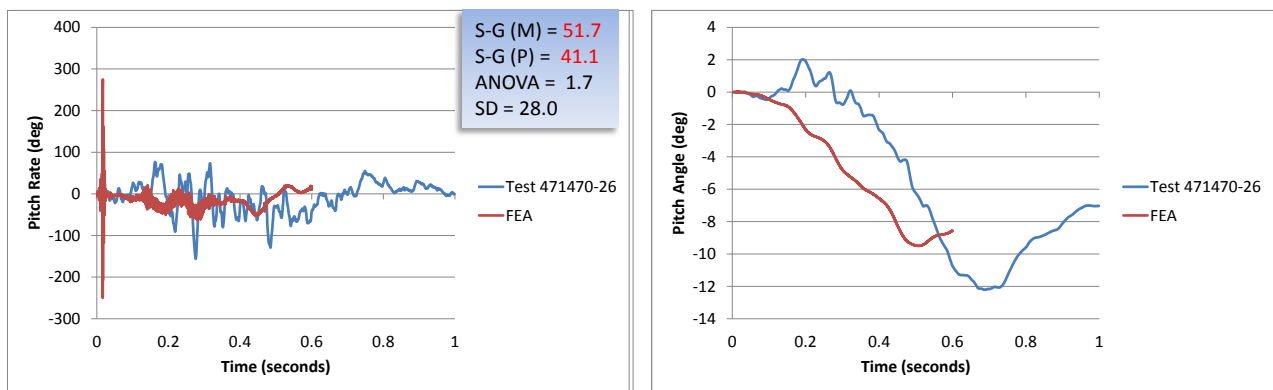


Figure 101. Pitch-time history plot from accelerometer at c.g. for full-scale test 471470-26 and FEA (angular rate and displacement).

Summary

The intent of this qualitative evaluation was to verify overall model response through a general comparison with a full-scale crash test. The general response of the FE model seemed reasonable in that the model provided the basic chain of phenomenological events that occurred in the full-scale crash test. The occupant risk measures computed from the time-history data collected at the c.g. of the vehicle also correlated reasonably well with the test data. As mentioned earlier, the higher pitch of the vehicle in the analysis in turn caused error in the yaw angle. The pitch angle was only 4 degrees higher in the analysis, but this was enough to allow the bumper to pass over the top of the rail. It was theorized that the increased pitch may have been a result of too high of friction forces between the vehicle and guardrail.

Quantitative Validation

The quantitative validation assessment of the model's results was based on validation procedures of NCHRP Web Document 179 (W179). [Ray10] The purpose of these guidelines is to establish accuracy, credibility, and confidence in the results of crash test simulations that are intended to support policy decisions, and to be used for approval of design modifications to roadside safety devices that were originally approved with full-scale crash testing.

The validation procedure has three steps:

1. Solution verification: Indicates whether the analysis solution produced numerically stable results (ensures that basic physical laws are upheld in the model).
2. Time-history evaluation: Quantitative measure of the level of agreement of time-history data (e.g., x, y, z accelerations and roll, pitch, and yaw rates) between the analysis and test.
3. Phenomena Importance Ranking Table (PIRT): A table that documents the types of phenomena that a numerical model is intended to replicate and verifies that the model produces results consistent with its intended use.

The PIRTs for the individual components were presented earlier in the "Calibration/Validation of Guardrail Components" section of this report. The following is a discussion of the time-history evaluation metrics, their acceptance criteria, and the Phenomena Importance Ranking Table (PIRT) for crash simulation.

Time-History Evaluation

The RSVVP (Roadside Safety Verification and Validation Program) software, which was developed as part of NCHRP Project 22-24, was used to compute the comparison metrics between analysis and full-scale test data. RSVVP computes fifteen different metrics that quantify the differences between a pair of curves. Since many of the metrics share similar formulations, their results are often identical or very similar. Because of this, it is not necessary to include all of the variations. The metrics recommended in Report W179 for comparing time-history traces from full-scale crash tests and/or simulations of crash tests are the Sprague & Geers metrics and the ANOVA metrics. The Sprague-Geers metrics assess the magnitude and phase of two curves while the ANOVA examines the differences of residual errors between them. The definitions of these metrics are shown below:

Sprague & Geers:

$$\text{Magnitude } (M) = \sqrt{\frac{\sum c_i^2}{\sum m_i^2} - 1}$$

$$\text{Phase } (P) = \frac{1}{\pi} \cos^{-1} \frac{\sum c_i m_i}{\sqrt{\sum c_i^2 \sum m_i^2}}$$

$$\text{Comprehensive } (C) = \sqrt{M^2 + P^2}$$

ANOVA:

$$\text{Residual Error } (\bar{e}^r) = \frac{\sum (m_i - c_i)}{m_{\max}} \cdot \frac{1}{n}$$

$$\text{Standard Deviation } (\sigma) = \sqrt{\frac{1}{n} \sum (m_i - c_i - \bar{e}^r)^2}$$

Where,

c_i = calculated quantities

m_i = measured quantities

m_{\max} = maximum measured experimental value

\bar{e}^r = relative average residual error

σ = relative standard deviation

Time-History Evaluation Acceptance Criteria

Once a measure of comparison is obtained using a quantitative metric, it is necessary to establish an acceptance criterion for deciding if the comparison is acceptable. Because of the highly nonlinear nature of crash events, there are often considerable differences in the results of essentially identical full-scale crash tests – this was demonstrated in the W179 report. Likewise, a computational model may not match “exactly” the results of a physical test, but the difference should be no greater than what is expected between physical tests. The approach taken in the W179 was to determine the realistic variation in the deterministic shape comparison metrics for a set of identical physical experiments and use that variation as an acceptance criterion. The current acceptance criteria is based on the results of a quantitative comparison of ten essentially identical full-scale crash tests that were performed as part of the ROBUST project involving small car impact into a vertical rigid wall at 100 km/hr and 25 degrees.[*ROBUST02; Ray08*] The resulting acceptance criteria recommended by W179 for assessing the similarity of two time-history curves are:

- Sprague-Geers
 - Magnitude should be less than 40 percent

- Phase should be less than 40 percent
- ANOVA metrics
 - Mean residual error should be less than 5 percent
 - Standard deviation should be less than 35 percent.

Phenomena Importance Ranking Tables (PIRT)

The PIRT includes evaluation criteria corresponding to *NCHRP Report 350* for TL-3 impacts and is patterned after the full-scale crash test evaluation criteria listed in Table 5.1 in *NCHRP Report 350*. [Ross93] The values for the individual metrics from the full-scale test and the computer analysis were reported and both the relative difference and absolute difference for each phenomenon were computed. If the relative difference is less than 20 percent or if the absolute difference is less than 20 percent of the acceptance limit in *NCHRP Report 350*, then the phenomena are considered to be replicated.

Results

The quantitative evaluation was based on comparison of acceleration-time histories and angular rate-time histories computed in the analysis to those measured in full-scale crash test 471470-26. The impact conditions for the simulation matched exactly those from the full-scale test (i.e., a 4572-lb pickup impacting the guardrail system at 62.6 mph (100.7 km/hr) at an angle of 24.3 degrees, at an impact point 2 ft (0.61 m) upstream of Post 14 in the guardrail system). These impact conditions correspond to *NCHRP Report 350* Test 3-11. A summary of the quantitative comparison results are provided herein. Additional comparison data can be found in Appendix C.

Solution Verification

The first step in the validation process is to perform global checks of the analysis to verify that the numerical solution is stable and is producing physical results (e.g., results conform to the basic laws of conservation). The analysis was modeled as a closed system, which means that energy is not being added or removed during the analysis. Thus, the total energy should remain constant throughout the analysis and should be equal to the initial kinetic energy of the impacting vehicle. The one exception in this case is any kinetic energy generated due to the gravity load (which should be minimal during the short time period of the crash event relative to the initial kinetic energy of the vehicle). Table 32 shows a summary of the global verification assessment based on criteria recommended in Report W179. Figure 102 shows a plot of the global energy-time histories from the analysis.

As shown in Table 32, all the solution verification parameters were satisfied except; for the hour glass energies in the truck model. The largest hourglass energies came from the frame rail of the pickup. The hourglass modes on the frame rail may have influenced the kinematics of the vehicle to some degree, but it is not likely that the error would have a significant influence on the overall results since the deformations and associated internal energies of the pickup are small compared to those of the guardrail system. Upon review of the truck model materials, the frame rail and many other components of the pickup model are modeled with under-integrated elements with no hourglass control. These were corrected prior to subsequent use of the model in this study.

Table 32. Analysis solution verification table.

Verification Evaluation Criteria	Change (%)	Pass?
<i>Total energy</i> of the analysis solution (i.e., kinetic, potential, contact, etc.) must not vary more than 10 percent from the beginning of the run to the end of the run.	5%	Y
<i>Hourglass Energy</i> of the analysis solution at the end of the run is less than <i>five percent</i> of the total <i>initial energy</i> at the <i>beginning</i> of the run.	5.2%	N
<i>Hourglass Energy</i> of the analysis solution at the end of the run is less than <i>ten percent</i> of the total <i>internal energy</i> at the <i>end</i> of the run.	9.7%	Y
The part/material with the highest amount of hourglass energy at the end of the run is less than ten percent of the total internal energy of the part/material at the end of the run.	Blockout (9.7%) Truck Frame (50%)	N
Mass added to the total model is less than five percent of the total model mass at the beginning of the run.	39 lb	Y
The part/material with the most mass added had less than 10 percent of its initial mass added.		Y
The moving parts/materials in the model have less than five percent of mass added to the initial moving mass of the model.	0.3%	Y
There are no shooting nodes in the solution?	Y	Y
There are no solid elements with negative volumes?	Y	Y

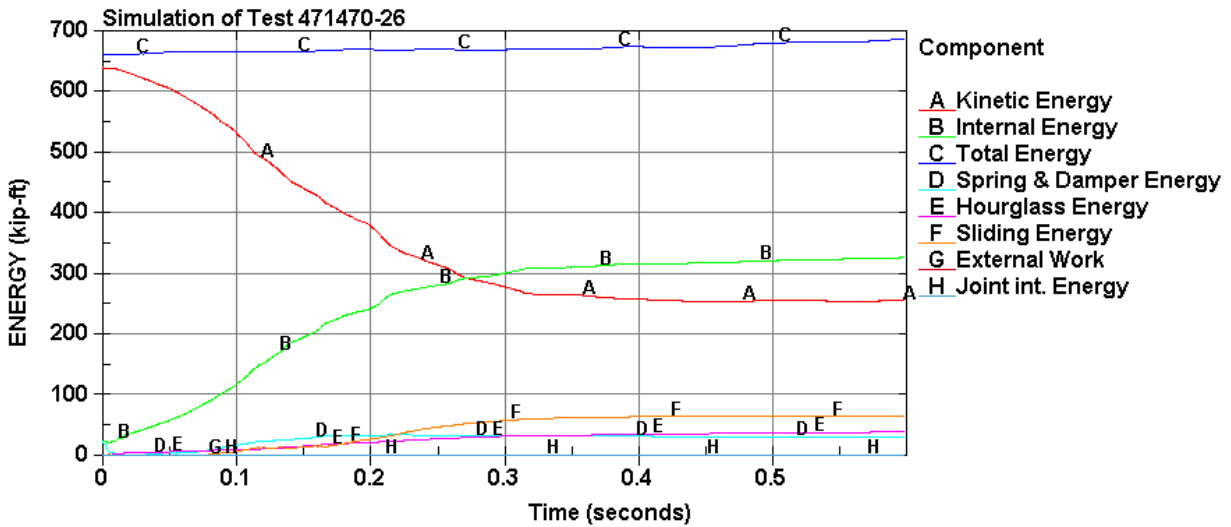


Figure 102. Plot of global energy-time histories from the analysis.

Time-History Validation

The RSVVP computer program was used to compute the Sprague-Geer metrics and ANOVA metrics using time-history data from the full-scale test (i.e., true curve) and analysis data (i.e., test curve). The multi-channel option in RSVVP was used since this option computes metrics for each individual channel as well as for the weighted composite of the combined channels. The data from each of the six data channels, which were located at the center of gravity of the vehicle, were input into RSVVP. These data included the x-acceleration, y-acceleration, z-acceleration, roll-rate, pitch-rate and yaw-rate. From Report W179 it was recommended that the raw data be used as input into the program. The data was then filtered in RSVVP using a CFC Class 60 filter. The shift and drift options in RSVVP were not used for the physical test data. From visual inspection, the physical test data appeared to show no initial offset of acceleration magnitude or drift. Since both the test and analysis data started at the time of impact with the barrier the synchronization of curves was determined to be unnecessary.

The default metrics evaluation options in RSVVP were used, which included the Sprague & Geers and the ANOVA metrics, as shown in Figure 103. The curves were evaluated over 0.6 seconds of the impact event, corresponding to the termination time of the analysis.

Metric profile: NCHRP 22-24 (suggested)

Metrics

MPC metrics

- Geers
- Geers CSA
- Sprague & Geers
- Russell
- Knowles & Gear

Single-value metrics

- Whang's inequality
- Theil's inequality
- Ziliacus error
- RSS error
- Weighted Integrated Factor
- Regression coefficient
- Correlation Coefficient
- Correlation Coefficient (NARD)

ANOVA metric

- Average & Stand. deviation

Figure 103. RSVVP metric selection for validation assessment.

Based on the validation metrics, a comparison of the individual components of acceleration indicated that the simulation was in good agreement for the x- and y-channels of acceleration, and for the roll-rate channel as well. The yaw-rate channel and the pitch-rate channel showed mixed results, while the z-acceleration channel showed poor correlation. The results are shown in Table 33 and are summarized below:

Sprague-Geers Metrics

- The Sprague-Geers metrics for the x-acceleration were good regarding both magnitude (i.e., $M=1.3\%$) and phase (i.e., $P=33.7\%$), which indicates that the simulation is in agreement with the test.

- The Sprague-Geers metrics for the y-acceleration were good regarding both magnitude (i.e., M=6.0%) and phase (i.e., P=31.7%), which indicates that the simulation is in agreement with the test.
- The Sprague-Geers metrics for the z-acceleration were poor for both magnitude (i.e., M=59.6%) and phase (i.e., P=51.1%), which indicates that the simulation is *not* in agreement with the test for this channel.
- The Sprague-Geers metrics for the yaw-rate were good regarding both magnitude (i.e., M=15.7%) and phase (i.e., P=8.3%), which indicates that the simulation is in agreement with the test.
- The Sprague-Geers metrics for the roll-rate were good regarding both magnitude (i.e., M=4%) and phase (i.e., P=23.3%), which indicates that the simulation is in agreement with the test.
- The Sprague-Geers metrics for the pitch-rate were poor for magnitude (i.e., M=51.7%) and phase (i.e., P=41.1%), which indicates that the simulation is in not agreement with the test.

ANOVA

- The ANOVA metrics for the x-acceleration were good regarding both the mean residual error (i.e., 1.42%) and the standard deviation of residual error (i.e., 26.4%), which indicated that the simulation is in agreement with the test.
- The ANOVA metrics for the y-acceleration were good regarding both the mean residual error (i.e., 1.29%) and the standard deviation of residual error (i.e., 27.3%), which indicated that the simulation is in agreement with the test.
- The ANOVA metrics for the z-acceleration were good regarding both the mean residual error (i.e., 0.92%) and the standard deviation of residual error (i.e., 17.4%), which indicated that the simulation is in agreement with the test.
- The ANOVA metrics for the yaw-rate were poor for the mean residual error (i.e., 8.99%) but good regarding the standard deviation of residual error (i.e., 11.8%).
- The ANOVA metrics for the roll-rate were good regarding both the mean residual error (i.e., 0.12%) and the standard deviation of residual error (i.e., 20.2%), which indicated that the simulation is in agreement with the test.
- The ANOVA metrics for the pitch-rate were good regarding both the mean residual error (i.e., 1.7%) and the standard deviation of residual error (i.e., 28.3%), which indicated that the simulation is in agreement with the test.

Since the metrics computed for the individual data channels did not all satisfy the acceptance criteria, the multi-channel option in RSVVP was used to calculate the weighted Sprague-Geer and ANOVA metrics for the six channels of data. The Area II method is the default method used in RSVVP for weighting the importance of each data channel. The Area (II) method determines the *weight* for each channel based on a pseudo momentum approach using the area under the curves.

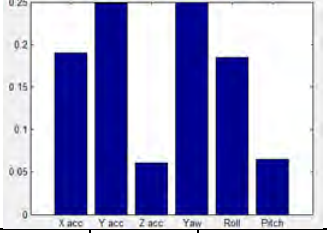
Table 34 shows the results from RSVVP for the multi-channel option using the Area (II) method. The resulting weight factors computed for each channel are shown in both tabular form and graphical form in the tables. The results indicate that the x-, y-, yaw rate-, and roll-rate channels dominate the kinematics of the impact event. Which implies that the velocity change in the z-direction was insignificant compared to the change in velocity in the x- and y-directions.

Similarly, the pitch angle magnitude was comparatively less than that for the yaw and roll channels (refer to Figure 99, Figure 100 and Figure 101). The weighted metrics computed in RSVVP in the multi-channel mode all satisfy the acceptance criteria; therefore, the time history comparison can be considered acceptable.

Table 33. Roadside safety validation metrics rating table – time history comparison (single-channel option).

Evaluation Criteria							Time interval [0.00 – 0.6 sec]		
<i>Sprague-Geers Metrics</i> List all the data channels being compared. Calculate the M and P metrics using RSVVP and enter the results. Values less than or equal to 40 are acceptable.									
	RSVVP Curve Preprocessing Options						M	P	Pass?
	Filter Option	Sync. Option	Shift		Drift				
			True Curve	Test Curve	True Curve	Test Curve			
X acceleration	CFC 60	none	none	none	none	none	1.3	33.7	Y
Y acceleration	CFC 60	none	none	none	none	none	6.0	31.7	Y
Z acceleration	CFC 60	none	none	none	none	none	59.6	51.1	N
Roll rate	CFC 60	none	none	none	none	none	4	23.3	Y
Pitch rate	CFC 60	none	none	none	none	none	51.7	41.1	N
Yaw rate	CFC 60	none	none	none	none	none	15.7	8.3	Y
P	<i>ANOVA Metrics</i> List all the data channels being compared. Calculate the ANOVA metrics using RSVVP and enter the results. Both of the following criteria must be met: <ul style="list-style-type: none"> The mean residual error must be less than five percent of the peak acceleration ($\bar{e} \leq 0.05 \cdot a_{Peak}$) and The standard deviation of the residuals must be less than 35 percent of the peak acceleration ($\sigma \leq 0.35 \cdot a_{Peak}$) 						Mean Residual	Standard Deviation of Residuals	Pass?
X acceleration/Peak									
Y acceleration/Peak							1.29	27.3	Y
Z acceleration/Peak							0.92	17.4	Y
Roll rate							0.12	20.2	Y
Pitch rate							1.7	28.0	Y
Yaw rate							9.0	11.83	N

Table 34. Roadside safety validation metrics rating table – (multi-channel option).

Evaluation Criteria (time interval [0.0 – 0.6 seconds])				
Channels (Select which were used)				
<input type="checkbox"/> X Acceleration	<input type="checkbox"/> Y Acceleration	<input type="checkbox"/> Z Acceleration		
<input type="checkbox"/> Roll rate	<input type="checkbox"/> Pitch rate	<input type="checkbox"/> Yaw rate		
Multi-Channel Weights - Area II method -	X Channel: 0.190 Y Channel: 0.249 Z Channel: 0.061 Yaw Channel: 0.249 Roll Channel: 0.185 Pitch Channel: 0.065			
	<i>Sprague-Geer Metrics</i> Values less or equal to 40 are acceptable.		M	P
		13.4	26.5	Pass?
				Y
<i>ANOVA Metrics</i> Both of the following criteria must be met: <ul style="list-style-type: none"> The mean residual error must be less than five percent of the peak acceleration $(\bar{e} \leq 0.05 \cdot a_{Peak})$ The standard deviation of the residuals must be less than 35 percent of the peak acceleration ($\sigma \leq 0.35 \cdot a_{Peak}$) 		Mean Residual	Standard Deviation of Residuals	Pass?
		2.8	21.4	Y

PIRT – Crash Specific Phenomena

The last step in the validation procedure was to compare the phenomena observed in both the crash test and the numerical solution. Table 35 contains the Report 350 crash test criteria with the applicable test numbers. The criteria that apply to Test 3-11 (i.e., corresponding to this particular test case) are marked with a red square. These include criteria A, D, F, L and M. Table 36 through Table 38 contain an expanded list of these same criteria including additional specific phenomena that were measured in the test and that could be directly compared to the numerical solution. Table 36 contains a comparison of phenomena related to structural adequacy, Table 37 contains a comparison of phenomena related to occupant risk, and Table 38 contains a comparison of phenomena related to vehicle trajectory.

Table 35. Report 350 crash test criteria with the applicable test numbers.

Evaluation Factors	Evaluation Criteria			Applicable Tests	
• Structural Adequacy	A	Test article should contain and redirect the vehicle; the vehicle should not penetrate, under-ride, or override the installation although controlled lateral deflection of the test article is acceptable.		10, 11, 12, 20, 21, 22, 35, 36, 37, 38	
	B	The test article should readily activate in a predictable manner by breaking away, fracturing or yielding.		60, 61, 70, 71, 80, 81	
	C	Acceptable test article performance may be by redirection, controlled penetration or controlled stopping of the vehicle.		30, 31,, 32, 33, 34, 39, 40, 41, 42, 43, 44, 50, 51, 52, 53	
Occupant Risk	D	Detached elements, fragments or other debris from the test article should not penetrate or show potential for penetrating the occupant compartment, or present an undue hazard to other traffic, pedestrians or personnel in a work zone.		All	
	E	Detached elements, fragments or other debris from the test article, or vehicular damage should not block the driver's vision or otherwise cause the driver to lose control of the vehicle. (Answer Yes or No)		70, 71	
	F	The vehicle should remain upright during and after the collision although moderate roll, pitching and yawing are acceptable.		All except those listed in criterion G	
	G	It is preferable, although not essential, that the vehicle remain upright during and after collision.		12, 22 (for test level 1 – 30, 31, 32, 33, 34, 35, 36, 37, 38, 39, 40, 41, 42, 43, 44)	
	H	Occupant impact velocities should satisfy the following:			10, 20, 30,31, 32, 33, 34, 36, 40, 41, 42, 43, 50, 51, 52, 53, 80, 81
		Occupant Impact Velocity Limits (m/s)			
Component		Preferred	Maximum		
Longitudinal and Lateral	9	12			
Longitudinal	3	5	60, 61, 70, 71		
I	Occupant ridedown accelerations should satisfy the following:			10, 20, 30,31, 32, 33, 34, 36, 40, 41, 42, 43, 50, 51, 52, 53, 60, 61, 70, 71, 80, 81	
	Occupant Ridedown Acceleration Limits (g's)				
	Component	Preferred	Maximum		
Longitudinal and Lateral	15	20			
Vehicle Trajectory	L	The occupant impact velocity in the longitudinal direction should not exceed 40 ft/sec and the occupant ride-down acceleration in the longitudinal direction should not exceed 20 G's.		11,21, 35, 37, 38, 39	
	M	The exit angle from the test article preferable should be less than 60 percent of test impact angle, measured at the time of vehicle loss of contact with test device.		10, 11, 12, 20, 21, 22, 35, 36, 37, 38, 39	
	N	Vehicle trajectory behind the test article is acceptable.		30, 31, 32, 33, 34, 39, 42, 43, 44, 60, 61, 70, 71, 80, 81	

Table 36. Roadside safety phenomena importance ranking table (structural adequacy).

Evaluation Criteria		Known Result	Analysis Result	Difference Relative/Absolute	Agree?	
Structural Adequacy	1	Test article should contain and redirect the vehicle; the vehicle should not penetrate, under-ride, or override the installation although controlled lateral deflection of the test article is acceptable. (Answer Yes or No)	Y	Y		Y
	2	Maximum dynamic deflection: - Relative difference is less than 20 percent or - Absolute difference is less than 6 inches	27.2 in	27.2 in	0 % 0 in	Y
	3	Length of vehicle-barrier contact: - Relative difference is less than 20 percent or - Absolute difference is less than 6.6 ft	22.7 ft	25.1 ft	10.6 % 2.4 ft	Y
	4	Number of broken or significantly bent posts is less than 20 percent.	0	0		Y
	5	Did the rail element rupture or tear (Answer Yes or No)	No	No		Y
	6	Number of detached post-rail connections.	2	2		Y
	7	Was there significant snagging between the vehicle wheels and barrier elements (Answer Yes or No).	Y	Y		Y
	8	Was there significant snagging between vehicle body components and barrier elements (Answer Yes or No).	N	N		Y

Table 37. Roadside safety phenomena importance ranking table (occupant risk).

Evaluation Criteria			Known Result	Analysis Result	Difference Relative/Absolute	Agree?	
Occupant Risk	D	Detached elements, fragments or other debris from the test article should not penetrate or show potential for penetrating the occupant compartment, or present an undue hazard to other traffic, pedestrians or personnel in a work zone. (Answer Yes or No)	N	N		Y	
	F	1	The vehicle should remain upright during and after the collision although moderate roll, pitching and yawing are acceptable. (Answer Yes or No)	Y	Y		Y
		2	Maximum roll of the vehicle at 0.6 seconds: - Relative difference is less than 20 percent or - Absolute difference is less than 5 degrees.	25 deg	30 deg	20% 5 deg	Y
		3	Maximum pitch of the vehicle at 0.6 seconds: - Relative difference is less than 20 percent or - Absolute difference is less than 5 degrees.	10.7 deg	9.1 deg	15% 1.6 deg	Y
		4	Maximum yaw of the vehicle at 0.6 seconds: - Relative difference is less than 20 percent or - Absolute difference is less than 5 degrees.	41.2 deg	50.4 deg	22% 9.2 deg	N
	L	1	Occupant impact velocities: - Relative difference is less than 20 percent or - Absolute difference is less than 2 m/s.				
			• Longitudinal OIV (m/s)	4.6	5.3	15 0.7 m/s	Y
			• Lateral OIV (m/s)	5.8	5.8	0% 0 m/s	Y
			• THIV (m/s)	6.9	7.4	7.2% 0.5 m/s	Y
		2	Occupant accelerations: - Relative difference is less than 20 percent or - Absolute difference is less than 4 g's.				
			• Longitudinal ORA	11.5	10.2	11.3 % 1.3 g	Y
			• Lateral ORA	11.2	11.1	0.9 % 0.1 g	Y
	• PHD		11.7	13.6	16.2 % 1.9 g	Y	
		• ASI	1.01	0.99	2% 0.02 g	Y	

Table 38. Roadside safety phenomena importance ranking table (vehicle trajectory).

Evaluation Criteria				Known Result	Analysis Result	Difference Relative/Absolute	Agree?
Vehicle Trajectory	M	1	The exit angle from the test article preferable should be less than 60 percent of test impact angle, measured at the time of vehicle loss of contact with test device.	55%	106%		N
		2	Exit angle at loss of contact: - Relative difference is less than 20 percent or - Absolute difference is less than 5 degrees.	13.5 deg	25.7 deg	90% 12.2 deg	N
		3	Exit velocity at loss of contact: - Relative difference is less than 20 percent or - Absolute difference is less than 6.2 mph.	44 mph	37.3 mph	15% 6.7 mph	Y
		4	One or more vehicle tires failed or de-beaded during the collision event (Answer Yes or No).	Y	Y		Y

All the applicable criteria in Table 36 through Table 38 agree (i.e., the relative difference between the numerical solution and the test was less than 20%) except for the criteria involving the vehicle yaw angle. As discussed earlier, the slight increase in pitch of the vehicle allowed the rear bumper to pass over the top of the w-beam during redirection, which significantly increased the yaw angle as the vehicle exited the system.

Conclusions

In general, the finite element analysis of the G4(2W) guardrail system under *NCHRP Report 350* Test Level 3 conditions demonstrated that the finite element model replicates the basic phenomenological behavior of the system in a redirection impact with a 2000P vehicle. There was good agreement between the test and the simulations with respect to event timing, overall kinematics of the vehicle, guardrail damage and guardrail deflections; although, the model did experience slightly higher pitch angle and higher yaw angle than occurred in the test.

There were some components of the truck model that experienced higher than acceptable zero-energy modes (i.e., hourglass energies). Although it is not likely that slight errors in the response of those components would affect overall results, it is possible that they could lead to further instability in the model. These issues were corrected and the vehicle model is thus considered stable for subsequent analyses in this study. Quantitative comparison of the time-history data indicated that the finite element model accurately replicates the results of the baseline crash test. Thus, the model is considered valid for use in assessing the effects of incremental modifications to the guardrail system.

CHAPTER 8 – EVALUATION OF GUARDRAIL POST DETERIORATION FOR THE G4(2W)

The guardrail post is a fundamental component of a guardrail system and its response during a crash event is important to the overall performance of the system. The posts are intended to absorb energy as they rotate through the soil during collisions. If the posts do not have sufficient strength they will fracture prematurely, resulting in excessive deflection of the w-beam rail element which may lead to rail forces that exceed its capacity. As posts deteriorate, the strength of the posts decline; thus, it is important to develop a field-assessment procedure for correlating strength degradation of guardrail posts to its effects on the crash performance of the guardrail system. The focus of this chapter is the evaluation of the G4(2W) guardrail with various levels of post deterioration to quantify their effects on system performance.

Wood posts are subject to decay and rot from several causes. The area at and just below the ground line is of great concern because the combination of moisture and air greatly promotes decay. Wood posts are also subject to inhabitation by ants and other small insects. The degradation of wood fibers takes place because insects create living spaces within the wood or by ingesting wood fibers for nutrients; in which case damage can occur within any portion of the wood post. There is no particular standard at this time for quantifying the degree of rot or deterioration in a guardrail post. The approach typically used is to simply replace any post with visible deterioration under the assumption that if rot is visible there is probably also a great deal of non-visible rot, especially just below the groundline. In many, if not most, cases however the rot begins just underneath the outer shell of the post and is thus hidden from view.

The power industry has experienced similar problems with wooden utility poles. Like guardrail posts, utility poles remain in service for many years and can sometimes rot and deteriorate, often below ground. There are some destructive test techniques that involve drilling multiple large (e.g., $\frac{3}{4}$ -inch diameter) holes in the pole and probing the interior but this would too greatly compromise strength if applied to guardrail posts. Several non-destructive techniques have been developed which have demonstrated reasonable accuracy in predicting breaking strength of utility poles based on the modulus of elasticity of the pole. These methods include static bending tests, stress wave propagation techniques, near infrared spectroscopy, and ultrasound to name a few.[*Hron11; Tallavo09; Green06; Hendrick03; Hascall07*] Another type of “non-destructive” test involves the use of a resistograph, which measures the torque of a 1/16” diameter drill bit as it is inserted into the wood. The torque is measured as a function of length along the drill bit so any interior rot, voids or areas of low density are reflected in the torque measurement. The results are compared to a baseline reading on healthy wood to determine level of degradation. The resistograph can also drill at a 45 degree angle to obtain an indication of the subsurface condition of the post. Since the drill bit is only 1/16-inch diameter it is not considered a destructive test and there is little negative effect on the post strength due to the very small size hole.

The objectives of this study task were to develop a process for estimating the degree of deterioration of a guardrail post and to quantify the effects of various levels of post deterioration on the crash performance of the guardrail system.

Scope

The scope of this study included: (1) obtaining field-extracted wood guardrail posts from State DOT maintenance garages, (2) measuring the degree of deterioration of the posts with a Resistograph, (3) performing pendulum impact tests to measure the strength and capacity of the posts with various levels of deterioration, (4) processing the pendulum tests and resistograph data to correlate levels of deterioration to strength degradation, and (5) using FEA to quantify the effects of various levels of post deterioration on overall guardrail crash performance.

Procurement of Guardrail Post Test Articles

The Ohio Department of Transportation (ODOT) provided 140 guardrail posts with various levels of deterioration for the test program. These posts were extracted from the ground from damaged guardrail installations in Ohio. It has not been confirmed, but all the posts are assumed to be of the Southern Yellow Pine (SYP) species, which is the post type primarily used in Ohio. The posts all had round cross-section with nominal diameter size of 8 inches. The actual diameter size varied from 6.45 inches to 9.15 inches with standard deviation of 0.62 inches. In some cases the smaller diameters were a result of shell loss due to deterioration. The post lengths varied from approximately 5 to 6 ft, with the two most common lengths being 5 ft – 6 inches and 5 ft – 10 inches. Figure 104 shows a photo of the guardrail posts provided by the Ohio DOT for use in the physical test program. In addition to the deteriorated posts, ODOT also donated three new (or unused) guardrail posts to the project so that the Resistograph measurements from the in-service posts could be compared directly to the corresponding values for new posts.



Figure 104. Posts from Ohio DOT procured for the Physical Test Program.

Resistograph Measurements and Processing

Resistograph Measurements

The deterioration of each post was measured using an IML Resi-F400 S Resistograph, shown in Figure 105. The resistograph was equipped with a 1/16 inch in diameter drilling needle 19 ⁵/₁₆ inches long. The resistograph measurements were recorded at increments of approximately 0.004 inches of drilling depth. The measurements were taken just below, or at, the groundline where the highest levels of deterioration were visually evident. With the posts extracted from ground, this critical area of the post was readily accessible, so the measurements were made at 90 degrees to the post.



Figure 105. IML Resi-F400 S Resistograph.

Data Processing and Interpretation

The data from the resistograph was then processed to develop a procedure to yield a single quantitative value representing the strength or capacity of the posts. The pendulum test program, which will be discussed later, involved the post mounted in a rigid foundation, in which the guardrail post was essentially a cantilevered beam with a concentrated load applied at the end of, and normal to, the post. The stresses in the post arise from the resulting bending moment, where the stress profile through the cross-section of a beam in pure bending can be calculated from the following equation:

$$\sigma = \frac{Mc}{I}$$

Where M is the bending moment, I is the moment of inertia of the beam, and c is the distance from the neutral axis of the beam. Since M and I are constants, the strain varies linearly through the cross-section, increasing from zero at the neutral axis to a maximum value at the outermost fiber of the beam. If the material is elastic and homogeneous then the stress also varies linearly through the cross-section. For a non-homogeneous material such as wood, on the other hand, the stress values vary through the cross-section as a function of the local wood modulus, as illustrated in the schematic in Figure 106.

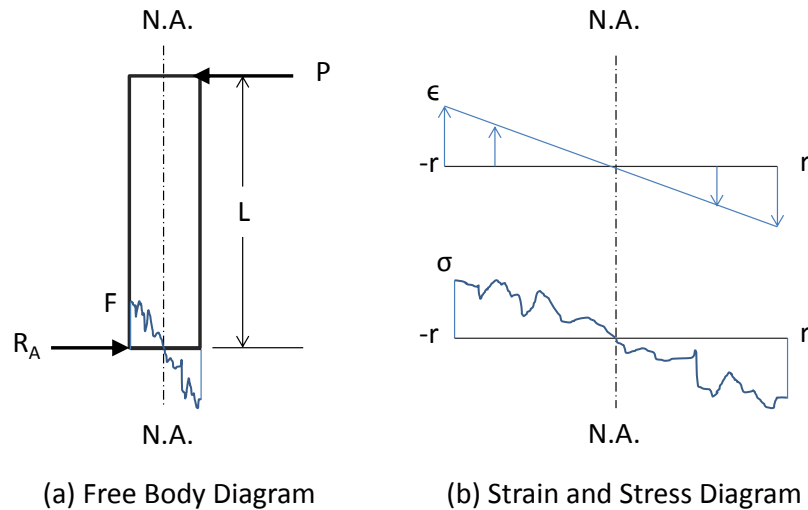


Figure 106. Schematic of typical (a) Free-body and (b) strain and stress diagrams for non-homogeneous beam under bending load.

From the free body diagram in Figure 106, equilibrium is achieved when the sum of the moments due to the internal forces at Point A are equal to the moment created by the applied force P times its distance L , as described by:

$$\int_{-r}^r F dy = PL$$

If the internal force at Point A in Figure 106 is approximated in terms of discrete forces, F_i , acting at fixed increments, y_i , through the cross-section of the post, as illustrated in Figure 107, then the equilibrium condition can be re-written as:

$$\sum_{i=1}^N F_i y_i = PL$$

Figure 108 shows the resistograph results for one of the new posts (i.e., Post A), illustrating a typical drill-torque vs. depth plot through the cross section of a guardrail post. Note that the torque resistance is not constant through the cross-section due to the non-homogeneous nature of wood, and also tends to oscillate considerably at each increment as the needle passes through each ring (or layer) of the post. For the following calculations, the data is used in its raw form (i.e., unfiltered).

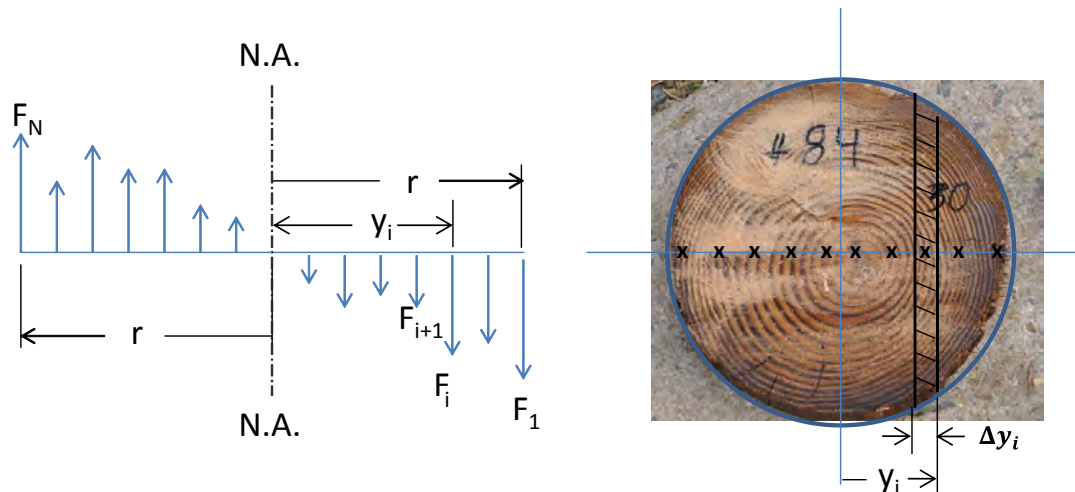


Figure 107. Schematic illustrating internal force distribution through cross-section of a circular shaped post.

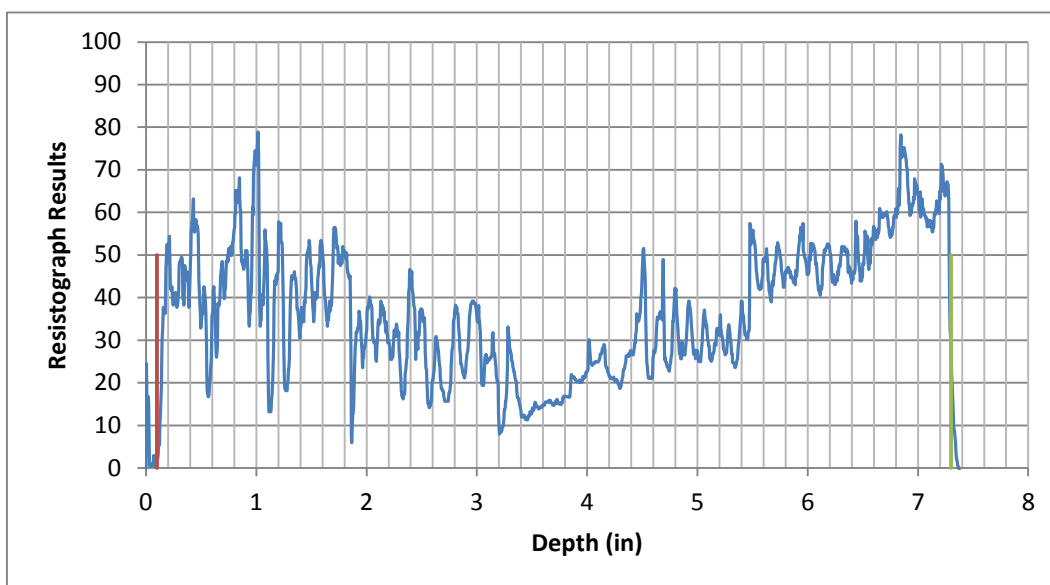


Figure 108. Resistograph results for Post A.

The resistograph data is measured along the centerline of the post’s cross-section. It is assumed that the torque resistance amplitude at each point is directly proportional to the modulus (or strength) of the torque post fibers at that radial depth within the post. For example, the hashed cross-section of Figure 107 shows the overall area for the representative force, F_i , acting at $y = y_i$. As wood posts age and deteriorate, the properties of the wood will differ depending on its depth within the post. As illustrated in Figure 109, the crosshatched region at $y = y_i$ includes points at multiple depth locations through the post, where the number of points increases as y_i approaches zero (i.e., the neutral axis). Each of these points is associated with a local modulus, E_j , and a representative subarea, A_{ij} , as illustrated in Figure 109. For example, the shaded area in Figure 109(a) is representative of the subarea bounded by the two outermost rings which correspond to radii $r = y_1$ and $r = y_2$ and the two vertical lines $y = y_i$ and $y = y_{i+1}$. The properties of the post at

this location are assumed to be the same as that measured at Point 1 (outer most data point circled in Figure 109), which was taken directly from the resistograph data. Likewise Figure 109(b) and Figure 109(c) illustrate the local subareas at $y = y_i$ associated with the resistograph data points measured at Point 2 and Point 3, respectively, for $i=3$.

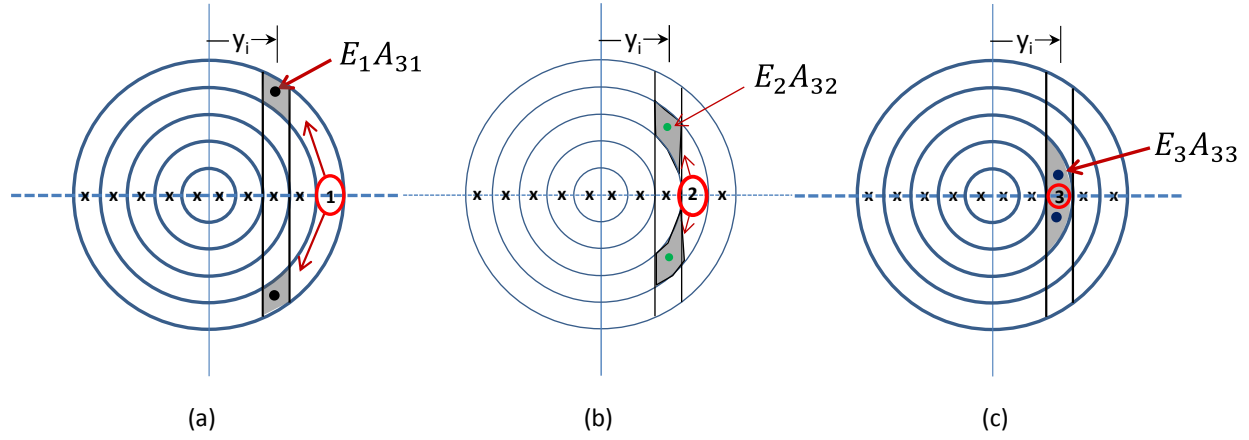


Figure 109. Schematic illustrating the local moduli and subareas associated with the various points through the post thickness at $y = y_i$.

Thus, for a given applied load, each data point from the resistograph can be converted to a “pseudo” force value using the following equation:

$$F_i^* = \sum_{j=1}^i E_j^* A_{ij} \frac{y_i}{R} \epsilon_R$$

Where, F_i^* are the pseudo forces, E_j^* are pseudo modulus values associated with the incremental subareas ΔA_{ij} , y_i is the distance of the force F_i from the neutral axis of the post, R is the radius of the post and ϵ_R is the value of strain at $y = R$. Note that the term $\frac{y_i}{R} \epsilon_R$ is the strain at y_i . The total resisting “moment” of the post is then proportional to the pseudo moment defined by:

$$M^* = \sum_{i=1}^N F_i^* y_i = \frac{\epsilon_R}{R} \sum_{i=1}^N \sum_{j=1}^i E_j^* A_{ij} y_i^2 \quad (1)$$

The relationship between the strain ϵ_R and E_j^* was not determined, so the value for ϵ_R was set to unity for calculations of M^* . The subarea A_{ij} , as illustrated previously in Figure 109, can be computed using the simple formula for defining the area bounded between two circles with limits of y_{i+1} to y_i as:

$$A_{ij} = \int_{y_{i+1}}^{y_i} \left[\sqrt{r_j^2 - y^2} - \sqrt{r_{j+1}^2 - y^2} \right] dy$$

The energy absorbed by the post is also meaningful for quantifying the performance of a guardrail post. The equation calculating internal strain energy is shown below. The constitutive behavior of wood is assumed linear for calculation of the strain energy (for the sake of simplification), which yields:

$$U = \int \sigma \epsilon dV \approx \sum_i A_i \sigma_i \epsilon_i = \sum_i \sum_j^i A_{ij} E_j \epsilon_i^2 = \sum_i \sum_j^i A_{ij} E_j \frac{y_i^2}{R^2} \epsilon_R^2$$

Where σ_i , ϵ_i and E_i are the stress, strain and modulus, respectively, of the wood post at each increment through the cross-section. Thus, a pseudo strain energy can be computed for the post by substituting E^* for E in the above equation and rearranging such that:

$$U^* = \frac{\epsilon_R^2}{R^2} \sum_i \sum_j^i A_{ij} E_j^* y_i^2 \quad (2)$$

Statistics for Resistograph Measurement of Test Articles

Resistograph measurements were taken for each of the 140 aged post specimens and the three new post specimens obtained from the Ohio DOT. The values for M^* ranged from 162 to 3251 with a mean value of 1123 and standard deviation of 11.3. The values for U^* ranged from 40.9 to 812.9 with mean of 294.6 and standard deviation of 140.9. Figure 110 and Figure 111 show the cumulative distribution function for M^* and U^* , respectively, which indicate relatively uniform distribution of scores.

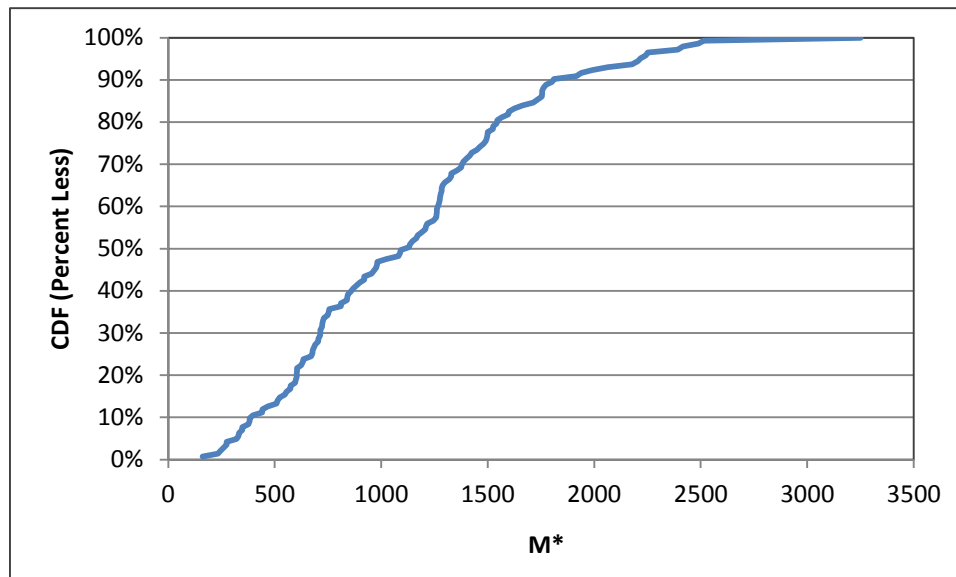


Figure 110. Cumulative distribution plot for M^* .

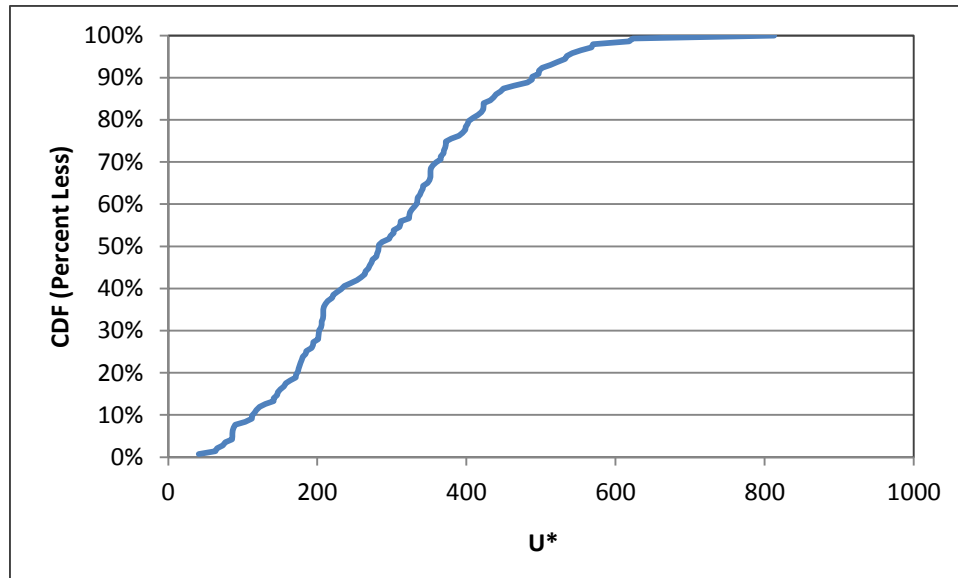


Figure 111. Cumulative distribution plot for U^* .

In some cases the resistograph data did not fall back to zero when the drilling needle passed through the back-side of the post. This indicated that the needle likely encountered a “check” or a knot at some point during the test that turned the needle from its straight path and affected subsequent results (e.g., friction and bending of the needle may have increased the resistance measurements). This was somewhat corrected in the data by estimating the most logical location for the start of the divergence and assuming that the error was increasing linearly for the duration of the test, as illustrated in Figure 112. A logical solution for avoiding this phenomenon would be to drill only half way through the diameter on each side of the post.

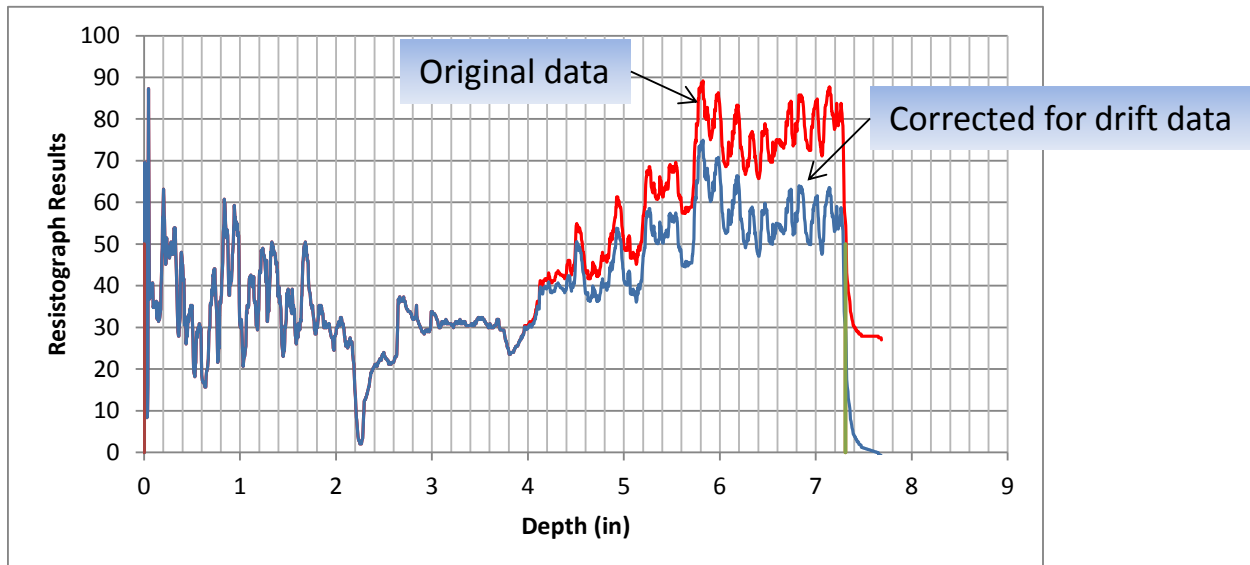


Figure 112. Resistograph data corrected for drift.

Pendulum Testing of Post-in-Rigid-Foundation

Scope

Pendulum tests were conducted at the FOIL to assess the dynamic failure properties of the deteriorated posts. Two series of tests were performed. The target impact conditions for the first series of tests were a 2,372-lb rigid pendulum impacting the posts at an impact speed of 20 mph at a height of 21.5 inches above ground. A review of the tests results indicated that the inertial response of the posts may have significantly influenced the pendulum mounted accelerometer data. The 20 mph impact speed resulted in much more energy than was required to break the post so the excess energy resulted in extraneous signal ringing. Finding an impact speed just fast enough to consistently break the post would help provide a cleaner signal with less noise. Thus, a second series of tests was conducted in which the target impact speed was reduced to 10 mph. A total of 22 tests were conducted at 20 mph and a total of 39 tests were conducted at 10 mph. The complete test matrices are shown below in Table 39 and Table 40.

In an earlier study by Hascal *et. al* t it was stated that,

“As the moisture content of a wood post increases up to 23 percent, the strength of the wood fibers within the post decreases. Beyond 23 percent, the wood strength is fairly constant. In their actual use, the moisture content may exceed 23 percent, and therefore the posts would be saturated.”[Hascal07]

In order to reduce the effects of moisture content, each wood post specimen was saturated prior to testing. Each specimen was cut to 66 inches long, weighed, and then soaked for several hours in an open water tank as shown in Figure 113. Only the portion of the posts that were to be embedded into the steel sleeve (i.e., below groundline) was submerged in the tank to achieve realistic saturation of the posts (i.e., saturation below the groundline and air-dried above the groundline). The pre-soaked post specimens were again weighed just prior to testing. The circumferences of the posts were measured at the top, at the groundline and at the bottom of the posts to estimate the average diameter of the post. The average diameter, post length and weight of the post were then used to calculate the wet density for each post. The number of rings for each post was counted and used to determine the average ring density for each post. The moisture content was measured immediately after each pendulum test at several points through the cross-section of the post along the break-line using an [MT-10](#) moisture meter developed by AMPROBE. The moisture meter was not able to obtain accurate readings when the moisture content exceeded 50 percent. In those cases the moisture content was reported as “greater than 50 percent”.

Table 39. Test Series 13009 Group 1 (2,372-lb pendulum, velocity = 20 mph, impact point = 21.5 inches).

Test No.	Test Date	Post No.	Length (in)	Initial Weight (lbs)	Soak Time (hours)	Soak Weight (lbs)	Circumference			Volume (in3)	Wet Density (lb/ft3)	Groundline Diameter (in)	Number of Rings	Ring Density (rings/in)
							bottom (in)	mid (in)	top (in)					
13009B	9/24/2013	3	66	-	-	61	23.5	24	24.5	3025.2	34.8	7.6	19	5.0
13009C	9/24/2013	1	66	-	-	88	23.25	21.25	24.75	2798.5	54.3	6.8	30	8.9
13009D	9/24/2013	2	66	-	-	52	22.375	22.38	22.875	2669.1	33.7	7.1	14	3.9
13009E	9/24/2013	7	66	-	-	69	23.5	23.5	23.75	2921.1	40.8	7.5	30	8.0
13009F	9/24/2013	12	66	-	-	67	22	20.75	22	2446.6	47.3	6.6	23	7.0
13009G	9/24/2013	4	66	-	-	85	24.375	24	24.25	3078.0	47.7	7.6	18	4.7
13009H	9/25/2013	36	66	-	-	74	23	20.5	22.5	2542.0	50.3	6.5	25	7.7
13009I	9/25/2013	14	66	-	-	104	25.5	25.5	25	3370.7	53.3	8.1	30	7.4
13009J	9/25/2013	15	66	-	-	58	21.25	22	23.75	2619.6	38.3	7.0	18	5.1
13009K	9/25/2013	B	66	-	-	71	23	22.75	22.75	2738.2	44.8	7.2	21	5.8
13009L	9/25/2013	A	66	-	-	72	23	22.75	22.75	2738.2	45.4	7.2	34	9.4
13009M	9/25/2013	13	66	-	-	87	26.25	24.5	24.5	3304.5	45.5	7.8	25	6.4
13009N	9/26/2013	62	66	37.0	17.0	64	24	24.25	24.25	3067.4	36.1	7.7	25	6.5
13009O	9/26/2013	40	66	60.0	18.0	87	26.25	24.5	24.5	3304.5	45.5	7.8	28	7.2
13009P	9/26/2013	19	66	53.0	19.0	69	24.75	24.75	26.75	3392.9	35.1	7.9	18	4.6
13009Q	9/26/2013	22	66	76.0	19.5	100	28.5	28	28.5	4216.3	41.0	8.9	30	6.7
13009R	9/26/2013	18	66	71.0	20.0	72	24.25	24.5	25	3174.1	39.2	7.8	24	6.2
13009S	9/26/2013	46	66	83.0	20.5	116	28.5	28.75	27.5	4191.5	47.8	9.2	40	8.7
13009T	9/27/2013	74	60	35.0	17.0	42	20	20.75	22	2088.9	34.7	6.6	23	7.0
13009U	9/27/2013	41	60	58.0	17.5	61	24.5	23.5	23	2674.3	39.4	7.5	26	7.0
13009V	9/27/2013	38	66	46.0	18.0	58	20.75	21.25	22.25	2409.0	41.6	6.8	19	5.6
13009W	9/27/2013	39	66	42.0	18.5	53	20.25	20.25	20.25	2153.7	42.5	6.4	14	4.3

Table 40. Test Series 13009 Group 2 (2,372-lb pendulum, velocity = 10 mph, impact point = 21.5 inches).

Test No.	Test Date	Post No.	Length (in)	Initial Weight (lbs)	Soak Time (hours)	Soak Weight (lbs)	Circumference			Volume (in ³)	Wet Density (lb/ft ³)	Groundline Diameter (in)	Number of Rings	Ring Density (rings/in)
							bottom (in)	mid (in)	top (in)					
13009Y	10/1/2013	43	66.0	65.0	17.0	85	24.3	23.8	24.3	3046.3	48.2	7.6	22	5.8
13009Z	10/1/2013	56	66.0	71.0	18.5	92	25.5	25.8	24.8	3370.7	47.2	8.1	30	7.4
13009A1	10/1/2013	50	66.0	69.0	19.0	74	24.5	23.0	25.5	3109.8	41.1	7.4	47	12.7
13009B1	10/1/2013	31	66.0	59.0	19.5	70	23.5	24.3	24.3	3025.2	40.0	7.6	17	4.5
13009C1	10/1/2013	47	66.0	69.0	20.0	93	27.0	25.5	24.8	3482.5	46.1	8.0	27	6.8
13009D1	10/1/2013	55	66.0	51.0	20.5	63	22.3	22.5	23.5	2718.3	40.0	7.3	26	7.1
13009E1	10/1/2013	32	60.0	103.0	21.0	119	26.8	26.8	27.8	3502.2	58.7	8.8	26	5.9
13009F1	10/1/2013	88	60.0	41.0	21.5	56	23.0	23.8	24.3	2674.3	36.2	7.6	20	5.3
13009G1	10/2/2013	71	60.0	61.0	18.0	70	26.0	23.5	23.3	2807.8	43.1	7.6	30	7.9
13009H1	10/2/2013	30	60.0	67.0	18.5	73	26.0	25.3	24.5	3044.1	41.4	8.0	28	7.0
13009I1	10/2/2013	76	60.0	70.0	19.0	75	28.3	26.3	25.5	3395.3	38.2	8.4	30	7.2
13009J1	10/2/2013	49	66.0	70.0	19.5	76	26.3	24.3	23.3	3174.1	41.4	7.5	30	8.0
13009K1	10/2/2013	29	66.0	72.0	20.0	80	23.0	22.0	23.3	2718.3	50.9	7.0	25	7.1
13009L1	10/2/2013	92	66.0	74.0	20.5	78	25.5	25.3	23.8	3239.0	41.6	8.0	32	8.0
13009M1	10/2/2013	68	66.0	65.0	21.0	69	24.0	23.3	22.8	2859.5	41.7	7.4	35	9.5
13009N1	10/3/2013	17	66.0	71.0	18.0	76	25.0	25.5	25.5	3370.7	39.0	8.0	30	7.5
13009O1	10/3/2013	94	66.0	37.0	18.5	47	21.3	20.8	20.8	2297.8	35.3	6.6	20	6.1
13009P1	10/3/2013	44	66.0	61.0	19.0	80	24.0	23.3	23.0	2879.9	48.0	7.6	30	7.9
13009Q1	10/3/2013	53	66.0	52.0	19.5	68	25.0	24.3	25.8	3282.6	35.8	7.6	24	6.3
13009R1	10/3/2013	84	66.0	72.0	20.0	84	24.5	22.3	22.5	2798.5	51.9	6.6	30	9.1
13009S1	10/3/2013	21	66.0	97.0	20.5	109	29.0	25.8	23.8	3596.1	52.4	8.0	50	12.6
13009T1	10/3/2013	63	66.0	57.0	21.0	62	24.0	23.5	23.5	2941.8	36.4	7.5	30	8.0
13009U1	10/3/2013	65	60.0	58.0	21.5	68	26.3	24.3	23.5	2905.1	40.4	7.6	32	8.4
13009V1	10/8/2013	90	66.0	37.0	18.0	49	21.8	22.3	22.5	2580.7	32.8	7.0	16	4.6
13009W1	10/8/2013	118	66.0	63.0	18.5	79	25.3	25.5	24.8	3326.5	41.0	7.7	28	7.3

Table 40. [CONTINUED] Test Series 13009 Group 2 (2,372-lb pendulum, velocity = 10 mph, impact point = 21.5 inches).

Test No.	Test Date	Post No.	Length (in)	Initial Weight (lbs)	Soak Time (hours)	Soak Weight (lbs)	Circumference			Volume (in ³)	Wet Density (lb/ft ³)	Groundline Diameter (in)	Number of Rings	Ring Density (rings/in)
							bottom (in)	mid (in)	top (in)					
13009X1	10/8/2013	81	66.0	69.0	19.0	87	24.0	22.5	22.3	2758.3	54.5	6.7	22	6.6
13009Y1	10/8/2013	123	66.0	74.0	19.5	92	26.0	26.3	25.0	3482.5	45.7	8.3	19	4.6
13009Z1	10/8/2013	61	66.0	73.0	20.0	90	27.0	26.0	27.0	3734.8	41.6	8.2	25	6.1
13009A2	10/8/2013	67	66.0	68.0	20.5	83	25.5	25.5	26.0	3460.0	41.5	8.2	21	5.1
13009B2	10/8/2013	126	66.0	77.0	21.0	93	25.8	26.3	26.0	3550.4	45.3	8.3	29	7.0
13009C2	10/8/2013	91	66.0	76.0	22.5	93	27.5	27.0	25.5	3734.8	43.0	8.6	37	8.6
13009D2	10/9/2013	105	66.0	52.0	17.0	63	24.0	23.0	22.8	2839.1	38.3	7.0	17	4.9
13009 E2	10/9/2013	117	66.0	73.0	17.5	81	27.0	27.0	26.5	3781.7	37.0	8.6	25	5.8
13009F2	10/9/2013	129	66.0	58.0	18.0	79	23.0	23.0	23.3	2798.5	48.8	7.3	28	7.7
13009G2	10/9/2013	24	66.0	81.0	18.5	84	25.3	25.8	27.3	3573.2	40.6	8.4	30	7.1
13009H2	10/9/2013	35	66.0	83.0	19.0	86	26.8	25.5	25.0	3482.5	42.7	8.1	22	5.4
13009I2	10/9/2013	78	66.0	68.0	19.5	78	23.5	24.0	26.0	3152.6	42.8	7.6	24	6.3
13009J2	10/9/2013	111	66.0	68.0	20.0	71	24.0	24.5	24.8	3131.2	39.2	7.6	28	7.4
13009K2	10/9/2013	114	60.0	63.0	20.5	69	24.3	25.0	25.0	2924.8	40.8	8.0	35	8.8



Figure 113. Photo of post specimen soaking in tank of water.

Test Specimen Mounting Condition

The tests were performed with the posts installed in a rigid steel sleeve, as shown in Figure 114. The sleeve was a 12 x 12 x ¼ inch steel tube fabricated from A500 Class B 58,000 psi structural steel. The top of the tube was reinforced with a 5-inch tall 13 x 13 x ½ inch steel tube welded to the main tube sleeve. The foundation sleeve was braced against the steel reinforced concrete wall on the inside of the ground-pit using a 7.4 ft long S20x86 structural steel section. The posts were mounted inside the sleeve at a nominal depth of 38 inches, except for the few cases in which the length of the post was too short (e.g., several of the posts were only 60 inches long, which resulted in an embedment of 32 inches). In all cases, the top mounting height of the posts was nominally 28 inches. The posts were held in place inside the sleeve using structural grade pine boards (e.g., 2x8) that were press-fit against the back-side of the sleeve using a 1.0-inch diameter grade 8 set-screw.



Figure 114. Rigid steel sleeve used for post mounting.

Equipment and Instrumentation

Pendulum Device

The striker for the tests was a 2,372-lb concrete pendulum with a semi-rigid nose, as shown in Figure 115. The semi-rigid nose, which was developed by researchers from Virginia Tech during the first phase of this study, was fabricated from a wooden block and covered with sheet metal. [Gabler10] The radius of chamfer at the center of the impactor face was 6 inches, which was based on measurements of a 2006 Chevrolet 1500 pickup truck. [Gabler10]



Figure 115. 2,372-lb pendulum device with semi-rigid nose.

Accelerometers

The pendulum was instrumented with three accelerometers mounted onto the backside of the pendulum mass. Two of the accelerometers recorded data in the x-direction (forward direction) and the third accelerometer recorded data in the z-direction (vertical direction). Figure 116 provides a schematic showing the locations of the accelerometers.



Pendulum top view with accelerometer blocks

CH.	LOCATION	X (cm) From frt.	Y (cm) From lft frt. corner	Z (cm) From ground	SERIAL NO.	AXIS
1	Rear Center of Pend.	43.0	127.0	71.0	D12153	-X
2	Rear Center of Pend.	43.0	127.0	71.0	D12748	-X
3	Rear Center of Pend.	43.0	127.0	71.0	D12820	-Z

Figure 116. Schematic of the accelerometer instrumentation for the pendulum tests.

Photography Cameras

The tests were also recorded using four high-speed cameras with an operating speed of 500 frames per second and a digital video camera (~30 fps). Figure 117 provides the specifications and the general placement of the high-speed cameras for the tests. The accelerometers and the high-speed video were triggered using pressure tape switches when the pendulum contacted the post. The test setup and results were also documented with photographs taken before and after each test.

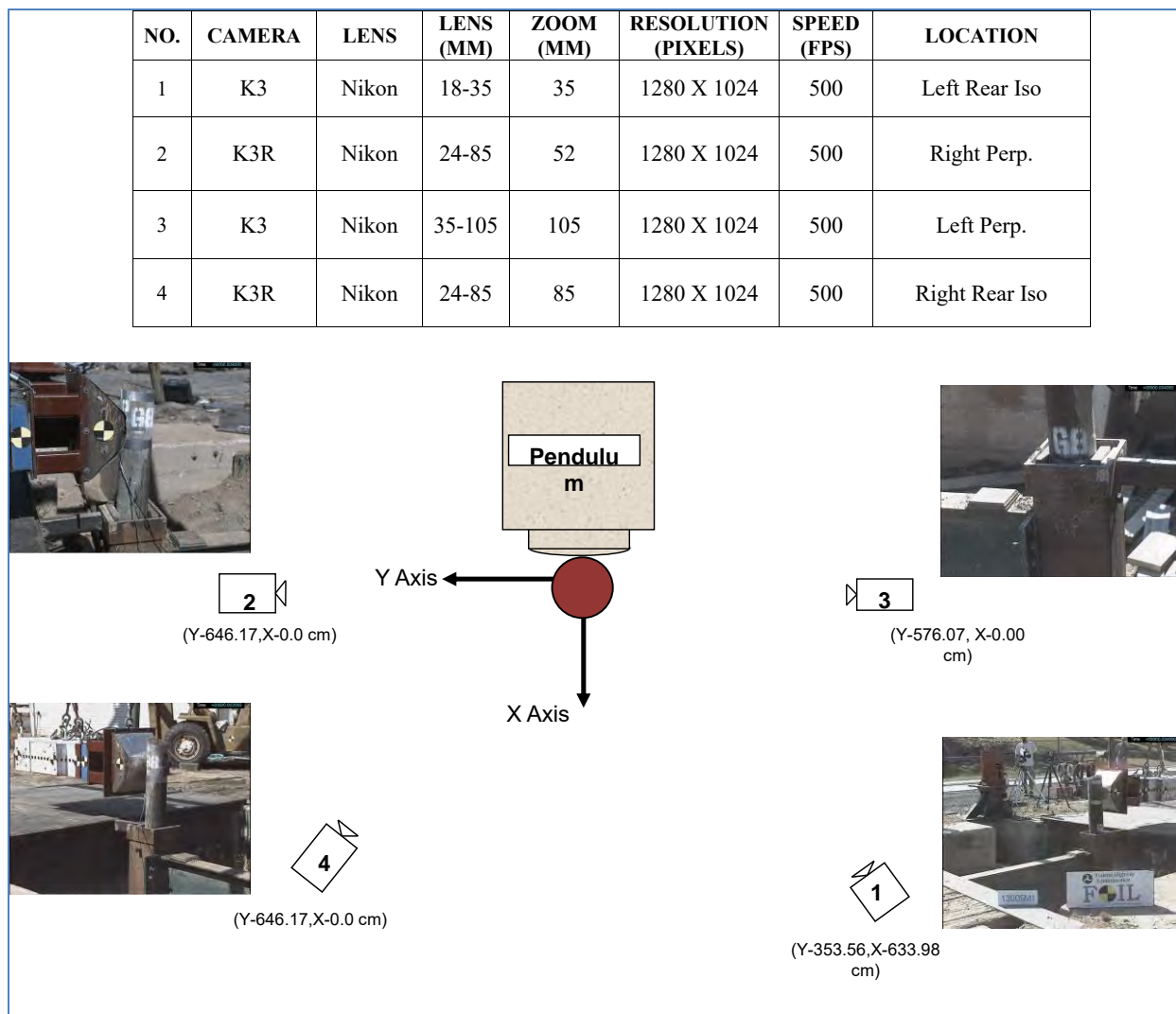


Figure 117. High-speed camera specifications and placement.

Impact Conditions

Two test series were performed. In the first series (i.e., Test Series 13009 Group 1), the 2,372-lb pendulum struck the post at 21.5 inches above grade at an impact speed of 20 mph, which resulted in a total kinetic energy of the striker of 31.7 ft-kips. In the second series of tests (i.e., Test Series 13009 Group 2), the impact velocity was reduced to 10 mph, which resulted in a total kinetic energy of 7.92 kip-ft. The posts were oriented such that the post bolt-hole was in-line with the pendulum; which also coincided with the direction of measurement in the resistograph tests.

Results

The x-channel accelerometer data was processed to obtain the accelerations of the pendulum during impact with the posts. The data was filtered using an SAE Class 60 filter with a cutoff frequency of 100 Hz. The impact force-time history response from each post was approximated by multiplying the acceleration-time history curves by the total mass of the pendulum. The acceleration data was then integrated to obtain velocity-time history, and again integrated to obtain the displacement-time history of the pendulum. This information was then used to generate force-deflection response of the posts during impact. The force-deflection curves were then integrated to obtain the energy-deflection curves. The results for each of the tests are shown in Appendix D for Test Series 1 and Appendix E for Test Series 2.

The diameter of the posts varied significantly among the test specimens (i.e., 6.45 inches to 9.15 inches with a standard deviation of 0.61 inches). In some cases the reduction in diameter was due to deterioration, but there were also significant differences regarding the nominal diameter of the posts. Since the effects of diameter have already been incorporated into the weighted resistograph scores (i.e., S_{MOR*} and S_{U*}), it was not necessary to adjust for post diameter in the pendulum test results. Note that the objective was to develop a relationship between the resistograph score and the strength properties of the posts.

Although the intent of the rigid foundation tube was to create a “fixed” condition on the post at the groundline, the posts sometimes failed inside the foundation tube below the groundline, as illustrate in Figure 118. As a result, the moment arm (i.e., the distance from the impact point to the break point) was slightly different in each test. It was therefore decided to compute post capacity in terms of maximum resistive moment rather than maximum force. One complication, however, was that the posts do not generally fail along plane sections, let alone a perpendicular plane. To obtain a rough estimate for the length of the moment arm in each test, the average distance from the impact point on the post to the break line on the front and back side of the post was used.



Figure 118. Photo of Test 13009G1 showing Post 71 breaking below groundline.

Test Series 13009 Group 1 (20 mph Impact Speed)

Table 41 provides the peak force, the strain energy at initiation of rupture, peak moment, and the energy at complete rupture for each post in Test Series 1. Figure 119 shows typical force and energy curves annotated to illustrate location of peak force, initial rupture energy, and rupture energy computed from the pendulum impact tests. The test summary sheets for this test series are shown in Appendix D.

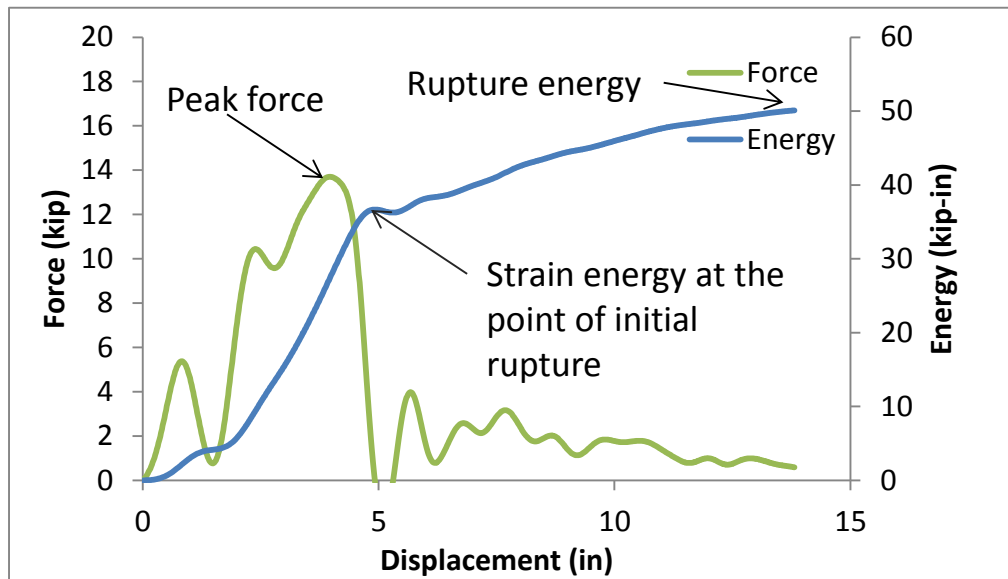


Figure 119. Typical force and energy curves annotated to illustrate location of peak force, initial rupture energy, and rupture energy computed from pendulum test results.

The results from this first series of tests raised a few concerns: 1) the kinetic energy of the striker greatly exceeded the energy required to break the posts, 2) the “inertial effects” of the impact seemed to dominate the impact event and overshadow the bending response of the posts and 3) a significant portion of the energy measured in the impact was transferred into kinetic energy of the broken post.

The term “inertial effects” is loosely defined here as the impulse required to initiate movement of the post’s mass upon impact. Also, from the high-speed video it was apparent that the broken posts were moving at significant speeds after the impact. It was not possible to accurately quantify the amount of energy expended in rupturing the post, since there was no convenient way to measure the speed of the broken post. From the test results, the highest energy expended in any test was 37 kip-in, while the majority of the tests expended less than 25 kip-in of energy. This was significantly less than the kinetic energy of the striker, which was 380.4 kip-in. Based on these issues along with the scatter in the test results, it was decided to reduce the impact speed to 10 mph for the second series of tests. The corresponding kinetic energy of the striker in the second series was 95 kip-in.

Table 41. Test Results for Test Series 13009 Group 1 (2,372-lb pendulum, velocity = 20 mph, impact point = 21.5 inches).

Test No.	Test Date	Post No.	Ring Density	Ground-Line (in)	Moisture Content (%)	Weight (lb)	Resistograph Score		At Peak Force				Rupture Energy (kip-in)
							S _M	S _U	Force (kip)	Deflection (in)	Energy (kip-in)	Moment* kip-in	
13009B	9/24/2013	3	5.0	7.6	43.0	61	0.2	0.2	5.8	1.5	6.4	131.2	6.7
13009C	9/24/2013	1	8.9	6.8	>50	88	0.1	0.1	9.1	0.8	6.7	205.7	7.4
13009D	9/24/2013	2	3.9	7.1	39.8	52	0.1	0.1	7.1	0.9	8.8	159.8	9.3
13009E	9/24/2013	7	8.0	7.5	-	69	0.6	0.6	9.4	0.8	11.9	212.4	12.0
13009F	9/24/2013	12	7.0	6.6	46.8	67	0.3	0.3	7.6	0.9	7.4	171.9	8.4
13009G	9/24/2013	4	4.7	7.6	-	85	0.8	0.7	10.5	0.8	14.6	235.8	17.8
13009H	9/25/2013	36	7.7	6.5	>50	74	0.3	0.3	8.2	2.4	8.7	184.2	9.3
13009I	9/25/2013	14	7.4	8.1	>50	104	0.3	0.3	13.6	1.0	14.2	305.6	17.7
13009J	9/25/2013	15	5.1	7.0	>50	58	0.2	0.2	8.2	1.0	6.4	184.9	8.5
13009K	9/25/2013	B	5.8	7.2	-	71	0.8	0.9	16.1	1.9	21.3	362.4	25.0
13009L	9/25/2013	A	9.4	7.2	-	72	0.8	0.9	19.1	2.2	32.2	429.4	37.2
13009M	9/25/2013	13	6.4	7.8	>50	87	0.4	0.4	15.0	2.2	16.6	336.9	16.7
13009N	9/26/2013	62	6.5	7.7	>50	64	0.2	0.2	-	-	-	-	-
13009O	9/26/2013	40	7.2	7.8	>50	87	0.3	0.3	2.4	1.1	4.9	54.8	7.2
13009P	9/26/2013	19	4.6	7.9	>50	69	0.3	0.3	7.1	0.8	5.1	159.0	6.6
13009Q	9/26/2013	22	6.7	8.9	47.7	100	0.5	0.5	8.5	5.0	31.1	191.1	35.1
13009R	9/26/2013	18	6.2	7.8	>50	72	0.6	0.6	10.1	0.8	11.6	227.2	12.4
13009S	9/26/2013	46	8.7	9.2	>50	116	0.6	0.5	9.5	0.9	7.1	214.2	10.3
13009T	9/27/2013	74	7.0	6.6	>50	42	0.1	0.2	6.4	2.3	8.7	144.8	9.9
13009U	9/27/2013	41	7.0	7.5	28.1	61	0.5	0.6	20.7	2.1	22.4	465.3	22.4
13009V	9/27/2013	38	5.6	6.8	>50	58	0.2	0.2	7.5	0.8	9.0	169.0	9.6
13009W	9/27/2013	39	4.3	6.4	>50	53	0.4	0.4	7.4	0.8	9.3	166.0	9.3

* Moment computed based on estimated moment arm of 22.5 inches.

- Data was not collected.

Test Series 13009 Group 2 (10 mph Impact Speed)

Table 42 provides the peak force, the strain energy at initiation of rupture, peak moment, and the energy at complete rupture for each post in Test Series 13009 Group 2. The test summary sheets for this test series are shown in Appendix E. For the 39 tests, the peak force ranged from 3.25 kips to 18.4 kips, with a mean of 9.32 kips and standard deviation of 3.75 kips. The strain energy of the post at the point of initial rupture ranged from 4 kip-in to 43.3 kip-in, with mean of 21.4 and standard deviation 11.5. The total energy absorbed by the post at the point of complete rupture ranged from 5.44 kip-in to 80.6 kip-in, with a mean of 27.7 and standard deviation of 16.0. These statistics are summarized in Table 43, and the cumulative distribution functions for these three strength capacity metrics are shown in Figures 120 through 122.

Correlation of Resistograph Measurements to Test Results

The data from Group 2 of Test Series 13009 were used to assess the relationship between the resistograph measurements to peak force and energy capacity of the posts. Figure 123 shows a plot of the peak impact force vs. M^* ; Figure 124 shows a plot of the maximum resistive moment vs. M^* ; Figure 125 shows a plot of the strain at initiation of rupture vs. U^* ; and Figure 126 shows a plot of the rupture energy vs. U^* . The linear regression of the data for the peak force and peak moment curves yielded R^2 values of 0.71 and 0.70, respectively, which indicated that both curves fit the data reasonably well. The linear regression fit of the energy at rupture initiation yielded an R^2 value of 0.66, which indicated that this curve was also a reasonable fit. The linear regression for the rupture energy data, however, yielded R^2 value of 0.43 which indicated a significant scatter in the data.

From visual inspection of the resistograph results (see Appendix E), it was apparent that at least two of the resistograph measurements were in error. These were for Post 53 of Test 13009Q1 and Post 21 of Test 13009 S1, as shown in Figure 127 and Figure 128, respectively. The resistograph data for these two posts showed abnormally high readings for very local sections of the posts, which indicate that the drilling needle likely encountered a knot at those locations or an error occurred when performing the resistograph test. This error was not discovered until after the post was destroyed in the pendulum test, so the resistograph reading could not be retaken. Excluding these data from the results yields better correlation with the test results. Figure 129 and Figure 130 show the results for Peak Force vs. M^* and Energy at Rupture Initiation vs. U^* , respectively, for the revised data set. The resulting R^2 values improved to 0.82 and 0.76 for these two correlation plots.

In the plot for U^* vs. Rupture Energy, there were two data points that appeared to be outliers (see Figure 126). These points correspond to Tests 13009T1 and 13009Y1. The rupture of the post was very ductile in those two cases, resulting in a relatively high energy absorption compared to the rupture energy in all other tests (refer to Appendix E). There were no obvious signs for why those two posts resulted in such marked difference in behavior compared to the other posts. For example, visual inspection of the resistograph data for these two posts did not indicate any apparent error in the data (see Figure 131 and Figure 132). Also, the impact test results did not show significant error regarding the plots for Force vs. M^* or Energy at Rupture Initiation vs. U^* (see circled data points in Figure 129 and Figure 130).

Table 42. Test Results for Test Series 13009 Group 2 (2,372-lb pendulum, velocity = 10 mph, impact point = 21.5 inches).

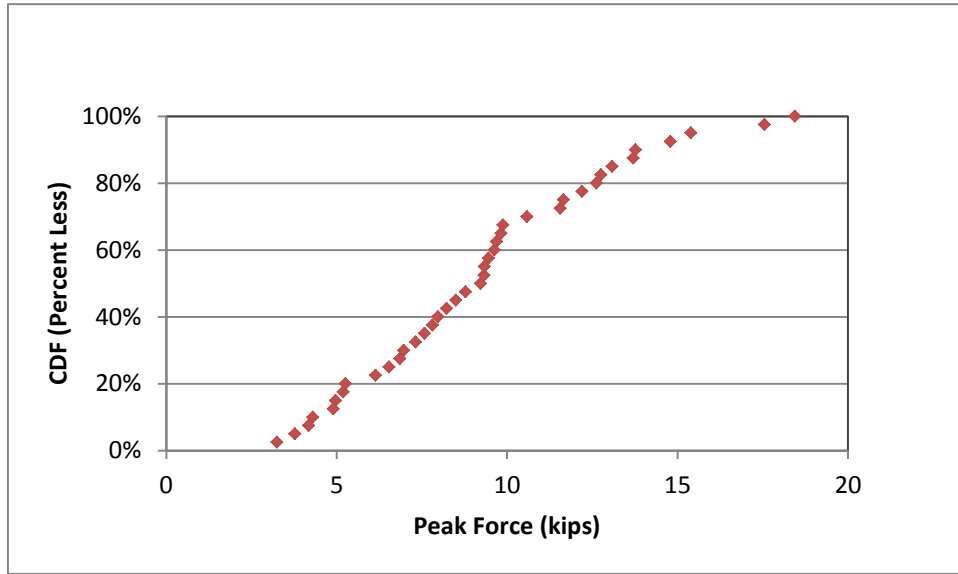
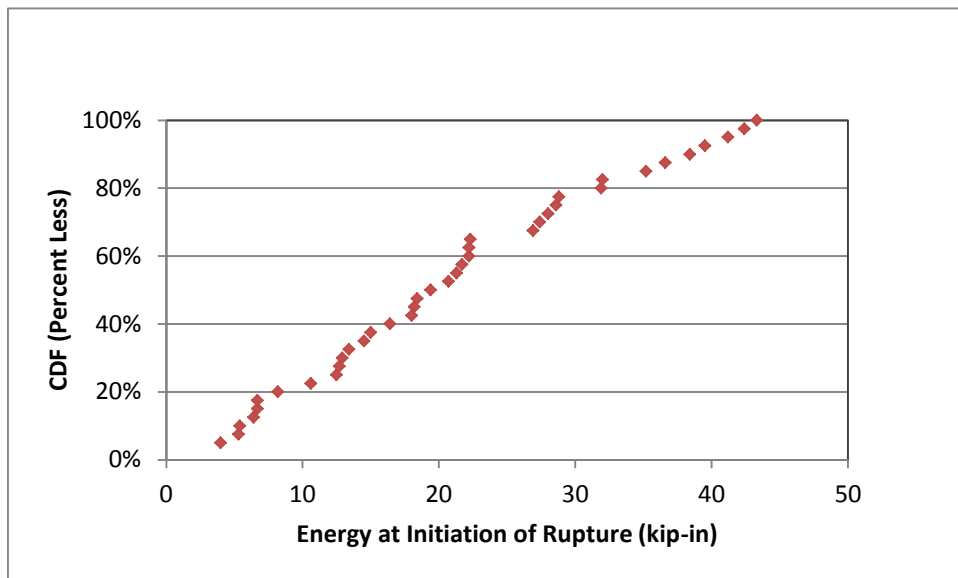
Test No.	Test Date	Post No.	Ring Density	Ground-Line (in)	Moisture Content (%)	Weight (lb)	Resistograph Score		At Peak Force				Rupture
							S _M	S _U	Force (kip)	Deflection (in)	Energy (kip-in)	Moment kip-in	Energy (kip-in)
13009Y	10/1/2013	43	5.8	7.6	-999.0	85	0.6	0.6	9.9	2.5	12.7	230.8	18.1
13009Z	10/1/2013	56	7.4	8.1	45.1	92	0.7	0.6	7.6	3.8	21.3	194.3	24.3
13009A1	10/1/2013	50	12.7	7.4	-999.0	74	0.4	0.4	6.9	2.8	8.2	158.6	12.8
13009B1	10/1/2013	31	4.5	7.6	-999.0	70	0.2	0.2	4.2	2.4	6.4	97.6	7.6
13009C1	10/1/2013	47	6.8	8.0	0.0	93	0.6	0.6	5.2	2.7	16.4	127.3	18.4
13009D1	10/1/2013	55	7.1	7.3	37.7	63	0.6	0.6	8.8	3.0	15.0	228.3	21.6
13009E1	10/1/2013	32	5.9	8.8	-999.0	119	1.1	1.0	15.4	4.7	38.4	402.0	43.8
13009F1	10/1/2013	88	5.3	7.6	-999.0	56	0.1	0.1	4.9	3.6	10.6	108.4	10.8
13009G1	10/2/2013	71	7.9	7.6	42.2	70	0.7	0.7	9.5	2.5	26.9	230.6	30.9
13009H1	10/2/2013	30	7.0	8.0	43.6	73	0.8	0.8	12.2	3.5	41.2	288.2	45.7
13009I1	10/2/2013	76	7.2	8.4	47.6	75	1.2	1.1	18.4	5.1	42.4	412.7	42.5
13009J1	10/2/2013	49	8.0	7.5	36.6	76	0.3	0.3	9.8	2.4	18.4	247.9	24.8
13009K1	10/2/2013	29	7.1	7.0	50.0	80	0.6	0.7	7.8	3.9	20.7	193.3	24.3
13009L1	10/2/2013	92	8.0	8.0	44.5	78	1.2	1.1	13.7	4.0	36.6	339.1	42.9
13009M1	10/2/2013	68	9.5	7.4	47.2	69	0.9	1.0	14.8	4.4	32.0	354.8	34.9
13009N1	10/3/2013	17	7.5	8.0	48.0	76	0.4	0.4	7.3	2.2	12.9	162.7	16.2
13009O1	10/3/2013	94	6.1	6.6	50.0	47	0.2	0.3	3.8	2.1	5.3	86.7	6.3
13009P1	10/3/2013	44	7.9	7.6	50.0	80	0.4	0.4	9.3	3.5	22.3	257.5	22.9
13009Q1	10/3/2013	53	6.3	7.6	47.6	68	0.7	0.7	4.3	1.1	4.0	97.2	7.8
13009R1	10/3/2013	84	9.1	6.6	49.7	84	0.4	0.5	8.0	2.7	21.7	175.3	23.0
13009S1	10/3/2013	21	12.6	8.0	50.0	109	0.8	0.8	8.5	2.3	12.5	217.8	18.5
13009T1	10/3/2013	63	8.0	7.5	37.3	62	0.7	0.7	9.7	7.6	28.0	213.2	61.5
13009U1	10/3/2013	65	8.4	7.6	50	68	0.3	0.3	8.2	3.6	14.5	186.0	17.8
13009V1	10/8/2013	90	4.6	7.0	50	49	0.1	0.1	3.2	2.4	6.7	70.6	6.8
13009W1	10/8/2013	118	7.3	7.7	50	79	0.3	0.3	5.3	2.1	6.7	121.0	9.7

Table 42. [CONTINUED] Test Results for Test Series 13009 Group 2 (2,372-lb pendulum, velocity = 10 mph, impact point = 21.5 inches).

Test No.	Test Date	Post No.	Ring Density	Ground-Line (in)	Moisture Content (%)	Weight (lb)	Resistograph Score		At Peak Force				Rupture Energy (kip-in)
							S _M	S _U	Force (kip)	Deflection (in)	Energy (kip-in)	Moment kip-in	
13009X1	10/8/2013	81	6.6	6.7	50	87	0.3	0.4	6.1	4.0	18.0	141.3	30.7
13009Y1	10/8/2013	123	4.6	8.3	50	92	0.7	0.6	9.2	3.2	19.4	217.8	80.6
13009Z1	10/8/2013	61	6.1	8.2	45.5	90	0.7	0.7	11.6	4.4	35.2	294.2	43.5
13009A2	10/8/2013	67	5.1	8.2	50	83	0.8	0.8	10.6	3.5	22.2	239.5	26.0
13009B2	10/8/2013	126	7.0	8.3	50	93	1.0	0.9	13.1	5.0	43.3	304.2	47.2
13009C2	10/8/2013	91	8.6	8.6	46.16	93	1.1	1.0	17.5	3.8	28.6	364.1	36.8
13009D2	10/9/2013	105	4.9	7	50	63	0.2	0.2	5.0	2.2	5.4	121.1	5.4
13009 E2	10/9/2013	117	5.8	8.6	46.2	81	0.4	0.4	9.6	3.5	18.2	227.5	18.3
13009F2	10/9/2013	129	7.7	7.25	50	79	0.4	0.4	6.5	3.4	13.4	165.0	19.9
13009G2	10/9/2013	24	7.1	8.4	50	84	0.6	0.6	12.6	3.6	27.4	290.4	29.6
13009H2	10/9/2013	35	5.4	8.1	50	86	0.7	0.7	7.0	2.2	22.2	160.3	25.8
13009I2	10/9/2013	78	6.3	7.6	36.28	78	0.9	0.9	13.8	5.0	39.5	330.4	44.5
13009J2	10/9/2013	111	7.4	7.6	50	71	0.7	0.8	12.8	4.0	28.8	309.3	40.4
13009K2	10/9/2013	114	8.8	8	47.84	69	0.8	0.8	11.6	4.6	31.9	268.8	33.3

Table 43. Statistics for Post Strength Capacity from Pendulum Test Series 13009 (Group 2).

Capacity Measure	Post Strength Statistics			
	Mean	Std. Dev.	Min	Max
Peak Force	9.32	3.75	3.25	18.44
Energy at Initial fracture	21.42	11.47	4.00	43.30
Energy at Complete Rupture	27.68	16.04	5.44	80.60

**Figure 120. Cumulative distribution plot for the peak force values measured in Test Series 13009 (Group 2).****Figure 121. Cumulative distribution plot for the strain energy in the post at initiation of rupture measured in Test Series 13009 (Group 2).**

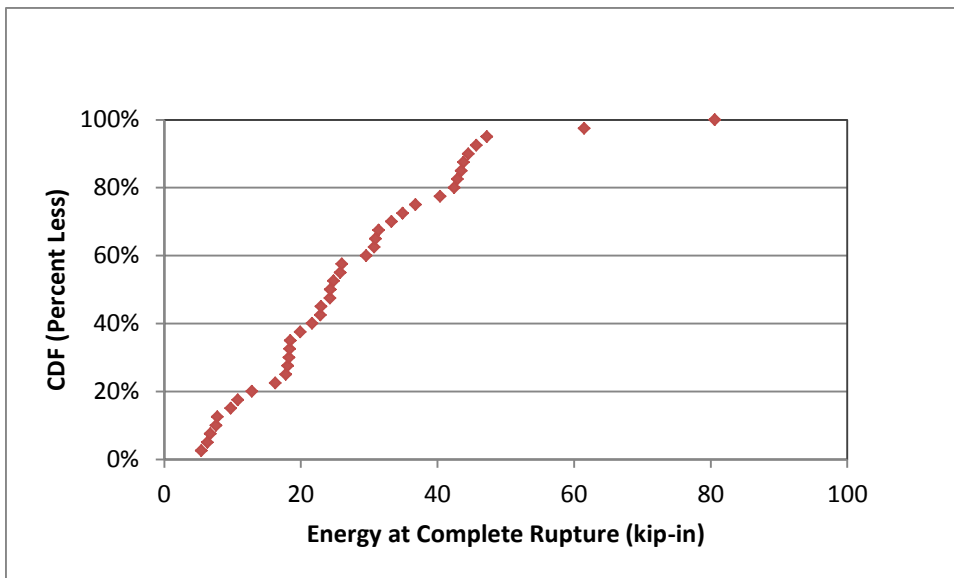


Figure 122. Cumulative distribution plot for the total energy absorbed by the post at complete rupture measured in Test Series 13009 (Group 2).

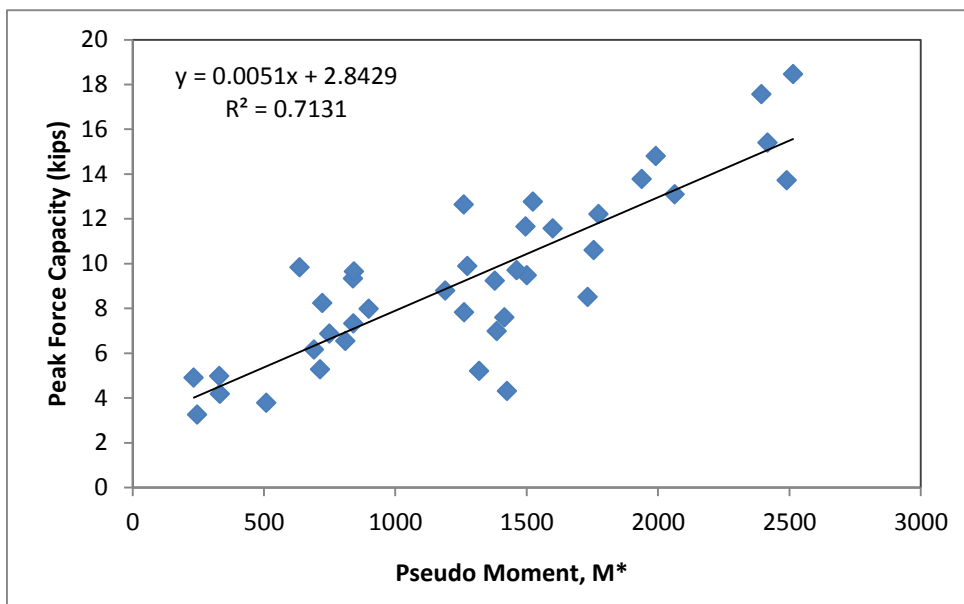


Figure 123. Peak Force vs. M^* for Test Series 13009 Group 2 (all data).

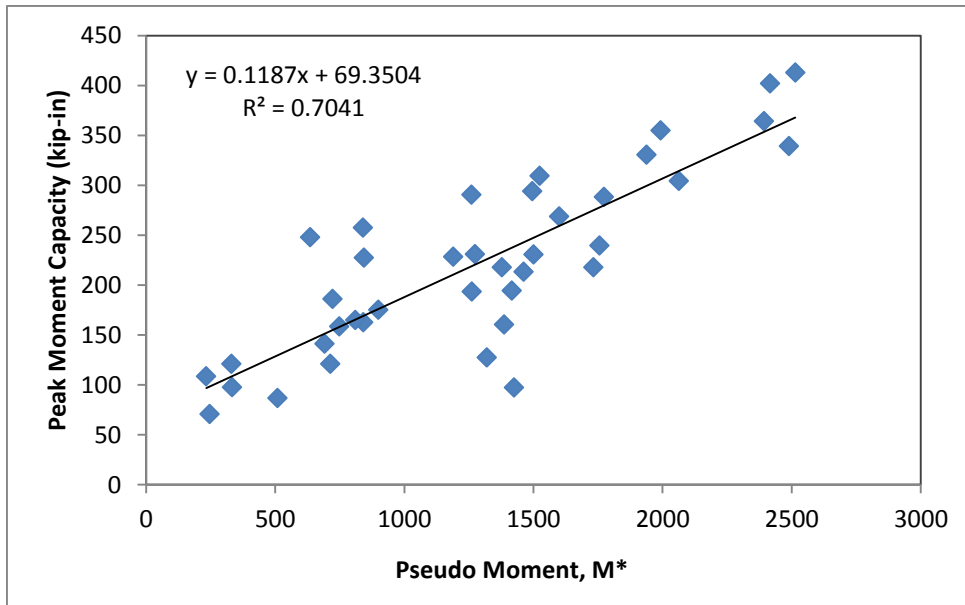


Figure 124. Peak Moment vs. M^* for Test Series 13009 Group 2 (all data).

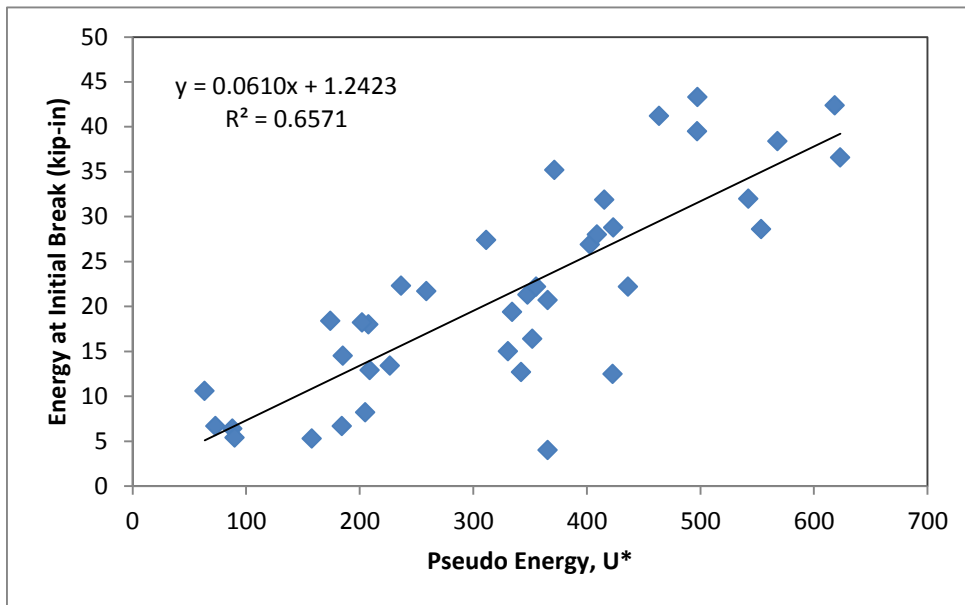


Figure 125. Energy at rupture initiation vs. U^* for Test Series 13009 Group 2 (all data).

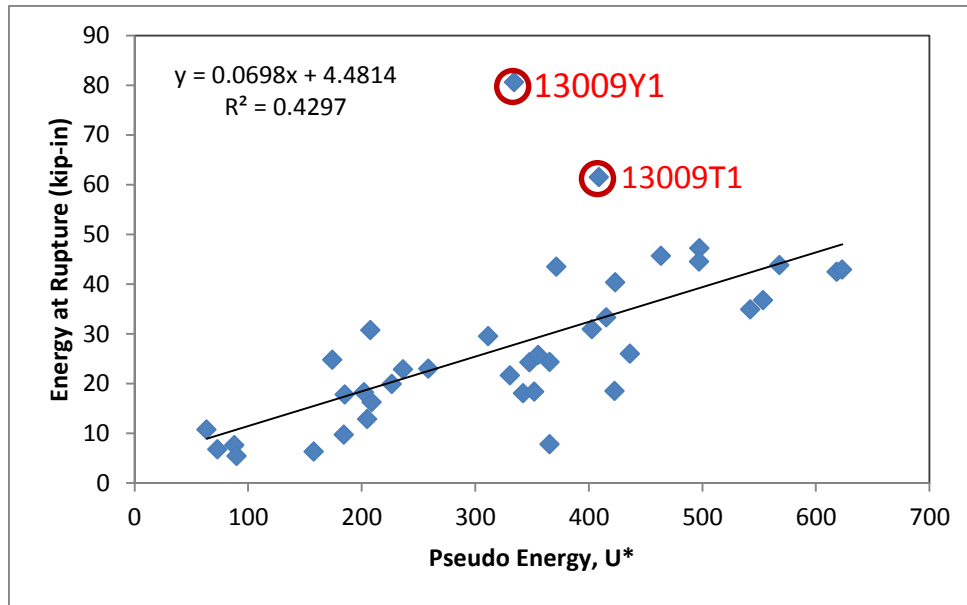


Figure 126. Rupture Energy vs. U^* for Test Series 13009 group 2 (all data).

Test Information	
Test Number:	13009Q1
Test Date:	03-Oct-2013
Post Properties	
Post Number:	53
Post Type:	Round SYP
Post Length:	66 inches
Post Diameter:	7.64 inches
Moisture Content:	47.62%
Ring Density (avg.):	6.2 per inch
Resi Score S_{MOR} :	0.68
Resi Score S_U :	0.67
Pendulum Properties	
Weight:	2,372 lb
Impact Speed:	10 mph
Impact Height:	21.5 inches



Ring density at bottom of post



Fractured Post

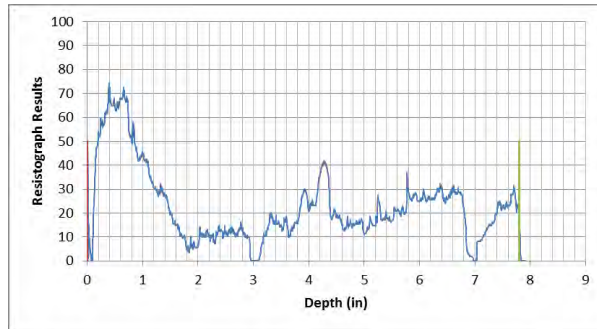
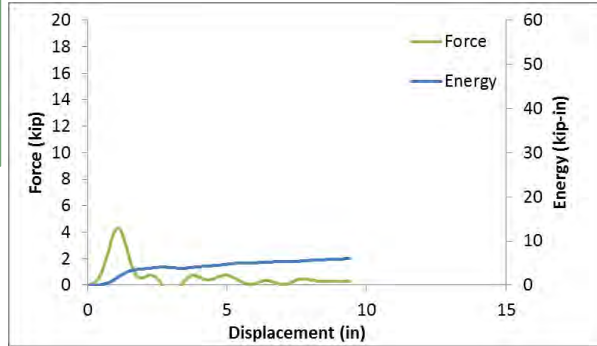
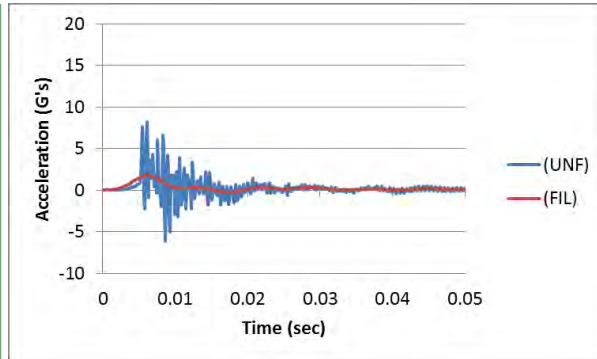


Figure 127. Test Summary Sheet for Test 13009Q1.

Test Information	
Test Number:	13009S1
Test Date:	03-Oct-2013
Post Properties	
Post Number:	21
Post Type:	Round SYP
Post Length:	66 inches
Post Diameter:	7.96 inches
Moisture Content:	< 50%
Ring Density (avg.):	12.2 per inch
Resi Score S_{MOR} :	0.82
Resi Score S_U :	0.77
Pendulum Properties	
Weight:	2,372 lb
Impact Speed:	10 mph
Impact Height:	21.5 inches



Ring density at bottom of post



Fractured Post

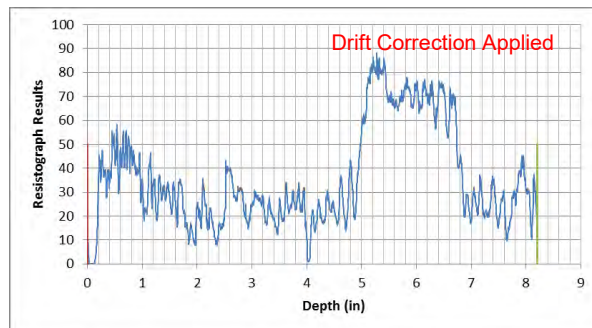
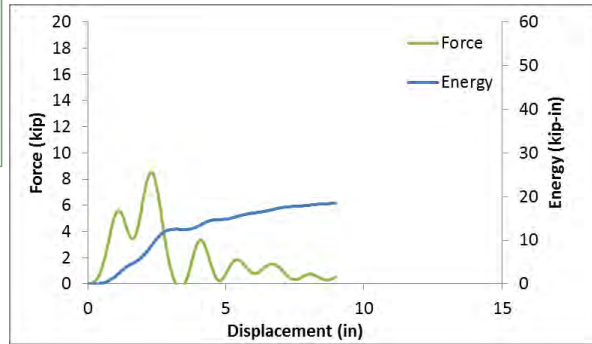
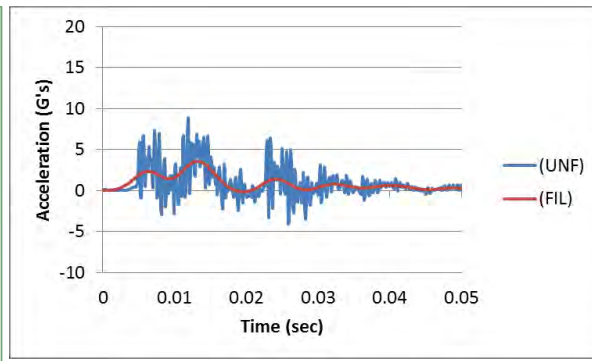


Figure 128. Test Summary Sheet for Test 13009S1.

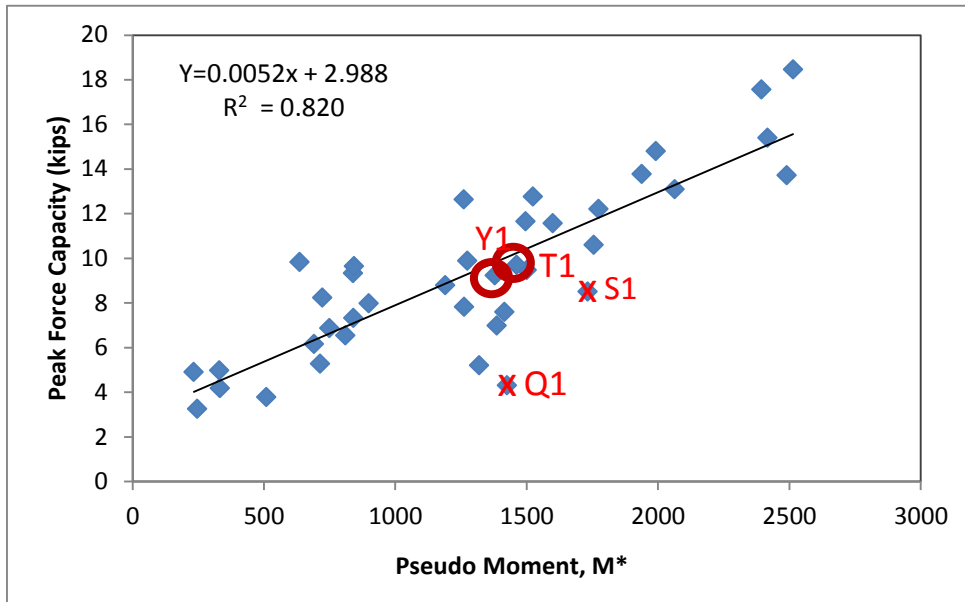


Figure 129. Peak Force vs. M^* for Test Series 13009 Group 2 (revised data set).

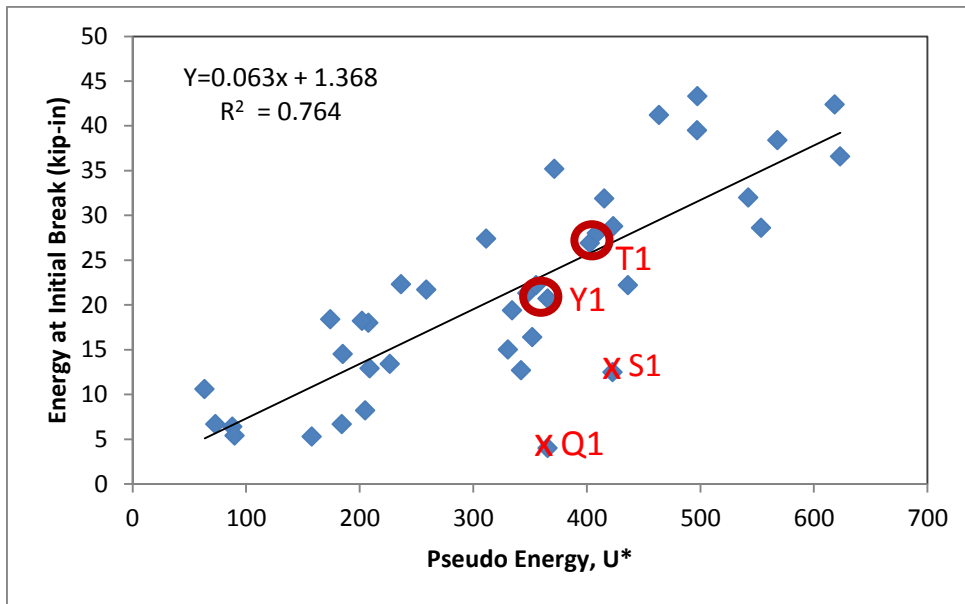
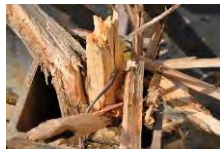


Figure 130. Energy at Initial Break vs. U^* for Test Series 13009 Group 2 (revised data set).

Test Information	
Test Number:	13009T1
Test Date:	03-Oct-2013
Post Properties	
Post Number:	63
Post Type:	Round SYP
Post Length:	66 inches
Post Diameter:	7.48 inches
Moisture Content:	37.26%
Ring Density (avg.):	8.0 per inch
Resi Score S_{MOR} :	0.69
Resi Score S_U :	0.75
Pendulum Properties	
Weight:	2,372 lb
Impact Speed:	10 mph
Impact Height:	21.5 inches



Ring density at bottom of post



Fractured Post

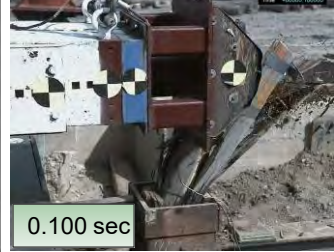
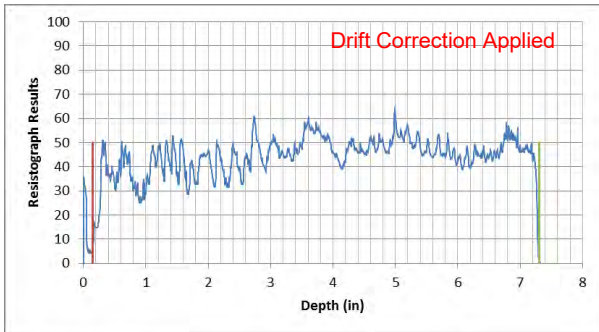
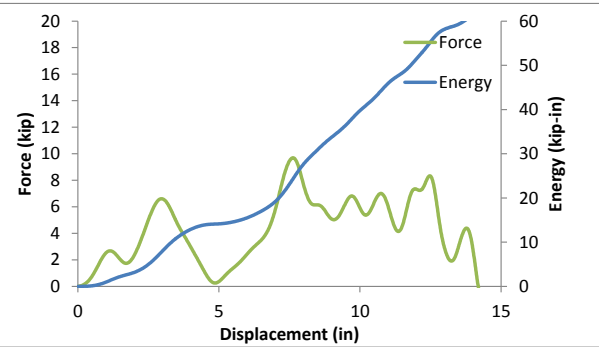
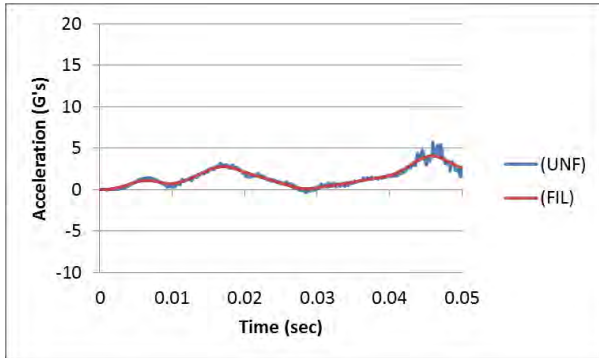


Figure 131. Test Summary Sheet for Test 13009T1.

Test Information	
Test Number:	13009Y1
Test Date:	08-Oct-2013
Post Properties	
Post Number:	123
Post Type:	Round SYP
Post Length:	66 inches
Post Diameter:	8.28 inches
Moisture Content:	< 50%
Ring Density (avg.):	4.6 per inch
Resi Score S_{MOR} :	0.66
Resi Score S_U :	0.61
Pendulum Properties	
Weight:	2,372 lb
Impact Speed:	10 mph
Impact Height:	21.5 inches



Ring density at bottom of post



Fractured Post

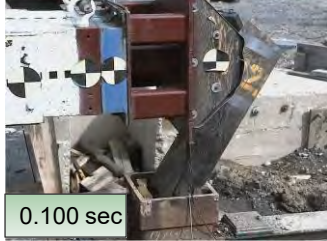
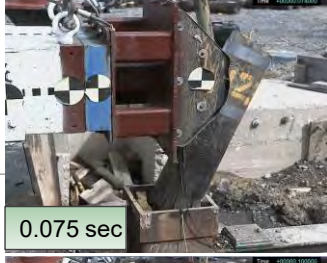
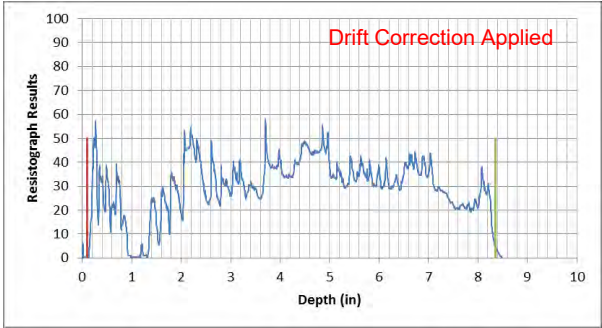
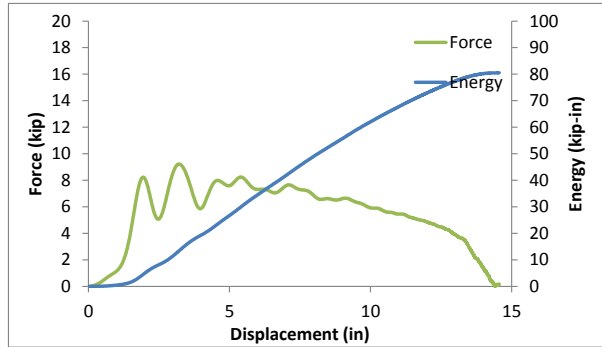
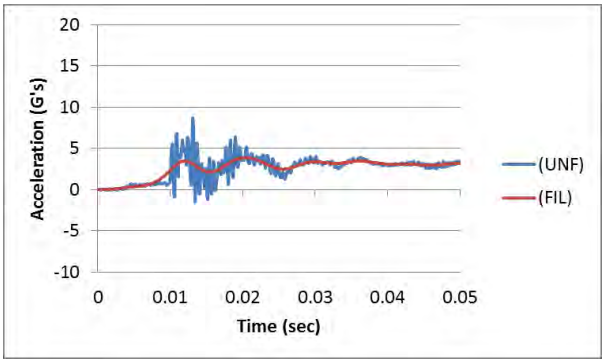


Figure 132. Test summary sheet for Test 13009Y1.

Quantifying Wood Post Deterioration Damage Levels

The pendulum impact tests conducted in Test Series 13009 were used to establish four levels of damage for deteriorated guardrail posts. For the assessment, only those tests with post diameters ranging from 8.0 to 8.2 inches were selected in order to eliminate the effects of post size. There were a total of 10 tests that met this criterion. These tests were then sorted based on strain energy absorbed by the post at the time of fracture initiation. The results are shown in Table 44 and in Figures 133 - 135. The four deterioration levels are summarized in Table 45 in terms of force capacity and energy capacity. Figure 136 shows examples of aged posts corresponding to deterioration levels DL1 through DL3.

For convenience the values for pseudo moment M^* and the pseudo energy U^* were normalized based on their values at the threshold of Damage Level 1 (DL1), such that for scores greater than 1 the post is considered undamaged. Figure 137 shows a graphical representation of damage levels with respect to resi-score S_{M^*} and load capacity; and Figure 138 shows a graphical representation of the damage levels with respect to resi-score, S_U , and strain energy capacity. The values for M^* and U^* are computed slightly differently, but when normalized the resulting scores corresponding to each of the damage levels are essentially identical; thus, either score may be used. The fourth column of Table 45 shows the damage level in terms of resistograph scores and the last column of Table 45 presents the damage levels in terms of relative capacity. Therefore, if post strength is measured or otherwise determined in the field via alternative means (e.g., stress wave techniques, force-deflection techniques, etc.) then the relative capacity may be used to identify damage level.

Table 44. Deterioration damage levels for posts in Test 13009 Series 2 based on strain energy.

Damage Level	Test No.	Test Date	Post No.	Ring Density	Ground-Line (in)	Moisture Content (%)	Weight (lb)	Resistograph Score		At Peak Force				Rupture Energy (kip-in)
								S_M	S_U	Force (kip)	Deflection (in)	Energy (kip-in)	Moment kip-in	
DL1	13009H1	10/2/2013	30	7.0	8.0	43.6	73	0.8	0.8	12.2	3.5	41.2	288.2	45.7
	13009L1	10/2/2013	92	8.0	8.0	44.5	78	1.2	1.1	13.7	4.0	36.6	339.1	42.9
	13009Z1	10/8/2013	61	6.1	8.2	45.5	90	0.7	0.7	11.6	4.4	35.2	294.2	43.5
	13009K2	10/9/2013	114	8.8	8.0	47.8	69	0.8	0.8	11.6	4.6	31.9	268.8	33.3
DL2	13009H2	10/9/2013	35	5.4	8.1	50.0	86	0.7	0.7	7.0	2.2	22.2	160.3	25.8
	13009A2	10/8/2013	67	5.1	8.2	50.0	83	0.8	0.8	10.6	3.5	22.2	239.5	26.0
	13009Z	10/1/2013	56	7.4	8.1	45.1	92	0.7	0.6	7.6	3.8	21.3	194.3	24.3
DL3	13009C1	10/1/2013	47	6.8	8.0	0.0	93	0.6	0.6	5.2	2.7	16.4	127.3	18.4
	13009N1	10/3/2013	17	7.5	8.0	48.0	76	0.4	0.4	7.3	2.2	12.9	162.7	16.2
	13009S1	10/3/2013	21	12.6	8.0	50.0	109	0.8	0.8	8.5	2.3	12.5	217.8	18.5

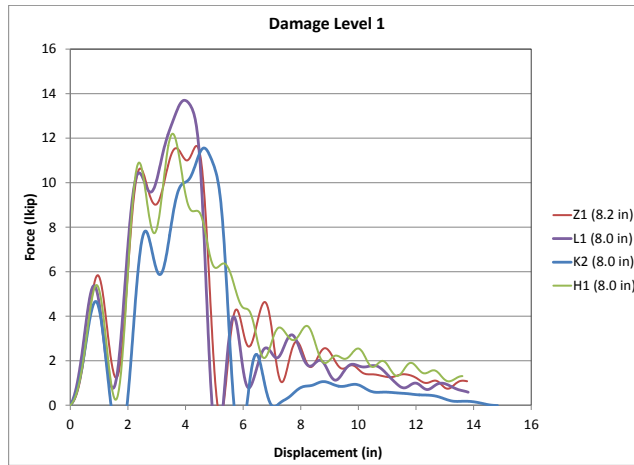


Figure 133. Pendulum impact tests from Series 13009 corresponding to deterioration damage level 1 (DL1).

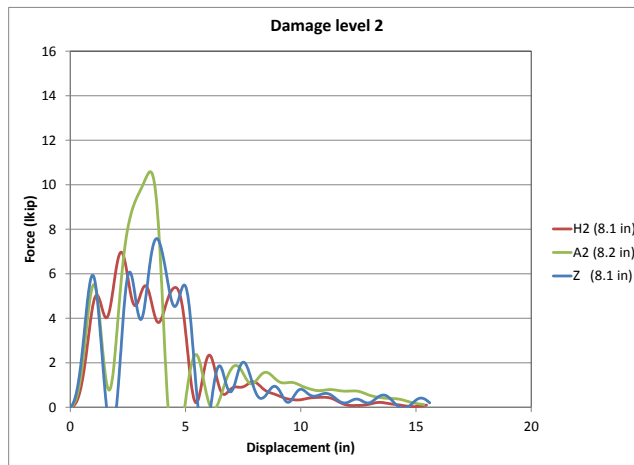


Figure 134. Pendulum impact tests from Series 13009 corresponding to deterioration damage level 2 (DL2).

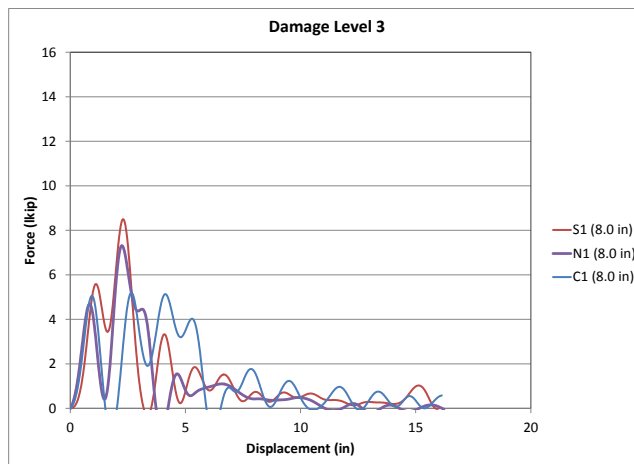


Figure 135. Pendulum impact tests from Series 13009 corresponding to deterioration damage level 3 (DL3).

Table 45. Damage levels for guardrail post deterioration.

Damage Level	8-inch Round Posts (nominal)			General
	Capacity		Resi Score	Relative Capacity
	Peak Force (kips)	Strain Energy (kip-in)	S_U or S_M	
0 (new)	> 14	> 35	>1	100%
1	12 - 15	26 - 40	0.83 - 1.0	83%
2	7 - 13	20 - 30	0.57 - 0.83	57%
3	< 9	< 20	< 0.57	< 57%



	DL3		DL2		DL1	
	<u>Score</u>	<u>Criteria</u>	<u>Score</u>	<u>Criteria</u>	<u>Score</u>	<u>Criteria</u>
Force (k):	3.8	< 9	7.6	7-13	14.8	12-15
Energy (k-in):	5.3	< 20	21.3	20-30	32	26-40
Resi:	0.24	< 0.57	0.67	0.57 - 0.83	0.95	0.83 - 1.0

Figure 136. Examples of aged posts corresponding to deterioration levels DL1 through DL3.

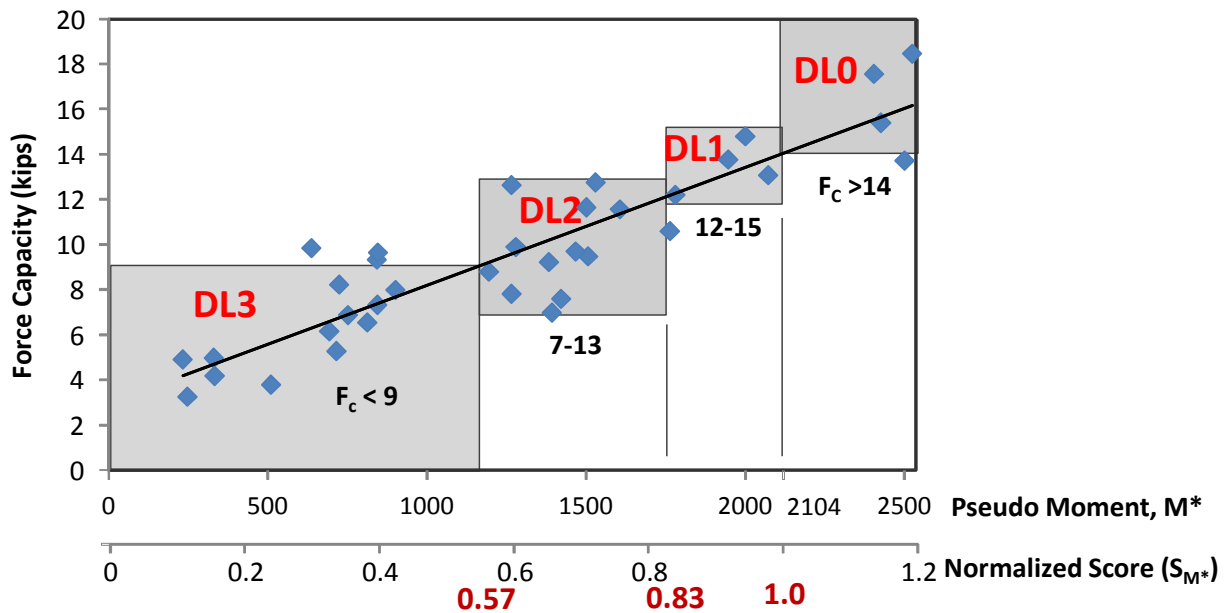


Figure 137. Graphical representation of damage levels with respect to resi-score, S_M , and load capacity.

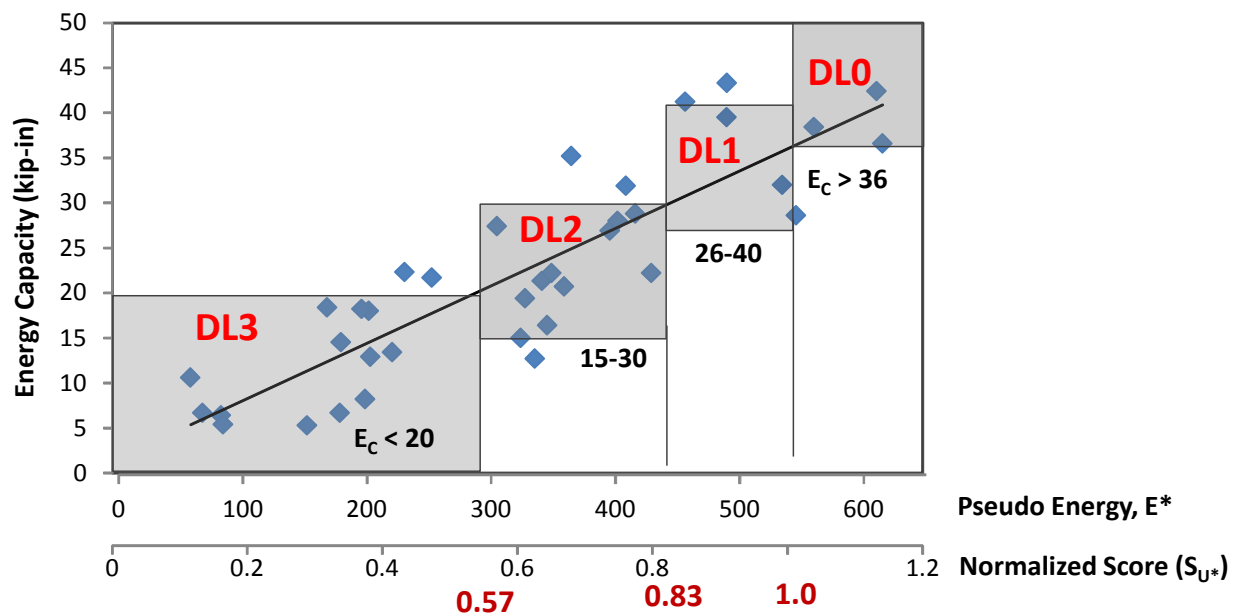


Figure 138. Graphical representation of damage levels with respect to resi-score, S_U , and strain energy capacity.

Visual and Auditory Cues

If strength and/or deterioration measurement tools are not available, then visual inspection and “sounding” procedures should be utilized by experienced maintenance personnel to assess the soundness of the posts. Refer to Figure 136 in regard to the following damage assessment cues.

DL3: Significant deterioration at top of post is usually evident. Deterioration is often deep (>1”) and covers the full cross-section of the post. Mildew or mold is often present on the side of the post near the ground line; and the post is audibly very soft (punky) when struck with a hammer near the groundline.

DL2: Often marked by shallow deterioration at top of post (<1”), extending over most if not all the cross-section. Post is audibly soft but not punky when struck by a hammer.

DL1: Generally there is no deterioration evident at the top of the post. In some cases, however, signs of deterioration may exist near the top-center of post, but will not extend to the outer shell. The post is relatively sound when struck with a hammer.

Pendulum Testing of Posts-in-Soil

Scope

The tests were categorized into two groups. Group 1 was conducted to establish a baseline soil density, percent compaction and moisture content to be used throughout the remainder of the study. The purpose of this group of tests was to ensure consistency in soil stiffness and also to confirm that the soil conditions met the minimum strength requirements set forth in MASH.[MASH09] The second group of tests were designed to evaluate the impact response of the post-soil system for various levels of post degradation. Based on the results from the first group of tests; however, it was decided that the second group of tests would not provide additional information and was therefore not performed.

The target impact conditions for *Test Group 1* included a 2,372-lb rigid pendulum impacting the posts at an impact speed of 20 mph at a height of 24.88 inches above ground, which was consistent with the test procedures in MASH for measuring soil strength. The posts were 72 inches long and embedded 40 inches in the soil. Two types of posts were used in the study: 1) a steel W6x16 post and 2) round wood posts with diameters ranging from 7.2 to 8.4 inches.

The target impact conditions for *Test Group 2* included a 2,372-lb rigid pendulum impacting the posts at an impact speed of 20 mph at a height of 21.5 inches above ground; a post-length of 68-72 inches, and a post-embedment depth of 40 inches in the soil. The post specimens in these tests were to include both *new* and *used* posts. Several additional *new* posts were donated to the study by Road Systems, Inc. The *used* posts were to be drawn from the lot of guardrail posts extracted from damaged guardrail systems in Ohio (refer to Figure 104). The test specimens were sub-categorized based on their resistograph scores. DL0 in Table 47 denotes damage level 0, which corresponds to *new* post conditions. DL1 denotes damage level 1 which represents a low level of deterioration. Likewise, DL2 and DL3 represent increasing levels of deterioration. The test matrices for the two test groups are shown below in Table 46 and Table 47.

The soil for all tests conformed to Grading B of AASHTO M147-95 and was compacted in 6-inch lifts using a pneumatic tamper. The density, moisture content and degree of compaction of the soil was measured in front of and behind the post after each compaction process using a Troxler-model 3440 Surface Moisture-Density Gauge. There were a total of twelve readings which were averaged to determine the effective soil conditions.

Table 46. Post-in-Soil Test Group 1 (2,372-lb pendulum, v = 20 mph, impact point = 24.88 inches, embedment 40 inches).

Test No.	Test Date	Post Data											Soil Data			Impact Conditions		
		Post No.	Resi Score		Length (in)	Initial Weight (lbs)	Soak Time (hours)	Soak Weight (lbs)	Volume (in ³)	Wet Density (lb/ft ³)	Groundline Diameter (in)	Ring Density (rings/in)	Dry Density (pcf)	Moisture Content (%)	Compaction (%)	Pendulum		Impact Point (in)
			S _M	S _U												Weight (lbs)	Speed (mph)	
Preliminary Tests																		
13010A	10/23/2013	102	0.63	0.69	68.0	96.0	18.0	106	1936.7	94.6	7.6	8.4	148.3	4.0	98.7	2372	20	21.5
13010B	10/24/2013	54	1.04	0.95	68.0	90.0	N/A	90	2179.5	71.4	8.4	12.0				2372	20	21.5
13010C	10/29/2013	C	0.51	0.54	68.0	65.0	17.0	69	1683.9	70.8	7.3	8.2	142.1	3.6	94.7	2372	20	21.5
Soil Strength Tests																		
13010D	10/31/2013	W6x16	-	-	72.0	-	-	-	-	-	-	0.0	143.5	3.8	95.6	2372	20	24.9
13010E	11/4/2013	W6x16	-	-	72.0	-	-	-	-	-	-	0.0	132.4	3.1	88.1	2372	20	24.9
13010F	11/6/2013	W6x16	-	-	72.0	-	-	-	-	-	-	0.0	138.4	3.3	92.1	2372	20	24.9
13010G	11/8/2013	57	0.86	0.97	68.0	71.0	17.0	69	1671.7	71.3	7.2	9.2	138.6	3.4	92.3	2372	20	24.9
13010H	12/16/2013	D			72.0	81.0	-	81	1745.4	80.2	7.5	6.4	142.4	6.2	94.8	2372	20	24.9
13010I	12/18/2013	E			72.0	82.0	-	82	1770.4	80.0	7.4	4.1	-	-	-	2372	10	24.9

Table 47. Post-in-Soil Test Group 2 (2,372-lb pendulum, v = 20 mph, impact point = 21.5 inches, embedment 40 inches).

Test No.	Test Date	Post Data											Soil Data			Impact Conditions		
		Post No.	Resi Score		Length (in)	Initial Weight (lbs)	Soak Time (hours)	Soak Weight (lbs)	Volume (in ³)	Wet Density (lb/ft ³)	Groundline Diameter (in)	Ring Density (rings/in)	Dry Density (pcf)	Moisture Content (%)	Compaction (%)	Pendulum		Impact Point (in)
			S _{MOR}	S _U												Weight (lbs)	Speed (mph)	
13010J	TBD	TBD	DL0													2372	20	21.5
13013L	TBD	TBD	DL0													2372	20	21.5
13013M	TBD	TBD	DL0													2372	20	21.5
13013N	TBD	TBD	DL1													2372	20	21.5
13013O	TBD	TBD	DL1										BASELINE SOIL STIFFNESS Density ≈ 138 pcf Compaction ≈ 92% Moisture Content ≈ 3.4%			2372	20	21.5
13013P	TBD	TBD	DL1											2372	20	21.5		
13013Q	TBD	TBD	DL2											2372	20	21.5		
13013R	TBD	TBD	DL2											2372	20	21.5		
13010S	TBD	TBD	DL2											2372	20	21.5		
13010T	TBD	TBD	DL3											2372	20	21.5		
13010U	TBD	TBD	DL3											2372	20	21.5		
13010V	TBD	TBD	DL3											2372	20	21.5		

Soil Strength Tests

Preliminary Tests

The first three tests (i.e., 13010A, 13010B and 13010C) involved wooden posts selected from the lot of *used* posts obtained from the Ohio DOT. The resistograph score for Post No. 54 in Test 13010B was relatively high, as shown in Table 47. As such, it was expected that the post would rotate through the soil during the test without fracturing the post, and that the results could then be used to quantify soil stiffness.

All the tests, however, resulted in complete rupture of the posts with relatively little disturbance of the soil, as illustrated in Figure 139. Additional results can be found in Appendix F. The soil for these tests was compacted to a dry density of 142-148 pcf, corresponding to 95-99 percent soil compaction. It was apparent from these results that the soil was considerably stronger than the standard soil conditions recommended in MASH. It was then decided that soil stiffness tests would be carried out using the recommended procedures in *MASH* (which involves a rigid W6x16 steel post) to establish the baseline soil conditions to be used in the remainder of the study.

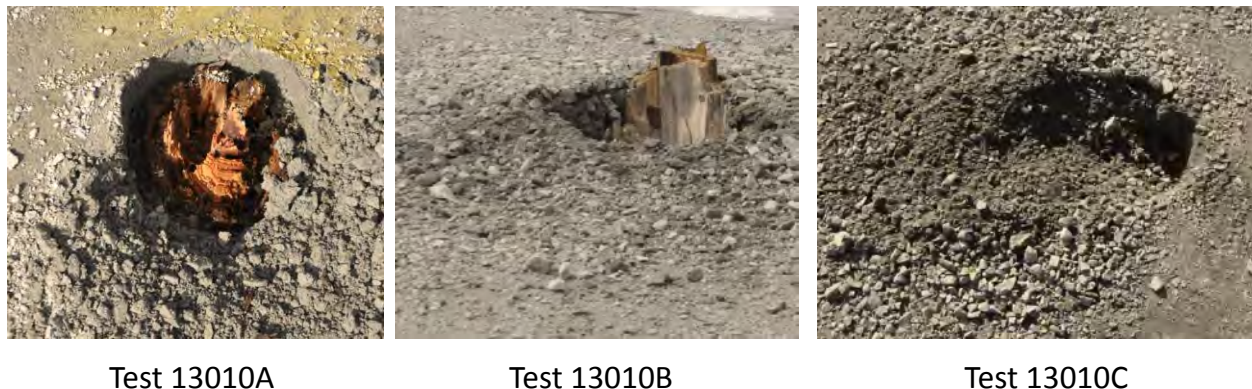


Figure 139. Tests 13010A, B and C resulted in relatively little soil displacement.

Steel W6x16 Post Tests

Tests 13010 D, 13010E and 13010F were performed using a W6x16 steel section post. The post was 72 inches long and embedded 40 inches in the soil. The 2,372-lb pendulum struck the posts at 24.88 inches above ground at an impact speed of 20 mph. Three levels of soil compaction were evaluated:

- Test 13010D: 96 percent soil compaction with an average soil density of 144 pcf.
- Test 13010E: 88 percent soil compaction with an average soil density of 132 pcf.
- Test 13010F: 92 percent soil compaction with average soil density of 138 pcf.

The results of these tests are shown in Figure 140 and Figure 141. The dashed line in Figure 140 represents the minimum strength requirements for the soil. The soil test with 96 percent compaction resulted in a peak impact force of 24 kips with total energy absorption of 317 kip-in. The soil test with 92 percent compaction resulted in a peak impact force of 13.2 kips with total energy absorption of 244 kip-in. The soil test with 88 percent compaction resulted in a peak

impact force of 12.3 kips with total energy absorption of 86.6 kip-in. The results clearly show that for 96 percent soil compaction (i.e., soil conditions used in the preliminary tests) the soil strength greatly exceeded the minimum strength conditions specified in *MASH*; at 92 percent soil compaction, the soil strength exceeded the minimum strength conditions by approximately 30 percent; and at 88 percent soil compaction the resulting strength was significantly less than *MASH* specifications. The soil conditions corresponding to 92 percent compaction were selected as the baseline for the remainder of the study.

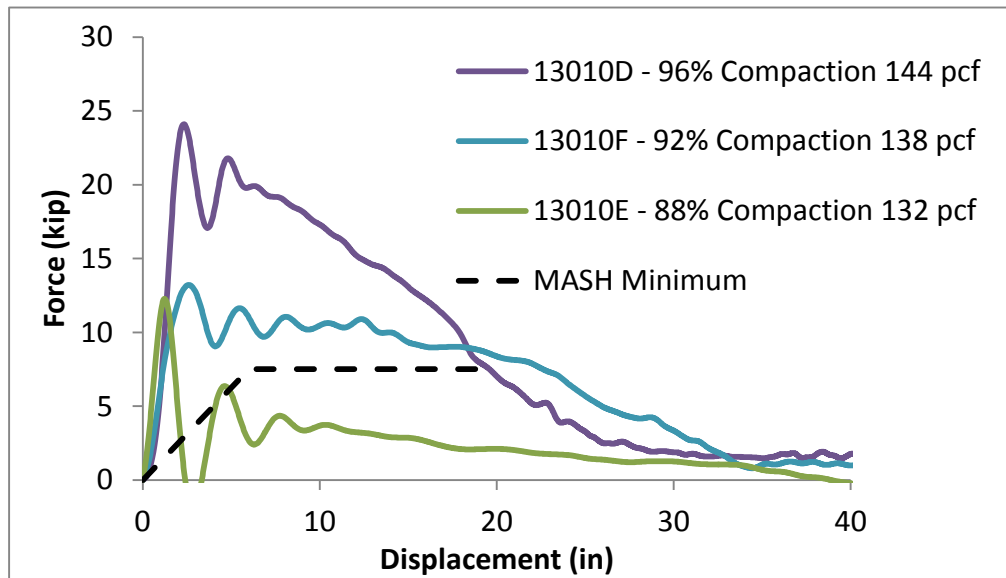


Figure 140. Force vs. deflection results for soil strength tests.

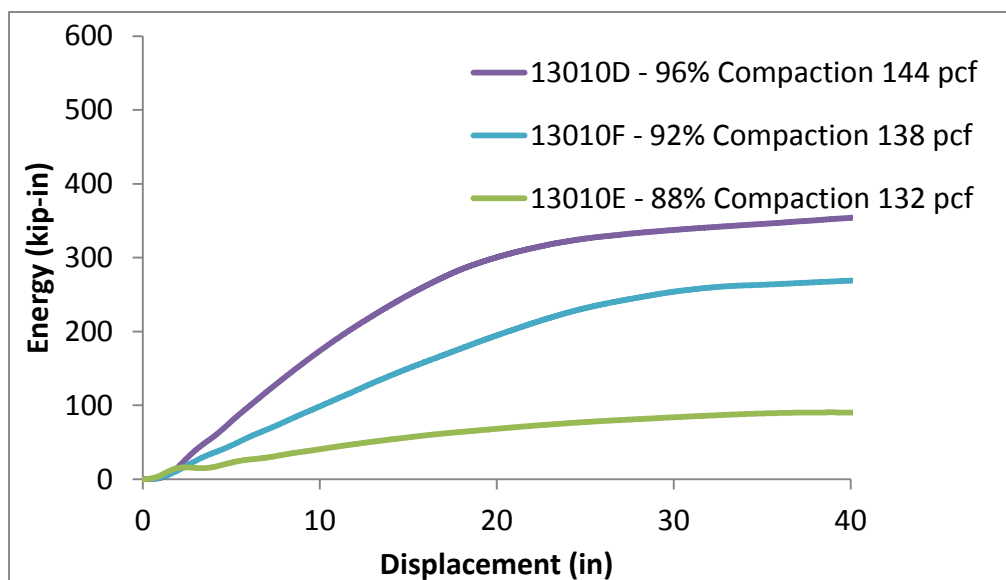


Figure 141. Energy vs. deflection results for soil strength tests.

Round Wood Post Tests

Tests 13010G, 13010H and 13010I were performed using a round wood posts. Test 13010G involved a 68-inch long post with a low level of deterioration (e.g., Resi Scores $S_M = 0.86$ and $S_U = 0.97$). Tests 13010 H and 13010I, involved new, *unused* posts 72 inches long. The posts were embedded 40 inches in the soil for all cases. The soil conditions for Test 13010G conformed to the baseline soil conditions with dry density of 138.6 pcf, moisture content of 3.4 percent and soil compacted to 92.3 percent. The soil conditions for Test 13010H, however, exceeded the baseline values with soil density equal 142.4 pcf, 6.2 percent moisture content and 94.8 percent compaction. The soil conditions were not measured for Test 13010I due to problems with soil density gauge; however, the same compaction procedure used in Test 13010G was followed.

In Tests 13010G and 13010H, the 2,372-lb pendulum struck the posts at 24.8 inches above ground at an impact speed of 20 mph. For Test 13010I, the impact speed was reduced to 10 mph. The results of these tests are shown in Figure 142 through Figure 144. The posts ruptured in each of the three tests. The peak force at rupture was 9.8 kips, 8.6 kips and 10.7 kips for Tests G, H, and I, respectively, compared to a maximum resistive force of 13.2 kips for the soil (refer to Figure 140). Based on the results of these tests, it appears that the round wood post with nominal diameter of 8 inches does not have sufficient strength to properly rotate through the soil, for this baseline soil strength. Further, it should be noted that these tests were conducted with an embedment depth of 40 inches, whereas the construction drawings in the AASHTO-AGC-ARTBA Barrier Hardware Guide show the standard embedment depth for the G4(2W) guardrail system to be 44 inches.[AASHTO04]

Wood Post Strength Test

Based on the results of Tests 13010G, 13010H and 13010I, which involved two new posts and one used (but very sound) post, it was decided that it would not be meaningful to perform the second group of tests. Over 85 percent of the posts tested in Test Series 13009 resulted in peak impact forces that were less than 13.2 kips (e.g., peak resistance of baseline soil), as shown in Figure 120; and those that exceeded this strength had very low deterioration and/or relatively large cross-section diameters.

Effects of Post Shape (Round vs. Rectangular) on Load Capacity

The bending load capacity of a guardrail post is proportional to its section modulus, which for a circular cross-section post is:

$$S_{round} = \frac{\pi r^3}{4}$$

For 6x8 rectangular posts, the section modulus is defined for the strong and weak directions by:

$$S_{6x8(strong)} = \frac{bh^2}{6} = 64in^3$$

$$S_{6x8(weak)} = \frac{hb^2}{6} = 48in^3$$

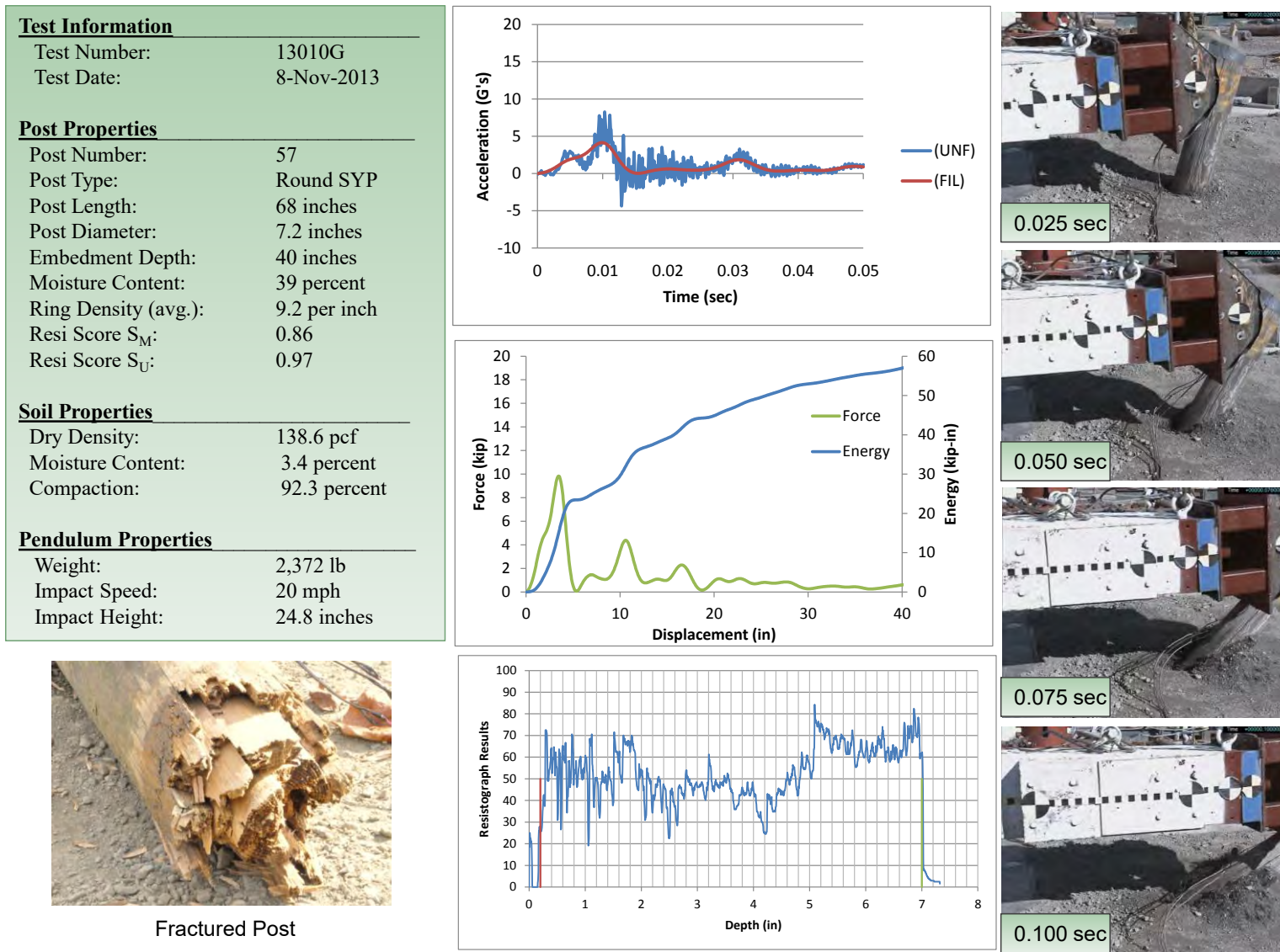
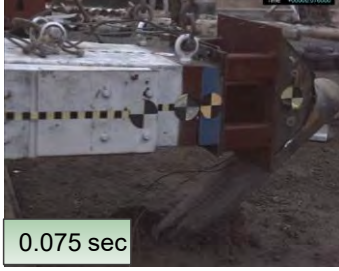
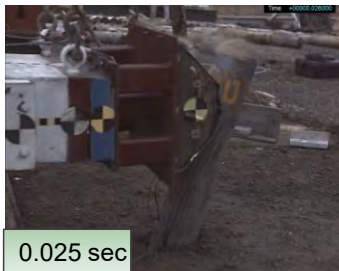
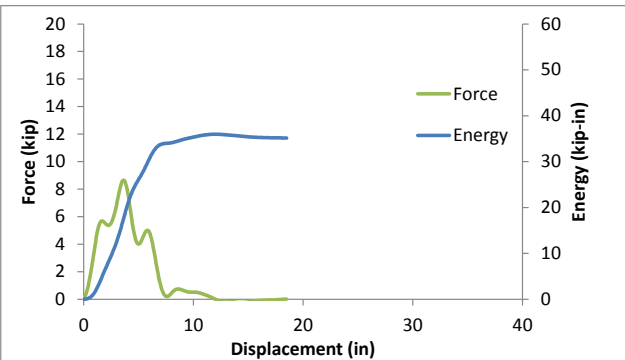
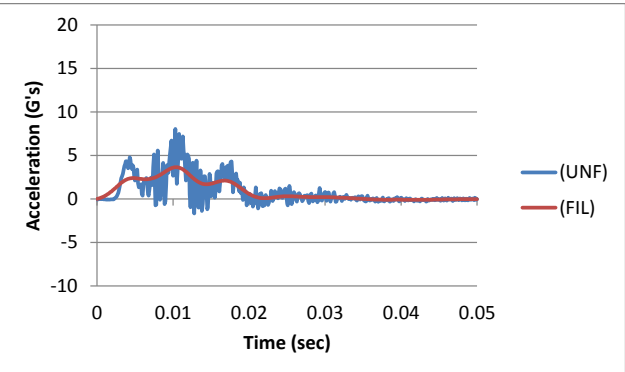


Figure 142. Summary sheet for Test 13010G.

Test Information	
Test Number:	13010H
Test Date:	16-Dec-2013
Post Properties	
Post Number:	D
Post Type:	Round SYP
Post Length:	72 inches
Post Diameter:	7.5 inches
Embedment Depth:	40 inches
Moisture Content:	35 percent
Ring Density (avg.):	6.4 per inch
Resi Score S_M :	
Resi Score S_U :	
Soil Properties	
Dry Density:	142.4 pcf
Moisture Content:	6.2 percent
Compaction:	94.8 percent
Pendulum Properties	
Weight:	2,372 lb
Impact Speed:	20 mph
Impact Height:	24.8 inches



Fractured Post

Figure 143. Summary sheet for Test 13010H.

Test Information	
Test Number:	13010I
Test Date:	18-Dec-2013
Post Properties	
Post Number:	E
Post Type:	Round SYP
Post Length:	72 inches
Post Diameter:	7.4 inches
Embedment Depth:	40 inches
Moisture Content:	19 percent
Ring Density (avg.):	4.1 per inch
Resi Score S_M :	
Resi Score S_U :	
Soil Properties	
Dry Density:	- pcf
Moisture Content:	- percent
Compaction:	- percent
Pendulum Properties	
Weight:	2,372 lb
Impact Speed:	10 mph
Impact Height:	24.8 inches

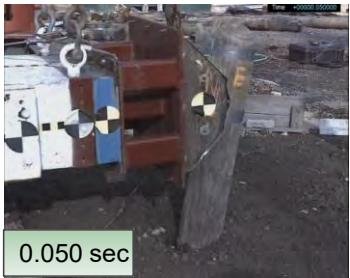
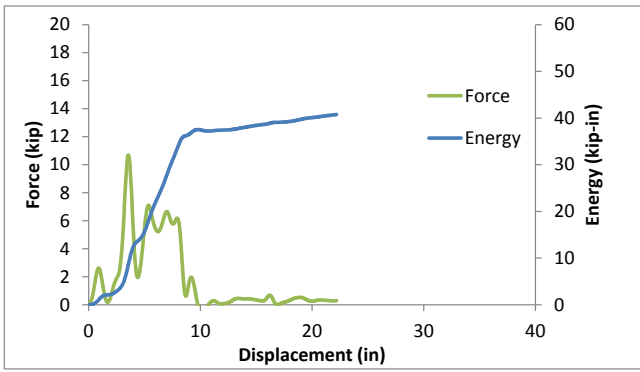
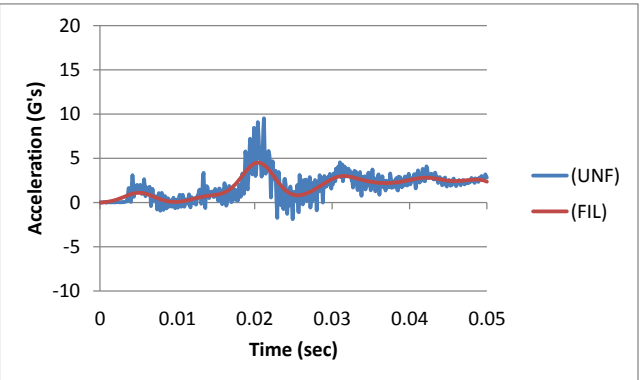


Figure 144. Summary sheet for Test 13010I.

Figure 145 shows a plot of section modulus vs. post diameter for the round wood post. The two dashed lines in the plot represent the section modulus for the 6x8 rectangular post in the strong direction (thick dashed line) and the weak direction (thin dashed line). The calculations show that a round post with a diameter of 8.67 inches has the same section modulus (i.e., strength) as the 6x8 rectangular post in the strong direction. Recall that the nominal diameter for the round wood post is 8 inches \pm 1 inch; thus, most of the round post sizes have less strength than the 6x8 post and in some cases half the strength. In the weak direction, on the other hand, the strength of the round post with 7.9-inch diameter is equal to that of the 6x8 post. When guardrail posts are struck on their side (e.g., wheel snag on the post) it is desired that the post readily breakaway in order to minimize impact forces. It is also important, however, for the posts have sufficient strength to sustain the lateral loading of the guardrail during impact to minimize guardrail deflections. Since the bending strength of a round post is equal in all directions, it is not possible to obtain optimum strength for the post in both the lateral and longitudinal directions.

Finite Element Analysis

Finite element models of wood guardrail posts with various levels of deterioration damage were developed. These models were then used in full-scale crash simulations of the G4(2W) guardrail under Report 350 Test 3-11 impact conditions to quantify the effects of post degradation on the performance of the guardrail system.

The development and validation of the finite element model of the G4(2W) guardrail was presented in Chapter 7. The various components of the validated G4(2W) guardrail were modeled according to their baseline conditions, including the wood post model. For example, the material properties for the baseline guardrail post model were determined through the process of trial and error by comparing the dynamic impact response of the post model to the results of full-scale pendulum impact tests on new guardrail posts (i.e., Tests 13009K and 13009L). This same approach was adopted here for calibrating the material properties for the posts with various levels of deterioration damage.

Calibration of FE Models for Deteriorated Posts

Damage Level 1 (DL1)

The impact conditions for Tests 13009 Series 2 were simulated using the finite element model shown in Figure 146. The guardrail post was modeled with a diameter of 8 inches. Two sets of material properties were developed for simulating damage level 1. One set was developed based on comparison to Test 13009H1 which resulted in a relatively low peak force with ductile post-peak failure response. Another set of material properties was developed based on comparison to Test 13009L1, which resulted in a relatively high peak force and brittle post-peak failure. The specific property values for these models are shown in Table 48 which correspond to material model *MAT_WOOD in LS-DYNA.

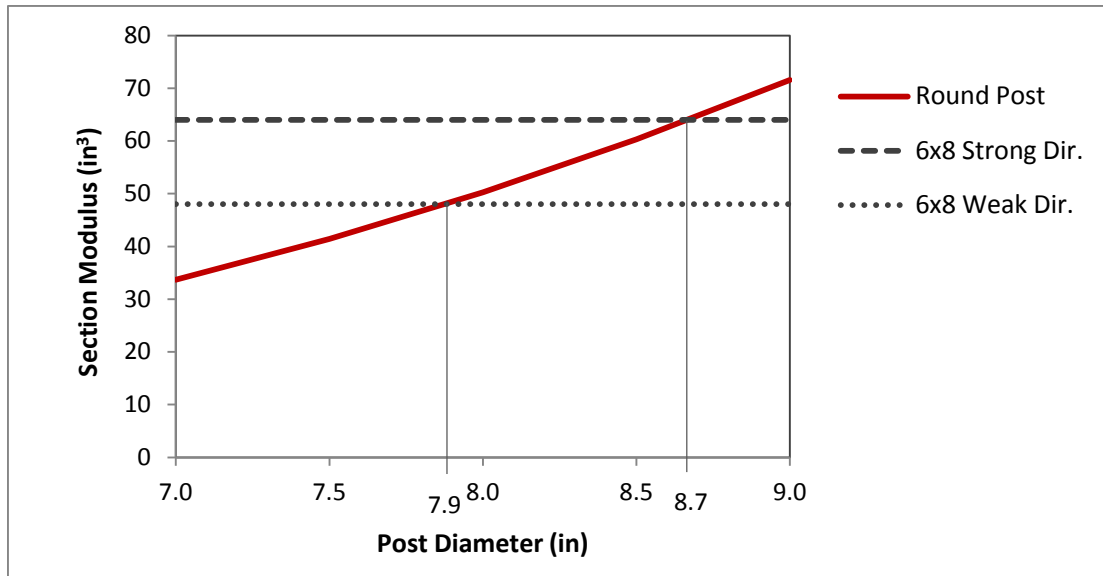


Figure 145. Section modulus for round posts with radius ranging from 7 to 8 inches compared to the 6x8 rectangular post.

The results of the model are compared to the full-scale impact tests in Figure 147 through Figure 150. Figures 147 and 148 show the force vs. deflection and energy vs. deflection results, respectively, for the FE model compared to Test 13009H1. The peak impact force from the analysis was 13 kips compared to 12.2 kips in the test. The total energy absorbed in the analysis at 13 inches displacement was 57 kip-inches compared to 56 kip-inches in the test. Figure 149 and Figure 150 show the force vs. deflection and energy vs. deflection response for the FE model compared to Test 13009L1. In this case the FE model resulted in a peak force of 17.3 kips compared to 13.6 kips in the test. The total energy absorbed in the analysis at 13 inches displacement was 46.5 kip-inches compared to 49.7 kip-inches in the test. Figure 151 and Figure 152 show sequential views comparing analysis results to dynamic impact tests 13009H1 and 13009L1, respectively.

An important point to consider regarding the differences between the tests and simulations is that the analyses and the tests have essentially the same number of peaks leading up to initiation of rupture, but the distance between peaks is considerably different. The reason for the differences is not well understood. From a review of the test video, the impact speed was confirmed to be 10 mph, which is the same as the impact speed that was simulated in the models. The most logical explanation is that the boundary conditions for the tests were effectively less “rigid” than those of the model. Thus, the test specimens were allowed greater movement upon impact at, and below, groundline, which consequently resulted in a greater distance between the initial inertial spike (i.e., first peak) and the start of the actual loading on the post (i.e., second peak). For comparison of the analysis results with the tests, the test data was shifted such that the initial loading of the second peak was coincident with that of the analysis.

Table 48. Material properties for wood post model corresponding to damage levels 1 through 3.

Variable	Description	DL1(a)	DL1(b)	DL2	DL3(a)	DL3(b)
		lower force more ductile	higher force more brittle	lower force more ductile	more ductile	more brittle
General						
RO	Density (Mg/mm ³)	6.73E-10	6.73E-10	6.73E-10	6.73E-10	6.73E-10
NPLOT	Parallel damage written to D3PLOT	1	1	1	1	1
ITERS	Number of plasticity iterations	1	1	1	1	1
IRATE	Rate effects (0=off; 1=on)	1	1	1	1	1
GHARD	Perfect plasticity override (0=perfect plasticity)	0.05	0.05	0.05	0.05	0.05
IFAIL	Erosion perpendicular to grain (0=No; 1=Yes)	1	1	1	1	1
IVOL	Erode on negative volume (0=No; 1=Yes)	0	0	0	0	0
Stiffness						
EL	Parallel Normal Modulus (MPa)	11352	9082	567.6	4540.8	4540.8
ET	Perpendicular Normal Modulus (MPa)	246.8	197.4	123.4	98.7	98.7
GLT	Parallel Shear Modulus (MPa)	715.2	572.2	357.6	286.1	286.1
GTR	Perpendicular Shear Modulus (MPa)	87.5	70	43.8	35	35
PR	Parallel Major Poisson's Ration	0.157	0.157	0.157	0.157	0.157
Strength						
XT	Parallel Tensile Strength (MPa)	35.8	35.8	30.7	27.3	25.5
XC	Parallel Compressive Strength (MPa)	12.7	13.7	8.88	7.83	7.4
YT	Perpendicular Tensile Strength (MPa)	0.86	0.86	0.74	0.66	0.61
YC	Perpendicular Compressive Strength (MPa)	2.5	2.7	1.7	1.5	1.4
SXY	Parallel Shear Strength (MPa)	3.8	3.8	3.3	2.9	2.7
SYZ	Perpendicular Shear Strength (MPa)	5.3	5.3	4.6	4.1	3.8
Damage						
GF1	Parallel Fracture Energy in Tension (MPa-mm)	35.8	35.8	15.4	13.7	12.8
GF2	Parallel Fracture Energy in Shear (MPa-mm)	74.1	74.1	31.8	28.2	26.5
BFIT	Parallel Softening Parameter	30	30	30	30	30
DMAX	Parallel Maximum Damage	0.9999	0.9999	0.9999	0.9999	0.9999
GF1 _⊥	Perpendicular Fracture Energy in Tension (MPa-mm)	0.8	0.8	0.4	0.4	0.4
GF2 _⊥	Perpendicular Fracture Energy in Compression (MPa-mm)	1.6	1.6	0.83	0.83	0.83
DFIT	Perpendicular Softening Parameter	30	30	30	30	30
DMAX _⊥	Perpendicular Maximum Damage	0.99	0.99	0.99	0.99	0.99
Rate Effects						
FLPAR	Parallel Fluidity Parameter Tension/Shear	3.96E-06	3.96E-06	3.39E-06	3.02E-06	2.83E-06
FLPARC	Parallel Fluidity Parameter Compression	5.65E-06	6.13E-06	3.96E-06	3.49E-06	3.30E-06
POWPAR	Parallel Power	0.107	0.107	0.107	0.107	0.107
FLPER	Perpendicular Fluidity Parameter Tension/Shear	8.29E-05	8.29E-05	7.10E-05	6.31E-05	5.92E-05
FLPERC	Perpendicular Fluidity Parameter Compression	1.18E-04	1.04E-04	8.29E-05	7.30E-05	6.91E-05
POWPER	Perpendicular Power	0.104	0.104	0.104	0.104	0.104
Hardening						
NPAR	Parallel Hardening Initiation	0.50	0.50	0.50	0.50	0.50
CPAR	Parallel Hareding Rate (/s)	111.1	500.0	226.8	292.2	326.5
NPER	Perpendicular Hardening Initiation	0.40	0.40	0.40	0.40	0.40
CPER	Perpendicular Hardening Rate (/s)	277.8	400.0	566.9	730.5	816.3

Units: Mg, mm, sec, N, MPa

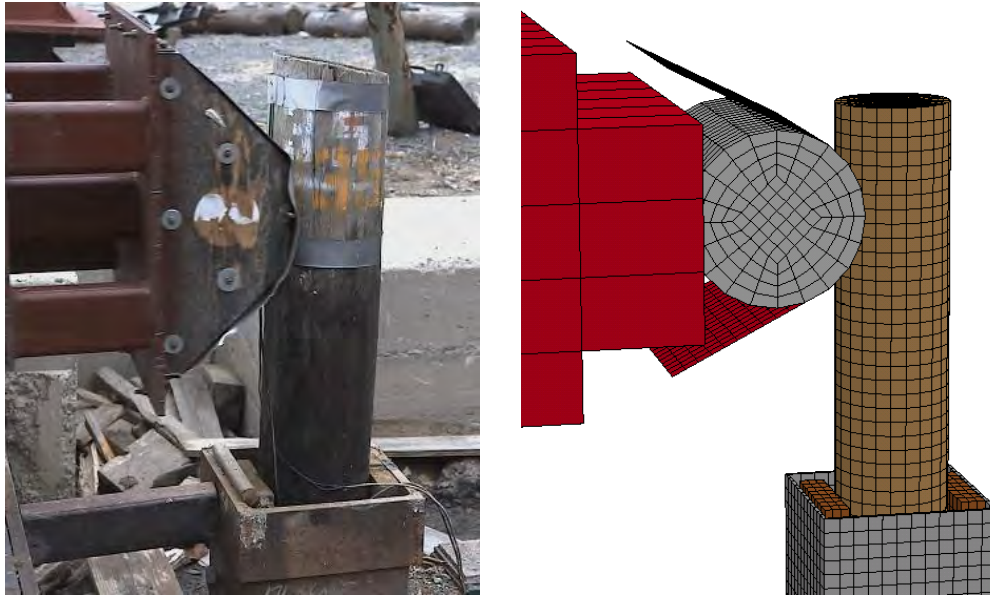


Figure 146. Finite element model used for calibrating material property values for various deterioration levels of wood posts.

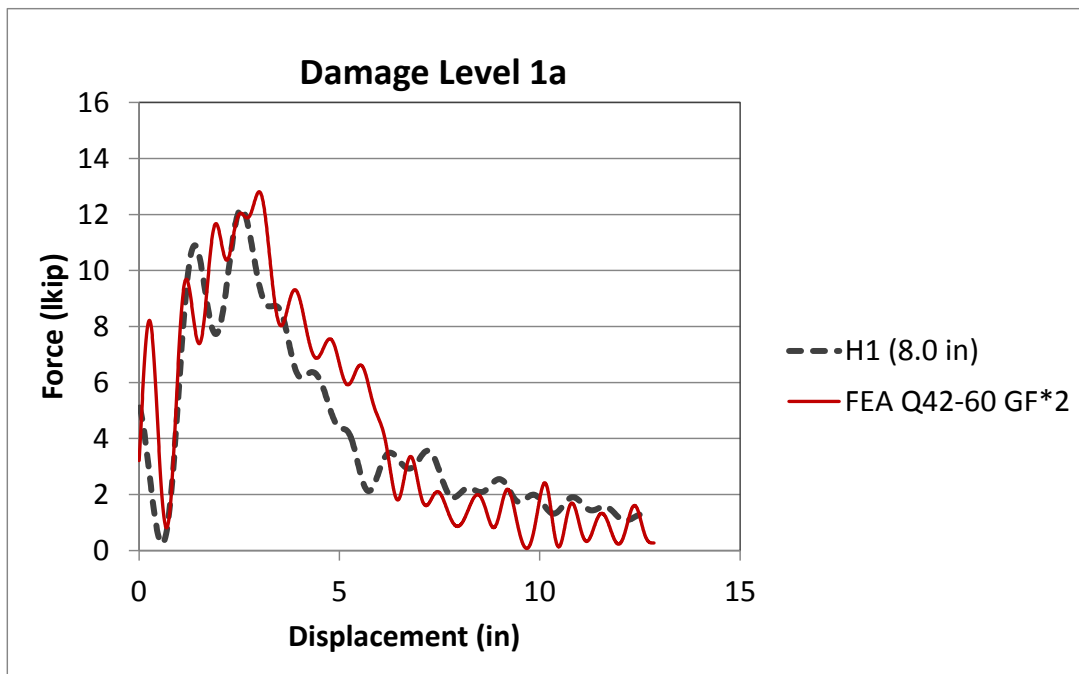


Figure 147. Force vs. deflection for DL1(a) wood post model corresponding to Test 13009H1 (ductile response).

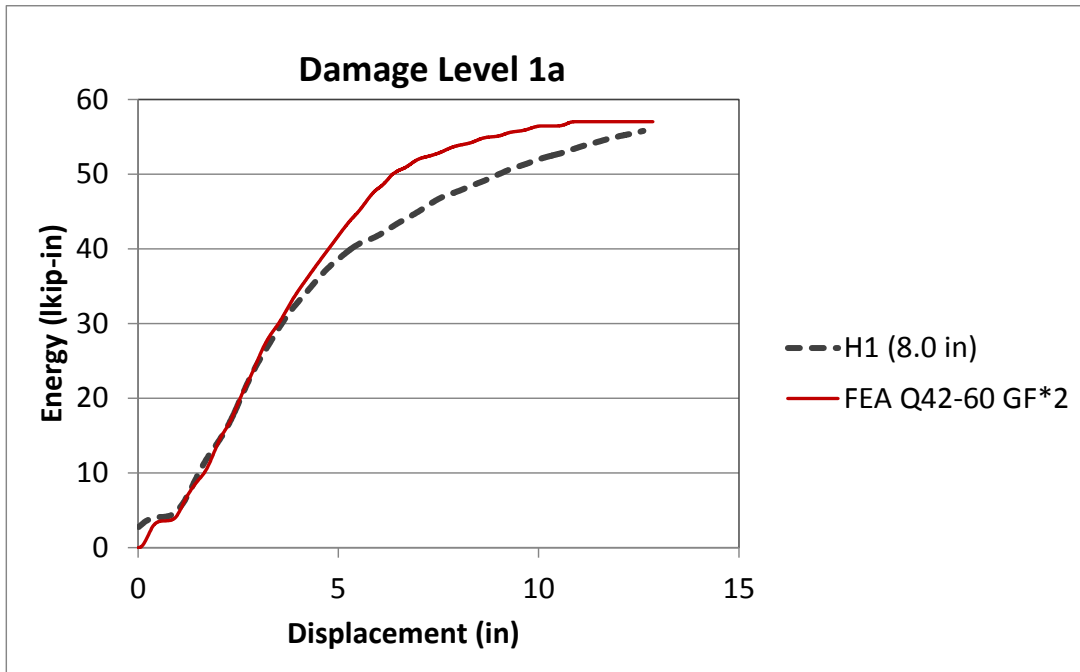


Figure 148. Energy vs. deflection for DL1(a) wood post model corresponding to Test 13009H1 (ductile response).

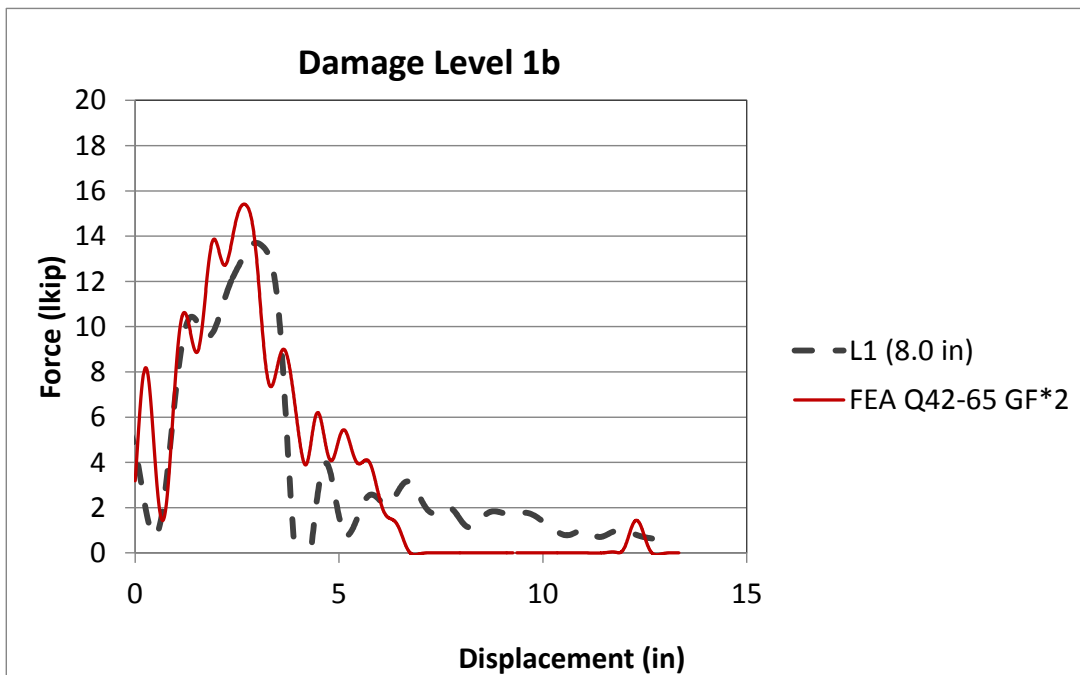


Figure 149. Force vs. deflection for DL1(b) wood post model corresponding to Test 13009L1 (brittle response).

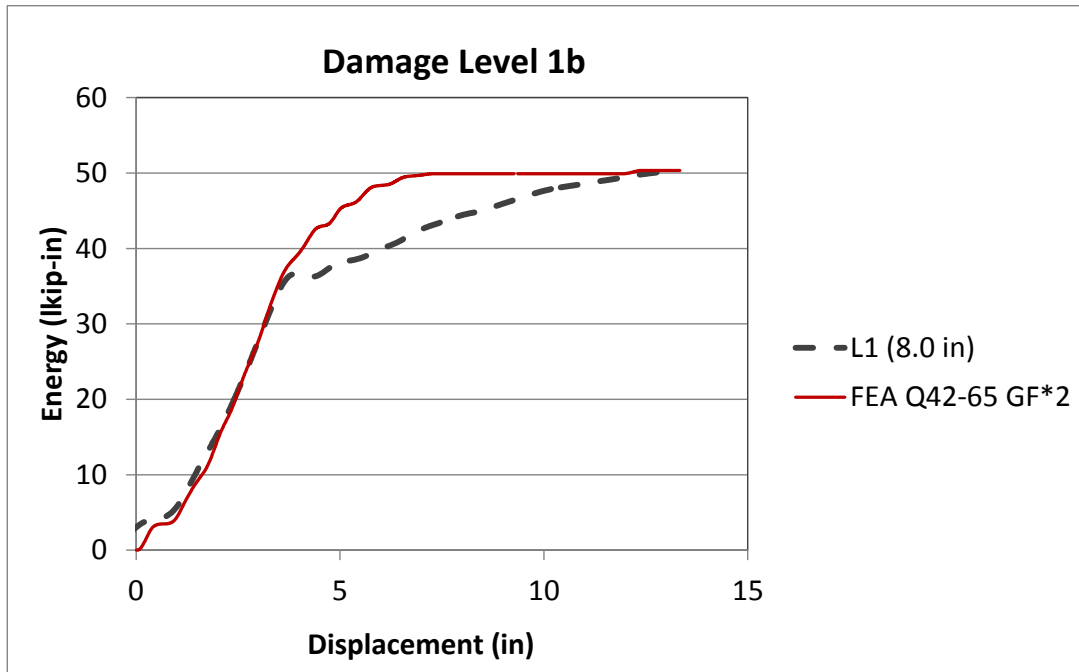
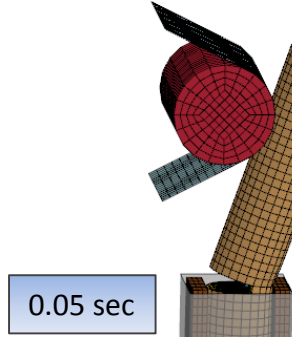
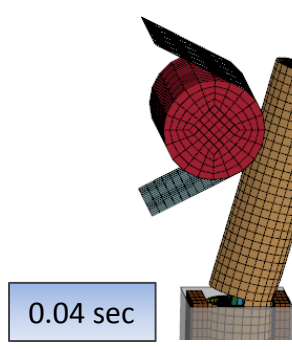
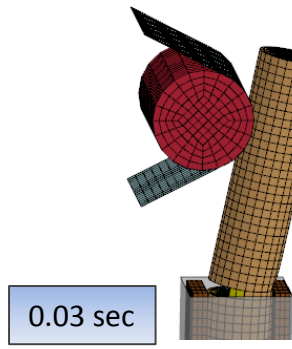
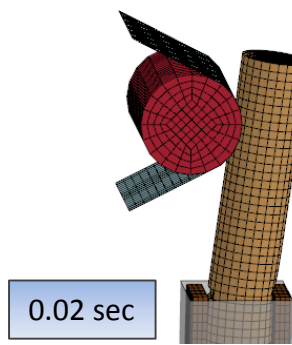


Figure 150. Energy vs. deflection for DL1(b) wood post model corresponding to Test 13009L1 (brittle response).



13009H1



FEA DL1(a)

Figure 151. Sequential views of Test 13009H1 and FE analysis DL1(a).

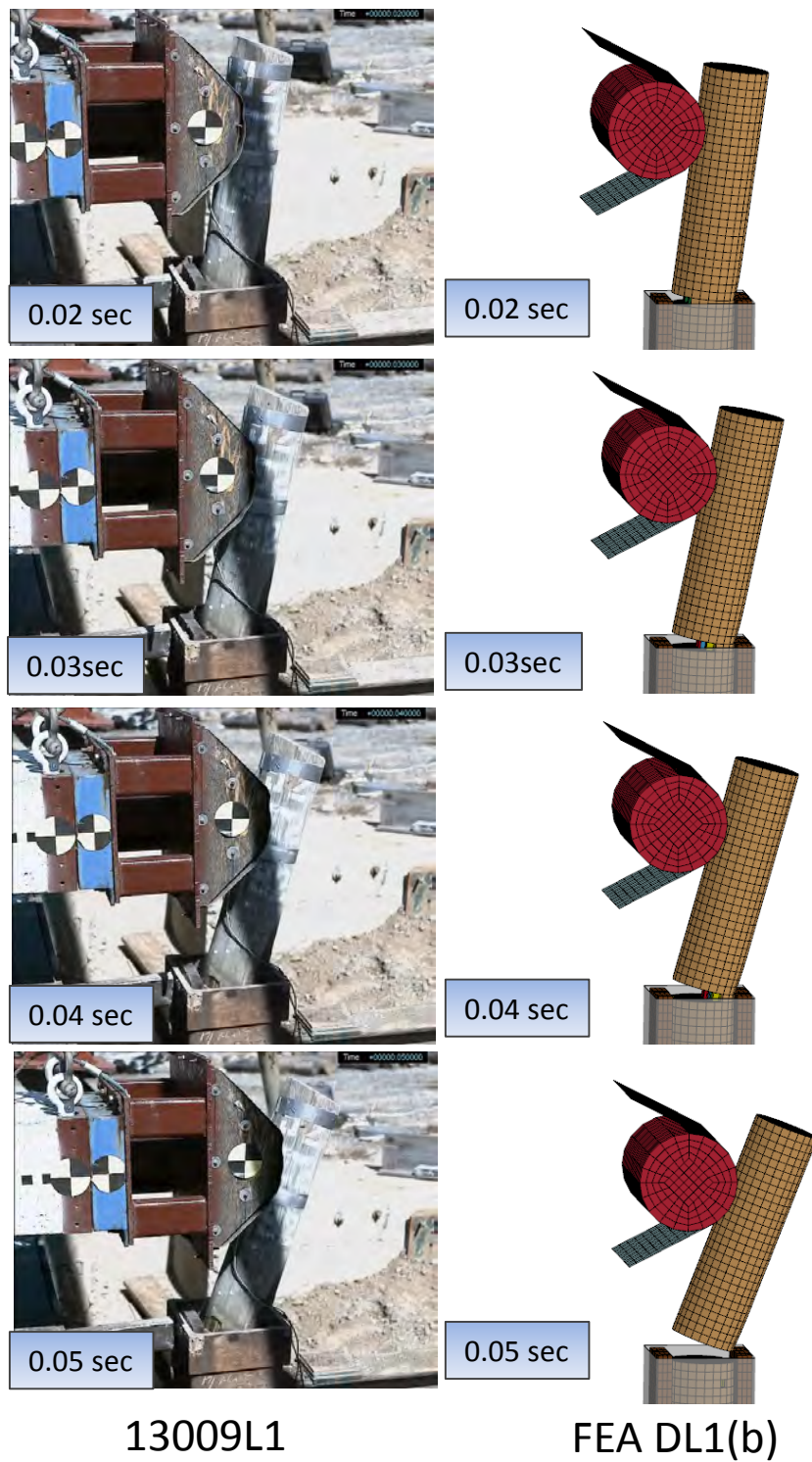


Figure 152. Sequential views for Test 13009L1 and FE analysis DL1(b).

Damage Level 2 (DL2)

A single set of material properties were developed for simulating damage level 2. These properties, shown in Table 48 under heading DL2, correspond to predefined values for *MAT_WOOD_PINE with $Q_T=0.36$ and $Q_C=0.42$, with the elastic properties scaled by 50 percent of the default undamaged wood values. The impact response for this model was very similar to the results from Tests 13009Z1 and 13009H2. Figure 153 and Figure 154 show the force vs. deflection and energy vs. deflection results for the FE model compared to the pendulum tests. The peak impact force from the analysis was 8.8 kips and the total energy absorbed in the analysis at 15 inches displacement was 27.3 kip-inches. Thus, response falls within the criteria defined for damage level 2.

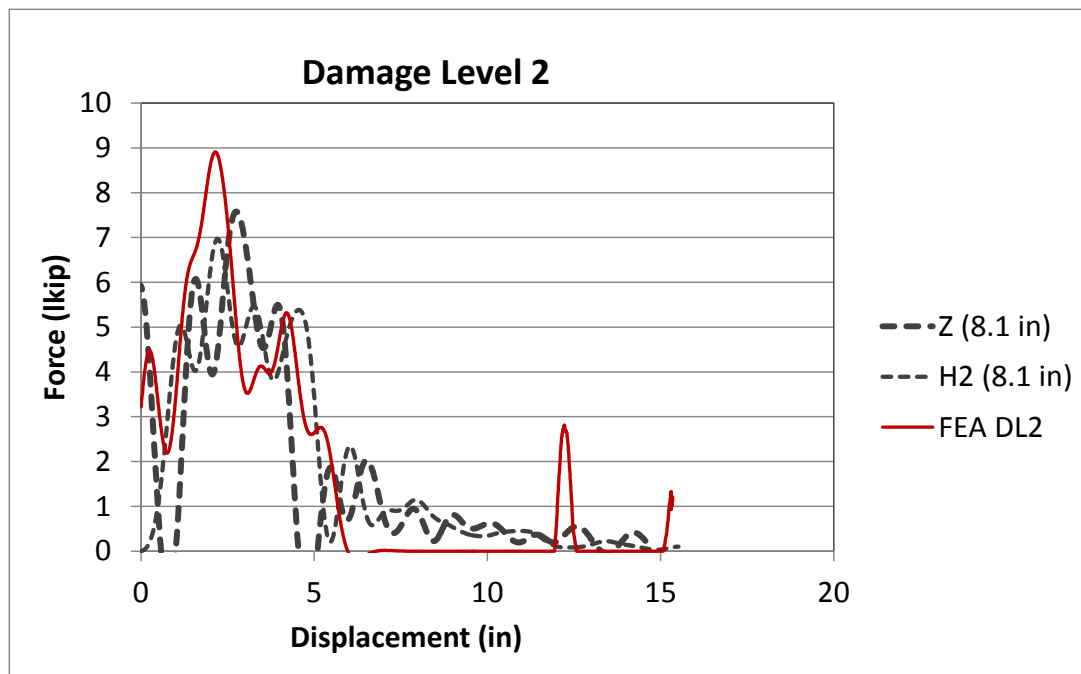


Figure 153. Force vs. deflection for DL1(a) wood post model corresponding to Test 13009H1 (ductile response).

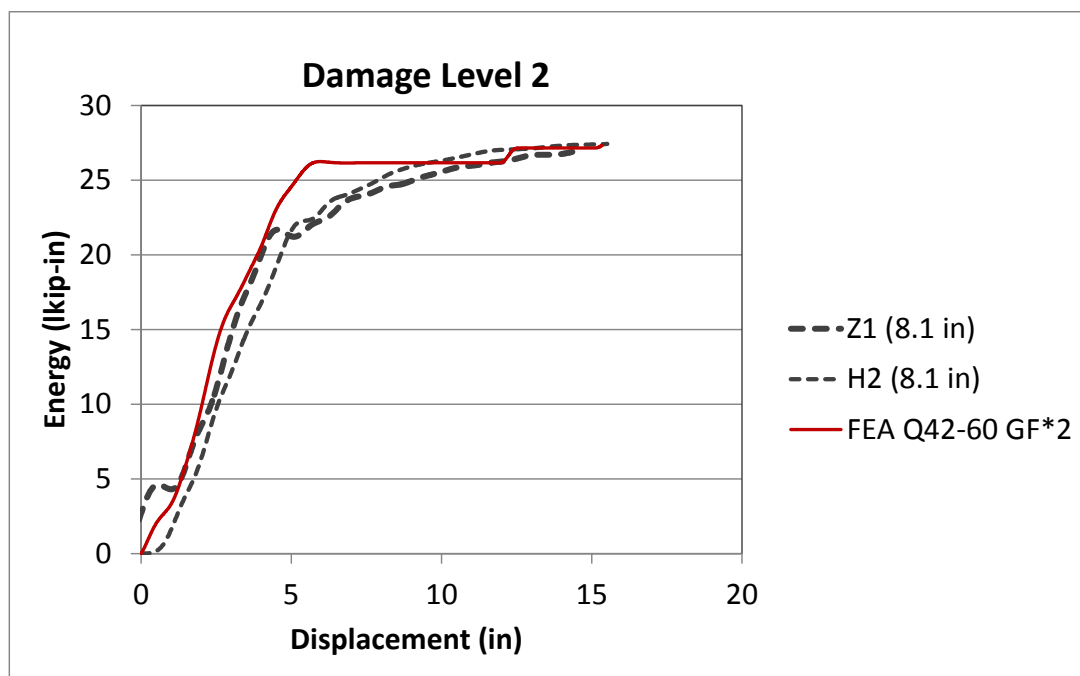


Figure 154. Energy vs. deflection for DL1(a) wood post model corresponding to Test 13009H1 (ductile response).

Damage Level 3 (DL3)

Two sets of material properties were developed for simulating damage level 3. The properties shown in Table 48 under heading DL3(a), correspond to predefined values for *MAT_WOOD_PINE with $Q_T=0.32$ and $Q_C=0.37$, with the elastic properties scaled by 40 percent of the default undamaged wood values. The impact response for this model was very similar to the results from Test 13009S1. The properties shown in Table 48 under heading DL3(b), correspond to predefined values for *MAT_WOOD_PINE with $Q_T=0.30$ and $Q_C=0.35$, with the elastic properties scaled by 40 percent of the default undamaged wood values. The impact response for this model was very similar to the results from Test 13009N1.

Figure 155 and Figure 156 show the force vs. deflection results for model DL3(a) and DL3(b), respectively, compared to the pendulum tests; and Figure 157 and Figure 158 show the energy vs. deflection results for model DL3(a) and DL3(b), respectively, compared to the pendulum tests. The peak impact force from the analysis was 8.4 kips for both models, and the total energy absorbed at 15 inches displacement was 19.4 kip-inches for model DL3(a) and 17.8 kip-inches for model DL3(b). Thus, the response of both models falls within the criteria defined for damage level 3.

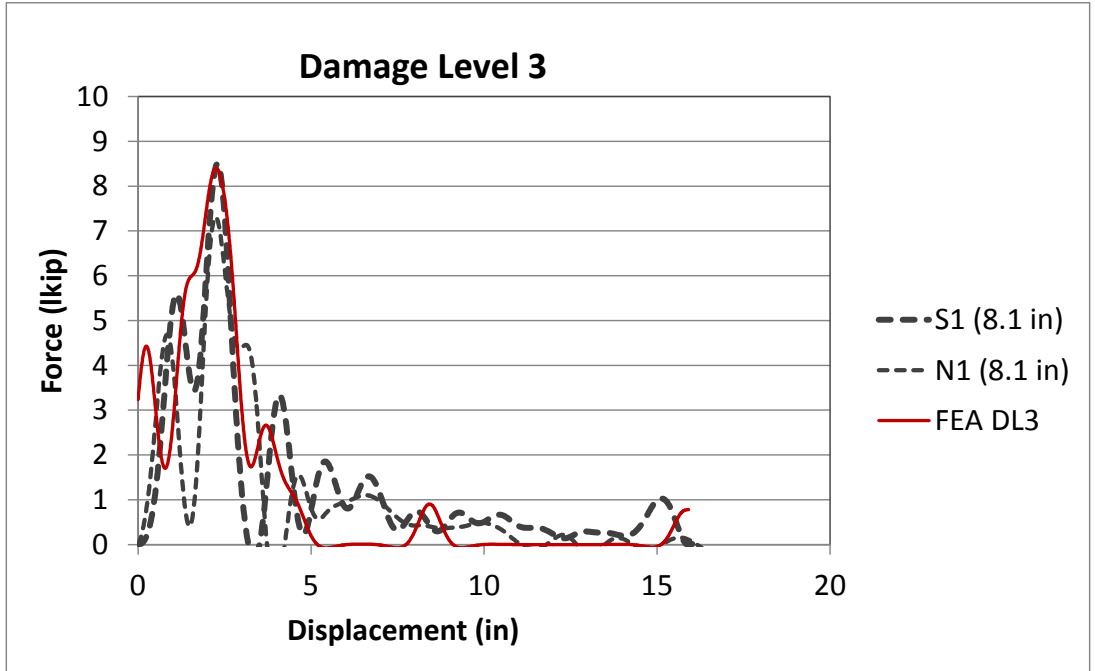


Figure 155. Force vs. deflection for DL3(a) wood post model and Tests 13009S1 and 13009N1 (more ductile response).

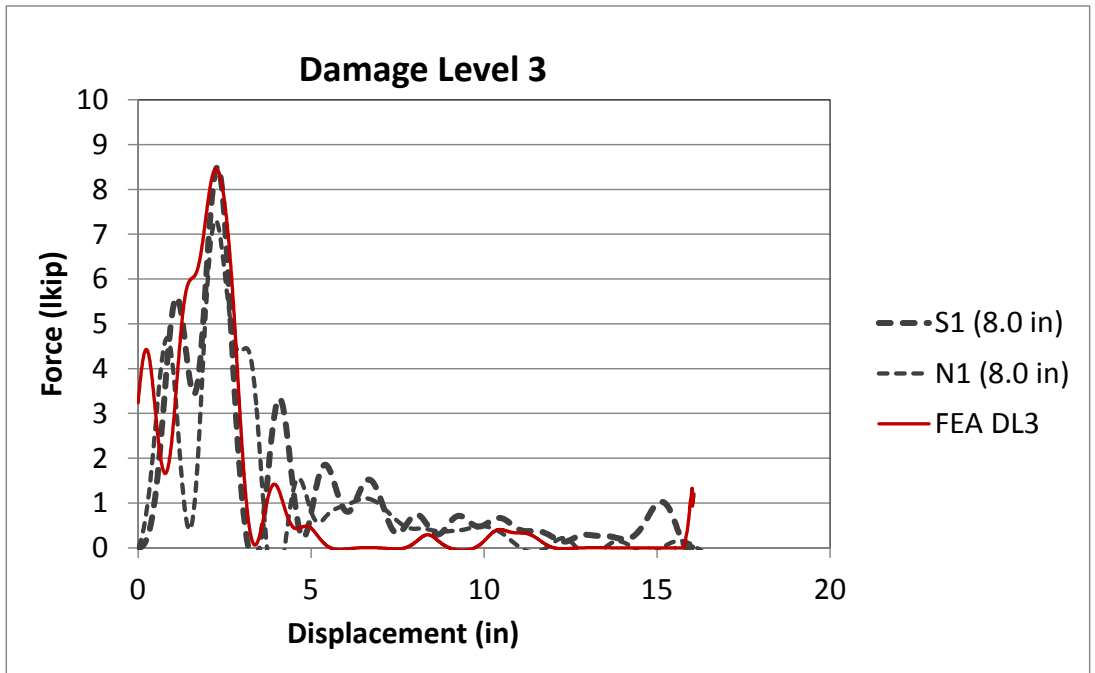


Figure 156. Force vs. deflection for DL3(b) wood post model and Tests 13009S1 and 13009N1 (more brittle response).

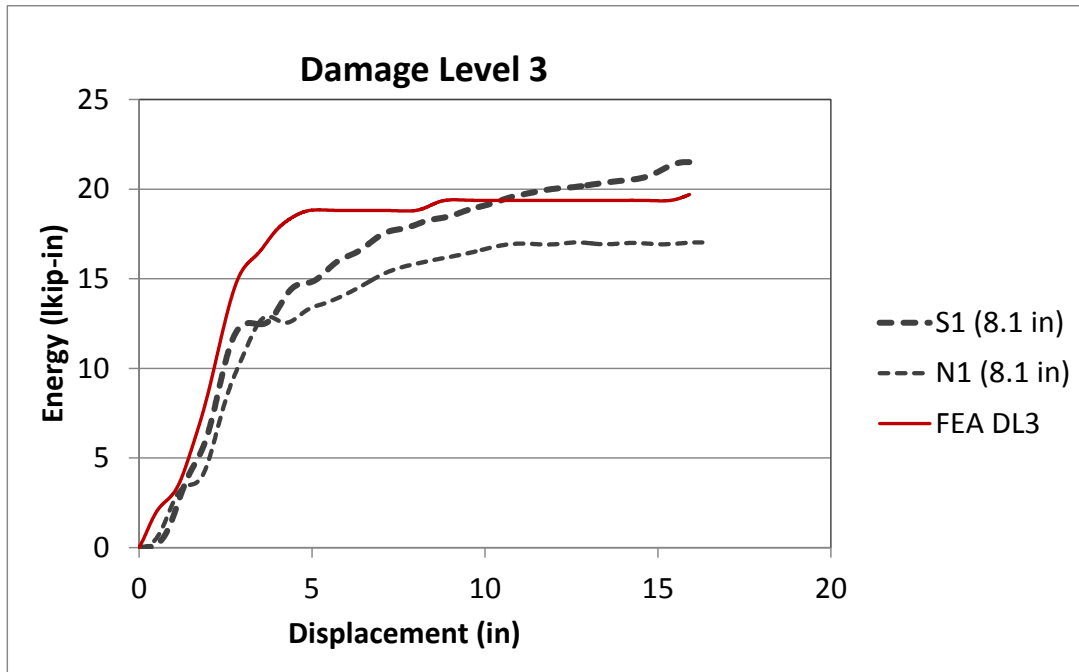


Figure 157. Energy vs. deflection for DL3(a) wood post model and Tests 13009S1 and 13009N1 (more ductile response).

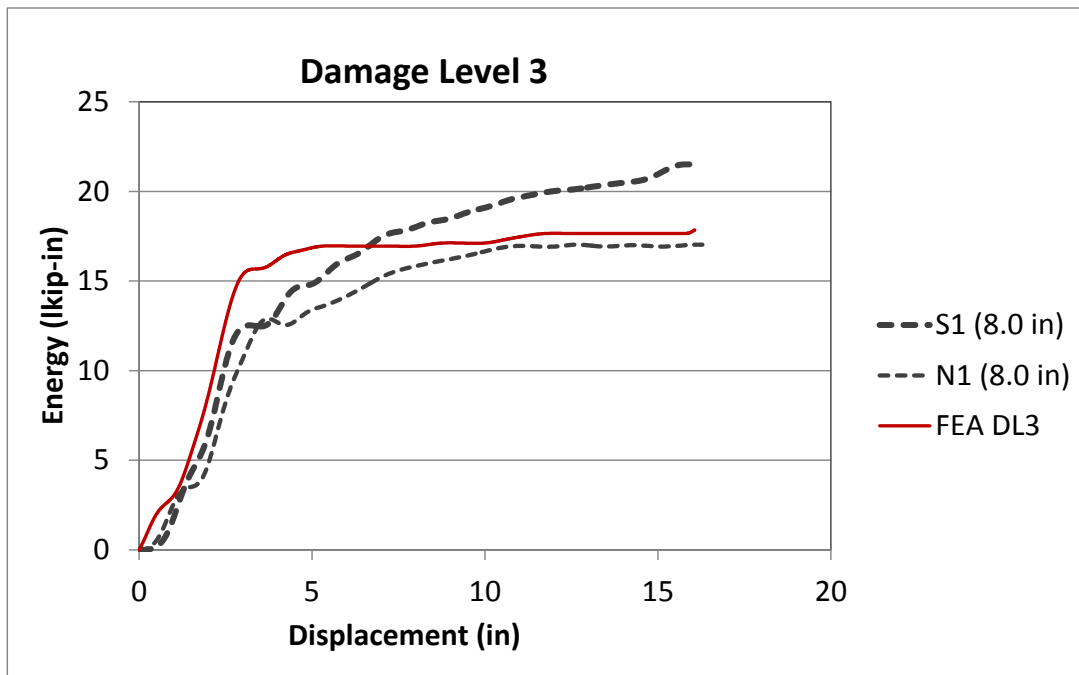


Figure 158. Energy vs. deflection for DL3(b) wood post model and Tests 13009S1 and 13009N1 (more brittle response).

Evaluate Effects of Post Deterioration on Guardrail Performance

The effects of post strength degradation on the crash performance of the G4(2W) guardrail was evaluated using FEA. Two damage scenarios were investigated. The first involved evaluation of the G4(2W) with uniform deterioration of the guardrail posts throughout the impact region. This scenario is analogous to an aged guardrail system with deteriorated posts, but otherwise the guardrail is undamaged. The second scenario involved evaluation of the G4(2W) in which a number of new posts were installed downstream and adjacent to a line of deteriorated posts. This scenario is representative of a local repair on an aged guardrail system, where a small number of the posts in a line of deteriorated posts have been replaced with new posts.

The analysis matrix for the study is shown in Table 49. The impact conditions were set to those of full-scale crash test 471470-26 and involved the 4,568-lb C2500D pickup model impacting the guardrail at 62.6 mph (100.8 km/hr) at an angle of 24.3 degrees.[Mak99] Due to time and budget constraints, the critical impact point (CIP) for each individual guardrail damage case was not determined. The impact point for all analysis cases was set at 22 inches upstream of Post 14, which corresponded to the CIP for the baseline G4(2W) guardrail in Test 471470-26.[Mak99] The analyses were conducted for 0.6 seconds of the impact event.

Table 49. Analysis matrix for deteriorated wood post study.

Damage Case Scenario	Damage Level for Guardrail Posts			
	(Baseline)			
	DL0	DL1	DL2	DL3
Uniform Post Deterioration in Impact Region	x	x	x	x
Deteriorated Posts Upstream of Undamaged Posts	x	x	x	x

Uniform Post Deterioration in Impact Region

The analysis model used for evaluating the effects of uniform deterioration of the guardrail posts is shown in Figure 159. The posts located within the impact region were modeled using MAT143 with material properties defined according to Table 48; while the posts located outside the impact region were modeled using MAT13, which was a much simpler, less computationally demanding material model. MAT13 was not calibrated for the various levels of post deterioration. Instead, the material parameters used for MAT13 were adopted from the earlier work by Plaxico, et.al.[Plaxico98] In effect, the posts outside the impact zone should be considered undamaged, or new.

The boundary conditions for the ends of the rail were modeled using non-linear springs with force-deflection response corresponding to a standard two-foundation-tube-and-strut type anchor, which was the type of anchor used in the baseline full-scale crash test.[Mak99]. The stiffness of the anchor for these analyses were notably less than that of the validation model in which the stiffness properties of the boundary springs were defined based on previous work presented in [Plaxico03]. As a result, the baseline model (i.e., model with Damage Level 0 posts) showed slightly higher deflections than the validation model. Both cases are included in the results below for relative comparisons.

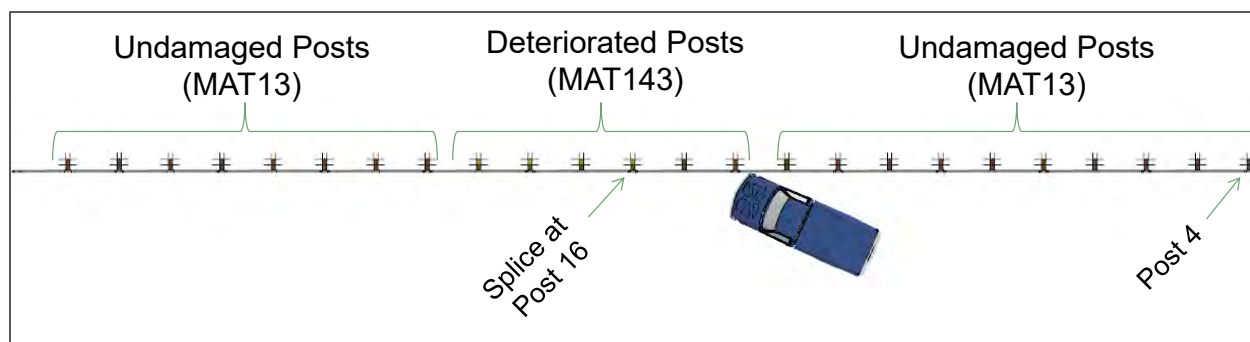


Figure 159. Analysis setup for evaluation of uniform deterioration of posts in the impact region.

Sequential views of the FE analysis results for each case are provided in Appendix G. Table 50 provides a summary of barrier damage from the analyses related to rail deflections, anchor movement and splice damage. This information is also presented graphically in Figure 160 and Figure 161. The maximum rail deflection increased significantly for each damage level. The deflections for DL2 and DL3 cases were more than 75 percent higher than the baseline case.

Table 50. Summary of barrier damage evaluation from uniform post deterioration analyses.

Event	Validation DL0	Analysis			
		DL0	DL1	DL2	DL3
Maximum Rail Deflection (in)	27.3	32.0	45.1	56.1	58.9
Location of Max Defl. (in) (Relative to Post 16)	-30.5	-14.8	23.8	64.4	75.0
Rail Deflection at Post 13 (in)	1.2	1.8	4.7	5.6	6.5
Rail Deflection at Post 14 (in)	11.3	13.1	20.4	22.8	24.1
Rail Deflection at Post 15 (in)	24.8	27.8	33.7	38.1	40.5
Rail Deflection at Post 16 (in)	25.4	31.1	44.3	51.4	53.9
Rail Deflection at Post 17 (in)	9.1	17.5	42.9	56.1	58.9
Rail Deflection at Post 18 (in)	0.3	1.2	32.3	54.2	56.2
Rail Deflection at Post 19 (in)	0.0	0.0	7.3	42.2	50.9
Upstream Anchor Deflection (in)	0.5	1.4	1.4	1.4	1.4
Downstream Anchor Deflection (in)	0.2	0.9	1.3	1.7	1.9
Maximum Strain in splice	0.89	0.84	1.05	1.13	1.10

For strong-post w-beam guardrails with rail splices located at the guardrail posts, the critical impact point is determined based on achieving maximum loading on a w-beam splice connection. This generally occurs when the maximum rail deflection occurs just upstream of the splice. Regarding the “location of maximum deflection” in Table 50, a negative number indicates that the maximum deflection occurred upstream of the splice at Post 16, while a positive number indicates that maximum deflection occurred downstream of the splice. The maximum rail deflection for the baseline DL0 case occurred at 14.8 inches upstream of the w-beam splice at Post 16 and can therefore be considered a critical impact case. The location of maximum deflection for the damaged post cases, on the other hand, all occurred downstream of the splice

connection; particularly for cases DL2 and DL3. Thus, the results for the deteriorated post cases would likely have been more severe had critical impact conditions been used.

Figure 161 shows the longitudinal displacement of the upstream and downstream ends of the w-beam at the anchor locations. For the validation case, the maximum deflection was only 0.5 inches compared to 1.4 inches computed for the baseline analysis case due to different anchor stiffness. For the deteriorated post cases, the loading on the upstream anchor was the same as the baseline analysis. The longitudinal rail deflections at the downstream anchor, however, increased significantly with each level of post deterioration. In general, higher lateral deflections in the impact region are associated with higher anchor forces. The fact that only the downstream anchor resulted in increased anchor forces is not clearly understood, but it was in part attributed to the fact that the location of maximum lateral deflection occurred farther downstream for each increase in post deterioration level.

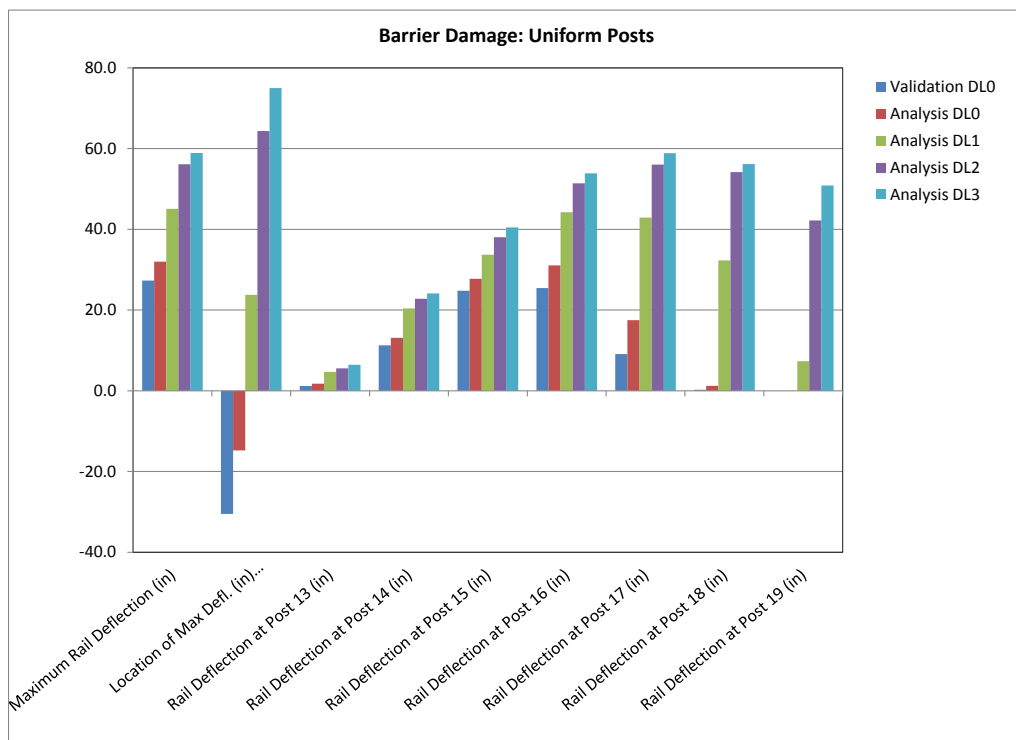


Figure 160. Summary of barrier damage evaluation from analysis of uniform post deterioration.

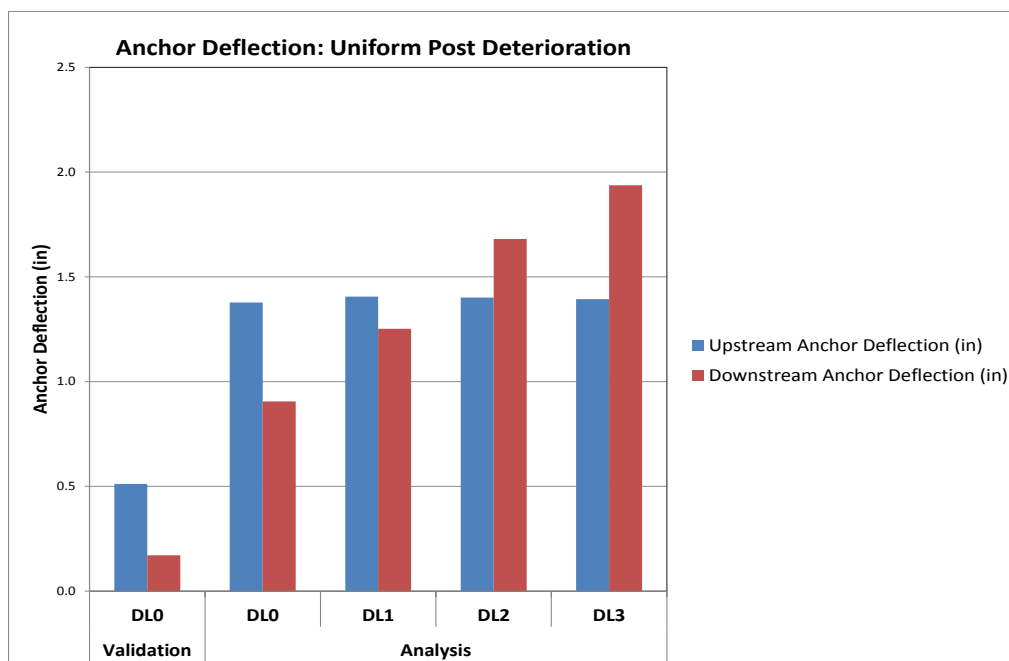


Figure 161. Summary of anchor displacement at rail height from analysis of uniform post deterioration.

A summary of occupant risk measures computed from the acceleration and angular rate time-histories at the vehicle's center of gravity is provided in Table 51. This data is also presented graphically in Figures 163 through 165. The difference in results between the validation case and the baseline case was considered minimal. The results of the analyses involving deteriorated posts indicated that as post deterioration increases (i.e., post strength decreases) the vehicle decelerations decreased, thereby reducing the occupant risk metrics. This seems logical since the system is effectively becoming less stiff, similar to weak-post w-beam systems.

The potential for rail rupture was assessed by comparing the plastic strains in the w-beam rail with those from the baseline case. Figure 162 shows the effective plastic strain contours for the w-beam splice connection at Post 16 from one of the analysis cases. As illustrated in the figure, the highest strains occurred at the splice-bolt holes while the strains in all other regions of the w-beam splice were relatively benign (note that the splice-bolt nuts were removed from view in Figure 162 in order to more clearly show the strains in the material around the bolt holes).

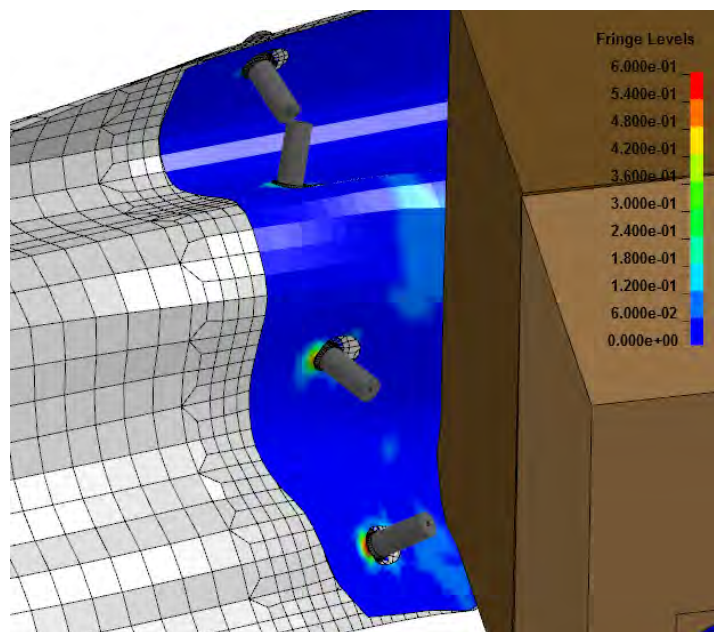


Figure 162. Effective plastic strain contour plot for w-beam in splice connection at Post 16.

A summary of the maximum effective plastic strains around the splice-bolt holes in the w-beam is shown in Figure 166. The results indicate that the plastic strain values were relatively high even for the baseline case with a magnitude of 0.84, while for analysis Case DL1, the plastic strain values were 25 percent higher with a magnitude of 1.05. It is assumed that the baseline G4(2W) guardrail case is near its performance capacity under these impact conditions, thus as the plastic strains increase beyond those of the baseline case, the potential for rupture increases accordingly.

Table 51. Summary of occupant risk measures from evaluation of uniform post deterioration analyses.

Occupant Risk Factors		Test 471470-26	DL0 (Validation)	DL0 (Baseline)	DL1	DL2	DL3
Occupant Impact Velocity (m/s)	x-direction	4.6	5.3	5.2	4.4	3.8	3.3
	y-direction	5.8	5.8	5.3	4.8	4.3	4.3
	at time	(0.1437 sec)	(0.1442 sec)	(0.1519 sec)	(0.1618 sec)	(0.1727 sec)	(0.1782 sec)
THIV (m/s)		6.9 (0.1404 sec)	7.4 0.1398	7 0.1471	6.1 (0.1559 sec)	5.6 (0.1667 sec)	5.4 (0.1723 sec)
Ridedown Acceleration (g's)	x-direction	11.5 (0.2025 - 0.2125 sec)	10.2 (0.1791 - 0.1891 sec)	10.3 (0.1519 - 0.1619 sec)	7.9 (0.1968 - 0.2068 sec)	7.0 (0.3578 - 0.3678 sec)	5.8 (0.27148 - 0.2814 sec)
	y-direction	11.2 (0.2381 - 0.2481 sec)	11.1 (0.2152 - 0.2252 sec)	10.7 (0.2198 - 0.2298 sec)	8.0 (0.2143 - 0.2243 sec)	6.9 (0.2825 - 0.2925 sec)	7.3 (0.5641 - 0.5741 sec)
PHD (g's)		11.7 (0.2025 - 0.2125 sec)	13.6 (0.2148 - 0.2248 sec)	13.7 (0.2003 - 0.2103 sec)	8.5 (0.2047 - 0.2147 sec)	8.1 (0.3571 - 0.3671 sec)	8.7 (0.2695 - 0.2795 sec)
ASI		1.01 (0.2176 - 0.2676 sec)	0.99 (0.1172 - 0.1672 sec)	0.93 (0.1219 - 0.1719 sec)	0.66 (0.2062 - 0.2562 sec)	0.63 (0.2822 - 0.3322 sec)	0.65 (0.2651 - 0.3151 sec)
Max 50-ms moving avg. acc. (g's)	x-direction	6.1 (0.1382 - 0.1882 sec)	6.2 (0.1390 - 0.1890 sec)	7.6 (0.1216 - 0.1716 sec)	4.6 (0.1166 - 0.1666 sec)	3.8 (0.3448 - 0.3948 sec)	3.2 (0.1808 - 0.2308 sec)
	y-direction	6.8 (0.0945 - 0.1445 sec)	7.7 (0.1179 - 0.1679 sec)	6.5 (0.1976 - 0.2476 sec)	5.4 (0.2071 - 0.2571 sec)	5.5 (0.2825 - 0.3325 sec)	5.4 (0.2661 - 0.3161 sec)
	z-direction	9.0 (0.2174 - 0.2674 sec)	2.4 (0.4155 - 0.4655 sec)	2.4 (0.3344 - 0.3844 sec)	1.9 (0.3900 - 0.4400 sec)	1.5 (0.3383 - 0.3883 sec)	1.9 (0.2985 - 0.3485 sec)

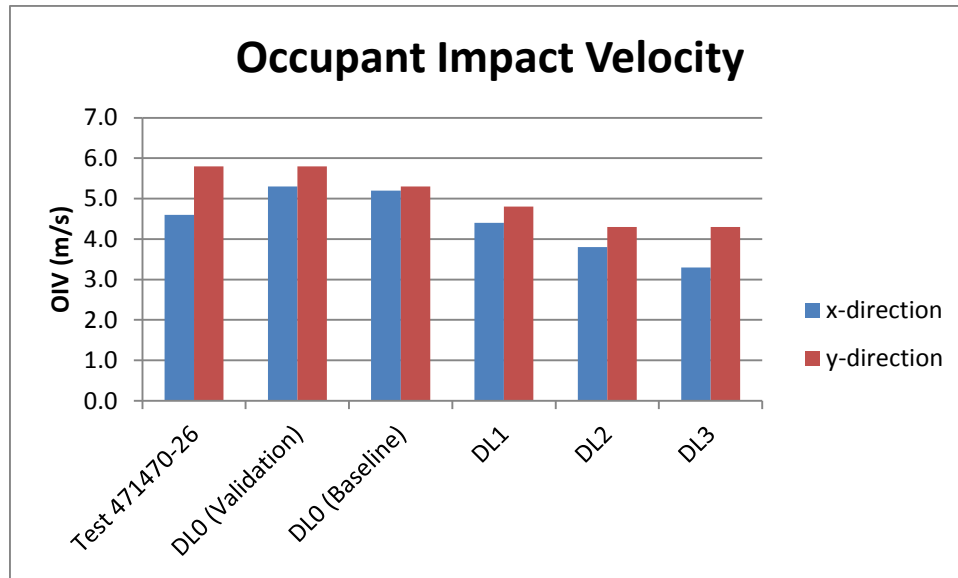


Figure 163. Summary of occupant impact velocity evaluation of uniform post deterioration.

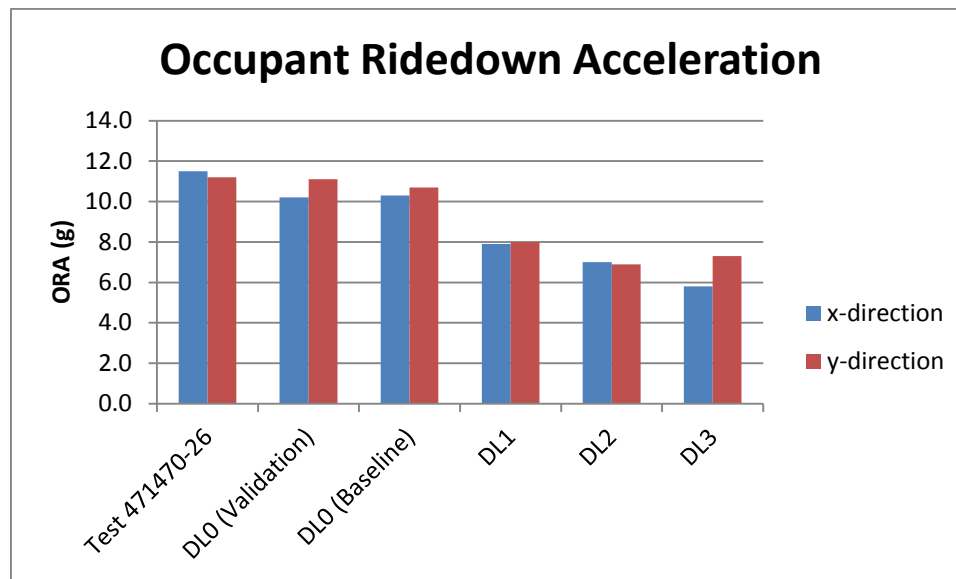


Figure 164. Summary of maximum occupant ridedown acceleration evaluation of uniform post deterioration.

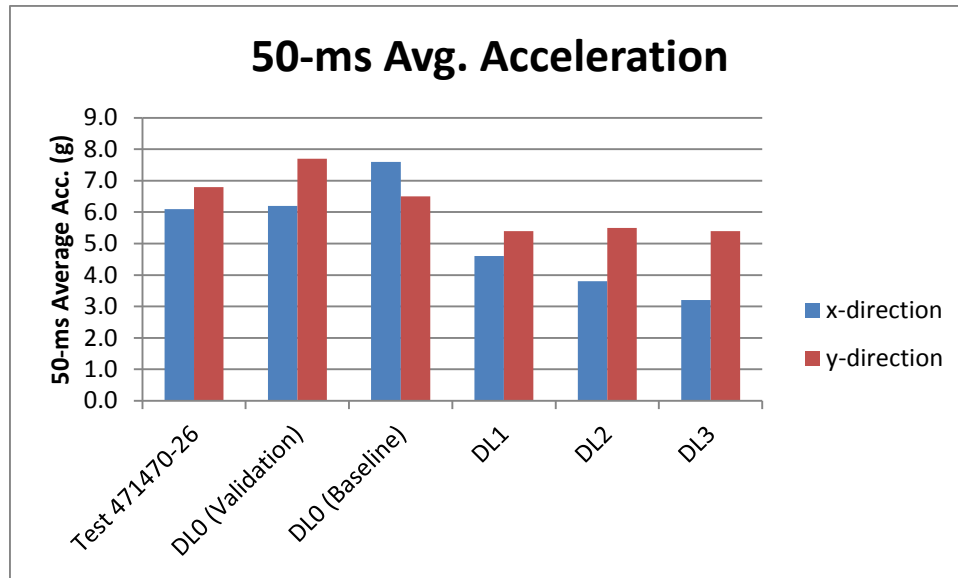


Figure 165. Summary of 50-ms running average acceleration evaluation of uniform post deterioration.

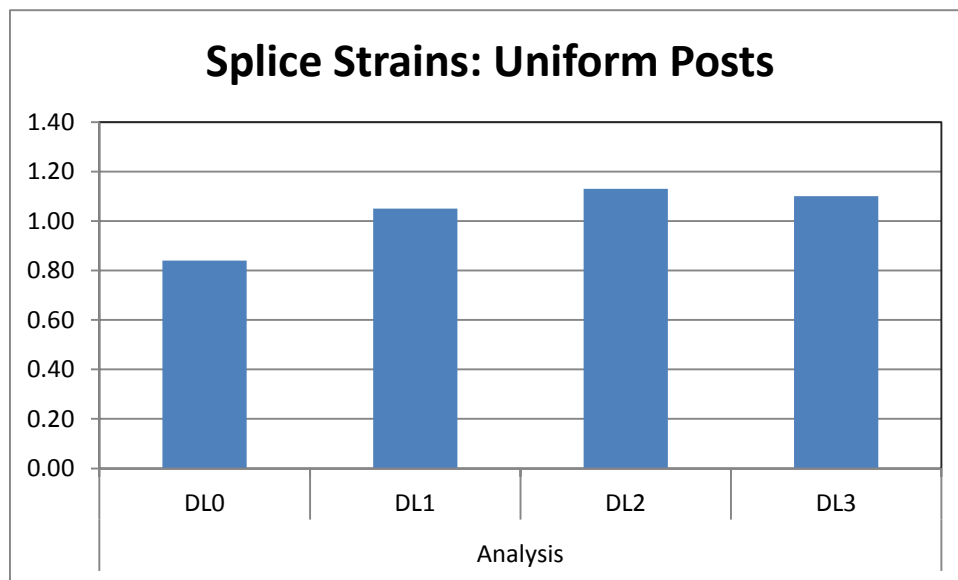


Figure 166. Summary of maximum effective plastic strains occurring at the splice-bolt locations at Post 16.

For analysis case DL2 and DL3 the plastic strains were slightly higher than the DL1 case. It is possible, although not confirmed, that the splice damage for cases DL2 and DL3 may be higher if evaluated at their critical impact points.

Deteriorated Posts Upstream of Undamaged Posts

The analysis model used for evaluating the effects of deteriorated posts upstream of undamaged posts is shown in Figure 167.

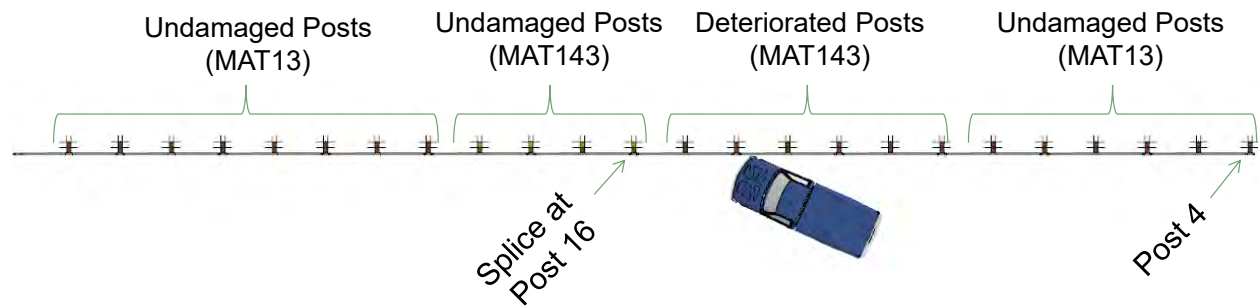


Figure 167. Analysis setup for evaluation of mixed deterioration of posts in the impact region.

Sequential views of the FE analysis results for each case are provided in Appendix H. Table 52 provides a summary of barrier damage from the analyses related to rail deflections, anchor movement and splice damage. This information is also presented graphically in Figure 168 and Figure 169. The maximum rail deflection increased only slightly for the DL1 case, compared with the baseline; while the maximum rail deflection for cases DL2 and DL3 were 46 percent and 56 percent higher, respectively, than the baseline analysis case. The location of maximum rail deflection for analysis Case DL1 was at 21.5 inches upstream of the splice connection at Post 16; thus the impact conditions for this analysis were representative of the critical impact conditions. The location of maximum rail deflection for cases DL2 and DL3, on the other hand, was at Post 16; thus, the critical impact point for these cases was probably not achieved. It is assumed that the results for Cases DL2 and DL3 would likely have been more severe had critical impact conditions been used. Based on the results from the evaluation of uniform deterioration of guardrail posts, the CIP for Case DL2 was estimated to be at approximately 20.8 feet upstream of the splice connection at Post 16, and the CIP for DL3 was estimated to be at approximately 21.7 feet upstream of the splice connection at Post 16. These impact conditions should result in maximum rail deflection occurring just upstream of the splice connection located at the first undamaged post at Post 16.

Figure 169 shows the longitudinal displacement of the upstream and downstream ends of the w-beam at the anchor location. For Case DL1 the loading on both the upstream and downstream anchors were essentially the same as those of the baseline analysis case. As the deterioration levels increased, the loading on the upstream anchor increased slightly, although deflections were not that significant (e.g., maximum deflections of 1.8 to 2 inches). The loading on the downstream anchor was essentially the same in all cases.

Table 52. Summary of barrier damage evaluation from mixed post deterioration analyses.

Event	Validation	Analysis			
		DL0	DL1-DL0	DL2-DL0	DL3-DL0
Maximum Rail Deflection (in)	27.3	32.0	35.5	46.6	49.8
Location of Max Defl. (in) (Relative to Post 16)	-30.5	-14.8	-21.5	0.0	0.0
Rail Deflection at Post 13 (in)	1.2	1.8	3.1	23.9	31.1
Rail Deflection at Post 14 (in)	11.3	13.1	14.2	33.2	40.3
Rail Deflection at Post 15 (in)	24.8	27.8	29.6	41.1	46.0
Rail Deflection at Post 16 (in)	25.4	31.1	34.9	46.6	49.8
Rail Deflection at Post 17 (in)	9.1	17.5	25.0	39.9	44.4
Rail Deflection at Post 18 (in)	0.3	1.2	4.6	18.9	24.6
Rail Deflection at Post 19 (in)	0.0	0.0	0.0	1.4	3.1
Upstream Anchor Deflection (in)	0.5	1.4	1.4	1.8	2.0
Downstream Anchor Deflection (in)	0.2	0.9	1.0	1.0	1.1
Maximum Strain in splice	0.89	0.84	1.00	1.16	1.27

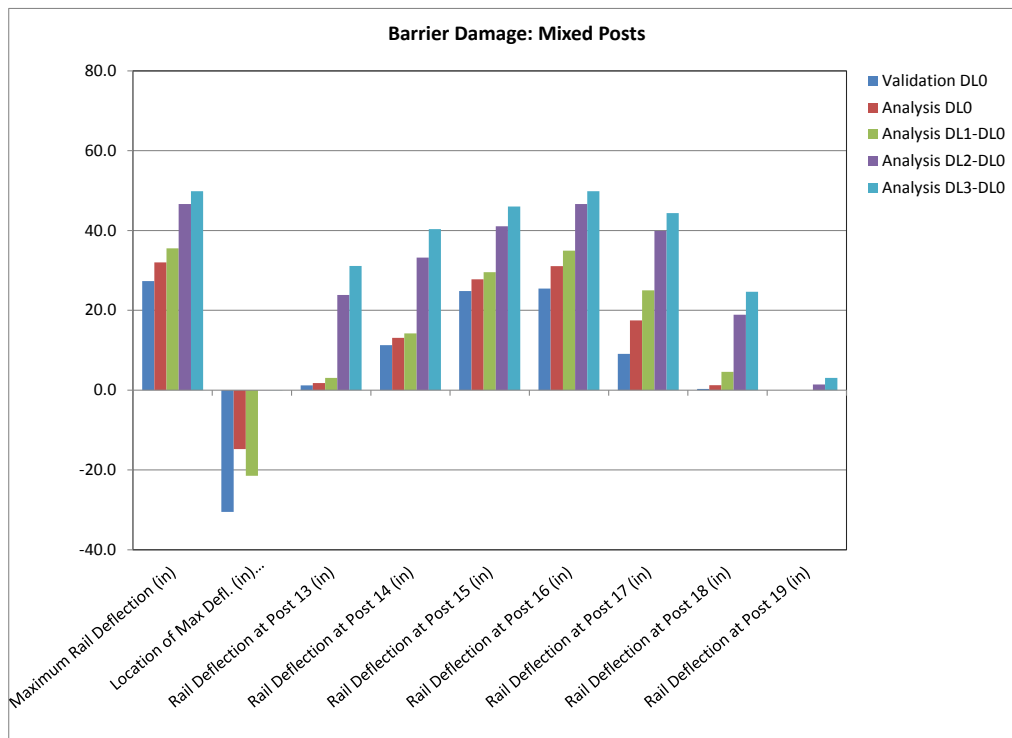


Figure 168. Summary of barrier damage evaluation from mixed post deterioration analyses.

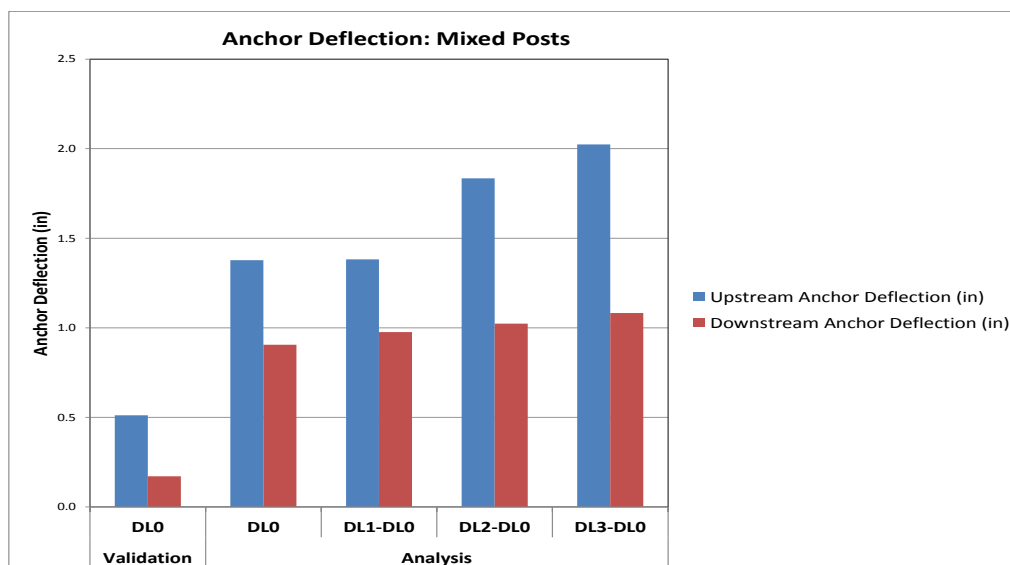


Figure 169. Summary of anchor displacement at rail height from mixed post deterioration analyses.

A summary of occupant risk measures computed from the acceleration and angular rate time-histories at the vehicle's center of gravity is provided in Table 53. This data is also presented graphically in Figures 170 through 172. The results indicate that the vehicle decelerations were very similar for all cases, with a slight trend toward decreasing values as post deterioration increased. These results seem counter intuitive and should be reassessed using a more appropriate impact point for the analyses.

A summary of the maximum effective plastic strains around the splice-bolt holes in the w-beam for each analysis case is shown in Figure 173. The results indicated that the potential for splice rupture increased as post deterioration increased. For example, the plastic strains at the splice-bolt holes reached magnitudes of 1.0, 1.2 and 1.3 for cases DL1, DL2 and DL3, respectively. It is assumed that the results for cases DL1 and DL2 actually under-predict the maximum strain values, since the critical impact point for these two cases was not evaluated.

Table 53. Summary of occupant risk measures from mixed post deterioration analyses.

Occupant Risk Factors		Test 471470-26	DLO (Validation)	DLO (Baseline)	DL1 - DLO	DL2 - DLO	DL3 - DLO
Occupant Impact Velocity (m/s)	x-direction	4.6	5.3	5.2	4.3	5.1	5.1
	y-direction	5.8	5.8	5.3	5.1	5.0	4.9
	at time	0.1437	(0.1442 sec)	(0.1519 sec)	(0.1535 sec)	(0.1683 sec)	(0.1701 sec)
THIV (m/s)		6.9 (0.1404 sec)	7.4 0.1398	7 0.1471	6.4 (0.1484 sec)	6.7 (0.1629 sec)	6.7 (0.1646 sec)
Ridedown Acceleration (g's)	x-direction	11.5 (0.2025 - 0.2125 sec)	10.2 (0.1791 - 0.1891 sec)	10.3 (0.1519 - 0.1619 sec)	11.2 (0.1546 - 0.1646 sec)	11.0 (0.1962 - 0.2062 sec)	9.1 (0.1988 - 0.2088 sec)
	y-direction	11.2 (0.2381 - 0.2481 sec)	11.1 (0.2152 - 0.2252 sec)	10.7 (0.2198 - 0.2298 sec)	10.2 (0.2124 - 0.2224 sec)	10.5 (0.2142 - 0.2242 sec)	7.2 (0.2836 - 0.2936 sec)
PHD (g's)		11.7 (0.2025 - 0.2125 sec)	13.6 (0.2148 - 0.2248 sec)	13.7 (0.2003 - 0.2103 sec)	13.6 (0.1547 - 0.1647 sec)	11.2 (0.1964 - 0.2062 sec)	10.0 (0.1996 - 0.2096 sec)
ASI		1.01 (0.2176 - 0.2676 sec)	0.99 (0.1172 - 0.1672 sec)	0.93 (0.1219 - 0.1719 sec)	0.89 (0.1936 - 0.2436 sec)	0.74 (0.1142 - 0.1642 sec)	0.72 (0.1145 - 0.1645 sec)
Max 50-ms moving avg. acc. (g's)	x-direction	6.1 (0.1382 - 0.1882 sec)	6.2 (0.1390 - 0.1890 sec)	7.6 (0.1216 - 0.1716 sec)	6.1 (0.1174 - 0.1674 sec)	5.9 (0.1583 - 0.2083 sec)	5.8 (0.1939 - 0.2439 sec)
	y-direction	6.8 (0.0945 - 0.1445 sec)	7.7 (0.1179 - 0.1679 sec)	6.5 (0.1976 - 0.2476 sec)	7.1 (0.1919 - 0.2419 sec)	5.6 (0.2037 - 0.2537 sec)	5.5 (0.2818 - 0.3318 sec)
	z-direction	9.0 (0.2174 - 0.2674 sec)	2.4 (0.4155 - 0.4655 sec)	2.4 (0.3344 - 0.3844 sec)	2.7 (0.3158 - 0.3658 sec)	2.3 (0.3944 - 0.4444 sec)	3.0 (0.4245 - 0.4745 sec)

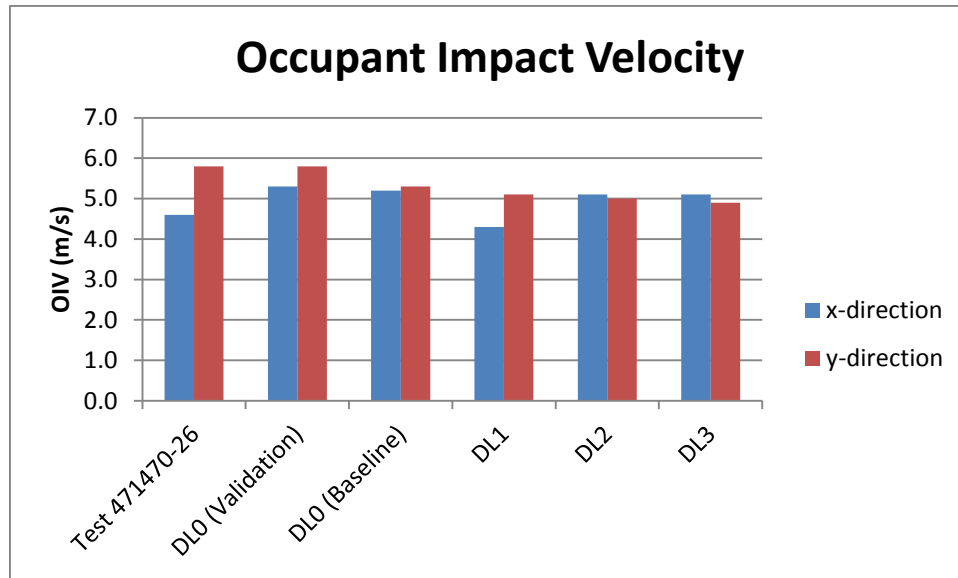


Figure 170. Summary of occupant impact velocity evaluation of uniform post deterioration.

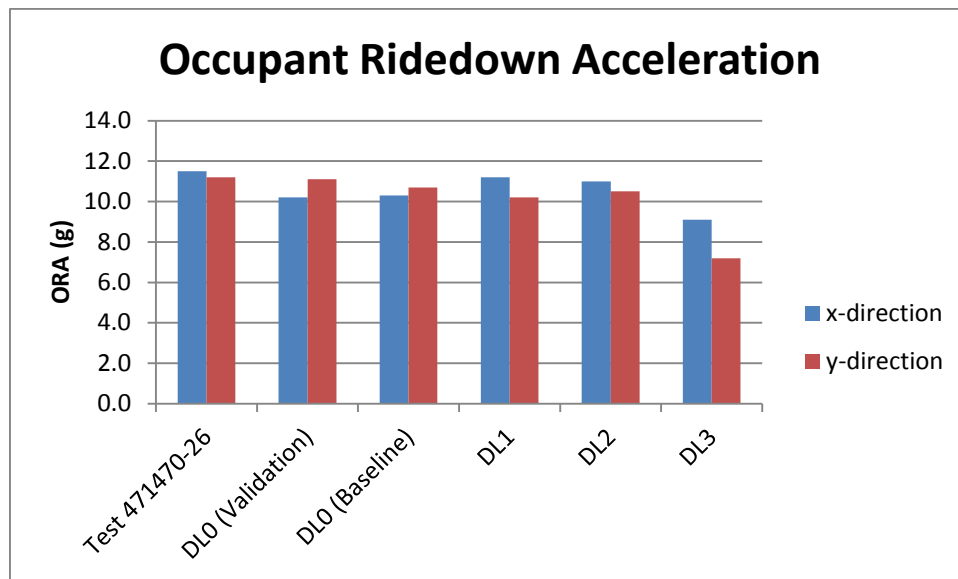


Figure 171. Summary of maximum occupant ridedown acceleration evaluation of uniform post deterioration.

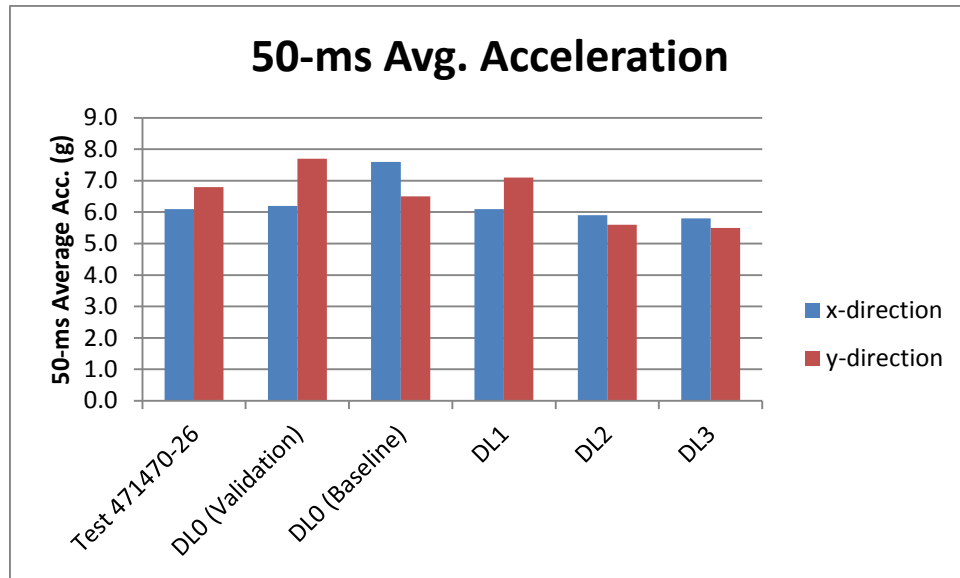


Figure 172. Summary of 50-ms running average acceleration evaluation of uniform post deterioration.

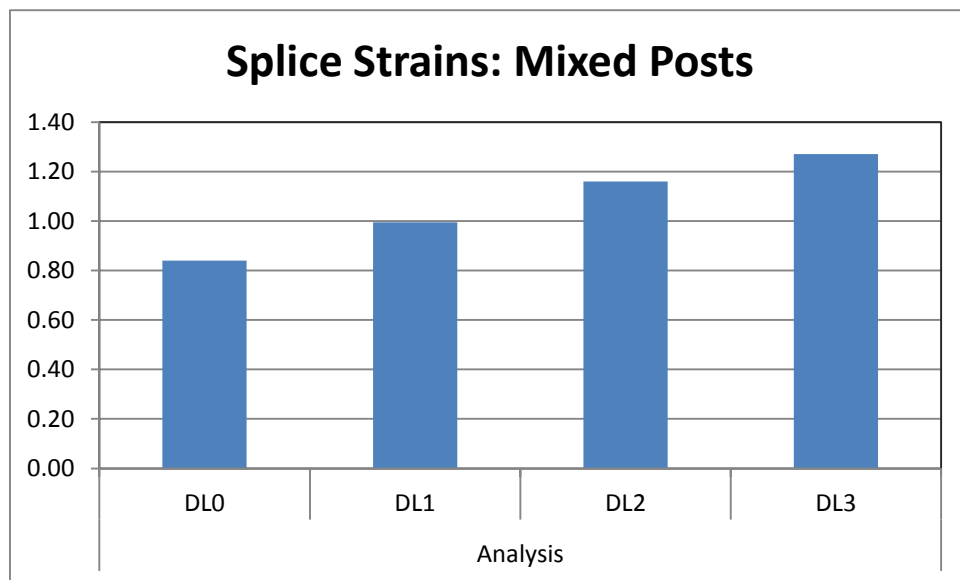


Figure 173. Summary of maximum effective plastic strains occurring at the splice-bolt locations at Post 16.

Summary and Discussion

The purpose of this study task was to quantify the effects of various levels of wood post deterioration on the crash performance of the G4(2W) strong-post guardrail system. The first phase involved (1) procuring guardrail post specimens with deterioration levels ranging from severe to essentially undamaged, (2) developing a procedure for quantifying the degree of deterioration, and (3) correlating the degree of deterioration to the dynamic properties of the posts.

The Ohio DOT provided 140 wooden guardrail posts for use in this study. The posts were extracted from damaged guardrail installations and represented a wide range of wood deterioration. A resistograph device was used to quantify the degree of deterioration of each post by drilling a 1/16th inch diameter drill bit through the full diameter of each post at groundline and recording the torque resistance on the drilling needle as a function of drilling depth. This information was then processed to determine a deterioration score that represented the effective degradation of post strength. The deterioration score was developed assuming that the resistograph data (i.e., torque amplitude on the drill bit) was linearly proportional to the local fiber strength (e.g., modulus) of the wood at each data point measured through the cross-section of the post. Accordingly, the resistograph data points were then processed to compute a pseudo moment and energy capacity value based on the effects of the measured strength and location within the cross-section with regard to the bending resistance and strain energy capacity of the post.

Pendulum tests were conducted to measure the dynamic impact response of the posts. Two series of tests were performed. The first series involved a 2,372-lb rigid pendulum impacting the posts at an impact speed of 20 mph at a height of 21.5 inches above ground. A review of the test results indicated that the inertial response of the posts may have significantly influenced the pendulum-mounted accelerometer data. The 20 mph impact speed resulted in much more energy than was required to break the post so the excess energy resulted in extraneous signal ringing. Thus, a second series of tests was conducted in which the target impact speed was reduced to 10 mph. A total of 22 tests were conducted for the first series at 20 mph and, a total of 39 tests were conducted for the second series at 10 mph. The test data from the second series of tests was found to correlate reasonably well with the resistograph scores. Based on a least-squares regression analysis of the data it was determined that the peak force, peak moment and energy at rupture initiation all increase as a linear function of the resistograph scores.

There was some scatter in the data which was expected to be due to the many variables that affect wood strength. The effects of moisture, however, were minimized in the tests by soaking all the posts to saturation levels prior to testing. Other possible causes for error may have been the result of faulty resistograph measurements. The resistograph measurements were made by drilling through the full diameter of the posts at the groundline at the front of the post. There were some cases in which the resistance did not fall back to zero when the drilling needle passed through the back-side of the post. This indicated that the needle likely encountered a “check” or a knot at some point during the test that turned the needle from its straight path and affected subsequent results. This was somewhat corrected in the data by estimating the most logical location for the start of the divergence and assuming that the error was increasing linearly for the remainder of the test. To minimize the effects of this drift phenomenon, it is recommended that the resistograph be used to drill only half way through the diameter on each side of the post. Due

to equipment cost and complexity of this method it may not be feasible for use in routine maintenance assessments for quantifying the degree of post degradation; thus future work should include development of more practical procedures for quantifying post deterioration.

Pendulum impact tests were also performed to evaluate the effects of various levels of post deterioration on the impact response of the post-soil system. The objectives for these tests were to determine the critical level of deterioration in which a guardrail post ruptures rather than rotates through the soil, and to gather data for validation/calibration of the finite element models. The soil was compacted to 92 percent with a moisture content of approximately 3.4 percent resulting in a dry density of 138 pcf. These soil conditions resulted in a stiffness response that exceeded the minimum strength requirements specified in *MASH* by approximately 30 percent. The results of the tests showed that the round wood post with nominal diameter of 8 inches does not have sufficient strength to properly rotate through the soil for these soil-strength conditions with post embedment depth of 40 inches or greater. Recall, that the embedment depth for the posts in full-scale crash Test 471470-26 was 36 inches.[Mak99a] The 6x8 inch wood posts used in that test were able to properly rotate through the soil without rupturing. The current standard embedment depth for the G4(2W) guardrail system is 44 inches. That version of the system, however, has not been tested under Report 350 conditions; and when it was tested under MASH conditions, it failed.[Bullard10]

Finite element models of round wood posts with various levels of deterioration damage were then developed and the constitutive behavior was calibrated based on the results of the test data from the pendulum impact study. These constitutive material models were incorporated into the validated G4(2W) guardrail model and the system was evaluated under *NCHRP Report 350* Test 3-11 impact conditions to quantify the effects of post degradation on the performance of the guardrail. Two damage scenarios were investigated. The first involved evaluation of the G4(2W) with uniform deterioration of the guardrail posts throughout the impact region. This scenario would be analogous to an aged guardrail system in which the posts are deteriorated but the guardrail is otherwise undamaged. The second scenario involved evaluation of the G4(2W) in which a number of new posts were installed adjacent to a line of deteriorated posts. This scenario is representative of a local repair on an aged guardrail system where a small number of the posts in an aged guardrail system have been replaced with new posts.

Regarding the first scenario, the analyses indicated that the lateral deflection of the rail increased significantly as post deterioration increased. As lateral rail deflection increased, the tension in the rail also increased and, consequently, resulted in higher loads on the downstream end-anchor. In this scenario, there were no indications that pocketing would be an issue. That is, as post deterioration levels increased, the system behaved more and more like a weak-post guardrail, where the posts upstream of the vehicle failed at an appropriate time, thereby preventing pocketing. However, the analyses did show that the loading on the w-beam splice at Post 16 (i.e., critical splice location for the analysis) resulted in relatively high local strains at the edges of the splice-bolt holes. The magnitude of these strains, for all cases, exceeded the failure strain of the material indicating a potential for a tear initiation. As post deterioration levels increased, the strain magnitudes increased to levels that indicated a high potential for rail rupture.

In the second damage scenario, the stiffer posts located downstream of the impact point helped to limit the lateral deflections of the rail, compared to those of the first damage scenario. In this case, the loading on the downstream anchor increased only slightly as the post

deterioration levels increased, while the loading on the upstream anchor was somewhat more notable. The potential for pocketing was higher for this damage scenario and increased as post deterioration levels increased.

The critical impact point (CIP) for the undamaged G4(2W) guardrail was used for all cases. That is, the CIP was not determined for the various guardrail damage cases; thus the results presented herein are to be considered *less severe* than they might otherwise have been.

Recommendations

Four levels of deterioration for wood guardrail posts were defined in terms of load and energy capacity of the post data, as well as in terms of relative capacity. Therefore, if post strength is measured or otherwise determined in the field (e.g., stress wave techniques, force-deflection techniques, resistograph, etc.) then the relative capacity may be used to identify damage level.[*Hron11*]

As a result of this study, the authors recommend that the repair threshold for wood post deterioration be those exceeding DL2 deterioration levels. If there are fixed/rigid objects located within 42 inches behind the guardrail, then posts with damage levels of DL2 or greater should be replaced with high priority. Otherwise, posts with damage level DL2 are considered to be of medium priority for replacement. Posts with damage level DL3 are essentially non-functional and are considered to be of high priority for replacement. If strength and/or deterioration measurement tools are not available, then visual inspection and “sounding” procedures should be utilized by experienced maintenance personnel to assess the soundness of the posts.

If it is determined that replacement of guardrail post(s) is warranted, (e.g., in a crash damaged section), then the posts immediately upstream and downstream of the repair section should also be checked for damage/deterioration to ensure stiffness compatibility of the repair section with the existing guardrail. If the adjacent posts are DL1 or better then only the posts in the damaged region need to be replaced. If the adjacent posts are DL2, then either (1) all posts in the system should be replaced with new posts or (2) the damaged posts in the immediate repair section should be replaced with posts of equivalent strength to DL1 (e.g., new posts with reduced cross-section). From available test data, new round wood posts with a diameter of 7.2 to 7.6 inches meet this condition. These diameters also meet the minimum size criteria for round posts (i.e., 8 ± 1 inches). If the adjacent posts are DL3 then, according to the aforementioned criteria, all posts in the system should be replaced since the deterioration state of the existing system renders it non-functional.

A summary of the recommendations regarding wood post deterioration are presented in Table 54.

Table 54. Recommendations for wood post deterioration damage.

Damage Mode	Repair Threshold	Relative Priority
Missing or Broken Posts	One or more posts: <ul style="list-style-type: none"> - Missing - Cracked across grain - Broken 	High
Rot or Insect Damaged Posts	Posts with damage level 3 (DL3) should be replaced with high priority (i.e., rotted posts). <u>These cases include:*</u> <ul style="list-style-type: none"> - Resi Score < 25 - Break strength < 9 kips - Rupture energy < 20 kip-in - Relative strength capacity < 45% - Young's modulus = TBD 	High
	If a hazard is located within 42 inches behind the face of the w-beam rail, then posts with damage level 2 (DL2) or worse should be replaced with high priority. <u>These cases include:*</u> <ul style="list-style-type: none"> - Resi Score < 35 - Break strength < 12 kips - Rupture energy < 26 kip-in - Relative strength capacity < 55% - Young's modulus = TBD 	High
	Otherwise, posts with damage level DL2 should be replaced with medium priority.	Medium
	<p>– If Repair is Warranted: –</p> <p>If post replacement is warranted (e.g., in a crash damaged section) then the posts immediately adjacent to the repair section should also be checked for damage/deterioration to ensure stiffness compatibility.</p> <ul style="list-style-type: none"> - <u>If adjacent posts are DL1 or better</u> then only the posts in the damage region need be replaced. - <u>If adjacent posts are DL2</u>, then: <ul style="list-style-type: none"> - Damaged posts should be replaced with posts of equivalent strength to DL1 (e.g., posts with reduced cross-section) ** - OR, all posts in the system should be replaced with new posts. - <u>If adjacent posts are DL3</u>, then the repair section should be expanded to include those posts as well (see above). 	!

If strength and/or deterioration measurement tools are not available, then visual inspection and "sounding" procedures should be utilized by experienced maintenance personnel to assess the soundness of the posts. Any posts with visual rot, mildew, or mold at the groundline should be further inspected for soundness.

From available test data, new posts with diameters equal 7.2 - 7.6 inches meet this condition. These diameter values also meet the minimum size criteria for round posts (e.g., 8 ± 1 inches).

CHAPTER 9 – EFFECTS OF ANCHOR STRENGTH ON PERFORMANCE OF THE G4(2W)

Finite element analysis was used to simulate *NCHRP Report 350* Test 3-11 impact conditions on the G4(2W) guardrail system. The analyses were performed using various levels of anchor strength in order to quantify the effects on anchor strength on guardrail performance. Although the end-terminal of a guardrail serves many purposes, one of its primary functions is to “anchor” the ends of the rail so that the resulting tension in the rail can help to limit lateral deflection of the system during impacts. Once the effect of anchor strength on guardrail performance was quantified, the various damage modes for end-terminals were then defined simply in terms of their effects on anchor strength (see Chapter 13).

Most guardrail end-terminals use the same basic arrangement that is illustrated in Figure 55. When the guardrail is struck, the anchor cable transfers the load to the foundation tubes to resist axial movement of the rail; the resulting tension in the rail helps to limit lateral deflections of the guardrail in the impact zone. Figure 56 shows a photo of the generic end-anchor for the modified G4(1S) with wood blockouts that was used in full-scale crash test 2214-WB1.[Polivka06a]

The effectiveness of the anchor is not dependent on the terminal type (i.e., a FLEAT, ET-PLUS, SKT, REGENT, SRT, etc.) since all these terminals include essentially the same anchorage details. So, for example, if the groundline strut is missing, broken or otherwise nonfunctional, regardless of specific end-terminal type, then that damage mode would be associated with a corresponding anchor stiffness and strength. Likewise, eroded soil around an anchor post or an anchor post installed with inappropriate embedment depth would be associated with a corresponding anchor stiffness and strength.

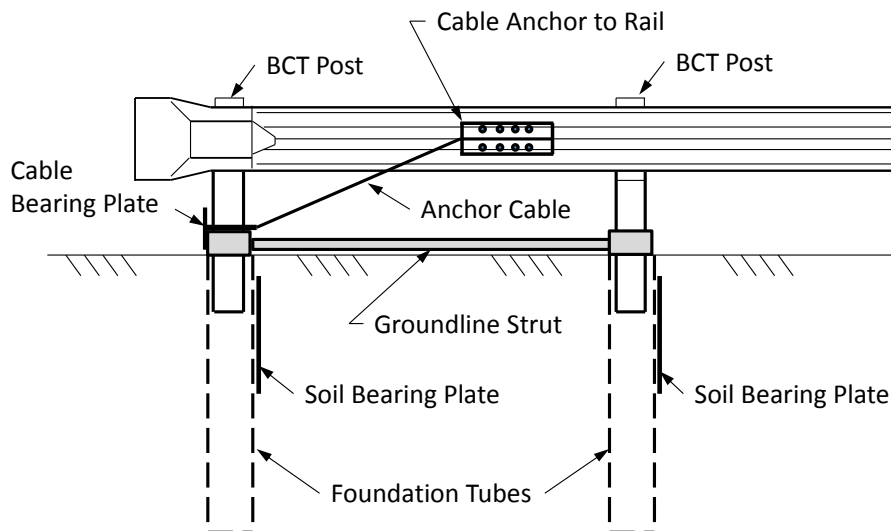


Figure 174. Sketch of typical guardrail anchor system.



Figure 175. Generic end-terminal used in full-scale crash test 2214-WB1 of a strong-post guardrail system.[Polivka06a]

Finite element analysis was used to quantify the effects of various levels of anchor strength degradation on the crash performance of the G4(2W) guardrail system. Two series of analyses were conducted. In the first series, an undamaged G4(2W) with various levels of end-anchor strength was evaluated. In the second series, the anchor strength was reduced by 47 percent (e.g., end-terminal with single foundation-tube anchor) and the posts were modeled with deteriorated strength properties.

Research Approach

The baseline anchor strength was determined through physical testing by measuring the force-deflection response of a standard two-post end-terminal anchor subjected to tensile loading, as illustrated in Figure 176. Ideally, the loading on the end of the rail would be applied dynamically with a loading rate similar to real-world vehicular collisions. However, there are many difficulties involved in designing a pendulum test experiment to “pull” on the end of the system. In general pendulums (and bogie vehicles) are used to strike and “push” an object rather than “pull”. Although it should be possible to construct a fixture (e.g., using pulleys or levers) to convert the compressive load of the pendulum to a tensile load on the rail, it would probably be difficult to separate out the dynamic effects of the mass, stiffness, energy absorption, etc. of the fixture from the test results. Also, the rail tension, which results from the lateral deflection of the guardrail during vehicular collisions, develops at a relatively low rate. For example, the maximum deflection of a guardrail in a TL3 event typically occurs over a period of approximately 0.2 to 0.3 seconds. If the resulting maximum rail deflection at the anchor is, say, 3 inches and assuming that the rail displaces at a constant rate, then the resulting deflection rate would be in the range of 10 in/s (0.6 mph) to 15 in/s (0.9 mph). To use a pendulum (or bogie) to achieve sufficient energy to displace the anchor system at such a low rate would require a very large mass and/or a fixture with significant mechanical advantage. Based on these facts and issues, it was decided that a more appropriate approach would be to perform a quasi-static test using a cable and winch system. The loading rate for the quasi-static tests was 1.0 to 1.5 in/s.



Figure 176. Example – finite element model for computing force-deflection response of the standard two-post guardrail anchor system.[Plaxico03]

Once the baseline anchor response was determined, finite element analysis was then used to quantify the effects of various levels of anchor strength degradation on the crash performance of the G4(2W) guardrail system. The end-anchor response was modeled using non-linear springs attached to the ends of the w-beam rail. The baseline end-anchor condition corresponded to the two-post cable-and-strut anchor system and was characterized by a force-deflection response measured directly from physical testing. To evaluate the effects of anchor strength, the stiffness and strength of the anchor was incrementally reduced to represent various levels of anchor damage. The incremental reduction in strength was achieved by simply scaling the baseline anchor stiffness. The crash performance of the guardrail was then evaluated for each damage level. Table 55 shows the analysis matrix used in this study.

Table 55. Analysis matrix for Task 4A-2.

Post Strength	Anchor Strength				
	167%	133%	Baseline	67%	47%
DL0	x	x	**	x	x
DL1			**		
DL2			**		
DL3			**		

** Analyses conducted in Task 4A-3 (See Chapter 8)

Physical Testing

Quasi-Static Pull-Test on End-Anchor

A quasi-static test was performed to measure the force-deflection response of a standard two-post guardrail anchor system, shown in Figure 177. The components of the test article were donated to the study by three guardrail distributors: Trinity Industries, Gregory Industries, Inc. and Road Systems, Inc. The test was performed on December 16, 2013 by the staff of the Federal Outdoor Impact Laboratory (FOIL) at the Federal Highway Administration's Turner Fairbank Highway Research Center in McLean, Virginia. Since the purpose of the test was to measure the

response of the anchor, only those components directly related to the anchor system were included in the test assembly.



Figure 177. Test set-up for measuring force-deflection response of a standard two-post guardrail end-terminal anchor.

Figure 178 shows a photo of the two foundation tubes with soil plates taken during the installation process. Because of the limited size of the soil pit at the test site, the test article was placed as far back as possible in the pit in order to minimize the influence of the rigid steel wall at the front of the soil pit. The distance from the front of the foundation tube at Post 2 to the front wall was approximately 30 inches; and the distance from the back of the foundation tube at Post 1 to the back of the soil pit was approximately 6 inches. It was not clear from the test results if the response of the system was influenced by the size limitation of the soil pit area.

The load was applied to the end of the test article using a winch and a cable-pulley system with a 2:1 mechanical advantage, as shown in Figure 179. The winch system used for the quasi-static test was an existing component of the pendulum test device – used primarily to hoist the pendulum into position for dynamic tests. For the test, the winch cable was run through a stationary pulley bracket aligned with the test article, then around another pulley that was attached to the end of the test article, and then back to a fixed anchor point near the stationary pulley bracket. This arrangement resulted in a 2:1 mechanical advantage for the winch. For the pulley located at the end of the test article, a 1-inch diameter steel rod was attached to the pulley and then fastened onto the end of the w-beam rail using a standard cable-anchor-bracket (i.e., RWE02), as shown in Figure 179.



Figure 178. Photograph of anchor tubes with soil plates during installation.

An additional wood post was fastened onto the rail near the load-point in order to maintain the proper height of the rail during the test. Recall that for most end-terminals a CRT post is fastened to the rail at this location. As a further precaution, additional materials were stacked underneath the end of the w-beam near the load point to ensure that the rail height did not drop during the test. The three vertical steel posts shown in the test set-up in Figure 177 were used for mounting (anchoring) the string-pot displacement transducers and were not part of the test article.

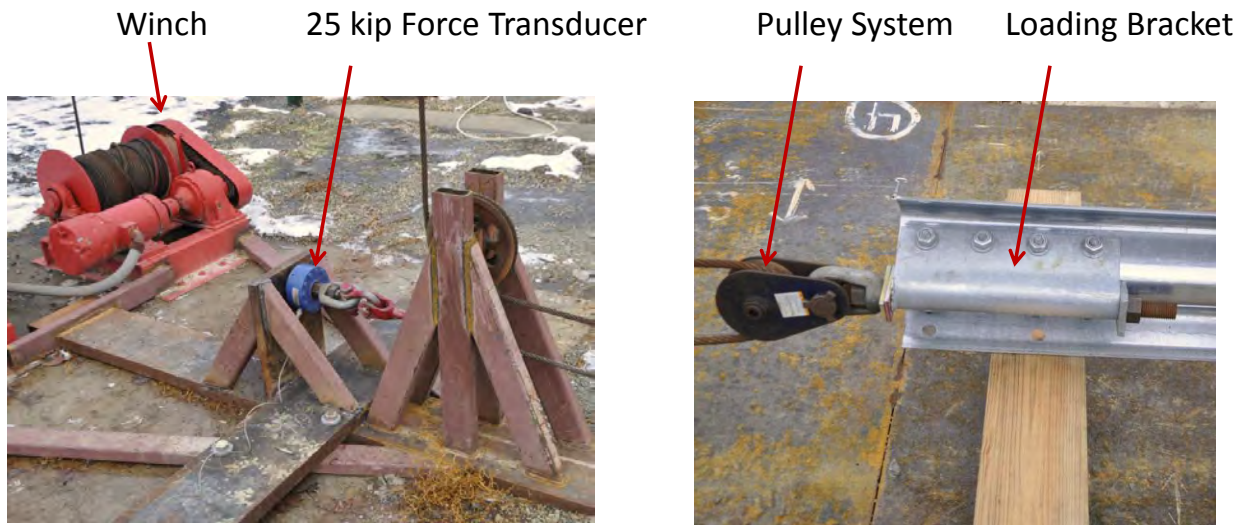


Figure 179. Cable and pulley system used to apply tensile loading on end-terminal anchor.

Equipment and Instrumentation

Force Transducer

The load on the cable was measured using an Interface Model 1220 standard load cell, rated at 25-kip. With the 2:1 mechanical advantage of the cable-pulley system, the load on the test article was two times the load measured by the load cell.


Displacement Transducers

SpaceAge Control, Inc. Series 162 Miniature Position Transducers (i.e., string-pots) were used to measure displacements at three key locations on the test article during the test. One was used to measure displacement at the end of the w-beam rail at the load point, another was used to measure the groundline displacement of the foundation tube at Post 1 (i.e., end post), and the third was used to measure the groundline displacement of the foundation tube at Post 2.


Photography

The tests were also recorded using three high-definition digital video cameras with operating speed set to 60 frames per second. Figure 180 provides the specifications and the general placement of the cameras for the test. The pre-test setup and the post-test results were also documented with photographs.


NO.	CAMERA	LENS	LENS (MM)	ZOOM (MM)	RESOLUTION (PIXELS)	SPEED (FPS)	LOCATION
1	GX-1	Nikon	24-85	30	1280 X 1024	60	Right Perp Post #1
2	Go Pro 1	Go Pro	24	24	Hi-Definition	60	Real Time Post #2
3	Go Pro	Go Pro	24	24	Hi-Definition	60	Real Time Guardrail End



3



1



2

Figure 180. Video camera specifications and placement.

Results

The loading on the anchor system was applied in two steps. In the first step, a displacement of 1 inch was applied to the end of the rail at a displacement rate of approximately 1 inch per second. The displacement was then held constant for 2.8 seconds. The test then proceeded at a displacement rate of approximately 1.5 inches per second until failure of the anchor system. Figure 181 shows the displacement- and displacement rate-time histories measured at the load point; Figure 182 shows the resulting force-deflection response. The displacement at the end of the rail and the displacement at the groundline of Post 2 are shown in Figure 183. The displacement at Post 1 was not measured due to the displacement transducer malfunctioning.

Sequential views of the test from two view-points are shown in Figure 184. The foundation tube at Post 1 began to displace vertically almost immediately at the start of the second loading step. The vertical component of displacement was not measured in the test; however, at 2 inches horizontal deflection of the rail element, the vertical displacement of Post 1 was estimated from the test videos to be 0.5 inches. At approximately 8.1 inches horizontal displacement of the rail element, the foundation tube fully extracted from the ground.

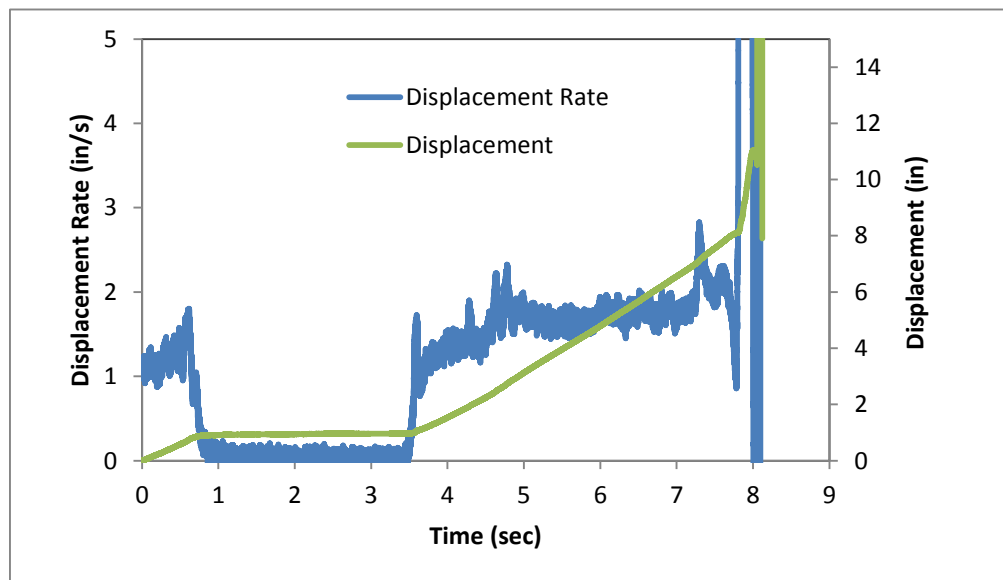


Figure 181. Displacement- and displacement rate-time histories measured at the load point on the end of the rail.

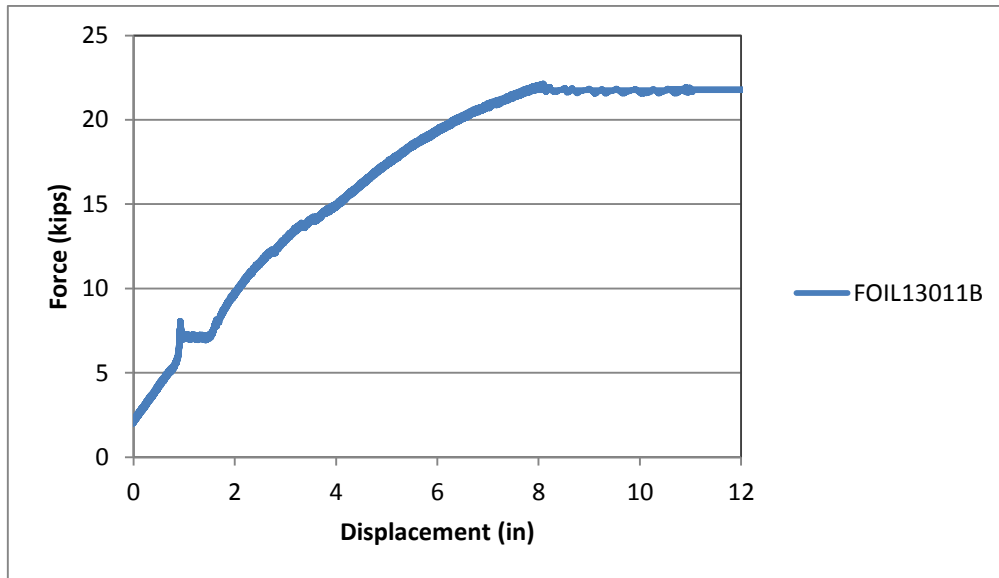


Figure 182. Force-displacement response of the anchor system measured at the load point on the end of the rail.

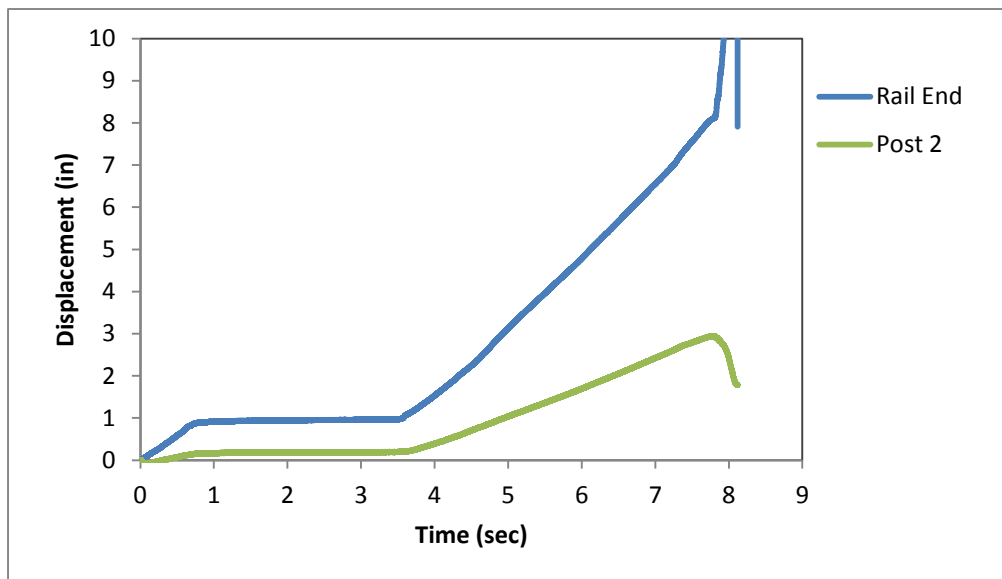


Figure 183. Displacement-time history at the end-of-the rail and at the groundline of Post 2.

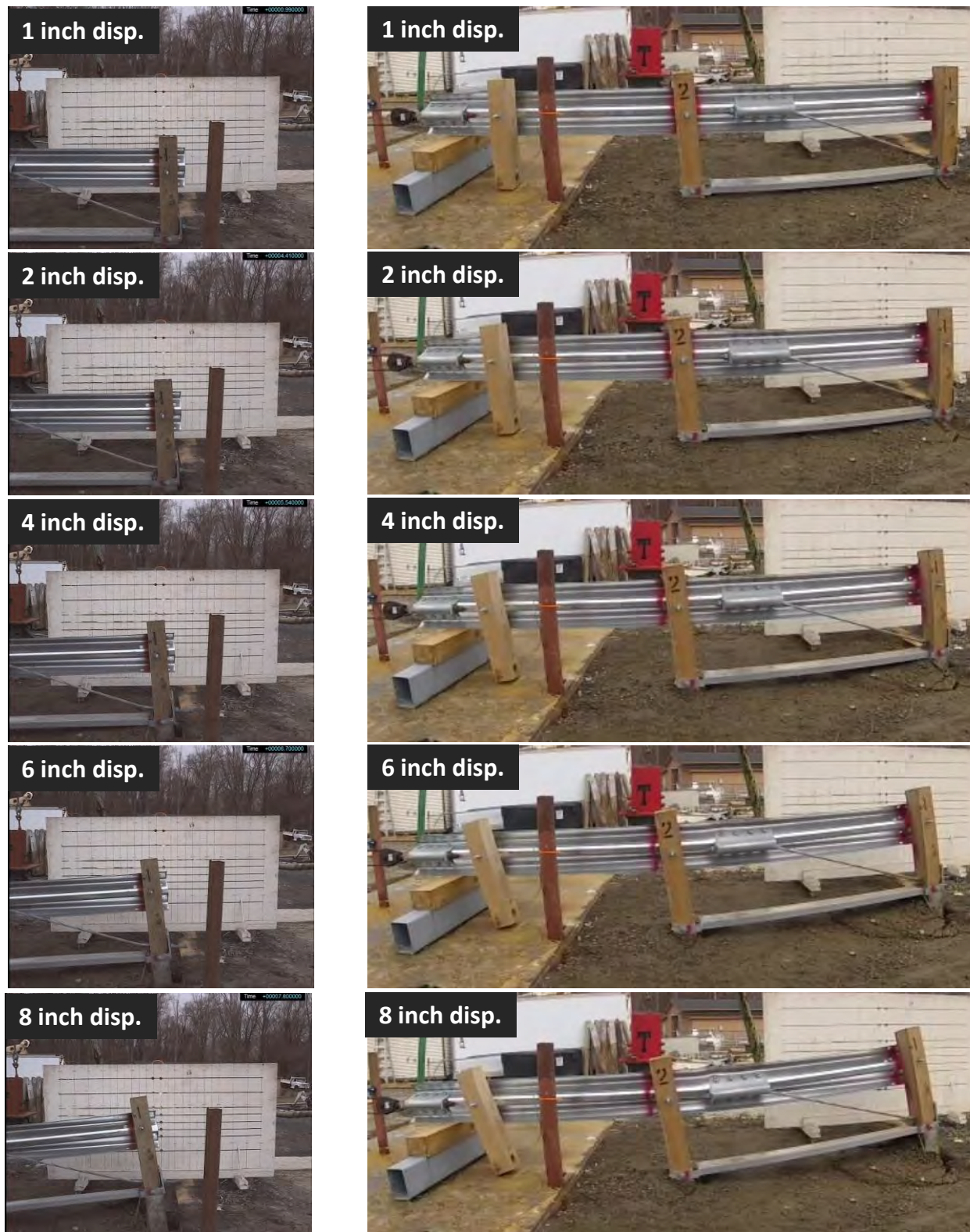


Figure 184. Sequential views of Test 13011B.

As the rail element was pulled during the test, the vertical force on the foundation tube (resulting from the vertical component of force of the anchor cable) was greater than the friction forces between the ground and foundation tube. This behavior, however, was not expected based on the results of previous full-scale crash tests in which vertical displacement of the foundation tube was generally negligible. For example, Figure 185 shows the damage to the upstream anchor system in full-scale crash Test MGSDF-1 conducted by the Midwest Roadside Safety Facility (MwRSF). The horizontal groundline displacement of the foundation tube in the crash test appears to be greater than that of quasi-static Test 13011B, and yet there was no measurable vertical deflection in the dynamic test.



Figure 185. Damage to end-terminal anchor in full-scale crash Test MGSDF-1.[Hascal07]

Due to the abnormal behavior of the anchor system in Test 13011B, the test results were considered to represent a lower bound for the force-deflection response of the system. Further, if the foundation tube had not extracted suddenly at 8 inches rail deflection, then it was assumed that the force would have continued to increase. Based on these assumptions, the effective static force-deflection response of the system was approximated, as shown in Figure 186. The effect of loading rate on the anchor response was accounted for in the finite element model using a dynamic magnification factor of 1.5 to scale the quasi-static force-deflection curve.

As a side note, the anchor strength tests performed in Task 4B included modifications to the test set-up which eliminated many of these issues. The baseline test was again conducted and produced slightly higher, but similar results (see Chapter 13 for more details).

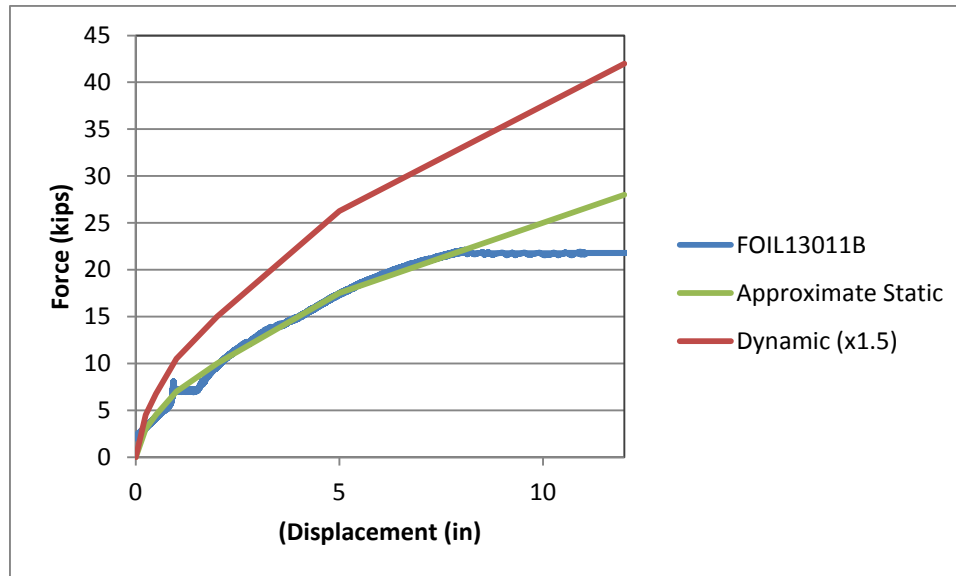


Figure 186. Measured and approximated force-deflection response for the end-anchor.

Evaluate Effects of Anchor Strength on Guardrail Performance

The finite element model of the standard G4(2W) guardrail system, which was developed and validated in an earlier part of this study (See Chapter 7), was used to evaluate the effects of end-anchor strength on the crash performance of the guardrail system. The baseline (undamaged) condition for the guardrail included the DL0 guardrail post model (refer to Chapter 7) and anchor strength corresponding to the results of the end-terminal in Test 13011B with force-deflection response scaled by 1.5 to account for loading rate³, as shown in Figure 186. The various levels of anchor strength were included in the model by simply scaling the baseline anchor force-deflection curve.

The crash performance of the guardrail was then evaluated using FEA to determine the effects of anchor strength degradation. The evaluation included anchor strengths ranging from 167 percent of the baseline anchor strength down to 47 percent of the baseline strength. The analysis matrix was shown previously in Table 55. The G4(2W) model used for this study was developed based on the *NCHRP Report 350 TL3* compliance test for the guardrail conducted at TTI (i.e., Test 471470-26).^[Mak99a] Refer to Chapter 7 for more details on model development.

The impact conditions were set to those of full-scale crash Test 471470-26 and involved the 4,568-lb C2500D pickup model impacting the guardrail at 62.6 mph (100.8 km/hr) at an angle of 24.3 degrees.^[Mak99a] Due to time and budget constraints, no attempt was made to determine the critical impact point (CIP) for each of the various anchor damage cases. The impact point for all analysis cases was set at 22 inches upstream of Post 14, which corresponded to the CIP for the baseline G4(2W) guardrail in Test 471470-26.^[Mak99a] The analyses were conducted for 0.6 seconds of the impact event.

³ The 1.5x scale factor used here was based on comparison of static vs. dynamic post-in-soil tests curves shown in Figure B-3 of MASH. It was later determined through physical tests in this project (not documented here) that the dynamic scale factor for the W6x16 post in soil with density of 144 pcf was 1.4x.

Results

The analysis model used for the evaluations is shown in Figure 187. Post 4 through Post 21 were modeled using MAT143; while the posts located upstream of the impact zone were modeled using a less computationally demanding material model, MAT13. The material parameters for MAT143 were defined according to deterioration level as described in Chapter 8. MAT13, however, was not calibrated for the various levels of post deterioration. Instead, the material parameters used for MAT13 were adopted from the earlier work by Plaxico, et.al.[Plaxico98] In effect, the line of posts near the downstream anchor should be considered undamaged, or new.

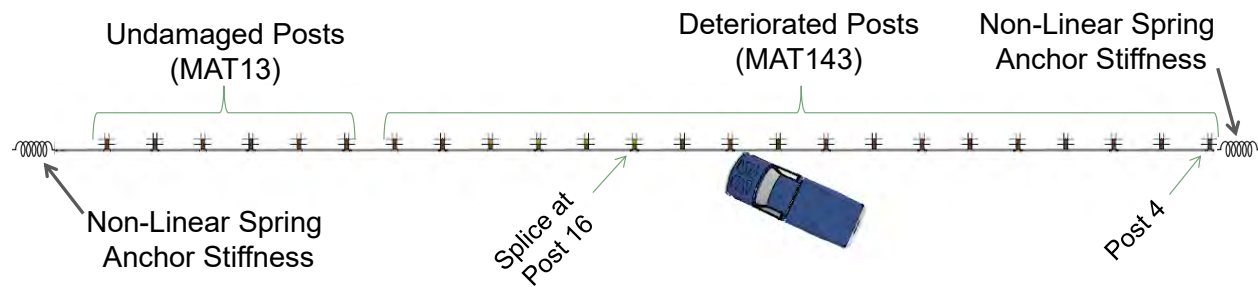


Figure 187. Analysis setup for evaluating effects of anchor strength on the performance of the G4(2W).

G4(2W) with Undamaged Posts and Various Anchor Strengths

The following is an evaluation of the G4(2W) guardrail with various levels of anchor strengths. Sequential views of the FE analysis results for each case are provided in Appendix I. Table 56 provides a summary of barrier damage from the analyses related to rail deflections, anchor movement and splice damage. This information is also presented graphically in Figure 188 and Figure 189. The maximum lateral rail deflection was essentially the same for all cases. This result was not expected, however, and was interpreted to indicate that the tension in the w-beam rail was carried primarily by the line-posts leading up to the end-terminals, resulting in minimal force on the anchor systems. Likewise, the maximum longitudinal deflection of the w-beam rail at the anchor was very similar for each case as well and ranged from 1.3 to 1.8 inches.

Regarding the “location of maximum deflection” in Table 56, a negative number indicates that the maximum deflection occurred upstream of the splice at Post 16, while a positive number indicates that maximum deflection occurred downstream of the splice. Since the maximum lateral deflection occurred just upstream of the splice connection at Post 16 for all cases, the impact point used in the analyses was considered to be representative of the critical impact point (CIP) for these damage cases.

Table 56. Summary of barrier damage evaluation from analyses of undamaged G4(2W) guardrail with various anchor strengths.

Event	Undamaged Posts (DL0)				
	Varying Anchor Strength				
	167%	133%	Baseline	67%	47%
Maximum Rail Deflection (in)	32.0	32.0	32.0	32.6	32.7
Location of Max Defl. (in) (Relative to Post 16)	-31.3	-20.3	-14.8	-6.0	-5.1
Rail Deflection at Post 13 (in)	1.9	1.7	1.8	1.6	1.8
Rail Deflection at Post 14 (in)	12.9	13.0	13.1	12.4	12.6
Rail Deflection at Post 15 (in)	27.7	27.5	27.8	28.2	27.7
Rail Deflection at Post 16 (in)	31.4	31.2	31.1	32.4	32.5
Rail Deflection at Post 17 (in)	17.4	17.8	17.5	18.0	20.7
Rail Deflection at Post 18 (in)	1.2	1.2	1.2	1.3	1.7
Rail Deflection at Post 19 (in)	0.0	0.0	0.0	0.0	0.0
Upstream Anchor Deflection (in)	1.3	1.4	1.4	1.8	1.8
Downstream Anchor Deflection (in)	0.9	0.9	0.9	1.1	1.1
Maximum Strain in splice	1.16	1.15	0.84	1.09	1.25

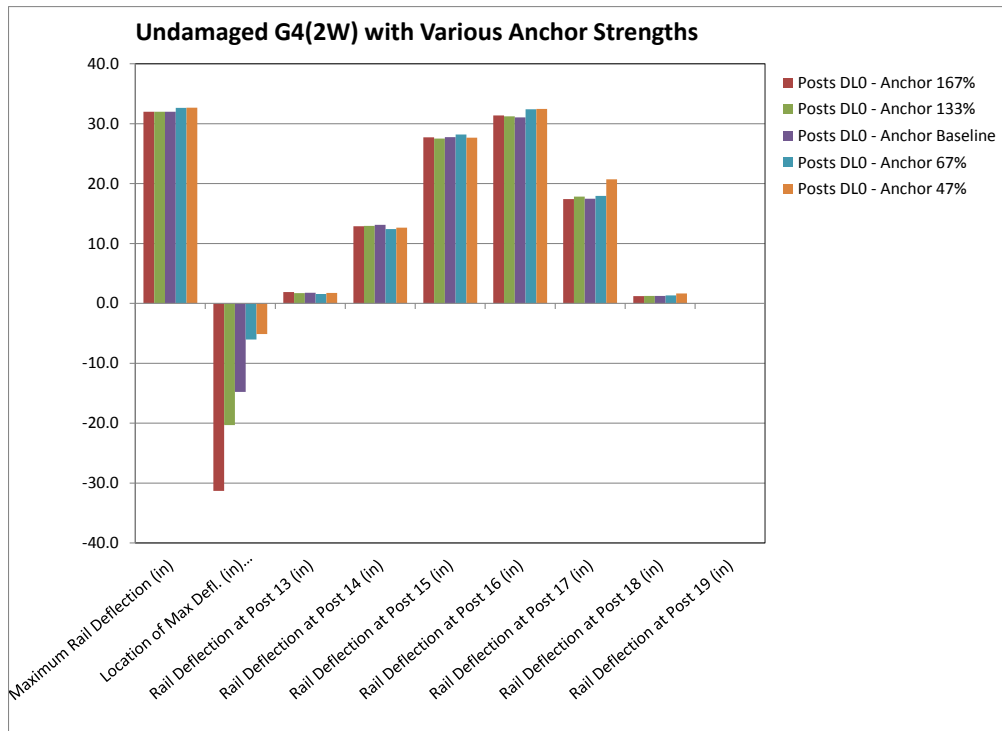


Figure 188. Summary of barrier damage evaluation from analyses of undamaged G4(2W) guardrail with various anchor strengths.

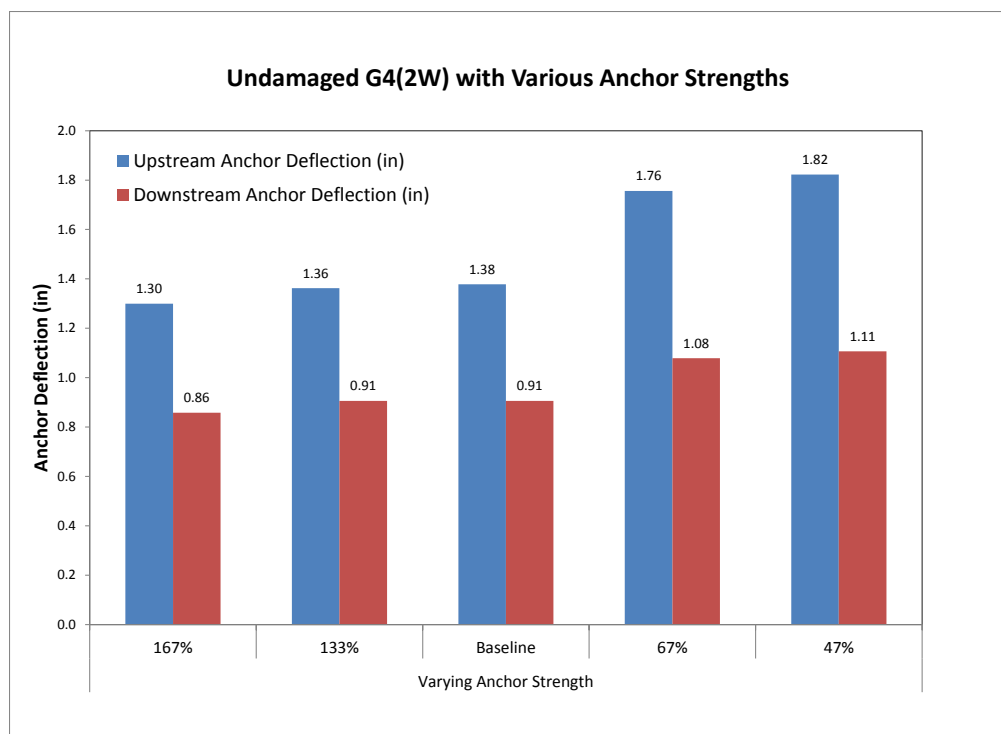


Figure 189. Summary of anchor displacement at rail height from analyses of undamaged G4(2W) guardrail with various anchor strengths.

A summary of occupant risk measures computed from the acceleration and angular rate time-histories at the vehicle's center of gravity is provided in Table 57. This data is also presented graphically in Figures 190 through 192. The results indicate that reduced anchor strength does not significantly affect occupant risk as the magnitude of maximum vehicle decelerations was very similar for all cases.

A summary of the maximum effective plastic strains around the splice-bolt holes in the w-beam for each analysis case is shown in Figure 193. The results showed that the potential for splice rupture increased as anchor strength increased or decreased from the baseline anchor strength case.

Table 57. Summary of occupant risk measures from analyses of undamaged G4(2W) guardrail with various anchor strengths.

Occupant Risk Factors		Undamaged Posts (DL0)				
		Varying Anchor Strength				
		167%	133%	Baseline	67%	47%
Occupant Impact Velocity (m/s)	x-direction	5.3	5.4	5.2	5.4	5.4
	y-direction	5.6	5.6	5.3	5.4	5.5
	at time	(0.1522 sec)	(0.1523 sec)	(0.1519 sec)	(0.1516 sec)	(0.1523 sec)
THIV (m/s)		7.3 (0.1473 sec)	7.3 (0.1477 sec)	7 (0.1471 sec)	7.1 (0.1466 sec)	7.2 (0.1476 sec)
Ridedown Acceleration (g's)	x-direction	10.3 (0.1623 - 0.1723 sec)	10.4 (0.1525 - 0.1625 sec)	10.3 (0.1519 - 0.1619 sec)	9.6 (0.1575 - 0.1675 sec)	9.0 (0.1650 - 0.1750 sec)
	y-direction	9 (0.2106 - 0.2206 sec)	9.7 (0.2196 - 0.2296 sec)	10.7 (0.2198 - 0.2298 sec)	9.7 (0.1516 - 0.1616 sec)	9.0 (0.2108 - 0.2208 sec)
PHD (g's)		12.3 (0.1507 - 0.1607 sec)	12.9 (0.1518 - 0.1618 sec)	13.7 (0.2003 - 0.2103 sec)	13.1 (0.1498 - 0.1598 sec)	11.6 (0.1488 - 0.1588 sec)
ASI		0.99 (0.1238 - 0.1738 sec)	1 (0.1242 - 0.1742 sec)	0.93 (0.1219 - 0.1719 sec)	0.97 (0.1235 - 0.1735 sec)	0.98 (0.1249 - 0.1749 sec)
Max 50-ms moving avg. acc. (g's)	x-direction	7.7 (0.1234 - 0.1734 sec)	7.6 (0.1225 - 0.1725 sec)	7.6 (0.1216 - 0.1716 sec)	7.6 (0.1230 - 0.1730 sec)	7.6 (0.1241 - 0.1741 sec)
	y-direction	6.8 (0.1254 - 0.1754 sec)	7.0 (0.1257 - 0.1757 sec)	6.5 (0.1976 - 0.2476 sec)	6.8 (0.1114 - 0.1614 sec)	6.8 (0.1258 - 0.1758 sec)
	z-direction	3 (0.3290 - 0.3790 sec)	2.6 (0.2631 - 0.3131 sec)	2.4 (0.3344 - 0.3844 sec)	4.6 (0.0929 - 0.1429 sec)	3.3 (0.3312 - 0.3812 sec)

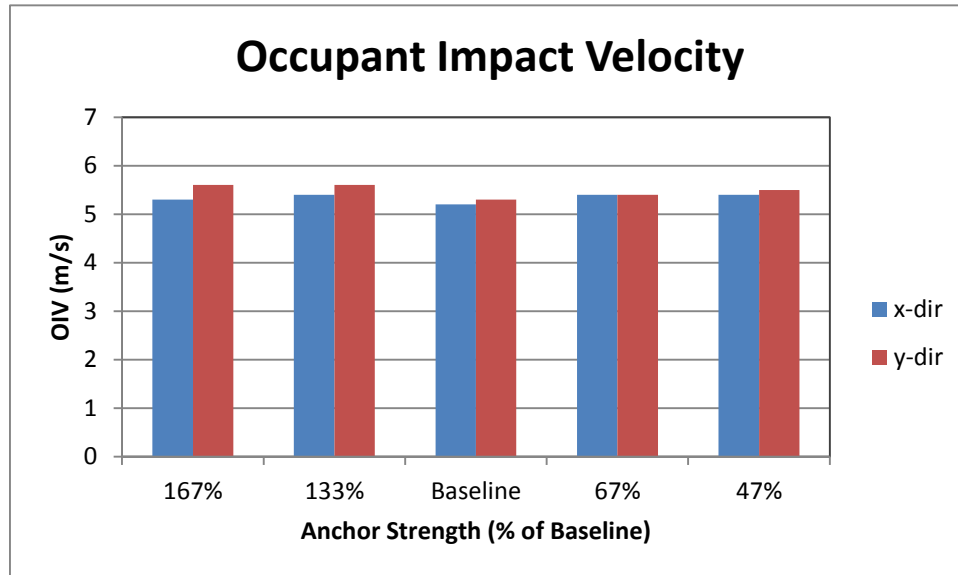


Figure 190. Summary of occupant impact velocity (OIV) from analyses of undamaged G4(2W) guardrail with various anchor strengths.

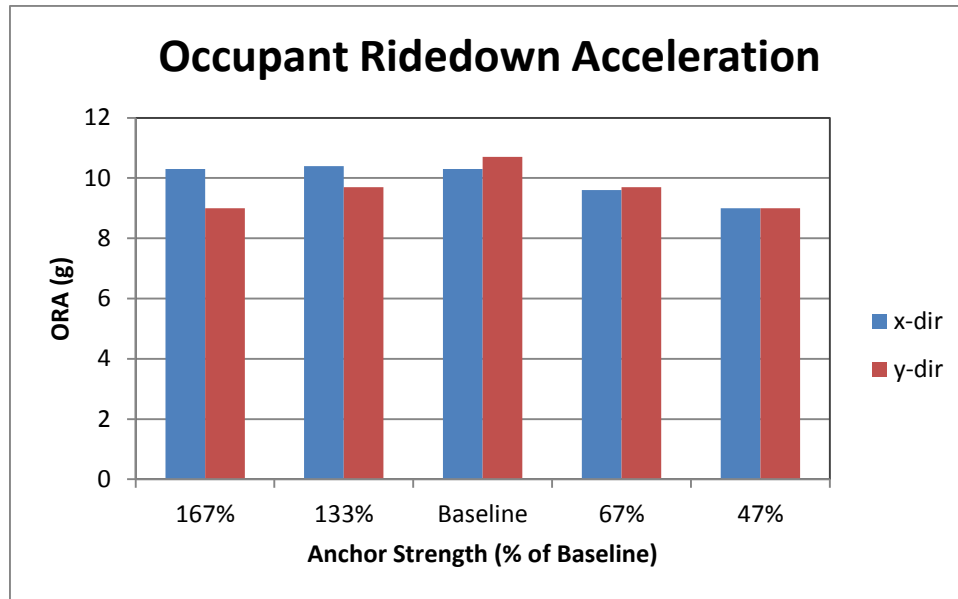


Figure 191. Summary of occupant ridedown accelerations (ORA) from analyses of undamaged G4(2W) guardrail with various anchor strengths.

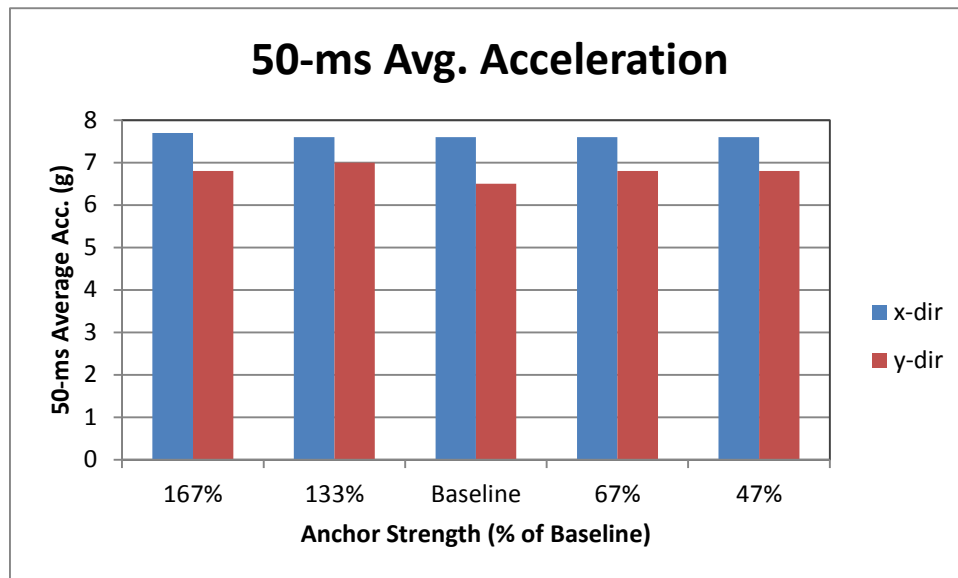


Figure 192. Summary of occupant risk measures from analyses of undamaged G4(2W) guardrail with various anchor strengths.

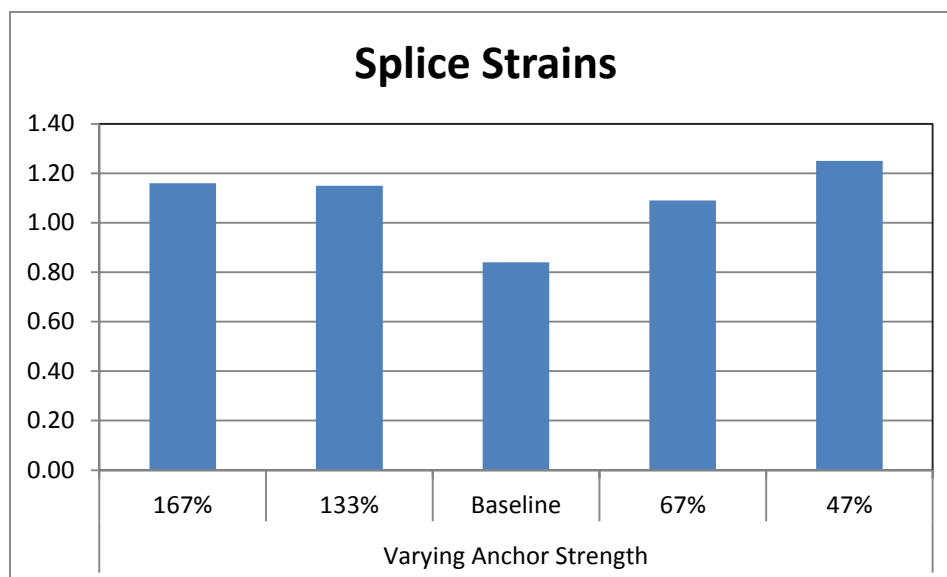


Figure 193. Summary of maximum effective plastic strains occurring at the splice-bolt locations at Post 16.

G4(2W) with 47 Percent Baseline Anchor Strength and Various Post Deterioration Levels

The following is an evaluation of the G4(2W) guardrail for the combination damage mode of reduced anchor stiffness and deteriorated guardrail posts. The anchor stiffness for this analysis was set to 47 percent of the baseline anchor strength and four different post deterioration levels were evaluated. Sequential views of the FEA results for each case are provided in Appendix J. Table 56 provides a summary of barrier damage from the analyses related to rail deflections, anchor movement and splice damage. This information is also presented graphically in Figures 188 and 189.

The maximum lateral rail deflection was 32 inches for case DL0 (i.e., undamaged posts) and increased significantly as post deterioration levels increased. This result was similar to that of the G4(2W) with baseline anchor strength and various levels of post-deterioration (see Chapter 8); however, the lateral deflection increased much more significantly for this combination damage mode case. The cause of the increased deflections was attributed to the fact that as deterioration levels for the guardrail posts increased, more and more posts fractured during the impact event. This resulted in fewer posts available to carry the tensile load in the w-beam rail and, thus, higher loads on the anchor systems. Likewise, the maximum longitudinal deflection of the w-beam rail at the anchor also increased significantly for this combination damage mode as post deterioration levels increased - compared to the results from the analyses involving the baseline anchor stiffness.

For these analyses cases, the maximum lateral deflection generally occurred downstream of the splice connection at Post 16; thus the impact point used in the analyses was *not* considered to be representative of the critical impact point (CIP) for these damage cases.

Table 58. Summary of barrier damage evaluation from analyses of G4(2W) with combination of weak anchor and deteriorated posts.

Event	Anchor Strength = 47% Baseline			
	Varying Post Deterioration			
	DL0	DL1	DL2	DL3
Maximum Rail Deflection (in)	32.7	49.5	73.5	107.0
Location of Max Defl. (in) (Relative to Post 16)	-5.1	43.5	75.0	0.0
Rail Deflection at Post 13 (in)	1.8	14.0	44.8	97.4
Rail Deflection at Post 14 (in)	12.6	28.1	53.1	103.2
Rail Deflection at Post 15 (in)	27.7	39.3	60.7	105.3
Rail Deflection at Post 16 (in)	32.5	47.2	69.3	107.0
Rail Deflection at Post 17 (in)	20.7	47.8	73.5	106.3
Rail Deflection at Post 18 (in)	1.7	37.5	71.6	103.5
Rail Deflection at Post 19 (in)	0.0	15.7	64.6	98.2
Upstream Anchor Deflection (in)	1.8	2.3	4.3	20.9
Downstream Anchor Deflection (in)	1.1	1.3	1.6	1.4
Maximum Strain in splice	1.25	1.22	1.15	1.04

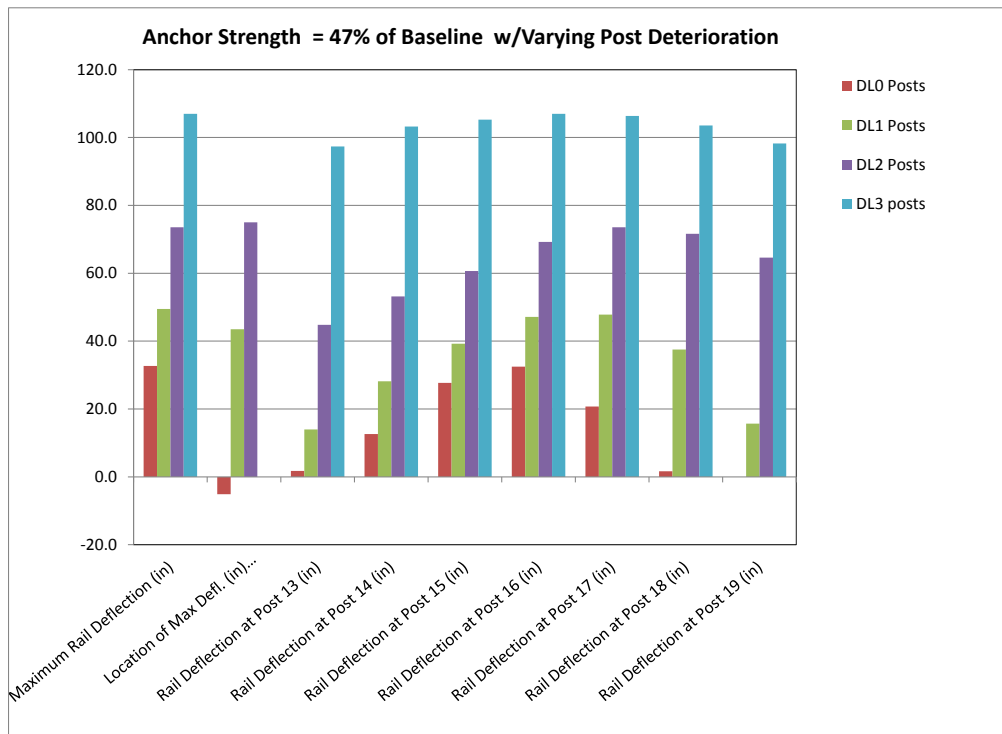


Figure 194. Summary of barrier damage evaluation from analyses of G4(2W) with combination of weak anchor and deteriorated posts.

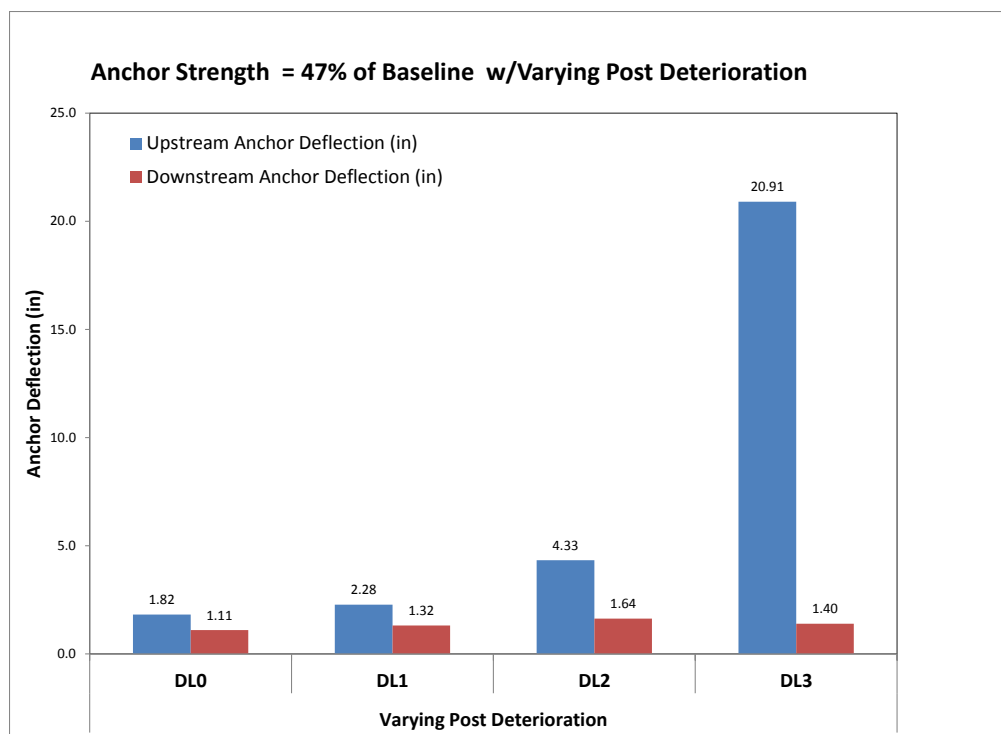


Figure 195. Summary of anchor displacement at rail height from analyses of G4(2W) with combination of weak anchor and deteriorated posts.

A summary of occupant risk measures computed from the acceleration and angular rate time-histories at the vehicle's center of gravity is provided in Table 59. This data is also presented graphically in Figures 196 through 198. The results indicated that reduced anchor strength did not significantly affect occupant risk; however there was a slight trend toward decreasing values as post deterioration levels increased.

A summary of the maximum effective plastic strains around the splice-bolt holes in the w-beam for each analysis case is shown in Figure 199. The results showed that the potential for splice rupture decreased slightly as post deterioration levels increased; this information may not be reliable, however, since the CIP was not used in the analyses. It is assumed that the results for Cases DL2 and DL3 would likely have been more severe had critical impact conditions been used. The CIP for these cases can be estimated based on the deflection data from Table 58 and assuming that the maximum potential for rail rupture occurs when maximum rail deflection is located at approximately 20 inches upstream of a splice connection. Future work should include analysis cases using the CIP (as estimated here or otherwise determined) for each damage case.

Table 59. Summary of occupant risk measures from analyses of G4(2W) with combination of weak anchor and deteriorated posts.

Occupant Risk Factors		Anchor Strength = 47% Baseline			
		Varying Post Deterioration			
		DL0	DL1	DL2	DL3
Occupant Impact Velocity (m/s)	x-direction	5.4	4.3	3.3	3.3
	y-direction	5.5	4.7	4.0	3.3
	at time	(0.1523 sec)	(0.1632 sec)	(0.1791 sec)	(0.1948 sec)
THIV (m/s)		7.2 (0.1476 sec)	5.9 (0.1573 sec)	5.1 (0.1727 sec)	4.5 (0.1853 sec)
Ridedown Acceleration (g's)	x-direction	9.0 (0.1650 - 0.1750 sec)	9.6 (0.2033 - 0.2133 sec)	5.3 (0.2487 - 0.2587 sec)	5.9 (0.4526 - 0.4626 sec)
	y-direction	9.0 (0.2108 - 0.2208 sec)	9.1 (0.2181 - 0.2281 sec)	8.0 (0.4893 - 0.4993 sec)	6.5 (0.3289 - 0.3389 sec)
PHD (g's)		11.6 (0.1488 - 0.1588 sec)	10.1 (0.1580 - 0.1680 sec)	9.0 (0.2413 - 0.2513 sec)	7.5 (0.3292 - 0.3392 sec)
ASI		0.98 (0.1249 - 0.1749 sec)	0.65 (0.1155 - 0.1655 sec)	0.57 (0.3053 - 0.3553 sec)	0.44 (0.4449 - 0.4949 sec)
Max 50-ms moving avg. acc. (g's)	x-direction	7.6 (0.1241 - 0.1741 sec)	5.1 (0.3408 - 0.3908 sec)	3.4 (0.2351 - 0.2851 sec)	3.4 (0.4299 - 0.4799 sec)
	y-direction	6.8 (0.1258 - 0.1758 sec)	4.8 (0.2179 - 0.2679 sec)	4.9 (0.3044 - 0.3544 sec)	3.5 (0.4496 - 0.4996 sec)
	z-direction	3.3 (0.3312 - 0.3812 sec)	2.0 (0.5022 - 0.5522 sec)	2.4 (0.5012 - 0.5512 sec)	1.6 (0.4371 - 0.4871 sec)

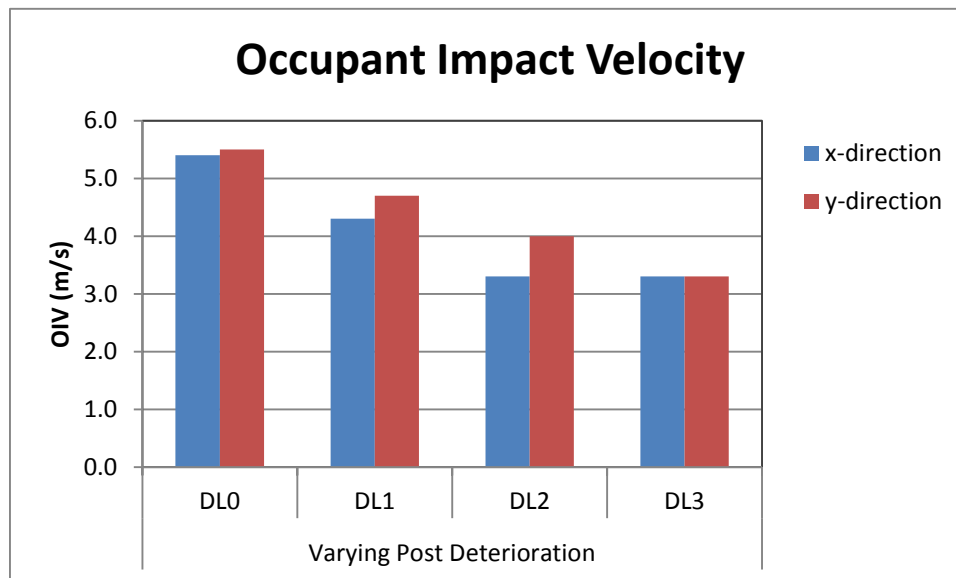


Figure 196. Summary of occupant impact velocity (OIV) from analyses of G4(2W) with combination of weak anchor and deteriorated posts.

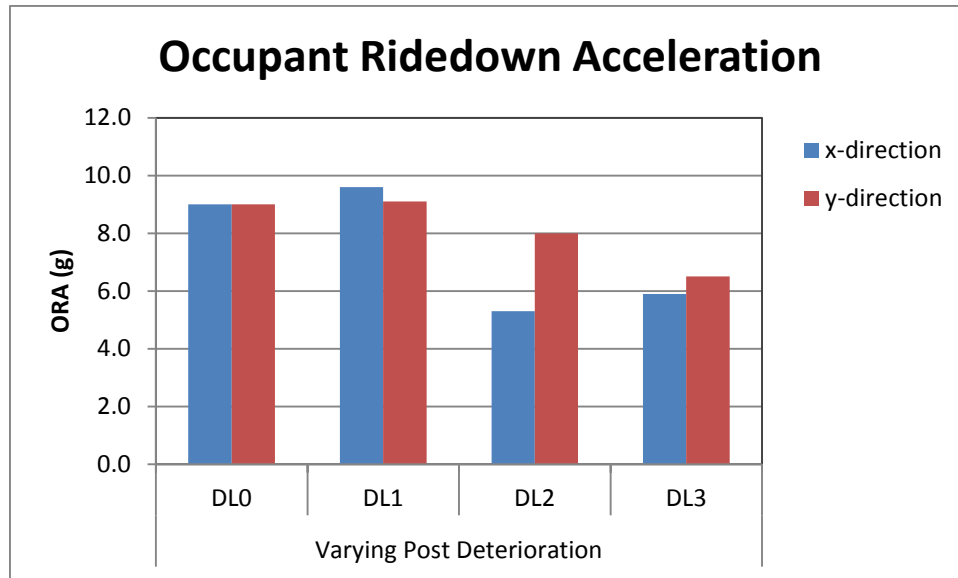


Figure 197. Summary of occupant ridedown accelerations (ORA) from analyses of G4(2W) with combination of weak anchor and deteriorated posts.

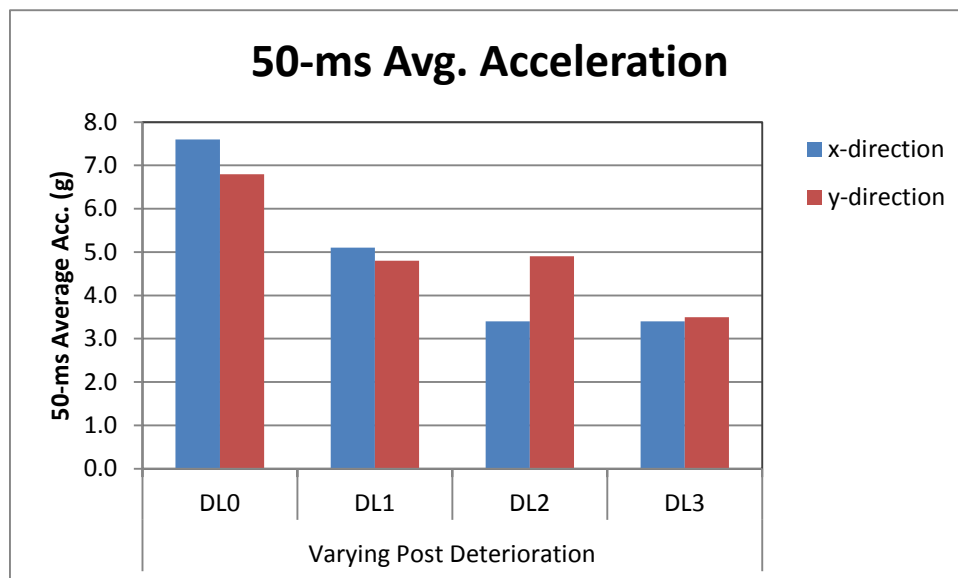


Figure 198. Summary of occupant risk measures from analyses of G4(2W) with combination of weak anchor and deteriorated posts.

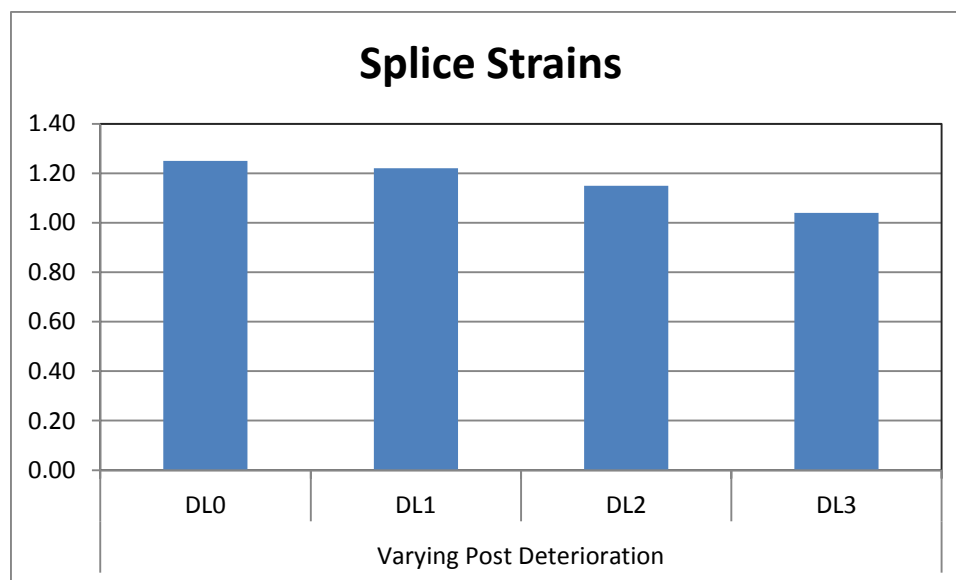


Figure 199. Summary of maximum effective plastic strains occurring at the splice-bolt locations at Post 16.

Summary and Discussion

The purpose of this study was to quantify the effects of various levels of anchor strength on guardrail performance. The focus was strictly on the use of FEA to evaluate the impact response of the G4(2W) guardrail system with various levels of end-anchor strength. The impact conditions for the analyses corresponded to those of *NCHRP Report 350* Test 3-11 (i.e., 4400 lb vehicle impacting at 62.2 mph and 25 degrees, nominally). The various causes of reduced anchor strength were evaluated and presented in Chapter 13 where physical testing was used to measure the anchor strength as a function of various damage modes for the end-terminal.

The baseline anchor strength used in these analyses was determined through physical testing by measuring the force-deflection response of a standard two-post cable-and-strut end-terminal subjected to tensile loading. An effective static force-deflection response for the baseline anchor system was derived from the results from Test 13011B, which was performed by pulling on the end-of the w-beam rail with a cable and winch system at a displacement rate of 1.0 to 1.5 in/s. For application in the dynamic impact study, the effects of loading rate on the anchor response was accounted for using a dynamic magnification factor of 1.5 to scale the quasi-static force-deflection curve; this response was then used as the baseline for the remainder of the study.

Finite element analysis was then used to quantify the effects of various levels of anchor strength degradation on the crash performance of the G4(2W) guardrail system. Two series of analyses were conducted. In the first series, the analyses involved an undamaged G4(2W) with various levels of end-anchor strength. In the second series, the anchor strength was reduced by 47 percent (e.g., end-terminal with single foundation-tube anchor) and the posts were modeled with deteriorated strength properties.

The results of the first series of analyses indicated that the performance of the G4(2W) with healthy posts (i.e., DL0 or DL1) was not significantly affected by anchor strength. This was interpreted to indicate that the tension in the w-beam rail was carried primarily by the line-posts leading up to the end-terminals, resulting in minimal force on the anchor systems.

This result may differ for the G4(1S) guardrail. The wood post (6x8-inch rectangular or 8-inch round cross-section) has a much higher torsional rigidity than the steel W6x9 steel post, and thus the posts of the G4(2W) guardrail do not experience torsional deflections like the posts of the G4(1S). For example, Figure 200 shows a snapshot from full-scale crash test C08C3-2 on the G4(1S) conducted by MGA Research Corporation on August 6, 2008, illustrating the relatively large torsional deflections of the guardrail posts upstream of the impact resulting from the tensile forces in the rail.[Fleck08] This test also resulted in relatively high deflection of the upstream anchor. Figure 201, on the other hand, shows a snapshot from full-scale crash test 471470-26 on the G4(2W) conducted by TTI on May 25, 1994.[Mak99a] In this test, the torsional deflection of the posts upstream of the impact was negligible and there was relatively low deflection of the anchor system.



Figure 200. Snapshot from Test C08C3-2 illustrating torsion behavior of posts upstream of impact on the G4(1S).[Fleck08b]



Figure 201. Snapshot from 471470-26 illustrating torsion behavior of posts upstream of impact on the G4(2W).[Mak99a]

As a further consideration, the impact point on the guardrail in these analyses was at approximately 62 feet downstream of the end-anchor. In this impact scenario, there were enough

posts upstream of the impact point carrying the tensile load of the rail such that the loading on the anchor was negligible. However, consideration should be given to the possibility of impact occurring at a point nearer to the anchor which would significantly increase the loading on the anchor. Also, if the w-beam rail detaches from the upstream posts during impact, or if posts upstream of the impact point fracture under the tensile loading of the w-beam, then anchor loads may increase significantly. For example, in full-scale crash test MGSDF-1 conducted by the MwRSF on a reduced-diameter wood post version of the MGS (i.e., 7.2-inch diameter Douglas Fir posts), the rail separated from all the posts upstream of the impact point to the anchor, as illustrated Figure 202, resulting in notable displacement of the anchor. This was, however, a successful test.



Figure 202. System damage at upstream anchor resulting from Test MGSDF-1.[Hascall07]

This result was demonstrated in this study by simulating Report 350 Test 3-11 impact on the G4(2W) in which the anchor strength was reduced by 47 percent (e.g., end-terminal with single foundation-tube anchor) and four different post deterioration levels. The results of this second analysis series indicated that lateral rail deflections increased significantly as post deterioration levels increased. Compared to the analysis results regarding post deterioration without anchor damage (e.g., see Chapter 8), the lateral deflection of the rail, as well as the load on the anchor system, increased much more significantly for this combination damage mode case. As discussed previously, the increased deflection was attributed to the fact that more posts upstream and downstream of the impact fractured as deterioration levels increased. This resulted in fewer posts available to carry the tensile load in the w-beam rail, thus causing higher loads on the anchor systems. The potential for rail rupture was also inconclusive for this series of analyses due to the fact that the impact point used for the analyses did not correspond to the critical impact point for the individual damage cases.

Future work should include analyses of the G4(2W) at impact points nearer to the anchor system. Due to the differences in the torsional rigidity of the W6x9 steel posts of the G4(1S) guardrail, an investigation similar to the one conducted herein should also be conducted to assess effects of anchor strength on the performance of that system; since it is expected that the G4(1S) would have a greater sensitivity to anchor strength.

Recommendations

As a result of this study, the research team recommends that the repair threshold for the end-terminal for the G4(2W) include damages that result in more than a 30% loss in anchor capacity relative to the baseline anchor strength. When the damage results in more than 50% loss of capacity then the relative priority for repair is high. For end-terminal damage that results in 30% to 50% loss of capacity for the anchor, the relative priority for repair is medium, unless a fixed object is located within 50 inches behind the face of the barrier. In that case, the line posts should also be checked for deterioration damage. If the damage level for the posts is DL1 or greater, then the priority for repair is high, based on lateral deflection limitations of the guardrail. A summary of the recommendations regarding end-terminal damage for the G4(2W) guardrail are presented in Table 60.

Table 60. Recommendations for end-terminal damage for the G4(2W).

Damage Mode	Repair Threshold	Relative Priority
Damaged End-Terminal for the G4(2W)	End-Terminal damage that results in more than 50% reduction in anchor capacity (relative to the baseline anchor strength) should be considered as high priority for repair.	High
	If a hazard is located within 50 inches behind the w-beam rail, then the end-terminal should be considered as high priority for repair for the <u>combination damage mode</u> of: <ul style="list-style-type: none"> - End-Terminal damage that results in more than 30% loss of anchor capacity and - Guardrail line-posts have deterioration levels of DL1 or greater. 	High
	Otherwise, end-terminal damage that results in a 30% to 50% loss of anchor capacity (relative to the baseline anchor strength) should be considered as medium priority for repair.	Medium

The repair criteria presented here provides assessment and repair criteria for the end-terminal of a G4(2W) guardrail in terms of anchor strength. The evaluation and repair criteria presented herein are later combined with the results of physical tests performed on the anchor system with various types and levels of measureable damage modes (see Chapter 13).

CHAPTER 10 – COMBINATION DAMAGE MODE OF RAIL DEFLECTION AND RAIL-POST CONNECTION FOR THE G4(2W)

In this chapter guardrail deflection in combination with rail-to-post connection strength are evaluated using finite element analysis to quantify their effects on the crash performance of the G4(2W) guardrail. The results of the study are then used to develop damage assessment and repair criteria for the guardrail system. The research approach was similar to that used by Gabler in Phase I for the evaluation of the G4(1S) guardrail with crash-induced damage. Finite element analysis was used to simulate impact of a 4568-lb pickup into the guardrail at low-impact speeds to obtain various levels of crash-induced damage. The damage resulting from these low-speed impacts also included various other non-critical damage modes such as rail flattening, slight anchor movement, slipping of post-bolt in the rail slot, moderate splice damage, etc. When additional critical damage modes resulted during the low-speed impacts, they were reported as such herein. For this study, the end-terminal was modeled using the baseline anchor response for a standard two-post anchor system as defined in Chapter 9. Finite element analysis was then used to simulate high-speed impact into the damaged guardrail to evaluate the performance of the system with low-severity, crash-induced rail deflections. The basic methodology involved using the finite element model validated in Chapter 7 to (1) simulate impact of the guardrail at low velocities (i.e., 30 mph, 35 mph and 40 mph); (2) save all deformations and residual stresses for the barrier components and soil; and (3) simulate high-speed impact on the damaged system under *NCHRP Report 350* Test 3-11 conditions.

Evaluate Effects of Rail Deflection and Rail-to-Post Connection Strength

The finite element model of the standard G4(2W) guardrail system developed in Chapter 7 was used to evaluate the effects of crash-induced rail deflection on the crash performance of the G4(2W) guardrail system. The baseline (undamaged) condition for the guardrail included the DL0 guardrail post model and anchor strength corresponding to the results of the end-terminal in Test 13011B with force-deflection response scaled by 1.5 to account for rate effects.

Low Severity Crash-Induced Damage

A total of six low severity, crash-induced damage cases were created by simulating the impact of a 4568-lb $\frac{3}{4}$ -ton pickup into the G4(2W) guardrail at an impact angle of 25 degrees using LS-DYNA. The simulation matrix is shown in Table 61 and includes three impact speeds (i.e., 30 mph, 35 mph and 40 mph) and two impact locations. The FEA models for these analysis cases are shown in Figure 203.

Impact Point 1 (IP01) was located at 2 feet upstream of Post 9. This impact point was chosen to create maximum deflection of the rail just upstream of the non-splice connection at Post 10, for investigating the effects of a rail-post connection at a non-splice location (e.g., at this connection point the bolt head only has a single layer of w-beam to pull-through in order to release). Impact Point 2 (IP02) was located at 2 feet upstream of Post 10. This impact point was chosen to create maximum rail deflection just upstream of the splice connection at Post 11, for evaluating the effects of the stronger rail-post connection at the splice where the bolt head must pull through two layers of w-beam to release. To facilitate reporting and data analysis, an

alternative reference system was used for labeling the posts within the impact region of the guardrail. This section of posts was labeled A through G, with Post A being the first post upstream of the impact point, as illustrated in Figure 203. This labeling system resulted in the rail-post connections at Posts C and D being the most critical for evaluating proper release of the rail from the posts for all impact scenarios. Recall that the greatest potential for vehicle override occurs when the rail is pulled down by the posts during deflection.

Table 61. Simulation matrix for creating low-severity guardrail deflection damage cases.

Impact Point	Impact Speed		
	30 mph	35 mph	40 mph
IP01	X	X	X
IP02	X	X	X

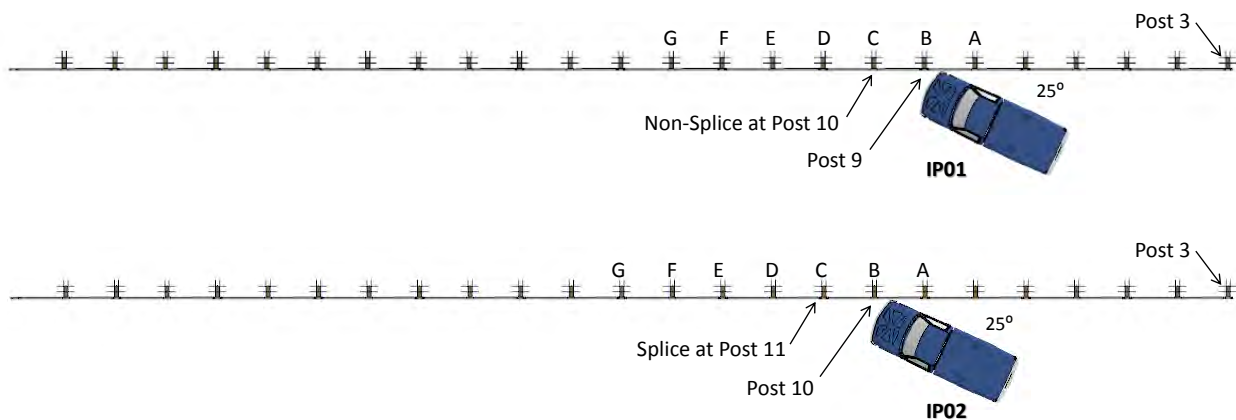


Figure 203. Impact locations, IP01 and IP02, for low-speed impact cases.

Table 62 provides a summary of barrier damages for the low-severity impact cases regarding lateral rail deflections, longitudinal rail deflection at the anchors, tensile forces in the w-beam rail, and final position of post-bolts in the slotted hole. Sequential views of the FE analysis results for each case are provided in Appendix K.

Table 62. Summary of results for the low-severity impact analyses.

Event		Impact Point 01			Impact Point 02		
		30 mph	35 mph	40 mph	30 mph	35 mph	40 mph
Rail Deflection	Maximum Dynamic (in)	13.7	17.0	18.8	12.2	16.6	18.9
	Maximum Permanent (in)	8.7	13.5	13.9	N.C.	13.3	13.3
	Location of Max Deflection (in) (Relative to Post C)	-37.0	-35.4	-35.0	-44.3	-30.5	-27.6
	Dynamic Deflection at Post A (in)	0.6	0.8	0.7	0.4	0.6	0.6
	Dynamic Deflection at Post B (in)	8.3	9.7	10.7	7.2	9.1	10.0
	Dynamic Deflection at Post C (in)	8.1	13.3	16.7	7.2	13.8	17.7
	Dynamic Deflection at Post D (in)	0.7	1.7	5.9	0.5	3.3	6.9
Rail Flattening	Maximum Rail X-Section Height (in)	16.0	16.9	17.3	16.9	17.8	17.9
Anchor Deflection	Upstream Anchor Permanent (in)	0.72	0.94	1.04	0.57	0.89	1.05
	Downstream Anchor Permanent (in)	0.07	0.18	0.33	0.04	0.24	0.36
Rail Load	Maximum Plastic Strain in Splice	0.19	0.24	0.83	0.32	0.58	0.57
	Maximum Rail Tension (kips)	N.C.	N.C.	N.C.	N.C.	N.C.	N.C.
Post Bolt Position	Final Position of Post-Bolt at Post B	USE	USE	USE	USE	USE	USE
	Final Position of Post-Bolt at Post C	DSE	CEN	DSE	CEN	CEN	CEN
	Final Position of Post-Bolt at Post D	DSE	DSE	DSE	DSE	DSE	DSE

USE - Upstream end of post-bolt slot

DSE - Downstream end of post-bolt slot

CEN - Center of post-bolt slot

N.A. - Not Applicable

N.C. - Not Computed

The maximum lateral dynamic deflections of the guardrail for the 30 mph, 35 mph and 40 mph impact cases were approximately 13 inches, 17 inches and 19 inches, respectively; the resulting maximum permanent deflections were approximately 9 inches, 13.5 inches, and 14 inches, respectively. Regarding the location of maximum deflection in Table 62, a negative number indicates that the maximum deflection occurred upstream of Post C, while a positive number indicates that maximum deflection occurred downstream of the post. In all cases, the maximum deflection occurred just upstream of the critical post-bolt connection at Post C, which was located at a w-beam splice for impact cases IP01 and at a non-splice location for IP02. The rail was flattened during the impact such that the maximum cross-section height of the w-beam ranged 16 to 17 inches for the analysis cases involving Impact Point 1, and 17 to 18 inches for the analysis cases involving Impact Point 2. According to Gabler et al., when the w-beam rail is flattened such that the cross-section height is greater than 17 inches, the damage severity rating is

considered “medium.” Thus, this damage mode was relatively significant for many of these cases.

The permanent longitudinal deflection of the rail element at the upstream anchor ranged from 0.6 inch for the 30 mph case to just over 1 inch for the 40 mph case. The movement of the rail at the downstream anchor was negligible for all cases. The maximum plastic strain in the rail element occurred at a splice-bolt location in all cases (typically at the downstream end of the splice at the lowest bolt hole). For simulation cases at IP01, the splice with highest strains was located at Post C; for simulation cases at IP02, the splice damage occurred at Post B. Unfortunately, the maximum tensile forces in the rail element were not recorded for these analysis cases.

At the start of the analyses, the post-bolts were positioned at the center of the slotted hole in the w-beam at all rail-to-post connections points. Due to the tension in the rail during impact, the post-bolts located upstream of the impact point tended to pull toward the upstream end of the slot, while the post-bolts downstream of the impact tended to pull toward the downstream end of the slot. At Post C, however, the post-bolt was first pulled to the downstream end of the slot as the vehicle approaches from the upstream direction; then as the vehicle passed by the post during redirection, the tension in the rail tended to pull the post-bolt back toward the center. In some cases, however, the bolt remained at, or very near to, the downstream end of the slot. The post-bolt positioned at the ends of the slotted hole result in a stronger, more critical connection for the study, since it results in a higher probability of the rail to remain attached to, and be pulled down with, the posts as they deflect.

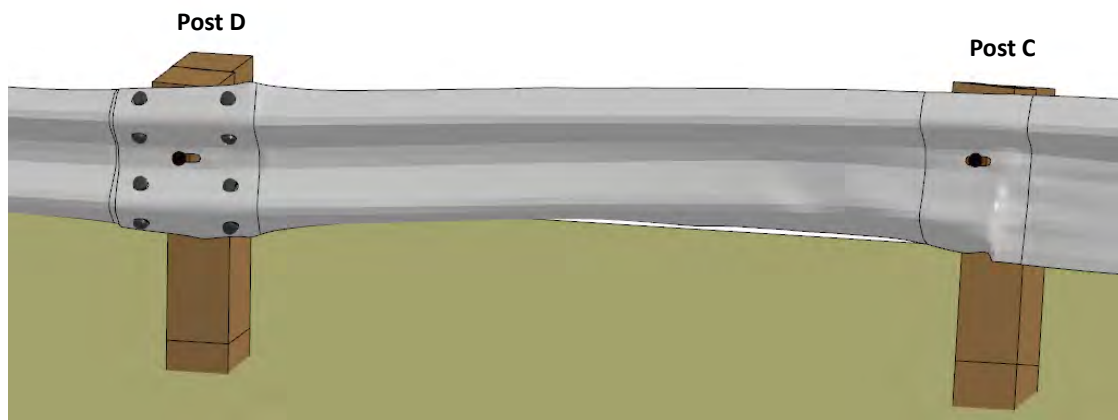


Figure 204. Example of low-severity impact damage illustrating final position of post-bolts relative to the slotted hole in w-beam.

The low-severity impact cases performed in this study involved low speeds and a high impact angle which resulted in damages to a relatively localized section of the guardrail, as illustrated in Figure 205. The length of damage shown in the figure includes only the section of rail with visually discernable lateral deflection. The full extent of damage actually involved a much longer section of the system and included low levels of permanent anchor deflections. It may be possible to achieve similar magnitudes of lateral deflection, spread over a greater length of guardrail, by using higher impact speeds and smaller impact angles. In such cases, the resulting capacity of the damaged guardrail may differ from those presented herein and should be considered in future evaluations of damage modes related to guardrail deflections.

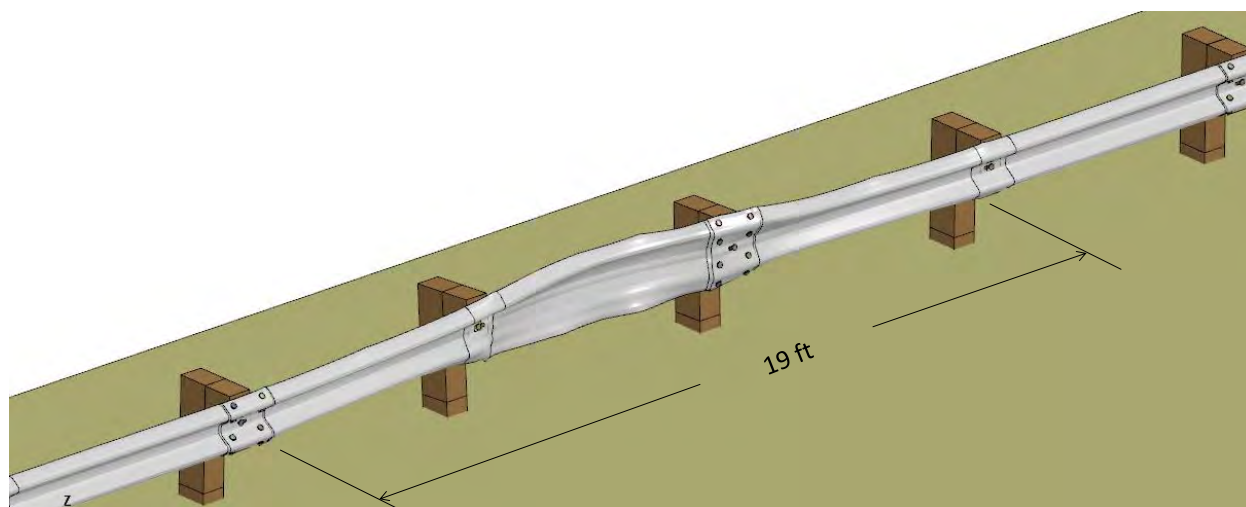
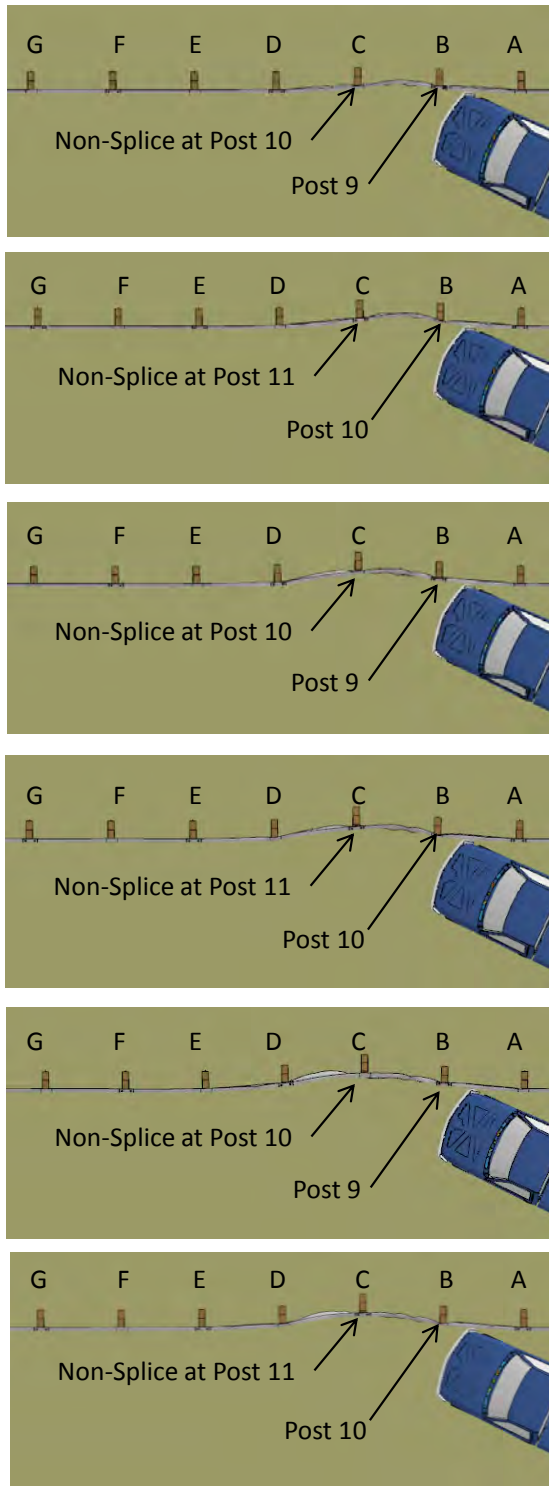


Figure 205. Extent of damage resulting from impact on G4(2W) at 30 mph at Impact Point.

High-Speed Impact into Pre-Damaged Guardrail

Finite element analysis was then used to simulate high-speed impact into the damaged guardrail to evaluate the performance of the system with various degrees of low-severity, crash-induced rail damage. The nodal deformations and residual stresses of the barrier components resulting from the low-speed impact cases were used as initial conditions for this phase of the study. The impact conditions for the high-speed impact simulations were set to those specified in *NCHRP Report 350* for Test 3-11 (i.e., 4409-lb pickup impacting at 62.2 mph and 25 degrees). The impact point for each analysis case was set to those of its corresponding low-severity impact analysis case (e.g., either IP01 or IP02). Figure 206 shows the FE model for the six analysis cases, denoting the impact point, extent of initial damage, and location of splice and non-splice positions relative to the critical post-bolt connection at *Post C*.

Sequential views of the FE analysis results for each of the high-speed impact cases are provided in Appendix L. Table 56 provides a summary of guardrail damages resulting from the analyses of the high-speed impacts, including rail deflections, anchor movement, splice damage, and release of post-bolt connections at Posts C and D. Portions of this information are also presented graphically in Figure 188 and Figure 189. The maximum lateral deflection of the rail during the high-speed impact cases increased as the severity of the pre-existing crash-induced deflection increased, with slightly higher deflections resulting from Impact Point 2. This trend was also prominent regarding maximum deflection of the rail at the post locations. The maximum rail deflection for the six cases ranged from 35.5 inches for the analysis case involving 8.7 inches initial deflection and Impact Point 1 to 41.3 inches for the analysis case involving 14 inches initial deflection and Impact Point 2. The maximum deflection for the baseline analysis of the undamaged G4(2W) was 32 inches (refer to Chapter 8). In all analysis cases, the maximum deflection of the rail occurred just upstream of Post D; thus Impact Point 1 was considered to be representative of the critical impact point (CIP) for the system.



Case 1: Impact Point - IP01
Critical post-bolt connection at non-splice

- Pre-Damage:
- Speed / angle = 30 mph / 25 deg.
 - Deflection = 8.7 in.
 - Length of damage = 19 ft.

Case 2: Impact Point - IP02
Critical post-bolt connection at splice

- Pre-Damage:
- Speed / angle = 30 mph / 25 deg.
 - Deflection = 8.7 in. (estimated)
 - Length of damage = 20 ft.

Case 3: Impact Point - IP01
Critical post-bolt connection at non-splice

- Pre-Damage:
- Speed / angle = 35 mph / 25 deg.
 - Deflection = 13.5 in.
 - Length of damage = 20 ft.

Case 4: Impact Point - IP02
Critical post-bolt connection at splice

- Pre-Damage:
- Speed / angle = 35 mph / 25 deg.
 - Deflection = 13.3 in.
 - Length of damage = 24.5 ft.

Case 5: Impact Point - IP01
Critical post-bolt connection at non-splice

- Pre-Damage:
- Speed / angle = 40 mph / 25 deg.
 - Deflection = 13.9 in.
 - Length of damage = 26 ft.

Case 6: Impact Point - IP02
Critical post-bolt connection at splice

- Pre-Damage:
- Speed / angle = 40 mph / 25 deg.
 - Deflection = 13.3 in.
 - Length of damage = 28 ft.

Figure 206. Initial conditions used in evaluating effects of low-level guardrail deflection on the performance of the G4(2W).

Table 63. Summary of barrier damage resulting from analysis of high-speed impact into the G4(2W) with pre-existing low-severity rail deflection.

Event		Initial Crash-Induced Deflection					
		Impact Point 01			Impact Point 02		
		8.7 inches	13.5 inches	14 inches	8.7 inches	13.5 inches	14 inches
Rail Deflection	Maximum Rail Deflection (in)	35.5	36.3	40.4	38.4	39.1	41.3
	Location of Max Deflection (in) (Relative to Post D)	-23.8	-8.5	-6.5	-14.6	-14.9	-7.9
	Rail Deflection at Post A (in)	3.1	3.9	4.0	3.9	3.7	4.5
	Rail Deflection at Post B (in)	15.0	16.7	17.7	17.2	16.5	17.7
	Rail Deflection at Post C (in)	31.9	33.4	35.4	33.2	33.7	35.0
	Rail Deflection at Post D (in)	34.3	36.2	40.0	37.9	38.7	40.1
	Rail Deflection at Post E (in)	21.2	22.7	30.5	25.4	27.3	27.4
	Rail Deflection at Post F (in)	2.0	2.5	9.0	3.8	4.4	4.9
	Rail Deflection at Post G (in)	0.0	0.0	0.9	0.0	0.0	0.0
Anchor Deflection	Upstream Anchor Deflection (in)	2.6	3.1	3.1	2.6	2.6	3.3
	Downstream Anchor Deflection (in)	0.9	0.9	1.0	0.9	1.1	1.2
Rail Load	Maximum Strain in splice	1.08	1.02	1.50	1.09	1.19	1.37
	Maximum Rail Tension (kips)	46.5	54.2	53.1	48.3	49.2	68.1
Post Bolt Release	Maximum Deflection at Time of Post-Bolt Release - Post C (in)	N.A.	32.1	27.5	27.1	28.5	32.2
	Maximum Deflection at Time of Post-Bolt Release - Post D (in)	32.2	33.5	37.3	29.6	28.7	31.3

The values presented in Table 56 for the “maximum deflection at time of post-bolt release” correspond to the lateral deflection of the rail measured at the post-bolt hole at the time when the connection separates. The shaded cells for this category in Table 56 represent those cases where the post-bolt is located at a w-beam splice, and the non-shaded cells correspond to cases where the post-bolt is at a non-splice location. For example, for IP01 the splice is located at Post D, while for IP02 cases the splice is located at Post C. The post-bolt connection at Post D was considered to be the most critical connection for these impact cases. This assumption was based on the fact that the lateral deflection of Post C did not reach critical magnitude until the vehicle was already at or past the post; whereas Post D reached critical deflections while the vehicle was still upstream of the post. For cases involving a w-beam splice at Post D, the release of the post-bolt connection tended to occur at higher post deflections, as the severity of the pre-existing crash-induced rail deflections increased. While for cases with a single w-beam layer at Post D, the connection failed rather consistently at 29-31 inches of post deflection, regardless of the severity of the pre-existing rail deflections.

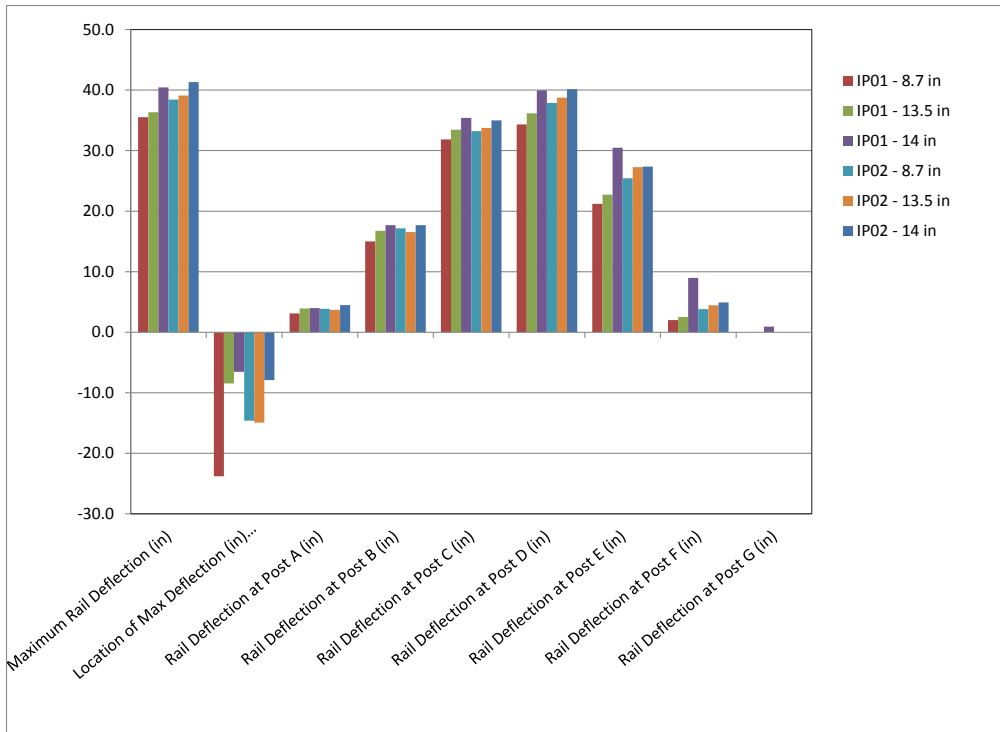


Figure 207. Summary of barrier damage resulting from analysis of high-speed impact into the G4(2W) with pre-existing low-severity rail deflection.

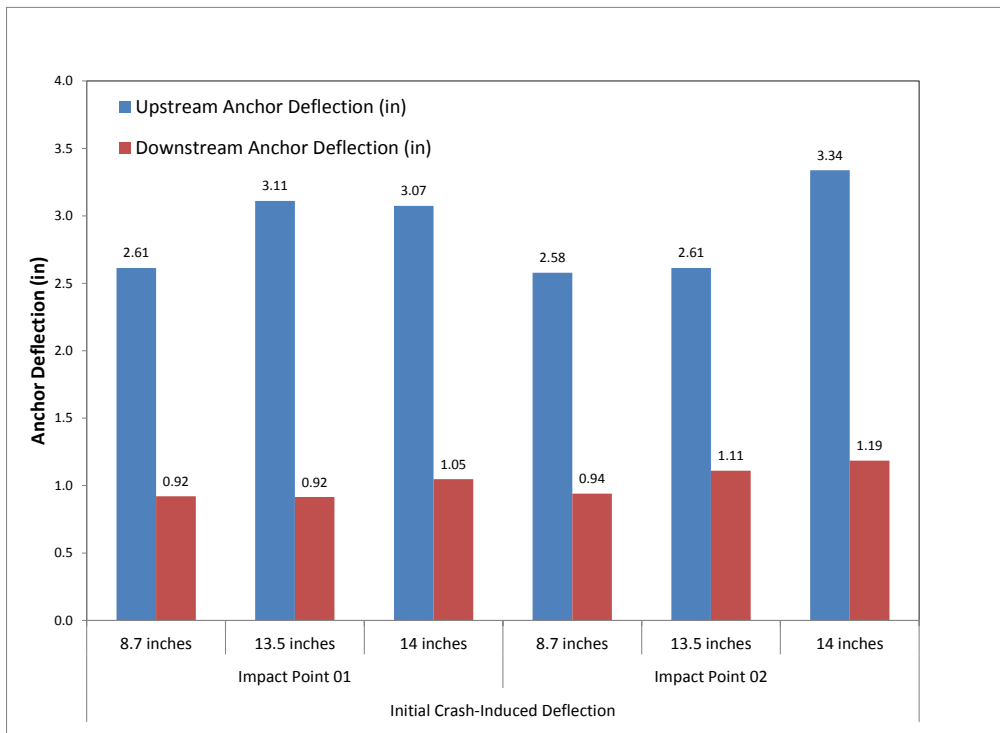


Figure 208. Summary of anchor displacement at rail height from analysis of high-speed impact into the G4(2W) with pre-existing low-severity rail deflection.

The movement of the anchors and the maximum tensile forces in the rail tended to increase as the severity of the pre-existing crash-induced rail deflections increased. The anchor deflections also tended to be higher for cases involving Impact Point 1, which was in part attributed to the fact that Impact Point 1 was closer to the downstream end-terminal (e.g., tensile force in rail were distributed to fewer upstream posts for IP01 cases). A summary of the maximum effective plastic strains around the splice-bolt holes in the w-beam is shown in Figure 209 for each analysis case. The results show that the potential for splice rupture tended to increase as the severity of the pre-existing crash-induced rail deflections increased. For all cases, the maximum splice damage occurred at Post 11; which, for those analysis cases involving Impact Point 2, was at Post C located upstream of point of maximum deflection. For reference, the maximum effective plastic strains in the splice for the undamaged baseline case was 0.84 (see Chapter 8).

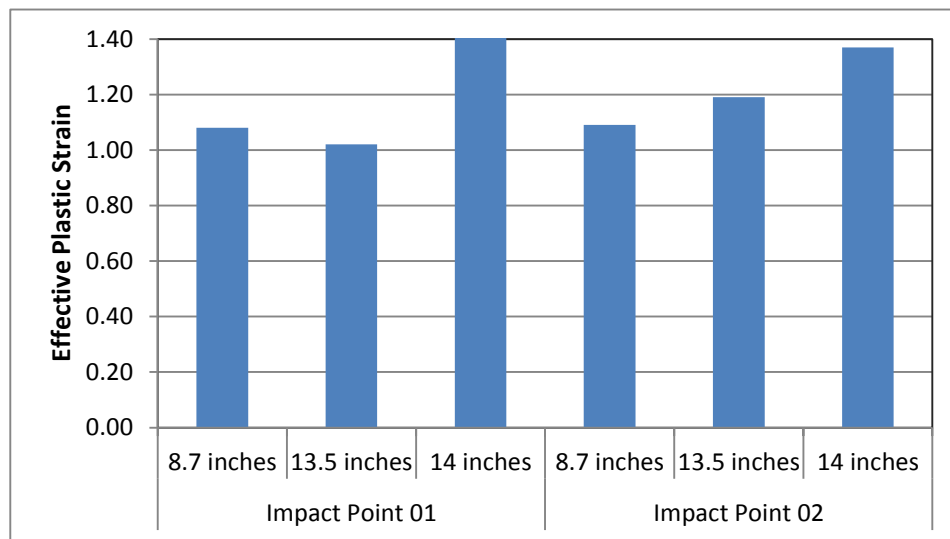


Figure 209. Summary of maximum effective plastic strains occurring at splice-bolt locations.

A summary of occupant risk measures computed from the acceleration and angular rate time-histories at the vehicle's center of gravity is provided in Table 64. This data is also presented graphically in Figures 190 through 192. The results indicate that occupant impact velocity (OIV) is not significantly affected by pre-existing low-level guardrail deflections. The maximum 10-millisecond occupant ridedown accelerations (ORA) in the longitudinal direction tended to increase as pre-existing guardrail deflections increased; however, they remained below critical limits of 20 g's for all cases. The ORA values in the lateral directions were less affected.

Table 64. Summary of occupant risk measures from analysis of high-speed impact into the G4(2W) with pre-existing low-severity rail deflection.

Occupant Risk Factors		Undamaged Posts (DL0) / Baseline Anchor Strength					
		Initial Crash-Induced Deflection					
		Impact Point 01			Impact Point 02		
		8.7 inches	13.5 inches	14 inches	8.7 inches	13.5 inches	14 inches
Occupant Impact Velocity (m/s)	x-direction	5.1	5.4	4.1	5.5	4.5	5.1
	y-direction	5.9	5.8	5.7	5.4	5.4	5.6
	at time	(0.1512 sec)	(0.1504 sec)	(0.1515 sec)	(0.1534 sec)	(0.1523 sec)	(0.1572 sec)
THIV (m/s)		7.6 (0.1472 sec)	7.3 (0.1468 sec)	6.9 (0.1480 sec)	7.3 (0.1487 sec)	7.1 (0.1483 sec)	7.1 (0.1534 sec)
Ridedown Acceleration (g's)	x-direction	8.8 (0.1665 - 0.1765 sec)	10.3 (0.1694 - 0.1794 sec)	15.4 (0.1986 - 0.2086 sec)	10.1 (0.2789 - 0.2889 sec)	12.9 (0.1551 - 0.1651 sec)	10.9 (0.1704 - 0.1804 sec)
	y-direction	10.7 (0.2301 - 0.2401 sec)	7.6 (0.1538 - 0.1638 sec)	9 (0.2149 - 0.2249 sec)	8.3 (0.2149 - 0.2249 sec)	10.8 (0.2390 - 0.2490 sec)	11.2 (0.2268 - 0.2368 sec)
PHD (g's)		11.4 (0.2300 - 0.2400 sec)	11.3 (0.1695 - 0.1795 sec)	17.3 (0.1985 - 0.2085 sec)	11.3 (0.1599 - 0.1699 sec)	14.5 (0.1552 - 0.1652 sec)	12.6 (0.1705 - 0.1805 sec)
ASI		1.03 (0.1231 - 0.1731 sec)	0.93 (0.1280 - 0.1780 sec)	0.89 (0.1958 - 0.2458 sec)	0.93 (0.1224 - 0.1724 sec)	0.92 (0.1212 - 0.1712 sec)	0.9 (0.1300 - 0.1800 sec)
Max 50-ms moving avg. acc. (g's)	x-direction	7.8 (0.1259 - 0.1759 sec)	7.8 (0.1289 - 0.1789 sec)	6.4 (0.1231 - 0.1731 sec)	7.5 (0.1229 - 0.1729 sec)	7.5 (0.1233 - 0.1733 sec)	7.0 (0.1395 - 0.1895 sec)
	y-direction	7.2 (0.1979 - 0.2479 sec)	6.6 (0.0925 - 0.1425 sec)	6.8 (0.1966 - 0.2466 sec)	6.2 (0.1216 - 0.1716 sec)	6.3 (0.0925 - 0.1425 sec)	6.5 (0.2060 - 0.2560 sec)
	z-direction	3 (0.2414 - 0.2914 sec)	2.9 (0.3358 - 0.3858 sec)	2.8 (0.3243 - 0.3743 sec)	2.5 (0.3479 - 0.3979 sec)	3.3 (0.3221 - 0.3721 sec)	2.9 (0.3374 - 0.3874 sec)

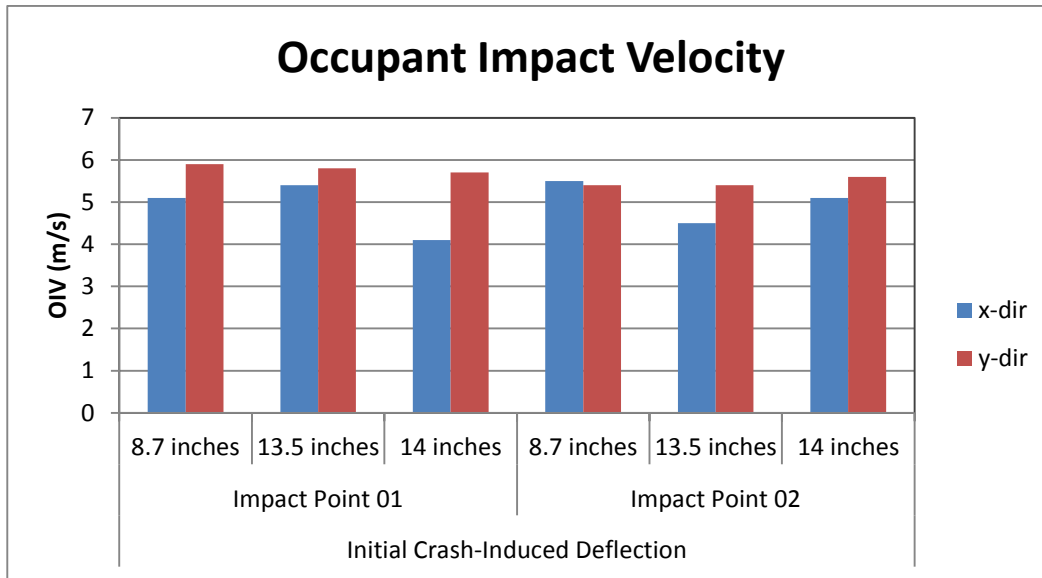


Figure 210. Summary of occupant impact velocity (OIV) from analysis of high-speed impact into the G4(2W) with pre-existing low-severity rail deflection.

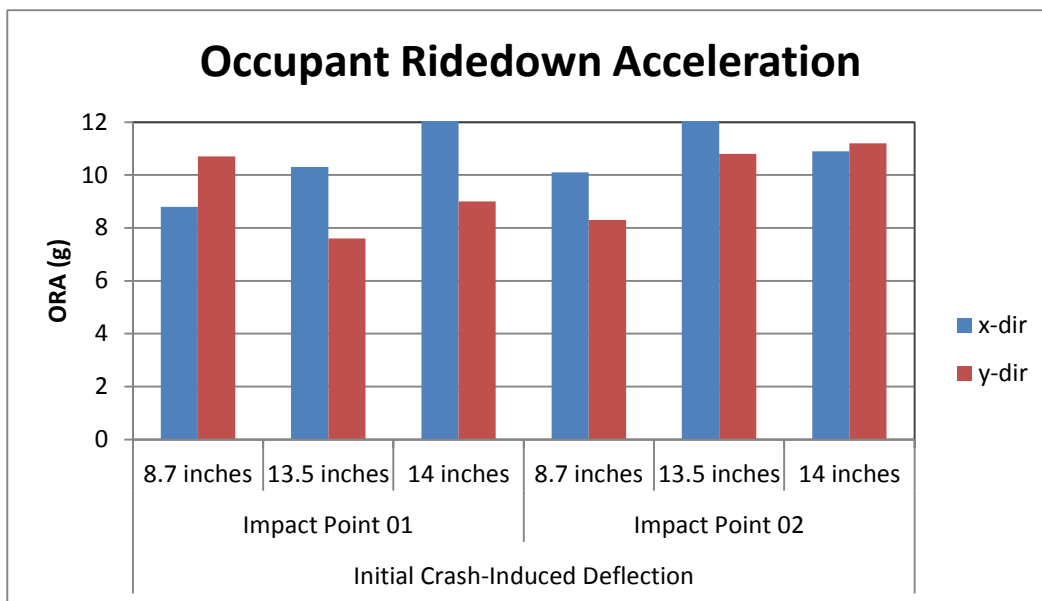


Figure 211. Summary of occupant ridedown accelerations (ORA) from analysis of high-speed impact into the G4(2W) with pre-existing low-severity rail deflection.

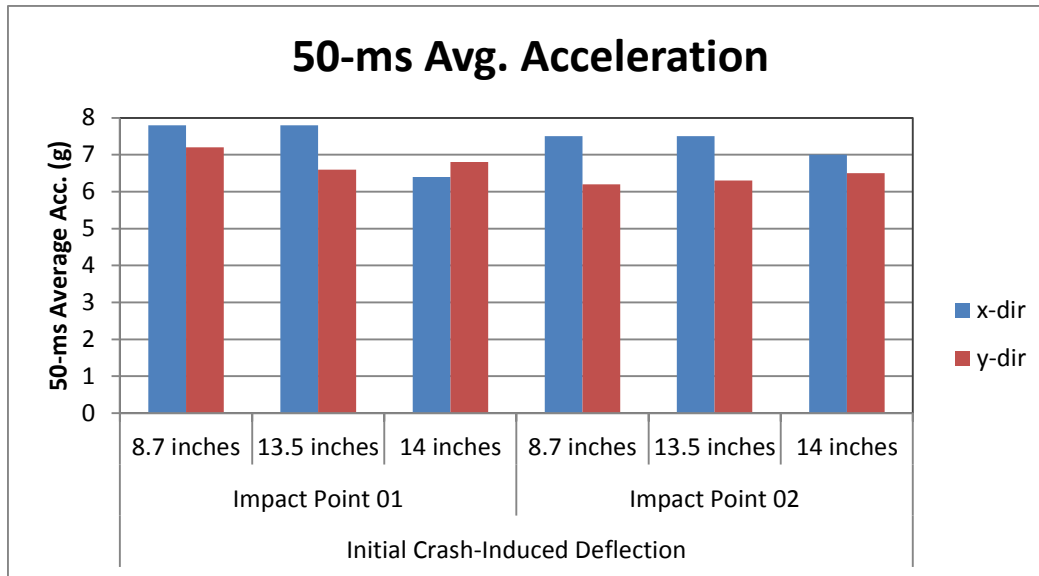


Figure 212. Summary of 50-ms average acceleration from analysis of high-speed impact into the G4(2W) with pre-existing low-severity rail deflection.

Summary and Discussion

The purpose of this task was to quantify the effects of crash-induced rail deflection in combination with rail-to-post connection strength on the crash performance of the G4(2W) guardrail system, and to use this information to develop assessment criteria for this very common guardrail damage mode. Finite element analysis was used to evaluate the impact performance of the G4(2W) guardrail system with various levels of pre-existing crash-induced rail deflection. The impact conditions used for the performance evaluations corresponded to those of *NCHRP Report 350 Test 3-11* (i.e., 4400 lb vehicle impacting at 62.2 mph and 25 degrees, nominally).

The initial crash-induced damage for the guardrail model was created by simulating low-speed impacts into the guardrail with the 4,568-lb pickup truck model at an impact angle of 25 degrees. Three impact speeds were used (i.e., 30 mph, 35 mph and 40 mph) which resulted in three levels of guardrail deflections (i.e., 8.7 inches, 13.5 inches, and 14 inches). Lower levels of damage were investigated by Gabler *et al.* in Phase I of this project and were therefore not considered in this study. The results from these low-speed impacts, which included guardrail component deformations and residual stresses, were then used as initial conditions for secondary high-speed impact simulations (i.e., Report 350 Test 3-11) into the damaged guardrail system. Two rail-to-post connection strength cases were investigated. In one case a w-beam splice was located at the critical connection point, in which the post-bolt head has to pull through two layers of w-beam in order to release; and in the second case the critical connection point was at a non-splice location, in which the post-bolt has to pull through only a single layer of w-beam in order to release.

Finite element analysis was then used to simulate a secondary impact into the damaged guardrail to evaluate the performance of the system with various degrees of low-severity, crash-induced rail damage. The results of the high-speed analyses indicated that as the severity of the pre-existing crash-induced rail deflections increased:

- The maximum lateral deflections of the rail increased,
- The tensile load in the rail increased,
- The deflection of the upstream anchor increased,
- The post-bolt connection at w-beam splice locations allowed greater post deflections before releasing,
- The post-bolt connection at non-splice locations released consistently regardless of pre-damage deflections,
- Potential for splice rupture increased,
- Occupant ridedown accelerations in the longitudinal direction increased (primarily due to increased wheel snag on posts), and
- All other occupant risk measures were less affected.

The results of the analyses also indicated that the potential for override was relatively low for all cases investigated. This is contradictory to the full-scale crash test results from Gabler's study, where a post-bolt did not release properly and allowed the rail to be pulled down with the post, resulting in the vehicle overriding the guardrail.[*Gabler10*] In that test the guardrail system was the G4(1S) (i.e., steel post w-beam guardrail) and the pre-existing crash-induced rail deflection was 14.5 inches. A possible explanation is that the G4(2W) and the G4(1S) respond differently to this particular damage mode. These two systems differ only by the type of guardrail post; i.e., the G4(2W) uses rectangular or round wood posts while the G4(1S) uses W6x9 structural steel section posts - all other aspects of these two systems are identical. Further, bogie impact tests have shown that the lateral force-deflection response for these two posts is essentially equivalent.[*Hascall07*] However, the results of full-scale crash tests have shown that the steel-post system results in lower impact forces. For example, tests on the modified G4(1S) with wood blockouts resulted in longitudinal ORA values of 7.9 G and 7.6 G [*Bullard96*; *Bligh97*]; while tests on the G4(2W) resulted in longitudinal ORA values of 10.2 G, 10.9 G and 11.6 G.[*Bullard09*; *Bligh95*; *Mak99a*]

In order to understand the differences in the performance of these two seemingly identical systems, it is first important to understand the differences in the response of the two different types of posts under loading conditions typical of real-world collisions. In particular, guardrail posts generally experience both lateral and torsional loads during vehicle collisions – whereas bogie impact tests induce only lateral loads onto the post. The lateral load from vehicle collision arises directly from the lateral deflection of the w-beam rail against the posts. The torsional loads on the posts result from the tensile load in the w-beam rail acting at the front of the blockouts; the blockouts are offset 8 inches from the front face of the posts, thus creating a torsional moment about the vertical axis of the posts. The wood posts tend to resist this torsion, while the W6x9 steel posts do not. The torsion of the steel posts not only reduces the breakout distance between the rail and the post, but also significantly reduces its resistance to lateral deflection. Figure 213 shows the results of full-scale Test C08C3-027.2 on the G4(1S) guardrail system conducted by the MGA Research Corporation in Gabler's study, illustrating the torsional deformation of the posts.[*Fleck08b*] The photo on the right in Figure 213 further illustrates the apparent reduction in lateral stiffness of the “twisted” post, where the post buckled at the groundline rather than displacing the soil. The combined effects of (1) reduced breakout

distance, (2) the post buckling at the groundline, and (3) loss of rail tension as the anchor failed resulted in the rail being pulled down with the post rather than releasing from the post as it was intended. In contrast, Figure 214 shows the results of full-scale Test 471470-26 on the G4(2W) guardrail conducted by TTI showing the general deformation mode of the posts during vehicle collision. In this case the posts do not show any apparent torsional deflections and tend to deflect only in the lateral direction. When wood posts fail under the torsional load, it is usually a brittle failure in which the posts split or fracture, as illustrated in Figure 215.



Figure 213. Results of Test MGA C08C3-027.2 illustrating torsional deformation of the W6x8 steel guardrail posts during vehicle collision.[Fleck08b]



Figure 214. Results of Test 471470-26 illustrating the response of the wooden guardrail posts during vehicle collision.[Mak99]



Figure 215. Results of Test 404201-1 illustrating brittle fracture of wood posts due to tensile forces in the w-beam rail.[Bullard00]




The research team is not aware of any tests on a wood post guardrail system in which a penetration occurred due to the vehicle overriding the barrier. Penetration of wood post guardrails tend to result from rupture of a w-beam splice; while penetrations of steel post guardrails are sometimes due to splice rupture and sometimes due to override. This is consistent with the results obtained in the current study, in which the most significant effect of pre-existing crash-induced rail deflection on the performance of the G4(2W) guardrail system is an increased potential for rail rupture.

Recommendations

The analysis results indicated that the performance of the G4(2W) with crash-induced rail damage was compromised when the initial damage included 8.7 inches or greater deflections. The capacity of the splice connection was the aspect of the system that was most affected by this damage mode. For example, the plastic strains around the splice-bolt holes resulting from *NCHRP Report 350* Test 3-11 impact was 0.84 for the baseline (undamaged) G4(2W) guardrail. The magnitude of effective plastic strains then increased as the magnitude of pre-damage deflections increased. At pre-damaged guardrail deflections of 8.7, 13.5 inches and 14 inches, the effective plastic strains in the splice-bolt holes reached magnitudes of 1.09, 1.19 and 1.5, respectively.

As a result of this study, the research team recommends that guardrail damage with rail deflections of greater than 9 inches constitute a high priority for repair for the G4(2W). Although the effects of rail damage differ between the G4(1S) steel post guardrail and the G4(2W) wood post guardrail, the threshold of damage that constitute need for repair are essentially the same for these two systems; thus the relative repair thresholds defined by Gabler *et al.* in Phase I are considered valid for the G4(2W) system as well and are adopted here, as shown in Table 65.

Table 65. Recommendations for post and rail deflection damage.

Damage Mode	Repair Threshold	Relative Priority	Measurement
Post and Rail Deflection	One or more of the following thresholds: <ul style="list-style-type: none"> • More than 9 in. of lateral deflection anywhere over a 25-ft length of rail • Top of rail height 2 or more inches lower than original top of rail height 	High	
	6-9 in. lateral deflection anywhere over a 25-ft length of rail	Medium	 (Weak Post W-Beam Shown Only for Clarity. Each measurement taken at the rail's middle fold)
	Less than 6 in. of lateral deflection over a 25-ft length of rail	Low	
Rail Deflection Only	6-9 in. of lateral deflection between any two adjacent posts <u>Note:</u> For deflection over 9 in., use post/rail deflection guidelines.	Medium	
	Less than 6 in. of lateral deflection between any two adjacent posts	Low	

Future work should include analyses of both the G4(2W) and G4(1S) with pre-existing crash-induced rail deflections in combination with varying anchor strength. Due to the differences in the torsional rigidity of the W6x9 steel posts of the G4(1S) guardrail and from the results of Test MGA C08C3-027-2 on that system which resulted in large anchor deflection and vehicle override, it is expected that the G4(1S) may have a greater sensitivity anchor strength. Also, the low-severity impact cases evaluated herein involved low speeds and a high impact angle which resulted in damages to a relatively localized section of the guardrail; i.e., the damaged area generally spanned only 3 to 4 posts, which increased the potential for pocketing. It is not known how the guardrail will respond to subsequent impacts when the rail deflections are spread over a longer length of the guardrail. It is recommended that future studies on the effects of pre-existing crash-induced rail deflections include higher impact speeds and smaller impact angles to create initial guardrail damage with similar magnitudes of rail deflection spread over a longer length of the guardrail.

In the following chapter, FEA is used to simulate Test C08C3-027.2 to reevaluate the cause of the vehicle overriding the barrier in that test.

CHAPTER 11 – RE-ASSESS CAUSE OF FAILURE IN TEST C08C3-027 FOR THE MODIFIED G4(1S) WITH PRE-CRASH-INDUCED DEFLECTION.

The undetached post-rail connection in Test C08C3-027.2 that led to the vehicle overriding the barrier was suspected by the authors to be a *symptom of low rail tension* resulting from the excessive movement of the anchor during the test. The focus of this chapter is to reevaluate the G4(1S) installation of Test C08C3-027.2 and investigate the cause for the improper rail detachment. The anchor system used in Test C08C3-027, shown in Figure 216(c) included only a single foundation tube, and was therefore not as stiff nor as strong as the standard anchor system used in the earlier tests of the G4(1S) (i.e., Figure 216 (a) and Figure 216 (b)), which included two foundation tubes connected via a groundline strut.

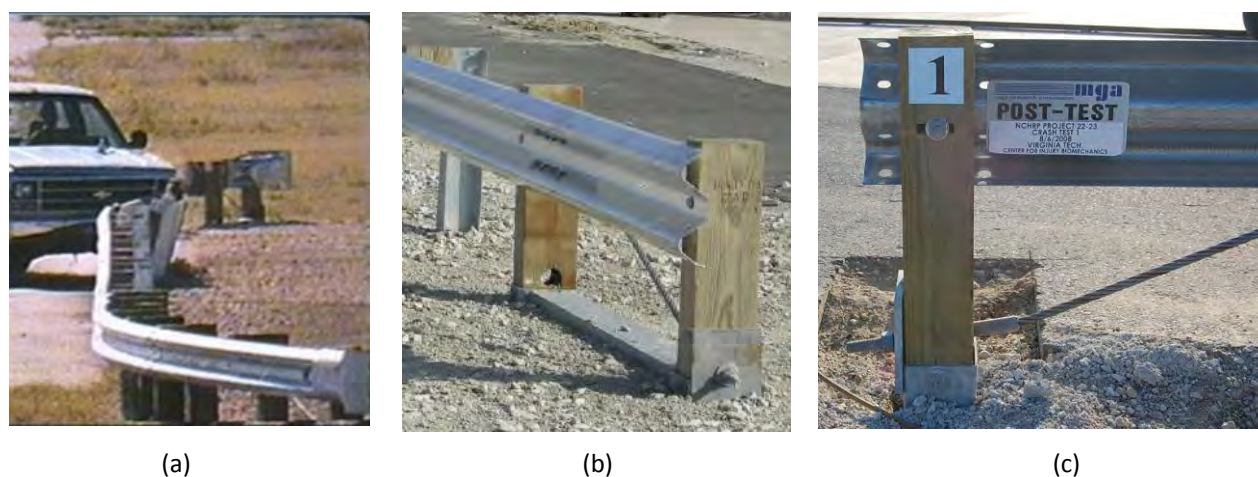


Figure 216. Anchor used in evaluation of the modified G4(1S) with wood blockouts in tests (a) 405421-1 [Bullard96], (b) 2214-WB2 [Polivka06b] and (c) C08C3-027 [Fleck08a;08b].

A model of the G4(1S) guardrail was developed and finite element analysis was used to simulate full-scale crash test C08C3-027-1 to create low-level crash-induced damage of the system. The results from this low-speed impact case, including guardrail component deformations and residual stresses, were then used as initial conditions in a secondary high-speed impact simulation of full-scale crash test C08C3-027-2. The upstream and downstream end-terminals for the system were modeled using non-linear springs attached to the ends of the rail. To represent the response of the single-foundation tube anchor system used in the full-scale tests, the force-deflection properties of the end-terminal springs were scaled to 47 percent of the baseline anchor stiffness defined in Chapter 9.

The results of the analysis were compared to those of the full-scale crash test to determine if the model reasonably reproduced the results of the full-scale test. If so, then it may be reasoned that the most likely cause for the override was the collective effects of the low-stiffness anchor system combined with the initial crash-induced rail deflections – rather than the rail deflections alone.

Simulation of Test C08C3-027-1

Test C08C3-027-1 Summary

Test C08C3-027-1 was conducted by MGA Research Corporation on August 6, 2008. The test article consisted of 12.5 feet long 12-gauge w-beam rail; the rail was supported with W6x9 structural steel posts that were 72 inches long, embedded 44 inches in the soil and spaced at 75 inches on center; the rail was blocked out from the post using 6x8x12 inch routed wood blockouts; the blockout and rail were attached to the post using 5/8-inch diameter carriage bolts. The top height of the guardrail was 27.8 inches. The overall length of the test installation for Test C08C3-027-1 was 162.4 feet including two single-foundation tube anchors – one at each end of the system.

Full-scale test C08C3-027-1 involved a 1997 Chevrolet 2500 pickup impacting the G4(1S) guardrail at 30.0 mph and at an impact angle of 26 degrees; the impact point was at 45.8 inches upstream of the splice connection at Post 11. The gross static mass of the test vehicle was 4,632 lb. The damage to the test installation is shown in Figures 217 and 218. The maximum deflection of the rail was 14.5 inches and occurred at the midspan between Post 11 and Post 12.



Figure 217. Damage to guardrail in low-speed impact test C08C3-027-1. [Fleck08a]

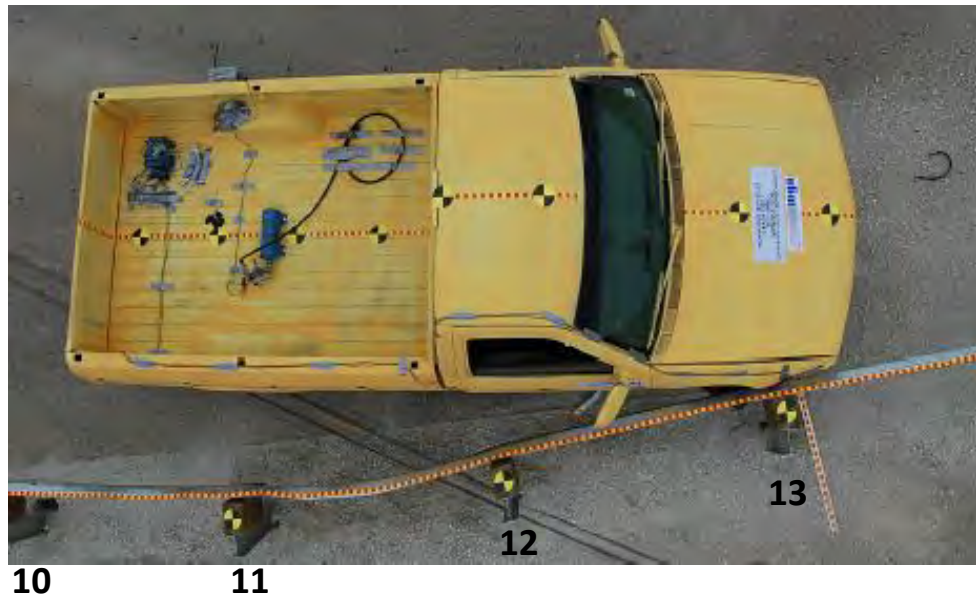


Figure 218. Damage to guardrail in low-speed test C08C3-027-1 (overhead view).[Fleck08a]

FEA Model Development

The finite element model of the G4(1S) guardrail is shown in Figure 219. The guardrail model consisted of eleven 13.5 foot lengths of 12-gauge w-beam rail, twenty-two W6x9 structural steel posts, and twenty-two 6x8x13 inch routed wood blockouts. The center-to-center distance between rail splices was 12.5 feet. The posts were spaced at 75 inches on center and the w-beam rail was positioned such that the top of rail was 27-5/8 inches above ground. The posts were embedded 44 inches in the ground. The model included 138.6 feet of the guardrail including Post 3 through Post 24. The boundary conditions at the ends of the rail were modeled using nonlinear springs with properties corresponding to 47 percent of the baseline anchor stiffness; this was based on the assumption that the single-foundation tube anchor would have approximately half the stiffness of the baseline two-foundation tube anchor system. The overall *effective* length of the model (including the simulated end-terminals) was 162.4 feet.

The finite element model for the rail element, the blockouts and the connection hardware were adopted from the G4(2W) guardrail model developed in Chapter 7. The blockout was modified by including the “routed” section that fits over the flange of the W6x9 steel posts. The finite element model of the W6x9 posts were modeled with the fully-integrated Type 16 shell elements in LS-DYNA with warping stiffness. The nominal element size was 0.4 x 0.5 inches for the post flange and 0.6 x 0.5 inches for the post web. The material properties for the post were characterized based on the properties determined in an earlier study by Wright and Ray.[Wright96] This material model has been used in numerous analyses and has been validated in simulations of full-scale crash tests.[Plaxico02] For consistency with the G4(2W) model, the soil response was modeled using the non-linear spring concept with the springs attached directly to the post. The properties of the spring elements were defined according to [Plaxico98] using a soil density of 134 pcf and no moisture content (refer to Chapter 7 for more details).

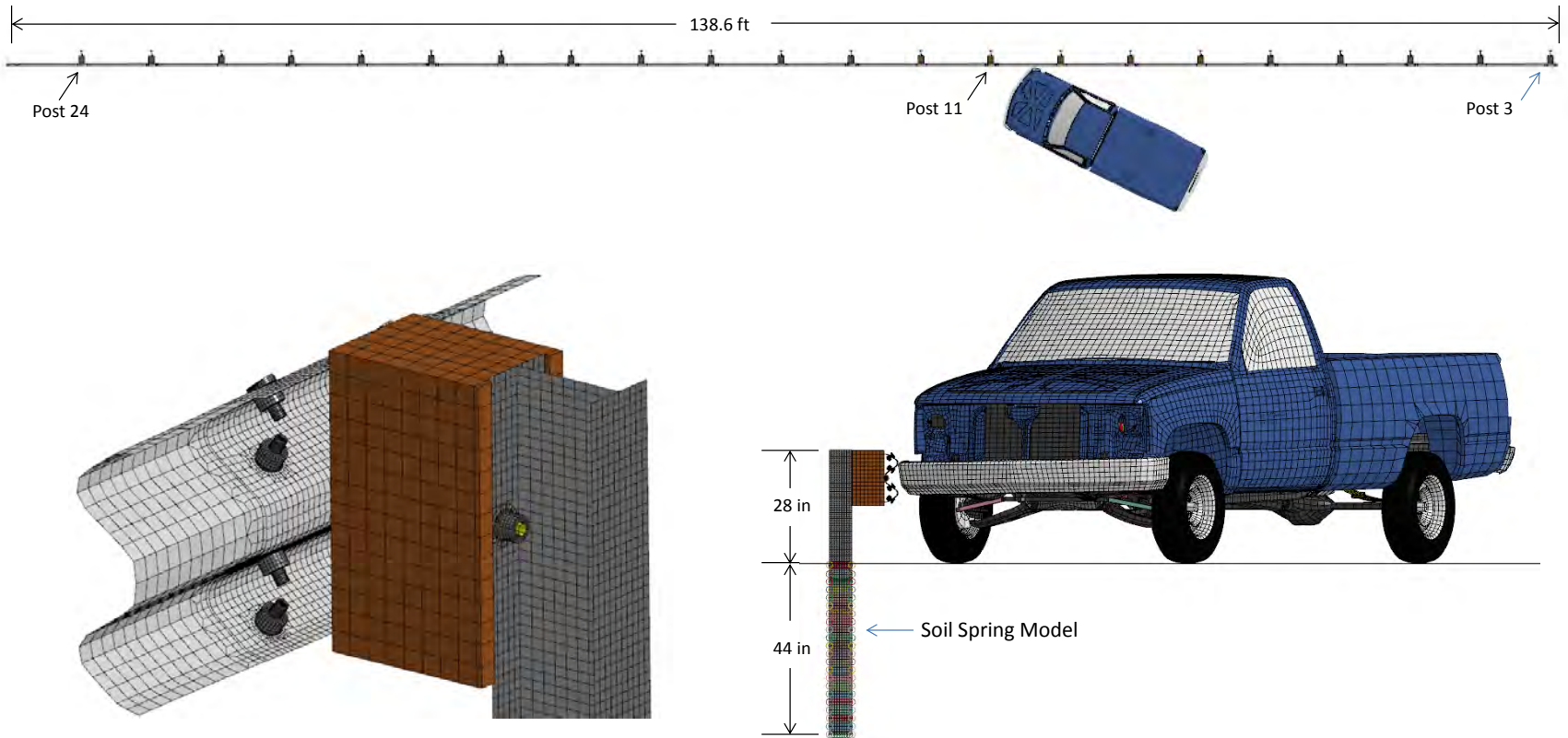


Figure 219. Finite element model of G4(1S) for simulation of Test C08C3-027-1.

FEA Simulation

Finite element analysis was then used to simulate the impact conditions of Test C08C3-027-1. At the beginning of the analysis the post-bolts that fasten the w-beam and blockouts to the post were tightened to approximately 2,000 lb axial force by imposing an initial strain-time history to the bolt elements via the LOAD_THERMAL card in LS-DYNA. The vehicle model used in the analysis was the NCAC C2500D version 5B with modifications described in Chapter 7. The total mass of the vehicle model was 4,568 lb. The vehicle model struck the guardrail at 45.8 inches upstream of the splice connection at Post 11 at an impact speed and angle of 30.0 mph and 26 degrees, respectively.

The analysis was conducted with a time-step of 1.26 microseconds for a time period of 0.6 seconds. Figure 220 shows sequential snapshots of the impact event from an overhead viewpoint comparing the results from the FE analysis with the full-scale test. The yaw angle of the model was greater than that of the test, due primarily to the difference in the response of the wheel assemblies during impact, as illustrated in Figure 221. In the full-scale test the wheel snagged on Post 11 causing the front wheels to turn “full-steer” toward the barrier; whereas in the simulation the wheel’s contact with the post was not sufficient to significantly alter the steer angle. In the full-scale test, the steer angle of the wheels resulted in higher deceleration of the vehicle and also altered the trajectory during the impact event, compared to the results of the FE analysis.

The W-Beam rail element was deformed from Posts 9 through 14 as shown Figure 222. The maximum permanent deflection of the rail in the FE analysis was 15.5 inches and occurred at 47 inches upstream of Post 12 (compared to 14.5 inches deflection at 37.5 inches upstream of Post 12 in the full-scale test). All the post-bolt connections remained attached throughout the impact for both the full-scale test and the FE analysis. The maximum permanent groundline deflections of Posts 10 through 13 in the FE analysis were 0.7 inches, 7 inches, 4.2 inches and 0.24 inches, respectively. Although it cannot be confirmed, it appears from visual inspection of the damaged test article that the deflections of the posts are of similar magnitude. The maximum deflection of the rail at the upstream boundary was 1.2 inches. Figure 223 shows the post-test photograph of the upstream anchor after Test C08C3-027-1. The separation between the back of the post and the soil in the photo is evidence of upstream anchor movement, but the actual amount of displacement was not included in the test report. Overall, the barrier damages resulting from the simulated impact were reasonably representative of that observed in the full-scale test.

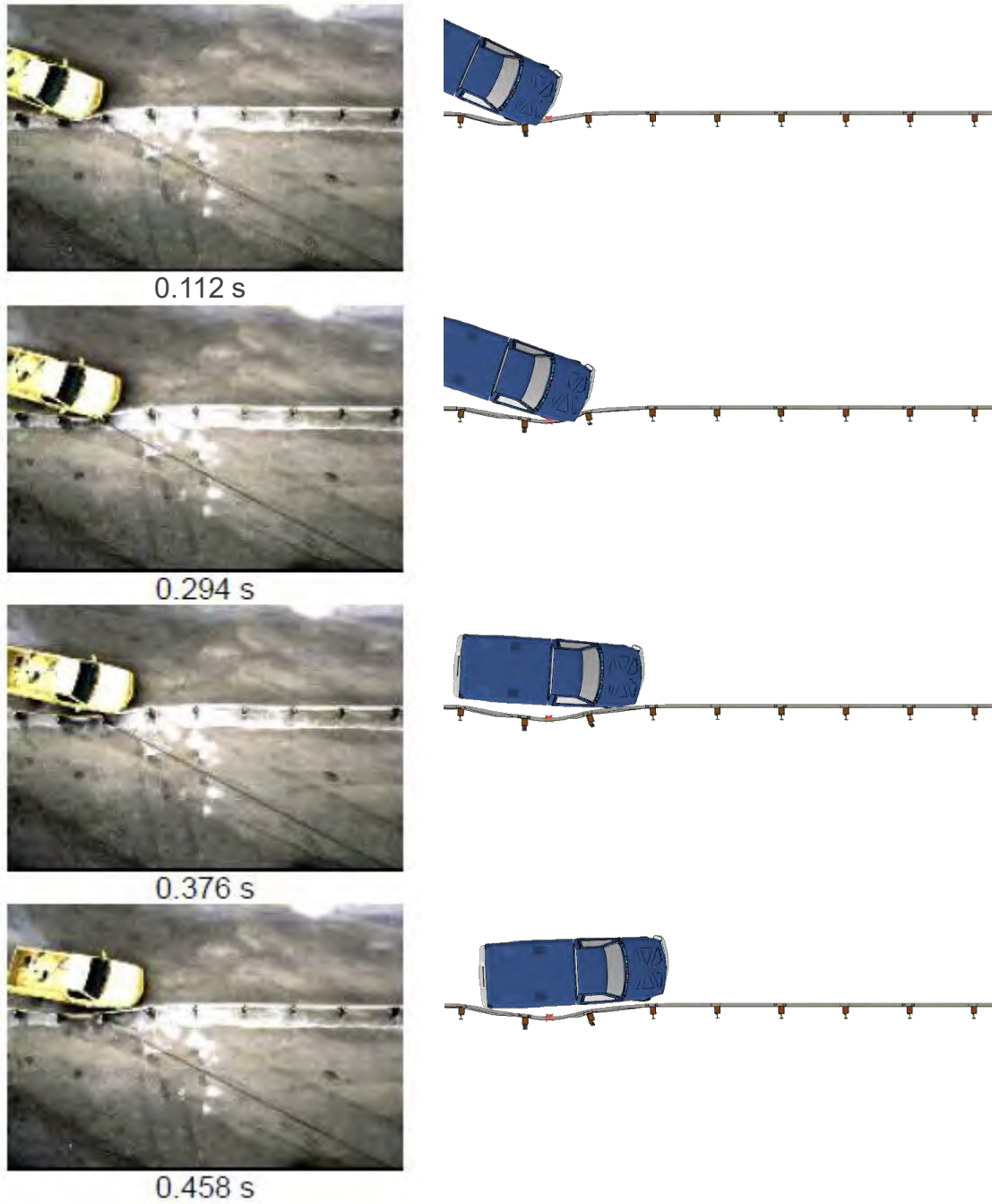
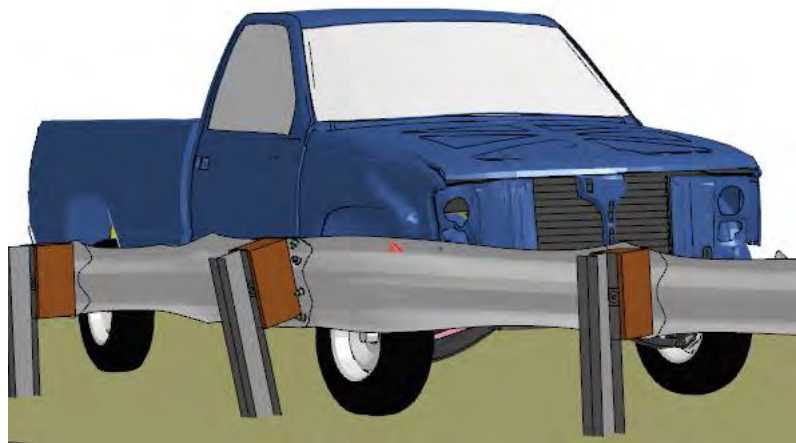


Figure 220. Sequential views of FEA results compared with Test C08C3-027-1.

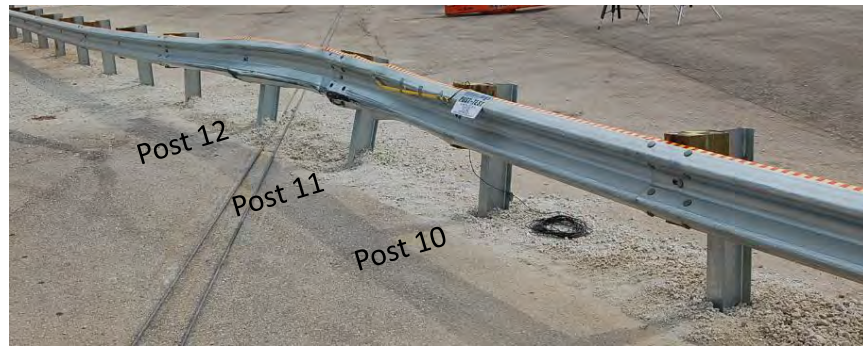


(a)

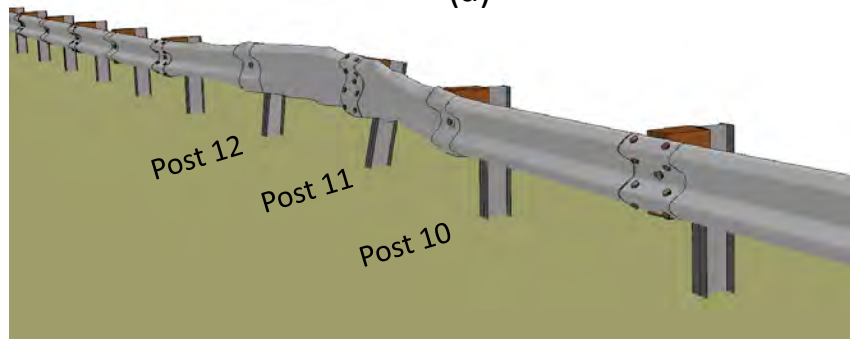


(b)

Figure 221. Impact response at 0.18 seconds for (a) full-scale test and (b) FEA illustrating wheel orientation.



(a)



(b)

Figure 222. Comparison of guardrail damage for (a) Test C08C3-027-1 and (b) FEA model.



Figure 223. Photo of upstream anchor after Test C08C3-027-1. [Fleck08a]

Simulation of Test C08C3-027-2

Test C08C3-027-2 Summary

The damaged guardrail from Test C08C3-027-1 was then subjected to a second impact at high-speed to evaluate the performance of the crash-damaged system. Test C08C3-027-2 was performed by MGA Research Corporation on August 7, 2008 under Report 350 Test 3-11 conditions. No repairs of the pre-damaged guardrail were made prior to this second test.

In Test C08C3-027-2, a 1997 Chevrolet 2500 pickup impacted the damaged rail at 38.5 inches upstream of Post 11 at an impact speed and angle of 62.1 mph and 26.4 degrees, respectively. At 16 milliseconds after impact Post 11 started to deflect back, and at 44 milliseconds Post 12 began to deflect. At 56 milliseconds the right-front tire impacted against Post 11, pushing the post over. As the tire interacted with the post, the tie-rod released and the tire steered 90 degrees toward the barrier. The left-front tire remained straight. At 60 milliseconds Post 10, which was upstream of the truck, began to twist such that the blockout was rotating in the downstream direction. At 98 milliseconds the front bumper was at Post 12. At 108 milliseconds the height of the w-beam at Post 12 began to reduce as the post and blockout began to rotate. At 112 milliseconds Post 12 was deflected significantly, the blockout on the post was rotated almost 90 degrees, and the post-bolt at Post 12 released. The rail began to drop and at 120 milliseconds the right-front corner of the truck bumper was visible above the rail. At 146 milliseconds Post 12 was pushed to the ground as the truck overrode the post and the front bumper of the truck at this time was completely over the top of the rail. At 174 milliseconds, the front of the truck was at Post 13; all the upstream posts had rotated essentially 90 degrees about their vertical axis at this time, which inferred substantial movement of the upstream anchor system. As the test continued, the front bumper continued to pass over the top of the rail. At 270 milliseconds Post 13 was pushed to the ground without releasing the post-bolt connection; the w-beam rail was pulled down with the post and the vehicle overrode the barrier.

Model Setup – Including Pre-Damage

The results from the low-speed impact case were used as initial conditions in a secondary high-speed impact simulation of full-scale crash test C08C3-027-2. The initial conditions for the pre-damaged guardrail included component deformations and residual stresses. These values were recorded for all shell, solid and beam elements in the model via the SPRINGBACK option in LS-DYNA. The residual forces for discrete elements (e.g., non-linear spring elements for the soil and rail end-boundaries), however, could not be recorded and saved with this option. For initialization of all the spring elements in the model, LS-PrePost was used to determine the final displacements of the spring nodes; these displacement values were then used to define the *initial* offset for each spring element in the FE model. This methodology directly imposed the force-deflection response of the spring elements for the soil and the end-anchor from the low-speed analysis onto the model for the high-speed impact case. Figure 224 shows a contour plot of effective plastic strain for the *initial* state of the guardrail model used in the simulation of Test C08C3-027-2.

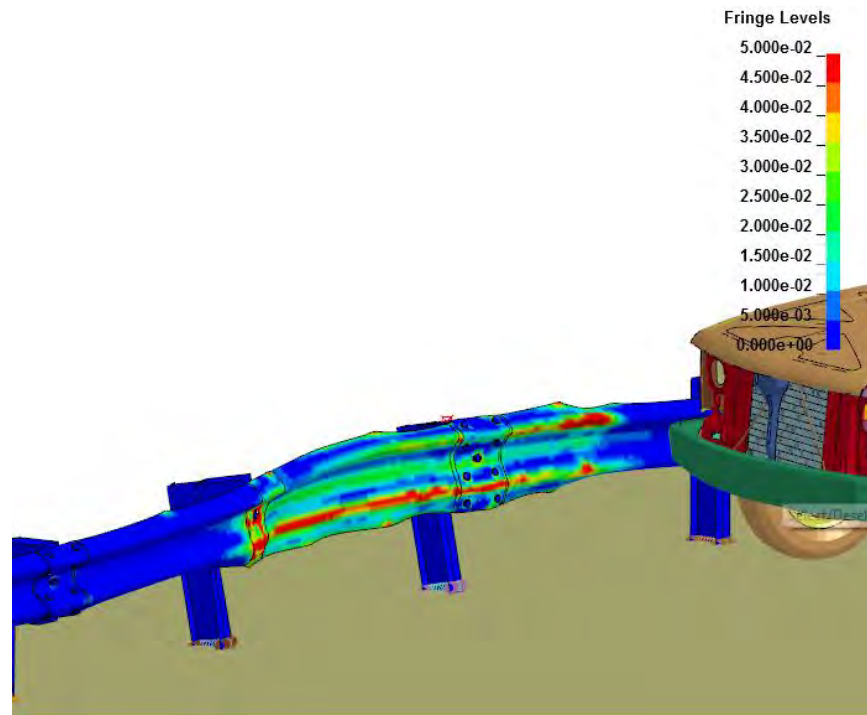


Figure 224. Contours of effective plastic strain for the initial state of the guardrail model for simulation of Test C08C3-027-2.

FEA Simulation

Finite element analysis was then used to simulate the impact conditions of Test C08C3-027-2. Two analysis cases were conducted:

- Case 1: The crash-induced damage of the guardrail (including displacements and residual stresses) from the analysis of C08C3-027-1 was imposed directly onto the model as initial conditions. The post-bolt position at Post 12 was then re-positioned to the corner of slotted hole in the w-beam (i.e., to be consistent with the test article) and re-tightened.
 - Analysis Model: FEA_C08C3-027_HS5
 - LS-DYNA version: smp s R6.1.2, revision 85139.
- Case 2: The same initial conditions as Case 1. The model used in Case 1 was modified to include a finite rigidwall which effectively simulated the boundary at the backside of the soil pit at the test site.
 - Analysis Model: FEA_C08C3-027_HS7a
 - LS-DYNA version: smp s R6.1.2, revision 85139.

Analysis Case 1

The vehicle model used in the analysis was the NCAC C2500D version 5B with modifications described in Task Report 4A-1. The vehicle model impacted the damaged rail at approximately 38.5 inches upstream of Post 11 at an impact speed and angle of 62.1 mph and

26.4 degrees, respectively (i.e., the same impact conditions as the full-scale test). At 25 milliseconds after impact, Post 11 started to deflect back, and at 55 milliseconds Post 12 began to deflect. At 60 milliseconds the right-front tire impacted against Post 11; however, there was no tire snag on the post and the tie-rod did not fail. At 80 milliseconds Post 11 reached its maximum lateral groundline deflection of 14 inches. At 50 milliseconds Post 10, which was upstream of the truck, began to twist such that the blockout was rotating in the downstream direction. At 100 milliseconds the front bumper was at Post 12, and Post 13 started to deflect. At 110 milliseconds the head of the post-bolt at Post 12 pulled through and released the rail; the rail did not begin to drop prior to release. At 120 milliseconds Post 14 began to deflect. At 130 milliseconds Post 12 reached its maximum groundline deflection of 12.3 inches; the post continued deflecting about the groundline until 135 milliseconds when the top of the post was pressed to the ground. The front tire of the vehicle contacted Post 12 at 140 milliseconds and proceeded to roll over the post and blockout.

At 185 milliseconds, the front of the truck was at Post 13. At this time all the upstream posts had rotated significantly and the post-bolt connection had released at all upstream non-splice locations. These factors inferred substantial movement of the upstream anchor system. At 200 milliseconds the post-bolt at Post 13 pulled through the double-slot of the splice and released the rail; at this time the rail was still at its original height. Post 15 also began to deflect slightly at this time. At 210 milliseconds Post 13 reached its maximum groundline deflection of 15 inches, and at 215 milliseconds the top of the post contacted the ground. At 225 milliseconds the front tire on the vehicle contacted Post 13 and its blockout; the tire proceeded to ride over the post and passed behind the blockout.

At 280 milliseconds the front of the vehicle was at Post 14. At 295 milliseconds the post-bolt at Post 14 released from the rail; at this time the rail was still at its original height. Also at this time deflection of Post 15 began to increase. The vehicle was parallel to the guardrail system at 315 milliseconds. Also at this time Post 14 reached its maximum groundline deflection of 10.5 inches. At 325 milliseconds the front tire on the vehicle contacted the post just as the top of the post contacted the ground; also, the deflection of Post 15 began to increase at this time.

At 395 milliseconds the front of the vehicle was at Post 15. At 405 milliseconds the front fender of the vehicle impacted against the blockout at Post 15, and at 435 milliseconds the front tire of the vehicle contact the post. The tire steered toward rail as the vehicle passed Post 15. At 455 milliseconds Post 16 began to deflect. At 490 milliseconds Post 15 reached its maximum groundline deflection of 8.3 inches. At 500 milliseconds the vehicle lost contact with the rail as it was redirected from the system. At 552 milliseconds the vehicle reached its highest roll angle of 18.5 degrees. The analysis was terminated at 0.6 seconds, at which time:

- The roll angle of the vehicle was 17.3 degrees and decreasing,
- The pitch angle was -18.4 degrees and stable,
- The yaw angle was 38.8 degrees relative to the barrier and increasing slightly, and
- The forward velocity of the vehicle was 25 mph.

Figure 238 and Figure 239 show sequential snapshots of the impact event from a downstream-oblique view point and an upstream viewpoint, respectively. The maximum plastic strain in the rail was 0.91 and occurred in the lower, down-stream splice-bolt hole at Post 13.

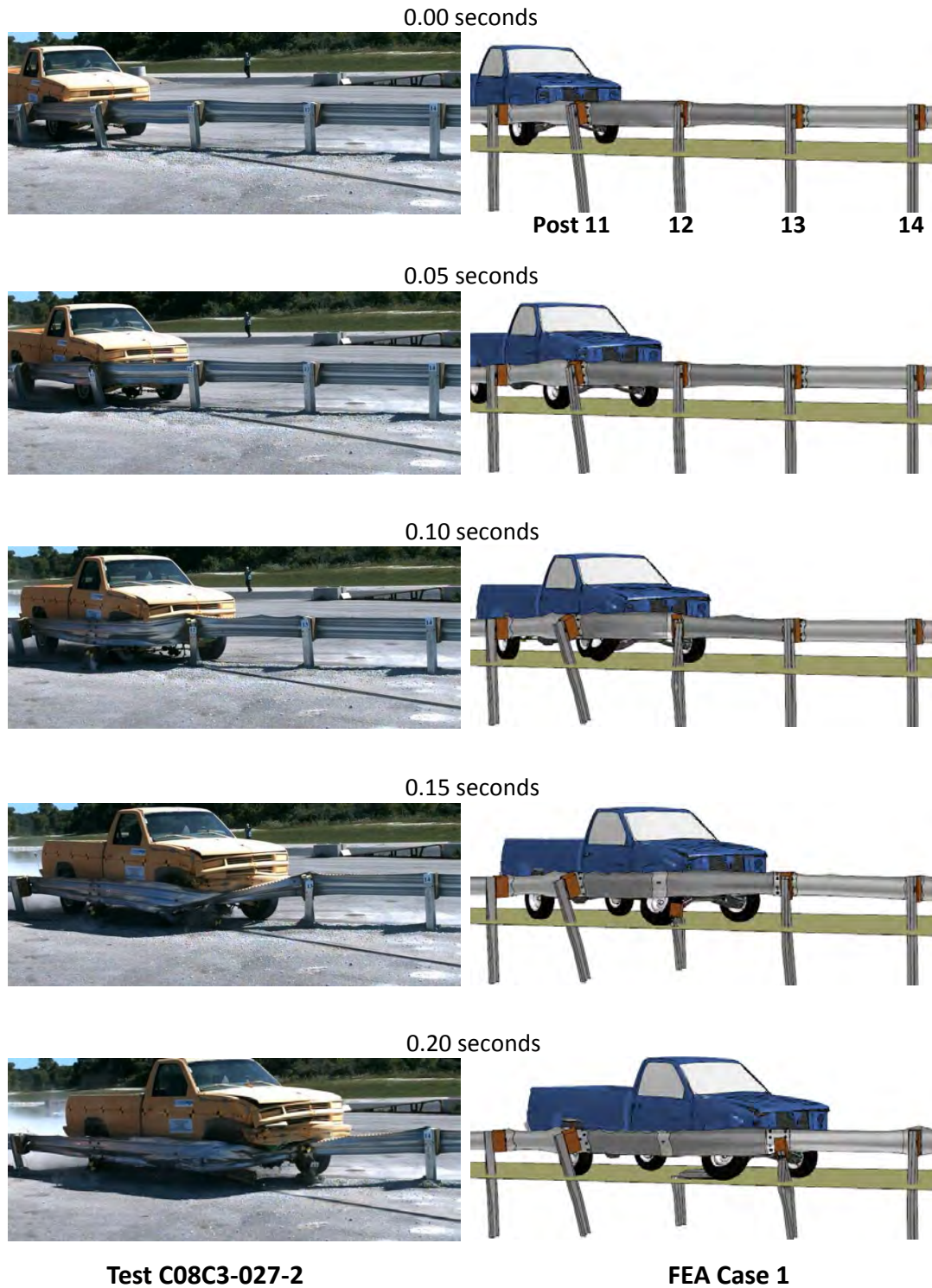


Figure 225. Sequential Views of Test C08C3-027-2 and FE analysis Case 1 from downstream-backside view perspective.

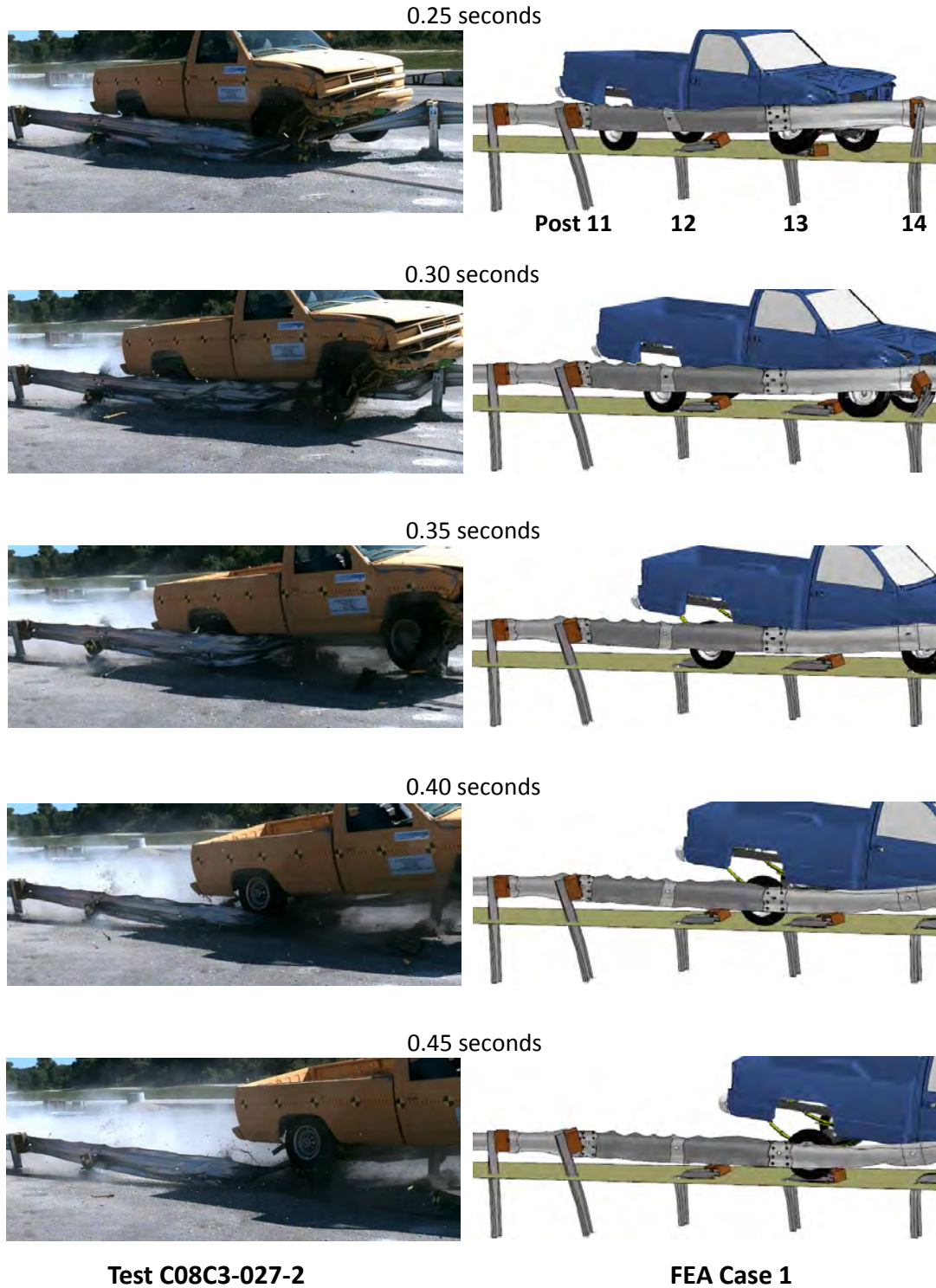


Figure 220. [CONTINUED] Sequential Views of Test C08C3-027-2 and FE analysis Case 1 from downstream-backside view perspective.

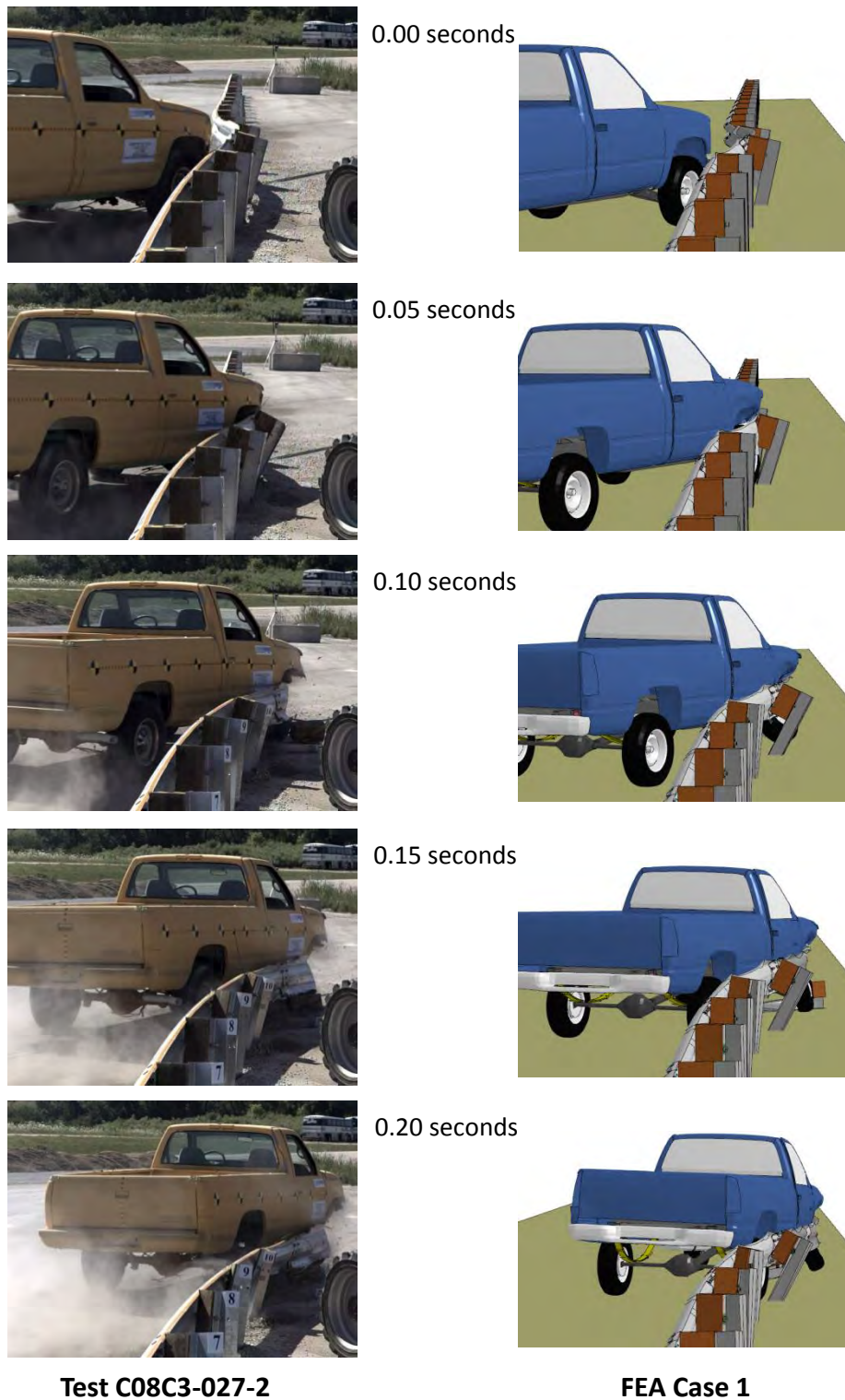


Figure 226. Sequential Views of Test C08C3-027-2 and FE analysis Case 1 from an upstream view perspective.

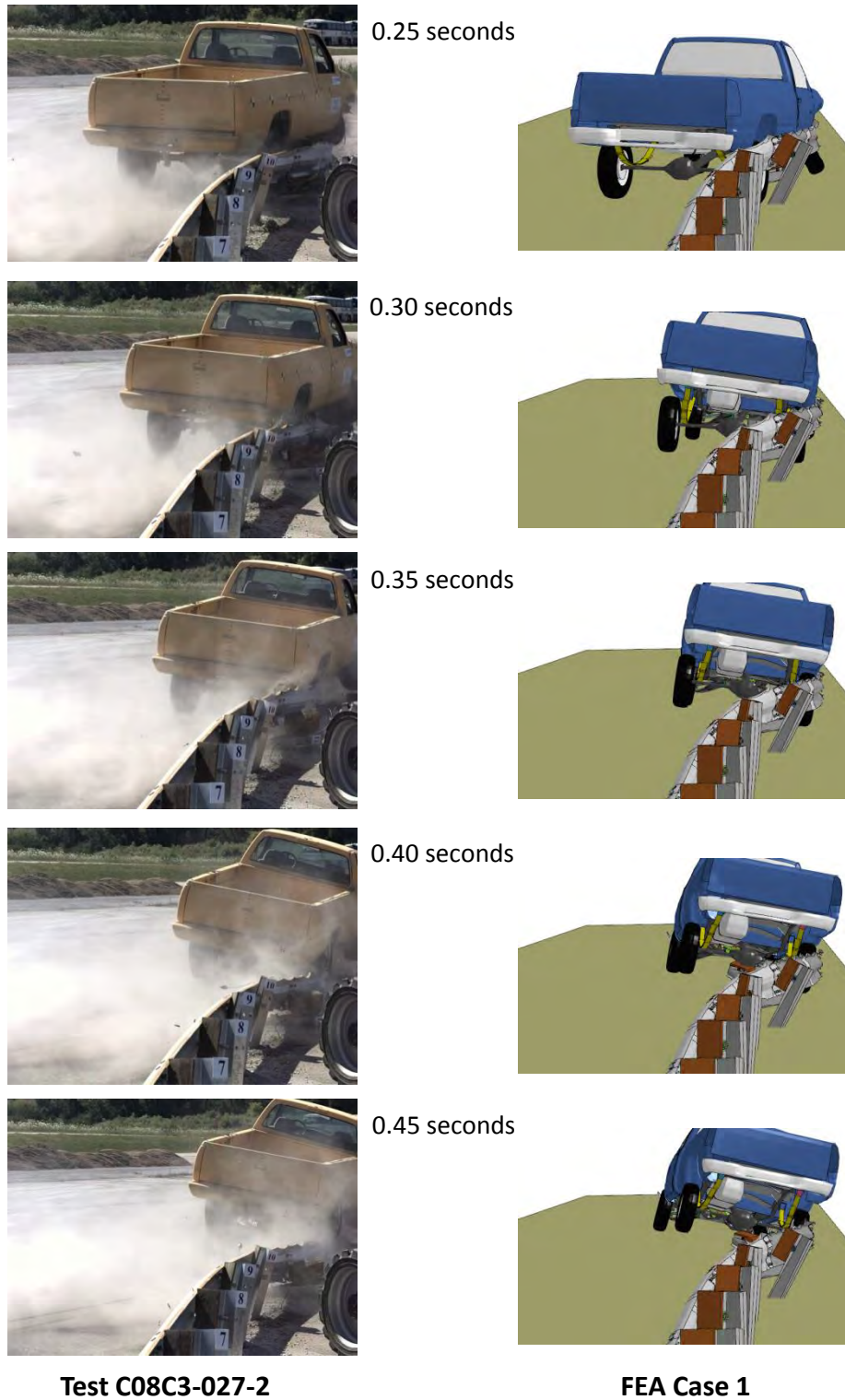


Figure 226. [CONTINUED] Sequential Views of Test C08C3-027-2 and FE analysis Case 1 from an upstream view perspective.

The acceleration time-histories of the vehicle during the event are shown in Figure 228 through Figure 230 and the angular displacement-time histories are shown in Figure 231. Data from the accelerometer located at the center of gravity of the vehicle were collected and input into the Test Risk Assessment Program (TRAP) Version 2.3.2 to determine occupant risk factors. The data as provided directly from TRAP is presented in Figure 232.

In the longitudinal direction, the occupant impact velocity was 16.4 ft/s (5.0 m/s) at 0.1584 seconds, the highest 0.010-second occupant ridedown acceleration was -8.5 g from 0.4146 and 0.4246 seconds, and the maximum 0.050-second average acceleration was -5.6 g between 0.3404 and 0.3904 seconds. The sudden drop in acceleration at times 0.13 seconds, 0.21 seconds, 0.27 seconds and 0.32 seconds corresponded to the release of post-bolts and buckling of posts. The maximum 0.010-second acceleration occurred when the vehicle impacted against Post 15, as shown in Figure 227.

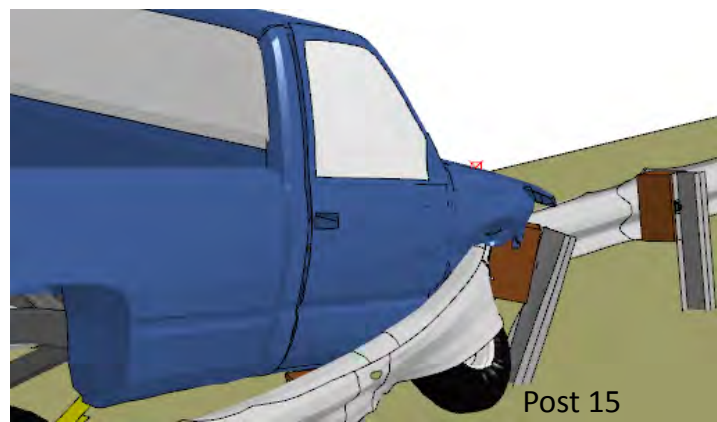


Figure 227. Vehicle impacts against Post 15 in analysis Case 1.

In the lateral direction, the occupant impact velocity was 15.4 ft/s (4.7 m/s) at 0.1584 seconds, the highest 0.010-second occupant ridedown acceleration was -8.9 g from 0.2575 and 0.2675 seconds, and the maximum 0.050-second average acceleration was -5.2 g between 0.2203 - 0.2703 seconds.

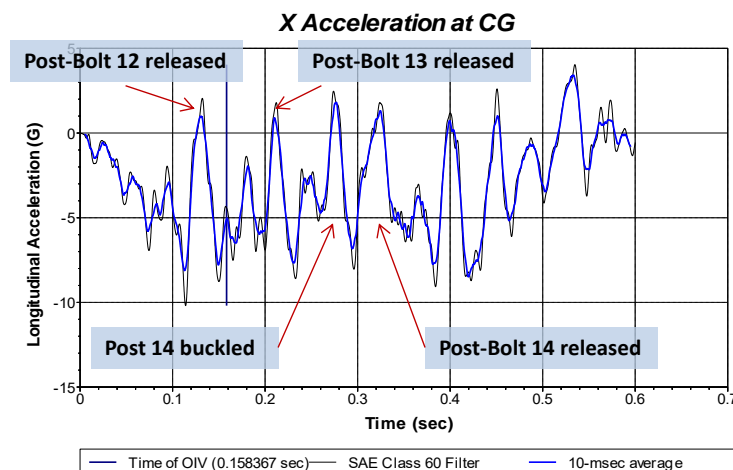


Figure 228. Longitudinal acceleration-time history at C.G. of pickup truck model in local coordinates for analysis Case 1.

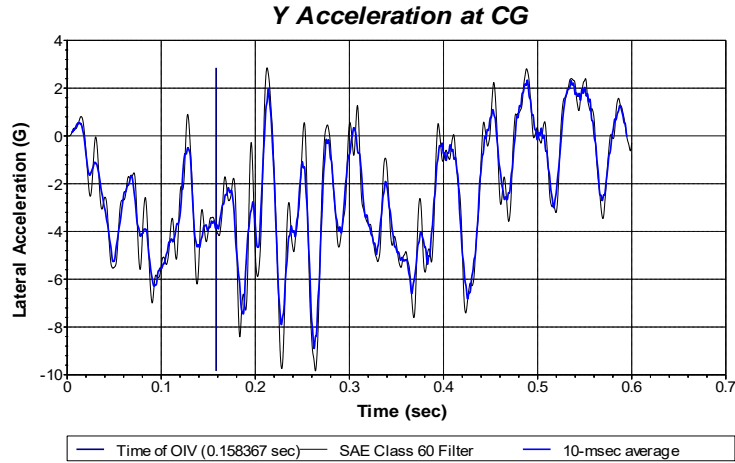


Figure 229. Lateral acceleration-time history at C.G. of pickup truck model in local coordinates for analysis Case 1.

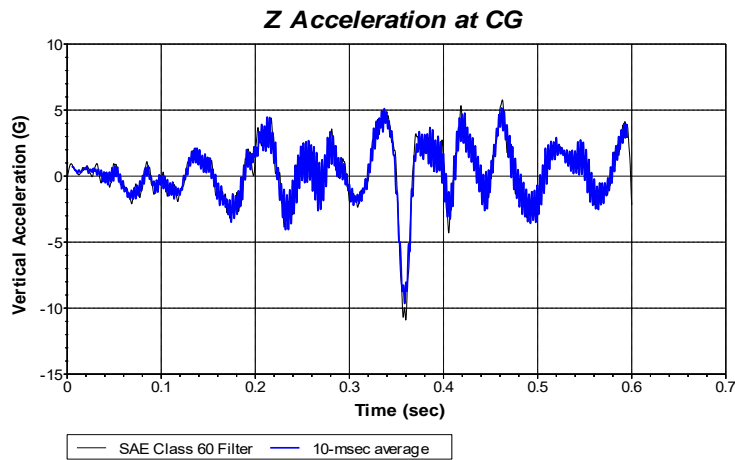


Figure 230. Vertical acceleration-time history at C.G. of pickup truck model in local coordinates for analysis Case 1.

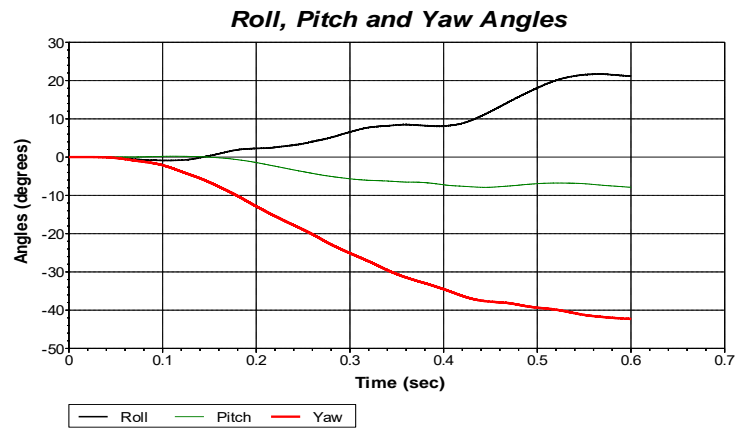


Figure 231. Acceleration-time history at C.G. of pickup truck model in local coordinates for analysis Case 1.

General Information			
	Test Agency:	RoadSafe, LLC	
	Test Number:	FEA_C08C3-027-2_5	
	Test Date:		
	Test Article:	Damaged G4(1S) with 15.5 inches initial deflection	
Test Vehicle			
	Description:	C2500D-v5b-R131202.k	
	Test Inertial Mass:	4472 lbm	
	Gross Static Mass:	4472 lbm	
Impact Conditions			
	Speed:	100.0 km/h	
	Angle:	26.4 degrees	
Occupant Risk Factors			
interior	Impact Velocity (m/s)	at 0.1584 seconds on right side of interior	
	x-direction	5.0	
	y-direction	4.7	
	THIV (km/hr):	23.4	at 0.1525 seconds on right side of
	THIV (m/s):	6.5	
	Ridedown Accelerations (g's)		
	x-direction	-8.5	(0.4146 - 0.4246 seconds)
	y-direction	-8.9	(0.2575 - 0.2675 seconds)
	PHD (g's):	10.7	(0.2231 - 0.2331 seconds)
	ASI:	0.72	(0.3411 - 0.3911 seconds)
	Max. 50msec Moving Avg. Accelerations (g's)		
	x-direction	-5.6	(0.3404 - 0.3904 seconds)
	y-direction	-5.2	(0.2203 - 0.2703 seconds)
	z-direction	2.0	(0.4172 - 0.4672 seconds)
Max Roll, Pitch, and Yaw Angles (degrees)			
Roll	21.7	(0.5603 seconds)	
Pitch	7.9	(0.4453 seconds)	
Yaw	-42.3	(0.5999 seconds)	

Figure 232. Summary report of occupant risk measures for the analysis Case 1.

Comparing the results of Analysis Case 1 to the full-scale test (C08C3-027-1) revealed that the *groundline* deflections of Posts 11 and 12 were notably higher in the analysis. This phenomenon resulted in the posts in the analysis rotating about a lower point below grade, which affected the tire's interaction with Post 11 and the height of the w-beam as the posts deflected and rotated back. After further review of the full-scale test it was determined that the limited width of the soil pit at the test site may have restricted the posts' deflection through the soil. Figure 233 shows the test setup for the low-speed Ttest C08C3-027-1 illustrating the limited distance between the back of the posts and the back edge of the soil pit. The ground surface outside the soil pit area was composed of asphalt material.

From a review of the high-speed video of the test, the lateral deflection of Post 11 was stopped abruptly at around 160 milliseconds of the impact event. Figure 234 shows snapshots from the test video for low-speed test C08C3-027-1 illustrating the position of the guardrail posts relative to the backside of the soil pit at the beginning of the test and at 0.16 seconds. Post 11 showed no signs of further deformation (e.g., torsional deflection, collapsing of the post cross-section, or further bending at the groundline). It was therefore assumed that the soil pit area was sufficient for the low-speed test.



Figure 233. Test setup for low-speed test C08C3-027-1 illustrating the limited distance to the back-edge of the soil-pit for the test article.

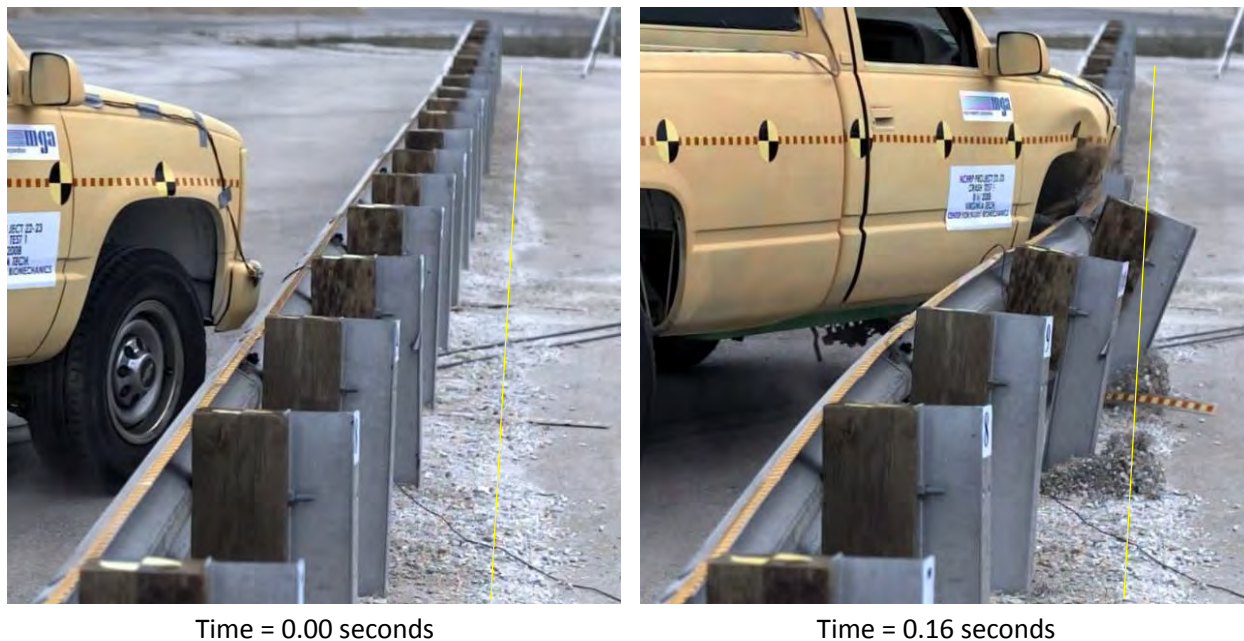


Figure 234. Snapshots from low-speed test C08C3-027-1 illustrating the position of the guardrail posts relative to the backside of the soil pit at the beginning of the test and at 0.16 seconds.

Figure 235 shows the test setup for high-speed test C08C3027-2. The initial deflections for Posts 11 and 12 were such that the back of the posts were already in contact (or nearly in contact) with the back edge of the soil pit prior to the start of the test. The reduced distance from the back of Posts 11 and 12 to the back-edge of the soil pit restricted the movement of the posts at the groundline.

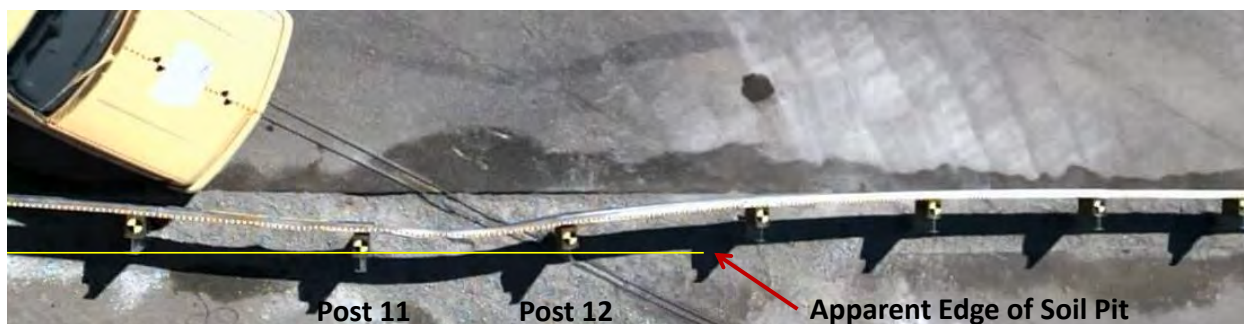


Figure 235. Test setup for high-speed test C08C3-027-2 illustrating the reduced distance from the back of Posts 11 and 12 to the back-edge of the soil-pit.

Analysis Case 2

As mentioned previously, analysis Case 2 included the same model used in analysis Case 1, except that the backside of the soil pit in the test article installation was included in the model. The soil-pit boundary was modeled using the “finite rigidwall” option in LS-DYNA. The lateral offset of the rigid wall relative to the guardrail was approximated based visual inspection of an

overhead view of the test article just before impact, as shown in Figure 235. The resulting model is shown in Figures 236 and 237 from an overhead and a downstream viewpoint, respectively.

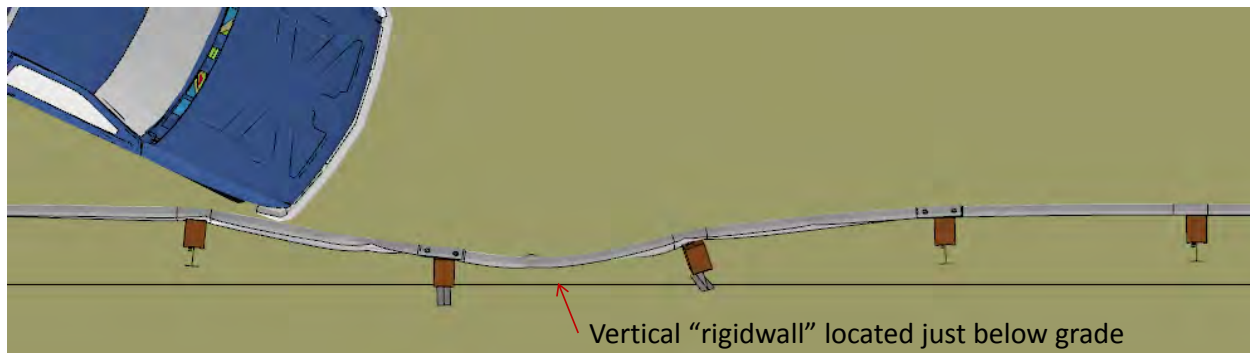


Figure 236. FE model for Case 2 with vertical "rigidwall" located just below grade to simulate back-edge of soil pit (overhead viewpoint).

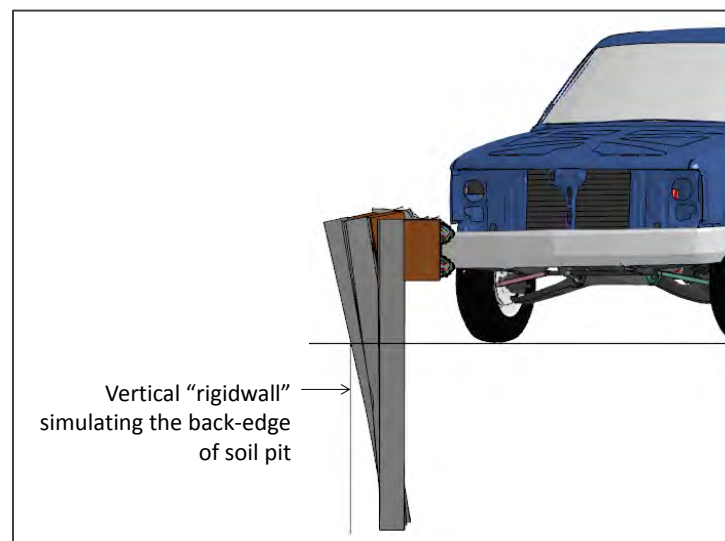


Figure 237. FE model for Case 2 with vertical "rigidwall" located just below grade to simulate back-edge of soil pit (downstream viewpoint).

At 30 milliseconds after impact Post 11 started to deflect back, and at 55 milliseconds Post 12 began to deflect. At 60 milliseconds the right-front tire impacted against Post 11 and began to push the post back as it rode over the post; the tie-rod did not fail as the wheel steered slightly toward the guardrail during interaction with the post. The post-bolt connection at Post 11 (location of a w-beam splice connection) released at 65 milliseconds. Post 11 was pushed completely to the ground at 95 milliseconds. At 50 milliseconds Post 10, which was upstream of the truck, began to twist such that the blockout was rotating in the downstream direction. At 85 milliseconds the posts upstream (e.g., Post 13, Post 14, etc.) began to twist, such that the blockouts were rotating in the upstream direction. At 100 milliseconds the front bumper was at Post 12. The w-beam at Post 12 began to drop at 110 milliseconds. At 115 milliseconds the upstream anchor reached its maximum deflection of 5.5 inches, and the post-bolt at Post 12

failed releasing both the rail and the blockout. Also at this time Post 12 was twisted almost 90 degrees. Between 115 and 120 milliseconds the right-front corner of the truck bumper was visible above the rail and Post 14 began to deflect laterally. The tire of the vehicle impacted Post 12 at 145 milliseconds and continued to push the post to the ground as it rode over the post. At 185 milliseconds, the front of the truck was at Post 13. At this time all the upstream posts had rotated significantly; however, none of the upstream post-bolt connections had released. Post 13 continued to deflect and at 220 milliseconds the top of the post contacted the ground with the w-beam still attached. At 225 milliseconds the right front tire of the vehicle impacted against the blockout of Post 13 and began to climb the rail (the top of the rail was 17 inches above ground at this time). At 275 milliseconds the front of the vehicle was at Post 14. At 320 milliseconds the right front tire overrode the rail. At 430 milliseconds the rear tire of the vehicle overrode the rail at Post 13 and the post-bolt at Post 13 released from the w-beam.

Figure 238 and Figure 239 show sequential snapshots of the impact event from a downstream-oblique view point and an upstream viewpoint, respectively. Table 2 provides a list of phenomenological events and their time of occurrence for both the full-scale test and the FE analysis. The model appears to reasonably simulate the basic kinematic behavior of the pickup until approximately 0.2 seconds of the impact event. After this time there was noticeable difference in the attitude of the vehicle, particularly in the yaw and pitch angles and the vertical trajectory. The front bumper and the front tire of the vehicle overrode the rail 0.05 seconds later in the analysis than it did in the full-scale test. As a result, the front of the vehicle remained in contact with the rail for a longer period of time in the analysis, resulting in greater yaw and pitch angles. This phenomenon is clearly evident in the sequential views beginning at 0.25 seconds.

Of primary concern, however, was that the post-rail connection at Post 13 did not release properly as the system deflected, which allowed the vehicle to override the guardrail in both the test and the analysis. Note that the only difference in this case, compared to Case 1, was the inclusion of the rigid boundary representing the soil pit wall, which limited the groundline deflection of the posts and resulted in the posts rotating about the top edge of the soil pit. Based on the results of the analysis, it is the authors' opinions that the override was likely the result of a combination of two events: 1) as the posts deflected laterally, the shorter radius of rotation of the posts resulted in the rail-height dropping more quickly, and 2) the low stiffness of the end-terminal resulted in lower tension in the rail, which consequently reduced the forces acting between the post-bolt and rail. That is, without sufficient tension in the rail there is not enough force to pull the post-bolt head through the w-beam slot and release the rail from the post, so the rail simply follows the deflection of the post to the ground – similar to a slack cable.

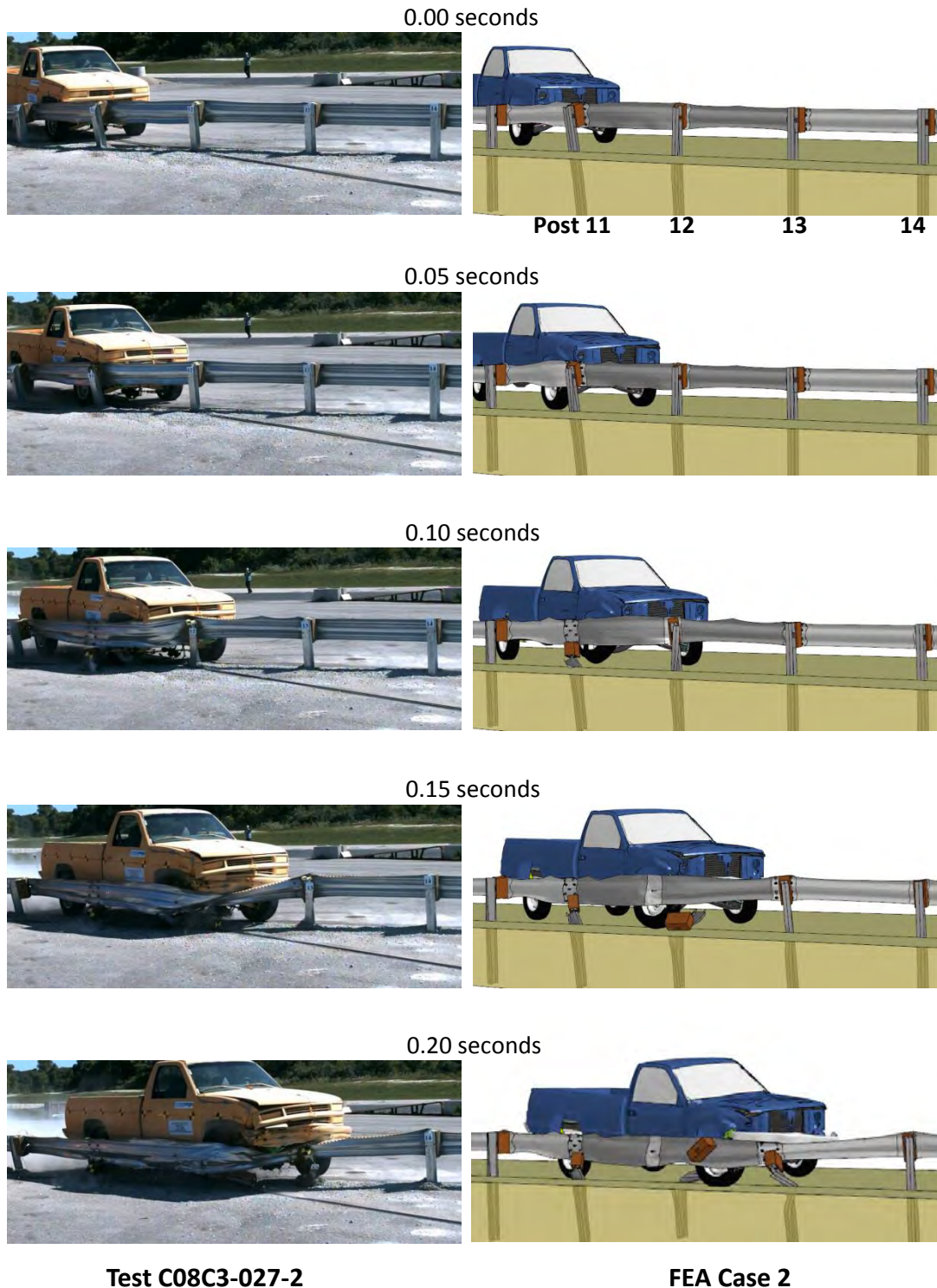


Figure 238. Sequential Views of Test C08C3-027-2 and FE analysis from downstream-backside view perspective.

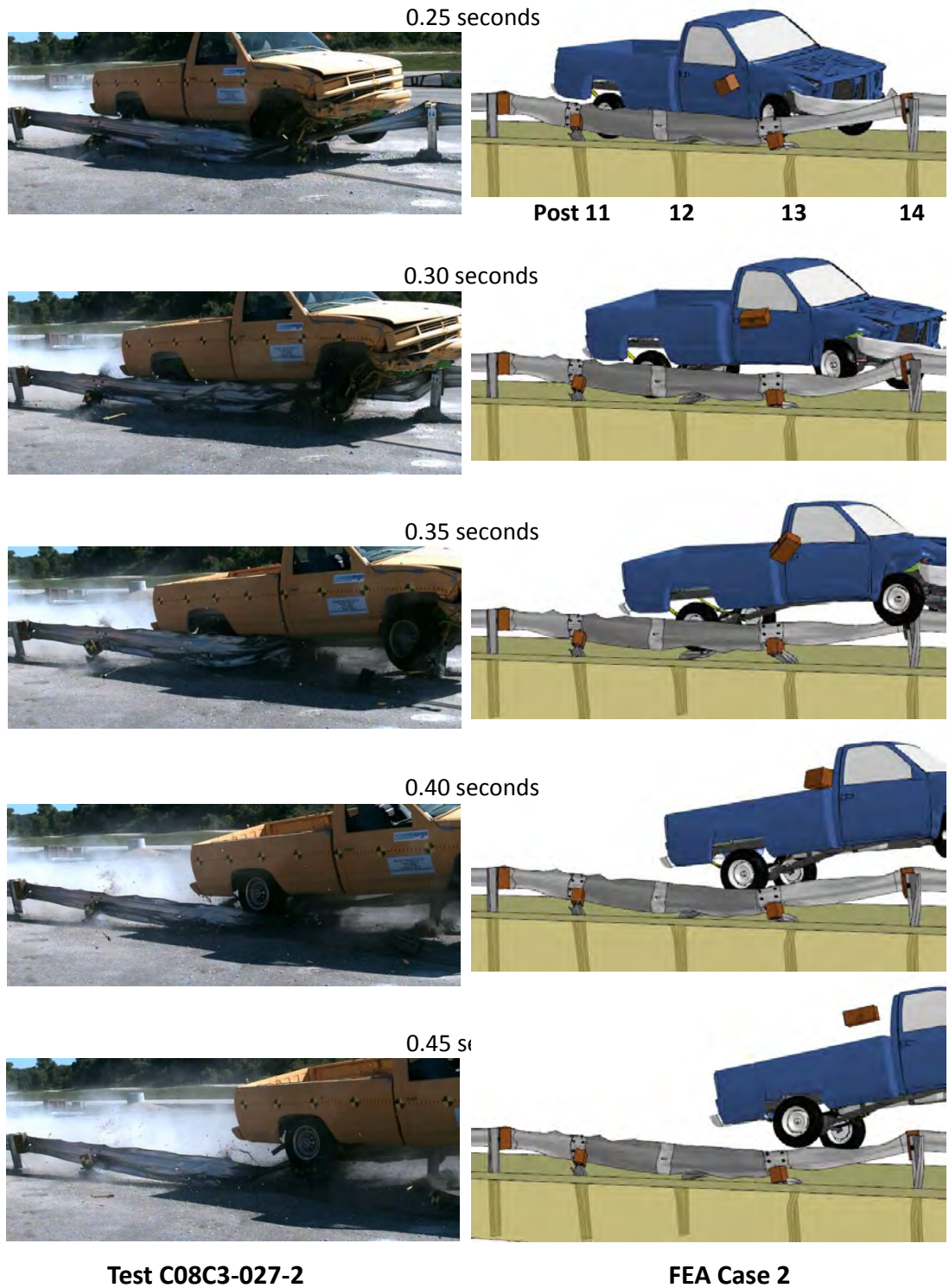


Figure 238. [CONTINUED] Sequential Views of Test C08C3-027-2 and FE analysis from downstream-backside view perspective.

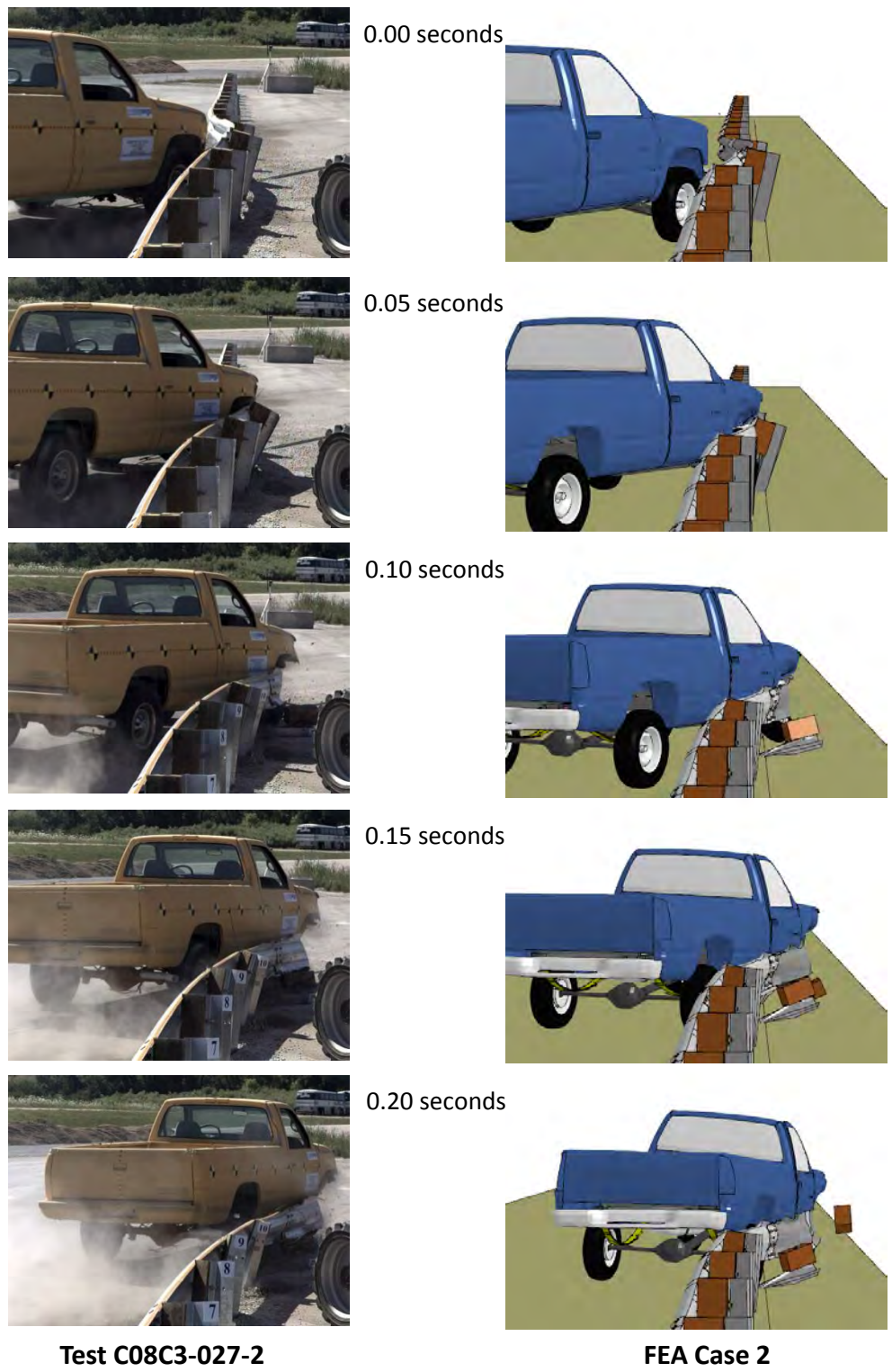


Figure 239. Sequential views of Test C08C3-027-2 and FE analysis from an upstream view perspective.

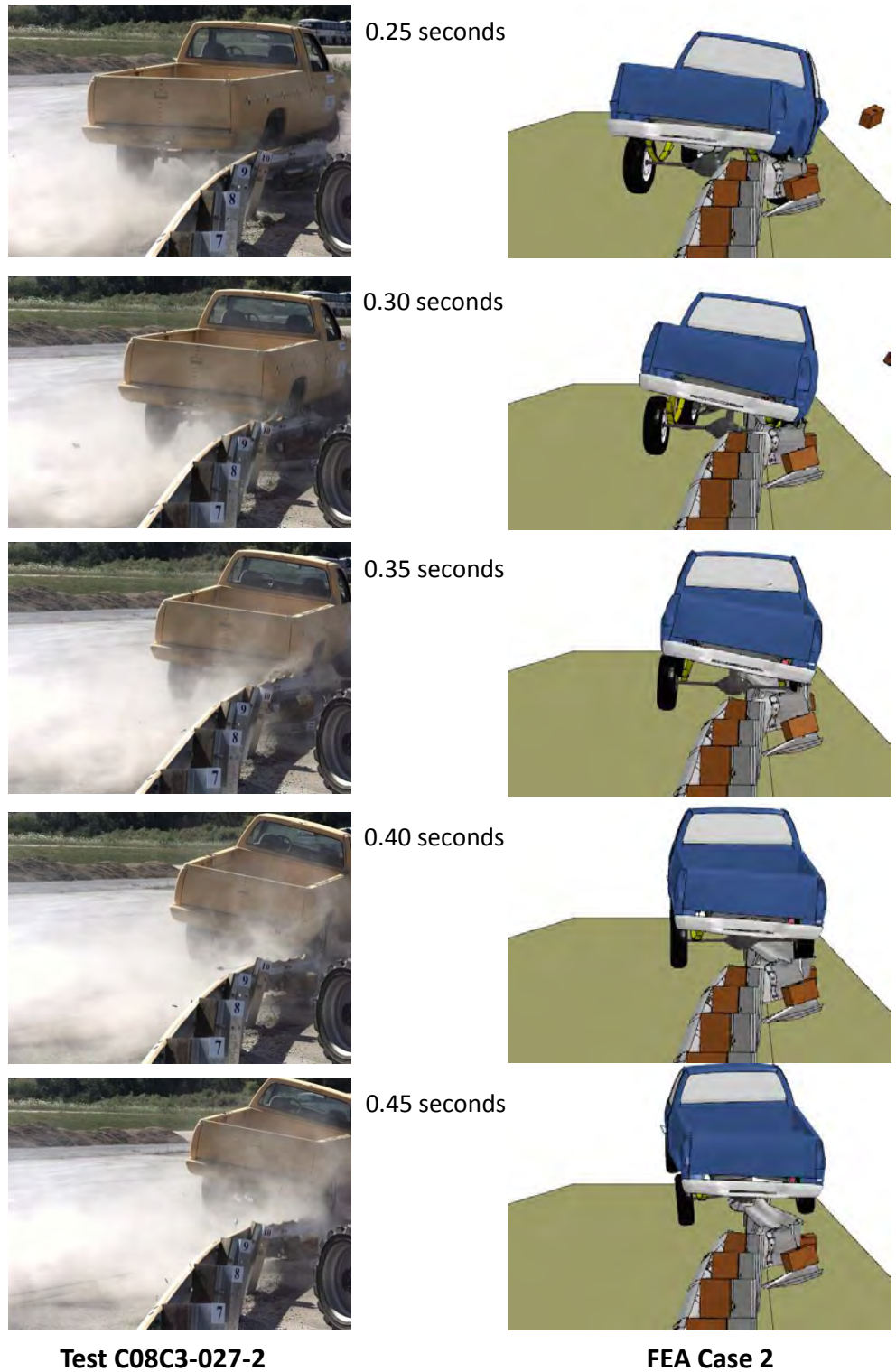


Figure 239. [CONTINUED] Sequential views of Test C08C3-027-2 and FE analysis from an upstream view perspective.

Table 66. Summary of phenomenological events of full-scale test C08C3-027-2 and FEA simulation.

Event	Test C08C3-027-2	FE Analysis
Post 11 began to deflect	0.016 sec	0.025 – 0.030 sec
Post 12 began to deflect	0.044 sec	0.050 – 0.055 sec
Right-front tire impacted Post 11	0.056 sec	0.055 – 0.060 sec
Post 10 began to twist clockwise	0.060 sec	0.050 – 0.055 sec
Post-bolt at Post 11 released	0.060 – 0.070 sec	0.060 – 0.065 sec
Post 11 pushed to the ground	0.088 sec	0.090 – 0.095 sec
Post 13 began to twist counter-clockwise	0.088 sec	0.085 – 0.090 sec
Front of vehicle was at Post 12	0.098 sec	0.095 – 0.100 sec
W-beam at Post 12 began to drop	0.108 sec	0.105 – 0.110 sec
Post-bolt at Post 12 released	0.112 sec	0.110 – 0.115 sec
Maximum displacement of upstream anchor	N.R.	5.5 in @ 0.115 sec
Right-front corner of bumper was visible over top of rail	0.120 sec	0.115 – 0.120 sec
Post 14 began to deflect laterally	0.128 – 0.130 sec	0.115 – 0.120 sec
Post 12 was pushed to the ground	0.146 sec	0.145 – 0.150 sec
Front bumper was completely overtop of rail	0.146 sec	0.225 – 0.230 sec
Front of vehicle was at Post 13	0.174 sec	0.180 – 0.185 sec
Post 13 was pushed to the ground without releasing rail	0.240 sec	0.220 – 0.225 sec
Maximum displacement of downstream anchor	N.R.	3.4 in @ 0.240 sec
Front-right tire overrode the rail	0.270 sec	0.320 – 0.325 sec
Rear-right tire overrode the rail	0.425 – 0.430 sec	0.425 – 0.430 sec
Post-bolt at Post 13 released	N.A.	0.425 – 0.430 sec

N.R.: Not reported.

Although the maximum deflection of the end-terminal was not reported in the full-scale tests, the magnitude could be approximated from the post-test photos of the deflected anchor post. Figure 240 shows the post-test photo of the upstream anchor in Test C08C3-027-2. The permanent deflection of the anchor post at the groundline was estimated from the photo to be approximately 8-9 inches, and the deflection of the post at the post-bolt location was approximately 13-14 inches.

The maximum dynamic and permanent deflections of the rail boundary in the analysis, as shown in Figure 241, were 5.5 inches and 3.7 inches, respectively, which were considerably lower than those of the full-scale test. This difference in anchor deflection is also apparent from the maximum rotation of the upstream posts, as illustrated in Figure 242. Since the end-terminal was modeled with less than half the stiffness of a standard two-post anchor system, it is not apparent why the displacement was so much greater in the test. Regardless, the seemingly low magnitude of rail tension in the full-scale test was likely a major contributing factor in how quickly and easily the rail was pulled down allowing the vehicle to override the guardrail.

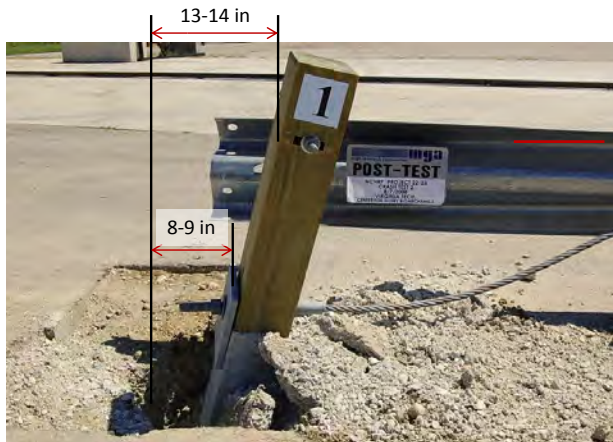


Figure 240. Permanent displacement of the upstream anchor in Test C08C3-027-2.

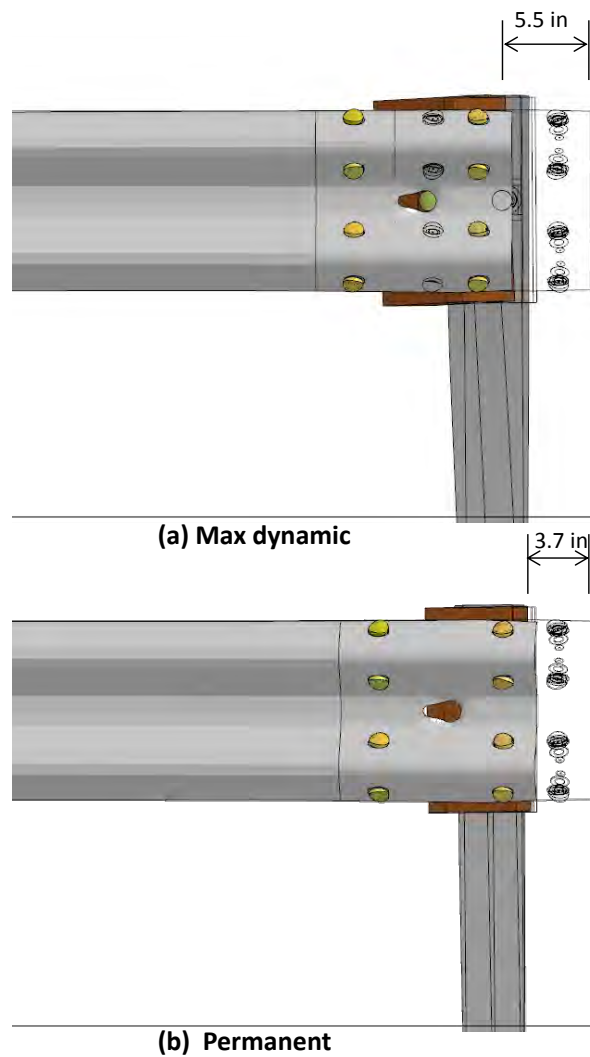


Figure 241. Displacement of upstream rail boundary in FEA analysis Case 2 (modeled with 47% baseline anchor stiffness).

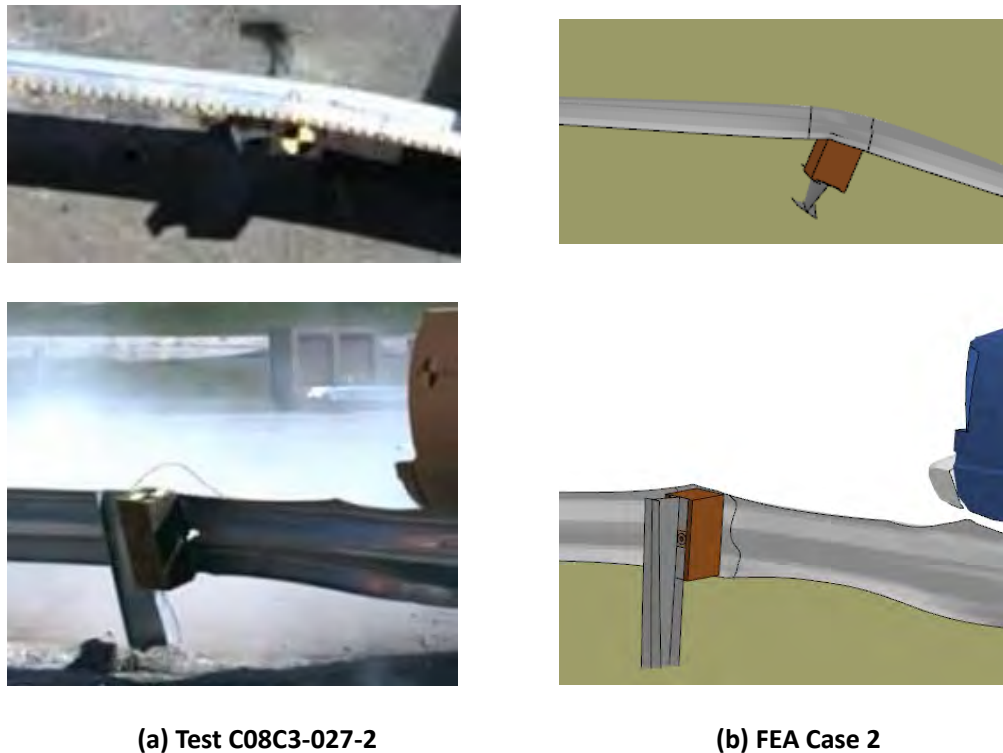


Figure 242. Maximum rotation displacement of Post 10 in (a) full-scale test and (b) FEA analysis Case 2.

Summary and Discussion

The purpose of this task was to resolve any discrepancies or to confirm the differences between the results in Chapter 10 for the G4(2W) guardrail and those in Report 656 which were based on damages to the G4(1S) guardrail. The primary discrepancy was related to the cause of failure. The results in Chapter 10 indicated that the most significant effect of pre-existing crash-induced rail deflection on the performance of the G4(2W) guardrail system was an increased potential for rail rupture. For example, Test 3-11 impact on the G4(2W) with an initial rail deflection of 14 inches resulted in maximum plastic strain values of 1.4 in the w-beam rail at the splice-bolt holes. The analyses for the G4(2W) also indicated that the potential for override was relatively low for all cases investigated. This was contradictory to the full-scale crash test results for the G4(1S) guardrail performed in Gabler's study, where a post-bolt did not release properly resulting in the rail being pulled down with one of the guardrail posts, allowing the vehicle to override the barrier.

The results in Chapter 10 lead to recommendations for future work to include analyses of both the G4(2W) and G4(1S) with pre-existing crash-induced rail deflections in combination with varying anchor strength. That activity was beyond the scope of this project; however, it was decided that the results of full-scale test C08C3-027-2 would be further investigated to determine if the cause of vehicle override was the combination of rail deflection and weak anchor rather than rail deflection and an "over-strong" post bolt connection. Due to the differences in torsional rigidity of the posts for these two systems it was expected that the G4(1S) would have a greater

sensitivity to anchor strength. This was further evidenced from the results of Test MGA C08C3-027-2 on that system which resulted in significant anchor deflection and vehicle override.

A model of the G4(1S) guardrail was developed and finite element analysis was used to simulate full-scale crash test C08C3-027-1 to create low-level crash-induced damage of the system. The results from this low-speed impact case, including guardrail component deformations and residual stresses, were then used as initial conditions in a secondary high-speed impact simulation of full-scale crash test C08C3-027-2. In these analyses, the upstream and downstream end-terminals for the system were modeled using non-linear springs attached to the ends of the rail. The single-foundation-tube anchor system in the full-scale tests was modeled via non-linear springs characterized by scaling the force-deflection properties of the baseline anchor defined in Chapter 9 by approximately 50 percent.

From review of the full-scale test video it was determined that there may have been an additional factor influencing the results of the test; specifically, an insufficient width of the soil pit behind the posts. It was apparent from the video that two of the posts contacted the backside of the pit during the test which arrested the lateral deflection of the posts at the groundline. Thus, two analysis cases were conducted: Case 1 which did not include the rigid boundary of the soil pit, and Case 2 which did include this boundary condition via the “finite rigidwall” option in LS-DYNA. For analysis Case 1 with 15.5 inches of initial guardrail deflection and without the influence of the restricted soil pit size, the system successfully contained and redirected the 2000P pickup under *NCHRP Report 350* impact conditions with no “apparent” likelihood for vehicle override. Case 2, on the other hand, which included the soil pit boundary, resulted in the vehicle overriding the barrier in a similar manner to that which occurred in the full-scale test.

In both analysis cases, however, the deflection of the anchor was significantly less than the anchor deflection in the full-scale test. The force-deflection characterization of the anchor used in the FEA model is shown in Figure 243. Also shown in the figure is the static force-deflection responses for a two-foundation-tube anchor (i.e., Test 13001B) and a single-foundation-tube anchor (i.e., Test 14001D on a standard anchor with groundline strut removed) measured via quasi-static tests in Chapter 12⁴. The plot shows that the anchor stiffness characterization of the FEA model was similar to that of Test 14001D up to approximately 5 inches deflection, at which point the resistance in the physical test suddenly dropped significantly. In the FE analyses, the deflection of the upstream anchor reached magnitudes of 11 inches and 5.5 inches for Case 1 and Case 2, respectively. It can therefore be assumed that the anchor system would likely have failed (i.e., experienced significant reduction in stiffness) in both of these analysis cases, which would have resulted in reduced tensile force in the w-beam and increased the potential for vehicle override.

4 The physical tests conducted in Task 4B were performed after this study was completed.

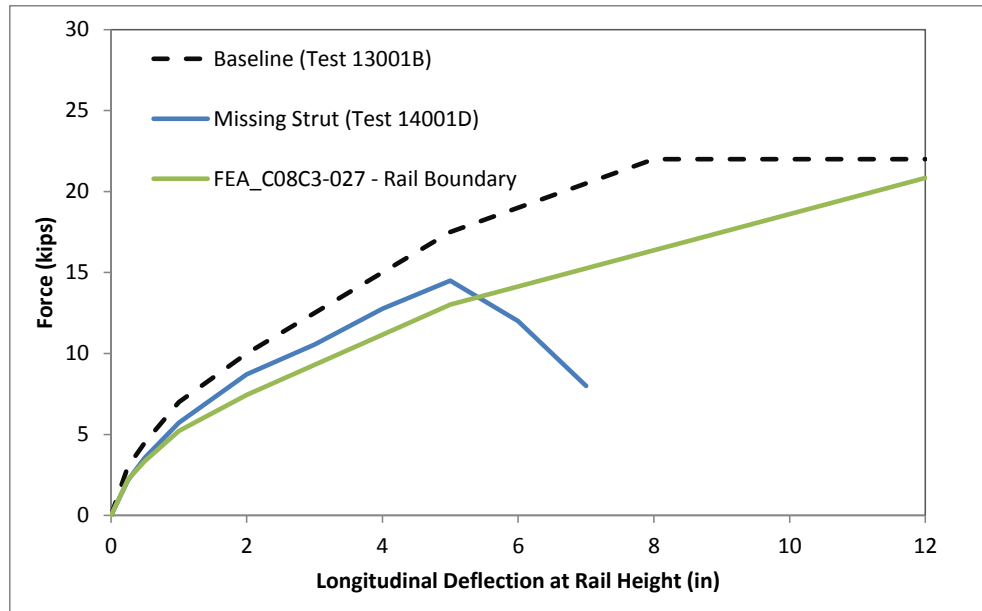


Figure 243. Anchor stiffness used in FEA model compared to anchor stiffness measured in physical tests.

The maximum plastic strain in the w-beam was 0.91 and was located at the edge of a splice-bolt hole. Strains of this magnitude for steel are generally associated with a high potential for material failure. These strains, however, are restricted to a very localized area at the end of the splice-bolt holes and are compressive (i.e., caused from the bearing load between the splice-bolt and the edge of the w-beam hole), which results in a lower potential for tear initiation – compared to the same magnitude of strain under tension. Further, the maximum strains in these analyses were considerably less than those from similar analysis cases involving the G4(2W). For example, the maximum effective plastic strains in the splice for the G4(2W) with 14 inches initial deflection was 1.4 (see Chapter 10); and the maximum effective plastic strains in the splice for the G4(2W) with weak anchor was 1.2 (see Chapter 9).

Conclusions

The analyses showed that the simulation of the full-scale test, including the effects of the single-foundation-tube anchor and the limited size of the soil pit in the model, resulted in essentially the same response as the test, in which the rail was pulled to the ground with Post 13 without releasing the post-bolt connection allowing the vehicle to override the rail. Thus, based on the results of the analyses presented herein and the subsequent assessment of the characterization of the anchor stiffness used in the FE model, it was concluded that the vehicle override in full-scale test C08C3-027-2 on the G4(1S) was likely augmented by the limited width of the soil pit as well as the reduced strength of the anchor system. However, further analyses or full-scale testing would be required to determine conclusively if the system would have been successful without these influences.

It was also ascertained that the influence of pre-existing crash-induced rail deflection was somewhat different for the G4(1S) compared to the G4(2W). That is, the G4(2W) has a higher probability for rail rupture for this damage mode; whereas, the G4(1S) is more likely to result in

the vehicle overriding the rail – particularly for cases when the movement of the posts in the soil is restricted (e.g., frozen soil, posts driven through asphalt, etc.).

Recommendations

Additional analyses should be conducted, in which the end-anchors are modeled using the revised stiffness and strength properties measured in Chapter 13 for the single-foundation-tube anchor system, to confirm the conclusions made herein regarding analysis results. Additional analyses may also be warranted to evaluate the performance of the G4(1S) with the standard anchor strength with and without the influence of the restricted soil pit size.

As discussed in Chapter 10, future work should also include analyses of both the G4(2W) and G4(1S) with pre-existing crash-induced rail deflections in combination with varying anchor strength. Due to the low torsional rigidity of the W6x9 steel posts of the G4(1S) guardrail it is expected that the G4(1S) may have a greater sensitivity to anchor strength. Also, the low-severity impact case evaluated herein involved low speed and a high impact angle which resulted in damage to a relatively localized section of the guardrail; i.e., the damaged area spanned only 3 to 4 posts. It is not known how the guardrail will respond to subsequent impacts when the rail deflections are spread over a longer length of the guardrail. It is recommended that future studies on the effects of pre-existing crash-induced rail deflections include higher impact speeds and smaller impact angles to create initial guardrail damage with similar magnitudes of rail deflection spread over a longer length of the guardrail.

CHAPTER 12 – EFFECTS OF SOIL EROSION AT GUARDRAIL POSTS FOR THE G4(2W)

The effects of various levels of soil loss around a guardrail post were evaluated for the G4(2W) guardrail in this study using a combination of pendulum testing and Finite Element Analysis (FEA). The post-soil assembly is a fundamental aspect of a guardrail and its response during a crash event is important to the overall performance of the system. Soil erosion effectively reduces the stiffness of the post-soil system and may have similar effects on guardrail performance as that of weakened posts described in Chapter 8. For cases in which soil confinement is reduced by the same degree at every post, such as when posts are installed at the edge of a foreslope, the increased deflection does not significantly degrade system performance.[*Polivka00b*] In such a case, the lateral stiffness of the guardrail is reduced uniformly across the entire system and results in increased rail deflection with reduced potential for pocketing (e.g., analogous to a weak-post guardrail system). A more critical situation may be when the soil is eroded away from one or two isolated posts, as shown in Figures 244 and 245. In this case, the increased deflection of the guardrail when struck at the lower stiffness section may result in pocketing as the vehicle approaches the stiffer downstream posts. Thus, a field-assessment procedure for assessing degradation of guardrail performance as a function of soil erosion around the guardrail posts was warranted to ensure proper performance of the guardrail system.



Figure 244. Example of soil erosion at a guardrail post.



Figure 245. Example of severe soil erosion at multiple posts.

The objectives of this study were to quantify the effects of soil erosion around guardrail posts on the crash performance of the G4(2W) guardrail system, and to develop recommendations for conducting field assessments for this damage mode for determining repair priority.

Research Approach

The basic research approach involved: (1) pendulum impact tests to measure the force-deflection response of the post-soil system for various levels of “manufactured” soil erosion; (2) developing finite element models for the various soil erosion cases and calibrating/validating the models using the test data; and (3) using FEA to quantify the effects of the various degrees of soil erosion on the crash performance of the G4(2W) guardrail system under Report 350 Test 3-11 impact conditions.

Physical Testing

The primary purpose of the physical test program was to measure the reduction in soil resistance as a function of soil erosion around the post for use in calibrating/validating the soil erosion FE models. The pendulum tests involved a W6x16 structural steel post embedded 36 inches in the soil, which was consistent with the embedment depth of the posts for full-scale crash test 471470-26 on the G4(2W) guardrail system.[Mak99] The soil for the tests conformed to Grading B of AASHTO M147-95 and was compacted in 6-inch lifts using a pneumatic tamper. The density, moisture content and degree of compaction of the soil was measured in front of, and behind the post after each compaction process using a Troxler-Model 3440 Surface Moisture-Density Gauge. There were a total of twelve soil readings – six on the front-side of the post and six on the back-side of the post – which were averaged to determine the effective soil

properties, as shown in Table 67. The target soil conditions included a dry density of 138 pcf, a moisture content of 3.4 percent, and a soil compaction of 92 percent.

The erosion condition was manufactured by removing a layer of soil behind and on the side of the post, as illustrated schematically in Figure 246. Four erosion depths were investigated: 3 inches, 6 inches, 9 inches, and 12 inches. The soil behind the post was flat and level and conformed to the desired erosion depth. The soil in front of the post tapered gradually from grade level down to the specified erosion depth, starting at approximately 10 inches in front of the post and ending at the back-face of the post. There were a total of 7 tests conducted. The complete test matrix is shown in Table 68.

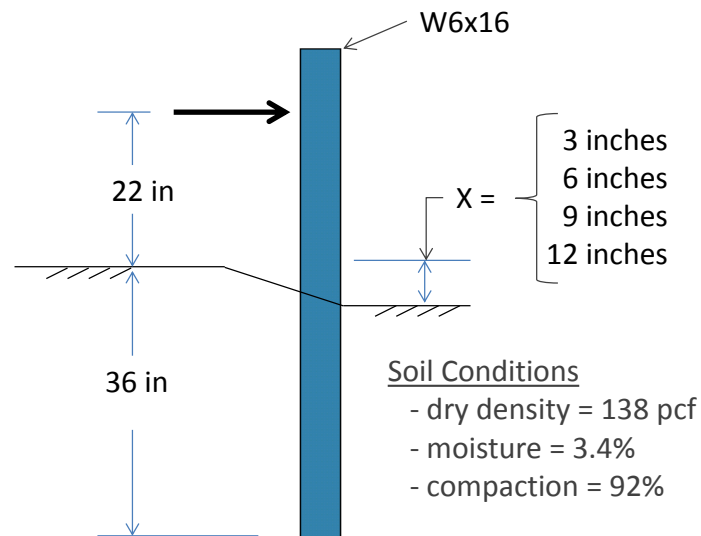


Figure 246. Test set-up for pendulum tests.

Table 67. Dry density of soil for each test case measured at 6-inch lifts.

Test No.	Damage Mode	Soil Properties														
		Dry Density														
		Front-Side of Post							Rear-Side of Post							Effective Density (pcf)
		Lift 1 (pcf)	Lift 2 (pcf)	Lift 3 (pcf)	Lift 4 (pcf)	Lift 5 (pcf)	Lift 6 (pcf)	Average (pcf)	Lift 1 (pcf)	Lift 2 (pcf)	Lift 3 (pcf)	Lift 4 (pcf)	Lift 5 (pcf)	Lift 6 (pcf)	Average (pcf)	
14003B	0" (Baseline)	143.7	140.1	142.9	143.9	143.8	145.2	143.3	143.3	140.6	146.4	143.7	140.8	141.7	142.8	143.0
14003A	3" Erosion	143.8	139.5	147.1	139.3	148.3	146.2	144.0	147.9	141.1	142.9	142.4	148.0	140.2	143.8	143.9
14003C	6" Erosion	144.0	147.5	145.0	141.5	140.9	147.3	144.4	145.1	140.8	145.8	144.0	142.5	144.9	143.9	144.1
14003D	9" Erosion	144.0	139.5	141.7	144.9	141.7	147.2	143.2	147.2	146.9	139.2	144.5	140.4	145.7	144.0	143.6
14003E	12" Erosion	140.0	140.6	143.4	146.5	140.8	145.2	142.8	144.6	140.7	142.6	145.7	141.0	145.2	143.3	143.0
14003F	0" (Baseline)	149.4	142.6	142.1	145.4	147.9	147.8	145.9	145.1	144.0	141.2	144.5	148.8	147.8	145.2	145.6
14003G	Supplemental	146.3	142.7	145.2	144.6	145.3	148.9	145.5	147.0	144.8	143.1	142.8	145.2	145.4	144.7	145.1

Table 68. Pendulum test matrix for erosion study showing post embedment, soil properties and impact conditions.

Test No.	Test Date	Damage Mode	Post Data			Effective Soil Properties			Impact Conditions		
			Type	Embedment Depth		Dry Density (pcf)	Moisture (%)	Compaction (%)	Pendulum		Impact Point (in)
				Front of Post (in)	Back of Post (in)				Weight (lbs)	Speed (mph)	
14003B	5/15/2014	Baseline	W6x16	36	36	143.0	3.6	92.6	2372	20	22.0
14003A	5/13/2014	3" Erosion	W6x16	34	33	143.9	4.1	93.1	2372	20	22.0
14003C	5/19/2014	6" Erosion	W6x16	34	30	144.1	4.2	93.3	2372	20	22.0
14003D	5/20/2014	9" Erosion	W6x16	32.5	27	143.6	3.8	92.9	2372	20	22.0
14003E	5/22/2014	12" Erosion	W6x16	35	24	143.0	3.6	92.6	2372	20	22.0
14003F	5/23/2014	Baseline	W6x16	36	36	145.6	3.0	94.2	2372	20	22.0
14003G	5/27/2014	Supplemental	W6x16	40	40	145.1	3.0	94.0	2372	20	22.0

Equipment and Instrumentation

Pendulum Device

The striker for the tests was a 2,372-lb concrete pendulum with a semi-rigid nose, which was the same striker used to evaluate the effects of post deterioration in Chapter 8 (see Chapter 8 for more details).



Figure 247. 2,372-lb pendulum device with semi-rigid nose.

Accelerometers

The pendulum was instrumented with three accelerometers mounted onto the backside of the pendulum mass. Accelerometers 1 and 3 recorded data in the x-direction (forward direction) and Accelerometer 2 recorded data in the z-direction (vertical direction). Figure 248 provides a schematic showing the locations of the accelerometers.

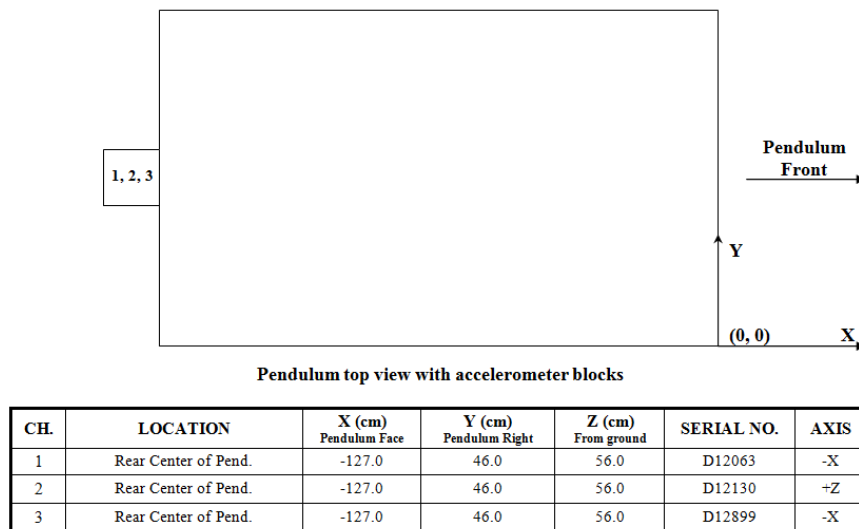


Figure 248. Schematic of the accelerometer instrumentation for the pendulum tests.

Photography Cameras

The tests were also recorded using four high-speed cameras with an operating speed of 500 frames per second and a digital video camera (~30 fps). Figure 249 provides the specifications and the general placement of the high-speed cameras for the tests. The accelerometers and the high-speed video were triggered using pressure tape switches when the pendulum contacted the post. The test setup and results were also documented with photographs taken before and after each test.

NO.	CAMERA	LENS	LENS (MM)	ZOOM (MM)	RESOLUTION (PIXELS)	SPEED (FPS)	LOCATION
1	GX-1	Nikon	18-35	35	1280 X 1024	500	Left Rear Iso
2	GX-1	Nikon	24-85	52	1280 X 1024	500	Right Perp.
3	GX-1	Nikon	35-105	105	1280 X 1024	500	Left Perp.
4	GX-1	Nikon	24-85	85	1280 X 1024	500	Right Rear Iso

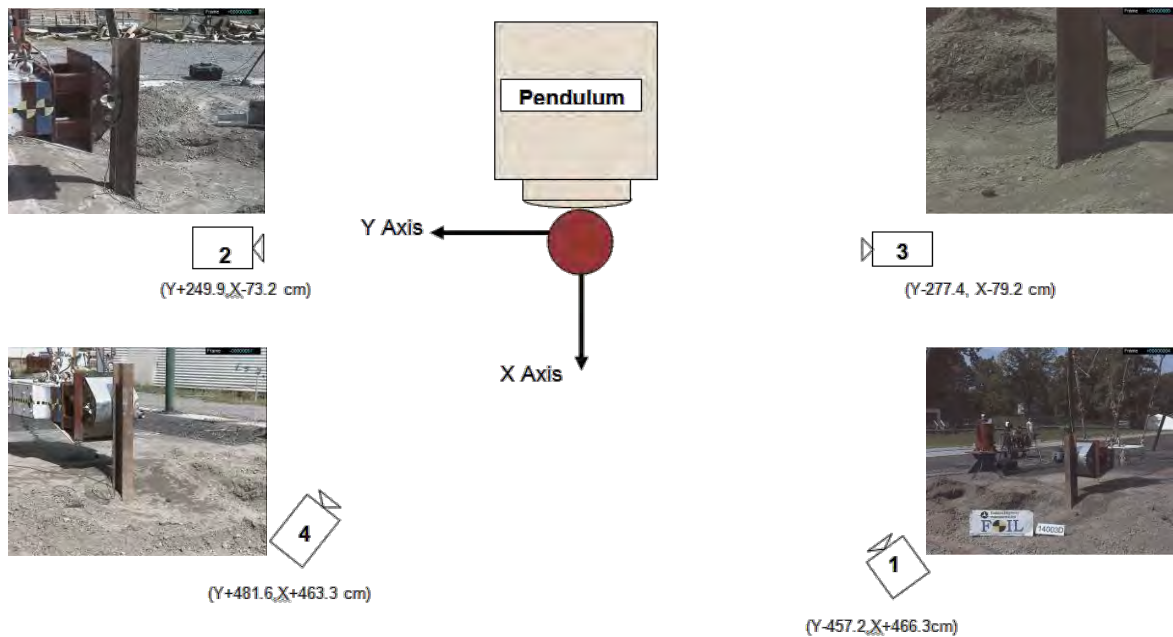


Figure 249. High-speed camera specifications and placement.

Impact Conditions

The 2,372-lb pendulum struck the post at 22 inches above grade at an impact speed of 20 mph, which resulted in 380.3 kip-in of kinetic energy for the striker. The posts were oriented in the strong direction such that the impact load was applied perpendicular to the flange of the post. The impact point height corresponded to the post-bolt location for the G4(2W) guardrail.

Results

The x-channel accelerometer data was processed to obtain the accelerations of the pendulum during impact with the posts. The data was filtered using an SAE Class 60 filter with cutoff frequency of 100 Hz. The impact force-time history response from each case was approximated by multiplying the acceleration-time history curves by the total mass of the pendulum. The displacement-time history of the pendulum was obtained by double integrating the acceleration-time history curve. These results were used to generate the force-deflection response of the post-soil system during impact. The force-deflection curve was then integrated to obtain the energy vs. deflection curves. Table 69 shows a summary of the test results. Plots of force vs. deflection and energy vs. deflection are shown in Figures 251 through 254. Test summary sheets for each erosion case are provided in Appendix M.

The data from the primary accelerometer (i.e., Channel 1) resulted in somewhat inconsistent results, as evidenced in the force-deflection plot in Figure 251 and the energy vs deflection plot in Figure 253. The data from the secondary accelerometer were much more consistent, as shown in Figure 252 and Figure 254. The two baseline tests from the secondary accelerometer resulted in essentially identical response; further, the results from the erosion tests showed that the resistance reduced monotonically as the erosion depth increased. Thus, the results from the secondary accelerometer (Channel 3) were considered to be more accurate and were used for the calibration/validation study for the finite element model in the next section.

The standard test procedure for measuring soil stiffness, as specified in MASH, entails a W6x16 post embedded 40 inches in the soil and impacted at 20 mph at 24.9 inches above grade. Recall that this test was previously performed in Test 13010F and was presented in Chapter 8. A supplemental test involving a W6x16 post embedded 40 inches with no manufactured erosion (i.e., Test 14003G) was included in the current test series. The impact point for the test was 22 inches (consistent with the mounting height of the G4(2W)), which was approximately 3 inches lower than that for the standard MASH test, and thereby provided a more direct comparison to the tests performed in this study.

The peak force in all cases was due to the initial inertial/impulse force between the pendulum head and the steel post. The magnitude of this peak was essentially the same for all cases regardless of post-soil stiffness, as shown in Figure 255. The one exception was Test 14003A corresponding to the 3-inch erosion case, which was the first test performed in this test series. During the “return swing” of the pendulum after striking the post in Test 14003A, the impact head snagged on the top of the post and was detached from the pendulum. The repair to the pendulum head included a steel “slide plate” mounted underneath the pendulum covering the gap between the head and the body of the pendulum, as shown in Figure 250. The plate was welded to the impact head and to the pendulum body. This modification resulted in a more rigid connection between the head and the pendulum mass which, consequently, increased the initial impulse/inertial spike for all the subsequent tests.



Figure 250. Repair to the pendulum head included adding a steel “slide Plate” underneath the head.

Figure 256 shows a plot of the total energy absorbed by the post-soil system as a function of erosion depth. The data in the plot corresponds to the total energy absorbed at the time when the pendulum overrode the post. As indicated in the plot, the data from the primary accelerometer generally resulted in slightly lower magnitudes than those from the secondary accelerometer. Since it has not been confirmed which of the accelerometers is correct, the data from both accelerometers were averaged and plotted in Figure 257. The data for the 40-inch embedment case was also included in the plot (e.g., the erosion depth was included as -4 inches). The results indicate that the energy capacity of the post-soil system reduces linearly with respect to erosion depth. Using an embedment depth of 36 inches as the baseline, the reduction in energy capacity as a function of erosion depth can be approximated using the following relationship:

$$\text{Energy Capacity} = 178.33 - 8.04 * (\text{erosion depth})$$

Table 69. Summary of results for Test Series 14003.

Test No.	Test Date	Damage Mode	Post Data			Effective Soil Properties			Impact Conditions			Results				
			Type	Embedment Depth		Dry Density (pcf)	Moisture (%)	Compaction (%)	Pendulum		Impact Point (in)	Primary Accel.		Secondary Accel.		Average Energy (kip-in)
				Front of Post (in)	Back of Post (in)				Weight (lbs)	Speed (mph)		Peak Force (kips)	Energy (kip-in)	Peak Force (kips)	Energy (kip-in)	
14003B	5/15/2014	Baseline	W6x16	36	36	143.0	3.6	92.6	2372	20	22.0	18.7	149.5	19.2	186.4	167.9
14003A	5/13/2014	3" Erosion	W6x16	34	33	143.9	4.1	93.1	2372	20	22.0	13.2	158.0	13.6	181.2	169.6
14003C	5/19/2014	6" Erosion	W6x16	34	30	144.1	4.2	93.3	2372	20	22.0	17.2	121.8	17.3	142.1	132.0
14003D	5/20/2014	9" Erosion	W6x16	32.5	27	143.6	3.8	92.9	2372	20	22.0	18.7	85.9	19.4	116.0	101.0
14003E	5/22/2014	12" Erosion	W6x16	35	24	143.0	3.6	92.6	2372	20	22.0	18.1	85.2	18.3	73.7	79.4
14003F	5/23/2014	Baseline	W6x16	36	36	145.6	3.0	94.2	2372	20	22.0	21.3	183.1	21.6	183.7	183.4
14003G	5/27/2014	Supplemental	W6x16	40	40	145.1	3.0	94.0	2372	20	22.0	17.7	197.4	18.4	214.8	206.1

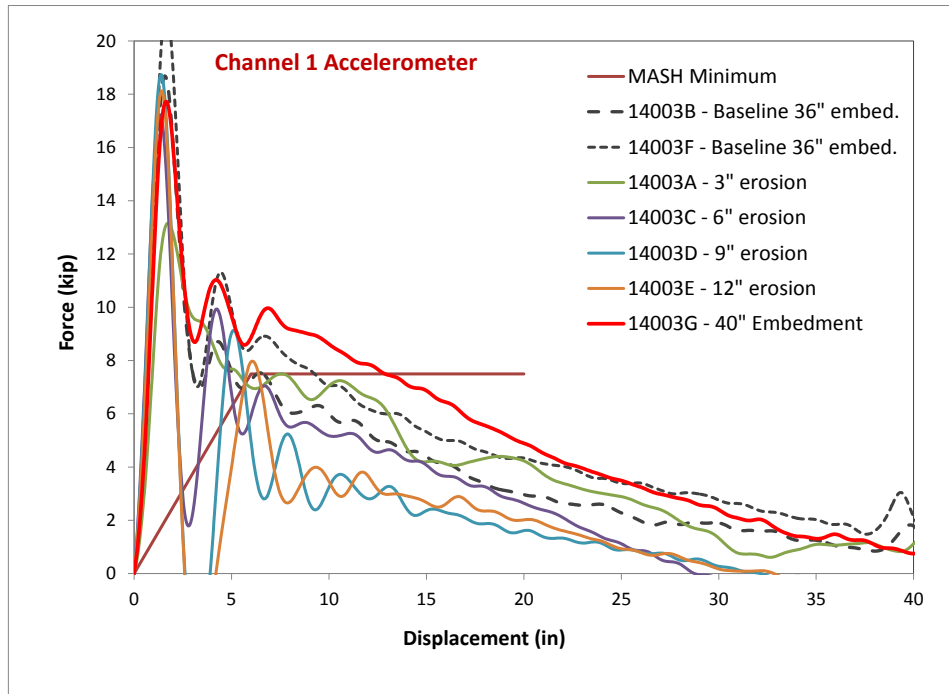


Figure 251. Force vs. deflection curves for Test Series 14003 from primary accelerometer.

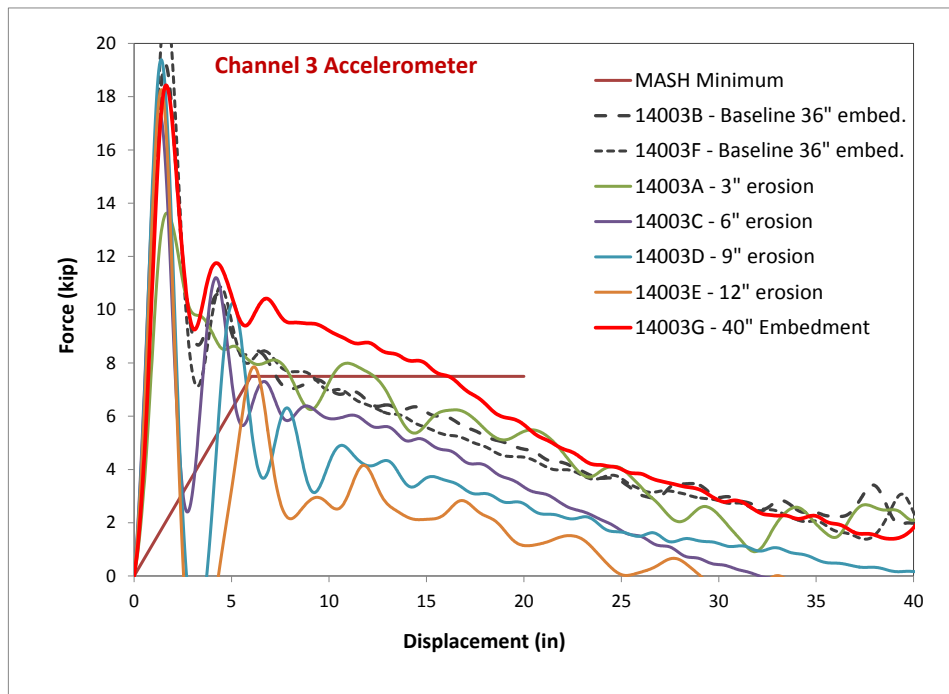


Figure 252. Force vs. deflection curves for Test Series 14003 from secondary accelerometer.

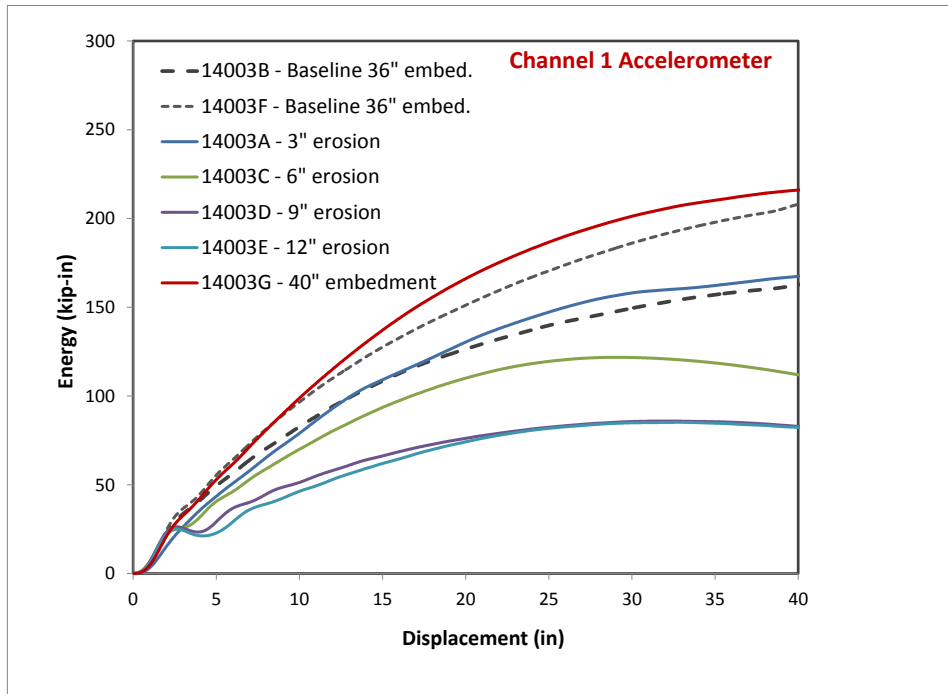


Figure 253. Energy vs. deflection curves for Test Series 14003 from primary accelerometer.

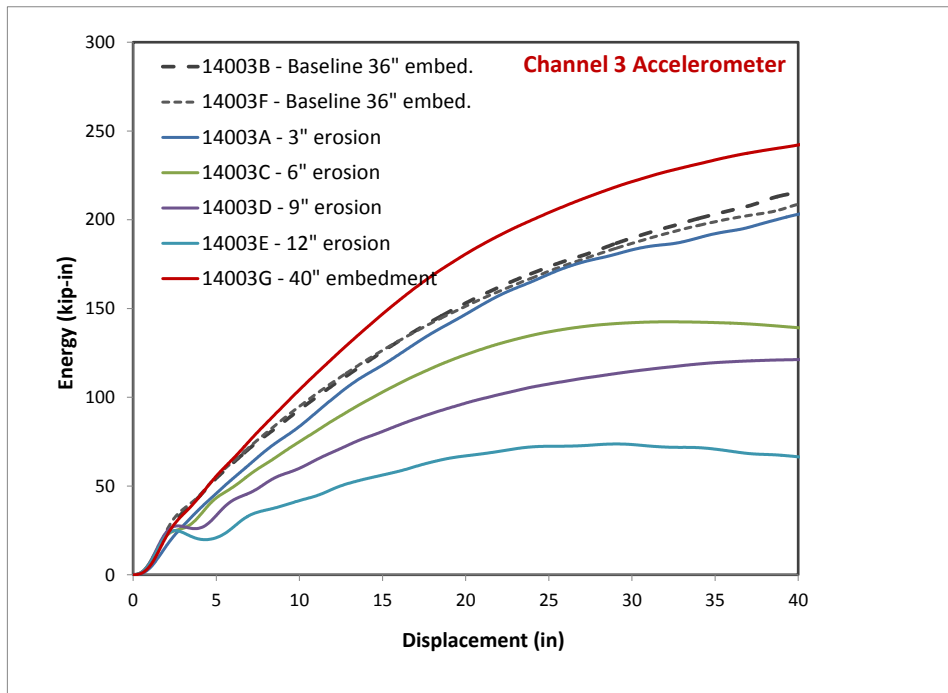


Figure 254. Energy vs. deflection curves for Test Series 14003 from secondary accelerometer.

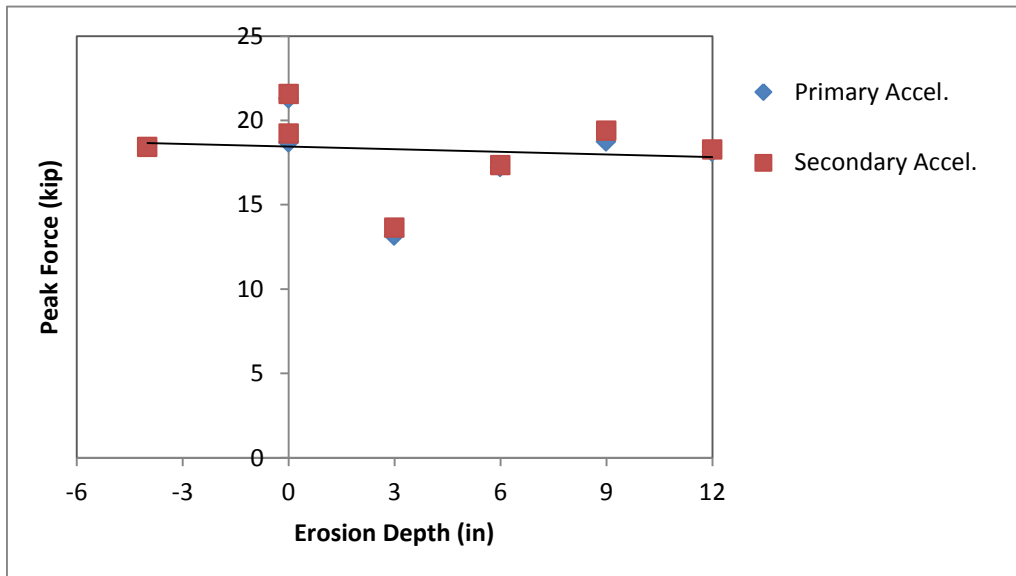


Figure 255. Peak “impulse” force in Test Series 14003.

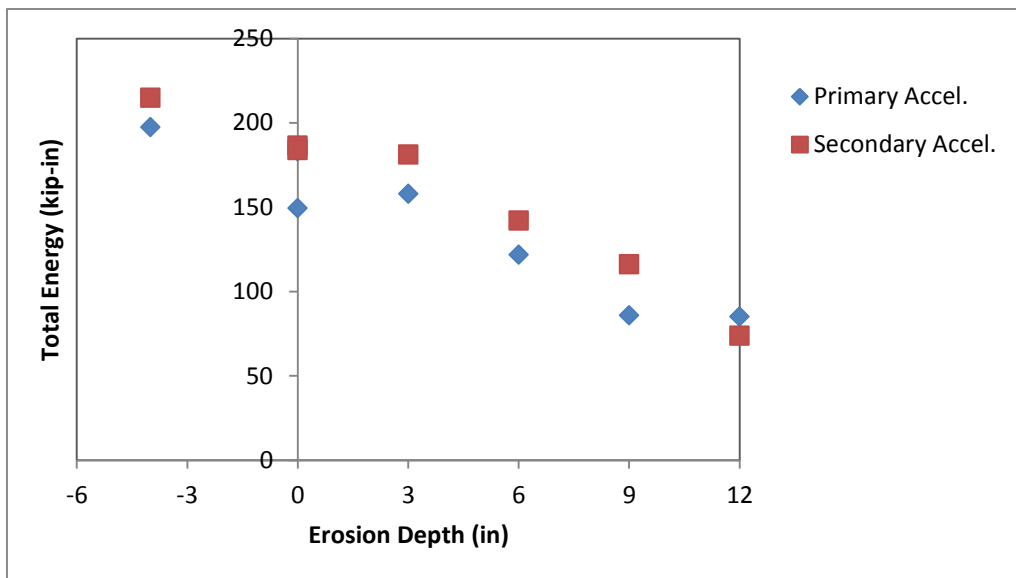


Figure 256. Total energy vs. erosion for Test Series 14003 – energy values correspond to point when pendulum overrides the post.

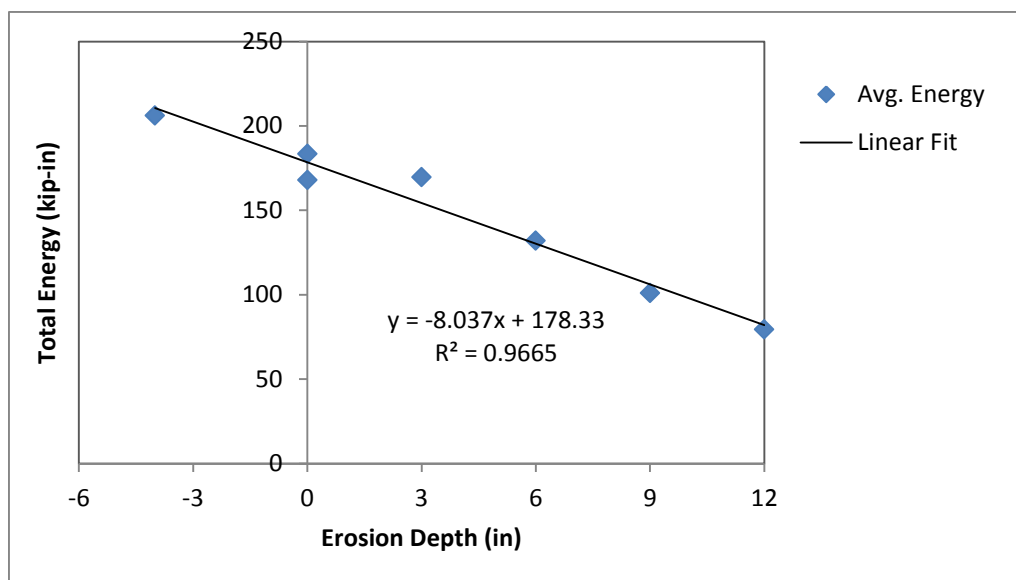


Figure 257. Total energy vs. erosion for Test Series 14003 – average of primary and secondary accelerometers – including linear curve fit to the data.

Finite Element Analysis

Finite element models with various levels of erosion were developed and included in the G4(2W) guardrail model. FEA was then used to simulate Report 350 Test 3-11 impact conditions to quantify the effects of soil erosion on the performance of the guardrail system. The development and validation of the finite element model of the G4(2W) guardrail was presented in Chapter 7. The various components of the G4(2W) guardrail were modeled according to their baseline conditions, including the wood post model. The soil models representing the various levels of erosion were calibrated/validated through comparison with pendulum test data from test Series 14003 presented earlier. The erosion levels were modeled by simply translating the soil-spring model to the appropriate erosion depth. The following sections discuss the methodology and results for calibrating/validating soil erosion models and evaluation of the effects of soil erosion on performance of the G4(2W) guardrail.

Calibration/Validation of FE Soil-Erosion Model

The impact conditions for Test Series 14003 were simulated using the finite element model shown in Figure 258. From the results of the pendulum tests, the initial spike at the beginning of the impact, as seen in Figures 251 and 252, was due in part to the impulse load between the pendulum and the post, but also to an increase in soil stiffness from “friction locking” of soil particles under high soil compaction. The soil-spring model developed in Chapter 7 was modified slightly to account for this “friction locking”. In particular, the force-deflection characterization for the soil springs was increased for the first 0.5 inches of soil deflection, and then then reverted back to their original stiffness. The following sections present a comparison of the FE model results compared to the physical tests for the baseline condition (i.e., 36-inch embedment depth) and various erosion depths.

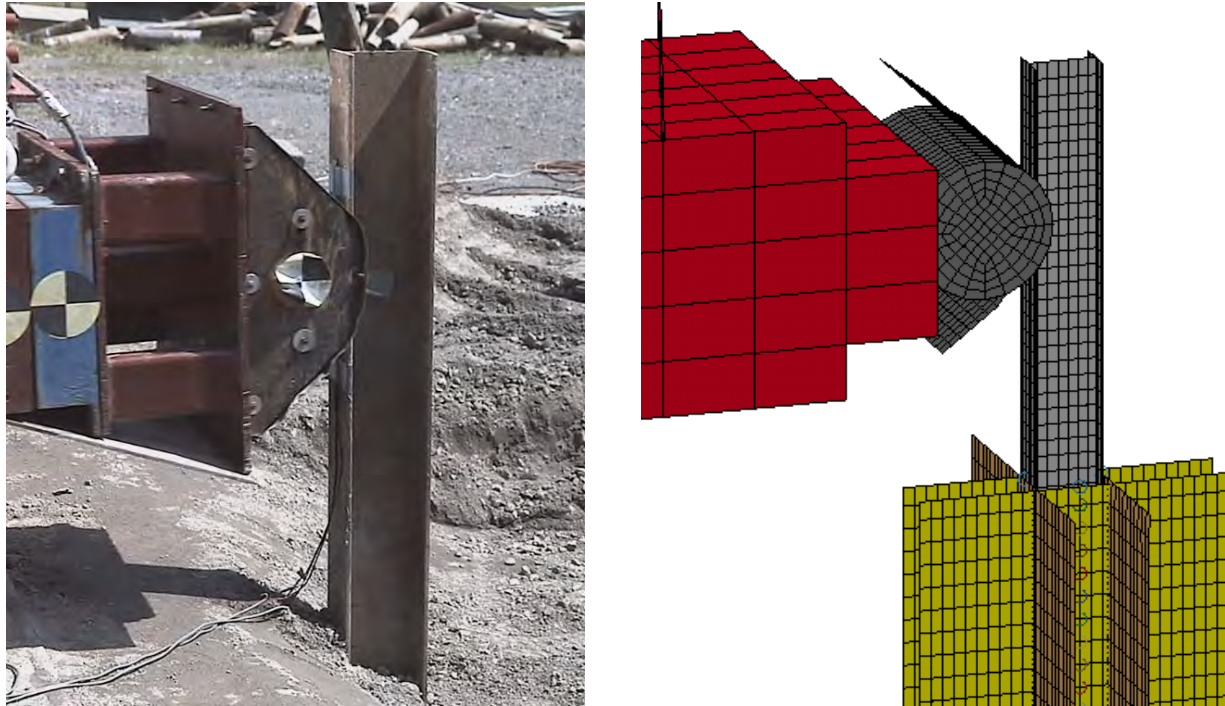


Figure 258. Finite element model used for validating/calibrating soil-spring stiffness corresponding to various levels of soil erosion.

Baseline Case – Damage Level 0 (DL0)

The results of the model for the baseline condition are compared to full-scale test results in Figures 259 through 261. The force vs. deflection curves and the energy vs. deflection curves are shown in Figure 259 and Figure 260, respectively. As indicated from these plots, the FE model does not accurately capture the magnitude of the initial force response; otherwise, the overall response of the model matches reasonably well to the physical test. The model shows slightly higher response than the tests at post deflections beyond 20 inches. From the high-speed videos of the physical tests, it is evident that the soil is loosened significantly as the post rotates through the soil at increasingly higher deflections; at that point the post is essentially moving through a loose soil mass. The characterization of the soil in FE model does not include this softening behavior; however, the friction between the post and soil in the model effectively results in a similar response as the post slides up and out of the soil plates.

The total energy absorbed at 12 inches displacement in the analysis was 95.4 kip-in compared to 109 kip-in in Test 14003F; the total energy absorbed at 20 inches displacement in the analysis was 149 kip-in compared to 152 kip-in in Test 14003F; and the total energy absorbed at 40 inches displacement in the analysis was 247 kip-in compared to 211 kip-in in Test 14003F. Figure 261 shows sequential views comparing analysis results to dynamic impact Test 14003F.

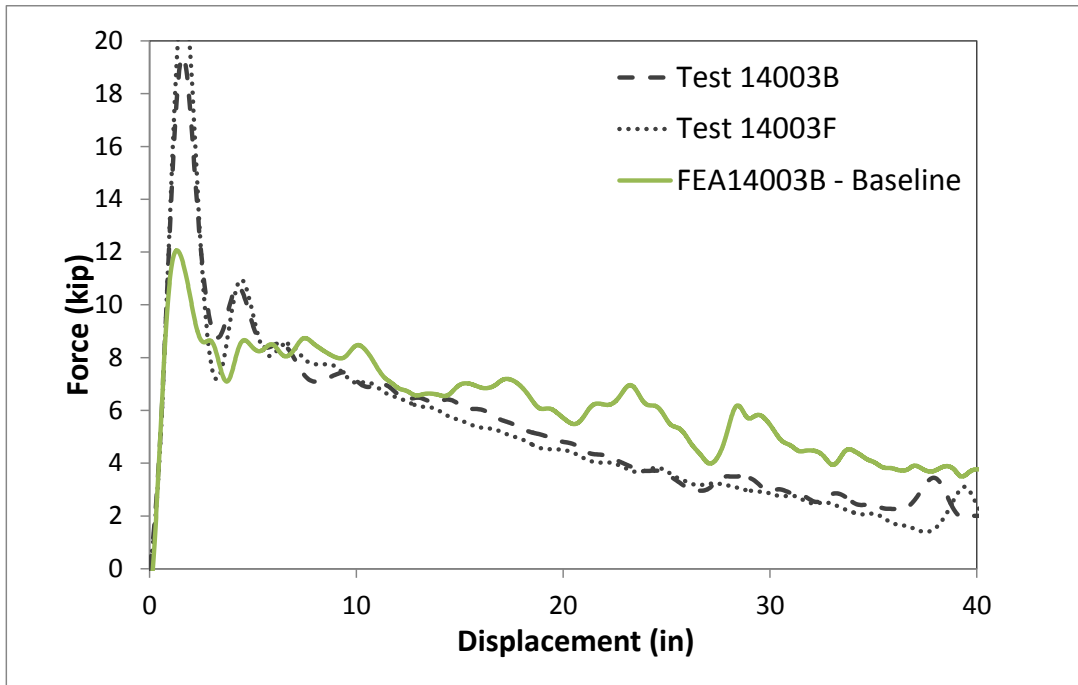


Figure 259. Force vs. deflection for DL0 soil model compared to Tests 14003B and 14003F.

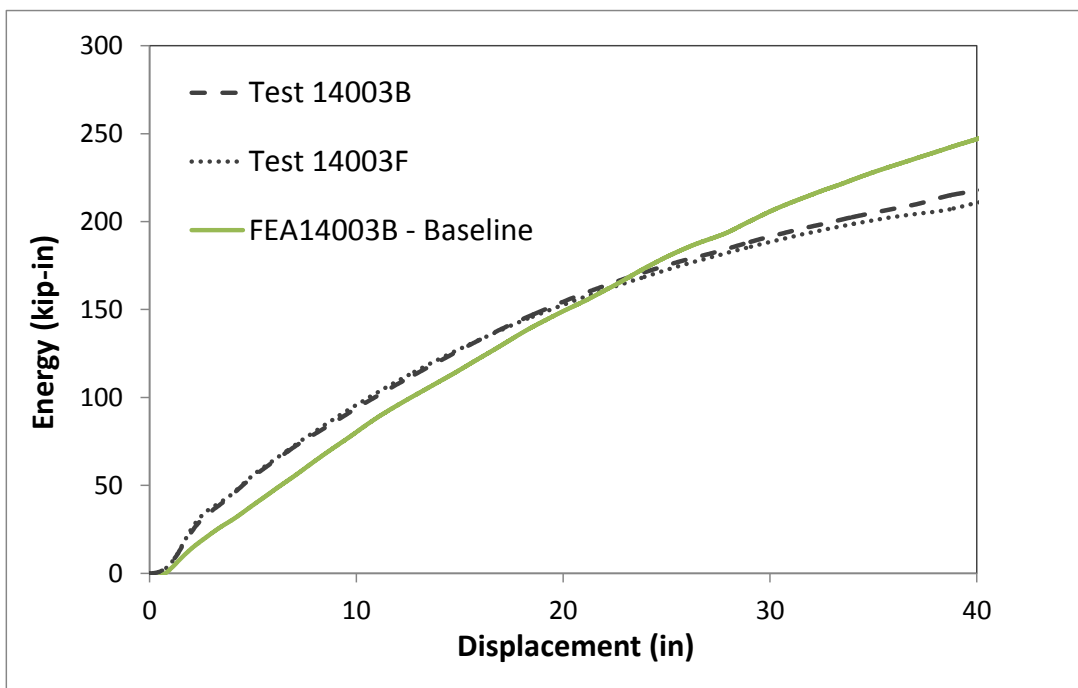


Figure 260. Energy vs. deflection for DL0 soil model compared to Tests 14003B and 14003F.

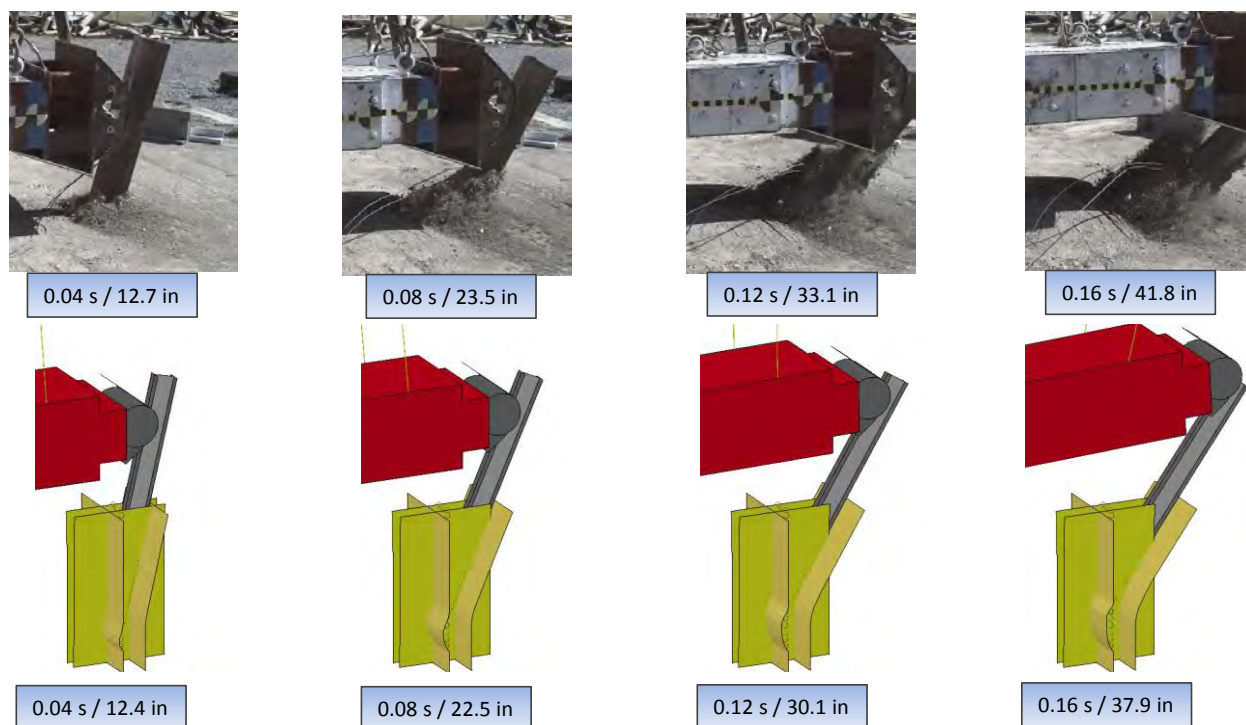


Figure 261. Sequential views of Test 14003F and FE analysis on baseline post-soil case, DL0.

3" Erosion Case

The impact conditions for Test 14003A were simulated using the finite element model shown in Figure 258 with the following modifications: In the physical test, the soil depth was at grade level starting at approximately 10 inches in front of the post and tapered gradually to 2 inch below grade at the front-face of the post. The soil continued to taper to three inches below grade at the back-face of the post. The soil then remained at 3 inches below grade level for several feet behind the post. As mentioned previously, the soil-spring model was shifted downward in the vertical direction to account for the erosion. For this case, the soil model was set three inches below grade on the backside of the post, while the soil level on the front side of the post was kept at its original position at grade level. This methodology was based on the fact that the post pushes against the soil much farther below grade on the front-side of the post, where the lateral stiffness of the soil is affected by the overbearing pressure of a greater volume of soil (e.g., considering an angle of internal friction >40 deg.). The volume of soil removed from this region when creating the manufactured erosion was considered negligible; particularly in this case where only 2 inches of soil was removed at the front edge of the post. On the backside the post, on the other hand, the post interacts with the soil nearer to the surface, where a much greater volume of soil was removed.

Figure 262 and Figure 263 show the force vs. deflection and energy vs. deflection results, respectively, for the FE model compared to pendulum Test 14003A. The overall response of the model matches reasonably well to the physical test, including the impulsive force spike at the beginning of the impact event. Recall that this test was performed using the original pendulum head (before the head was repaired), which resulted in a lower impulse/inertial spike compared to subsequent tests with the repaired head.

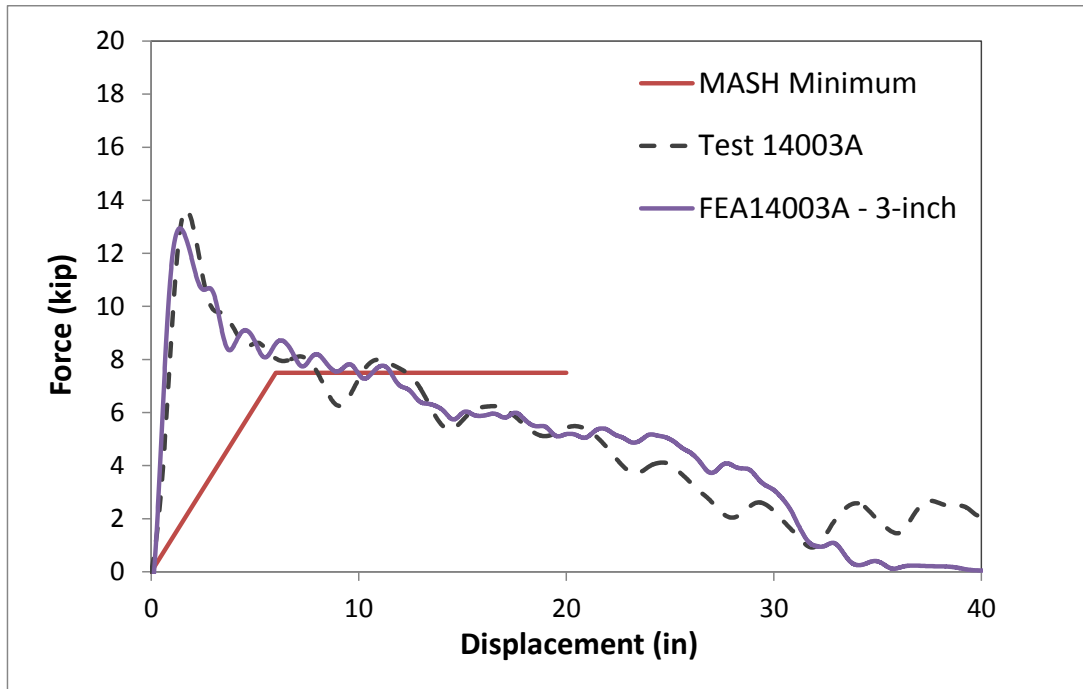


Figure 262. Force vs. deflection for soil model with 3” erosion compared to Test 14003A.

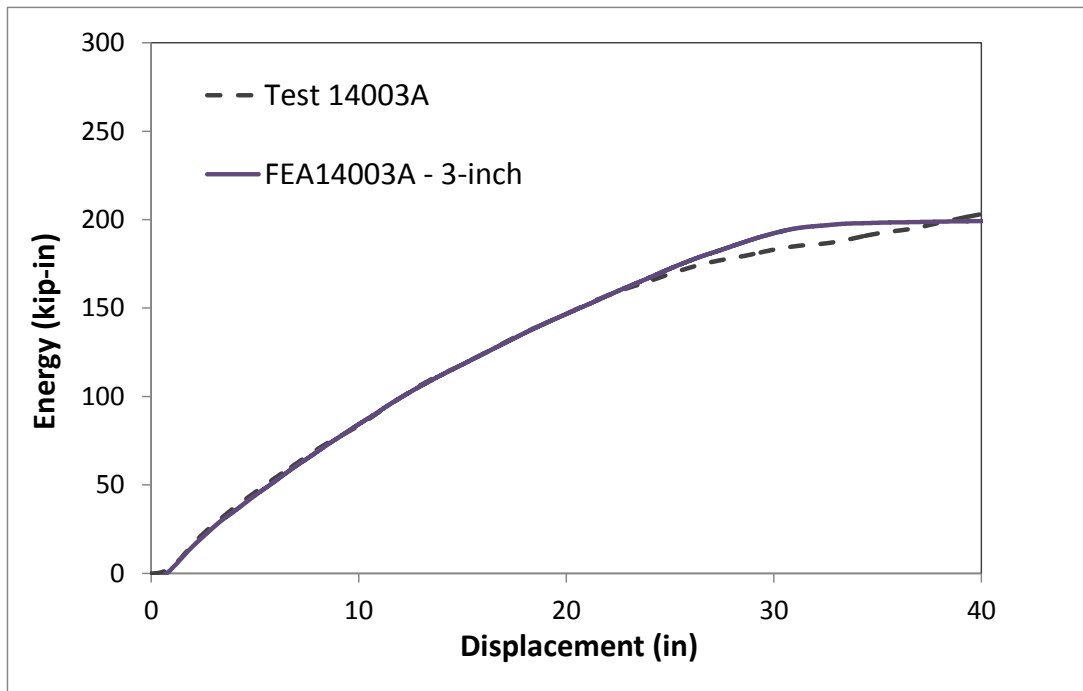


Figure 263. Energy vs. deflection for soil model with 3” erosion compared to Test 14003A.

The total energy absorbed at 12 inches displacement in the analysis was 99 kip-in, which was the same as that measured in Test 14003A; the total energy absorbed at 20 inches displacement in the analysis was 146 kip-in compared to 147 kip-in in Test 14003A; and the total energy absorbed at 40 inches displacement in the analysis was 199 kip-in compared to 203 kip-in in Test 14003A. Figure 264 shows sequential views comparing analysis results to dynamic impact test 14003A.

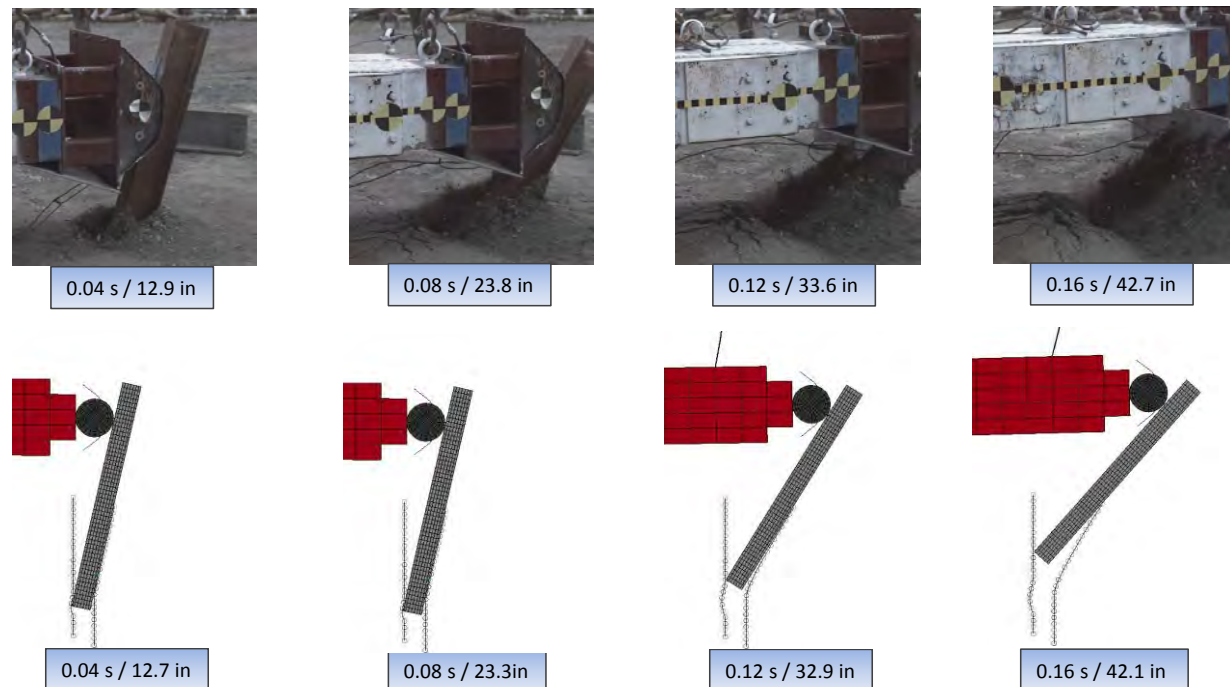


Figure 264. Sequential views of Test 14003A and FE analysis for 3-inch erosion case.

6" Erosion Case – Damage Level 1 (DL1)

The impact conditions for Test 14003C were simulated using the finite element model shown in Figure 258 with the following modifications. In the physical test, the soil depth was at grade level starting at approximately 10 inches in front of the post and tapered gradually to 2 inches below grade at the front-face of the post. The soil continued to taper to 6 inches below grade at the back-face of the post. The soil then remained at 6 inches below grade level for several feet behind the post. For this case, the soil model was set six inches below grade on the backside of the post, while the soil level on the front side of the post was kept at its original position at grade level.

Figure 265 and Figure 266 show the force vs. deflection and energy vs. deflection results, respectively, for the FE model compared to pendulum Test 14003C. The overall response of the model matches reasonably well to the physical test, except for the impulse/inertial spike at the beginning of the impact. Note that this test was performed using the repaired pendulum head which resulted in higher impulse/inertial force magnitude compared to the original head.

The total energy absorbed at 12 inches displacement in the analysis was 75.2 kip-in compared to 87.6 kip-in in Test 14003C; the total energy absorbed at 20 inches displacement in the analysis was 109 kip-in compared to 125 kip-in in Test 14003C; and the total energy absorbed at 40 inches displacement in the analysis was 124 kip-in compared to 140 kip-in in Test

14003C. Figure 267 shows sequential views comparing analysis results to dynamic impact Test14003C.

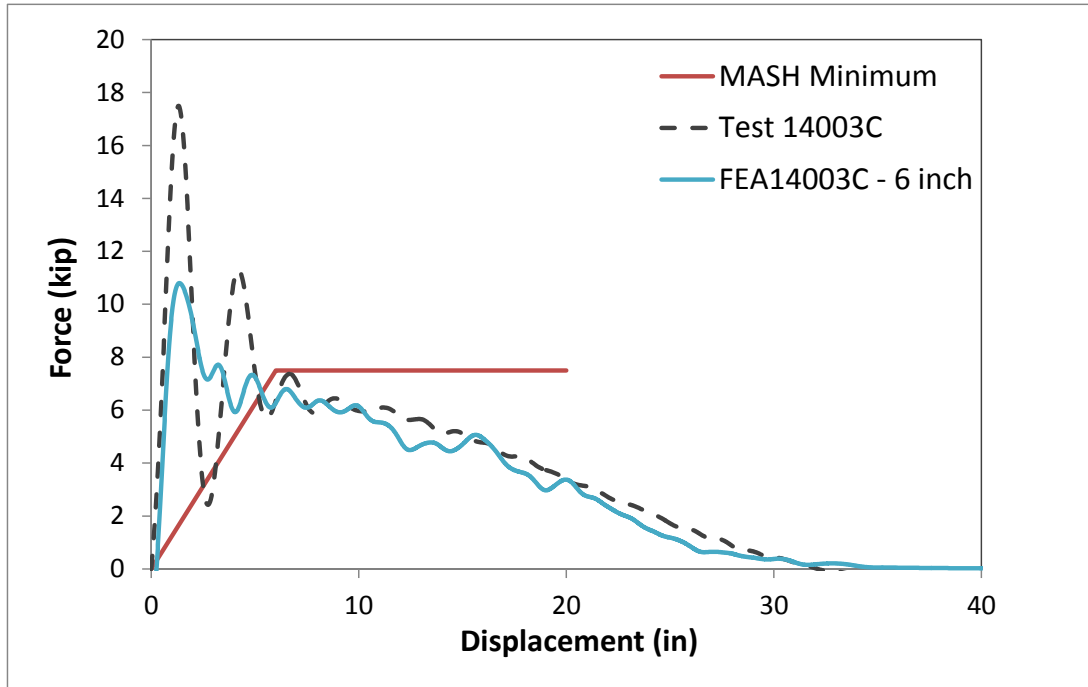


Figure 265. Force vs. deflection for soil model with 6” erosion compared to Test 14003C.

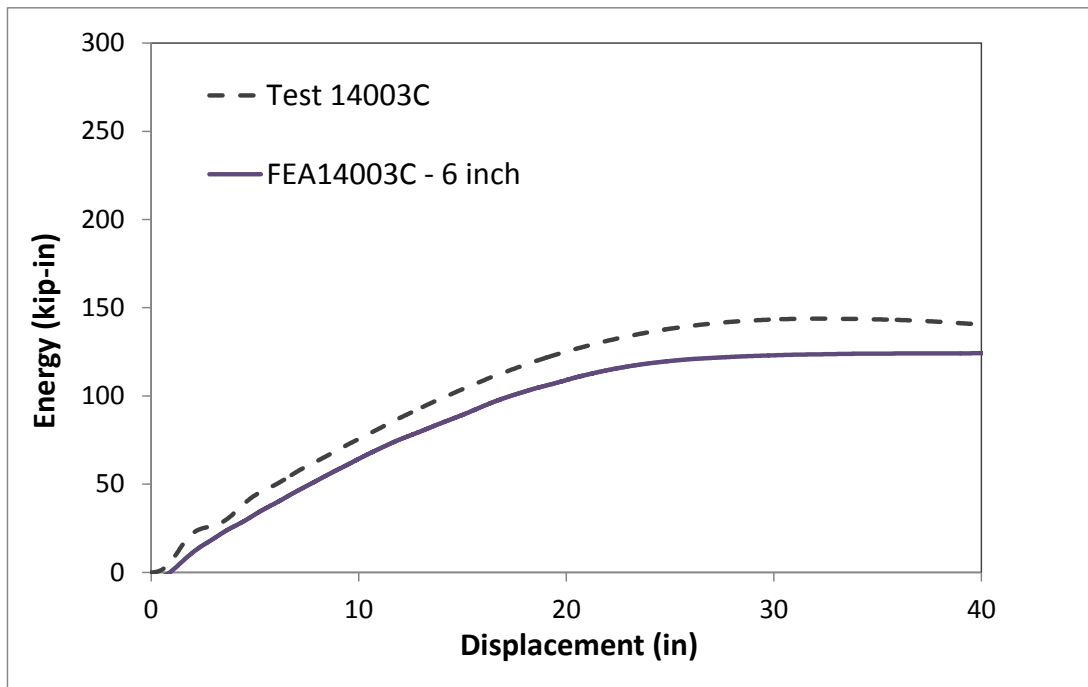


Figure 266. Energy vs. deflection for soil model with 6” erosion compared to Test 14003C.

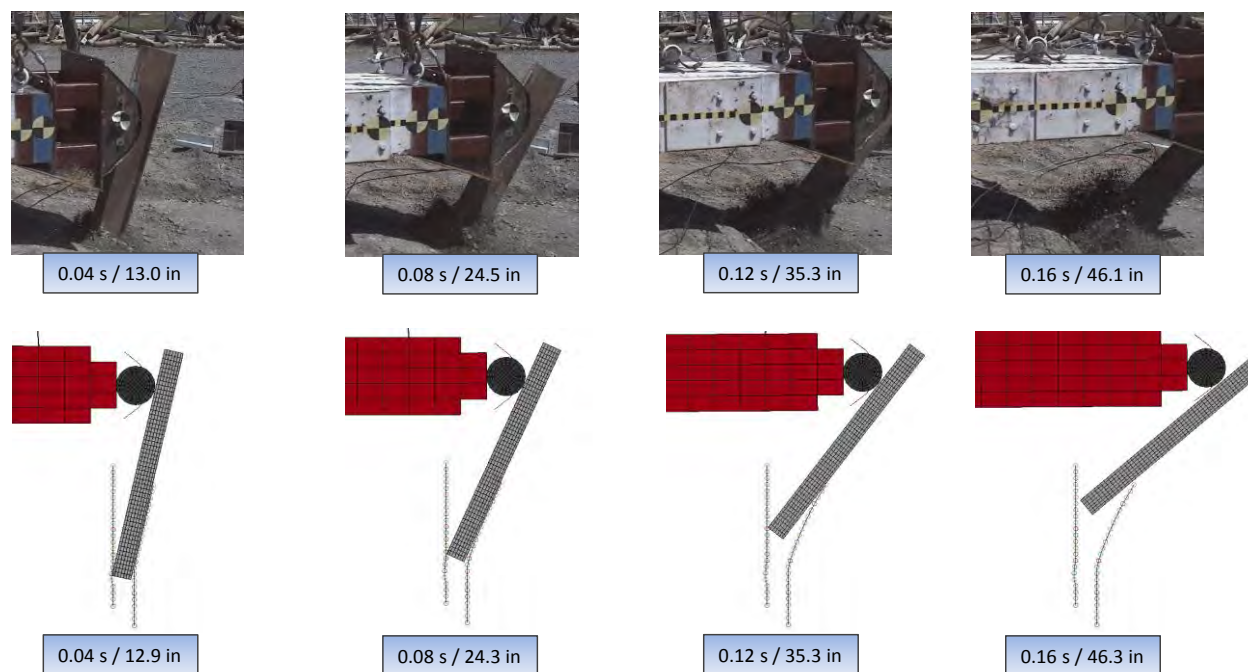


Figure 267. Sequential views of Test 14003C and FE analysis for 6-inch erosion case.

9" Erosion Case – Damage Level 2 (DL2)

The impact conditions for Test 14003D were simulated using the finite element model shown in Figure 258 with the following modifications. In the physical test, the soil depth was at grade level starting at approximately 10 inches in front of the post and tapered gradually to 3.5 inches below grade at the front-face of the post. The soil continued to taper gradually to 9 inches below grade at the back-face of the post. The soil then remained at 9 inches below grade level for several feet behind the post. For this case, the soil model was set 9 inches below grade on the backside of the post, while the soil level on the front side of the post was set at 2 inches below grade.

Figure 268 and Figure 269 show the force vs. deflection and energy vs. deflection results, respectively, for the FE model compared to pendulum Test 14003D. The overall response of the model matches reasonably well to the physical test, except for the impulse/inertial spike at the beginning of the impact. Again, this test was performed using the repaired pendulum head which tended to result in higher impulse/inertial force magnitude compared to the original head.

The total energy absorbed at 12 inches displacement in the analysis was 55.9 kip-in compared to 69.8 kip-in in Test 14003D; the total energy absorbed at 20 inches displacement in the analysis was 81.5 kip-in compared to 97.7 kip-in in Test 14003D; and the total energy absorbed at 40 inches displacement in the analysis was 93.1 kip-in compared to 122 kip-in in Test 14003D. Figure 270 shows sequential views comparing analysis results to dynamic impact Test 14003D.

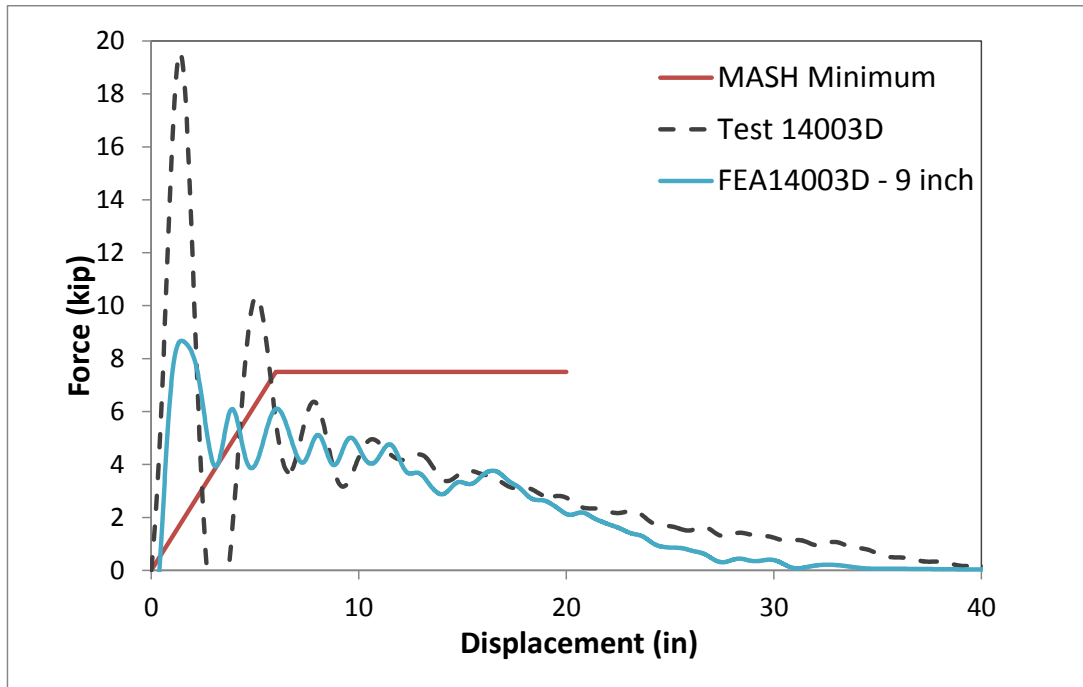


Figure 268. Force vs. deflection for soil model with 9” erosion compared to Test 14003D.

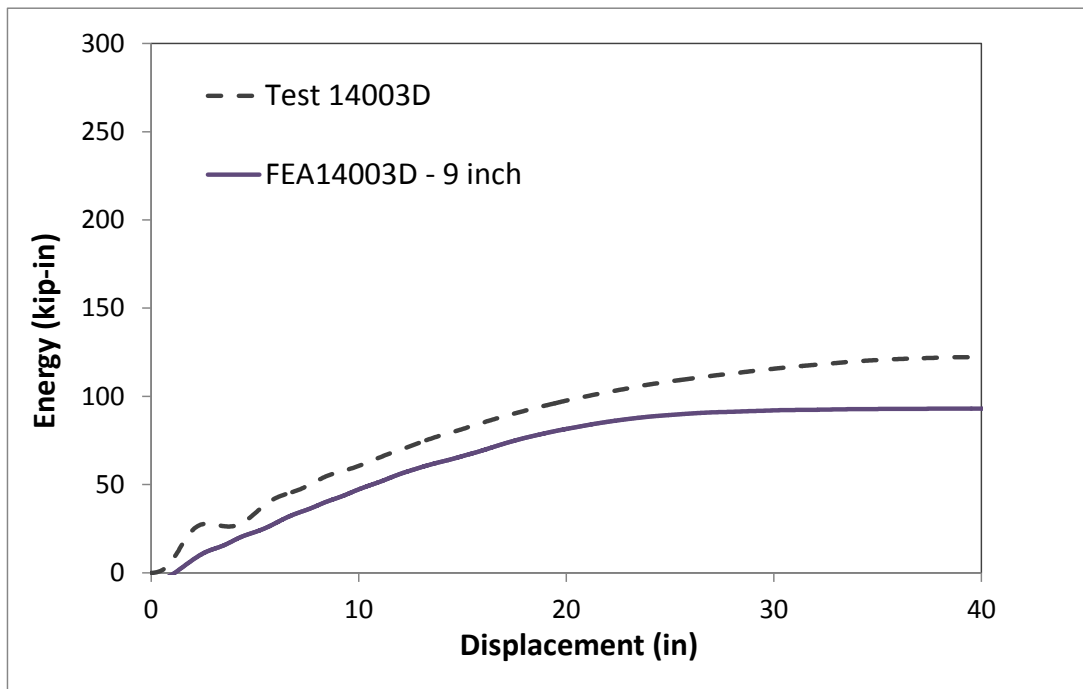


Figure 269. Energy vs. deflection for soil model with 9” erosion compared to Test 14003D.

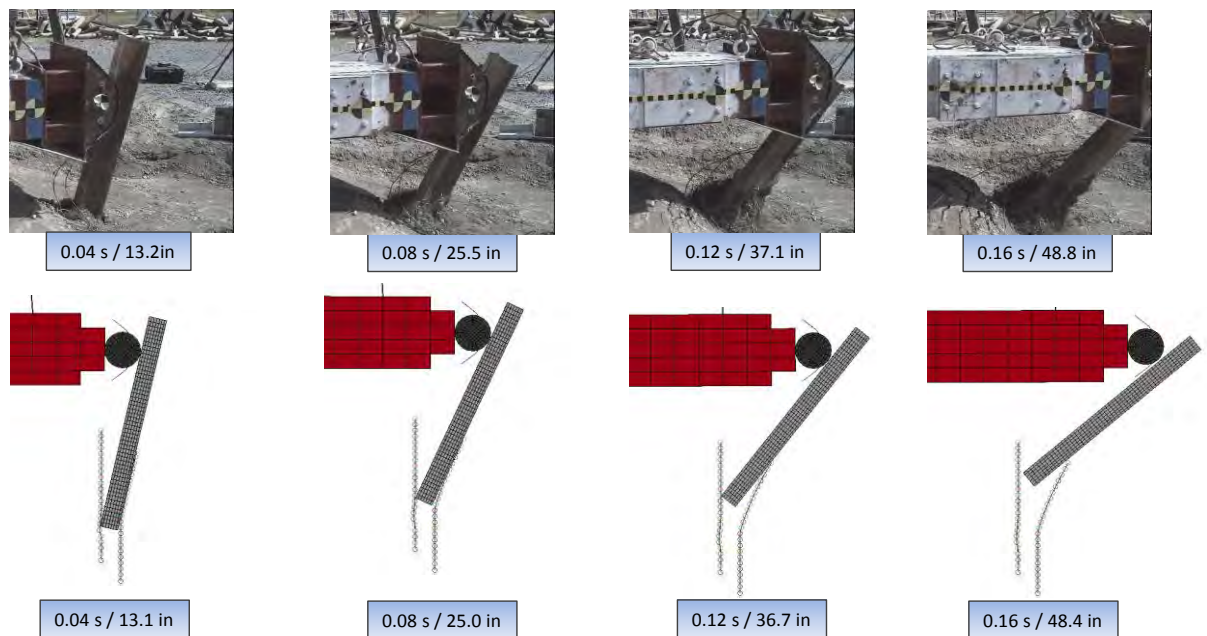


Figure 270. Sequential views of Test 14003D and FE analysis for 9-inch erosion case.

12" Erosion Case – Damage Level 3 (DL3)

The impact conditions for Test 14003E were simulated using the finite element model shown in Figure 258 with the following modifications: In the physical test, the soil depth was at grade level starting at approximately 10 inches in front of the post and tapered gradually to 4 inches below grade at the front-face of the post. The soil continued to taper gradually to 12 inches below grade at the back-face of the post. The soil then remained at 12 inches below grade level for several feet behind the post. For this case, the soil model was set at 12 inches below grade at the backside of the post, while the soil level on the front side of the post was set at 2 inches below grade.

Figure 271 and Figure 272 show the force vs. deflection and energy vs. deflection results, respectively, for the FE model compared to pendulum Test 14003E. This test was performed using the repaired pendulum head, and the overall response of the model matched reasonably well to the physical test, except for the impulse/inertial spike at the beginning of the impact.

The total energy absorbed at 12 inches displacement in the analysis was 40.4 kip-in compared to 48.8 kip-in in Test 14003E; the total energy absorbed at 20 inches displacement in the analysis was 58.6 kip-in compared to 67.6 kip-in in Test 14003E; and the total energy absorbed at 40 inches displacement in the analysis was 66.1 kip-in compared to 67.1 kip-in in Test 14003E. Figure 273 shows sequential views comparing analysis results to dynamic impact Test 14003E.

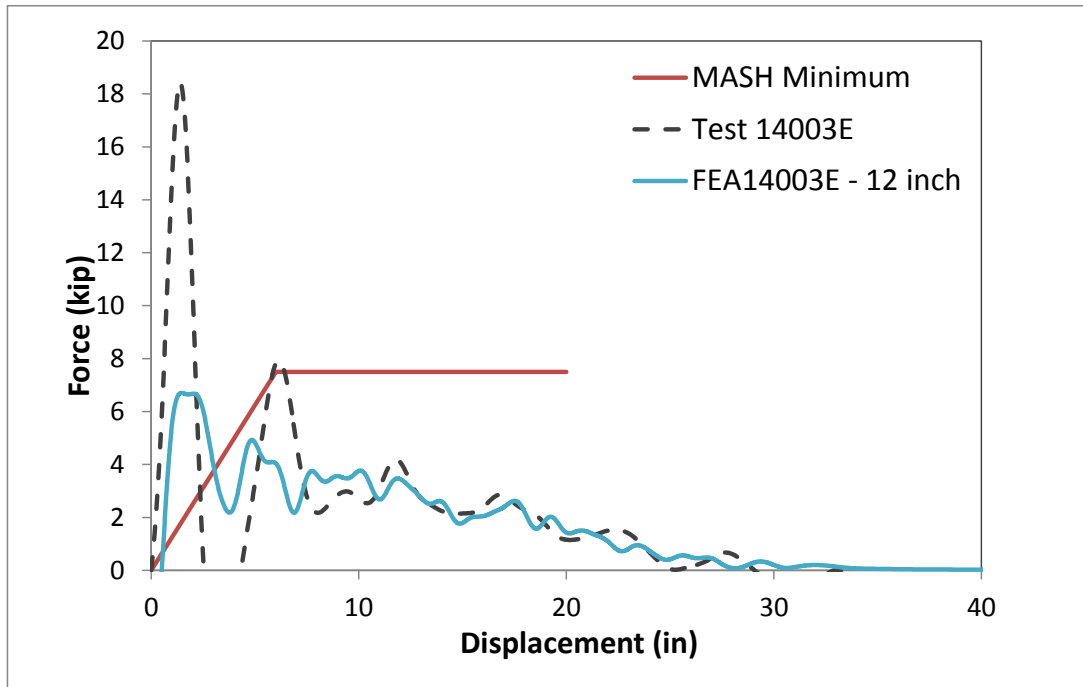


Figure 271. Force vs. deflection for soil model with 12” erosion compared to Test 14003E.

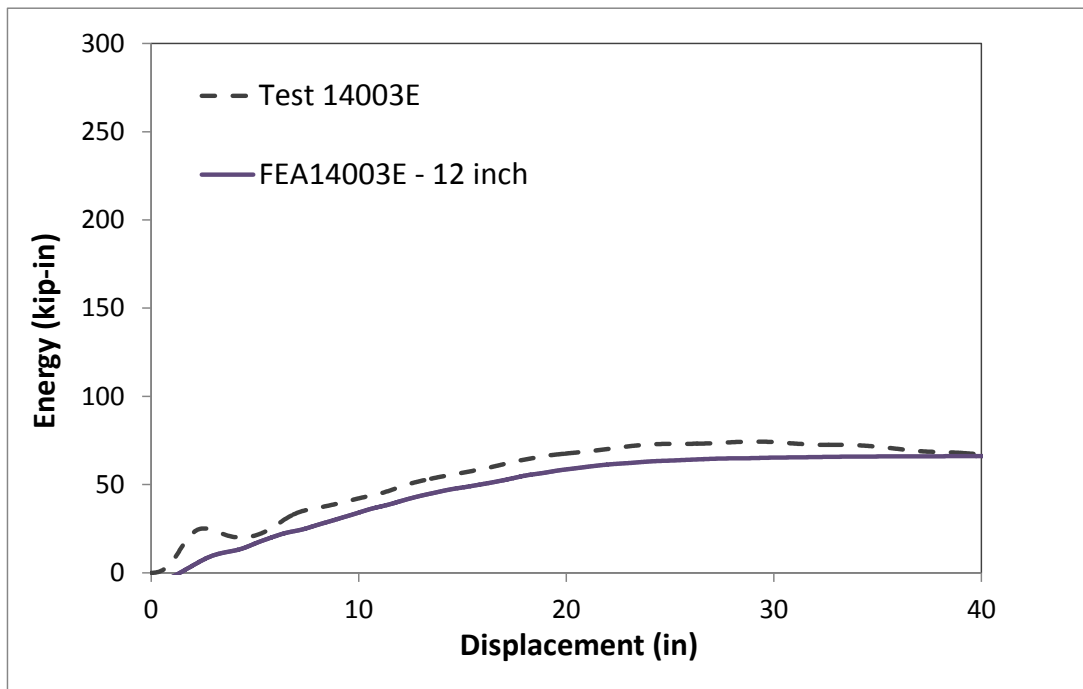


Figure 272. Energy vs. deflection for soil model with 12” erosion compared to Test 14003E.

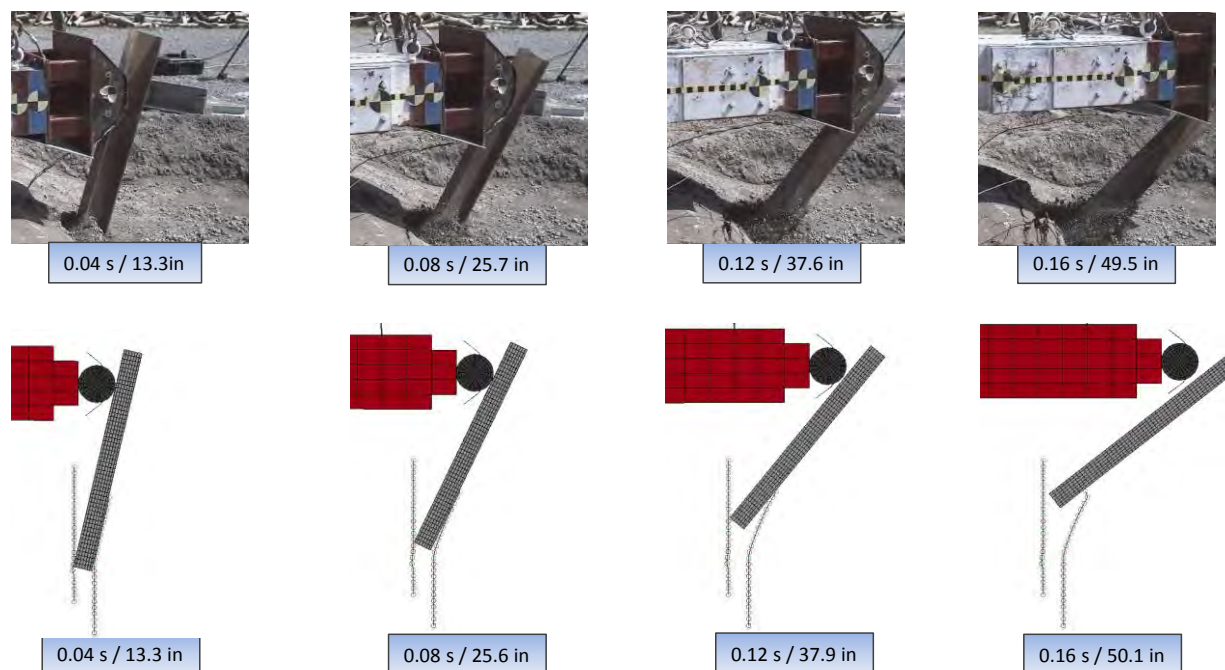


Figure 273. Sequential views of Test 14003E and FE analysis for 12-inch erosion case.

Effects of Soil Erosion on Guardrail Performance

Finite element analysis was used to evaluate the effects of soil erosion around guardrail posts on the crash performance of the G4(2W) guardrail system. The baseline (undamaged) condition for the guardrail included the DL0 guardrail post model (refer to Chapter 8); and anchor strength corresponding to the results of the end-terminal in Test 13011B with force-deflection response scaled by 1.5 to account for loading rate (refer to Chapter 9). The various levels of erosion were included in the model by simply shifting the soil-spring model in the vertical direction to the appropriate position according to erosion depth, as discussed in the preceding section.

Three levels of erosion were considered, including erosion depths of 6, 9 and 12 inches. The study included the effects of erosion at a single post and also erosion at two consecutive posts. The analysis matrix is shown in Table 70.

Table 70. Simulation matrix for evaluating soil erosion around creating low-severity guardrail deflection damage cases.

Number of Posts	Varying Erosion Depth		
	6 inches	9 inches	12 inches
Single Post	x	x	x
2 Consecutive Posts	x	x	x

Refer to Chapter 7 regarding details of the development and installation length of the G4(2W) guardrail model. The impact conditions were set to those of full-scale crash test 471470-26 and involved the 4,568-lb C2500D pickup model impacting the guardrail at 62.6 mph (100.8 km/hr) at an angle of 24.3 degrees. [Mak99] The critical impact point (i.e., regarding the maximum potential for pocketing and rail rupture) for the 6-inch erosion case was determined

using FE analysis to be 45 inches (1.16 m) upstream of the w-beam rail splice connection at Post 14. Due to time and budget constraints, the CIP for the 6-inch erosion case was used for all subsequent cases in this study. The analyses were conducted for 0.6 seconds of the impact event.

The analysis model used for the evaluations is shown in Figure 274. Posts 4 through 21 were modeled using MAT143 in LS-DYNA; while the posts located upstream of the impact zone were modeled using MAT13. The material properties corresponded to undamaged wood posts (i.e., no deterioration) for all posts in the model. Refer to Chapter 8 for more details on wood post model development and validation.

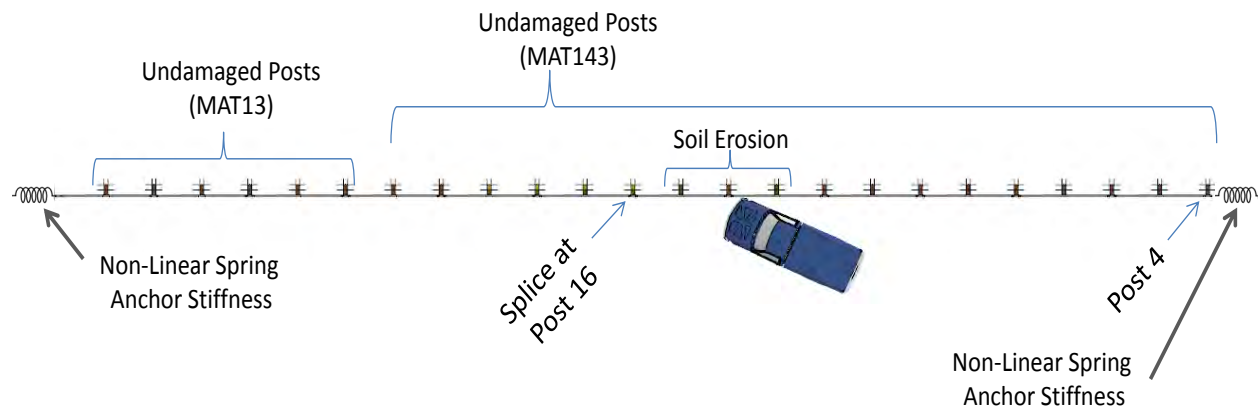


Figure 274. Analysis setup for evaluating effects of anchor strength on the performance of the G4(2W).

Soil Erosion at a Single Post

The following is an evaluation of the G4(2W) guardrail with various levels of soil erosion at a single post location. Sequential views of the FE analysis results for each case are provided in Appendix N. Table 71 provides a summary of barrier damage from the analyses related to rail deflections, anchor movement and splice damage. This information is also presented graphically in Figures 275 and 276. The maximum lateral rail deflection was 32 inches for the baseline case and increased to 35.5 inches at 12 inches of erosion (i.e., 9.2 percent higher than the baseline case).

Regarding the “location of maximum deflection” in Table 71, a negative number indicates that the maximum deflection occurred upstream of the w-beam splice located at Post 16, while a positive number indicates that maximum deflection occurred downstream of the splice. For the 6-inch erosion case, the maximum lateral deflection occurred at 29 inches upstream of the splice connection at Post 16. For the 9-inch and 12-inch cases the maximum deflection occurred exactly at Post 16. Figure 276 shows the longitudinal displacement of the upstream and downstream ends of the w-beam at the anchor locations. In all erosion cases, the loading on the upstream anchor was of similar magnitude as the baseline case. The longitudinal rail deflections at the downstream anchor increased slightly with each level of erosion. In general, higher lateral deflections in the impact region were associated with higher anchor deflections.

Table 71. Summary of barrier damage evaluation from analyses of undamaged G4(2W) guardrail with various levels of soil erosion at a single post.

Event	Varying Erosion Depth at 1 Post			
	Baseline	6 inches	9 inches	12 inches
Maximum Rail Deflection (in)	32.0	32.5	34.4	35.5
Location of Max Defl. (in) (Relative to Post 16)	-14.8	-28.9	0.0	0.0
Rail Deflection at Post 13 (in)	1.8	1.3	1.7	2.5
Rail Deflection at Post 14 (in)	13.1	11.3	13.9	15.1
Rail Deflection at Post 15 (in)	27.8	27.9	28.1	28.9
Rail Deflection at Post 16 (in)	31.1	31.3	34.4	35.5
Rail Deflection at Post 17 (in)	17.5	22.7	25.5	27.1
Rail Deflection at Post 18 (in)	1.2	1.7	4.6	5.8
Rail Deflection at Post 19 (in)	0.0	0.0	0.0	0.0
Upstream Anchor Deflection (in)	1.4	1.5	1.5	1.7
Downstream Anchor Deflection (in)	0.9	1.1	1.1	1.1
Maximum Strain in splice	0.84	1.05	1.04	1.12

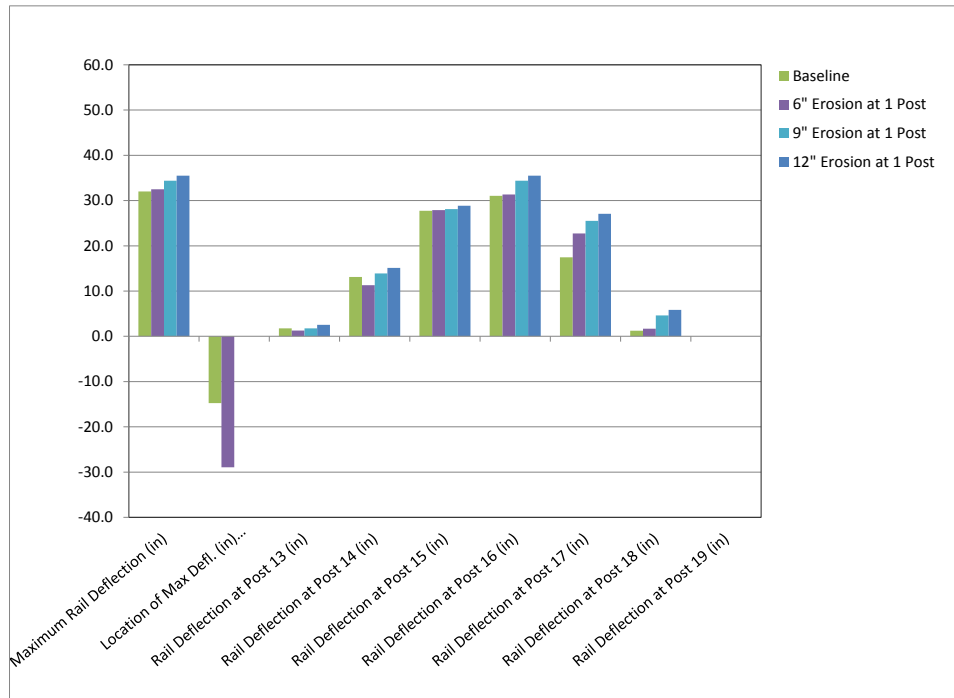


Figure 275. Summary of barrier damage evaluation from analyses of undamaged G4(2W) guardrail with various levels of soil erosion at a single post.

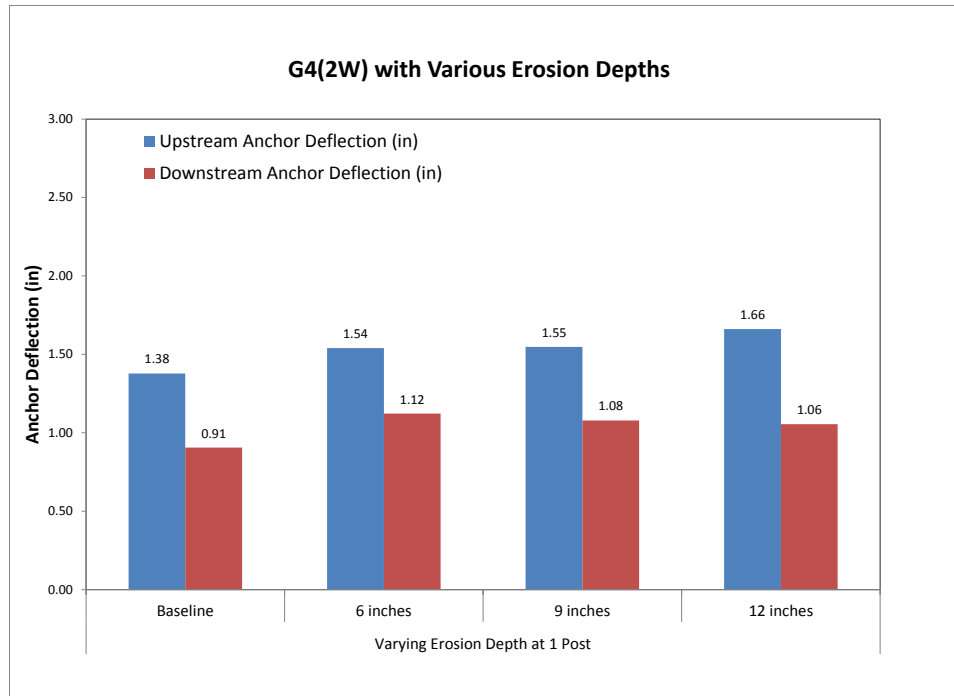


Figure 276. Summary of anchor displacement at rail height from analyses of undamaged G4(2W) guardrail with various levels of soil erosion at a single post.

A summary of occupant risk measures computed from the acceleration and angular rate time-histories at the vehicle's center of gravity is provided in Table 72. This data is also presented graphically in Figures 277 through 279. The results indicated that increased levels of erosion at a single post did not significantly affect occupant risk; and, in general, the values were slightly lower for the erosion cases. A summary of the maximum effective plastic strains around the splice-bolt holes in the w-beam for each analysis case is shown in Figure 280. The results indicated that the potential for splice rupture increased as erosion levels increased. For example, the plastic strains at the splice-bolt holes reached magnitudes of 1.05, 1.04, and 1.12 for cases of 6, 9 and 12 inches of erosion, respectively. The values computed from the 9-inch and 12-inch analysis case likely under-predict the actual strains, since the critical impact point was not achieved.

Table 72. Summary of occupant risk measures from evaluation of undamaged G4(2W) guardrail with various levels of soil erosion at a single post.

Occupant Risk Factors		Erosion at Single Post			
		Varying Erosion Depth			
		Baseline	6 inches	9 inches	12 inches
Occupant Impact Velocity (m/s)	x-direction	5.2	4.8	4.1	3.6
	y-direction	5.3	5.2	5.3	5.3
	at time	(0.1519 sec)	(0.1473 sec)	(0.1483 sec)	(0.1427 sec)
THIV (m/s)		7.0 (0.1471 sec)	6.9 (0.1424 sec)	6.7 (0.1432 sec)	6.5 (0.1428 sec)
Ridedown Acceleration (g's)	x-direction	10.3 (0.1519 - 0.1619 sec)	10.6 (0.2179 - 0.2279 sec)	10.4 (0.2734 - 0.2834 sec)	10.1 (0.2900 - 0.3000 sec)
	y-direction	10.7 (0.2198 - 0.2298 sec)	8.6 (0.1488 - 0.1588 sec)	8.2 (0.2164 - 0.22264 sec)	9.2 (0.2187 - 0.2287 sec)
PHD (g's)		13.7 (0.2003 - 0.2103 sec)	13.5 (0.2174 - 0.2274 sec)	12.3 (0.2739 - 0.2839 sec)	12.7 (0.2947 - 0.3047 sec)
ASI		0.93 (0.1219 - 0.1719 sec)	0.84 (0.1812 - 0.2312 sec)	0.78 (0.1951 - 0.12451sec)	0.79 (0.2657 - 0.3157 sec)
Max 50-ms moving avg. acc. (g's)	x-direction	7.6 (0.1216 - 0.1716 sec)	5.6 (0.1798 - 0.2298 sec)	5.5 (0.1589 - 0.2089 sec)	6.0 (0.1540 - 0.2040 sec)
	y-direction	6.5 (0.1976 - 0.2476 sec)	6.6 (0.1099 - 0.1599 sec)	6.4 (0.1955 - 0.2455 sec)	6.1 (0.2675 - 0.3175 sec)
	z-direction	2.4 (0.3344 - 0.3844 sec)	2.2 (0.2320 - 0.2820 sec)	3.2 (0.3164 - 0.3664 sec)	3.0 (0.3186 - 0.3686 sec)

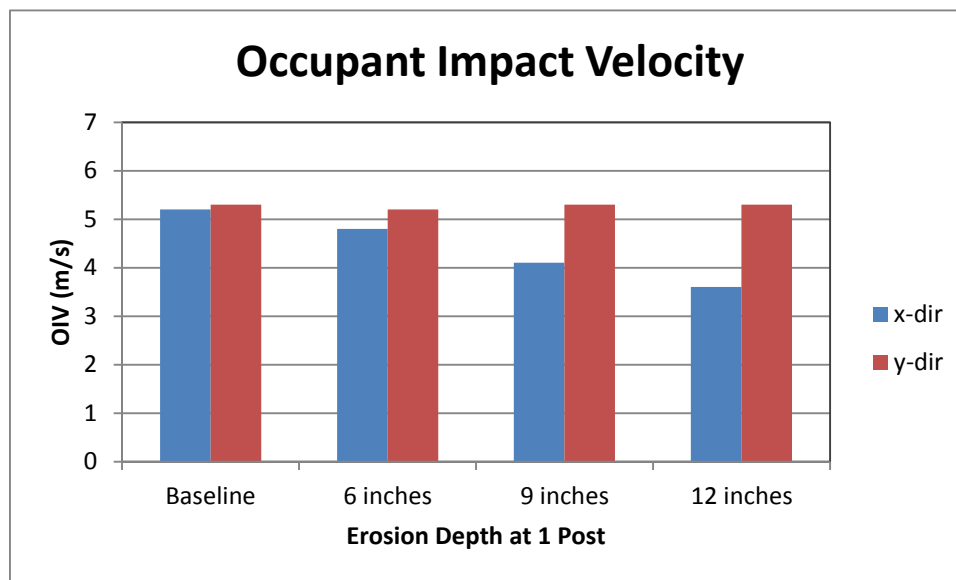


Figure 277. Summary of occupant impact velocities for undamaged G4(2W) guardrail with various levels of soil erosion at a single post.

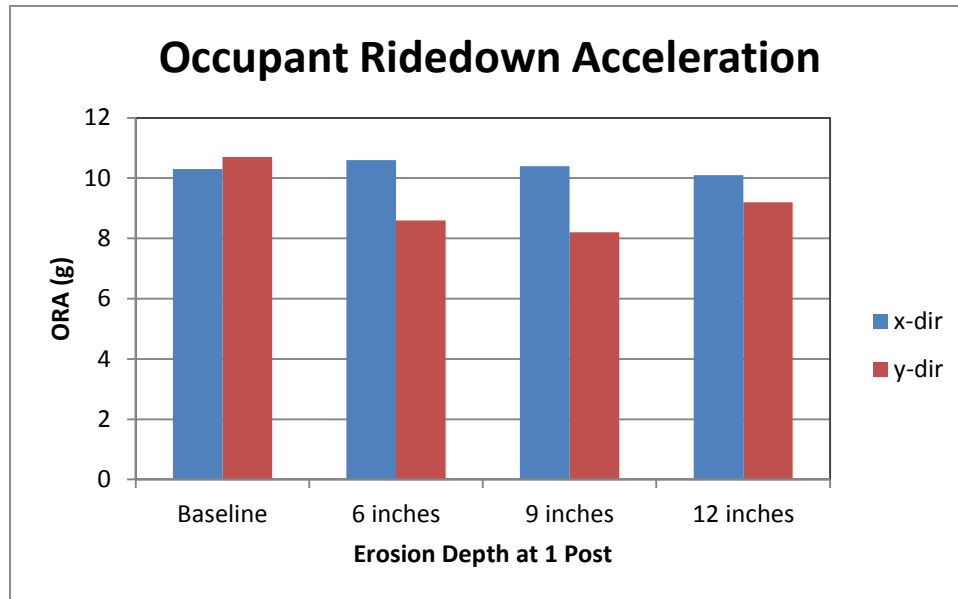


Figure 278. Summary of maximum occupant ridedown accelerations for undamaged G4(2W) guardrail with various levels of soil erosion at a single post.

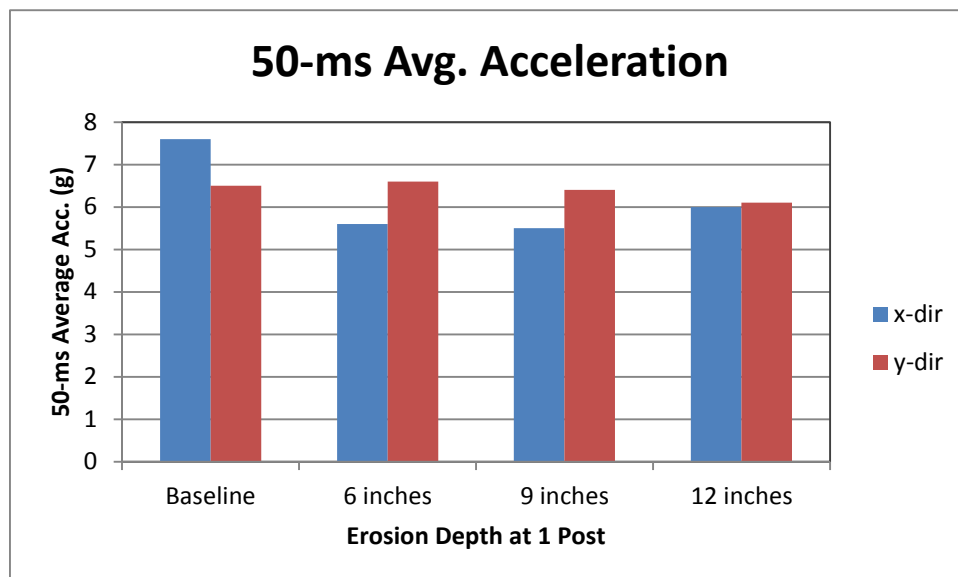


Figure 279. Summary of maximum 50-ms running average accelerations for undamaged G4(2W) guardrail with various levels of soil erosion at a single post.

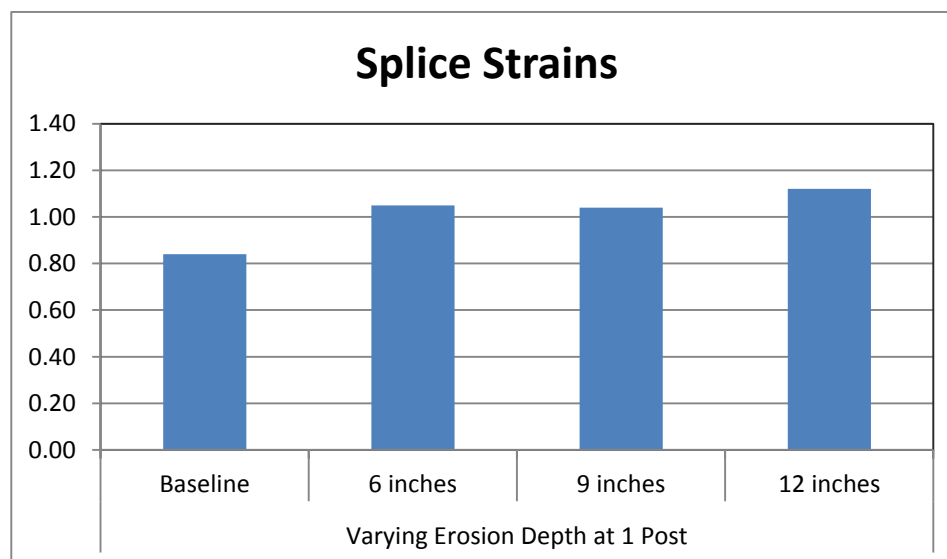


Figure 280. Summary of maximum effective plastic strains occurring at the splice-bolt locations at Post 16.

Soil Erosion at Two Consecutive Posts

The following is an evaluation of the G4(2W) guardrail with various levels of soil erosion at two consecutive post locations. Sequential views of the FE analysis results for each case are provided in Appendix O. Table 73 provides a summary of barrier damage from the analyses related to rail deflections, anchor movement and splice damage. This information is also presented graphically in Figures 281 and 282. The maximum lateral rail deflection was 32 inches for the baseline case and increased to 40.1 inches at 12 inches of erosion (i.e., 25.3 percent higher than baseline case).

As shown in Table 73, the maximum lateral deflection generally occurred within 34 inches upstream of the splice connection at Post 16. Thus, the impact conditions were considered to correspond to critical impact conditions for the various cases. Figure 282 shows the longitudinal displacement of the upstream and downstream ends of the w-beam at the anchor locations. In all erosion cases, the loading on the upstream anchor was of similar magnitude as the baseline case; while the longitudinal rail deflections at the downstream anchor increased slightly with each level of erosion. In general, higher lateral deflections in the impact region were associated with higher anchor deflections.

Table 73. Summary of barrier damage evaluation from analyses of undamaged G4(2W) guardrail with various levels of soil erosion at two consecutive posts.

Event	Varying Erosion Depth at 2 Posts			
	Baseline	6 inches	9 inches	12 inches
Maximum Rail Deflection (in)	32.0	35.5	37.4	40.1
Location of Max Defl. (in) (Relative to Post 16)	-14.8	-28.1	-34.4	-21.9
Rail Deflection at Post 13 (in)	1.8	4.4	7.1	10.1
Rail Deflection at Post 14 (in)	13.1	21.7	21.7	25.0
Rail Deflection at Post 15 (in)	27.8	33.7	35.2	37.1
Rail Deflection at Post 16 (in)	31.1	34.9	36.4	39.8
Rail Deflection at Post 17 (in)	17.5	25.4	20.2	26.1
Rail Deflection at Post 18 (in)	1.2	4.1	1.7	4.3
Rail Deflection at Post 19 (in)	0.0	0.0	0.0	0.0
Upstream Anchor Deflection (in)	1.4	1.7	1.7	1.8
Downstream Anchor Deflection (in)	0.9	1.1	1.1	1.1
Maximum Strain in splice	0.84	1.07	1.16	1.22

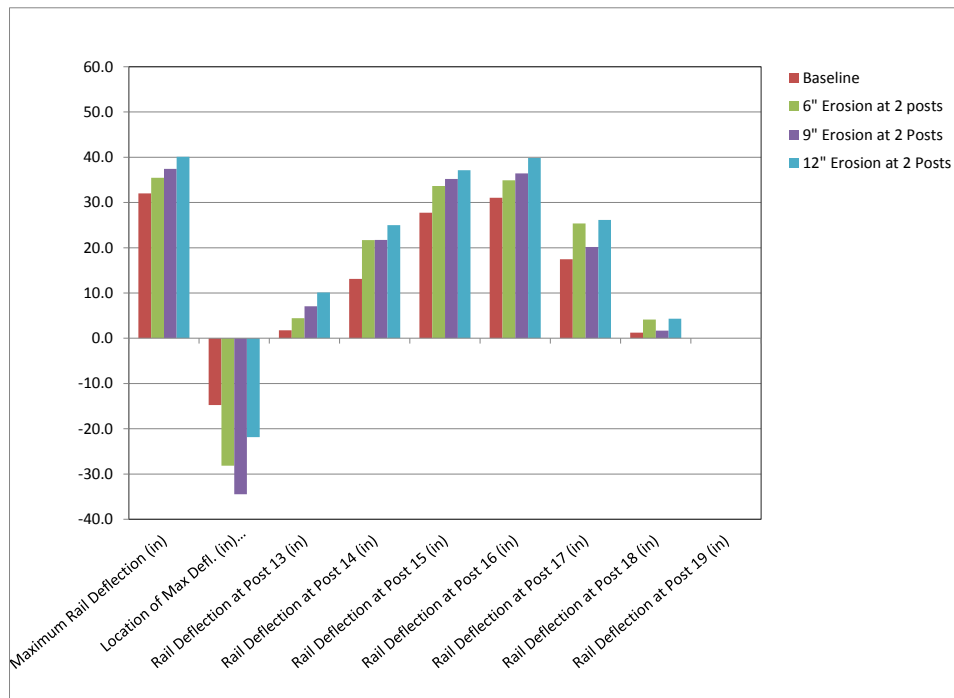


Figure 281. Summary of barrier damage evaluation from analyses of undamaged G4(2W) guardrail with various levels of soil erosion at two consecutive posts.

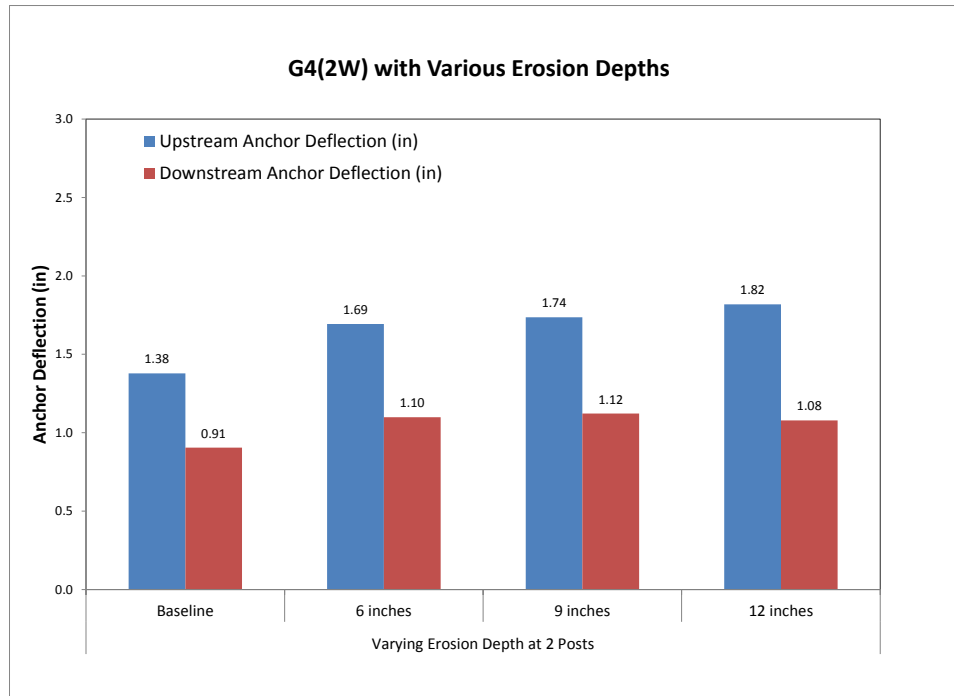


Figure 282. Summary of anchor displacement at rail height from analyses of undamaged G4(2W) guardrail with various levels of soil erosion at two consecutive posts.

A summary of occupant risk measures computed from the acceleration and angular rate time-histories at the vehicle's center of gravity is provided in Table 74. This data is also presented graphically in Figures 283 through 285. The results indicate that increased levels of erosion at two consecutive posts do not significantly affect occupant risk; and, in general, the values were again slightly lower for the erosion cases.

A summary of the maximum effective plastic strains around the splice-bolt holes in the w-beam for each analysis case is shown in Figure 286. The results indicated that the potential for splice rupture increased as erosion levels increased. For example, the plastic strains at the splice-bolt holes reached magnitudes of 1.07, 1.16, and 1.22 for cases of 6, 9 and 12 inches of erosion, respectively. As was discussed in Chapter 11, strains of this magnitude for steel are generally associated with a high potential for material failure. In these cases, however, the strains are restricted to a very localized area at the end of the splice-bolt holes and are compressive (i.e., caused from the bearing load between the splice-bolt and the edge of the w-beam hole). Thus, the potential for tear initiation is much lower than the same magnitude of strain in a tensile region of the w-beam (e.g., on the lateral edge of the upper or lower edge of the splice-bolt holes).

Table 74. Summary of occupant risk measures from evaluation of undamaged G4(2W) guardrail with various levels of soil erosion at two consecutive posts.

Occupant Risk Factors		Erosion at 2 Posts			
		Varying Erosion Depth			
		Baseline	6 inches	9 inches	12 inches
Occupant Impact Velocity (m/s)	x-direction	5.2	4.9	4.8	4.4
	y-direction	5.3	5.4	5.6	5.4
	at time	(0.1519 sec)	(0.1541 sec)	(0.1580 sec)	(0.1625 sec)
THIV (m/s)		7.0 (0.1471 sec)	7.2 (0.1493 sec)	7.1 (0.1532 sec)	6.8 (0.1579 sec)
Ridedown Acceleration (g's)	x-direction	10.3 (0.1519 - 0.1619 sec)	6.9 (0.1789 - 0.1889 sec)	9.7 (0.2713 - 0.2813 sec)	7.0 (0.3036 - 0.3136 sec)
	y-direction	10.7 (0.2198 - 0.2298 sec)	8.7 (0.2223 - 0.2323 sec)	9.2 (0.2333 - 0.2433 sec)	8.5 (0.2179 - 0.2279 sec)
PHD (g's)		13.7 (0.2003 - 0.2103 sec)	10.9 (0.2223 - 0.2323 sec)	12.4 (0.3209 - 0.3309 sec)	10.2 (0.3004 - 0.3104 sec)
ASI		0.93 (0.1219 - 0.1719 sec)	0.75 (0.0990 - 0.1490 sec)	0.8 (0.1244 - 0.1744 sec)	0.81 (0.1065 - 0.1565 sec)
Max 50-ms moving avg. acc. (g's)	x-direction	7.6 (0.1216 - 0.1716 sec)	4.8 (0.0980 - 0.1480 sec)	5.1 (0.1741 - 0.2241 sec)	4.8 (0.1069 - 0.1569 sec)
	y-direction	6.5 (0.1976 - 0.2476 sec)	6.0 (0.1166 - 0.1666 sec)	6.4 (0.1244 - 0.1744 sec)	6.4 (0.1230 - 0.1730 sec)
	z-direction	2.4 (0.3344 - 0.3844 sec)	2.0 (0.3460 - 0.3960 sec)	4.2 (0.3467 - 0.3967 sec)	3.8 (0.3425 - 0.3925 sec)

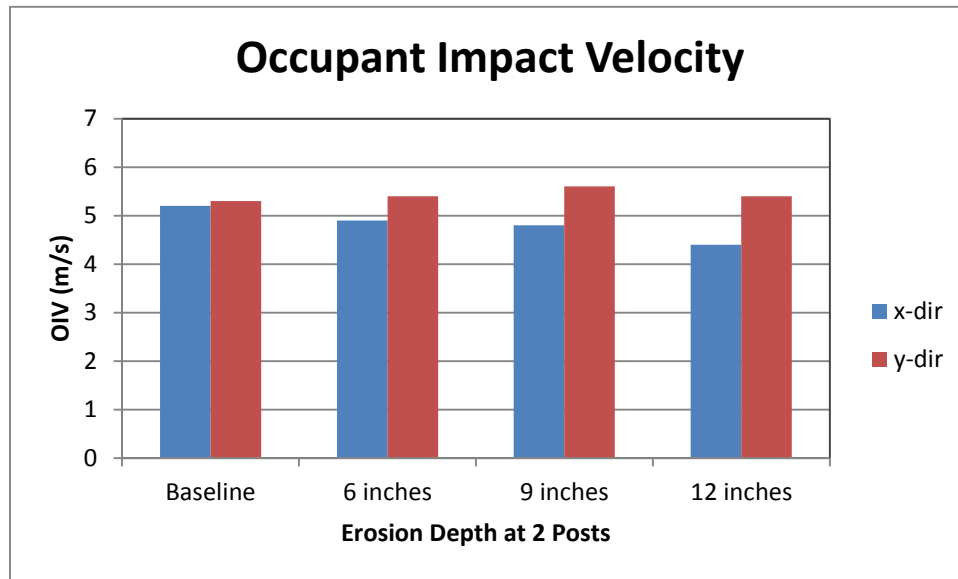


Figure 283. Summary of occupant impact velocities for undamaged G4(2W) guardrail with various levels of soil erosion at two consecutive posts.

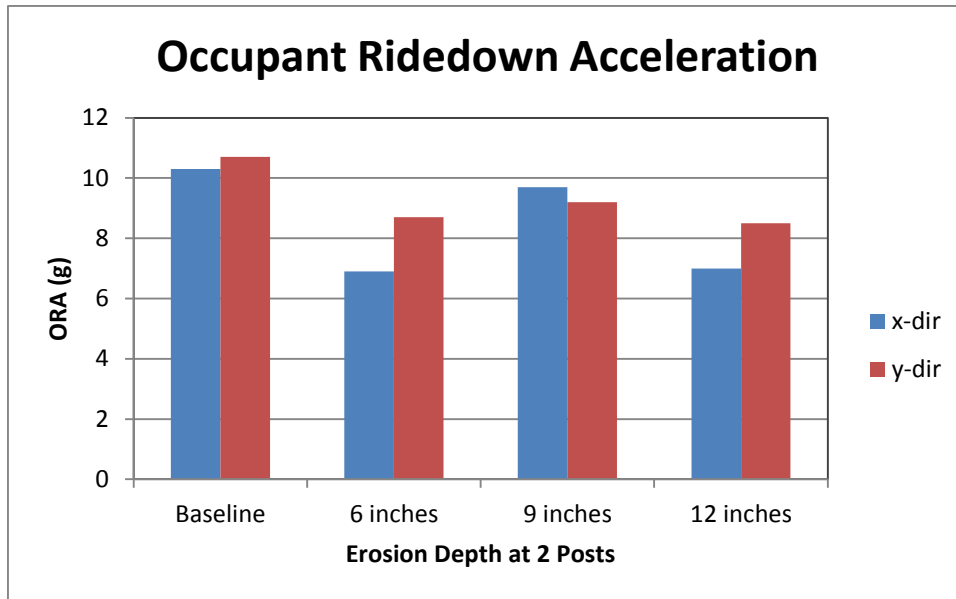


Figure 284. Summary of maximum occupant ridedown accelerations for undamaged G4(2W) guardrail with various levels of soil erosion at two consecutive posts.

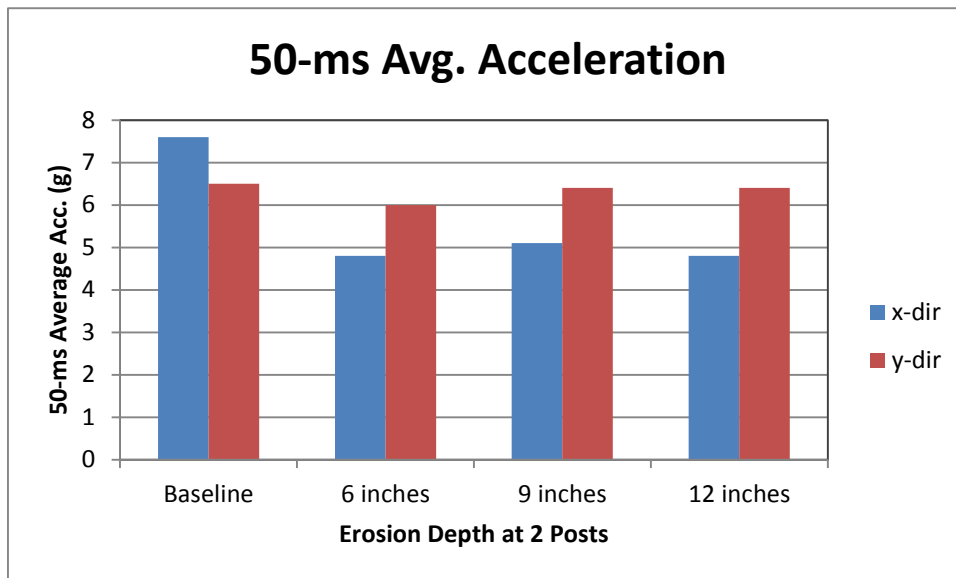


Figure 285. Summary of maximum 50-ms running average accelerations for undamaged G4(2W) guardrail with various levels of soil erosion at two consecutive posts.

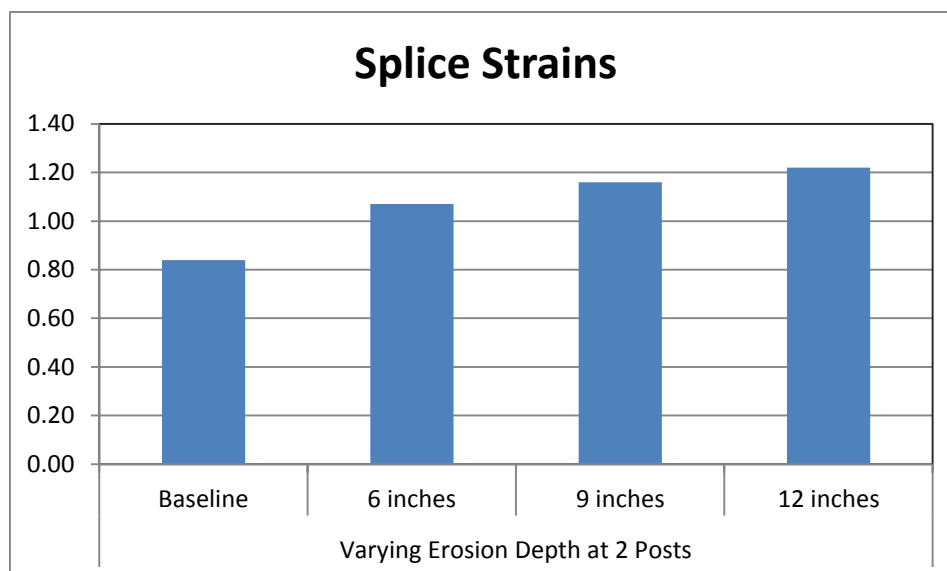


Figure 286. Summary of maximum effective plastic strains occurring at the splice-bolt locations at Post 16.

Summary and Discussion

The purpose of this study was to quantify the effects of various levels of soil erosion around guardrail posts on system performance. The study involved: (1) performing pendulum impact tests to measure the force-deflection response of the post-soil system for various levels of “manufactured” soil erosion; (2) developing finite element models for the various soil erosion cases and calibrating/validating the models using the test data; and (3) using FEA to quantify the effects of the various degrees of soil erosion on the crash performance of the G4(2W) guardrail system under Report 350 Test 3-11 impact conditions.

The pendulum tests involved a W6x16 structural steel post embedded 36 inches in the soil. The W6x16 post was used because of its rigidity, so that the energy absorption measured in the test would be attributable only to soil deformation. The erosion condition was manufactured by removing a layer of soil behind and on the sides of the posts.

Four erosion conditions were evaluated in the physical test program: 3 inches, 6 inches, 9 inches and 12 inches of erosion. The impact conditions involved a 2,372-lb pendulum impacting the post at 22 inches above grade at an impact speed of 20 mph. The posts were oriented in the strong direction. The results showed that the energy capacity of the post-soil system reduced as a linear function of erosion depth, in which:

$$\text{Energy Capacity (kip-in)} = 178.33 - 8.04 * (\text{erosion depth})$$

Where the constant, 178.33 kip-in corresponds to the energy capacity of the post at an embedment depth of 36 inches with no erosion (i.e., consistent with the post embedment depth used in full-scale crash test 471470-26 which has been used as the baseline system throughout this study.)

Finite element models for the various soil erosion cases were then developed and validated based on comparison to the physical tests. In each soil-erosion case, the characterization of the soil model was exactly the same; that is, the same model was used in each case. The various levels of erosion were modeled by simply translating the soil-spring model to the appropriate erosion depth.

The finite element model of the standard G4(2W) guardrail system was then used to evaluate the effects of soil erosion around guardrail posts on the crash performance of the guardrail system. The impact conditions were set to those of full-scale crash test 471470-26 and involved the 4,568-lb C2500D pickup model impacting the guardrail at 62.6 mph (100.8 km/hr) at an angle of 24.3 degrees.[*Mak99*] The critical impact for the 6-inch erosion case was determined using FE analysis to be 45 inches (1.16 m) upstream of the w-beam rail splice connection at post 14. Due to time and budget constraints, the CIP for the 6-inch erosion case was used for all subsequent cases.

A total of six analysis cases were evaluated. These included two erosion scenarios (i.e., erosion at a single post and erosion at two consecutive posts) with three erosion depths (i.e., 6, 9 and 12 inches). The results indicated that rail deflection increased as erosion depth increased. For the baseline case (i.e., no erosion) the maximum rail deflection was 32 inches. For the case of erosion at a single post, the lateral deflection increased 7.5 percent at 9 inches erosion and 11 percent at 12 inches erosion. For the case of erosion at two posts, with erosion depths of 6, 9, and 12 inches the lateral deflection increased 11 percent, 17 percent, and 25 percent, respectively.

The analyses further indicated that the erosion does not significantly affect occupant risk measures, and in general the values were slightly lower for the erosion cases. The most critical effect of erosion was related to the potential for rupture of a rail-splice connection. For the case of erosion at a single post, the three levels of erosion (i.e., 6, 9 and 12 inches) resulted in an increase of 25 percent, 24 percent, and 33 percent increase in plastic strain levels, respectively, relative to the baseline case. Given that the G4(2W) is near its capacity under these impact conditions, the effective increase in plastic strain in the splice, indicates that the potential for rail rupture is relatively high for all cases, but particularly for the 12-inch erosion case.

For the case of erosion at two consecutive posts, the three levels of erosion resulted in an increase of 27 percent, 38 percent, and 45 percent increase in plastic strain levels, respectively, relative to the baseline case. Again, the effective increase in plastic strain indicated that the potential for rail rupture was relatively high for all three erosion levels, but particularly so for the 9-inch and 12-inch erosion cases.

Recommendations

As a result of this study, the research team recommends that the repair threshold for soil erosion at a single post include depths 9 inches or greater measured at the backside of the posts. For erosion depths ranging from 9 to 12 inches, the recommended priority for repair is medium. For erosion depths of 12 inches or greater, the relative priority for repair is high, based on potential for excessive pocketing and increased potential for rail rupture.

For soil erosion at two consecutive posts, the research team recommends that the repair threshold include depths 4 inches or greater measured at the backside of the posts. For erosion depths ranging from 4 to 6 inches, the recommended priority for repair is medium. The lower bound for the medium priority was based on engineering judgment, since the analysis matrix did

not include erosion depths less than 6 inches. The upper bound was based on the high magnitude of strain in the splice-bolt holes for the 6-inch erosion analysis case, which was considered borderline regarding high potential for rail rupture. For erosion depths of 6 inches or greater, the relative priority for repair is considered high, based on potential for excessive pocketing and increased potential for rail rupture. A summary of the recommendations regarding soil erosion for the G4(2W) guardrail are presented in Table 75.

Table 75. Recommendations for soil erosion around guardrail posts for the G4(2W).

Damage Mode	Repair Threshold	Relative Priority
Erosion at a Single Post	Erosion depth \geq 12 inches (erosion depth is measured at the back-face of the posts)	High
	Erosion depth $>$ 9 inches and $<$ 12 inches	Medium
Erosion at Two or More Consecutive Posts	Erosion depth \geq 6 inches (erosion depth is measured at the back-face of the posts)	High
	Erosion depth $>$ 4 inches and $<$ 6 inches	Medium

CHAPTER 13 – ANCHOR STRENGTH QUANTIFIED IN TERMS OF ANCHOR DAMAGE

In Chapter 9 the performance of the G4(2W) guardrail system was quantified in terms of anchor strength. In this chapter, anchor strength will be defined in terms of various anchor damage modes and levels of damage. Combining the results of Chapter 9 with the results presented in this chapter will provide a means of correlating “measurable” damage modes directly to a corresponding level of degradation in guardrail performance. Recall from Chapter 3 that essentially all end-terminals, with the exception of the buried-in-backslope end-terminal, share the same basic features and components which function to ensure that the guardrail maintains proper tension during impacts. The basic features of these systems were presented earlier and will not be repeated here.

The focus of this chapter is on the development of procedures for assessing damage modes that directly affect the anchor strength of end-terminals. *NCHRP Report 656* provides assessment criteria for generic end-terminals based on a “check list for repairing energy absorbing end terminals” developed by the Ohio Department of Transportation.[*Gabler10*] The assessment criteria in Report 656 covered damaged end-posts, missing or slack anchor cable, improper stub height, missing or failed lag bolts on impact head, and missing or misaligned bearing plate. A summary of generic end terminal repair guidance from Report 656 is shown in Table 76. These criteria were “based solely on engineering judgment; no finite element simulations or pendulum tests evaluating these end terminal damage modes were conducted.”[*Gabler10*]

Table 76. Summary of generic end terminal repair guidance. [*Gabler10*]

Damage	Repair Threshold	Relative Priority
Damaged end post	Not functional (sheared, rotted, severely cracked)	High
Anchor cable	Missing	High
	Loose—more than 1 inch of movement when pushed down by hand	Medium
Cable Anchor Bracket	Loose or not firmly seated in rail	Medium
Stub height of steel tube or hinged post	Height which exceeds 4 inches	Medium
Lag bolts on impact head (Energy Absorbing Terminals Only)	Missing or failed lag bolts	High
Bearing Plate	Loose or Misaligned	Medium
	Missing	High

Due to the importance of the end-terminal to guardrail performance, it was decided that several of these damage modes, in addition to a few others, should be quantified through

physical testing, including: embedment depth of foundation tubes (i.e., stub height); missing or damaged groundline strut; slack anchor cable; and rotted/weakened posts. These damage modes could affect the end-terminal's ability to properly anchor the guardrail during impacts, which may increase the potential for excessive rail deflection, improper release of rail-post connection, and pocketing. Further, whereas local damage to a guardrail results in a relatively isolated damage-affected section of the guardrail (i.e., limited exposure to future impacts in the damage region), a damaged anchor will affect the performance of the entire guardrail system (i.e., increased risk of exposure).

Research Approach

The force-deflection response of a standard two-post anchor system with various types and levels of damage was determined through physical testing by applying a displacement-time history to the w-beam rail at the downstream end of the system and measuring the force-deflection response, as illustrated in Figure 287.



Figure 287. Example – finite element model for computing force-deflection response of the standard two-post guardrail anchor system.[Plaxico03]

Ideally, the loading on the end of the rail should be applied dynamically with a loading rate similar to real-world vehicular collisions. However, there are many difficulties involved in designing a pendulum test experiment to “pull” on the end of the system. In general, pendulums (as well as other impact devices) are used to strike and “push” an object rather than “pull” on it. Although it may be possible to construct a fixture (e.g., using pulleys or levers) to convert the compressive load of the pendulum to a tensile load on the rail, it would be difficult to separate out the dynamic effects of the mass, stiffness, energy absorption, etc. of the fixture from the test results. Also, the tension in the rail, resulting from lateral deflection of the guardrail during vehicular collisions, develops at a relatively low rate. For example, the maximum deflection of a guardrail in a TL3 event typically occurs over a period of 0.2 to 0.3 seconds. If the resulting maximum rail deflection at the anchor is, say for example, 3 inches and assuming that the rail displaces at a constant rate, then the resulting deflection rate would be in the range of 10 in/s (6.8 mph) to 15 in/s (10.2 mph). To use a pendulum (or bogie) to achieve sufficient energy to displace the anchor system at such a low rate would require a very large mass and/or a fixture

with significant mechanical advantage. Based on these difficulties, it was decided to use a more practical approach by performing a quasi-static test using a cable-and-winch system.

A total of 10 tests were performed, in which the system was subjected to displacement-time history applied to the downstream end of the w-beam at a nominal rate of 0.5 – 1.4 in/s. The test matrix for the study is shown in Table 77 and includes evaluation of the undamaged system as well as three damage modes: (1) Missing groundline strut, (2) reduced embedment depth, and (3) slack in anchor cable.

Test Set-up

The tests were performed by the staff of the Federal Outdoor Impact Laboratory (FOIL) at the Federal Highway Administration's Turner Fairbank Highway Research Center in McLean, Virginia. Figure 288 shows the typical test setup used for the study. The components of the test articles were donated by three guardrail distributors: Trinity Industries, Gregory Industries, Inc. and Road Systems, Inc. Since the purpose of these tests was to measure the force-displacement response of the anchor, only those components directly related to the anchor system were included in the test article. After each test, the components were inspected for damage. Those that showed no signs of damaged were reused in subsequent tests.

Figure 289 shows a photo of the two foundation tubes with soil plates taken during the installation process. Because of the limited size of the primary soil pit, it was necessary to also utilize the adjacent soil pit to accommodate installation of the test article. This allowed sufficient distance between the posts and the edges of the soil pit for mitigating the influence of the soil pit walls on the response of the system. The distance from the front of the foundation tube at Post 1 to the front wall of Soil Pit 1 was approximately 88 inches; and the distance from the front of the foundation tube at Post 2 to the front wall of Soil Pit 2 was approximately 43 inches. The soil for all tests was classified as 21A, which conformed to Grading B of AASHTO M147-95, and was compacted in 6-inch lifts using a pneumatic tamper. The density, moisture content and degree of compaction of the soil was measured in front of and behind the post after each compaction process using a Troxler-Model 3440 Surface Moisture-Density Gauge. There were a total of twelve readings which were averaged to determine the effective soil conditions.

The posts were spaced at 6.25 feet (typical). The w-beam rail was bolted to Post 2 using a 5/8-inch diameter bolt (ASTM F568) that was 10 inches long. A bracket, similar to the design used for most end-terminals, was mounted onto the end-post (Post 1), as shown in Figure 290, to allow the w-beam to slide freely in the longitudinal direction relative to the rail element. The w-beam was not bolted at the end-post. Construction drawings for the baseline generic end-terminal are provided in Appendix P.

Table 77. Test matrix for the anchor system damage study.

Case No.	FOIL Test No.	Description	Notes:
4B1_004	14001E	Baseline System Test	Undamaged generic end-terminal with two-foundation tubes, anchor cable, and groundline strut.
4B2_001	14001D	No groundline strut	Baseline system with groundline strut removed.
4B1_002	14001M	2 inches reduced embedment depth	Baseline system with foundation tubes installed with 2 inches less embedment.
4B1_003	14001F	4 inches reduced embedment depth	Baseline system with foundation tubes installed with 4 inches less embedment.
4B1_004	14001L	6 inches reduced embedment depth	Baseline system with foundation tubes installed with 6 inches less embedment.
4B1_005	14001G	8 inches reduced embedment depth	Baseline system with foundation tubes installed with 8 inches less embedment.
4B3_001	14001H	1 inch slack in anchor cable	Slack was measured as 1/2 the maximum vertical range of cable deflection when pushed down and pulled up using a force of 7-lbs. Measurement taken at the center of the cable length.
4B3_002	14001I	2 inches slack in anchor cable	
4B3_003	14001K	3 inches slack in anchor cable	
4B3_004	14001J	4 inches slack in anchor cable	



Figure 288. Typical test set-up for measuring force-deflection response of the guardrail end-terminal anchor.



Figure 289. Photograph of anchor tubes with soil plates during installation (from preliminary Test 14011B).

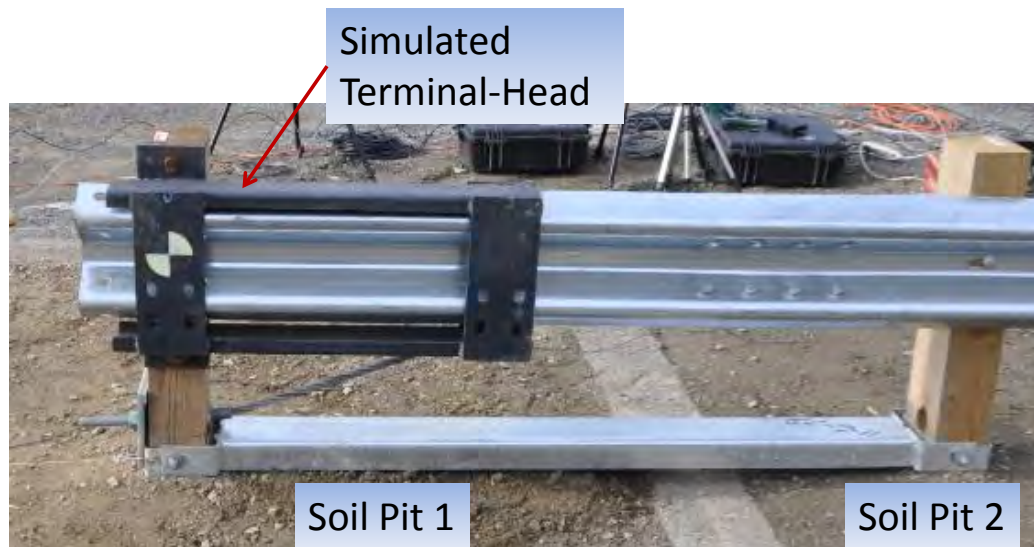


Figure 290. Photo of the simulated terminal-head bracket mounted onto the end-post.

The load was applied to the end of the test article using a winch and a cable-pulley system with a 3:1 mechanical advantage, as shown in Figure 291. The winch system used for the quasi-static test was an existing component of the pendulum test device – used primarily to hoist the pendulum into position for dynamic tests. For the tests, the winch cable was run through a pulley aligned with the top corrugation of the w-beam on the test article, around another stationary pulley that was attached to a fixed bracket near the winch system, and then back to the test article and attached to the lower corrugation of the w-beam rail. For the attachment to the end of the test article, a 1-inch diameter steel rod was attached to the pulley, and another was attached to the end of the force transducer. These two rods were then fastened to the end of the w-beam rail using a standard cable-anchor-bracket (i.e., RWE02), as shown in Figure 291. A bracket-and-idler-pulley system was also mounted just downstream of the test article, as shown in Figure 292, to maintain vertical position of loading cables during the tests (e.g., simulate the continuation of the w-beam mounted to the downstream posts).

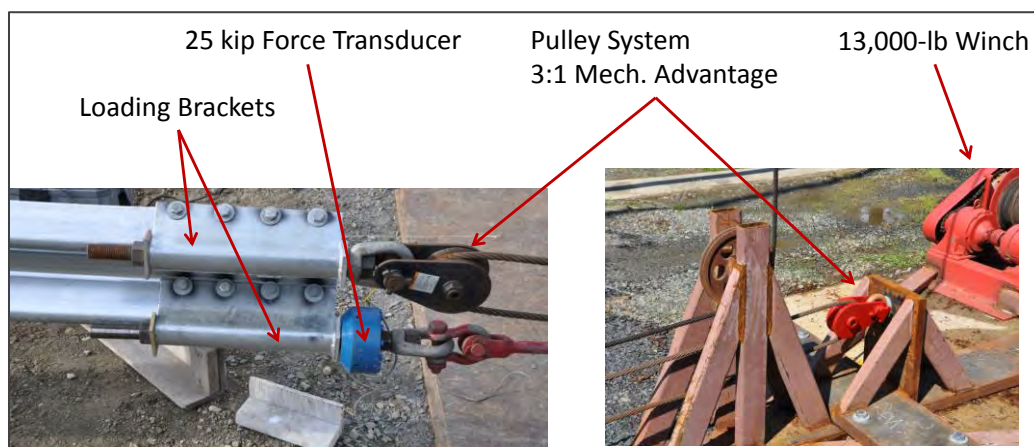


Figure 291. Cable and pulley system used to apply tensile loading on end-terminal anchor.



Figure 292. Idler-pulley mount used to maintain vertical position of loading cable.

Two types of posts were used for the tests. The primary differences in the two post types were that one had a round post-bolt hole with a diameter of 0.625 inches, and the other had a slotted hole 0.75 inches tall and 2.5 inches long, as shown in Figure 293.

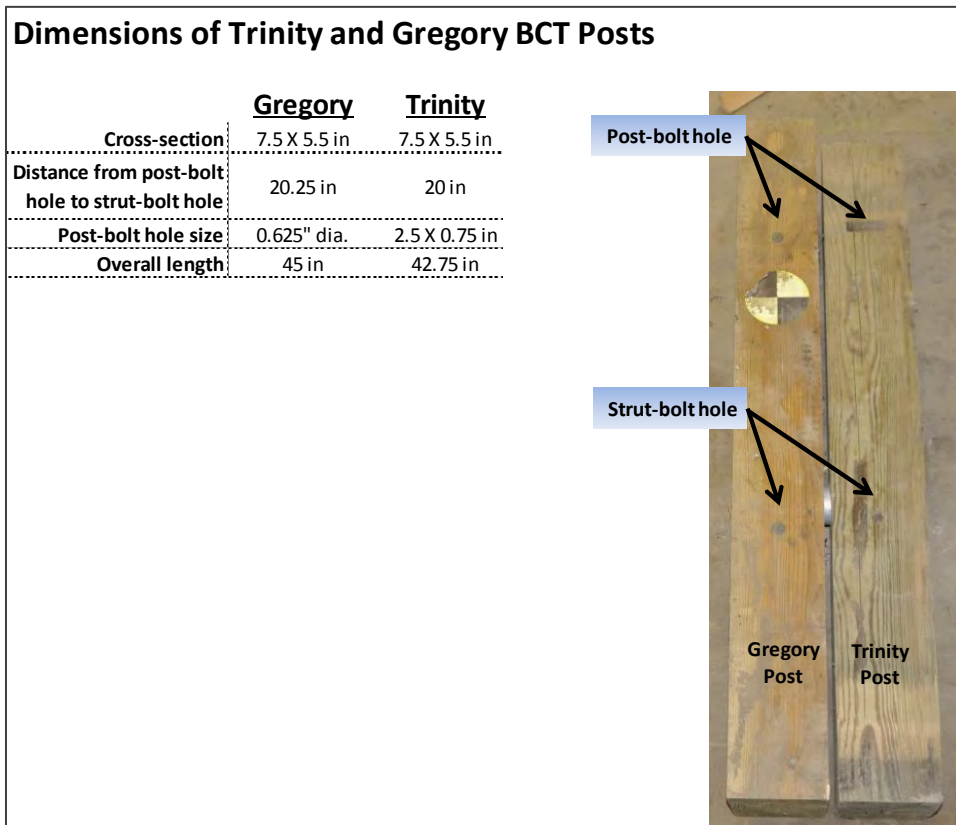


Figure 293. Comparison of the two post types used in the end-terminal tests.

Equipment and Instrumentation

Force Transducer

The load on the cable was measured using an Interface Model 1220 standard load cell, rated at 25-kip. With the 3:1 mechanical advantage of the cable-pulley system, the resulting load on the test article was thus three times greater than the load measured by the load cell.

Displacement Transducers

SpaceAge Control, Inc. Series 162 Miniature Position Transducers (i.e., string-pots) were used to measure displacements at two key locations on the test article during the test, as shown in Figure 294. One string-pot was used to measure displacement at the downstream end of the w-beam rail at the load point, and another was used to measure the groundline displacement of the foundation tube at Post 1 (i.e., end post).



Figure 294. Displacement transducers mounted to (a) w-beam rail at load point and (b) top of foundation tube at Post 1.

Photography

The tests were recorded using seven digital video cameras. Figure 295 provides the specifications and the general placement of the cameras for the test. The pre-test setup and the post-test results were also documented with “still” photographs.

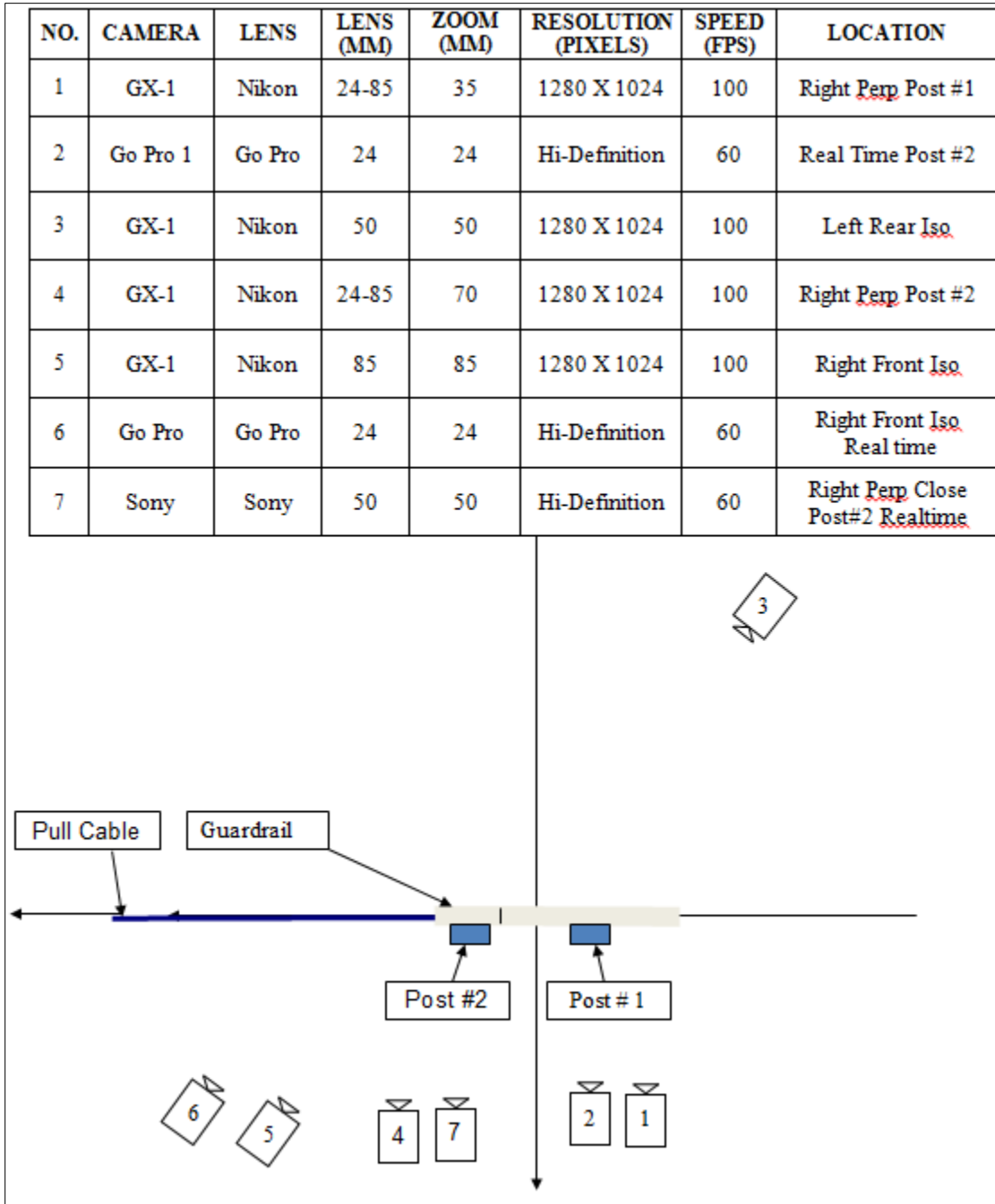


Figure 295. Video camera specifications and placement.

Test Procedure

A quasi-static displacement-time history was applied to the end of the w-beam rail of the end-terminal at a rate of approximately 0.5 – 1.4 in/sec. The test continued until there was a sudden decrease in resistance (e.g., failure of an end-terminal component) or when the displacement of the rail reached 10 inches, whichever came first. Figure 296 shows the displacement- and displacement rate-time histories measured at the load point on the end of the rail and at the groundline of Post 1 for the undamaged end-terminal case. The blue curve in Figure 297 shows the resulting force-deflection response of the end-terminal measured at the end-of the w-beam rail. The test data was resampled to obtain the “apparent” force-deflection response of the system denoted by the green curve in Figure 297. To account for the effects of loading rate on the anchor response in the finite element model, a dynamic magnification factor of 1.45 was used to scale the quasi-static force-deflection curve denoted by the red curve in Figure 297. Only two displacement transducers were available, so the displacement-time history at Post 2 was not measured in the tests. Sequential views of the undamaged end-terminal case from two view-points are shown in Figure 298.

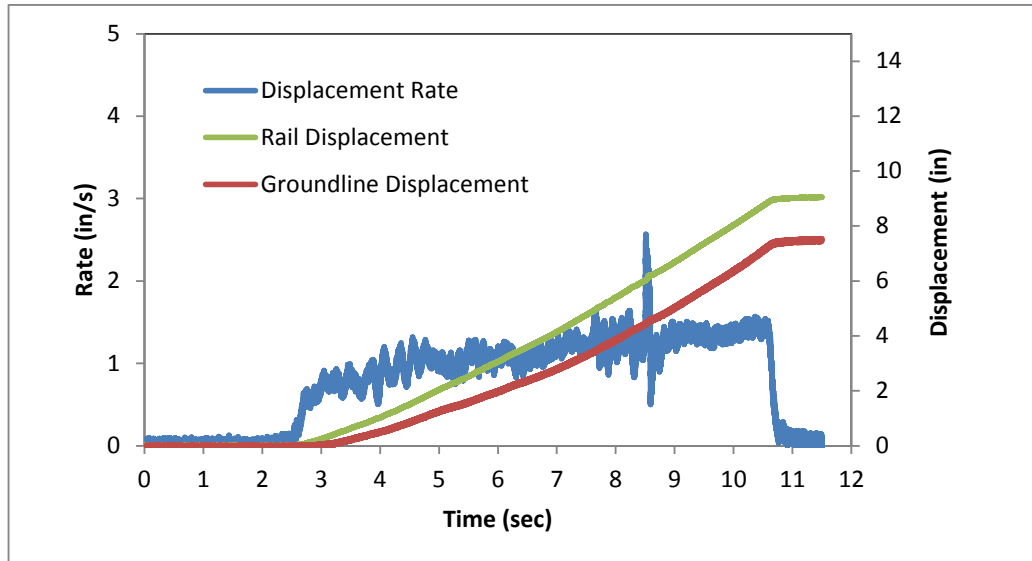


Figure 296. Displacement- and displacement rate-time histories measured at the load point on the end of the rail and at the groundline of Post 1 for baseline case.

⁵ The 1.4x scale factor used here was based on physical tests performed in this project (not documented here) involving static and dynamic tests on a W6x16 post in soil with density of 144 pcf.

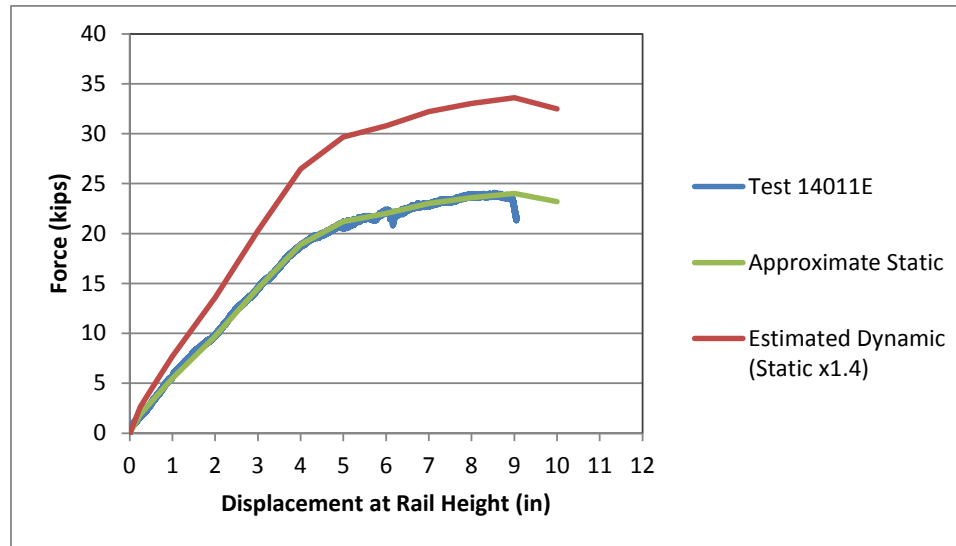


Figure 297. Force-displacement response of the anchor system measured at the load point on the end of the rail for undamaged end-terminal case.

Test Results

A summary of the test results for Test Series 14001 are shown in Tables 78 and 79. Table 78 includes the damage mode case, installation conditions, the resulting component failures that occurred during the test, the displacement of the rail at the load point at the time of maximum load, the apparent stiffness of the anchor system during the first two inches of rail displacement, and the apparent strength of the anchor system. Table 79 includes test setup information regarding post spacing, rail height, loading point locations, embedment depth of the foundation tubes, and post-test information regarding groundline deflection of the end-terminal posts. The individual test-summary sheets are included in Appendix Q. Other than soil displacement, there were three common types of component failures that occurred during the tests: (1) Post 2 split, (2) the end-foundation tube extracted from the ground, and (3) the groundline strut buckled near the joint at Post 2.

Also included in Table 78 are the results for Test 13011B, which were used to characterize the baseline anchor system model for the damaged-system-performance evaluations performed throughout the project. The primary differences in the test setup for Series 14001, compared to Test 13011B, included adding the surrogate terminal head, removal of the post-bolt at Post 1, and utilization of two soil pit areas for the installation of the post and foundation tubes (e.g., to mitigate effects of soil pit boundaries). Refer to Chapter 9 for more details regarding test setup and results of Test 13011B.

The following sections discuss the effects of specific end-terminal damages on the force-deflection response of the anchor system, including the effects of missing groundline strut, reduced embedment of the foundation tubes, and slack in the anchor cable. For relative comparison, the results from the undamaged system (i.e., Test 14001E) and the baseline system (i.e., Test 13011B) are also included in the force-deflection plots for each case.

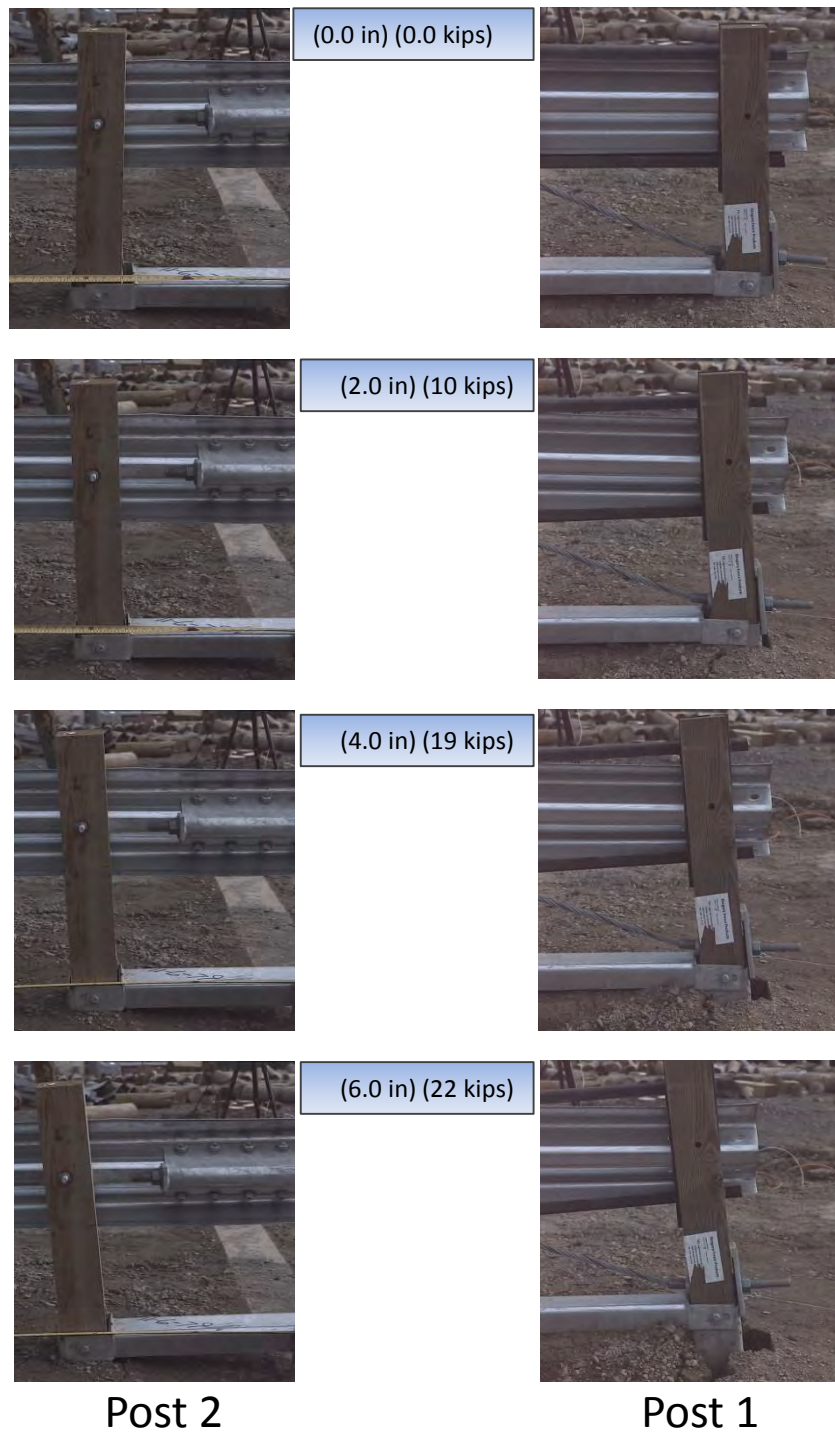


Figure 298. Sequential views of quasi-static test conducted for undamaged end-terminal case (Test 14011E).

Table 78. Quasi-static test results for end-terminal damage modes (Table 1 of 2).

Case No.	Test No.	Test Date	Damage Mode	Soil Properties						RESULTS							
				Post 1			Post 2			Stiffness			Force				Failure
				Dry Density (pcf)	Moisture (%)	Compaction (%)	Dry Density (pcf)	Moisture (%)	Compaction (%)	0"-2" (k/in)	2"-4" (k/in)	4"-6" (k/in)	@2" (k/in)	@4" (k/in)	@6" (k/in)	Peak (k)	
4B1_000	13011B	12/16/2013	Baseline Test (used in Task 4A-2)	142.2	6.3	94.7	-	-	-	6.0	2.4	2.1	12.0	16.8	21.0	22.2	Post 1 Extraction
4B1_004	14001E	4/18/2014	Undamaged System Test	142.1	6.4	94.6	144	4.6	93.2	4.9	4.5	1.7	9.7	18.9	22.0	24.0	Soil Only
4B2_001	14001D	4/16/2014	No groundline strut	143.4	5.4	95.5	143.5	4.4	93.2	4.5	1.9	1.8	8.7	12.8	12.0	14.8	Post 2 Split
4B1_002	14001M	6/23/2014	2" reduced embedment	138.8	5.3	92.5	140.3	4.1	90.8	4.8	1.9	0.8	9.7	13.4	15.0	18.8	Post 1 Extraction
4B1_003	14001F	5/6/2014	4" reduced embedment	145.2	5.7	96.6	143.4	4.0	92.8	5.0	1.5	0.6	9.9	12.8	14.0	15.7	Post 1 Extraction
4B1_004	14001L	6/20/2014	6" reduced embedment	141.3	5.1	94.1	142.8	4.5	92.4	5.2	0.9	1.3	10.4	12.3	15.0	22.6	Post 2 Split
4B1_005	14001G	5/12/2014	8" reduced embedment	144.2	5.3	95.7	143.7	5.1	93.0	5.8	4.2	2.8	11.7	20.1	19.0	23.2	Strut Bent
4B3_001	14001H	6/4/2014	1" slack in anchor cable	143.7	5.3	95.7	143.8	3.7	93.1	5.4	4.1	2.1	10.9	19.1	23.3	29.9	Post 2 Split Strut Bent
4B3_002	14001I	6/6/2014	2" slack in anchor cable	140.4	5.7	93.5	143.4	4.3	92.8	5.4	2.8	1.3	10.8	16.4	19.0	19.3	Post 2 Split Strut Bent
4B3_003	14001K	6/18/2014	3" slack in anchor cable	140.2	5.8	93.3	144.6	4.6	93.5	2.2	3.6	2.1	4.4	11.6	15.8	22.5	Post 2 Cracked
4B3_004	14001J	6/16/2014	4" slack in anchor cable	141.8	4.6	94.4	145.1	5.3	93.9	1.3	2.3	3.5	2.6	7.3	14.2	25.2	Post 2 Split Strut Bent

Table 79. Quasi-static test results for end-terminal damage modes (Table 2 of 2).

Test No.	Test Date	Damage Mode	PRE-TEST MEASUREMENTS									POST-TEST RESULTS			
			Distance Post 2 to Soil Pit Front (in)	Distance Post 2 to Soil Pit Rear (in)	Distance Post 1 to Soil Pit Front (in)	Distance Post 1 to Soil Pit Rear (in)	Distance Center to Center Posts (in)	Height to Top of Rail (in)	Height to Load Point Top (in)	Height to Load Point Bottom (in)	Post Embedment Depth (in)	Distance Center to Center Posts (in)	Groundline Deflection Post #1 (in) Post #2 (in)		
13011B	12/16/2013	Baseline Test (used in Task 4A-2)													
14001E	4/18/2014	Undamaged System Test	88.0	16.0	43.0	30.0	75.5	28.5	25.5	17.5	57.0	74.0	5.8	4.0	
14001D	4/16/2014	No groundline strut	86.0	18.0	45.0	28.0	74.0	-	-	-	-	70.0	4.3	<0.125	
14001L	5/20/2014	2" reduced embedment	88.5	17.8	42.0	30.5	75.3	29.5	26.5	18.5	55.0	75.0	8.0	7.0	
14001F	5/6/2014	4" reduced embedment	85.8	18.3	41.3	31.8	74.5	31.5	28.5	17.3	53.0	73.3	4.8	4.0	
14001L	6/20/2014	6" reduced embedment	87.0	19.3	42.0	30.5	76.5	34.5	31.5	23.5	51.0	73.3	9.0	6.5	
14001G	5/12/2014	8" reduced embedment	85.5	18.5	44.5	28.5	75.0	31.0	28.0	20.0	49.0	71.5	4.5	3.0	
14001H	6/4/2014	1" slack in anchor cable	87.5	18.3	41.5	25.0	75.3	26.0	23.0	16.0	57.0	69.0	9.5	3.0	
14001I	6/6/2014	2" slack in anchor cable	86.8	19.5	40.8	31.8	75.5	26.5	22.8	15.0	57.0	69.5	9.8	5.0	
14001K	6/18/2014	3" slack in anchor cable	87.0	19.3	42.0	30.5	75.0	29.0	26.0	18.0	57.0	72.8	8.0	6.5	
14001J	6/16/2014	4" slack in anchor cable	86.8	19.5	40.8	31.8	76.3	27.3	24.3	17.0	57.0	68.8	9.5	3.0	

Missing or Non-Functioning Groundline Strut

Pre-test and post-test photos of Test 14011D are shown in Figures 299 and 300, respectively. The data from the test were resampled to obtain the “approximate static” force-deflection response, which is compared to that of the undamaged system in Figure 301. Refer to the test-summary sheets in Appendix Q for the “unprocessed” force-deflection results. Figure 302 shows the displacement-time history measured at the load-point on the rail and at the groundline of Post 1.

The “apparent” initial stiffness⁶ of the anchor was 4.5 kips/in for the first 2 inches of displacement measured at the load point, compared to 4.9 kips/in for the undamaged system. Between 2-4 inches displacement the stiffness dropped to 1.9 kips/in, compared to 4.5 kips/in for the undamaged system. Post 2 split at approximately 5 inches displacement at which point the loading on the system was 14.8 kips resulting in a sudden loss of the anchor resistance. The test was terminated immediately after the loss of Post 2 with a maximum displacement of 6.4 inches measured at the load point; thus, the response of the system beyond this displacement was not determined. The apparent strength of the anchor was 14.8 kips and occurred at 5 inches deflection.



Figure 299. Pre-test photo of Test 14001D (front view).

⁶ Apparent initial stiffness was computed as the force at 2 inches displacement divided by 2 inches; the apparent stiffness from 2-4 inches was calculated as the difference in force from 2-4 inches divided by 2 inches; etc.



Post 2



Post 1

Figure 300. Post-test photo of Test 14001D (back view).

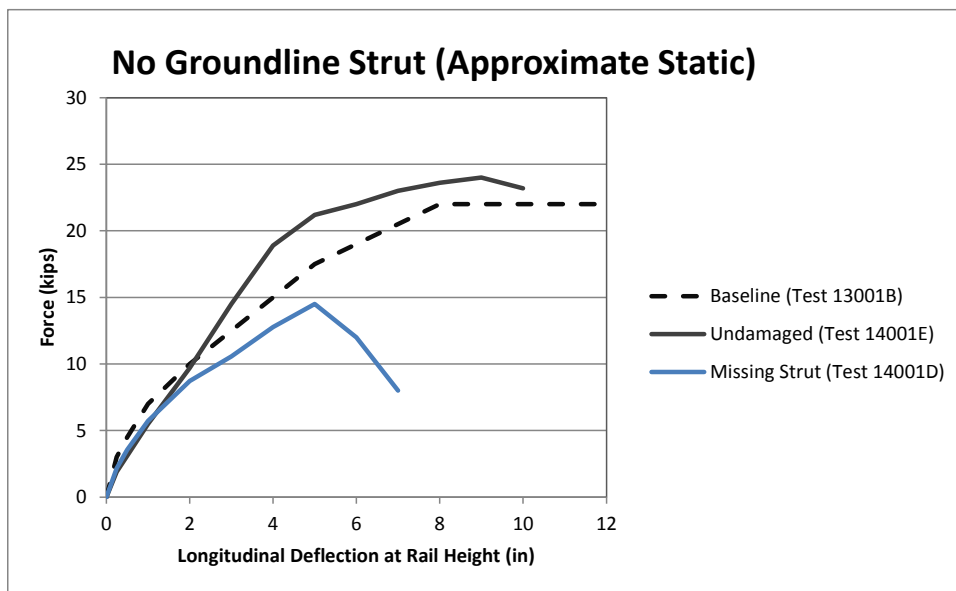


Figure 301. Force vs. deflection response for the standard end-terminal with missing groundline strut.

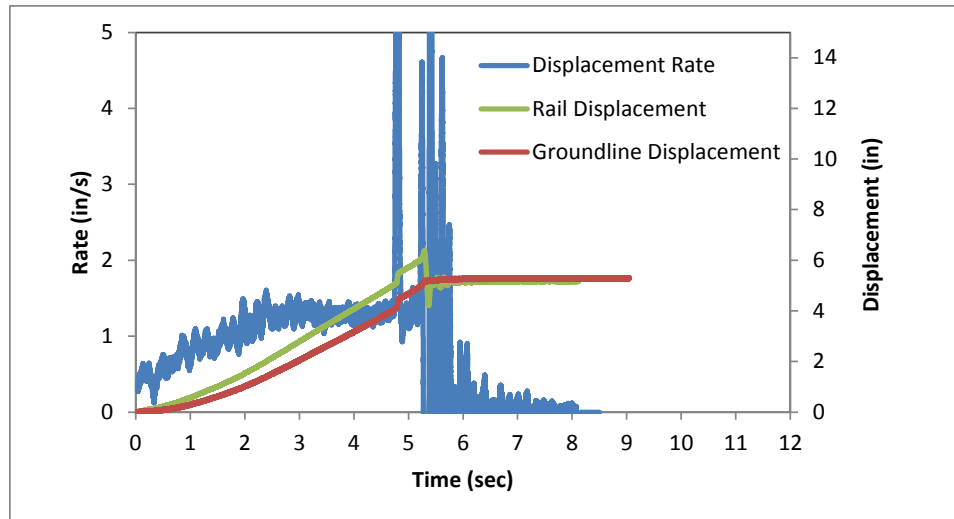


Figure 302. Displacement and displacement rate vs. time for Test 14001D.

The results for the test involving the missing groundline strut showed that the initial stiffness of the end-terminal was similar to that of the undamaged system for approximately the first 1.5 inches of longitudinal rail movement. This was because the length of the groundline strut was 67 inches, compared to the distance of 68 inches measured between the two foundation tubes for the undamaged test case (refer to Test 14001E in Table 79). This resulted in a total gap of 1.0 inch between the strut and foundation tubes, as shown in Figure 303. Thus, the foundation tube at Post 1 during the test on the undamaged system experienced 1 inch of movement before the groundline strut engaged the foundation tube at Post 2.

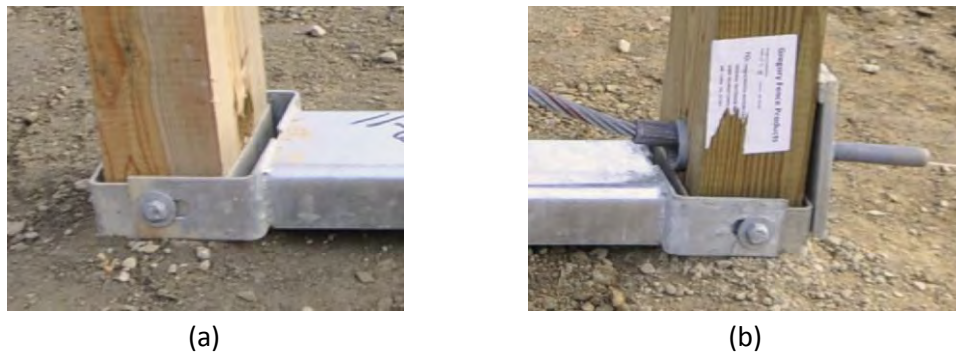


Figure 303. Typical position of groundline strut in a standard two-post-strut anchor system relative to (a) Post 2 and (b) Post 1.

Reduced Embedment Depth

A total of four tests were performed to quantify the effects of reduced embedment depth on the force-deflection response of the standard anchor system. These tests included installations with 2, 4, 6 and 8 inches of reduced embedment depth. At the standard embedment depth for the system, the top of the foundation tube protrudes 3 inches above the ground. Thus, amount of reduced embedment was determined by measuring the distance from the top of the soil to a point three inches from the top of the foundation tube at Post 1. Figure 304 shows an example of the procedure for the case of 6 inches reduced embedment.



Figure 304. Procedure for measuring reduced embedment depth.

Pre-test photos for the four reduced-embedment cases are shown in Figures 305 through 308, and post-test photos are shown in Figures 309 through 312. The “approximate static” force-displacement results from the tests are shown in Figure 313, including the undamaged cases. The results from this series of tests were somewhat inconclusive. The initial stiffness (i.e., between 0-2 inches displacement) for all reduced embedment cases was essentially identical to the undamaged case (i.e., 4.9 kips/in). The stiffness at deflections of 2 to 4 inches, however, was significantly lower for reduced embedment cases of 2, 4 and 6 inches, and reduced slightly for each successive reduction of embedment (i.e., 1.9, 1.5 and 0.9 kips/in, respectively, compared to 4.5 kips/in for the undamaged case). For the 8-inch reduced embedment depth, on the other hand, the stiffness at this second level of displacement was essentially the same as the undamaged case (e.g., 4.2 vs. 4.5 kips/in).

For the case involving 2 inches of reduced embedment of the foundation tubes, the “apparent” initial stiffness of the anchor was 5.0 kips/in for the first 2 inches of displacement measured at the load point, compared to 4.9 kips/in for the undamaged system. Between 2-4 inches displacement the stiffness dropped to 1.5 kips/in, compared to 4.5 kips/in for the undamaged system. Between 4-6 inches displacement the stiffness dropped further to 0.6 kips/in, compared to 1.7 kips/in for the undamaged case. The maximum load measured during the test was 15.7 kips at 10.5 inches displacement. Post 1 foundation tube began to extract from the ground at a rail deflection of approximately 7.3 inches. At approximately 13 inches displacement the foundation tube at Post 1 was fully extracted. Refer to the test-summary sheets in Appendix Q for more details.

For the case involving 4 inches of reduced embedment of the foundation tubes, the “apparent” initial stiffness of the anchor was 4.8 kips/in for the first 2 inches of displacement measured at the load point. Between 2-4 inches displacement the stiffness dropped to 1.9 kips/in. Between 4-6 inches displacement the stiffness dropped further to 0.8 kips/in. The maximum load

measured during the test was 18.4 kips at 16 inches displacement. Post 1 foundation tube began to extract from the ground at a rail deflection of approximately 3 inches (based on assessment of real-time video and force-displacement data). Refer to the test-summary sheets in Appendix Q for more details.

For the case involving 6 inches of reduced embedment of the foundation tubes, the “apparent” initial stiffness of the anchor was 5.2 kips/in for the first 2 inches of displacement measured at the load point. Between 2-4 inches displacement the stiffness dropped to 0.9 kips/in. Between 4-6 inches displacement the stiffness increased to 1.3 kips/in. The maximum load measured during the test was 22.6 kips at 12 inches displacement. Post 2 split at approximately 5.1 inches of rail deflection. The rail then dropped at Post 2. The foundation tube at Post 1 showed no signs of pulling out of the ground for this case. Refer to the test-summary sheets in Appendix Q for more details.

For the case involving 8 inches of reduced embedment of the foundation tubes, the “apparent” initial stiffness of the anchor was 5.8 kips/in for the first 2 inches of displacement measured at the load point. Between 2-4 inches displacement the stiffness was 4.2 kips/in. Between 4-6 inches displacement the stiffness was 2.8 kips/in. The maximum load measured during the test was 23.2 kips at 5.0 inches displacement. The foundation tube at Post 1 began to extract from the ground at approximately 5 inches rail deflection. At approximately 8 inches deflection the groundline strut buckled near Post 2, resulting in a sudden loss of anchor resistance. Refer to the test-summary sheets in Appendix Q for more details.

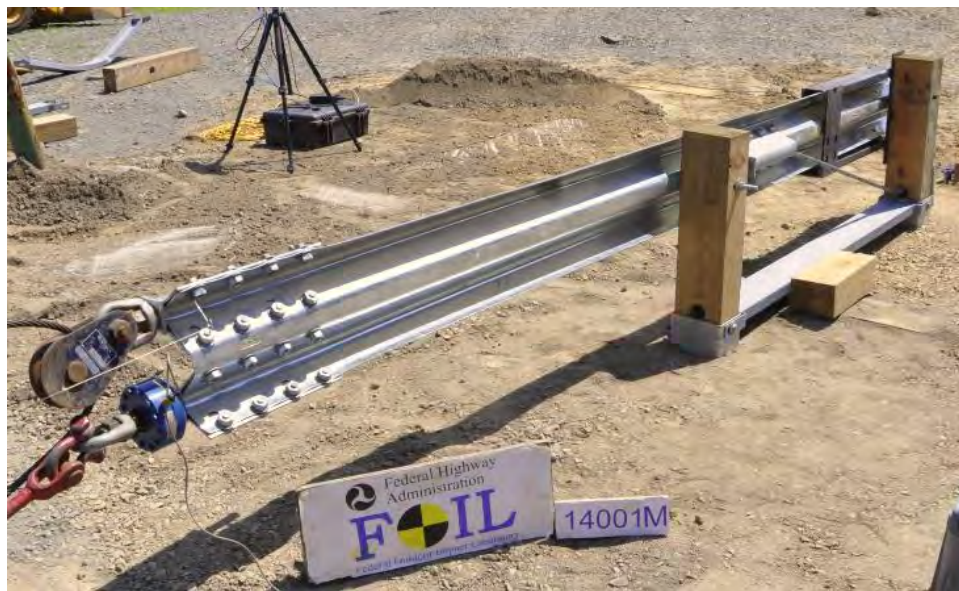


Figure 305. Pre-test photo of Test 14001M for 2-inch reduced embedment case.



Figure 306. Pre-test photo of Test 14001F for 4-inch reduced embedment case.



Figure 307. Pre-test photo of Test 14001L for 6-inch reduced embedment case.



Figure 308. Pre-test photo of Test 14001G for 8-inch reduced embedment case.



Figure 309. Post-test photo of Test 14001M for 2-inch reduced embedment case.



Figure 310. Post-test photo of Test 14001F for 4-inch reduced embedment case.



Figure 311. Post-test photo of Test 14001L for 6-inch reduced embedment case.



Figure 312. Post-test photo of Test 14001G for 8-inch reduced embedment case.

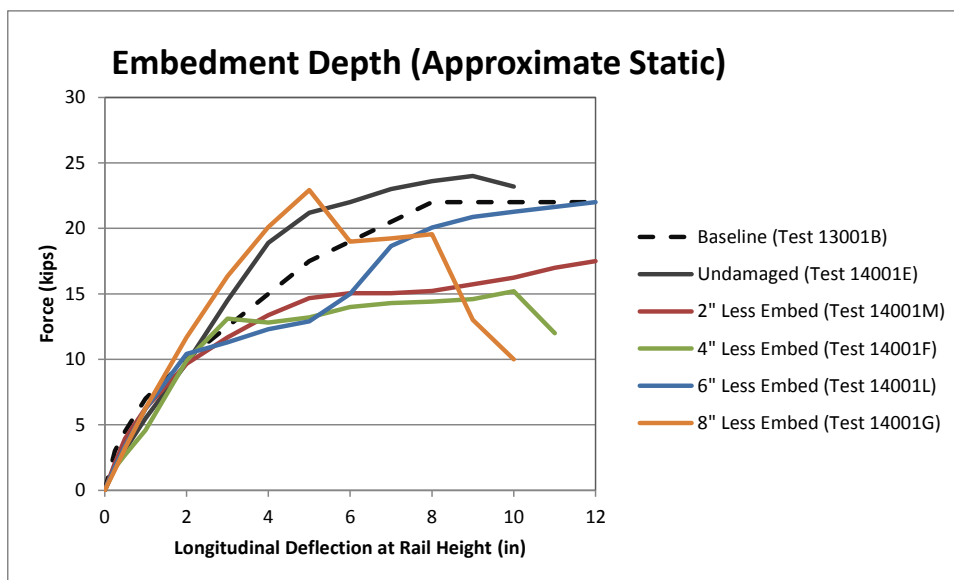


Figure 313. Force vs. deflection response for the standard end-terminal with 0 to 8 inches reduced embedment depth of foundation tubes.

Slack Anchor-Cable

A total of four tests were performed to quantify the effects of slack in the anchor-cable on the force-deflection response of a standard anchor system. These tests included installations with 1, 2, 3 and 4 inches of slack in the anchor cable. The procedure for measuring the amount of slack in the cable involved applying a downward vertical force of 7 lbs. at the center of the cable length and then measuring the vertical distance from the top of the cable to the ground. The cable was then pulled upward with a vertical force of 7 lbs. and again the distance from the top of the cable to the ground was measured. The amount of slack in the cable was then calculated as the difference in these two values divided by 2. In other words, slack was defined as one-half the maximum vertical range of cable's deflection when pushed down then pulled up using a force of 7-lbs, as shown schematically in Figure 314. This definition of slack is consistent with that specified by most manufacturers of proprietary end-terminals. The 7-lb force is representative of the amount of force required when applying reasonable pressure with one's index finger to push down or pull up on the cable. When performing this procedure, care was taken to ensure that all the slack was taken out of the cable by visually confirming that the bearing plate on the front of Post 1 was seated firmly against the post under the applied pressure.

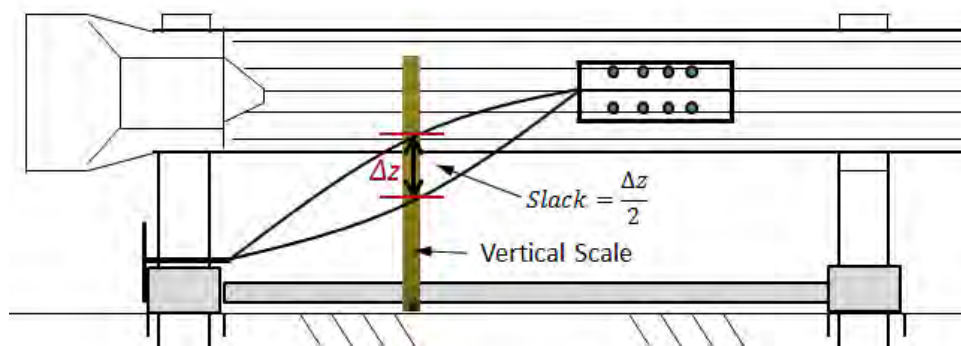


Figure 314. Illustration showing procedure for measuring slack in cable-anchor.

Pre-test photos for the four slack-cable cases are shown in Figures 315 through 318, and post-test photos of are shown in Figures 319 through 322. The “approximate static” force-displacement results from the tests are shown in Figure 323, including the undamaged cases. The results show that the initial force-deflection response of the end-terminal was essentially unaffected until the slack in the cable exceeded 2 inches. At 3 inches of slack, there was a significant drop in the force-deflection response, particularly during the first 1-inch of displacement. This was partly due to the fact that Post 2 for that test included a 2.5-inch long slotted post-bolt hole (rather than the 0.625” diameter post-bolt hole for all other tests). The slotted hole effectively delayed the point at which the post-bolt engaged the edge of the hole and began to load the post. The end result was that Post 2 was able to survive significant rail displacement without failure, but also with the effect of slightly reducing the initial stiffness of the anchor system.



Figure 315. Pre-test photo of Test 14001H for 1" slack-cable case.



Figure 316. Pre-test photo of Test 14001I for 2" slack-cable case.



Figure 317. Pre-test photo of Test 14001K for 3” slack-cable case.



Figure 318. Pre-test photo of Test 4001J for 4” slack-cable case.

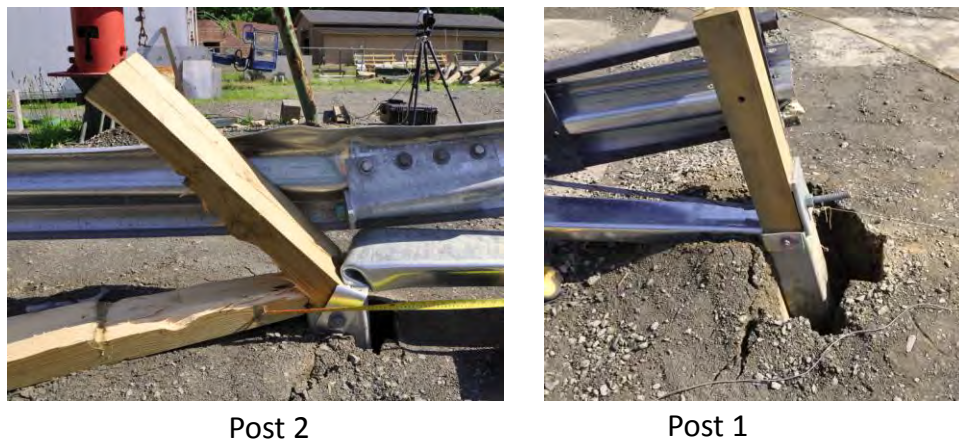


Figure 319. Post-test photos of Test 14001H for 1” slack-cable case.

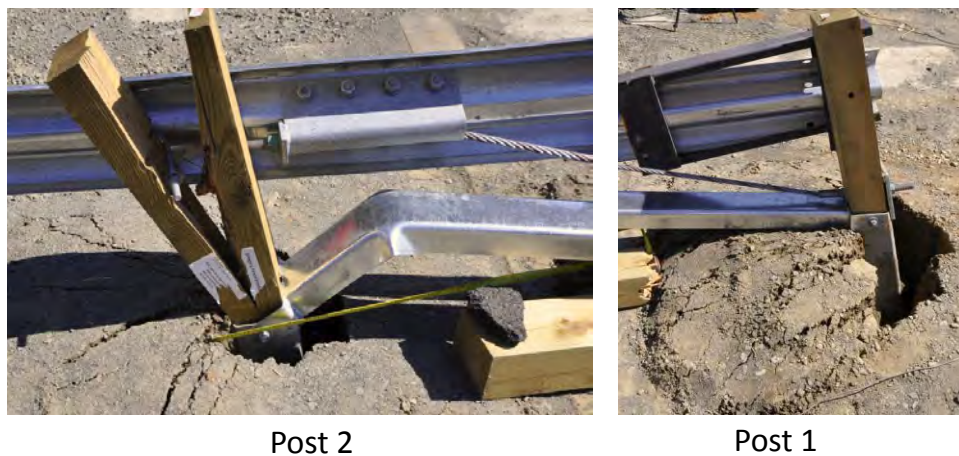


Figure 320. Post-test photos of Test 14001I for 2” slack-cable case.



Figure 321. Post-test photos of Test 14001K for 3” slack-cable case.

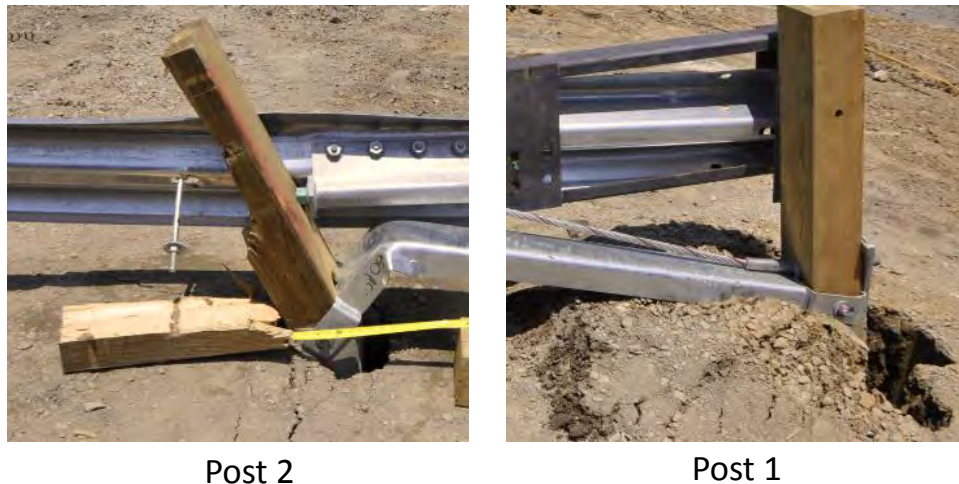


Figure 322. Post-test photos of Test 14001J for 4" slack-cable case.

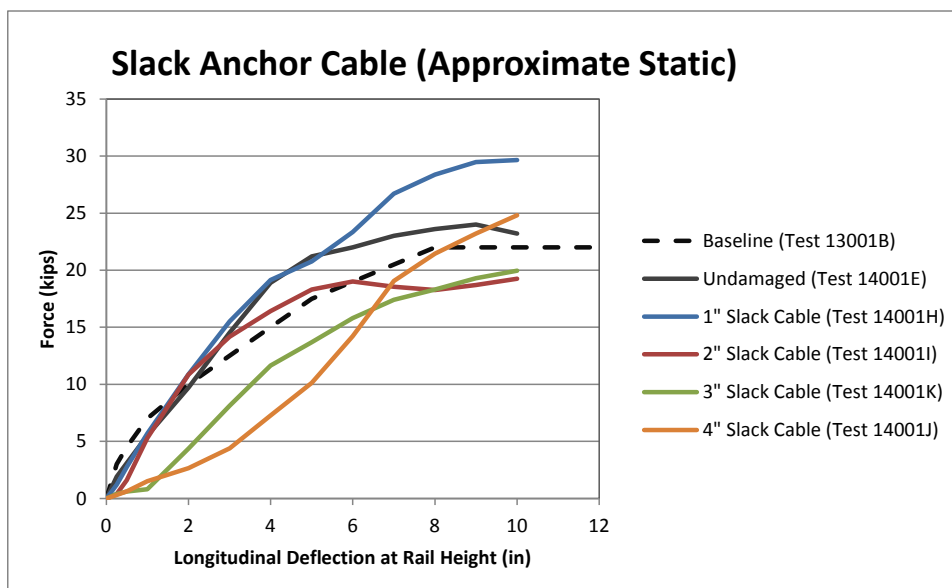


Figure 323. Force vs. deflection response for the standard end-terminal with 0 to 4 inches of slack in the anchor-cable.

For the case involving 3 inches of slack in the cable, the “apparent” initial stiffness of the anchor was 2.2 kips/in for the first 2 inches of displacement measured at the load point, compared to 4.9 kips/in for the undamaged system. Between 2-4 inches displacement the stiffness increased to 3.6 kips/in, compared to 4.5 kips/in for the undamaged system. Between 4-6 inches displacement the stiffness dropped back to 2.1 kips/in, compared to 1.7 kips/in for the undamaged case. The maximum load measured during the test was 22.5 kips at 12 inches displacement. No significant failures occurred during the test. Refer to the test-summary sheets in Appendix Q for more details.

For the case involving 4 inches of slack in the cable, the “apparent” initial stiffness of the anchor was 1.3 kips/in for the first 2 inches of displacement, compared to 4.9 kips/in for the

undamaged system. Between 2-4 inches displacement the stiffness increased to 2.3 kips/in, compared to 4.5 kips/in for the undamaged system. Between 4-6 inches displacement the stiffness increased to 3.5 kips/in, compared to 1.7 kips/in for the undamaged case. The maximum load measured during the test was 25.2 kips at 10 inches displacement. Post 2 split at 3.3 inches of rail displacement at 5.8 kips, and the groundline strut buckled at 10.8 inches of rail deflection at 20.7 kips. Refer to the test-summary sheets in Appendix Q for more details.

Summary and Discussion

Although the end-terminal of a guardrail serves many purposes, one of its primary functions is to “anchor” the ends of the rail so that the resulting tension in the rail can help to limit lateral deflection of the system during impacts. The objectives of this study were to (1) quantify the effects of various types and levels of end-terminal damage on the force-deflection response of standard generic guardrail end-terminals using physical testing, and (2) to then correlate those effects to guardrail performance. In Chapter 9 the response of the G4(2W) guardrail system was evaluated for various levels of reduced anchor strength. In the current study quasi-static tests were performed to quantify the force-deflection response of a standard two-post-and-strut anchor system with three modes of damage: (1) missing or otherwise non-functional groundline strut, (2) reduced embedment depths of 2, 4, 6, and 8 inches, and (3) slack anchor cable with 1, 2, 3, and 4 inches of slack. The tests were performed by pulling on the downstream end of the rail element with a cable and winch system at a displacement rate of 0.5 to 1.4 in/s. The force-deflection response was measured via a force transducer and string-pot which were attached to the rail at the load point. The following is a brief summary and discussion of the results.

Discussion of Failure Modes

There were basically three types of anchor component failures that occurred during the test series: (1) Post 2 splitting, (2) the foundation tube at Post 1 pulling out of the ground, and (3) buckling of the groundline strut. Based on the test results, however, there was no conclusive evidence that the failure of Post 2 in any way degraded anchor performance; and is therefore not considered a failure mode for the system. In fact, in all cases for which the test was allowed to continue after Post 2 failed, the effective stiffness of the system remained more or less continuous, as illustrated in Figure 324 (also see results for Tests 14001L, 14001H, and 14001J in Appendix Q). In field installations the failure of Post 2 would, however, be an indication that other aspects of the system may be compromised, such as significant movement of the anchor foundation tubes or slack in the anchor cable.

For cases in which the foundation tube at Post 1 began pulling out of the ground, there was noticeable reduction in stiffness of the system during the extraction process (e.g., refer to Tests 14001M, 14001F, and 14001G). This failure mode was primarily associated with reduced embedment of the foundation tubes. When the foundation tube was fully extracted there was an abrupt loss of the anchor. There was also an abrupt loss of anchor resistance for cases in which the groundline strut buckled. Although there was one case of this failure mode occurring for the reduced embedment cases, it was principally associated with slack in the anchor cable, and generally occurred when *groundline* deflections at Post 1 reached approximately 7-8 inches.

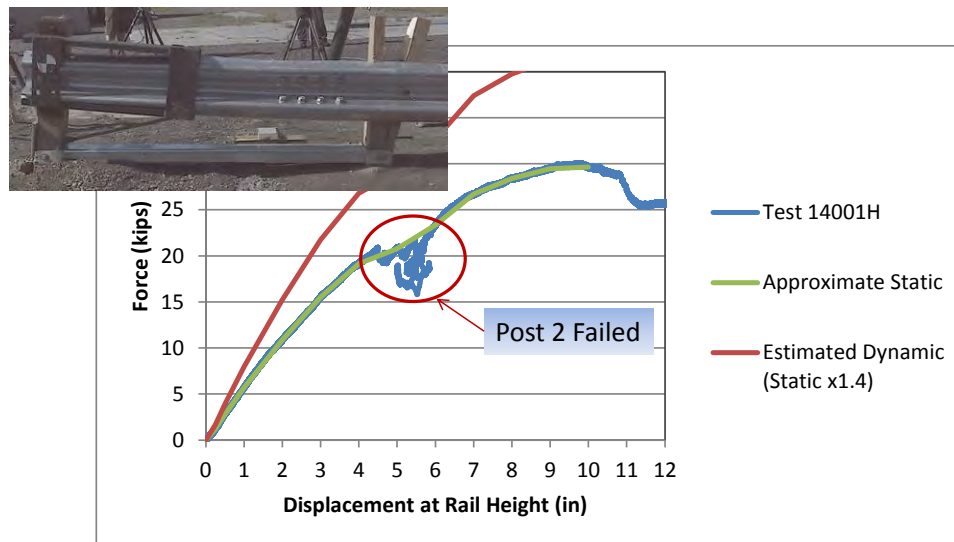


Figure 324. Test 14001H showing continuing effectiveness of anchor after Post 2 fails.

Missing Groundline Strut

The results of the tests showed that the missing groundline strut resulted in a reduction in anchor capacity of approximately 50%; however, the initial stiffness of the anchor was very similar to the undamaged case. Also, the test was terminated prematurely (i.e., soon after Post 2 split), thus the full range of effective anchor response was not measured for this case. Regarding the effects on guardrail performance, it is expected that the damage mode involving a missing (or otherwise non-functional) groundline strut would be similar to that of the FE analysis for the 47% percent anchor strength case in Chapter 9.

Recall from Chapter 9 that when end-terminal damage results in more than 50% reduction in anchor capacity, the recommended repair priority was “high”. This was particularly true for the G4(1S), due to the low torsional strength of the W6x9 steel posts; and for wood post guardrail systems when the posts had a degradation level of DL1 or higher. For example, the analysis of the G4(1S) in Chapter 11, which involved an end-terminal with no groundline strut and 14 inches of pre-crash-induced rail deflections, the upstream anchor deflected 5.5 inches, which lead to the vehicle overriding guardrail. Test C080C3-027-2 of this same system, also resulted in excessive anchor movement and vehicle override.

Reduced Embedment Depth for the Foundation Tubes

The results from this series of tests were somewhat inconclusive. The initial stiffness (i.e., corresponding to displacements from 0-2 inches) on the anchor for all of the reduced embedment cases was essentially identical to that of the undamaged case (i.e., 4.9 kips/in). The stiffness at deflections of 2 to 4 inches, however, was significantly lower for the reduced embedment cases and tended to progressively decrease as a function of embedment depth, with the exception of the 8-inch reduced embedment case. The effective stiffness values were 1.9, 1.5, 0.9, and 4.2 kips/in for the 2”, 4”, 6” and 8” reduced embedment cases, respectively. The stiffness at this second level of displacement for the 8-inch reduced embedment case was, unexpectedly, of similar magnitude as for the undamaged case (i.e., 4.5 kips/in).

In *NCHRP Report 656*, Gabler et al. stated that when the stub height above ground level exceeds 4 inches (i.e., reduced embedment of 1 inch) then the breakaway mechanism of the end-terminal may not activate properly during end-on hits. [Gabler10] Gabler further stated that stub heights exceeding 4 inches could lead to small vehicles snagging on the top of the foundation tube. Based on those observations, Gabler recommended that stub heights of more than 4 inches above ground be assigned a repair priority of “medium”. In those assessments, however, only the performance of the end-terminal in regard to direct impact on the end of the system was considered. Whereas, in the current study, the focus was on the effects of reduced embedment (i.e., or stub height) with regard to the force-deflection response of the anchor, which would thus affect the entire length of need of the guardrail system.

From the evaluations of the effects of varying anchor strengths on the performance of the G4(2W) guardrail in Chapter 9, it was determined that for undamaged wood posts (i.e., DL0) the performance of the system was not significantly affected by anchor strength. In those cases, the torsional rigidity of the line posts effectively allowed the posts to carry a large proportion of the tensile load in the guardrail. However, when the deterioration level for the posts were DL1 or higher, the performance of the system was compromised when anchor strength was reduced by 30 percent (relative to the baseline case). From the tests performed in this study, the response of the anchor with 2 inches reduced embedment indicated negligible reduction in strength for the first 2 inches of rail deflection, and only 16 percent reduction in strength at 6 inches deflection. Beyond 6 inches deflection the reduction in strength gradually approached 31 percent, but it is expected that the system would have provided sufficient anchorage to successfully contain and redirect most vehicle impact situations prior to reaching such magnitudes of deflection.

The response of the anchor with 4 inches reduced embedment was similar to that at 2 inches reduced embedment, but for this case the resistance of the system at approximately 3 inches of displacement was 13 kips, and remained at this level up to approximately 10 inches displacement. The response at 6 inches reduced embedment began to experience lower resistance at approximately 2 inches deflection, but not significantly less than that of the 4 inches reduced embedment case. At 8 inches reduced embedment, the initial response was undistinguishable from that of the undamaged case, but the loss of anchor resistance occurred abruptly at only five inches rail displacement, which corresponded to 2.6 inches groundline deflection.

Based on the results of these tests combined with those from Gabler’s study, it was concluded that:

- When the “stub height” of the foundation tube, as measured from the top of the foundation tube to the ground, is greater than 4 inches and less than 9 inches (i.e., reduced embedment of 1 to 6 inches), repair should be considered if other system maintenance is being performed. The performance of the anchor is not compromised when stub height is less than 7 inches; however, there is an increased potential for small cars snagging on the top of the foundation tube as well as an increased potential for the breakaway mechanism of the end-terminal to not activate properly during end-on hits at stub heights exceeding 4 inches.
- When stub height exceeds 9 inches (i.e., reduced embedment exceeds 6 inches) the performance of the anchor may be significantly compromised due to significant reduction in anchor strength and the high probability of complete anchor loss at relatively low anchor displacement.

Slack in Anchor Cable

For the damage mode defined by slack in the anchor cable, the tests showed that the force-deflection response of the end-terminal was essentially unaffected for up to approximately 6 inches of rail deflection for cases where the initial slack in the cable was two inches or less. At 3 and 4 inches of slack, however, there was a significant drop in the force-deflection response. In fact, the resistance during the first 1 inch of displacement was essentially negligible for both of these cases. At two inches of displacement the effective resistance was reduced by 65 percent for the case of 3 inches slack, and reduced by 73 percent for the case of 4 inches slack, relative to the baseline case. At four inches of displacement the effective resistance was reduced 39 percent for the case of 3 inches slack; and 62 percent for the case of 4 inches slack. For these two test cases the ultimate strength of the anchor tended to approach a similar magnitude as that of the undamaged case as the displacement approached 10 inches. During a crash event, however, the reduced tension in the rail at the early stages of the crash would likely have resulted in excessive lateral deflections and possibly severe pocketing of the guardrail system by the time the anchor became effective.

Based on the results from the evaluations of anchor strength on the performance of the G4(2W) guardrail in Chapter 9, when the slack in the anchor cable is greater than 2.0 inches and less than 3 inches the performance of the anchor system may be somewhat compromised; and when the slack in the cable exceeds 3 inches, the performance of the anchor may be significantly compromised. According to manufactures recommendations, the anchor cable should be tightened when there is more than 1 inch of slack. When possible this simple repair should be performed during the inspection process.

Recommendations

The following recommendations are based on the collective results from (1) evaluations of the G4(2W) guardrail with varying anchor strength (i.e., Chapter 9), (2) the force-deflection response of the standard two-post-and-strut anchor subjected to tensile loading and (3) the recommendations by Gabler et al. in *NCHRP Report 656*. [Gabler10]

The analysis results from Chapter 9 indicated that the performance of the G4(2W) with healthy posts (i.e., DL0 or DL1) was not significantly affected by anchor strength for the case of an impact on the system at approximately 62 feet downstream of the anchor – this impact point was adopted from full-scale Test 471470-26 which was used as the baseline system throughout this study. In this impact scenario, there were enough posts upstream of the impact point carrying the tensile load of the rail such that the loading on the anchor was negligible. However, consideration should be given to the possibility of impact occurring at a point nearer to the anchor which would significantly increase the loading on the anchor. Also, if the w-beam rail detaches from the upstream posts during impact, or if posts upstream of the impact point fracture under the tensile loading of the w-beam, then anchor loads may increase significantly. This result was demonstrated in this study by simulating Report 350 Test 3-11 impact on the G4(2W) in which the anchor strength was reduced by 47 percent (e.g., end-terminal with single foundation-tube anchor) and the posts were modeled with deteriorated strength properties. The results indicated that as post deterioration levels increased, there was an increase in the number of posts upstream of the impact that fractured, resulting in increased loading on the anchor.

As a result of this study, the research team recommends that the repair threshold for the end-terminal for the G4(2W) be those in which the damage results in more than a 30% loss in anchor capacity relative to the baseline anchor strength. When the damage results in more than 50% loss of capacity then the relative priority for repair is high. These cases include:

- High Priority:
 - Missing or otherwise non-functional groundline strut,
 - Reduction in embedment depth exceeding 6 inches for foundation tubes (i.e., stub height exceeding 9 inches), and
 - Anchor cable slack exceeding 3 inches.

For end-terminal damage that results in 30% to 50% loss of capacity for the anchor, the relative priority for repair is medium, unless a fixed object is located within 50 inches behind the face of the barrier. In that case, the line posts should also be checked for deterioration damage. If the damage level for the posts is DL1 or greater, then the priority for repair is high, based on lateral deflection limitations of the guardrail. These cases include:

- High Priority:
 - Fixed/rigid object located within 50 inches of guardrail, reduced embedment of foundation tube exceeding 4 inches (i.e., stub height exceeding 7 inches) and line posts with deterioration level of DL1 or greater.
- Medium Priority:
 - No fixed objects located within 50 inches of guardrail, reduced embedment of foundation tube exceeding 4 inches but less than 6 inches (i.e., stub height protruding 7 to 9 inches above grade).

A summary of the recommendations regarding end-terminal damage for the G4(2W) guardrail are presented in Table 80. For completeness, the recommendations from *NCHRP Report 656* for damage modes involving the end post, cable bracket, lag bolts on impact head, and bearing plate are also included. The recommendations derived from the current study pertain, primarily, to the upstream anchor. The downstream end-terminal does not generally experience the same magnitude of loading as does the upstream terminal. For this reason, many guardrail systems use a standard “trailing end terminal” (i.e., a single foundation tube and anchor cable) at the downstream end of the guardrail.

For undivided highways, where the impact on a guardrail may occur from either the primary or opposing directions of traffic, the anchor at either end of the guardrail should meet the recommendations of Table 80. For divided roadways, on the other hand, guardrails are only exposed to impacts from traffic in one direction (the primary direction), thus the downstream anchor will require less stiffness/strength compared to the upstream anchor.

Table 80. Recommendations for end-terminal damage for the G4(2W).

Damage Mode	Repair Threshold	Relative Priority
Damaged End Post	Not functional (Sheared, rotted, severely cracked)	High
Anchor Cable	Missing	High
	More than 3 inches slack.	
	Greater than 2 inches and less than 3 inches	Med
Cable Anchor Bracket	Loose or not firmly seated in rail	Medium
Foundation Tube	- Stub height exceeds 9 inches (e.g., soil plate is visible above grade)	High
	- Stub height exceeds 4 inches but less than 9 inches	Medium
Groundline Strut	Missing or otherwise nonfunctional	High
Bearing Plate	Missing	High
	Loose or misaligned	Med
Lag Bolts (Energy Absorbing Terminals Only)	Missing or failed	High
Other	- End-Terminal damage that results in more than 50% reduction in anchor capacity (relative to the baseline anchor strength).	High
	- If a hazard is located within 50 inches behind the w-beam rail, and includes the combination damage mode of: - End-Terminal damage that results in more than 30% loss of anchor capacity and - Guardrail line-posts with deterioration levels of DL1 or greater. <u>These cases include:</u> - Reduced embedment exceeding 4 inches (i.e., stub height exceeding 7 inches) and line posts with deterioration level of DL1 or greater.	High

Future Work

- Test Instrumentation
 - A displacement transducer should be installed on the upstream end of the rail to provide a more accurate representation of the longitudinal displacement. The problem with measuring displacement at the load point is that there are many cases when there is significant lateral and vertical displacement of the rail (e.g., when Post 2 breaks and the rail suddenly drops). The displacement transducer only measures the change in length of the “string” and thus can’t discern direction of motion.

- Crash Performance Evaluations
 - Future work should include analyses of the G4(2W) at impact points nearer to the anchor system.
 - Due to the differences in the torsional rigidity of the W6x9 steel posts of the G4(1S) guardrail, an investigation similar to the one conducted in Chapter 9 should also be conducted to assess effects of anchor strength on the performance of that system, since it is expected that the G4(1S) would have a greater sensitivity to anchor strength.

CHAPTER 14 – EFFECTS OF W-BEAM SPLICE DAMAGE ON RAIL CAPACITY

The effects of crash-induced damage on the residual capacity of w-beam splices were evaluated using physical impact testing. In Report 656 a single damage mode was evaluated for the w-beam splice, which involved a “cut out” of w-beam material around the lower upstream splice bolt. From review of full-scale tests (see Chapter 3) it was determined that a more critical location for splice rupture may be at the downstream splice-bolts. The goal of this study was to supplement the splice damage assessment criteria in Report 656 by quantifying the effects of additional damage modes on the capacity of the splice connection.

The most difficult challenge of this task was in determining how to measure the degree of damage for many of the damage modes, particularly in regards to field assessments. There are several obvious damage modes, such as a missing bolts, that are both easy to assess in the field and also easy to quantify; however, damage modes for splice connections are usually more complicated and are more commonly caused by high stress concentrations in the splice connection and small tears/cuts in the w-beam caused by the w-beam contacting other components with relatively sharp edges during crash events.

Since small tears in the splice bolt holes are likely to be hidden by the bolt head and/or nut, the degree of damage must be quantified by parameters such as degree of flattening, angle of bend in the splice, measure of separation between the two w-beam elements at the upstream and downstream ends of the splice, noticeable indentation/gouging of bolt head into w-beam (e.g., rotation of splice bolt), and slip of bolt in splice-bolt-hole. Most of these damage modes would be difficult to fabricate in the laboratory; therefore, damaged sections of w-beam from crash sites in the state of Maine were collected and assessed for use in this study.

Research Approach

The basic research approach involved:

1. Identifying and measuring the visible damage modes from a number of crash-damaged splice connections from field installations,
2. Correlating the measurable visible damage to the potential for crack initiation in the splice-bolt holes via disassembly and non-destructive inspection techniques (e.g., ultrasonic or magnetic particle) (those specimens selected for pendulum testing were not disassembled),
3. Use pendulum testing to measure the reduction in splice capacity due to various damage modes and levels of damage for a select number of damaged splices, and
4. Associate various splice damage modes with “priority for repair” for inclusion in a Field Guide to assist DOT maintenance personnel in making decisions about repairing damaged guardrail installations.

Procurement and Assessment of Damaged W-Beam Splices

A total of fifteen damaged splice samples were provided to the study by the Maine Department of Transportation (MEDOT); however, a number of those did not have sufficient damage for consideration in the test program. The damaged splice samples were extracted from various crash-damaged field installations in Oxford County, Maine. Most of the damaged articles were delivered fully-assembled to nearby MEDOT maintenance facilities. The research team traveled to these collection-sites to identify and measure the various damages for each specimen.

Inspection of Fully Assembled Splice (General Field-Type Measurements)

The first phase of this assessment involved measurement-procedures that could readily be performed by maintenance personnel at a crash site and included:

1. *Percent Rail Flattening/Crush* – The condition of rail flattening was measured at each of the four quadrants of the splice connection, since it was not known how deformation at each of these locations would affect capacity. In particular, measurements were taken at the:
 - a. Downstream, top section – The distance from the center of the w-beam to the top edge was measured from the back-side of the w-beam splice at the downstream splice bolts, as shown in Figure 325.
 - b. Downstream, bottom section – The distance from the center of the w-beam to the bottom edge was measured from the back-side of the w-beam splice at the downstream splice bolts.
 - c. Upstream, top section – Measurement was taken in the same manner as described above at the upstream splice bolts on the upper half of the w-beam splice.
 - d. Upstream, bottom section – Measurement was taken in the same manner as described above at the upstream splice bolts on the lower half of the w-beam splice.
 - The degree of flattening was then computed using the following equation:

$$\text{Percent Rail Flattening} = \frac{x - x_0}{x_{flat} - x_0} * 100$$

- Where x is the deformed $\frac{1}{2}$ -cross-sectional height from the center of the w-beam to the top-edge of the rail measured from the back-side of the w-beam splice; x_0 is the undeformed $\frac{1}{2}$ -cross-section height taken as 6.125 inches; x_{flat} is the $\frac{1}{2}$ -cross-section height of the w-beam when completely flattened taken as 9.6 inches.
- For cases where the value of x was less than x_0 (i.e., vertical crushing of the splice), the degree of crush was computed as the percent difference of the deformed height (x) to that of the undeformed height (x_0) using the following relationship:

$$\text{Percent Rail Crush} = \frac{x - x_0}{x_0} * 100$$

2. *Rail Separation* – Two types of rail separation were measured:
 - a. The lateral gap opening at the upstream edge of the splice (traffic face of rail) and at the downstream edge of the splice (back face of rail). The measurements were taken at eight points, adjacent to the splice-bolt locations, as illustrated in Figure 326.
 - b. The longitudinal slip in the splice – taken as the distance measured from the original position of the rail (discernible in most cases) to the current position, as illustrated in Figure 327.
3. *Condition of Splice Bolts* – The condition for each splice bolt was recorded as missing, loose, gouging, or torn-through. The term gouging refers to the condition of a splice-bolt rotated about the vertical axis of the rail, where the edge of the bolt-head is pressed into the w-beam panel. This damage mode generally results from high tensile load in the rail during a crash event. An example of “light gouging” is shown in Figure 328 evidenced by visible rotation of the splice-bolt.
4. *Condition of Splice Bolt Holes* – Each splice bolt hole was inspected for visible stretching and tearing. Figure 329 shows an example of a splice bolt hole with evident stretching (resulting from high tension loading in the rail during crash) which was measured by taking the longitudinal distance from the edge of the splice bolt to its apparent original position. In some cases the only visual cue to indicate that a bolt hole is “stretched” is when the edge of the bolt hole is visible beside the bolt head.
5. *Condition of Post Bolt Holes* – Each post bolt hole was inspected for visible damages which included (listed in order of increasing severity) stretching, horizontal tears, and vertical tears. Figure 330 shows an example of a splice bolt hole with evident stretching and a horizontal tear. In this case, the worse condition was recorded, which was the horizontal tear.
6. *Vertical and Horizontal Tears* – When a tear was evident within the splice region (i.e., region encompassing the out-to-out distance from the ends of the rail sections in the splice) the length of the tear was measured and reported in the appropriate category. The possible categories include tears in the upstream or downstream panels at the top section, bottom section, middle section, top edge or bottom edge, as illustrated in Figure 331. For tears that intersect the top or bottom edge of the rail, in which case the tear locations would also fall into the category of top section or bottom section, only the “edge” category was reported - since edge tears in general have been shown to be the more critical condition.[Gabler10]



Figure 325. Rail flattening – Rail flattening and rail crush at each quadrant of the splice is measured from the center of the w-beam to the top/bottom edge at the splice bolts.



Figure 326. Rail separation - Lateral gap between rail elements at splice connection (measurements taken at locations adjacent to the eight splice bolts).

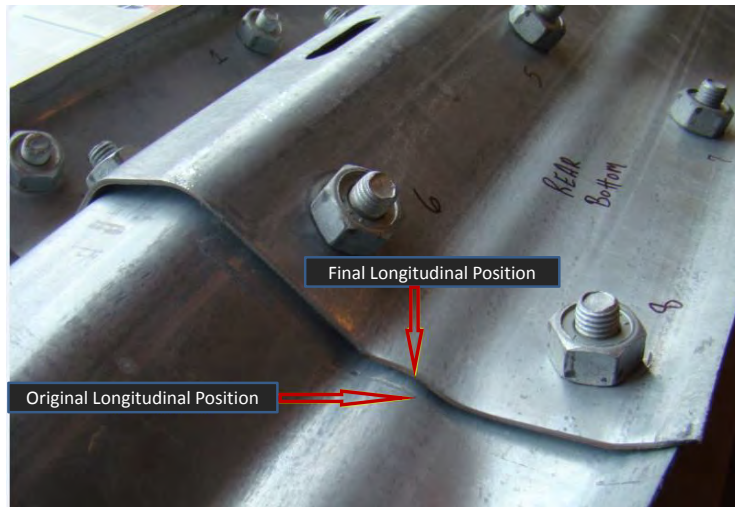


Figure 327. Rail separation – Longitudinal slip in splice connection.



Figure 328. Gouging – Gouging of splice-bolts into w-beam panel is evidenced by rotation of the bolt about the vertical axis.

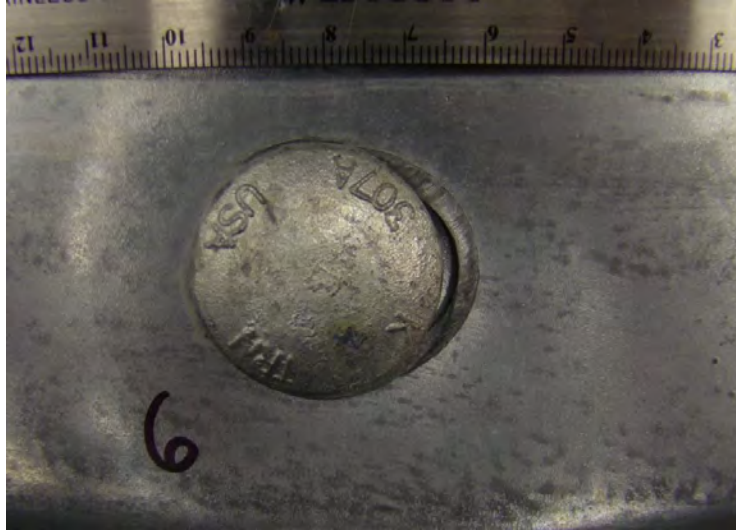


Figure 329. Splice bolt hole stretching – Stretching of the splice bolt hole is evidenced in this photo by the apparent longitudinal movement of the splice bolt relative to its original position.



Figure 330. Horizontal tear in post bolt hole – This photo shows evidence of both stretching and a horizontal tear in the post bolt hole.

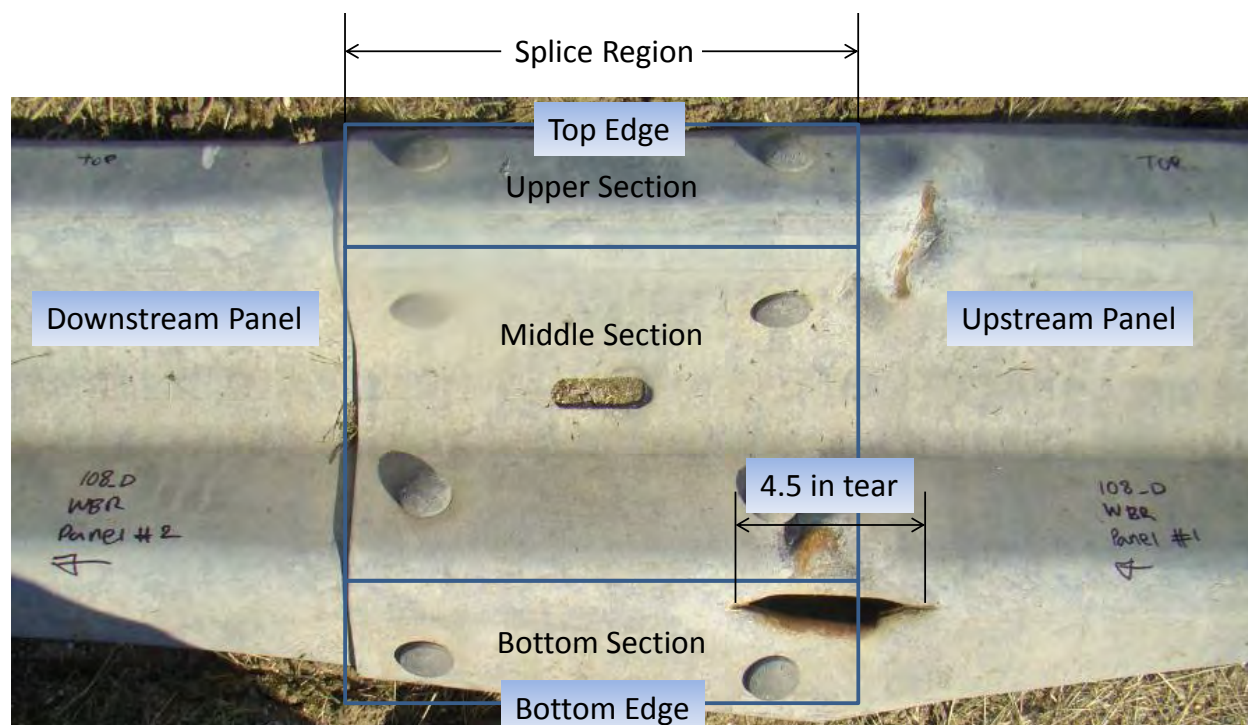


Figure 331. Horizontal and vertical tears – tears were measured and categorized according to location on upstream and downstream panel as denoted here.

A damage summary sheet was created for each damaged splice specimen (see Appendix R). The summary sheets include damage measurements as described above and photos of the damaged splices. When there were no measurable damages for a particular damage mode, the corresponding damage-field was left blank in the assessment table. Tables 81 through 85 show the results of the damage measurements. Each table focuses on a single damage mode and lists the specimens in descending order with respect to the maximum level of the corresponding damage. Since splice damage generally involves multiple damage modes, each damage-mode table also includes a summary of all other damages identified for reference.

Regarding the physical test program, there were not a sufficient number of specimens with a single mode of damage for each damage mode case, which made it difficult to accurately quantify the effect of each isolated damage mode on capacity of the splice. For example, there was some amount of rail flattening, rail crush or both in essentially all damage splice cases, as shown in Table 81. So, when evaluating the effects of any specific damage mode on the capacity of the splice, the response was also influenced by the effects of any other existing damages, such as flattening/crushing. It also appears that some of the damage modes are strongly linked with others. For example, from Table 83, high levels of rail separation generally occur in combination with high levels of rail flattening and also gouging of the splice bolts into the w-beam (e.g., compare columns for “*Max Separ.*”, “*Rail Flattening*” and “*Gouging*” in Table 83). There were no *apparent* correlations between rail tears (i.e., non-hole tears) and other splice damage modes (at least from the damaged specimens collected in this study). From visual inspection, these horizontal and vertical tears in the splice were likely caused by a part on the vehicle cutting into the rail during the crash (see Figure 331 for example).

Table 81. Summary of “rail flattening” damage mode for MEDOT crash-damaged splice specimens – listed in descending order, w.r.t maximum degree of flattening.

Specimen No.	% Rail Flattening / Crush					Other Damages									
	@ upstream bolts		@ downstream bolts		Max Deg. of Flattening	Rail Separation (in)		Splice Bolts and Hole				Post Bolt Hole		Tears (in)	
	Top Section	Bottom Section	Top Section	Bottom Section		Long.	Lateral	Loose	Missing	Gouging	Torn	Stretched	Torn	Vertical	Horizontal
4A5-ME010	97.1%	-2.0%	86.3%	-4.1%	97.1%	0.20	0.55			*					
4A5-ME006	89.9%	68.3%	97.1%	82.7%	97.1%	N.A.	N.A.	N.A.	N.A.						
4A5-ME013	93.5%	3.6%	89.9%	3.6%	93.5%	0.20	0.35			*					11.8
4A5-ME008	86.3%	10.8%	75.5%	10.8%	86.3%	0.20	0.28								
4A5-ME011	82.7%	10.8%	68.3%	18.0%	82.7%	N.A.	N.A.	N.A.	N.A.						
4A5-ME007	75.5%	61.2%	82.7%	61.2%	82.7%		0.50			*					
4A5-ME001	68.3%	3.6%	68.3%	-14.3%	68.3%	0.20	0.13	*				*			
4A5-ME005	18.0%	68.3%	10.8%	32.4%	68.3%	0.12	0.25								4.5
4A5-ME017	32.4%	68.3%	46.8%	61.2%	68.3%	0.25	0.25			*					22.5
4A5-ME003	61.2%	10.8%	25.2%	-2.0%	61.2%		0.25							1.0	
4A5-ME018	46.8%	39.6%	39.6%	32.4%	46.8%	0.25	0.50		*	*					
4A5-ME002	25.2%	3.6%	3.6%	39.6%	39.6%	N.A.	N.A.	N.A.	N.A.		*				5.0
4A5-ME014	25.2%	7.3%	25.2%	-8.7%	25.2%	0.28		*							11.8
4A5-ME004	-26.5%	-30.6%	-30.6%	3.6%	3.6%		0.25								
4A5-ME015	0.0%	0.0%	0.0%	-4.1%				*							

Table 82. Summary of “rail crush” damage mode for MEDOT crash-damaged splice specimens – listed in descending order, w.r.t maximum degree of crush.

Specimen No.	% Rail Flattening / Crush					Other Damages										
	@ upstream bolts		@ downstream bolts		Max Deg. of Crush	Rail Separation (in)		Splice Bolts and Hole				Post Bolt Hole		Tears (in)		
	Top Section	Bottom Section	Top Section	Bottom Section		Long.	Lateral	Loose	Missing	Gouging	Torn	Stretched	Torn	Vertical	Horizontal	
4A5-ME004	-26.5%	-30.6%	-30.6%	3.6%	-30.6%		0.250									
4A5-ME001	68.3%	3.6%	68.3%	-14.3%	-14.3%	0.197	0.125	*				*				
4A5-ME014	25.2%	7.3%	25.2%	-8.7%	-8.7%	0.276		*							11.8	
4A5-ME010	97.1%	-2.0%	86.3%	-4.1%	-4.1%	0.197	0.551			*						
4A5-ME015	0.0%	0.0%	0.0%	-4.1%	-4.1%			*								
4A5-ME003	61.2%	10.8%	25.2%	-2.0%	-2.0%		0.250							1.0		
4A5-ME002	25.2%	3.6%	3.6%	39.6%		N.A.	N.A.	N.A.	N.A.		*					5.0
4A5-ME005	18.0%	68.3%	10.8%	32.4%		0.118	0.250									4.5
4A5-ME006	89.9%	68.3%	97.1%	82.7%		N.A.	N.A.	N.A.	N.A.							
4A5-ME007	75.5%	61.2%	82.7%	61.2%			0.500			*						
4A5-ME008	86.3%	10.8%	75.5%	10.8%		0.197	0.276									
4A5-ME011	82.7%	10.8%	68.3%	18.0%		N.A.	N.A.	N.A.	N.A.							
4A5-ME013	93.5%	3.6%	89.9%	3.6%		0.197	0.354			*						11.8
4A5-ME017	32.4%	68.3%	46.8%	61.2%		0.250	0.250			*						22.5
4A5-ME018	46.8%	39.6%	39.6%	32.4%		0.250	0.500		*	*						

Table 83. Summary of “rail separation” damage mode for MEDOT crash-damaged splice specimens – listed in descending order, w.r.t maximum separation.

Specimen No.	Rail Separation								Other Damages													
	Gap at Downstream End (in)				Gap at Upstream End (in)				Max. Separ. (in)	Long. Slip (in)	Rail Flattening (%)	Rail Crush (%)	Splice Bolts and Hole				Post Bolt Hole		Tears (in)			
	@ bolt1	@ bolt2	@ bolt3	@ bolt4	@ bolt5	@ bolt6	@ bolt7	@ bolt8					Loose	Missing	Gouging	Torn	Stretched	Torn	Vertical	Horizontal		
4A5-ME010	0.236	0.551	0.157		0.118				0.551	0.197	97%	-4%			*							
4A5-ME007		0.5	0.3125	0.25					0.500		83%				*							
4A5-ME018		0.5	0.5						0.500	0.250	47%			*	*							
4A5-ME013	0.276	0.354			0.157				0.354	0.197	94%			*								11.8
4A5-ME008	0.276	0.118							0.276	0.197	86%											
4A5-ME003	0.25				0.25				0.250		61%	-2%										1.0
4A5-ME004	0.25								0.250		4%	-31%										
4A5-ME005				0.25					0.250	0.118	68%											4.5
4A5-ME017		0.25	0.25				0.25		0.250	0.250	68%			*								22.5
4A5-ME001				0.125					0.125	0.197	68%	-14%	*					*				
4A5-ME002	N.A.	N.A.	N.A.	N.A.	N.A.	N.A.	N.A.	N.A.	0.000	N.A.	40%		N.A.	N.A.		*						5.0
4A5-ME006	N.A.	N.A.	N.A.	N.A.	N.A.	N.A.	N.A.	N.A.	0.000	N.A.	97%		N.A.	N.A.								
4A5-ME011	N.A.	N.A.	N.A.	N.A.	N.A.	N.A.	N.A.	N.A.	0.000	N.A.	83%		N.A.	N.A.								
4A5-ME014									0.000	0.276	25%	-9%	*									11.8
4A5-ME015									0.000		0%	-4%	*									

Table 84. Summary of “visible splice bolt and splice bolt hole” damage mode for MEDOT crash-damaged splice specimens.

Specimen No.	Visible Splice Bolt and Splice-Bolt Hole Damage																																Other Damages							
	Loose Bolts								Missing Bolts								Visible Gouging								Visible Tear								Rail Flattening (%)	Rail Crush (%)	Rail Separation		Post Bolt Hole		Non Bolt-Hole Tears	
	#1	#2	#3	#4	#5	#6	#7	#8	#1	#2	#3	#4	#5	#6	#7	#8	#1	#2	#3	#4	#5	#6	#7	#8	#1	#2	#3	#4	#5	#6	#7	#8			Long. (in)	Lateral (in)	H-Tear	V-Tear	Vertical (in)	Horizontal (in)
4A5-ME001			*			*	*																								68%	-14%	0.20	0.13		*				
4A5-ME007																	*			*	*										83%			0.50						
4A5-ME010																		*		*											97%	-4%	0.20	0.55						
4A5-ME013																*	*			*	*										94%		0.20	0.35				11.8		
4A5-ME014					*																										25%	-9%	0.28					11.8		
4A5-ME015						*																									0%	-4%								
4A5-ME003																															61%	-2%		0.25			1.0			
4A5-ME004																															4%	-31%		0.25						
4A5-ME005																															68%		0.12	0.25				4.5		
4A5-ME008																															86%		0.20	0.28						
4A5-ME002	-	-	-	-	-	-	-	-	-	-	-	-	-	-	-	-	-	-	-	-	-	-	-	-	-	-	-	-	-	40%		N.A.	N.A.				5.0			
4A5-ME006	-	-	-	-	-	-	-	-	-	-	-	-	-	-	-	-	-	-	-	-	-	-	-	-	-	-	-	-	-	97%		N.A.	N.A.							
4A5-ME011	-	-	-	-	-	-	-	-	-	-	-	-	-	-	-	-	-	-	-	-	-	-	-	-	-	-	-	-	-	83%		N.A.	N.A.							
4A5-ME018								*	*			*			*				*											47%		0.25	0.50							
4A5-ME017															*	*	*		*	*										68%		0.25	0.25				22.5			

Inspection of Unassembled Splice (for Hidden Damages in the Splice-Holes)

The next step of the research approach involved disassembly of the damaged splice samples in order to assess damages to the splice-bolt holes. These areas cannot be directly inspected in the field since they are hidden by the splice-bolt head and nut. The purpose of this task was to correlate visible, measurable damages to the potential for crack initiation in the splice-bolt holes.

The intent was to first select specimens for use in the pendulum test program. Those specimens would *not* be disassembled for inspection because it was highly unlikely that the damaged splice could be reassembled exactly to its original state, which included residual stress in the splice restrained by the bolted connection. Once the specimens for the pendulum test program were selected, the remaining specimens would then be disassembled and inspected for damages around the edges of the splice-bolt holes via non-destructive inspection techniques. Any damage mode, as well as the level of damage for that mode, that resulted in notable damage to the splice-bolt holes would be determined. The potential for crack initiation in the splice-bolt holes could then be correlated to the various types of measurable damage modes.

It was decided, however, that this task would not be performed due to the low number of samples collected for the study. Instead, all available damaged splice specimens were used for the pendulum test program.

Physical Testing

Equipment and Instrumentation

Pendulum Device

The striker used in the tests was a 4,360-lb concrete pendulum with a semi-rigid nose, which is shown in Figure 332. The semi-rigid nose was developed by researchers from Virginia Tech during the first phase of this study and was fabricated from a wooden block and covered with sheet metal.[Gabler10] The radius of chamfer at the center of the impactor face was 6 inches, which was based on measurements of a 2006 Chevrolet 1500 pickup truck. [Gabler10]

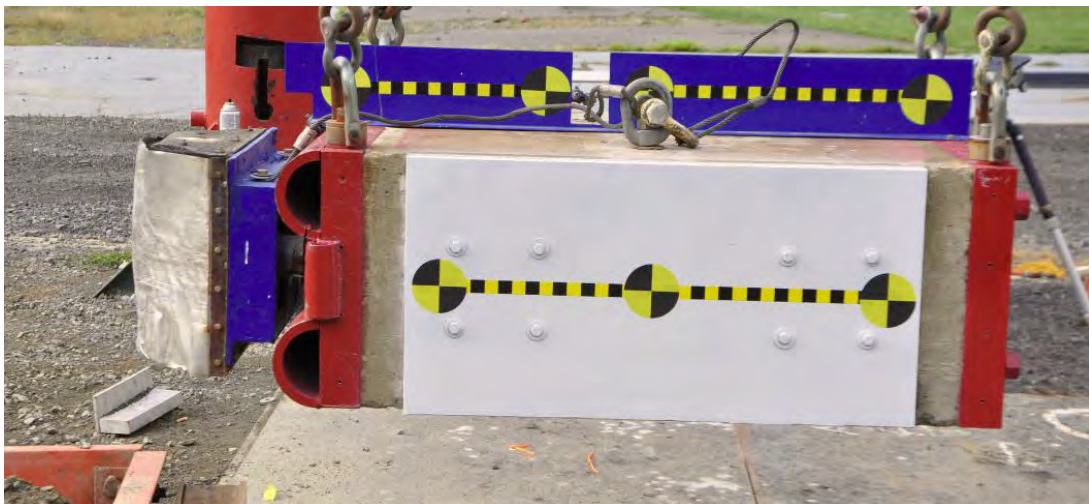
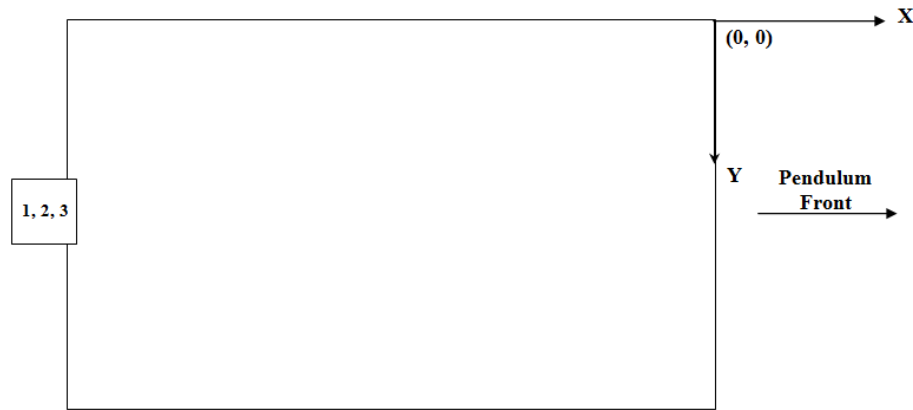


Figure 332. 4,360-lb pendulum device with semi-rigid nose.

Accelerometers

The pendulum was instrumented with three accelerometers mounted onto the backside of the pendulum mass. Accelerometers 1 and 3 recorded data in the x-direction (forward direction) and Accelerometer 2 recorded data in the z-direction (vertical direction). Figure 333 provides a schematic showing the locations of the accelerometers.



Pendulum top view with accelerometer blocks

CH.	LOCATION	X (cm) Guardrail	Y (cm) Center Pend. Nose	Z (cm) From ground	SERIAL NO.	AXIS
1	Rear Center of Pend.	-43.0	127.0	71.0	D12063	-X
2	Rear Center of Pend.	-43.0	127.0	71.0	D12130	-Z
3	Rear Center of Pend.	-43.0	127.0	71.0	D12899	-X

Figure 333. Schematic of the accelerometer instrumentation for the pendulum tests.

Photography Cameras

The tests were also recorded using five high-speed cameras with an operating speed of 500 frames per second and two digital video cameras (~60 fps). Figure 334 provides the specifications and the general placement of the high-speed cameras for the tests. The accelerometers and the high-speed video were triggered upon impact using pressure tape switches when the pendulum contacted the post. The test setup and results were also documented with pre- and post-test photographs.

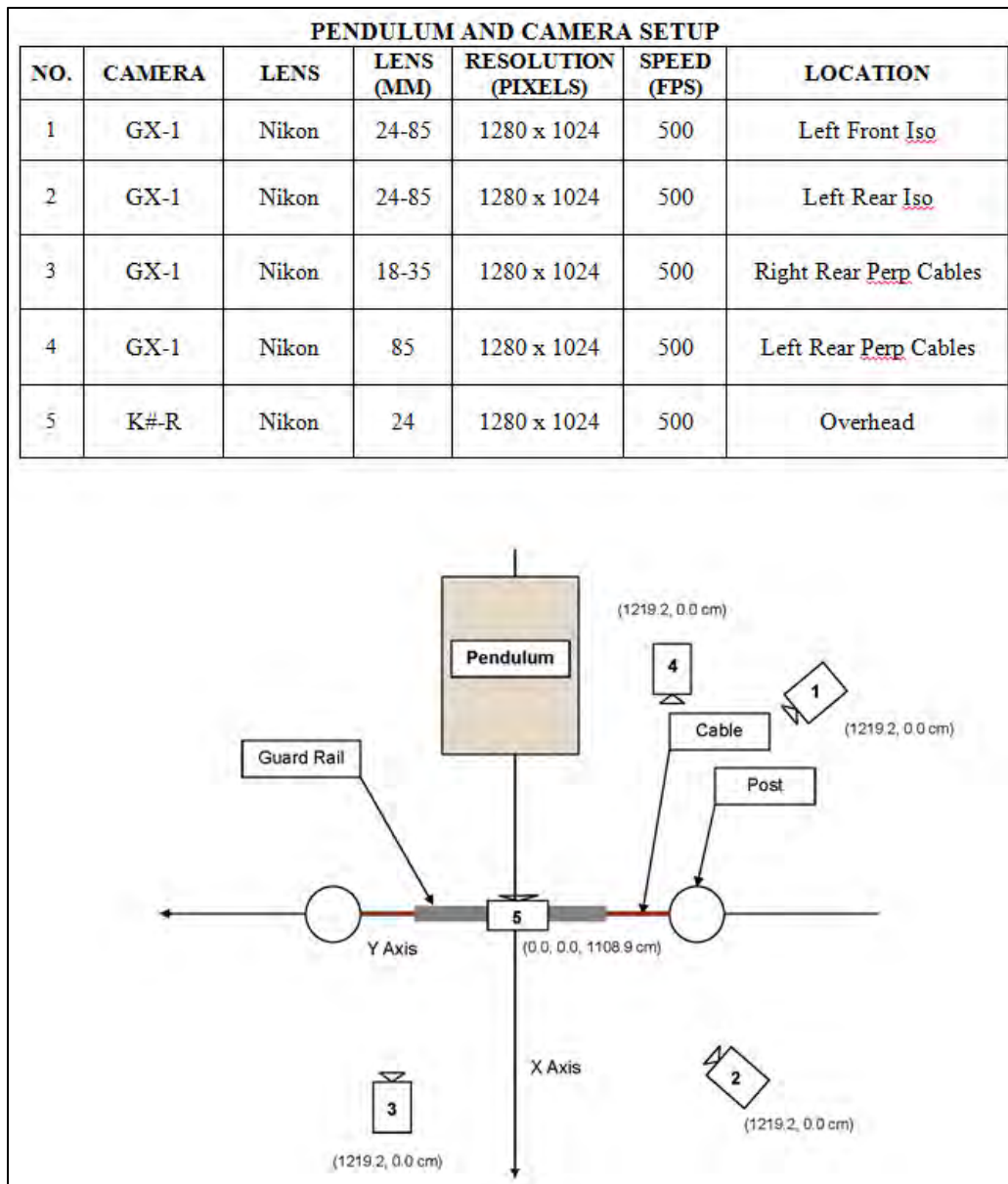


Figure 334. High-speed camera specifications and placement.

Test Setup

The original plan was to use the same test setup that Gabler *et al* used for testing the damaged splice in Phase I.[*Gabler10*] After critical review of the test videos from Gabler's study, it was determined that the test setup tended to result in a tensile rupture of the splice, which is not generally the mode of failure mode witnessed in full-scale tests. Because of the short length of rail and the "rigid" constraint on the boundaries in Gabler's study, the rail developed very high tensile forces at relatively low rail deflections. Figure 335 shows sequential views extracted from the high-speed video in one of Gabler's tests. The upper image shows the test article immediately before splice rupture and the lower image is the test article shortly after rupture.

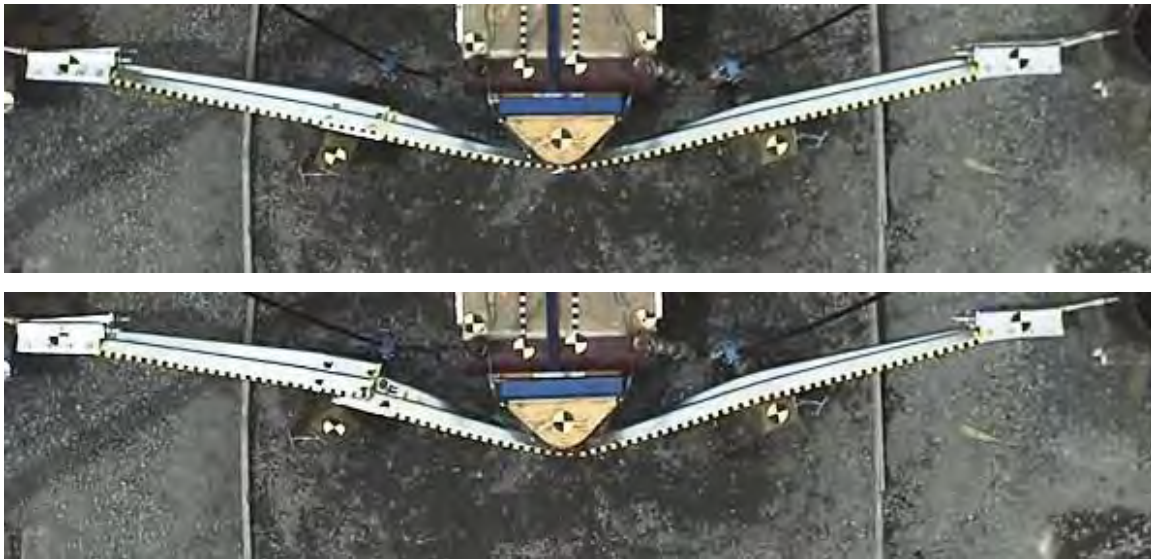


Figure 335. Sequential views of a pendulum test performed in Gabler's study.

Unfortunately, the length of rail could not be extended beyond these limits due to the limited space at the test site. One alternative would be to design the boundary conditions to mimic the longitudinal and lateral stiffness behavior of an extended guardrail, but such an effort was beyond the scope of this study. It was therefore decided to modify the test setup such that the rail would bend at the post (typical of a normal pocket that develops in a crash event), as illustrated in Figure 336.



Figure 336. Pocketing during full-scale crash test C08C3-27.2.[Fleck08b]

The test set up is shown in Figure 337. The test article was a 13-ft long section of w-beam rail with a w-beam splice located at 65 inches from the downstream end. Each end of the rail was constrained from longitudinal displacement using two 0.75-inch diameter cables (i.e., AASHTO-AGC-ARTBA FCA01) fastened onto the ends of the rail. On the downstream end, the cables were fastened to two standard cable anchor brackets (i.e., AASHTO-AGC-ARTBA

FPA01). Each bracket was bolted onto the rail using eight ½-inch bolts and nuts with 1-1/16 inch diameter washers under the bolt heads and two 2.5 x 15 x ¼-inch steel bearing plates under the nuts, as shown in Figure 338. On the upstream end, the cables were fastened to the rail by welding three modified anchor cable brackets directly to the end of the w-beam, as shown in Figure 339. The two legs of each of the cable anchor brackets were removed and a continuous weld along the top and bottom side of each bracket was used to fasten the bracket to the rail.

The test setup involved a single W6x16 structural steel post with wood blackout installed downstream of the impact location at the splice connection. There was no post installed upstream of the impact point in order to permit the maximum amount of deflection prior to developing full tension in the rail. The rigid W6x16 post was used to limit the amount of deflection of the post and force the bending mode of the splice around the post. The post was 72 inches long and was embedded 44 inches in the soil. The 6x8x12 inch routed wood blackout was used to separate the w-beam rail from the post, and a standard 10-inch long 5/8-inch diameter bolt and nut (i.e., AASHTO-AGC-ARTBA FBB03) was used to fasten the rail to the blackout and post. The post-bolt was positioned at the downstream end of the slotted hole in the w-beam to emulate the typical position of the bolt resulting from an impact upstream of the splice, as shown in Figure 340. The rail height was 28 inches measured from the ground to the top of the rail.

The soil for all tests conformed to Grading B of AASHTO M147-95 and was compacted in 6-inch lifts using a pneumatic tamper. The density, moisture content and degree of compaction of the soil was measured in front of and behind the post after each compaction process using a Troxler-Model 3440 Surface Moisture-Density Gauge. There were a total of twelve readings which were averaged to determine the effective soil conditions.



Figure 337. Test set-up for Test Series 14004.



Figure 338. Anchoring of the downstream end of the rail for Test Series 14004.

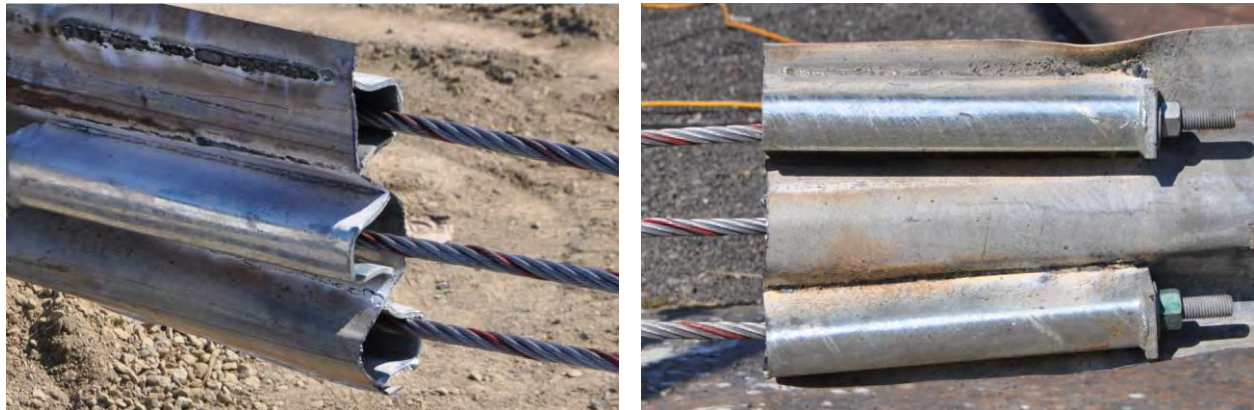


Figure 339. Anchoring of the upstream end of the rail for Test Series 14004.



Figure 340. Typical mounting position for post-bolt was on the downstream side of the slotted hole on the rail.

Impact Conditions

The 4,360-lb pendulum struck the w-beam rail at 37.5 inches upstream of the splice connection. The nominal impact speed was 20.5 mph, which resulted in 734 kip-in of kinetic energy for the striker. Several preliminary tests were performed to determine the appropriate impact and boundary conditions for the study. The results of those preliminary tests are included in the test summary sheets in Appendix S as Tests 14004A-E. Note that the test conditions for Test 14004E were consistent with those used in the primary test program, except that the post-bolt was positioned at the upstream end of the slotted hole in the rail. This test involved a new, undamaged rail splice connection, but resulted in relatively low capacity. Since it could not be determined if the position of the post bolt affected the results, the test was excluded from the study.

Scope

Three damage modes were investigated: (1) rail flattening, (2) longitudinal slip in the splice, and (3) splice separation (gap between panels at the downstream splice bolts). There were a total of fifteen tests, including the five preliminary tests performed using “spare” test specimens to help finalize the test setup and impact conditions. The complete test matrix is shown in Table 86. Because of the general nature of crash damage, most of the test specimens contained multiple damage modes. The primary damage mode evaluated for each test case is shown in Table 86. In most cases the primary damage mode corresponded to the predominate damage mode observed for that case.

Of the ten primary tests (Tests 14004F-O), two were performed on splices with significant rail flattening, two were performed on splices with notable longitudinal slip in the splice connection, one was performed on a splice with significant rail crush, two were performed on splices with significant lateral separation of the w-beam rails at the downstream splice bolts, and two were performed on undamaged (new) splices. One supplemental test (i.e., Test 14004M) was also performed which involved a damaged splice with a combination of three damage modes with notable damage levels (i.e., 0.35 inches of splice separation, 0.2 inch of longitudinal slip, and 93.5% flattening).

Table 86. Pendulum test matrix for the splice damage study.

Primary Damage Mode	Test #	Specimen #	Complete Damage Summary	Damage Level	Target Impact Conditions		
					Mass (kips)	Velocity (mph)	Energy (kip-in)
Rail Flattening	14004M	4A5-ME013	Rail Flattening Long. Slip Splice Separation Horizontal Tear Splice-Bolts Gouging	94% 0.2 inches 0.35 inches 11.81 in. 4 locations	4.36	20.5	734
	14004G	4A5-ME011	Rail Flattening	83%	4.36	20.5	734
	14004F	4A5-ME001	Rail Flattening Rail Crush Long. Slip Splice Separation Loose Splice-Bolts	68% 14% 0.20 inches 0.13 inches 3 locations	4.36	20.5	734
Long. Slip in Splice	14004H	4A5-ME014	Long. Slip Rail Flattening Rail Crush Loose Splice-Bolts	0.28 inches 25% 9% 1 location	4.36	20.5	734
	14004I	4A5-ME017	Long. Slip Rail Flattening Horizontal Tear Splice-Bolts Gouging	0.25 inches 68% 22.8 inches 5 locations	4.36	20.5	734
Rail Crush	14004J	4A5-ME004	Rail Crush Splice Separation	31% 0.25 inches	4.36	20.5	734
Lateral Gap in Splice	14004K	4A5-ME010	Splice Separation Rail Flattening Rail Crush Long. Slip Splice-Bolts Gouging	0.55 inch 97% 4% 0.2 inches 2 locations	4.36	20.5	734
	14004L	4A5-ME007	Splice Separation Rail Flattening Splice-Bolts Gouging	0.5 inch 83% 3 locations	4.36	20.5	734
Undamaged	14004N	New02	-	-	4.36	20.5	734
	14004O	New03	-	-	4.36	20.5	734

Results

A summary of the test results for Test Series 14004 are shown in Table 87, including damage mode case, damage level, impact velocity, failure mode, peak force during the impact, and the maximum energy absorbed by the guardrail system up to the point of rail rupture. The resulting peak impact force and peak energy for each case is also shown graphically in Figures 341 and 342. The impact force and energy vs. rail deflection for the various damage mode cases is compared to the results for the undamaged rail in Figures 343 through 346. Sequential views of the tests are shown in Figures 347 through 351. The individual test-summary sheets are included in Appendix S.

Table 87. Results of pendulum test series 14004.

Primary Damage Mode	Test #	Specimen #	Complete Damage Summary	Damage Level	Impact Conditions		Results		
					Velocity (mph)	Energy (kip-in)	Failure Mode	Force (kips)	Energy (kip/in)
Rail Flattening	14004M	4A5-ME013	Rail Flattening Long. Slip Splice Separation Horizontal Tear Splice-Bolts Gouging	94% 0.2 inches 0.35 inches 11.81 in. 4 locations	20.6	741.6	Splice-Bolt Tear-Out	48.2	503
	14004G	4A5-ME011	Rail Flattening	83%	21.2	734.0	Splice-Bolt Tear-Out	45.4	550
	14004F	4A5-ME001	Rail Flattening Rail Crush Long. Slip Splice Separation Loose Splice-Bolts	68% 14% 0.20 inches 0.13 inches 3 locations	20.2	734.0	Rail Tear	43.2	437
Long. Slip in Splice	14004H	4A5-ME014	Long. Slip Rail Flattening Rail Crush Loose Splice-Bolts	0.28 inches 25% 9% 1 location	19.7	734.0	Splice-Bolt Tear-Out	41.7	443
	14004I	4A5-ME017	Long. Slip Rail Flattening Horizontal Tear Splice-Bolts Gouging	0.25 inches 68% 22.8 inches 5 locations	20.3	734.0	Boundary Failure	50.1	542
Rail Crush	14004J	4A5-ME004	Rail Crush Splice Separation	31% 0.25 inches	20.2	734.0	Boundary Failure	52.1	561
Lateral Gap in Splice	14004K	4A5-ME010	Splice Separation Rail Flattening Rail Crush Long. Slip Splice-Bolts Gouging	0.55 inch 97% 4% 0.2 inches 2 locations	20.5	734.0	Splice-Bolt Tear-Out	39.5	501
	14004L	4A5-ME007	Splice Separation Rail Flattening Splice-Bolts Gouging	0.5 inch 83% 3 locations	20.6	734.0	Splice-Bolt Tear-Out	54.6	512
Undamaged	14004N	New02	-	-	20.4	734.0	Splice-Bolt Tear-Out	49.9	573
	14004O	New03	-	-	20.6	734.0	Splice-Bolt Tear-Out	46.1	520

The force, energy and displacement values were back-calculated using the accelerometer data from the impacting mass, and thus relate indirectly to the lateral motion of the rail at the point of impact. The force values reported herein should not be interpreted as tensile forces in the splice. Also, the reported energy values are a function of deformations within the overall guardrail test section, which include not only the deformations of the rail and splice, but also the energy dissipated through deformations of the post and soil.

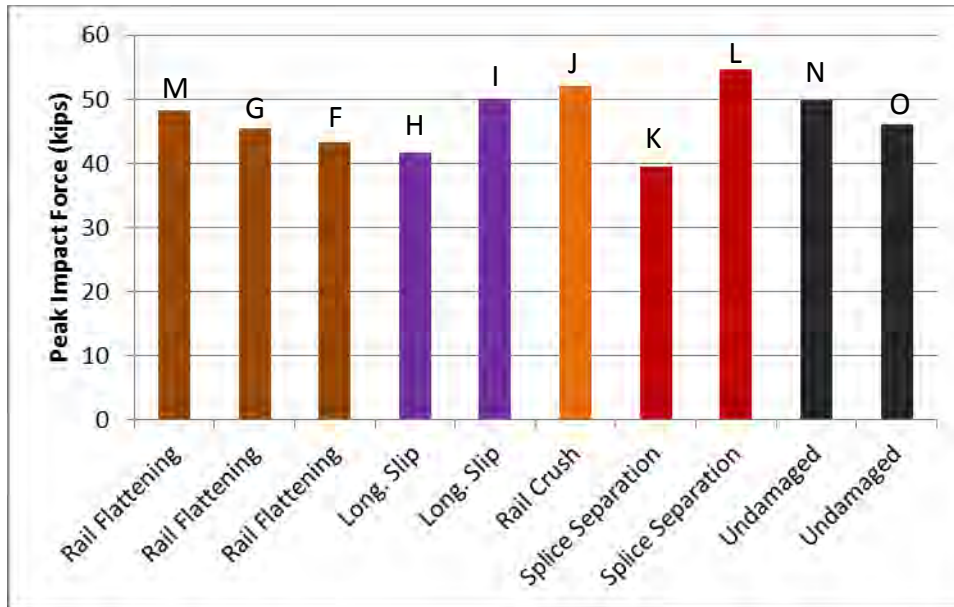


Figure 341. Peak impact force for each damage mode case investigated in test series 14004F-O.

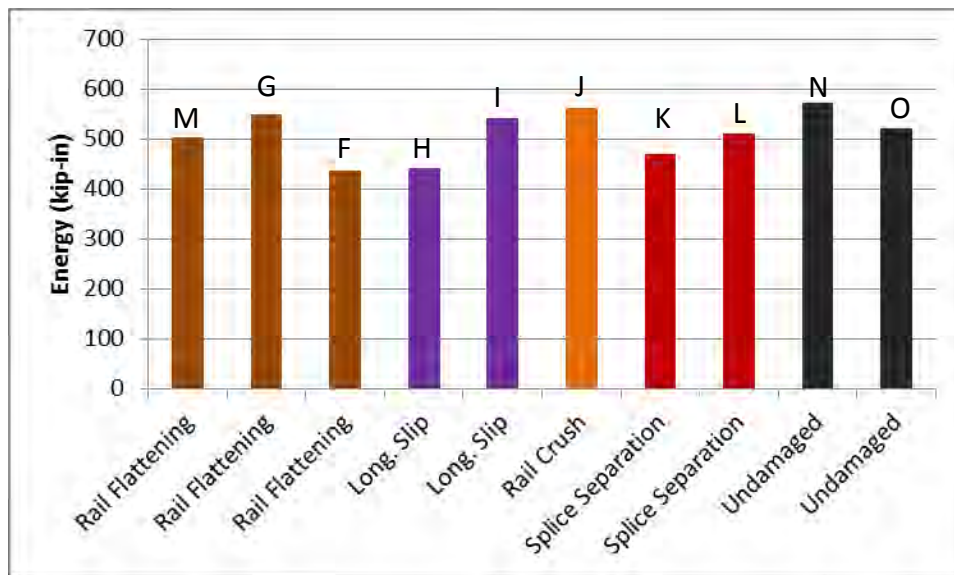
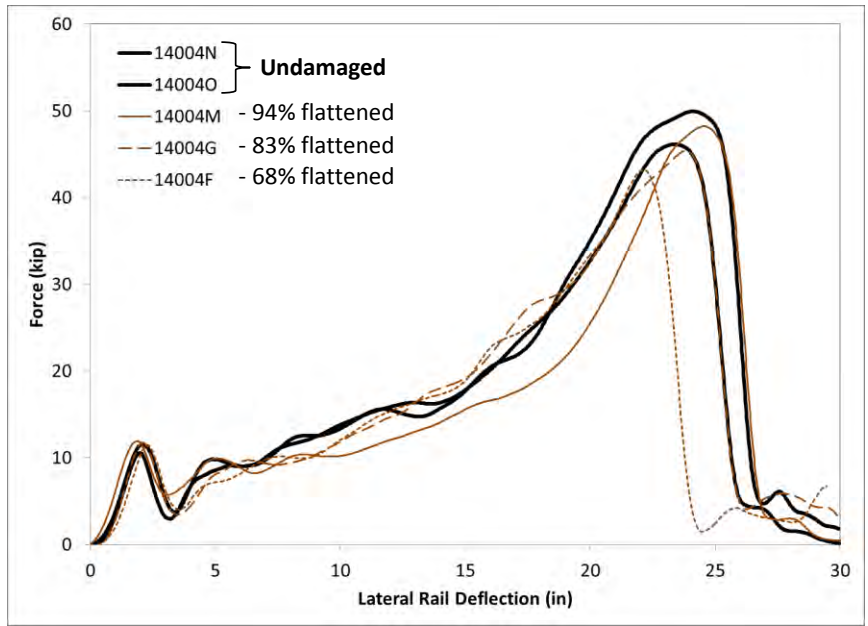
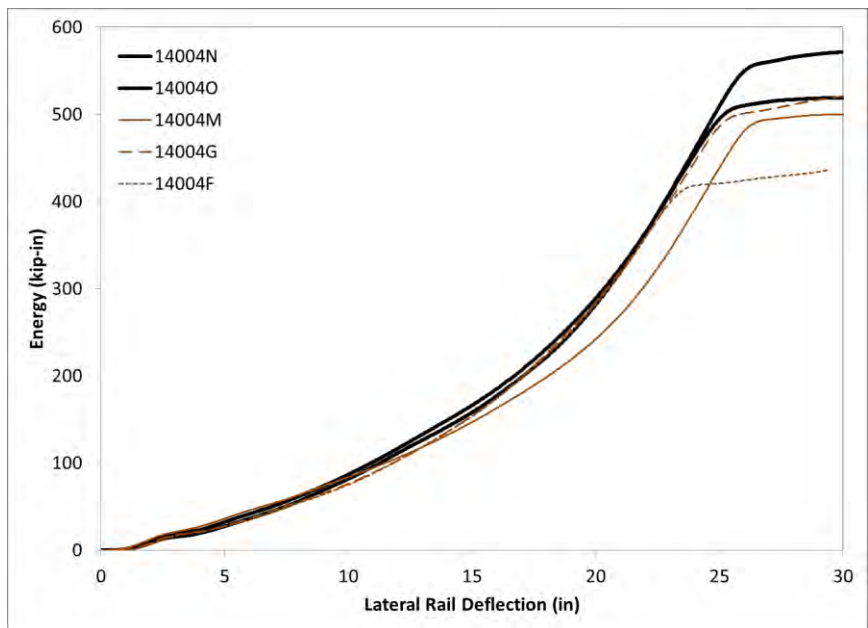


Figure 342. Peak impact energy for each damage mode case investigated in test series 14004F-O.

•

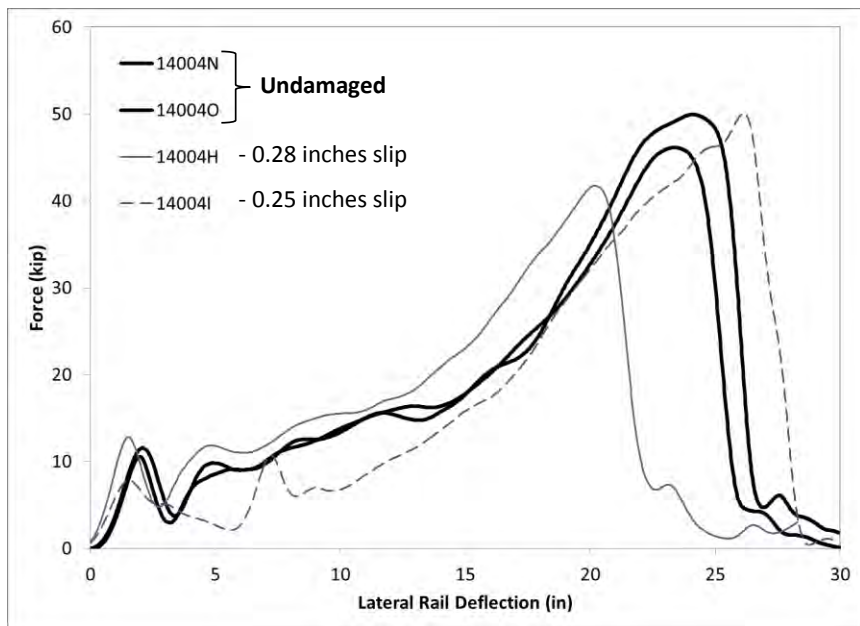


(a)

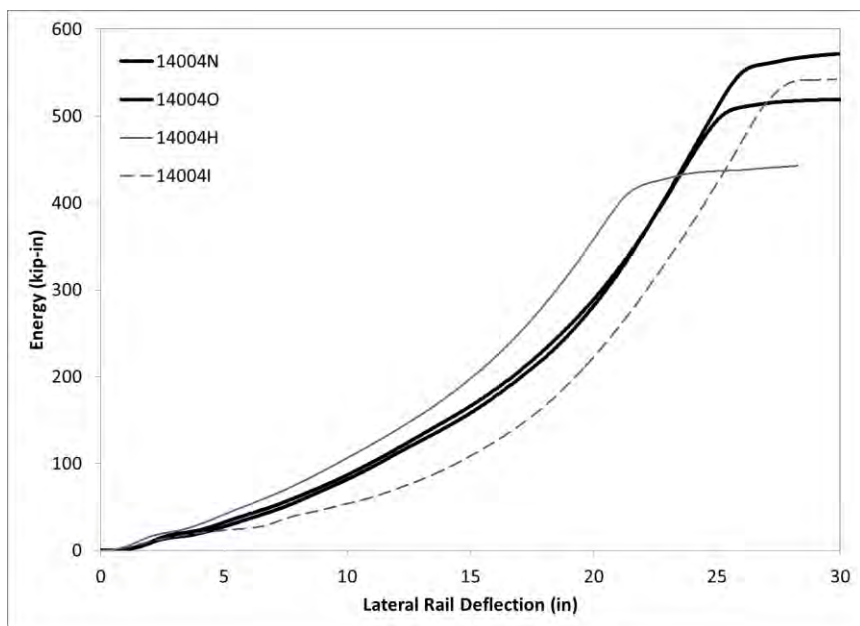


(b)

Figure 343. (a) Force vs. Deflection and (b) Energy vs. Deflection curves for damaged splices with flattened cross-section compared to undamaged cases.



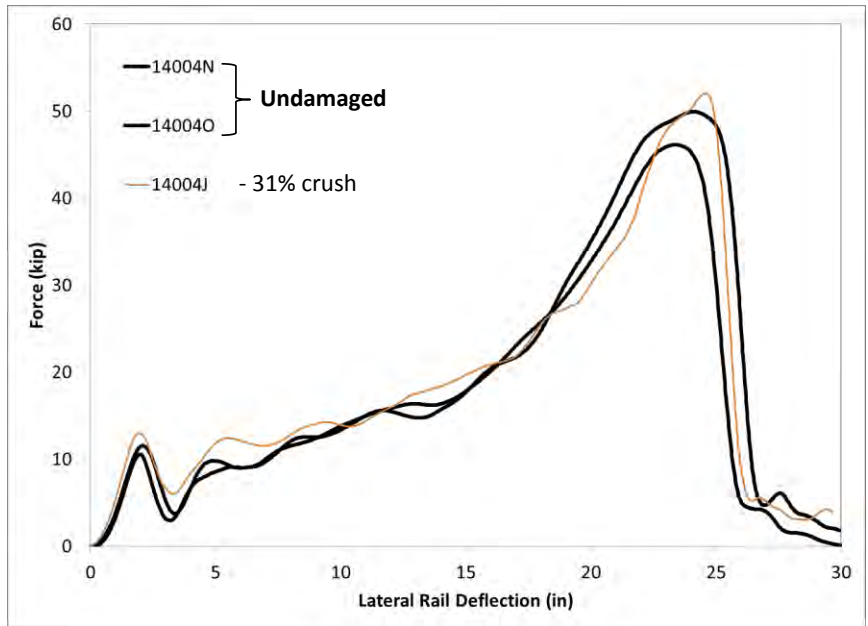
(a)



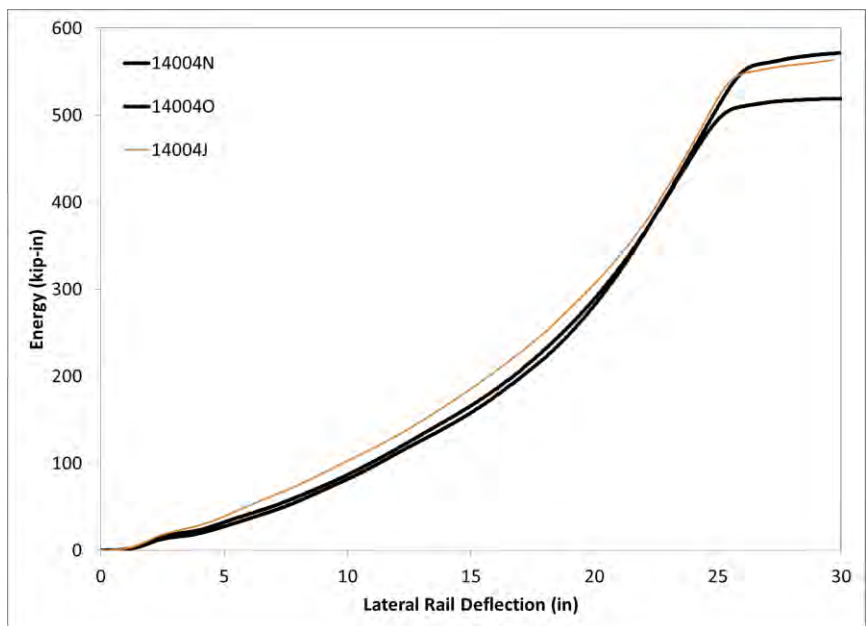
(b)



Figure 344. (a) Force vs. Deflection and (b) Energy vs. Deflection curves for damaged splices with longitudinal slip compared to undamaged cases.

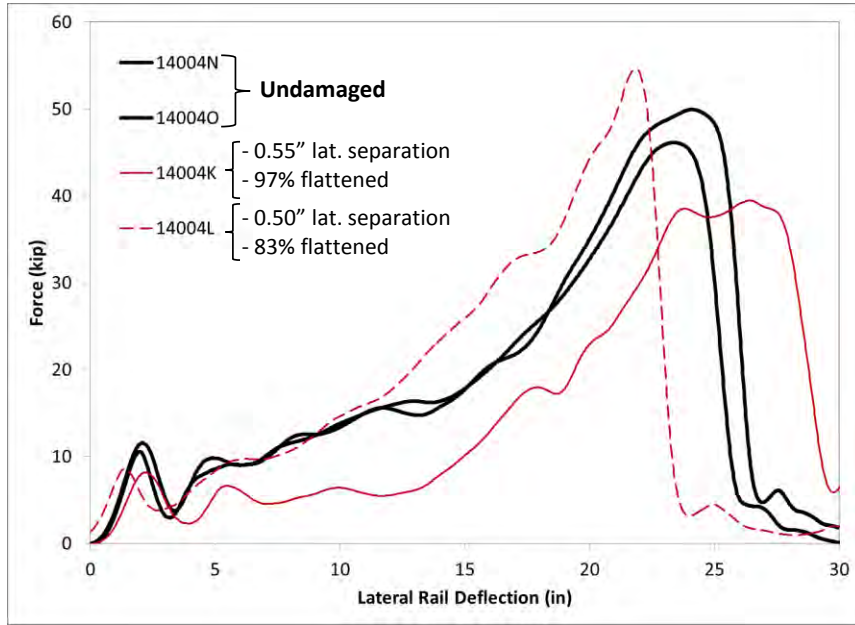


(a)

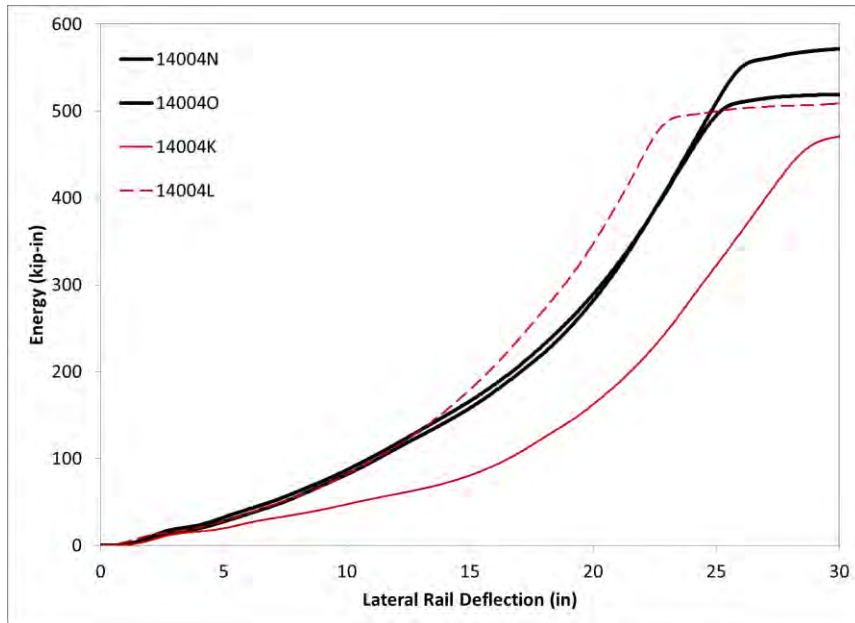


(b)

Figure 345. (a) Force vs. Deflection and (b) Energy vs. Deflection curves for damaged splice with vertical crush compared to undamaged cases.



(a)



(b)

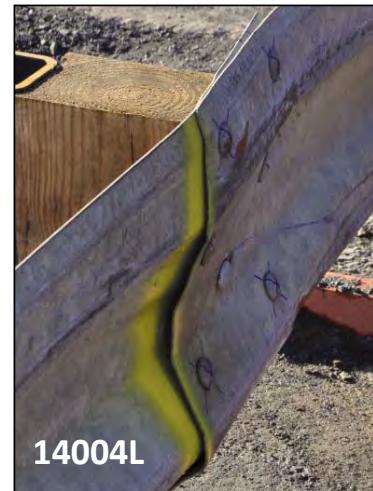


Figure 346. (a) Force vs. Deflection and (b) Energy vs. Deflection curves for damaged splice with combination of lateral rail separation and flattened rail compared to undamaged cases.



Test 14004F



Test 14004G

Figure 347. Sequential views of Tests 14004F and 14004G.



Test 14004H

0.018 s



0.036 s



0.054 s



0.072 s



0.090 s



Test 14004I
(rail tear at left boundary)

Figure 348. Sequential views of Tests 14004H and 14004I.



Test 14004J
(cable rupture at left
boundary)

Test 14004K

Figure 349. Sequential views of Tests 14004J and 14004K.



0.018 s



0.036 s



0.054 s



0.072 s



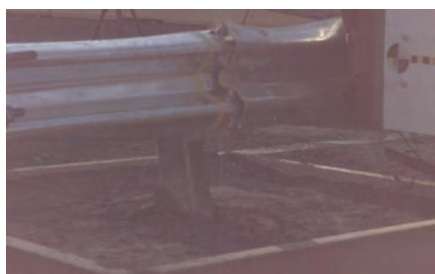
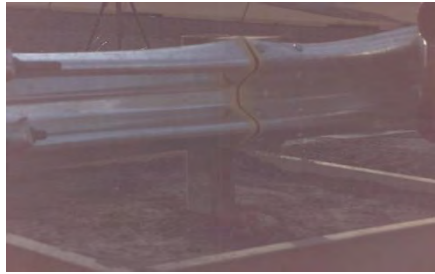
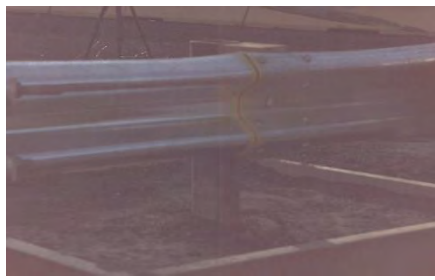
0.090 s



Test 14004L

Test 14004M

Figure 350. Sequential views of Tests 14004L and 14004M.



Test 14004N

Test 14004O

Figure 351. Sequential views of Tests 14004N and 14004O.

Discussion of Test Results

Pendulum impact tests were performed to evaluate the effects of crash-damage on the capacity of w-beam rail splices. For standard strong-post guardrail systems, such as the modified G4(1S) and the G4(2W) guardrails, the w-beam splices are located at the guardrail posts. During impact, one or more of the splice connections are often subjected to multidirectional loading as the splice bends around a guardrail post while the rail is under relatively high tensile force. As a result, relatively high stress concentrations occur at the splice-bolt holes which can sometimes initiate a small fracture or tear at those locations. Once a tear is initiated, the tension in the rail may cause the tear to propagate vertically through the w-beam section causing the rail to rupture.

The pendulum tests performed in this study were designed to create “pocketing” of the rail immediately upstream of a splice connection at the guardrail post in an attempt to emulate typical real-world conditions that lead to splice ruptures. Unfortunately, the tests were not able to accurately duplicate these conditions. Figure 352 shows an overhead view from Test 14004K demonstrating the typical pocketing behavior that occurred in the tests. The image was taken from one of the high-speed cameras at 0.002 seconds before rupture. The degree of pocketing was moderate and may have been sufficient for this study had the tension in the rail not developed so abruptly and so severely. Only one test (i.e., Test 14004F) resulted in rail rupture due to tearing the rail through its cross-section. In all other tests the rupture was due to the splice-bolts tearing through the splice-bolts holes or due to boundary failure.



Figure 352. Overhead view of Test 14004K from high-speed video camera.

This was basically the same issue that Gabler faced in Phase I, i.e., having a relatively short length of rail with a fixed longitudinal constraint at each end.[*Gabler10*] As a result very high tensile forces developed in the rail at relatively low rail deflections during the impact tests. As discussed earlier, the test setup did not permit a longer length of rail because of the limited space within the pendulum test area. So, future pendulum impact studies on rail splices should consider designing boundary conditions to more accurately emulate the longitudinal and lateral stiffness behavior of an extended guardrail.

Even though the tests did not produce the type of loading that was intended for the splice study, the results still provided some insight into the effects of the various damages on the tensile capacity of the splice connection. These are discussed in the following sections.

Rail Flattening

The results from Tests 14004F, 14004G and 14004M were used to evaluate the effects of flattening of the rail at the splice connection. Referring to Table 87, the only test article that had rail flattening as the sole damage mode was that of Test 14004G with 83% flattening at the top

section of the rail splice. The force and energy curves shown in Figure 343 indicate that this test article resulted in essentially the same capacity as the undamaged test article in Test 14004O. Test 14004M had the highest degree of rail flattening (i.e., 94%) but resulted in no reduction in load capacity and negligible reduction in energy capacity compared to the undamaged cases. Test 14004F, on the other hand, had only 68% flattening but resulted in a 6 percent decrease in load capacity and a 16 percent decrease in energy capacity. Test articles 14004M and 14004F both had the same amount of longitudinal slip in the splice (i.e., 0.2 inches); but 14004F, which resulted in the highest capacity, had greater lateral separation between the rail elements (i.e., 0.35 inches vs. 0.13 inches). The most notable outlier in Test 14004M was the fact that three of the splice-bolts were loose. It is possible that the loose bolts caused higher forces at one or more of the neighboring splice bolt connections which lead to the premature rupture of the splice. Recall that 14004F was the only test article that failed by tearing the rail through the cross-section, with the tear passing through all the downstream splice bolt holes, as shown in Figure 353.



Figure 353. Results of Test 14004F with rail tear passing through all four downstream splice-bolt holes.

Longitudinal Displacement (Slip) in the Splice Connection

The test articles for Tests 14004H and 14004I included the highest levels of lateral separation between rail elements at the downstream edge of the splice connection. The results from these tests yielded mixed results regarding the effects of longitudinal slip on the capacity of the splice, as shown in Table 87 and Figure 344. Test 14004H which had 0.28 inches of longitudinal slip in the splice resulted in 9.5 percent decrease in load capacity and 15 percent decrease in energy capacity. This test specimen also included a 25 percent flattened rail and one loose splice-bolt. Test 14004I, which included 0.25 inches of longitudinal slip, showed no decrease in capacity. This test article also included a 68 percent flattened rail, 0.25 inches of lateral separation between the two rails at the downstream edge of the splice and a large

horizontal tear downstream of the splice connection. Since the horizontal tear was located downstream of the splice connection, its effect was considered negligible in the test. It was also concluded that rail flattening was not likely the cause for reduced rail capacity based on the results from the previous group of tests (i.e., Tests 14004M, G and F). As in Test 14004F, it appears that the most notable outlier in Test 14004H was a loose splice-bolt.

Vertical Crush

There was only one test specimen available that had significant vertical crush of the splice. The damages for Test Article 14004J included 31 percent rail crush and 0.25 inches of lateral separation of the two rail sections at the downstream edge of the splice. The results from the test showed slightly higher load capacity for this damage mode than either of the undamaged cases, as shown in Table 87 and Figure 345. Although there was only a single test conducted for this damage mode, it was concluded that rail crush does not adversely affect rail capacity.

Lateral Separation of Rails at Splice

Tests 14004K and 14004L both included significant lateral separation between the two rail elements at the downstream edge of the splice (i.e., 0.55 inches and 0.5 inches, respectively). Both test articles also included significant rail flattening (i.e., 97% and 83%, respectively) as well as slight gouging of the splice bolts into the w-beam rail. In addition, Test 14004K also included 0.2 inches of longitudinal slip.

The results from these two tests were inconclusive. Test 14004L resulted in little or no decrease in capacity. Test 14004K, on the other hand, resulted in a 14 percent decrease in load capacity and a 4 percent decrease in energy capacity (refer to Table 87 and Figure 346). It was apparent, however, from the sudden drop in force shown in Figure 346 that the splice failed at approximately 30 inches of lateral rail displacement, which corresponded to approximately 470 kip-in of energy absorbed by the rail system (i.e., 10% less energy than the undamaged case). The additional energy absorbed in Test 14004K after splice rupture was due to the post-bolt tearing through the w-beam, based on review of the high-speed test video. It should be noted that the Test Article 14004K did include additional damage modes, but the level of damage was considered low to moderate for those cases. In fact the damages of Test Article 14004K are very similar to those of Test Article 14004M, with the exception of the lateral separation of the rails at the splice; but the results of Test 14004M showed no reduction of splice capacity for that case.

Conclusions

The effects of crash-induced damages on the residual capacity of w-beam splices were evaluated using dynamic impact testing. The tests were carried out at the Federal Outdoor Impact Laboratory at the Turner-Fairbank Highway Research Center in McLean, Virginia. The tests involved a 4,360-lb pendulum impacting a representative section of w-beam rail with various types and levels of splice damage at an impact speed of approximately 20.5 mph. The test samples were extracted from various crash-damaged field installations by the Maine DOT. The damaged rail specimens were delivered with the splice connections intact (i.e., still assembled) in order to preserve the original damage state of the splice, which include residual stresses in the splice restrained by the bolted connection.

Four primary splice damage modes were evaluated: (1) rail flattening, (2) rail crush, (3) longitudinal displacement (slip) between the rail elements at the splice and (4) lateral separation

(gap) between the two rail elements at the downstream edge of the splice. A total of 10 test specimens were used in the evaluations. The results from the test program were not very conclusive, due in large part to the low number of test samples available. Further complicating the effort was the fact that, due to the nature of crash damaged rails, each test sample included multiple damage modes - making it difficult to accurately quantify the effects of each isolated mode.

The results from the limited test data, however, indicated that rail fattening and rail crush do not significantly affect capacity of the splice connection. The results from the tests involving longitudinal displacement (slip) between the two rail elements at the splice connection indicated that, for the levels of damage investigated in this study (e.g., ¼-inch displacement), this damage mode also did not significantly affect rail capacity. Since longitudinal displacement in the splice is directly associated with high tensile loads in the rail, then relatively high magnitudes of longitudinal displacement would signify an increased potential for damage in the w-beam material at the bolt holes. With that said, such high levels of tension in the rail would likely be associated with other high level damage modes, such as excessive lateral deflections of the w-beam rail or post, that would have already denoted high priority for repair. In other words, once guardrail damage has been deemed severe enough to warrant repair, further assessment of the splice would be moot.

Although the damage mode of “loose splice-bolts” was not directly evaluated in the study, two of the test specimens included one or more loose bolts. In both of these test cases there was notable reduction in splice capacity. Based on those results, it is recommended that repair is warranted when one or more splice-bolts are loose or missing. This particular damage mode is not easily evidenced by such obvious signs as crash damage, thus loose bolts will not be easy to identify in the field without conducting close, detailed inspections of the splice. Since it is not feasible to perform such inspections on a routine basis, care should be taken to ensure that the splice-bolts are properly tightened when installing or repairing w-beam rails.

Recommendations

The following recommendations are based on the results presented herein and on the recommendations by Gabler et al. in *NCHRP Report 656*. [Gabler10] As a result of these studies, the research team recommends that the repair threshold for splice damage include splice-bolts missing, loose, damaged, severely gouging or torn through the rail, or visibly missing any rail material under the bolt. When any of these damages occur at a single splice-bolt location the recommended repair priority is medium. When any of these conditions occur at two or more splice-bolt locations the recommended repair priority is high. A summary of these recommendations are located in Table 88.

Further, all other damage assessment criteria presented throughout this study related to w-beam railing also apply to the w-beam splices; including rail height, rail flattening, rail crush, lateral rail deflection, holes in the rail, horizontal tears and vertical tears.

Table 88. Recommendations for assessment criteria for w-beam splice damage.

Damage Mode	Repair Threshold	Relative Priority
Splice Bolts - Missing - Visibly missing any underlying rail - Severely gouging rail - Torn through rail - Damaged - Loose	Two or more splice-bolt locations	High
	At a single splice-bolt location	Medium
W-Beam - Height - Flattening - Crush - Deflection - Non-manufactured holes - Horizontal Tears - Vertical Tears	Refer to assessment criteria for each corresponding damage mode for the w-beam rail element.	

CHAPTER 15 – DEVELOPMENT OF FIELD GUIDE MATERIALS AND FIELD TESTING

A field guide for assessing the repair priority for damaged guardrail was assembled based on the evaluation procedures and criteria presented in the preceding chapters; the guide also includes the recommendations developed in *NCHRP Report 656*, “Criteria for Restoration of Longitudinal Barriers.” The materials were assembled in two basic formats: (1) a field manual, which is available in pdf format for printing to hardcopy and (2) an online interactive website. These two versions are meant to be used together; the online version is intended to facilitate and automate the assessment procedure, while the field manual provides additional details and commentary on how to carry out the assessments. A cell phone app was also developed which connects directly to the online guide. The app provides a more user friendly graphical user interface for Android phone users.

Once the materials were assembled they were then submitted to various state DOTs and professional organizations (e.g., TRB subcommittee AFB20, ATTSA, and AASHTO) to make sure that the evaluation procedures were presented in a way that is useful and informative for maintenance engineers and supervisors in the state DOTs. The guide has been continuously revised and updated throughout the project based on the feedback from these groups.

The Field Manual

The field manual, which is provided in Appendix A, includes detailed procedures for carrying out the damage evaluations as well as criteria for determining repair priority based on quantitative metrics. Three classifications were used to denote the relative priority for repair – High, Medium and Low. These nomenclatures were adopted from *NCHRP Report 656* and are defined as follows:

- **High Priority:** Indicates severe damage. The crash performance of the barrier has been compromised to such a degree that a second impact to the damaged barrier would likely result in unacceptable performance.
- **Medium Priority:** Indicates moderate damage. The crash performance of the barrier has likely been compromised to some degree, but the system should perform effectively for a majority of impact conditions.
- **Low Priority:** Indicates that the damaged guardrail is expected to remain fully functional.

The field manual presents the evaluation procedures in a graphical format to facilitate the assessment process. For each damage mode, a commentary is also provided to support the evaluation criteria. A worksheet is provided at the end of the manual as a guide to aid highway maintenance personnel in assessing guardrail damage and for identifying materials needed for repair. Only those damage modes that have been shown to warrant high priority for repair were included in the assessment worksheet. When damages do not meet the critical threshold, then the damaged guardrail should be expected to perform effectively for a majority of impact conditions. That is, if the assessment indicates that a repair is *not warranted*, then the damages would be categorized as either “medium” or “low” priority for repair. However, sound

engineering judgment should always be used in making final repair decisions. If the user is unsure of the assessment result then they should reference the field manual to verify that those particular guardrail damages have been addressed in the assessment. For example, some damage modes, such as a flattened or a crushed rail panel, are not considered to be “high” priority repair and, therefore, are not directly included in the assessment questionnaire. However, a review of the field manual would confirm that these particular damage modes are indeed included in the assessment process, but have been determined to not have significant effect on guardrail performance (e.g., a w-beam panel completely flattened is only considered *medium priority* for repair).

The damage assessment worksheet, as shown in Appendix A, is divided into six levels of damage assessments:

- Level 1: Corresponds to a system level damage, related to lateral deflection of the system and overall height of the rail. If these damage modes meet critical repair criteria, then all damaged components should be included in the repair.
- Level 2: Is associated with damages to w-beam splice connections. If this damage mode meets critical repair criteria, then only the splice-bolts need be replaced unless the w-beam near the splice-bolt holes is critically damaged.
- Level 3: Is associated with damages to the w-beam panel including holes, horizontal tears and vertical tears.
- Level 4: Is associated with damages to the guardrail posts and soil erosion around the posts.
- Level 5: Is associated with damages to the end-terminal that affect the anchor-mechanism for the guardrail.
- Level 6: Simply involves recommendations for upgrading non-conforming systems to meet current FHWA approved designs (e.g., replacing non-conforming steel blockouts with FHWA approved blockouts, etc.).

Online Interactive Field Guide

The number of damage modes included in *NCHRP Report 656* was relatively small and thus manageable for use in routine inspections. However, as additional damage modes and additional guardrail types were included, the evaluation process became more complex and time consuming. To make the assessment process as accurate and efficient as possible, an on-line, context sensitive version of the field guide was developed using standard web development language. HTML and PHP were used to create a user interface and to store users’ answers to questions as variables. At the end of the automated assessment, the results were: 1) displayed directly on the screen of the device being used, 2) sent in an email to the address provided by the user at the beginning of the assessment, and 3) stored in a central MySQL database maintained by the research team. The online guide was coded such that the time required to perform assessments are minimized by avoiding unnecessary questions based on user inputs. The flow chart for the online guide is show in Figure 354. Example field assessments are provided in the next chapter to illustrate the use of the on-line field guide.

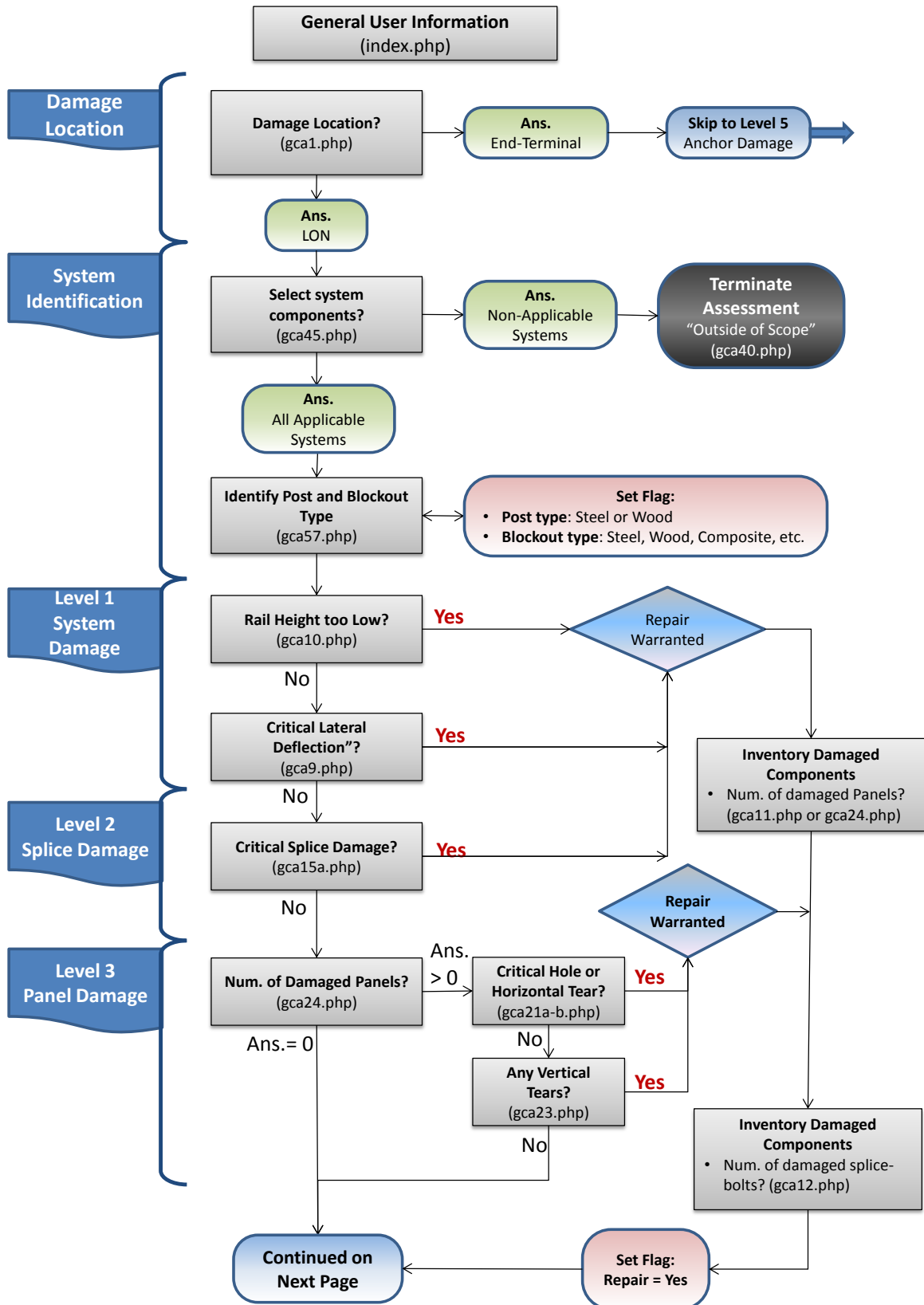


Figure 354. Flow chart for the online guide's guardrail assessment.

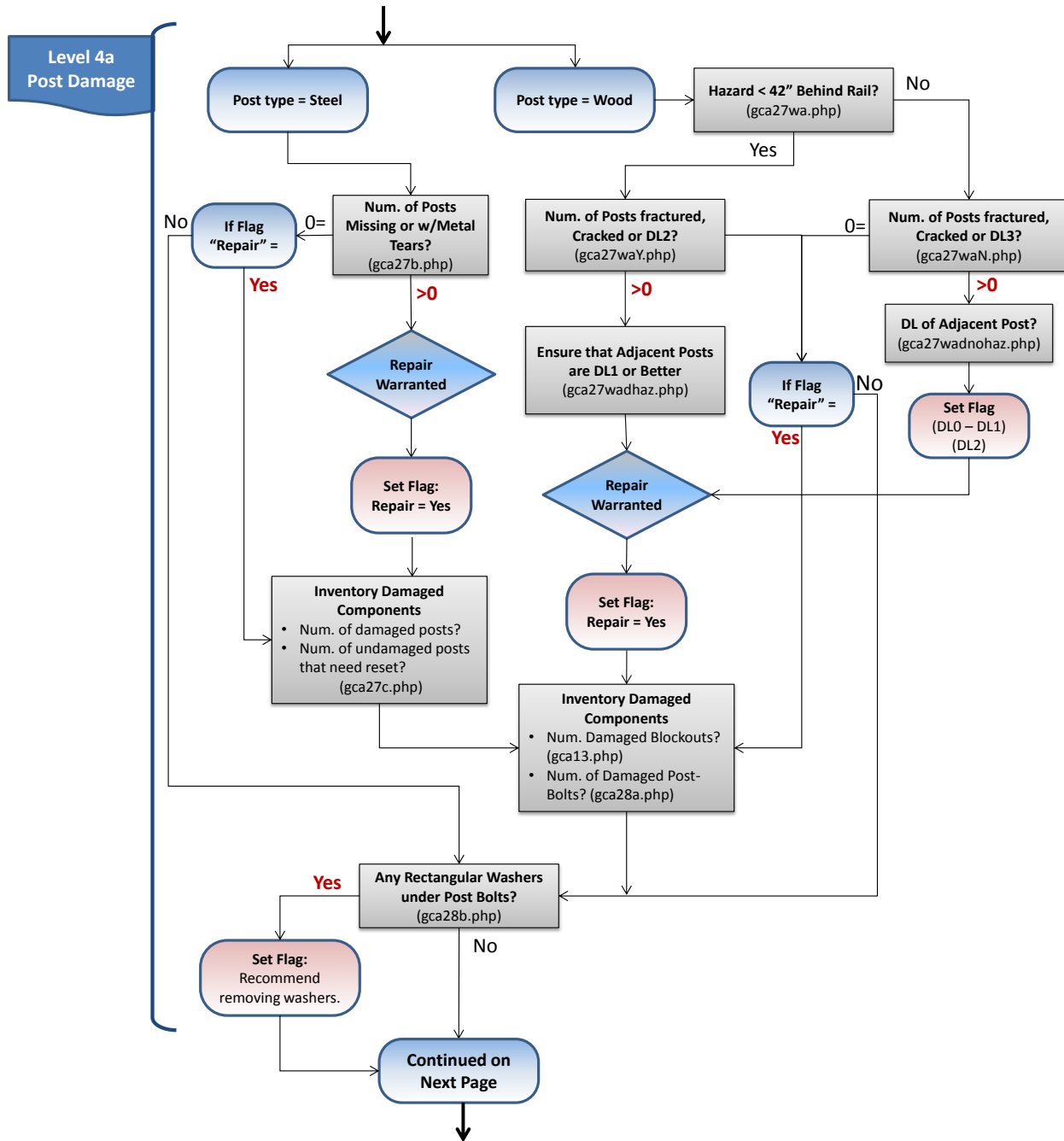


Figure 354. [CONTINUED] Flow chart for the online guide’s guardrail assessment.

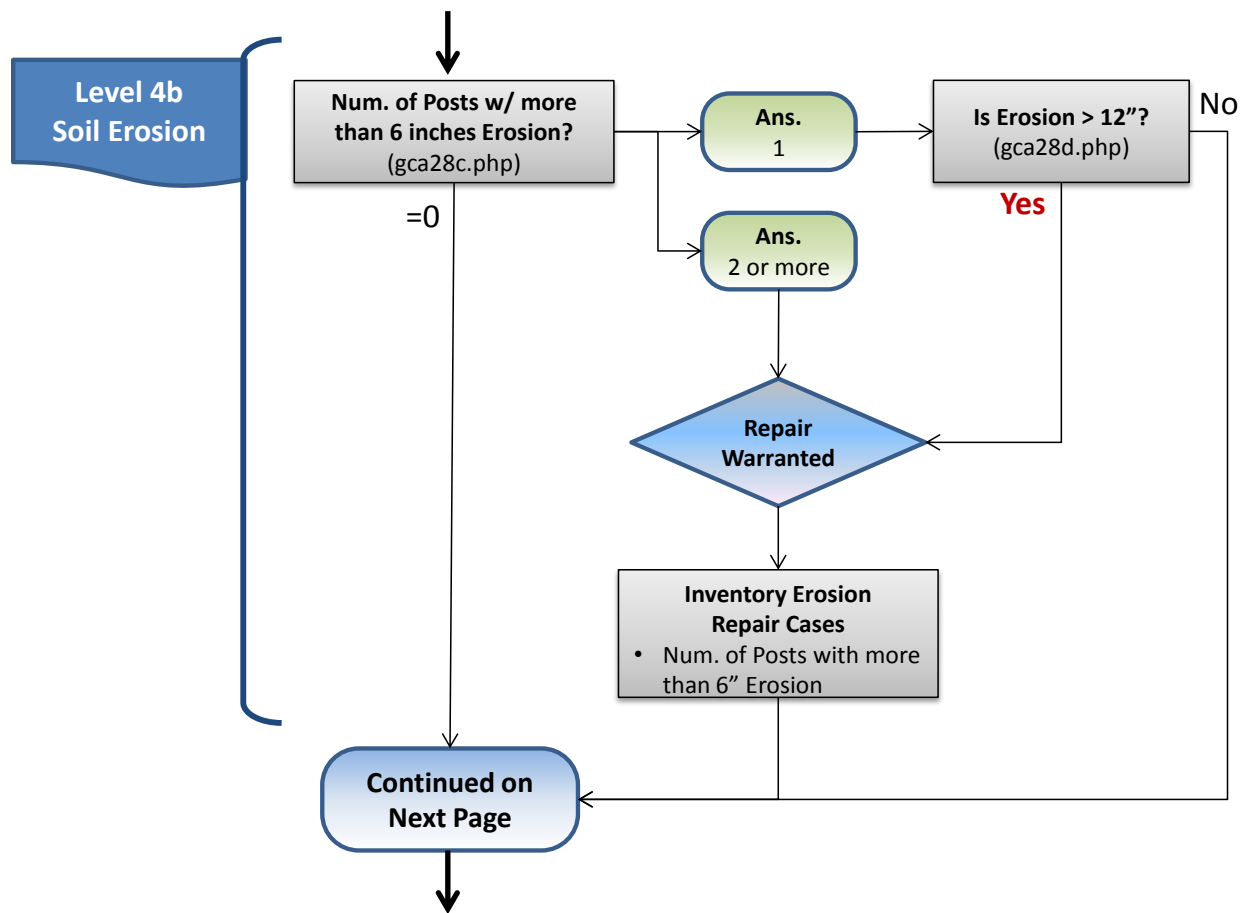


Figure 354. [CONTINUED] Flow chart for the online guide's guardrail assessment.

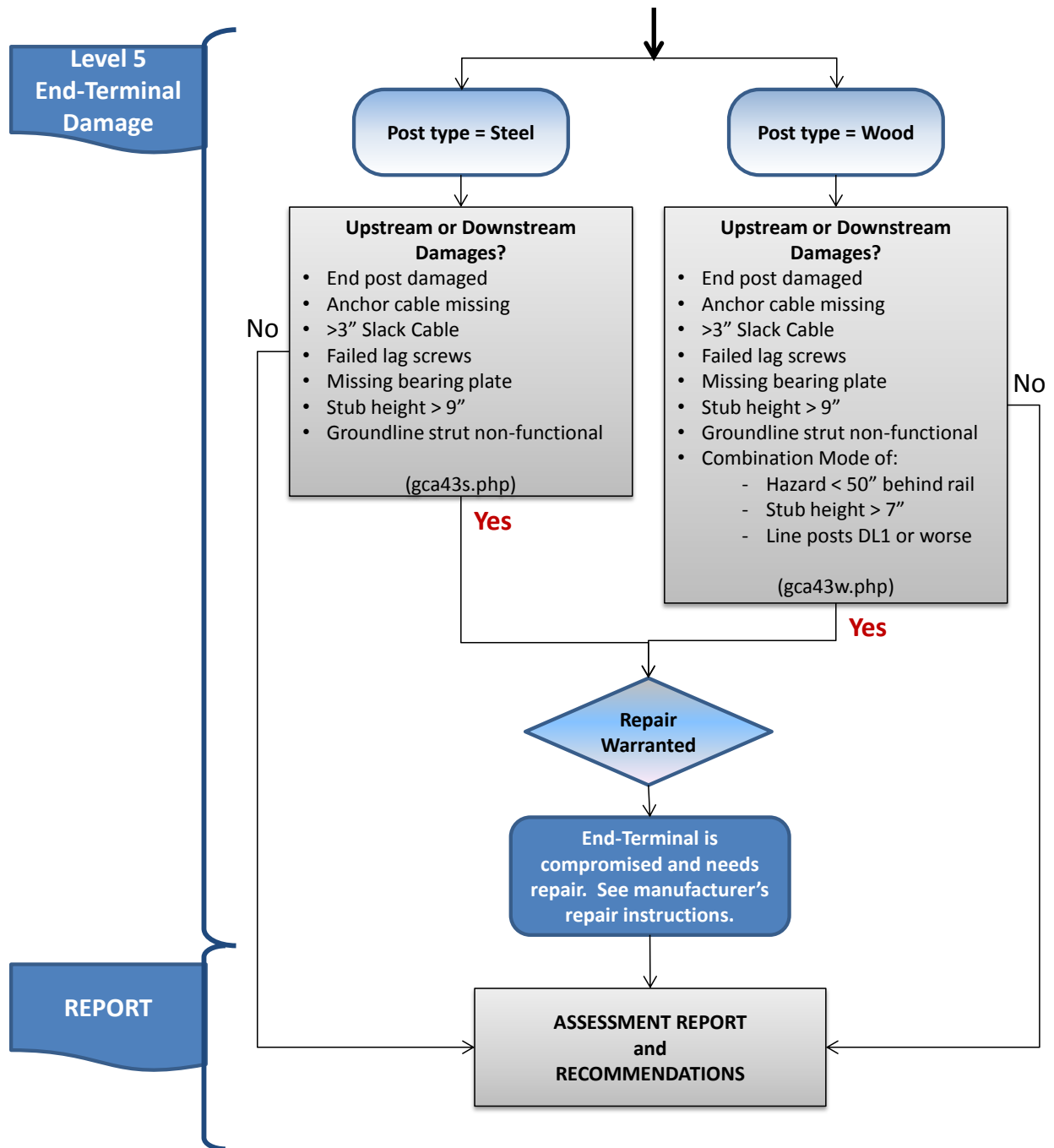


Figure 354. [CONTINUED] Flow chart for the online guide's guardrail assessment.

CHAPTER 16 –FIELD GUIDE APPLICATION EXAMPLES

The assessment procedures are designed to identify the types and levels of damage that will likely compromise the barrier's crash performance in subsequent impacts on the unrepaired system. In other words, the assessment process is designed to determine if the damage warrants high priority for repair. When the damages do not meet critical damage conditions, then the damaged guardrail should be expected to perform effectively for a majority of impact conditions; therefore, the assessment process does not directly evaluate damages that have been classified as "medium" or "low" priority for repair. However, sound engineering judgment should always be used in making final repair decisions.

A series of field assessments were performed using the on-line version of the Field Guide at <http://www.roadsafellc.com/GCA/index.php> to illustrate the basic assessment procedure. The example cases presented herein were based on damaged guardrails from actual crash sites in Oxford County, Maine.

The on-line field guide was developed as a logic-based questionnaire; therefore, the specific questions asked for each example case below differ depending on the types and levels of damages identified. The format of the questionnaire was designed to be as user friendly as possible. For example, questions that have a limited number of response options are generally structured as multiple choice questions with radio buttons, yes/no questions with mouse-click response, or check-boxes to minimize and simplify the required inputs for the user. Further, the questionnaire was designed so that a "yes" response is expected whenever the level of damage meets a critical damage threshold to avoid confusion for new users, as well as, to allow experienced users to quickly speed through the assessment questions by relying on visual cues in the questionnaire (e.g., question title) for determining the proper response. Also, the answers for many of the questions are automatically pre-selected based on the most common responses, to help speed through the process. For questions that require numeric input or that require a response using check-boxes, leaving the answer-field blank indicates that the answer is "zero" or "none" (i.e., the default answer for those questions is zero).

Example 1

This example involves a modified G4(1S) guardrail with crash damage extending over two rail panels, including the w-beam splice, as shown in Figure 355. The following images show the step-by-step evaluation procedure using the on-line *Guardrail Condition Assessment* (GCA) program developed in Chapter 15.



Figure 355. Photos of the crash site for Example 1.

<div style="border: 1px solid black; padding: 5px;"> <p>Help RoadSafe LLC Transportation Engineering and Research</p> <p style="text-align: center;">Location Information</p> <p>Full Name <input type="text" value="Chuck"/></p> <p>E-mail <input type="text" value="Chuck@roadsafellc.com"/></p> <p>Date <input type="text" value="11/21/2014"/></p> <p>State <input type="text" value="Maine [ME]"/></p> <p>State Route <input type="text" value="Example 1"/></p> <p>Side of Road <input type="text" value="West"/></p> <p>Approximate mile post <input type="text" value="15"/></p> <p>GPS <input type="text"/></p> <p style="text-align: center;">Limited Use Document The Guardrail Conditions Assessment App and Webpage are furnished only for review by members of the NCHRP project panel and selected field testers and is regarded as fully privileged. Dissemination of information included herein must be approved by NCHRP.</p> <p style="text-align: center;"><input type="button" value="Next"/></p> </div>	<p><i>User Input for Question 1:</i> Name, date, contact information, and crash site location was entered on the location information page.</p>
---	--

Help **RoadSafe LLC** Transportation Engineering and Research [Back](#)

Applicable Damage Site Selection

Is the damage located on the length-of-need section of the guardrail?

(i.e., damage is located more than 37.5 ft from either end of the system)

Yes No

User Input for Question 2:

The damage was on the length-of-need section of the guardrail (i.e., not on the end-terminal), so the “yes” response was selected.

Help **RoadSafe LLC** Transportation Engineering and Research [Back](#)

System Component Type Selection

Rail Type	Post Spacing	Blockout	Splice Location
<input checked="" type="radio"/> W-beam	<input checked="" type="radio"/> 6' 3"	<input checked="" type="radio"/> Yes	<input checked="" type="radio"/> At Blockout
<input type="radio"/> Thrie	<input type="radio"/> 12' 6"	<input type="radio"/> No	<input type="radio"/> Midspan
<input type="radio"/> Other	<input type="radio"/> Other		

User Input for Question 3:

The default radio buttons were selected, which correspond to the components of the G4(1S) with 6’-3” post spacing .



Help **RoadSafe LLC** Transportation Engineering and Research [Back](#)

Post and Blockout Type Selection

Post Type	Blockout Type
<input checked="" type="radio"/> W6x9 steel posts	<input type="radio"/> 6x8" wood
<input type="radio"/> 6x8" wood posts	<input checked="" type="radio"/> 6x8" composite
<input type="radio"/> 8" diameter wood posts	<input type="radio"/> W6x9 steel
<input type="radio"/> Other	<input type="radio"/> Other

User Input for Question 4:

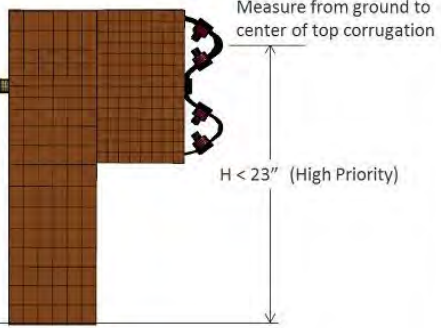
The system in this case was the modified G4(1S) with W6x9 posts and composite blockouts.



[Help](#) **RoadSafe LLC** [Back](#)
Transportation Engineering and Research

System Damage - Rail Height

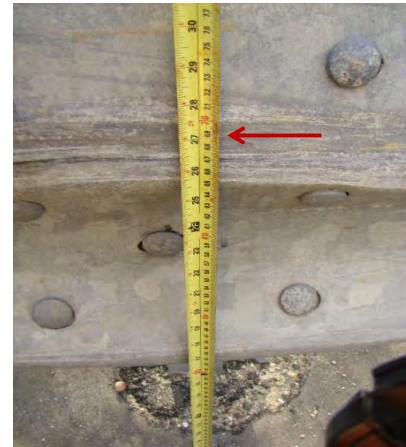
Is the height measured from the ground to the center of the top corrugation of the w-beam less than 23 inches?



Yes No

User Input for Question 5:

The rail height was 26.5 inches measured from the ground to the middle-point of the top w-beam corrugation, so the “No” response was selected.



[Help](#) **RoadSafe LLC** [Back](#)
Transportation Engineering and Research

System Damage

Is the lateral deflection more than 9 inches?

Yes No

User Input for Question 6:

The lateral deflection was less than 9 inches, so the “No” response was selected.



[Help](#) **RoadSafe LLC** [Back](#)
Transportation Engineering and Research

Splice Damage

Are there any rail splices with two or more splice-bolt deficiencies? Do not count more than one deficiency per splice bolt.

- Missing splice-bolt
- Visibly missing rail material under splice-bolt
- Splice-bolt torn through rail
- Loose bolt
- Bolt severely gouging rail

Yes No

User Input for Question 7:

There was only moderate longitudinal displacement in the splice connection. The “No” response was selected.



Help **RoadSafe LLC** Back
Transportation Engineering and Research

Number of Damaged Panels

of damaged straight panels

of damaged curved panels

Next Step

User Input for Question 8:

The extent of damage included two straight rail panels. The number “2” was entered in the appropriate text box; the other box was left blank.



Help **RoadSafe LLC** Back
Transportation Engineering and Research

Rail Panel Damage
Holes and Horizontal Tears

Are there any horizontal tears or non-manufactured holes that meet one or more of the following conditions:

- Intersect either the top or bottom edge of the rail,
- Height > 1", or
- Three or more holes or tears on a single panel

Yes No

User Input for Question 9:

The rail was free of horizontal holes and tears. The “No” response was selected.

Help **RoadSafe LLC** Back
Transportation Engineering and Research

Rail Panel Damage

Does the rail have any vertical tears?

Yes No

User Input for Question 10:

The damage included a 5.5 inch vertical tear on the top of the rail, so the “Yes” response was selected for this damage mode question.



Help **RoadSafe LLC** [Back](#)
Transportation Engineering and Research

Post Condition Assessment

of posts that are bent, deformed, or have metal tears

of posts in good condition but need to be reset (e.g. raise post height, straighten deflected posts, etc.)

Next Step

User Input for Question 11:

The posts experienced negligible deformations. No input is required on this page since the default values are “zero”.



Help **RoadSafe LLC** [Back](#)
Transportation Engineering and Research

Post Washers

Are there any rectangular washers under the post-rail bolt heads anywhere in the system?

Yes No

User Input for Question 12:

The post-bolts did not have washers under the bolt-heads.



Help **RoadSafe LLC** [Back](#)
Transportation Engineering and Research


Soil Erosion at Guardrail Posts

of posts with more than 6" of soil erosion (within a four post span length)

Next Step

User Input for Question 13:

There was no soil erosion since the posts were all embedded in asphalt. No input was required, because the default response is “zero”.

Help  Back


Upstream End Terminal

Select all that apply

- The end post is sheared, rotted, cracked across the grain, bent, deformed, or has metal tears
- The anchor cable is missing
- There is more than 3 inches of slack in the anchor cable
- There are missing or failed lag screws for the end terminal
- The terminal bearing plate is missing
- The foundation tube stub height exceeds 9 inches
- The groundline strut is missing or otherwise non-functional
- Any other end-terminal damage that would result in more than 50% reduction in anchor capacity
- Combination Mode of:
 - Hazard located with 50 inches behind w-beam rail
 - Stub height exceeds 7 inches
 - Line posts have deterioration level of DL1 or greater

User Input for Question 14:

There were no damages noted for the upstream end-terminal. The response boxes were left “unchecked” (i.e., indicating no damage).

Help  Back


Downstream End Terminal

Select all that apply

- The end post is sheared, rotted, cracked across the grain, bent, deformed, or has metal tears
- The anchor cable is missing
- There is more than 3 inches of slack in the anchor cable
- There are missing or failed lag screws for the end terminal
- The terminal bearing plate is missing
- The foundation tube stub height exceeds 9 inches
- The groundline strut is missing or otherwise non-functional
- Any other end-terminal damage that would result in more than 50% reduction in anchor capacity
- Combination Mode of:
 - Hazard located with 50 inches behind w-beam rail
 - Stub height exceeds 7 inches
 - Line posts have deterioration level of DL1 or greater

User Input for Question 15:

There were no damages noted for the downstream end-terminal. Again, the response boxes were left “unchecked”.

<p>Help  <small>Transportation Engineering and Research</small></p> <p>Guardrail Damage Assessment Results</p> <p>This guardrail is not likely to perform correctly if hit again. You should repair the damaged section immediately.</p> <p>**Please scroll down for more information and to complete the assessment.**</p> <p>General Information: Name: Email: Date: State: State Route: Side of Road: Approximate Milepost: GPS: Rail Type: System Height: Post Type: Post Spacing: Blockout Type:</p> <p>The following components need to be replaced: 2 Straight Rails</p> <p>Recommendations:</p> <p>This guardrail is not likely to perform correctly if hit again because: The rail has at least one vertical tear.</p>	<p><i>Assessment Results:</i></p> <p>The damage assessment is now complete. The results of the assessment are provided on the final page of the online guardrail condition assessment guide. The results are also sent to the e-mail address provided on the Question 1 page.</p> <p>The assessment results indicate that the guardrail is not likely to perform correctly if hit again, because of the vertical tear. It is recommended that the damages be repaired immediately.</p> <p>There may have been other critical damages on the system that were not evaluated in the assessment. According to the evaluation procedures, once the extent of damage to any aspect of the system has been shown to warrant repair, then no further investigations are necessary. It is only necessary to collect inventory of all components that will be replaced in the repair.</p> <p>Since the posts and connection hardware were not damaged, it is assumed that those components can be reused. The materials needed for the repair only include the two damaged w-beam rail elements.</p>
---	--

Example 2

This example also involves a modified G4(1S) guardrail with crash damage extending over two rail panels on the length-of-need section of the guardrail, as well as a portion of the end-terminal, as shown in Figure 356. The following images show the step-by-step evaluation procedure using the on-line GCA program.



Figure 356. Photos of the crash site for Example 2.

<p>Help RoadSafe LLC Transportation Engineering and Research</p> <p>Location Information</p> <p>Full Name <input type="text" value="RoadSafe"/></p> <p>E-mail <input type="text" value="User@Roadsafellc.com"/></p> <p>Date <input type="text" value="11/26/2014"/></p> <p>State <input type="text" value="ME"/></p> <p>State Route <input type="text" value="Example 2"/></p> <p>Side of Road <input type="text"/></p> <p>Approximate mile post <input type="text"/></p> <p>GPS <input type="text"/></p> <p>Limited Use Document The Guardrail Conditions Assessment App and Webpage are furnished only for review by members of the NCHRP project panel and selected field testers and is regarded as fully privileged. Dissemination of information included herein must be approved by NCHRP.</p> <p><input type="button" value="Next"/></p>	<p>User Input for Question 1: Name, date, contact information, and crash site location was entered on the location information page.</p>
---	---

Help **RoadSafe LLC** Transportation Engineering and Research [Back](#)

Applicable Damage Site Selection

Is the damage located on the length-of-need section of the guardrail?

(i.e., damage is located more than 37.5 ft from either end of the system)

Yes No

User Input for Question 2:

The damage was extended over a portion of the end-terminal and onto the length-of-need section of the guardrail, so the “yes” response was selected.

Help **RoadSafe LLC** Transportation Engineering and Research [Back](#)

System Component Type Selection

Rail Type	Post Spacing	Blockout	Splice Location
<input checked="" type="radio"/> W-beam	<input checked="" type="radio"/> 6' 3"	<input checked="" type="radio"/> Yes	<input checked="" type="radio"/> At Blockout
<input type="radio"/> Thrie	<input type="radio"/> 12' 6"	<input type="radio"/> No	<input type="radio"/> Midspan
<input type="radio"/> Other	<input type="radio"/> Other		

User Input for Question 3:

The radio buttons corresponding to components of the G4(1S) with 6’-3” post spacing were selected (i.e., default options)



Help **RoadSafe LLC** Transportation Engineering and Research [Back](#)

Post and Blockout Type Selection

Post Type	Blockout Type
<input checked="" type="radio"/> W6x9 steel posts	<input type="radio"/> 6x8" wood
<input type="radio"/> 6x8" wood posts	<input checked="" type="radio"/> 6x8" composite
<input type="radio"/> 8" diameter wood posts	<input type="radio"/> W6x9 steel
<input type="radio"/> Other	<input type="radio"/> Other

User Input for Question 4:

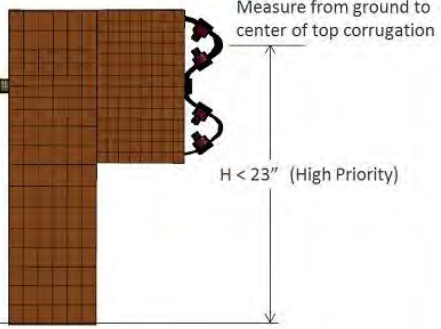
The system was the modified G4(1S) with W6x9 posts and composite blockouts.



[Help](#) **RoadSafe LLC** [Back](#)
Transportation Engineering and Research

System Damage - Rail Height

Is the height measured from the ground to the center of the top corrugation of the w-beam less than 23 inches?



Yes No

User Input for Question 5:

The rail height was 28 inches measured from the ground to the middle-point of the top w-beam corrugation, so the answer was “No”.



[Help](#) **RoadSafe LLC** [Back](#)
Transportation Engineering and Research

System Damage

Is the lateral deflection more than 9 inches?

Yes No

User Input for Question 6:

The lateral deflection was only 4 inches, so the “No” response was selected.



[Help](#) **RoadSafe LLC** [Back](#)
Transportation Engineering and Research

Splice Damage

Are there any rail splices with two or more splice-bolt deficiencies? Do not count more than one deficiency per splice bolt.



- Missing splice-bolt
- Visibly missing rail material under splice-bolt
- Splice-bolt torn through rail
- Loose bolt
- Bolt severely gouging rail

Yes No

User Input for Question 7:

The damage was limited to flattening with moderate longitudinal displacement in the splice connection. The “No” response was selected.



 <p>Help RoadSafe LLC Transportation Engineering and Research Back</p> <p>Number of Damaged Panels</p> <p># of damaged straight panels <input type="text" value="3"/></p> <p># of damaged curved panels <input type="text"/></p> <p>Next Step</p>	<p>User Input for Question 8:</p> <p>The extent of damage included two straight rail panels on the length of need section and one rail panel on the end-terminal. The number “3” was entered in the appropriate text box; the other box was left blank.</p> 
 <p>Help RoadSafe LLC Transportation Engineering and Research Back</p> <p>Rail Panel Damage</p> <p>Holes and Horizontal Tears</p> <p>Are there any horizontal tears or non-manufactured holes that meet one or more of the following conditions:</p> <ul style="list-style-type: none"> • Intersect either the top or bottom edge of the rail, • Height > 1", or • Three or more holes or tears on a single panel <p>Yes No</p>	<p>User Input for Question 9:</p> <p>The rail was free of horizontal holes and tears. The “No” response was selected.</p>
 <p>Help RoadSafe LLC Transportation Engineering and Research Back</p> <p>Rail Panel Damage</p> <p>Does the rail have any vertical tears?</p> <p>Yes No</p>	<p>User Input for Question 10:</p> <p>The rail was free of vertical tears. The “No” response was selected.</p>

Help  Back

Post Condition Assessment

of posts that are bent, deformed, or have metal tears


of posts in good condition but need to be reset (e.g. raise post height, straighten deflected posts, etc.)

Next Step

User Input for Question 11:

There are a total of 3 posts that need replacement. Two line posts were damaged and one CRT post.



Help  Back


Replacement Blockouts

of blockouts missing, broken, rotted, cracked across the grain, deformed, or have metal tears

Next

User Input for Question 12:

One of the composite blocks on the line posts need replacement and the wooden blockout on the CRT post needs replacement (see photo above).

Help  Back

Replacement Bolts

of missing or damaged post bolts

Next Step

User Input for Question 13:

Two post bolts are needed. The post-bolt for one line-post and one CRT was damaged.



Help **RoadSafe LLC** Transportation Engineering and Research [Back](#)

Post Washers

Are there any rectangular washers under the post-rail bolt heads anywhere in the system?

Yes No

User Input for Question 14:

The post-bolts did not have washers under the bolt-heads.



Help **RoadSafe LLC** Transportation Engineering and Research [Back](#)

Soil Erosion at Guardrail Posts

of posts with more than 6" of soil erosion (within a four post span length)

User Input for Question 15:

There was no soil erosion since the posts were all embedded in asphalt. No input was required, because the default response is "zero".

Help **RoadSafe LLC** Transportation Engineering and Research [Back](#)

Upstream End Terminal

Select all that apply

- The end post is sheared, rotted, cracked across the grain, bent, deformed, or has metal tears
- The anchor cable is missing
- There is more than 3 inches of slack in the anchor cable
- There are missing or failed lag screws for the end terminal
- The terminal bearing plate is missing
- The foundation tube stub height exceeds 9 inches
- The groundline strut is missing or otherwise non-functional
- Any other end-terminal damage that would result in more than 50% reduction in anchor capacity
- Combination Mode of:
 - Hazard located with 50 inches behind w-beam rail
 - Stub height exceeds 7 inches
 - Line posts have deterioration level of DL1 or greater

User Input for Question 16:

There were no damages noted for the upstream end-terminal. The response boxes were left "unchecked" (i.e., indicating no damage).



Help **RoadSafe LLC** Back
Transportation Engineering and Research

Downstream End Terminal

Select all that apply

- The end post is sheared, rotted, cracked across the grain, bent, deformed, or has metal tears
- The anchor cable is missing
- There is more than 3 inches of slack in the anchor cable
- There are missing or failed lag screws for the end terminal
- The terminal bearing plate is missing
- The foundation tube stub height exceeds 9 inches
- The groundline strut is missing or otherwise non-functional
- Any other end-terminal damage that would result in more than 50% reduction in anchor capacity
- Combination Mode of:
 - Hazard located with 50 inches behind w-beam rail
 - Stub height exceeds 7 inches
 - Line posts have deterioration level of DL1 or greater

Next

User Input for Question 17:

There were no damages noted for the downstream end-terminal. Again, the response boxes were left “unchecked”.


Help **RoadSafe LLC** Back
Transportation Engineering and Research

Field Guide for Guardrail Damage Assessment

You have completed the guardrail damage assessment for this damaged section. Please make any notes or comments regarding the section of guardrail being assessed in the text box below, then tap the results button to continue.

Results

This completes the damage assessment. Click the “Results” button to continue.

<p>Help  <small>Transportation Engineering and Research</small></p> <p>Guardrail Damage Assessment Results</p> <p>This guardrail is not likely to perform correctly if hit again. You should repair the damaged section immediately.</p> <p>**Please scroll down for more information and to complete the assessment.**</p> <p>General Information: Name: Email: Date: 11/26/2014 State: State Route: Side of Road: Approximate Milepost: GPS: Rail Type: w-beam System Height: Post Type: W 6 X 9 steel post Post Spacing: 6ft 3in Blockout Type: 6 X 8 inch wood</p> <p>The following components need to be replaced: 2 Panel-Post Bolts 3 Posts 2 Blockouts</p> <p>Recommendations:</p> <p>This guardrail is not likely to perform correctly if hit again because: At least one metal post has a tear in it, or needs to be reset.</p>	<p><i>Assessment Results:</i></p> <p>The results of the assessment are provided on the final page of the online guardrail condition assessment guide. The results are also sent to the e-mail address provided on the Question 1 page.</p> <p>The assessment results indicate that the guardrail is not likely to perform correctly if hit again, because of the damaged line post. It is recommended that the damaged section of guardrail be repaired immediately.</p> <p>Although the guardrail condition assessment does not yet include damage assessments for CRT posts, the broken CRT post, blockout and damaged rail panel on the end-terminal section were included in the inventory of materials needed for the repair.</p>
--	---

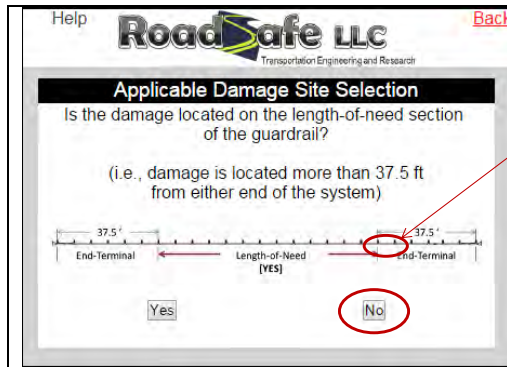
Example 3

This example also involves damages to a FLEAT guardrail end-terminal section, as shown in Figure 357. The following images show the step-by-step evaluation procedure using the on-line GCA program.



Figure 357. Photos of the crash site for Example 3.

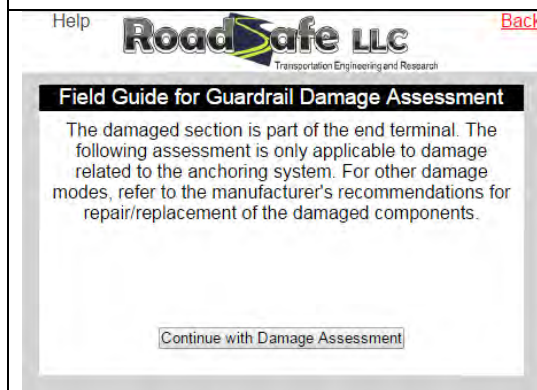
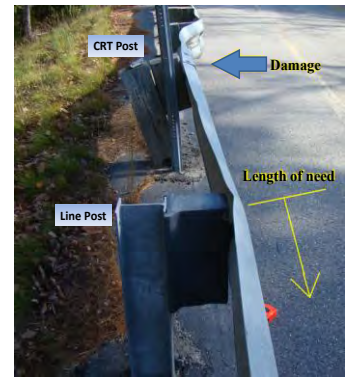
<div style="border: 1px solid black; padding: 5px;"> <p>Help RoadSafe LLC Transportation Engineering and Research</p> <p style="text-align: center;">Location Information</p> <p>Full Name <input type="text" value="RoadSafe"/></p> <p>E-mail <input type="text" value="User@Roadsafellc.com"/></p> <p>Date <input type="text" value="12/01/2014"/></p> <p>State <input type="text" value="ME"/></p> <p>State Route <input type="text" value="Example 3"/></p> <p>Side of Road <input type="text"/></p> <p>Approximate mile post <input type="text"/></p> <p>GPS <input type="text"/></p> <p style="text-align: center;">Limited Use Document</p> <p style="font-size: small;">The Guardrail Conditions Assessment App and Webpage are furnished only for review by members of the NCHRP project panel and selected field testers and is regarded as fully privileged. Dissemination of information included herein must be approved by NCHRP.</p> <p style="text-align: center;"><input type="button" value="Next"/></p> </div>	<p><i>User Input for Question 1:</i></p> <p>Name, date, contact information, and crash site location was entered on the location information page.</p>
--	---



Damaged Section

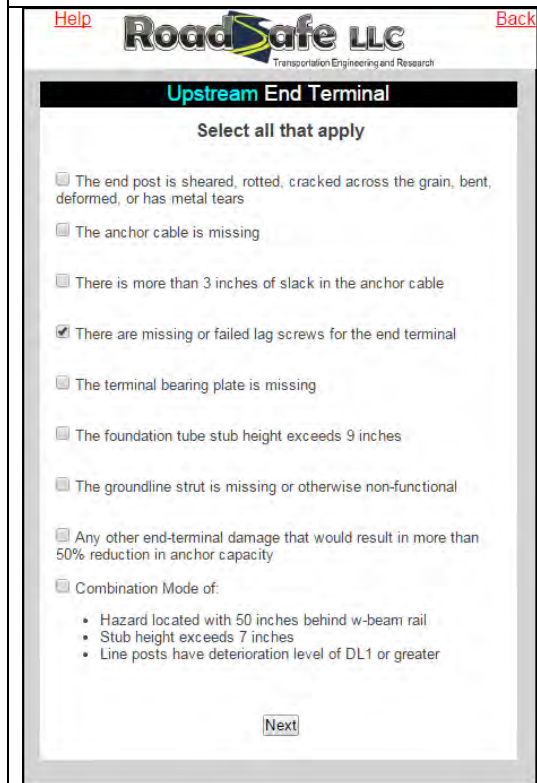
User Input for Question 2:

The damage was located at the last CRT post of the end-terminal section, so the “no” response was selected.



User Input for Question 3:

The GCA field guide does not currently include assessment criteria for this section of the end-terminal, and the user is referred to the manufacturer’s recommendations for repair. By clicking on the “Continue with Damage Assessment” button, the assessments for the end-terminal head and anchor system are then evaluated.



User Input for Question 4:

The lag screws fastening the terminal head to the end-post were pulled out of the post.



Help **RoadSafe LLC** Back
Transportation Engineering and Research

Downstream End Terminal

Select all that apply

- The end post is sheared, rotted, cracked across the grain, bent, deformed, or has metal tears
- The anchor cable is missing
- There is more than 3 inches of slack in the anchor cable
- There are missing or failed lag screws for the end terminal
- The terminal bearing plate is missing
- The foundation tube stub height exceeds 9 inches
- The groundline strut is missing or otherwise non-functional
- Any other end-terminal damage that would result in more than 50% reduction in anchor capacity
- Combination Mode of:
 - Hazard located with 50 inches behind w-beam rail
 - Stub height exceeds 7 inches
 - Line posts have deterioration level of DL1 or greater

Next

User Input for Question 5:

The downstream end-terminal was not an energy absorbing terminal and thus the assessment criteria is not applicable. However, there were no visual damages to the system.




Help **RoadSafe LLC** Back
Transportation Engineering and Research

Field Guide for Guardrail Damage Assessment

You have completed the guardrail damage assessment for this damaged section. Please tap the results button to continue.

Results

This completes the damage assessment. Click the “Results” button to continue.

<p>Help  <small>Transportation Engineering and Research</small></p> <p>Guardrail Damage Assessment Results</p> <p>The damage you have is part of the end terminal. See the manufacturer's recommendations regarding specific instructions for repair/replacement of the damaged components and additional damage assessments specific to the end-terminal type.</p> <p>**Please scroll down for more information and to complete the assessment.**</p> <p>General Information: Name: RoadSafe Email: User@Roadsafellc.com Date: 12/01/2014 State: ME State Route: Example 3 Side of Road: Approximate Milepost: GPS: Rail Type: System Height: Post Type: Post Spacing: Blockout Type:</p> <p>Recommendations:</p> <p>The upstream end terminal is compromised and needs to be repaired. See the manufacturer's recommendations regarding specific instructions for repair/replacement of the damaged components and additional damage assessments specific to the end-terminal type.</p>	<p><i>Assessment Results:</i></p> <p>The results of the assessment are provided on the final page of the online guardrail condition assessment guide. The results are also sent to the e-mail addressed provided on the Question 1 page.</p> <p>The assessment results state that the damage is part of the end-terminal and instruct the user to see the manufacturer's recommendations for repair.</p> <p>The general assessment of the terminal head, however, indicated that the end-terminal was compromised and needs to be repaired.</p>
---	--

CHAPTER 17 – CONCLUSIONS

One of the oft-touted advantages of strong-post w-beam guardrails is that they can retain some effectiveness even after having been struck and damaged. It is not always easy to discern, however, when the extent of damage warrants repair and when the damaged barrier is still largely functional. Occasionally, the damage is severe and the need to repair is evident. More frequently though the damage is the result of low-speed collisions and side-swipes which cause only minor or moderate damage for which the need to repair is not obvious. Guardrails also suffer deterioration from environmental factors and frequently incur minor impact damage during roadway maintenance operations such as snow plowing and mowing. Unfortunately, very little information has been available to quantify degradation of barrier performance that these seemingly minor damages cause.

Assessing guardrail damage is ultimately the responsibility of maintenance and repair personnel within each state's DOT. Making proper damage assessments maximizes the overall safety of the roadway by ensuring that the limited resources of the DOT are applied only to those guardrails that are no longer deemed effective. The result of this research study was a Field Guide that provides quantitative criteria for assessing guardrail damage and repair priority based on measureable damage metrics for use by maintenance personnel.

Phase I of this study was performed by Gabler *et. al* at Virginia Tech and was focused on damage assessments for the modified G4(1S) guardrail; those results were published in *NCHRP Report 656*. The work performed in the current study expands on Report 656 by including assessment criteria for the G4(2W) guardrail as well as additional damage assessment criteria for the modified G4(1S). The overall result is a relatively comprehensive field guide for assessing damages for these two very common strong-post guardrail systems. Further, the assessment criteria for the G4(2W) is considered applicable for all wood-post w-beam guardrails that are of the same basic design and that use guardrail posts of similar dimensions. For example, the G4(1W), G4(2W), and the ODOT Type 5 guardrail all use slightly different shaped wooden posts, but otherwise share the same system components. Although the posts are different (e.g., square, rectangular, and round, respectively), they are similar in that they are all wood and are of similar dimensions (i.e., 8-10 inches in width/diameter and 6 ft in length).

Damage Modes Investigated

The damage modes evaluated in this study included:

- Guardrail post deterioration (e.g., rot and insect damage),
- End-terminal damages that may affect anchor strength,
- Combination damage modes of rail deflection and rail-to-post connection,
- Soil erosion around guardrail posts, and
- Additional splice damages that were not investigated in Phase I.

The basic research approach was similar to that used in Report 656 and involved a combination of pendulum testing and computational analyses to assess performance degradation of the G4(2W) guardrail for various damage modes. Pendulum testing was used to quantify strength degradation of various guardrail components subjected to varying types and levels of damage, to evaluate failure modes that are not well suited for finite element analysis; and also to validate the accuracy of the finite element models and gain confidence in their results. Finite

element analysis was then used to investigate the effects of damage modes on overall system performance. For example, pendulum tests were used to quantify reduction in post strength as a function of deterioration (e.g., rot or insect damage); the results of the pendulum tests were used to validate/calibrate the finite element model of the post-soil system(s); FEA was then used to evaluate the effects of the various levels of damage on system performance. All crash performance evaluations of the damaged systems were carried out based on the crash testing procedures used in evaluation of the original undamaged systems, so that performance degradation could be directly assessed. For the systems evaluated in this study, the impact conditions corresponded to *NCHRP Report 350* Test Level 3.

The recommended procedures and assessment criteria for evaluating each damage mode are presented at the end of each corresponding chapter and are also assembled in Appendix A in the format of a “field guide.” The evaluation procedures in Appendix A are presented in a graphical format to facilitate the assessment process. For each damage mode, a commentary is also provided to support the evaluation criteria.

The guidance presented herein is based solely on the effectiveness of the damaged guardrail to safely contain and redirect errant vehicles. Three classifications are used to denote the relative priority for repair – High, Medium and Low. These were adopted from *NCHRP Report 656* and are defined as follows:

- **High Priority:** Indicates damage where the crash performance of the barrier has been compromised to such a degree that a second impact to the damaged barrier would result in unacceptable vehicle and/or barrier performance. This would include vehicle penetration of the barrier (via rail rupture, vehicle override, or vehicle underride) and vehicle rollover.
- **Medium Priority:** Indicates damage where the crash performance of the barrier has likely been compromised to some degree but the system should perform effectively for a majority of impact conditions.
- **Low Priority:** Indicates that the damaged guardrail is expected to remain fully functional.

The probability of a second impact on a previously damaged guardrail is dependent on many factors related to traffic exposure, including: crash history, ADT, operating speeds, roadway type, road curvature, roadway grade and pavement conditions to name a few. Determining the risk of a second impact was beyond the scope of this study, but is an important factor to consider when determining priority for repair.

Recommendations for Future Work

In developing these guidelines several areas for improvement were identified that should be considered in future research:

- A more simplified *in situ* procedure for quantifying the level of deterioration of wood guardrail posts needs to be developed. The procedure developed herein appears to be reasonably accurate for use in research studies, but due to equipment cost and complexity of the method it may not be feasible for use in routine maintenance assessments.
- Additional analyses or full-scale testing should be performed to evaluate the effects of anchor strength using an impact point located nearer to the upstream anchor system. Additionally, an investigation similar to the one conducted herein for assessing effects of anchor strength on the performance of the G4(2W) should be conducted to assess effects of anchor strength on the performance of the G4(1S). It is expected that the G4(1S) will have a greater sensitivity

to anchor strength due to the low torsional rigidity of the W6x9 steel posts of the G4(1S) guardrail.

- The impact conditions used herein to generate pre-existing crash-induced rail deflections involved low speeds and a high impact angle which resulted in damage to a relatively localized section of the guardrail; i.e., the damaged area generally spanned only 3 to 4 posts, which increased the potential for pocketing. It is not known how the guardrail will respond to subsequent impacts when the rail deflections are spread over a longer length of the guardrail. It is recommended that future studies on the effects of pre-existing crash-induced rail deflections include higher impact speeds and smaller impact angles to create initial guardrail damage with similar magnitudes of rail deflection spread over a longer length of the guardrail.
- Additional analyses or full-scale testing should be conducted to reevaluate the performance of the G4(1S), in which a standard anchor system (i.e., two foundation tubes and groundline strut) is installed on both the upstream and downstream end and a soil pit with adequate width to accommodate the full range of guardrail post deflections in the impact area.
- A more comprehensive study of damaged w-beam splice connections should be considered in future studies. The small number of damaged test articles available for the study was not sufficient to represent the complete range of damage levels for each damage mode case.
- Also, future impact studies for evaluating the capacity of rail splices should include boundary conditions that more accurately emulate the longitudinal and lateral stiffness behavior of the extended guardrail.

Recommendations for Additional Barrier Types

The guidance presented in Appendix A (i.e., the Field Guide) addresses a number of the most frequently encountered damage modes for the two most common guardrail systems (i.e., G4(1S) and G4(2W)). In Chapter 5 several additional guardrail systems were identified with relatively high rating for inclusion in the Field Guide, but had to be excluded from this study due to funding limitations. These systems include the G2 weak post guardrail, the G9 thrie-beam guardrail and the MGS. The G2 weak-post guardrail was the highest rated system for future study, followed very closely by the thrie-beam guardrail. The thrie-beam is not as popular as the strong-post w-beam, but almost all states have a number of thrie-beam installations. Although the G2 weak-post guardrail received the second highest rating from the survey respondents for inclusion in the study, the rating for the thrie-beam guardrail was very similar (see Appendix A), thus a case could be made for selecting either system. Consideration should also be given to the fact that the thrie-beam guardrail will require fewer damage mode evaluations for developing a comprehensive set of assessment criteria, compared to the weak-post system. As of this reporting date, there are currently not as many MGS guardrail installations compared to other strong-post guardrail systems; however, many states are now requiring that the MGS system be used in all new guardrail installations. Therefore, the MGS is also considered to have a relatively high rating for inclusion in future updates to the field guide.

REFERENCES

- AASHTO04 AASHTO-AGC-ARTBA Joint Committee, “A Guide to Standardized Hardware,” American Association of State and Highway Officials, Association of General Contractors, and American Road and Transportation Builder’s Association, Web-Document, https://www.aashtotf13.org/guide_display.php (2004).
- AASHTO09 American Association of State Highway and Transportation Officials, Manual for Assessing Safety Hardware, AASHTO Subcommittee on Bridges and Structures, Washington, D.C. (2009).
- Bielenberg07 Bielenberg, R.W., Faller, R.K., Rohde, J.R., Reid, J.D., Sicking, D.L., Holloway, J.C., Allison, E.M., and Polivka, K.A., Midwest Guardrail System for Long-Span Culvert Applications, Final Report to the Midwest States' Regional Pooled Regional Pooled Fund Program, Transportation Research Report No. TRP-03-187-07, Project No.: SPR-3(017), Project Code: RPPF-05-04 -Year 15, Midwest Roadside Safety Facility, University of Nebraska-Lincoln (November 16, 2007).
- Bligh95 Bligh, R.P. and W.L. Menges, “Crash Testing and Evaluation of Round, Wood Post, W-Beam Guardrail System,” Report No. 405391, Texas Transportation Institute, College Station, Texas (1995).
- Bligh97a Bligh, R.P., W.L. Menges, B.G. Butler, “Evaluation of a Modified Steel Post W-Beam Guardrail System,” Report No. TX-98/3963-S, Performed for the Texas Department of Transportation, Performing Agency: Texas Transportation Institute, College Station, Texas (January 1997).
- Bligh97b Bligh, R.P. and W.L. Menges, “Testing and Evaluation of Modified Steel Post W-Beam Guardrail with Recycled Polyethylene Blockouts,” TTI Project 400001-MPT, Texas Transportation Institute, College Station, Texas (1997).
- Brewer90 Brewer, K., “W-Beam Guardrail Repair and Maintenance: A Guide for Street and Highway Maintenance Personnel,” FHWA-RT-90-001, Federal Highway Administration, Washington, D.C. (1990).
- Bronstad71 Bronstad, M.E. and R.B. Burket, “Evaluation of timber weak-post guardrail systems,” Highway Research Record 343, Washington, D.C. (1971).
- Bronstad88 Bronstad, M.E., Calcote, L.R., Ray, M.H., and Mayer, J.B., Guardrail-Bridge Rail Transition Designs Volume 1, Research Report. Publication No. FHWA/RD-86/178 (1988).
- Brown91 CM Brown, ‘Pendulum Testing of BCT Wood Posts, FOIL Tests: 91P039 through 91P045’, Federal Outdoor Impact Laboratory (FOIL), McLean, Virginia (August 1991).
- Bullard96 Bullard, D.L., Jr., W.L. Menges, and D. Alberson, “NCHRP Report 350 Compliance Test 3-11 of the Modified G4(1S) Guardrail with Timber Blockouts,” FHWA Contract DTFH61-95-C-00090, Research Project 405421-1, Texas Transportation Institute, College Station, Texas (January 1996).

- Bullard00 Bullard, D.L., W.L. Menges, “NCHRP Report 350 Test 3-11 on the G4(2W) Strong Post W-Beam Guardrail with 100 mm High Asphaltic Curb,” Report 404201-1, Texas Transportation Institute, College Station, Texas (June 2000).
- Bullard09 Bullard, D.L., Jr., R.P. Bligh, and W.L. Menges, “MASH TL-3 Testing and Evaluation of the G4(2W) W-Beam Guardrail,” Report No. 476460-1-5, Texas Transportation Institute, College Station, Texas (January 2009).
- Bullard10 Bullard, D.L., Jr., R.P. Bligh, W.L. Menges, and R.R. Haug, *NCHRP Web-Only Document 157, Volume I: Evaluation of Existing Roadside Safety Hardware Using Updated Criteria – Technical Report*, Transportation Research Board of the National Academies, Washington, D.C. (2010).
- Buth99a Butth, E.C., R.A. Zimmer and W.L. Menges, “Testing and Evaluation of a Modified G4(1S) guardrail with W150x17 Steel Blockouts,” Test Report No. 405421-2, Texas Transportation Institute, Texas A&M University, College Station, Texas (1999).
- Buth99b Butth, E.C., R.A. Zimmer and W.L. Menges, “NCHRP Report 350 Test 3-11 of the Strong Wood Post Thrie Beam Guardrail,” Report No. FHWA-RD-99-061, Test Report No. 404211-11, Texas Transportation Institute, Texas A&M University, College Station, Texas (1999).
- Buth99c Butth, E.C. and W.L. Menges, “NCHRP Report 350 Test 4-12 of the Modified Thrie Beam Guardrail,” Report No. FHWA-RD-99-065, Test Report No. 404211-5a, Texas Transportation Institute, Texas A&M University, College Station, Texas (1999).
- Buth00a Butth, C.E., W.L. Menges, and S.K. Schoeneman, “NCHRP Report 350 Test 3-11 on the Modified PennDOT Type 2 Guide Rail, Test No. 473750-1, Texas Transportation Institute, College Station, Texas (January 2000).
- Buth00b Butth, C.E., W.L. Menges, and S.K. Schoeneman, “NCHRP Report 350 Test 3-11 on the Modified PennDOT Type 2 Guide Rail – Test 2, Test No. 473750-2, Texas Transportation Institute, College Station, Texas (February 2000).
- Buth00c Butth, C.E., W.L. Menges, and S.K. Schoeneman, “NCHRP Report 350 Test 3-11 on the Modified PennDOT Type 2 Guide Rail – Test 3, Test No. 473750-3, Texas Transportation Institute, College Station, Texas (2000).
- Buth00d Butth, C.E., W. L. Menges, S. K. Schoeneman, “NCHRP Report 350 Assessment of Existing Roadside Safety Hardware,” Research Report 404211-F, Texas Transportation Institute, College Station, Texas (November 2000).
- Buth00e Butth, C.E., W.L. Menges, and S.K. Schoeneman, “NCHRP Report 350 Test 3-10 on the Modified PennDOT Type 2 Guide Rail – Test 4, Test No. 473750-4, Texas Transportation Institute, College Station, Texas (2000).
- Buth00f Butth, C.E., D.L. Bullard, and W.L. Menges, “NCHRP Report 350 Test 3-11 on the Modified PennDOT Type 2 Guide Rail – Test 3, Test No. 473750-3, Texas Transportation Institute, College Station, Texas (2000).
<http://www.wsdot.wa.gov/research/reports/fullreports/662.1.pdf>

- Buth06 Buth, C.E., W.L. Menges, and S.K. Schoeneman, “NCHRP Report 350 Test 3-11 of the Long-Span Guardrail with 5.7 m Clear Span and Nested W-Beams Over 11.4 m,” Report/Test No.405160-1-1, Texas Transportation Institute, College Station, Texas (May 2006).
- Coon99 Coon, B.A., Reid, J.D., and Rohde, J.R., Dynamic Impact Testing of Guardrail Posts Embedded in Soil, Research Report TRP-03-77-98, Midwest Roadside Safety Facility, The University of Nebraska-Lincoln, Lincoln, Nebraska (July 1999).
- Dolci12 Dolci, Stefano, “Design of Suspension Component Testing for Chevy Silverado Model,” Unpublished Power Point document, Presentation made to the Computational Mechanics Workshop, Turner Fairbank, McLean, VA (January 2012).
- Engstrand00 Engstrand, K.E., M.H. Ray, C.A. Plaxico and R.G. McGinnis, “Testing of PennDOT Type 2 Guide Rail,” Work Order No. 50, Final Report to the Pennsylvania Department of Transportation, Work performed at Worcester Polytechnic Institute, Worcester, Massachusetts (December 2000).
- Faller04 Faller, R.K., K.A. Polivka, B.D. Kuipers, R.W. Bielenberg, J.D. Reid, J.R. Rohde, and D.L. Sicking, Midwest Guardrail System for Standard and Special Applications, *Transportation Research Record: Journal of the Transportation Research Board*, No. 1890, pp 19-33 (2004). <https://doi.org/10.3141/1890-03>
- Faller07 Faller, R.K., D.L. Sicking, R.W. Bielenberg, J.R. Rohde, K.A. Polivka, and J.D. Reid, Performance of Steel-Post, W-Beam Guardrail Systems, *Transportation Research Record: Journal of the Transportation Research Board*, No. 2025, pp 18-33 (2007). <http://pubsindex.trb.org/view.aspx?id=802321>
- Faller09 Faller, R.K., J.D. Reid, D.E. Kretschmann, J.A. Hascall, and D.L. Sicking, Midwest Guardrail System with Round Timber Posts, *Transportation Research Record: Journal of the Transportation Research Board*, No. 2120, pp 47-59 (2009). http://www.fpl.fs.fed.us/documnts/pdf2009/fpl_2009_faller001.pdf
- Fleck08a Fleck, “1997 Chevrolet C2500 Pickup Impact with the Strong Steel Post W-Beam Guardrail – Part 1,” Test Report C08C3-027-1, MGA Research Corporation, Burlington, WI (2008).
- Fleck08b Fleck, “1997 Chevrolet C2500 Pickup Impact with the Strong Steel Post W-Beam Guardrail – Part 2,” Test Report C08C3-027-2, MGA Research Corporation, Burlington, WI (2008).
- Gabler10 Gabler, H.C., D.J. Gabauer, and C.E. Hampton, *NCHRP Report 656: Criteria for Restoration of Longitudinal Barriers*, Transportation Research Board of the National Academies, Washington, D.C. (2010). <https://dx.doi.org/10.17226/14374>
- Garret98 Riley, “Light Vehicle Inertial Parameter Database,” (http://www.nrd.nhtsa.dot.gov/vrtc/ca/nhtsa_inertia_database_metric.pdf), National Highway Traffic Safety Administration, Washington, D.C. (1998).

- Hampton10 Hampton, C.E., and Gabler, H.C., “Crash Performance of Strong-Post W-Beam Guardrail with Missing Blockouts,” Virginia Tech – Center for Injury Biomechanics, Blacksburg, VA 24061, Proceedings of the 2010 ICRASH Conference, Paper No. 2010-118, Washington, D.C. (September 2010). <http://www.me.vt.edu/gabler/publications/ICRASH-2010-118.pdf>
- Hascall07 Hascall, J.A., R.K. Faller, J.D. Reid, D.L. Sicking, and D.E. Kretschmann, “Investigating the Use of Small-Diameter Softwood as Guardrail Posts (Dynamic Test Results),” MwRSF Research Report No. TRP-03-179-07, Midwest Roadside Safety Facility, Lincoln, Nebraska (2007).
- HRB62 HRB, “Proposed Full-scale Testing Procedures for Guardrails,” Highway Research Board Circular 482, Highway Research Board, Washington, D.C. (1962).
- Jeyapalan84 Jeyapalan, J.K., J.F. Dewey, T.J. Hirsch, H.E. Ross, and H. Cooner, Soil-Foundation Interaction Behavior of Highway Guardrail Posts, *Transportation Research Record*, No. 970, pp 37-47 (1984). <http://onlinepubs.trb.org/Onlinepubs/trr/1984/970/970-006.pdf>
- Karlsson00 Karlsson, J., Design of a Non-Snagging Guardrail Post, Master’s Thesis, Worcester Polytechnic Institute, Worcester, MA (June 2000).
- Kilarski99 Kilarski, W. P., M. El-Gindy, B. D. St. John and B. Peacheux, “Type 2 Weak Post Guardrail Testing,” Pennsylvania Transportation Institute, Pennsylvania State University, State College, PA (1999).
- Kuipers03 Kuipers, B.D. and Reid, J.D., Testing of W152x23.8 (W6x16) Steel Posts - Soil Embedment Depth Study for the Midwest Guardrail System (Non-Proprietary Guardrail System, Final Report to the Midwest States' Regional Pooled Fund Program, Transportation Research Report No. TRP-03-136-03, Midwest Roadside Safety Facility, University of Nebraska-Lincoln (June 12, 2003).
- Kuipers05 Kuipers, B.D., R.K. Faller, and J.D. Reid, Critical Flare Rates for W-Beam Guardrail - Determining Maximum Capacity Using Computer Simulation, Final Report, NCHRP Project No. 17-20(3), Transportation Research Report No. TRP 03-157-04, Midwest Roadside Safety Facility, University of Nebraska-Lincoln (January 24, 2005).
- LS-DYNA13 User’s Manual Volumes 1 and 2 Version R7.0, Livermore Software Technology Corporation, Livermore, California (February 2013).
- Mak93 Mak, K.K, R.P Bligh, D.L. Bullard, “Crash Testing and Evaluation of a Low-Speed W-Beam Guardrail System”, Final Report Number WA-RD 325.1, Texas Transportation Institute, College Station, Texas (1993).
- Mak94 Mak, K.K. and W.C. Menges, “Crash Testing and Evaluation of Strong-Post W-beam Guardrails,” Texas Transportation Institute, College Station, Texas (1994).
- Mak95 Mak, K.K., R.P. Bligh, and W.L. Menges, “Crash Testing and Evaluation of Existing Guardrail Systems.” Texas Transportation Institute, Test Report No.

- 471470-26, The Texas A & M University, College Station, Texas (December 1995).
- Mak96a Mak, K.K., R. Bligh, and W. C. Menges, "Testing of State Roadside Safety Systems," FHWA Contract DTFH61-89-C-00089, Research Study RF471470, Texas Transportation Institute, College Station, Texas (1996).
- Mak96b Mak, K.K., and Menges, W.L., "Testing of State Roadside Safety Systems Volume X: Appendix I – Crash Testing and Evaluation of a Mini-Melt Terminal for a W-Beam, Weak-Post (G2) Guardrail System (Draft Report)". Texas Transportation Institute, Texas A&M University System, College Station, Texas (June 1996).
- Mak96c Mak, K.K., Bligh, R.P., and Menges, W.L., "Testing and evaluation of the MELT-2 Terminal (Draft final report)". Texas Transportation Institute, Texas A&M University System, College Station, Texas (August 1996).
- Mak99a Mak, K.K., Bligh, R.P., and Menges, W.L., "Testing of State Roadside Safety Systems Volume XI: Appendix J – Crash Testing and Evaluation of Existing Guardrail Systems," Report No. FHWA-RD-98-046, Texas Transportation Institute, Texas A&M University System, College Station, Texas (April 1999).
- Mak99b Mak, K.K., Bligh, R.P., and Menges, W.L., "Crash Testing of Ford Taurus, Chevrolet Lumina, Plymouth Neon, and Dodge Caravan – In Support of Finite Element Computer Modeling (Draft Report)", Project No. 472580, Texas Transportation Institute, Texas A&M University System, College Station, Texas (May 1999).
- Marzougui07a Marzougui, P., Mohan, D., S. Kan and K. Opiela, "Evaluation of Rail Height Effects of the Safety Performance of W-Beam Barriers," Working Paper NCAC 2007-W-002, National Crash Analysis Center, Ashburn, VA (October 2007). <http://www.ncac.gwu.edu/research/pubs/NCAC-2007-W-002.pdf>
- Marzougui07b Marzougui, D., S. Kan and K. Opiela, "Evaluating W-Beam Guardrail Height Tolerances," Technical Summary NCAC 2007-T-003, Report prepared for FHWA, National Crash Analysis Center, Ashburn, VA (November 2007). <http://www.ncac.gwu.edu/research/pubs/NCAC-2007-T-003.pdf>
- Marzougui09 Marzougui, D., S. Kan and K. Opiela, "Safety Performance Evaluation of G4(2W) W-Beam Guardrail with Blockouts Raised by 3 Inches," Technical Summary NCAC 2009-T-002, Report prepared for FHWA, National Crash Analysis Center, Ashburn, VA (April 2009). <http://www.ncac.gwu.edu/research/pubs/NCAC-2008-T-002.pdf>
- Marzougui10 Marzougui, U. Mahadevaiah and K. Opiela, "Development of a Modified MGS Design for Test Level 2 Impact Conditions Using Crash Simulation," Working Paper NCAC 2010-W-005, National Crash Analysis Center, Ashburn, VA (June 2010). <http://www.ncac.gwu.edu/research/pubs/NCAC-2010-W-005.pdf>
- MASH09 Manual for Assessing Safety Hardware (MASH), American Association of State Highway and Transportation Officials (2009).

- Mayer99 Mayer, J.B., "Full-Scale Crash Evaluation of a Modified Eccentric Loader Terminal", Final Report, Report Number FHWA-RD-99-031, Federal Highway Administration, Washington, D.C. (September 1999). <http://ntl.bts.gov/lib/15000/15600/15676/PB2000100277.pdf>
- Michie71 Michie, J.D., L.R. Calcote, M.E. Bronstad, *NCHRP Report 115: Guardrail Performance and Design*, HRB, National Research Council, Washington, D.C. (1971). http://onlinepubs.trb.org/Onlinepubs/nchrp/nchrp_rpt_115.pdf
- Michie81 Michie, J.D., *NCHRP Report 230: Recommended Procedures for the Safety Performance Evaluation of Highway Appurtenances*, TRB, National Research Council, Washington, D.C. (March 1981). https://onlinepubs.trb.org/Onlinepubs/nchrp/nchrp_rpt_230.pdf
- Murray07 Murray, Y.D., "Manual for LS-DYNA Material Model 143," Report Number FHWA-HRT-04-097, APTECK, Inc., Colorado Springs, CO (2007).
- NCAC08 Finite Element Model of C1500 Pickup Truck, <http://www.ncac.gwu.edu/vml/archive/ncac/vehicle/c2500pickup-0.7.pdf>
- Patzner97 Patzner, G.S. "Effect of Wood Post Strength and Soil Strength on the Performance of the Modified Eccentric Loader Breakaway Cable Terminal (MELT) Under Impact Conditions Prescribed by NCHRP Report 350, Test3-35," Master's Thesis, University of Iowa (December 1997).
- Patzner99 Patzner, G.S., C.A. Plaxico, and M.H. Ray, Effect of Post and Soil Strength on the Performance of the Modified Eccentric Loader Breakaway Cable Terminal (MELT), *Transportation Research Record: Journal of the Transportation Research Board*, No. 1690, pp 78-83 (1999). <https://doi.org/10.3141%2F1690-08>
- Plaxico95 Plaxico, C.A., Hackett, R.M., Uddin, W. and Adeff, S.E. "Crashworthiness Analysis of a Modified Thrie-Beam Guardrail," Proceedings of the 32nd Annual Technical Meeting of the Society of Engineering Science, New Orleans, October 29 - November 2, 1995, pp 201-202.
- Plaxico97 Plaxico, C.A., R.M. Hackett, and W. Uddin, Simulation of Vehicle Impacting a Modified Thrie-Beam Guardrail, *Transportation Research Record*, No. 1599, pp 1-10 (1997). <https://doi.org/10.3141%2F1599-01>
- Plaxico98 Plaxico, C.A., G.S. Patzner, and M.H. Ray, Finite Element Modeling of Guardrail Timber Posts and the Post-Soil Interaction, *Transportation Research Record*, No. 1647, pp 139-146, Paper No. 980791 (1998). <https://doi.org/10.3141%2F1647-17>
- Plaxico00 Plaxico, C.A., M.H. Ray, and K. Hiranmayee, Comparison of the Impact Performance of the G4(1W) and G4(2W) Guardrail Systems Under Report 350 Test 3-11 Conditions, *Transportation Research Record: Journal of the Transportation Research Board*, No. 1720, pp 7-18 (2000). <https://doi.org/10.3141%2F1720-02>
- Plaxico02 Plaxico, C.A., Design Guidelines for the Use of Curbs and Curb/Guardrail Combinations along High-Speed Roadways, Ph.D. Dissertation, Worcester Polytechnic Institute, Worcester, MA (2002).

- Plaxico03 Plaxico, C.A., F. Mozzarelli and M.H. Ray, “Tests and Simulation of a W-Beam Rail-to-Post Connection,” *International Journal of Crashworthiness*, Vol.8, No. 3, pp. 001-009, Woodhead Publishing Ltd 0257 (2003).
- Plaxico07 Plaxico, C.A., Kennedy, J.C., and Miele, C.R., “Evaluation and Redesign of a Culvert Guardrail and Transition System,” Technical Report, Ohio Department of Transportation (2007).
- Plaxico09 Plaxico, C., Miele, C., Kennedy, J., Simunovic, S. and Zisi, N., Enhanced Finite Element Analysis Crash Model of Tractor-Trailers (Phase B), National Transportation Research Center, Inc., Knoxville, TN (August 2009).
- Polivka99 Polivka, K.A., R.K. Faller, D.L. Sicking, J.R. Rhode, J.D. Reid and J.C. Holloway, .Guardrail and Guardrail Terminals Installed Over Curbs,. MwRSF Research Report No. TRP-03-83-99, Midwest Roadside Safety Facility, University of Nebraska-Lincoln (September 23, 1999).
- Polivka00a Polivka, K.A., R.K. Faller, D.L. Sicking, J.R. Rohde, J.D. Reid, and J.C. Holloway, “Guardrail and Guardrail Terminals Installed Over Curbs”, Final Report to the Midwest States' Regional Pooled Fund Program, Transportation Research Report No. TRP-03-83-99, Project No. SPR-3(017)-Year 8, Midwest Roadside Safety Facility, University of Nebraska-Lincoln (2000).
- Polivka00b Polivka, K.A., Faller, R.K., Sicking, D.L., Rohde, J.R., Holloway, J.C., and Keller, E.A., Development of a W-Beam Guardrail System for Use on a 2:1 Slope, Final Report to the Midwest States' Regional Pooled Fund Program, Transportation Research Report No. TRP-03-99-00, Project No. SPR-3(017)-Years 9 & 10, Midwest Roadside Safety Facility, University of Nebraska-Lincoln (October 16, 2000).
- Polivka06a Polivka, K.A., R.K. Faller, D.L. Sicking, J.R. Rohde, B.W. Bielenberg, J.D.Reid, “Performance Evaluation of the Modified G4(1S) Guardrail – Update to NCHRP Report 350 Test No. 3-11 (2214WB-1),” Report No., TRP-03-168-06. Midwest Roadside Safety Facility, University of Nebraska-Lincoln (October 2006).
- Polivka06b Polivka, K.A., R.K. Faller, D.L. Sicking, J.R. Rohde, B.W. Bielenberg, J.D.Reid, “Performance Evaluation of the Modified G4(1S) Guardrail – Update to NCHRP Report 350 Test No. 3-11 with 28” C.G. Height (2214WB-2),” Report No. TRP-03-169-06, Midwest Roadside Safety Facility, University of Nebraska-Lincoln (October 2006).
- Polivka06c Polivka, K.A., R.K. Faller, D.L. Sicking, J.R. Rohde, B.W. Bielenberg, J.D.Reid, “Performance Evaluation of the Midwest Guardrail System – Update to NCHRP Report 350 Test No. 3-11 (2214MG-1),” Report No. TRP-03-170-06, Midwest Roadside Safety Facility, University of Nebraska-Lincoln (October 2006).
- Polivka06d Polivka, K.A., R.K. Faller, D.L. Sicking, J.R. Rohde, B.W. Bielenberg, J.D.Reid, “Performance Evaluation of the Midwest Guardrail System – Update to NCHRP Report 350 Test No. 3-11 with 28” C.G. Height (2214MG-2),” Report No. TRP-03-171-06, Midwest Roadside Safety Facility, University of Nebraska-Lincoln (October 2006).

- Polivka06e Polivka, K.A., R.K. Faller, D.L. Sicking, J.R. Rohde, B.W. Bielenberg, J.D.Reid, “Performance Evaluation of the Midwest Guardrail System – Update to NCHRP Report 350 Test No. 3-10 (2214MG-3),” Report No. TRP-03-172-06, Midwest Roadside Safety Facility, University of Nebraska-Lincoln (October 2006).
- Ray01a Ray, M.H., K.E. Engstrand, C.A. Plaxico, and R.G. McGinnis, Improvements to the Weak-Post W-Beam Guardrail, *Transportation Research Record: Journal of the Transportation Research Board*, No. 1743, pp 88-96, Paper No. 01-2282 (2001). <https://doi.org/10.3141%2F1743-12>
- Ray01b Ray, M.H., C.A. Plaxico, and K.E. Engstrand, Performance of W-Beam Splices, *Transportation Research Record: Journal of the Transportation Research Board*, No. 1743, pp 120-125, Paper No. 01-2420 (2001). <https://doi.org/10.3141%2F1743-16>
- Ray04 Ray, M.H., C.A. Plaxico and E. Oldani, “Finite Element Simulations of the Performance of the Alberta Weak-Post W-Beam Guardrail,” Performed for the Province of Alberta, Canada, Performed by Worcester Polytechnic Institute, Worcester, MA (November 2004).
- Ray08 Ray, M.H., Anghileri, M., Mongiardini, M., “Comparison of Validation Metrics Using Full-Scale Automobile Crash Tests,” 8th World Congress on Computational Mechanics, Venice, Italy (June 30 – July 5, 2008).
- Ray10 Ray, M.H., M. Mongiardini, C.A. Plaxico, and M. Anghileri, *NCHRP Web-Only Document 179: Procedures for Verification and Validation of Computer Simulations Used for Roadside Safety Applications*, Transportation Research Board of the National Academies, Washington, D.C. (2010).
- Reid97 Reid, J.D., D.L. Sicking, R.K. Faller, and B.G. Pfeifer, Development of a New guardrail System, *Transportation Research Record*, No. 1599, pp. 72-80 (1997).
- Reid07 Reid, J.D, B.D. Kuipers, D.L. Sicking, and R.K. Faller, Guardrail Flare Rates, Presented at 86th Annual Meeting of the Transportation Research Board, Washington, D.C. (2007).
- Rhohde95 Rohde, J.R. and Reid, J.D., Evaluation of the Performance Criteria for Wood Posts in Strong-Post W-Beam Guardrail, Research Report, Midwest Roadside Safety Facility, University of Nebraska-Lincoln, Lincoln, Nebraska (1995).
- Rhohde96 Rohde, J.R., B.T. Rosson and R. Smith, Instrumentation for Determination of Guardrail-Soil Interaction, *Transportation Research Record*, No. 1528, pp 109-115 (1996). <https://doi.org/10.1177%2F0361198196152800111>
- ROBUST02 Road Barrier Upgrade of Standards (ROBUST), “Deliverable 4.1.1 – Full scale test results – An analysis,” ROBUST PROJECT, GRD-2002-70021 (2002).
- Ross93 Ross, H.E., D.L. Sicking, R.A. Zimmer, and J.D. Michie, *NCHRP Report 350: Recommended Procedures for the Safety Performance Evaluation of Highway Features*, TRB, National Research Council, Washington, D.C. (1993). http://onlinepubs.trb.org/onlinepubs/nchrp/nchrp_rpt_350-a.pdf

- Ross99 Ross, H.E. Jr., Bligh, R.P. and Menges, W.L., "Evaluation of Roadside Features to Accommodate Vans, Minivans, Pickup Trucks, and 4-Wheel Drive Vehicles" (Preliminary Draft). Texas Transportation Institute, Texas A&M University System, College Station, Texas, November (1999).
- Rosenbaugh07 Rosenbaugh, S.K, Sicking, D.L., and Faller, R.K., "Development of a TL-5 Vertical Faced Concrete Median Barrier Incorporating Head Ejection Criteria," Test Report No. TRP- 030194-07, Midwest Roadside Safety Facility, University of Nebraska-Lincoln, 12/10/2007. [Test No. TL5CMB-2]
- Rosenbaugh12 Rosenbaugh, S., "Research Update from MwRSF," Presented at the Transportation Research Board AFB20 Subcommittee Mid-Year Meeting, Irvine, California (August 1, 2012).
- Rosson96 Rosson, B.T., M.G. Bierman, and J.R. Rohde, Assessment of Guardrail-Strengthening Techniques, *Transportation Research Record*, No. 1528, pp 69-77 (1996). <https://doi.org/10.1177%2F0361198196152800107>
- Sheikh09 Sheikh, N.M., R. Ferdous, R.P. Bligh and A.Y. Abu-Odeh, "Analysis of Roadside Safety Devices for use on Very High-Speed Roadways," Report No. FHWA/TX-09/0-071-1, Technical report prepared for Texas Department of Transportation, Performing Agency Texas Transportation Institute, College Station Texas (September 2009).
- Sicking02 Sicking, D.L., J.D. Reid and J.R. Rohde, Development of the Midwest Guardrail System, *Transportation Research Record: Journal of the Transportation Research Board*, No. 1797, pp 44-52 (2002). <https://doi.org/10.3141/1797-06>
- Sicking87 Sicking, D.L. and H.E. Ross, Jr., Structural Optimization of Strong-Post W-Beam Guardrail, *Transportation Research Record*, No. 1133, pp 42-50 (1987).
- Strybos97 Strybos, J., and J. Mayer. "Full-Scale Crash Evaluation of a Modified Eccentric Loader Terminal", NCHRP Report 350 Test Designation 3-35, SwRI Test No. MLT-3. Federal Highway Administration, Washington, D.C., (February 1997).
- TTI98 TTI, "Test Risk Assessment Program (TRAP) Version 1.01: User's Manual," Texas Transportation Institute, College Station, TX (1998).
- Vignjevic Vignjevic, J., "Review of Development of the Smooth Particle Hydrodynamics (SPH) Method," Crashworthiness, Impact and Structural Mechanics (CISM), Cranfield University, UK.
http://naca.central.cranfield.ac.uk/dcsss/2004/A4_RadeKeynoteEDITfinal.pdf
- Wright96 Wright, A., and M.H. Ray, Characterizing Roadside Hardware Materials for LSDYNA Simulations, Report No. FHWA-RD-96-108, Federal Highway Administration (1996)

Appendices A-S are not published here but can be found on the TRB website (www.trb.org) by searching for *NCHRP Web-Only Document 304: Criteria for Restoration of Longitudinal Barriers, Phase II*.